

NASA Conference Publication 2265

**Proceedings of the Fourteenth
Annual Precise Time and
Time Interval (PTTI) Applications
and Planning Meeting**

**A meeting held at the
NASA Goddard Space Flight Center
Greenbelt, Maryland
November 30, December 1-2, 1982**

Sponsored by

Naval Observatory
NASA Goddard Space Flight Center
Naval Electronic Systems Command
Naval Research Laboratory
Defense Communications Agency
Chief of Naval Operations
National Bureau of Standards
Army Electronics Technology
and Devices Laboratory
Rome Air Development
Center

NASA
National Aeronautics and
Space Administration

**Scientific and Technical
Information Branch
1983**

EXECUTIVE COMMITTEE

Schuyler C. Wardrip, Chairman
NASA Goddard Space Flight Center

Ralph T. Allen
Naval Electronic Systems Command

Charles A. Bartholomew
Naval Research Laboratory

Dr. William J. Klepczynski
Naval Observatory

Dr. Arthur O. McCoubrey
National Bureau of Standards

James A. Murray, Jr.
Naval Research Laboratory

Dr. Samuel R. Stein
National Bureau of Standards

Dr. Harris A. Stover
Defense Communications Agency

Straton M. Spyropoulos
Naval Observatory

Dr. John R. Vig
Army Electronics Technology
and Devices Laboratory

Dr. Nicholas F. Yannoni
Rome Air Development Center

Sheila C. Faulkner
Naval Observatory
Administrative Assistant

GENERAL CHAIRMAN

DR. RICHARD L. SYDNOR
Jet Propulsion Laboratory

TECHNICAL PROGRAM COMMITTEE

DR. NICHOLAS F. YANNONI, CHAIRMAN
Rome Air Development Center

RALPH T. ALLEN
Naval Electronic Systems Command

DR. SAMUEL R. STEIN
National Bureau of Standards

DR. ROBERT J. COATES
NASA Goddard Space Flight Center

DR. JOHN R. VIG
Army Electronics Technology and
Devices Laboratory

ALFRED KAHAN
Rome Air Development Center

DR. GERNOT M. R. WINKLER
Naval Observatory

EDITORIAL COMMITTEE

L. J. RUEGER, CHAIRMAN
Johns Hopkins University
Applied Physics Laboratory

MS. SANDRA HOWE
National Bureau of Standards

MARK J. LISTER
Naval Research Laboratory

ANDREW C. JOHNSON
Naval Observatory

SCHUYLER C. WARDRIP
NASA Goddard Space Flight Center

PAUL F. KUHNLE
Jet Propulsion Laboratory

CHARLOTTE M. HARRIGAN - SECRETARY
Applied Physics Laboratory

SESSION CHAIRMEN

SESSION I

DR. GERNOT M. R. WINKLER
Naval Observatory

SESSION II

ALFRED KAHAN
Rome Air Development Center

SESSION III

DR. SAMUEL R. STEIN
National Bureau of Standards

SESSION IV

DR. ROBERT J. COATES
NASA Goddard Space Flight Center

SESSION V

DR. JOHN R. VIG
Army Electronics Technology and Devices Laboratory

SESSION VI

PROFESSOR I. I. RABI
Columbia University

ARRANGEMENTS

William C. Brown, GSFC
Schuyler C. Wardrip, GSFC

FINANCE COMMITTEE

Straton M. Spyropoulos, USNO
Schuyler C. Wardrip, GSFC

PUBLICATIONS

Bonnie Dustin, SASC
Charlotte M. Harrigan, APL
L. J. Rueger, APL

TECHNICAL ASSISTANCE

William A. Adams, GSFC
Paul J. Kushmeider, GSFC
Richard J. Gatto, GSFC
Thomas A. Dixon, GSFC

PRINTING

Charles V. Hardesty, GSFC
Donald E. Ellis, GSFC

RECEPTIONISTS

Bonnie Dustin, SASC
Sheila Faulkner, USNO
Charlotte Harrigan, APL
Donna Kline, NBS
Stella Scates, NRL
Betty Schwartz, NESC
Emma Thomas, GSFC
Betty Wardrip, GSFC

BANQUET SPEAKER

Professor I. I. Rabi, Nobel Laureate
Columbia University
Subject: Scientist and Society

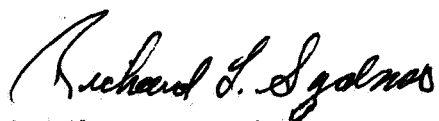
FOREWORD

These proceedings contain the papers presented at the Fourteenth Annual Precise Time and Time Interval Applications and Planning Meeting which was held on November 30 through December 2, 1982 at NASA Goddard Space Flight Center. The discussions following the presentations are also included. There were 252 registered attendees, of which 34 were from 13 foreign countries.

The objective of the meeting was to give the various sectors of the PTTI community (managers, systems engineers, program planners and industry) a forum for presentation and discussion of current and future programs and requirements, a general and in-depth review of plans and trends in PTTI applications, a review of new time and frequency developments which influence PTTI applications and an opportunity to discuss results, accomplishments and problem areas in the application of PTTI technology.

This year the emphasis on planning and applications with panel discussions by leaders in these fields was supplemented with a panel of the Distinguished Scientists who were originators of the various techniques which are at the heart of the field of frequency and time. The technical and political history of the developments was very timely and interesting. A further addition to this year's meeting was the opening of the new exhibit on atomic clocks at the National Museum of American History. All PTTI attendees were invited to a reception at the museum on the last evening of the PTTI meeting.

The Executive Committee wishes to express its appreciation of the excellent work of the Session Chairmen and the Technical Program Committee under the leadership of Dr. N. F. Yannoni. The quality of the program remains excellent as is evidenced by the increasing registration and continuing support of our sponsors. The key to the success of a meeting such as this depends on the unstinting support of the volunteers. We are fortunate to have such support by the secretaries and other personnel. In particular, the efforts of Mr. S. C. Wardrip must be recognized, as well as the hospitality of the Goddard Space Flight Center.



RICHARD L. SYDNOR
General Chairman

IN MEMORIAM

ANDREW R. CHI

From its inception, Andy Chi was an active, vocal and respected member of the PTTI Executive Committee. His background in the field of frequency and time, coupled with long and varied association with many national and international technical organizations, gave Andy a unique set of skills which complemented and enhanced the expertise embodied in the other Committee members.

Andy was born in Tiensin, China on September 12, 1920. He earned his B.S. degree in physics and mathematics from Western Maryland College in 1944, the M.A. in physics from Columbia University in 1946, and continued in graduate studies at Columbia until 1947. From that time until 1953, he was Instructor in physics at the Cooper Union School of Engineering in New York City.

Andy began his work in frequency and time in 1953 at the U.S. Army Signal Research and Development Laboratories, Fort Monmouth, New Jersey as a physicist doing research in the fundamental properties of quartz. His work contributed to the understanding of crystal growth and the effects of impurities injected into the crystal lattice. At the Naval Research Laboratory, beginning in 1957, Andy studied atomic resonance devices and precision frequency standards. Andy and his colleagues at the National Bureau of Standards developed the atomic gas cell frequency standard using optical pumping techniques. He was part of the group which first identified the hyperfine transition frequencies of Rubidium-87 and Cesium-133. The hyperfine transition of Cesium-133 eventually became the basis for the definition of the International System (SI) of the unit of time, the SI second.

In 1963, Andy joined the Goddard Space Flight Center and became head of the Timing Systems Section. He was fundamental in organizing the first symposium for the purpose of defining the short-term frequency stability of precision oscillators. He chaired both the symposium and the Technical Program Committee. Andy contributed to the Apollo Program as a member of the Navigation Working Group. Further work included developing NASA's time code standards and a time synchronization technique using the OMEGA Navigation System's Very Low Frequency transmissions.

DEDICATION

The Executive Committee and officers of the PTTI wish to dedicate these proceedings to the memory of Andy Chi, whose untimely death has deprived us of a good friend, tireless co-worker, and trusted councillor. Andy spent most of his professional life in the frequency and time area and was active in the PTTI from its beginning. His guidance and help will be greatly missed.

CONTENTS

	<u>Page</u>
CALL TO SESSION	1
Dr. Richard L. Sydnor	
WELCOME ADDRESS	3
John J. Quann	
OPENING COMMENTS	5
Dr. Nicholas F. Yannoni	

SESSION I PANEL DISCUSSION ON FUTURE TIMING REQUIREMENTS

Introduction to Planners Panel	9
Planners Panel	11
John C. Cittadino, Chairman	
Planners Panel	15
Dr. Harris A. Stover	
Planners Panel	18
Dr. Thomas Goblick	
Planners Panel	22
Dr. Michael Garvey	
Planners Panel	26
John C. Cittadino	
Two-Way Satellite Time Transfer Using Low Power CW Tones	31
C. C. Costain, H. Daams and J. -S. Boulanger	
Time Maintenance of User Clocks Via the Tracking and Data Relay Satellite System	39
Gary Whitworth, J. W. McIntyre, and R. E. Downs	
GOES Satellite Time Code Dissemination	57
R. E. Beehler	

SESSION II RUBIDIUM FREQUENCY STANDARDS

Influence of Modulation Frequency in Rubidium Cell Frequency Standards	87
C. Audoin, J. Viennet, N. Cyr, and J. Vanier	
Laser Induced Asymmetry and Inhomogeneous Broadening of the Microwave Lineshape of a Gas Cell Atomic Frequency Standard	113
J. C. Camparo, R. P. Frueholz, and C. H. Volk	

CONTENTS (continued)

	<u>Page</u>
Study of Multiple Optical Transitions in Rb ₈₇ Using Laser Diodes C. L. J. Newton and H. G. Robinson	133
A Rubidium Clock for Seek-Talk William J. Riley	141
A New Calibration Method for Time Delay Standard and its Application Bing-Wei Su and Su-Xiu Song	155
NAVEX - A Space Shuttle Experiment with Atomic Clocks S. Starker, H. Nau, J. Hammesfahr and H. Tschiesche	181
High-Accuracy Global Time and Frequency Transfer with a Space-Borne Hydrogen Maser Clock R. Decher, D. W. Allan, C. O. Alley, C. Baugher, B. J. Duncan, R. F. C. Vessot, and G. M. R. Winkler	205
Design of the Satellite Time and Frequency Transfer (STIFT) Microwave Ground Terminal H. Penfield, E. Imbier, and R. F. C. Vessot	223
Time Transfer Between the Goddard Optical Research Facility and the U.S. Naval Observatory Using 100 Picosecond Laser Pulses C. O. Alley, J. D. Rayner, C. A. Steggerda, J. V. Mullendore, L. Small, and S. Wagner	243
Open Discussion on Satellite Time Transfer Dr. G. M. R. Winkler, Moderator	269
SESSION IIIA NOISE STUDIES AND ATOMIC STANDARDS	
The Fundamental Structure Function of Oscillator Noise Models Charles A. Greenhall	281
Stochastic Models for Atomic Clocks J. A. Barnes, R. H. Jones, P. V. Tryon, and D. W. Allan	295
Narrow Rb ₈₇ and Cs ₁₃₃ Hyperfine Transitions in Evacuated Wall-Coated Cells H. G. Robinson and C. E. Johnson	307
Cesium Standard for Satellite Application M. Bloch, M. Meirs, I. Pascaru, and B. Weinstein	315

CONTENTS (continued)

	<u>Page</u>
SESSION IIIB PANEL DISCUSSION ON APPLICATIONS	
Applications Panel	325
Dr. Arthur O. McCoubrey, Moderator	
Commander William K. May	326
John D. Illgen	331
David A. Clayton	333
Dr. Mohan Ananda	335
L. Edward Stein	337
Milton Boutte	340
William Walker	341
Discussion	343
SESSION IV HYDROGEN MASER TECHNOLOGY	
Evaluation of Modern Hydrogen Masers	359
Albert Kirk, Paul Kuhnle, and Richard Sydnor	
First Experiences with the H-Maser EFOS 1	393
Wolfgang Schlüter, Klemens Nottarp, Dieter Feil, and Giovanni Busca	
A Commercial Hydrogen Maser, Progress Report	409
M. Dials and L. Wert	
The NASA/GSFC Hydrogen Maser Program: A Review of Recent Data	421
Mary Chiu, Alvin G. Bates, Lauren J. Rueger, Victor S. Reinhardt, Peter Dachel, Richard Kunski, Robert Kruger, and S. Clark Wardrip	
Timing Subsystem Development - Network Synchronization Experiments	451
K. R. Backe	
Aerospace Guidance and Metrology Center (AGMC) Inertial Navigation/ Calibration/Precise Time and Frequency Capabilities	479
Larry M. Galloway and James F. Barnaba	
Portable Clock Analyses	483
F. Neville Withington	

CONTENTS (continued)

	<u>Page</u>
Some Time Transfer Experiences with Indian Experimental Satellite APPLE	487
B. S. Mathur, P. Banerjee, A. sen Gupta, Mithlesh Saxena, A. K. Hanjura, A. K. Suri, C. L. Jain, K. Kumar, M. R. Sivaraman, and Sheela	

SESSION V
SYNCHRONIZATION
RADIATION STUDIES AND QUARTZ TECHNOLOGY

Systematic Effects in GPS Time Transfer	491
W. J. Klepczynski	
Architecture and Performance of a New GPS Time Transfer and Positioning Receiver	495
T. I. Kido, P. C. Ould, and R. J. Van Wechel	
Intercontinental Time and Frequency Transfer Using a Global Positioning System Timing Receiver	517
Philip A. Clements	
Test Results of the STI GPS Time Transfer Receiver	529
David L. Hall, Jim Handlan, and Paul Wheeler	
Radiation Hardness of Efratom M-100 Rubidium Frequency Standard	547
Thomas C. English, Henry Vorwerk, and Norman J. Rudie	
AK-cut Crystal Resonators	577
Alfred Kahan and Ferdinand K. Euler	
Some New Results on Irradiation Characteristics of Synthetic Quartz Crystals and Their Application to Radiation Hardening	593
Harish Bahudur and R. Parshad	
One Nanosecond Time Synchronization Using Series and GPS	605
L. A. Buennagel, D. J. Spitzmesser, and L. E. Young	
New Auto-Tuning Technique for the Hydrogen Maser	621
R. L. Sydnor and L. Maleki	

SESSION VI
DISTINGUISHED SCIENTIST PANEL DISCUSSION

Introduction to Distinguished Scientist Panel	631
Dr. R. L. Sydnor	
Professor I. I. Rabi	632

CONTENTS (continued)

	<u>Page</u>
Distinguished Scientist Panel (continued)	
Professor Norman F. Ramsey	635
Professor Charles A. Townes	641
Professor Robert H. Dicke	646
Professor Robert V. Pound	650
Professor Hans Dehmelt	655
14th Annual PTI Registration	659

CALL TO SESSION

Dr. Richard L. Sydnor
General Chairman
Jet Propulsion Laboratory

CHAIRMAN SYDNOR: I welcome you all to the Fourteenth Annual Precise Time and Time Interval Planning Meeting. I think you'll find that this year we have a very interesting and enjoyable meeting plan. If you haven't noticed yet, there is a reception to be held Thursday evening. I hope most of you can come to that. It's being held at the Smithsonian downtown. It's the opening of the Atomic Clock Exhibit. I realize that this extends some of your trips but I think it will be quite worthwhile. We've had some bad news this year. Andy Chi died unexpectedly. He has been a major contributor to this meeting for a number of years and as a consequence we're dedicating this year's proceedings to him. We will all miss him very much.

I'd like to introduce the host, John J. Quann, Deputy Director, NASA Goddard Space Flight Center.

WELCOME ADDRESS

John J. Quann
Deputy Director
NASA Goddard Space Flight Center

MR. QUANN: Thank you, Dr. Sydnor. I was hoping I would be able to say, "good morning, ladies and gentlemen," but it appears I can say, "good morning, lady and gentlemen." On behalf of NASA and the other sponsoring agencies, it's my pleasure to welcome you to the Fourteenth Precise Time and Time Interval Applications and Planning Meeting. This is the seventh time Goddard has hosted the PTTI, and it's been a pleasure to do so each time. Just before you came in, I was curious as to whether or not NASA had anything to do with picking the acronym of PTTI and tried to pronounce it, but I don't think you can pronounce this with any sort of reasonableness, although NASA has in the past been able to create some things that the first time I heard them pronounced, I couldn't believe. There was one called the Heat Capacity Mapping Machine, which turned out to be HCMM. The first time I heard HCMM pronounced, I could not believe that anybody could actually do it. There were scores of others, but I'm not sure how you'd say it. This is a difficult one. I'd like to acknowledge the attendance of several people from other countries. Your presence here makes the PTTI meetings that much more meaningful. Goddard looks forward to continued cooperation with each of you and, of course with the people at home. I think it's significant to note that of the 32 papers in the program, 8 will be presented by authors from other countries. This worldwide participation is evidence of the importance that the PTTI community and the attendees place on these annual meetings. I encourage you to continue the cooperative effort. I'd also like to welcome Professor Rabi and the other distinguished visitors who will participate in the panel discussions that are scheduled for the next three days.

So, once again, I thank you for coming and for the opportunity to greet you, and I wish you a very successful three days. Thank you.

OPENING COMMENTS

Dr. Nicholas F. Yannoni, Chairman
Technical Program Committee
Rome Air Development Center

DR. YANNONI: Good morning. I'd like to second all the welcomes you have heard today. We hope this will be a very nice meeting. The first activity of the meeting is going to be what we call the Planner's Panel. And I want to introduce to you the members of that panel. As I do so, perhaps they would come up and sit here. The Chairman of the panel is Mr. John Cittadino who is from the Office of Secretary of Defense and Director of Theater and Tactical C³. Accompanying Mr. Cittadino is Dr. Tom Goblick from Lincoln Laboratories. And Dr. Harris Stover from Defense Communication's Engineering Center and Dr. Michael Garvey from Frequency and Time Systems. I'd like also to introduce to you, although for many of you he needs no introduction, Dr. Gernot Winkler from the U.S. Naval Observatory, who will take over the Chairmanship of the morning session. Thank you.

SESSION I

PANEL DISCUSSION ON FUTURE TIMING REQUIREMENTS

Dr. Gernot M. R. Winkler, Chairman
Naval Observatory

INTRODUCTION TO PLANNERS PANEL

DR. WINKLER: Thank you, Nick. I think we should go right ahead and ask the panel to comment on future time requirements as they can be expected from the point of view of systems. May I ask the first.

MR. CITTADINO: Okay. Thank you. What we will attempt to do is to try to give you a view as we see it of the requirements for timing from four different perspectives. I will speak very briefly on the perspective of the Department of Defense with respect to communications, command and control and intelligence systems. I'll be followed by Dr. Stover who will speak on the requirements from the communications point of view as seen from the Defense Communications Agency. Dr. Goblick will talk from his experience in the laboratory which is working on numerous projects which rely very greatly on precise timing. And then Dr. Garvey will speak from an industry point of view, what he sees coming down the pike in the relatively near term from his viewpoint in industry. So, without further ado, let me get into what I'd like to say.

PLANNERS PANEL

Panel Chairman: John C. Cittadino, Director, Theater and Tactical C³,
Office of Secretary of Defense

When Nick Yannoni asked me to participate on this panel, we agreed that it would make sense that I talk about the importance of precise timing to military operations and military command, communication and control (C³) systems. All my life I've read and heard war stories and how important timing has been in the winning and losing of the key battles in most of the world's great wars. But being an expert in neither warfare or the science of precise timing, I felt compelled to go to the history books in an attempt to establish the origin of the use of timing in warfare. And as near as I can pinpoint it, it all began with Alexander the Great early in his career during the war with Tyre in 332 B.C.

It seems that Alexander was having a very hard time with the Tyrians who had for seven months resisted the siege of his forces. It eventually became apparent that his difficulties were caused by the failure of the various legions under his command to coordinate their attack. Those of you familiar with Alexander's accomplishments will recall that he was the first advocate of truly balanced and combined arms warfare; bringing together legions of sword carrying infantry with those made up of spear carriers, archers, javelin throwers and finally cavalry. Sitting despondently in his tent one evening after another severe setback, he racked his brains trying to come up with the solution to his dilemma. He knew that he must synchronize his attack, but exactly how remained the question. Then recalling the teachings of his mentor Aristotle, to always look to science for the answer to seemingly unsolvable problems, he remembered the discovery of one of the alchemists who was part of the large entourage of scientists and engineers who were an integral part of Alexander's army. It seems that a dye had been produced which possessed the remarkable characteristic of always changing color from red to green with the same precise time interval after the mixing of the individual components.

He summoned his alchemists and had them mix a large amount of the dye and then used it to color strips of rag. He next summoned his combined arm commanders and laid out the plan for a new attack the next day on the Tyrian forces. He emphasized that the attack must be initiated, enmasse, at precisely the right time. They would know the right time by watching the rag bands, which they would each tie around their wrists - and he proceeded to hand out the rags with the special dye.

Of course, I'm sure you've already guessed the rest of the story, the battle was a rout; Alexander overthrew Tyre and with his use of finely coordinated combined forces, using the newly invented technique for precise timing he went on to conquer the lands from Southern Europe across the Mediterranean and as far east as India. And it all happened because of the world's first Alexander's rag time band.

But in thinking seriously about time, it seems that those of us in the systems business tend to take it for granted. We generally tend to put timekeeping into one of two categories. The first is when we take a quick glance at our wrist, where we see a device that has served us pretty well over the years. In this day and age even those watches we used to see in the TV commercials strapped to the tip of a ski jumper's ski or submerged for days under the ocean have gone to quartz technology. They boast of accuracy on the order of one or two seconds per month. As long as it continues ticking after unspeakably inhumane treatment and provides reasonable accuracy, what more could be asked of our trusty time-pieces. Or on the other hand, we may not take quite such a cavalier attitude toward time. We recognize that accuracy and precision are necessary in certain walks of life. We tend to think, however, that precise time is somehow the province of the research scientist secluded away somewhere in his laboratory, who needs to split the second into ever shrinking, but more precise, increments to satisfy his scholarly pursuits.

I'd like this morning to depart from both of these views of time and assure you that we in the systems business need to become much more cognizant of the absolutely critical role precise time will play in the "Real World" of future military operations.

Accurate time is indispensable for numerous technological, commercial and scientific purposes. Closer to home, command, control, communications and intelligence (or C³I) systems -- both those currently in operation and those still on the drawing boards -- and our very ability to successfully employ sophisticated electronic systems in battle is intimately tied to the timing sources dispersed through the various echelons of our military forces. In general, C³I systems timing requirements fall into either one or two of two major categories. First, are the various communications systems requiring synchronization to on the order of tens of microseconds, or less, due to the increasingly high data modulation rates, time division multiplexing, and the use of precisely synchronized spread spectrum transmission techniques. Second are users of synchronization for positioning systems. Time and frequency are also essential for identification systems such as Identification Friend or Foe (IFF) or collision avoidance systems.

I'm told that a famous astronomer once observed that, "We don't know what data astronomers will want in the next twenty years, but we are sure that they want it with much greater accuracy." I can't speak for the astronomers of the world, but I do know that a similar statement could be made of needs for increased timing accuracy with DoD C³I systems. Moreover, I don't expect it to take twenty years before we see extremely stringent timing demands becoming an integral part of the specification for all of our evolving command and control systems.

Today the state-of-the-art in the timing world will support, and consequently we have to be satisfied with, atomic frequency standards which provide precisions of a few parts in 10^{11} and support time synchronization to 100 nanoseconds, this only on a local level. Emerging C^3 systems will require rugged frequency standards with much greater long-term stability and with global time synchronization to 100 nanoseconds. NAVSTAR GPS hold real promise for global time synchronization to the 100 nanosecond level. In fact, prototype receivers have been checked out that provide time transfers on the order of 30 nanoseconds.

A study of future timing requirements across the US government has recently been completed. This study confirmed that timing accuracy requirements are, in fact, expected to become even more severe. Generally speaking, the most stringent requirements would appear to be associated with research and calibration facilities. This is probably a fortunate happenstance since these activities are generally fixed installations where controlled, stable environments for the timing standards can normally be made available. It was interesting to note that on the unclassified requirements in this category, NASA's were generally the most stringent for a variety of programs such as Space Tracking, Geodesy and other investigative projects.

However, there is a wide range of emerging systems to be fielded that will impose requirements nearly as stringent as those imposed on the calibration or laboratory instruments. Already on the drawing boards and, in some cases, nearing actual deployment to the field is a wide range of communications' systems and data links that rely on timing for security, integrity, and jam resistant digital transmission of a large volume of data.

On the positive side is the fact that the emerging operational requirements and the nature of the timing problems are converging to a common ground. This is driven primarily by the sophisticated communications systems and position location equipment which will be widely dispersed in tactical deployments. For example, the Army is developing the Single Channel Objective Tactical Terminal (SCOTT). This system will require time of day with ± 20 microseconds and could conceivably necessitate the fielding of several hundred atomic -- cesium or rubidium -- clocks. Other planned Army systems such as the Single Channel Ground Air Radio System (SINCGARS) could also add cesium or rubidium clocks to the operational forces. Such additional programs as Have Quick, JTIDS, PLRS, TRI-TAC, and the Combat Identification System will all carry with them stringent requirements for accurate time synchronization in order to function effectively in their planned environments.

As these and other planned C^3I systems move from the drawing board into the operational inventory, the complexion of the DoD's timing program will clearly change from that of a Laboratory, fixed installation problem to the problem of supporting deployed operational forces. As the complexion of the program switches from the relatively benign controlled laboratory environment, a whole new set of design and performance criteria must come into play.

Consideration must be afforded such additional criteria as size, weight, acceleration sensitivity, temperature range, warm-up time, and power consumption. The timing sources must be reliable under field operationing conditions and supportable when deployed. Most importantly, our timing sources must be affordable. We are taking measures to encourage the services to standardize on a family of common timing components, so that costs of both production and logistics will be reduced.

The need is there. Electronic systems of all kinds, navigation systems, communications systems, weapons systems, radar systems, missile systems, computers, and many others are going to be increasingly dependent upon precise time. If our weapons systems of the future are going to be able to do their job, either singly or collectively, a precision timing system is of the essence. Both the timing system and the host systems themselves will need to be affordable, economic in operation, and capable of worldwide use. This challenge is there for all of us, then. It will take individual expertise in our respective areas and a close harmonization of our efforts to assure meeting this challenge and deploying the effective and affordable C³I systems that will be needed to support our combat forces on any future battlefield.

PLANNERS PANEL

Panel Member: Dr. Harris A. Stover, Defense Communication Agency

A worldwide switched digital communications system has never existed, but in the future the Defense Communications System (DCS) is expected to be such a system. This will result in timing problems not faced before.

At the present time, the DCS is an analog system that uses considerable digital transmission. The signals are returned to analog form at switches, and they can be retimed during analog to digital conversion. Also, at the present time, those signals which must pass through the system in digital form are usually applied to modems for transmission over these analog channels. There are many advantages to replacing these analog channels with digital channels so that all signals will be carried in digital form throughout the network. When this is done, the opportunity for retiming during analog to digital conversion at switches will be gone, time division multiplexing will be more extensively used, and digital switching will employ time slot interchange. Digital channels from many origins will have their bit streams interleaved in a pattern that changes as the connections through the network change. In such a digital network it is very important that a bit originating anywhere in the world be available at the instant when it is needed at every communications node through which it passes. Note that this is a phase (or time) control problem and not just a frequency control problem.

There are many methods by which the required phase coordinations can be provided. However, most of them will not satisfy the requirements of a wartime defense communications system. All of the different methods employ buffers for the temporary storage of bits to accommodate variations in signal propagation time and small clock errors. When the phase errors exceed the capacity of the storage buffers, a slip occurs. This is a timing event that will disturb the normal flow of traffic. In civilian digital voice systems slips are normally made exactly one frame at a time. In these systems, by doing it this way, the result is either the deleting or repeating in each channel of just one of the 8000 Pulse-Code Modulation (PCM) voice samples that occur every second. This is a minor disturbance. When other types of voice coding are employed, which do not use PCM samples, the effect can be much more severe, and it can also be more important for some types of data transmission. Furthermore, when encryption is used, it isn't so simple to slip exactly one frame at a time. This becomes particularly important if both link encryption and end-to-end encryption are employed. In a switched digital military communications system, where all channels are digital, a timing slip might commonly cause the interruption of traffic while several pieces of equipment are sequentially resynchronized. Therefore, timing slips are much more serious in a military application than in a civilian application.

The major difference between military and civilian applications comes from the requirement for military communications to survive in a wartime environment, even in the face of a concerted enemy effort to destroy them. The survivability of nearly slip-free communications in a switched digital communications system is dependent on the survivability of accurate system timing. Accurate

timing can also be an aid to reestablishing communications that have been lost. At present we employ precise clocks at major terminals of the Defense Satellite Communications System (DSCS) to aid the rapid synchronization of spread spectrum receivers in the presence of jamming.

Because of the importance of survivable system timing to a worldwide switched digital military communications system, at this meeting in 1979, I presented a set of "attributes for timing in a digital DCS" and explained the importance of each attribute. Those attributes were later published by the Defense Communications Engineering Center in Engineering Publication 1-80. Our studies have shown that the technology to provide these attributes exists. No breakthroughs are required, and the cost is not much greater than for any of the other approaches considered.

These desired attributes can be listed briefly as: (1) reference to Coordinated Universal Time (UTC) whenever such a reference is available, (2) specification of tolerances in time or continuous phase, (3) freedom from dependency on any particular facility, (4) self-organization, (5) availability of timing so long as any communications link to a node survives, (6) ability of nodes to rapidly reenter the network, (7) timing disturbances not propagated through the network, (8) avoidance of traffic interruption to reset buffers, (9) capable of most effective use of a free-running mode, (10) systematic self-monitoring, and (11) open options to apply new technology as it develops.

These attributes can be interpreted as saying that our network must be self-sufficient in its timing capability. Each major node must have its own clock together with those alternates required for reliability. These clocks should be coordinated with a timing reference distributed through the communications network. The master clock for the network and paths by which timing is distributed must be automatically selected. Even this selection process must be distributed throughout the network so that every node can automatically make its own decisions with no centralized decisions made anywhere in the timing system. Then any facilities can be lost, and the network can undergo massive destruction, but both the selection process and the rest of the timing system will still work properly. If the network becomes fragmented, each fragment will automatically select its own master and the paths for timing distribution. That master will be referenced to UTC when such a reference is available. This has the advantage of permitting any node to use an optional UTC timing reference from a navigation system if it is available. Referencing to UTC could sometimes be helpful in restoring operation between fragmented portions of the network.

Since any major node in the network is capable of serving as master for the entire network or any fragment of it, the system does not require UTC in order to operate properly. By maintaining timing system accuracy and preventing timing disturbances from propagating through the network, both of which are practical, a high degree of timing stability can be maintained. This could be very useful in a free-running mode to help a node reenter the network after temporarily being separated from it, particularly if spread spectrum signals must be acquired in a jamming environment.

All of these things put together will provide synchronized clocks at each major node in the network for so long as any communications link to the node is operational and for a considerable period of time following the loss of the last link to the node.

It might seem that providing all of these things would be very complicated. It is not! Most of the algorithms employed are very simple, once they are understood. However, a microprocessor is required at each node to carry out the algorithms and provide the needed automation. It would not be possible for the system operators to do this.

In present civilian practice, the lowest level of digital voice multiplexing, which carries 24 voice channels, provides 8000 synchronization bits every second. Once synchronization bits are available, the addition of a few hundred bits per second on each transmission link will make possible the network timing capability that I have just discussed. Since a system with stable timing capability needs but a small fraction of the 8000 bits per second for link synchronization, some of those unneeded synchronization bits could be used for the other system timing bits. Alternatively the other timing bits could use a portion of a service channel.

The most complex algorithm under consideration for communications system timing is one related to predicting clock errors and removing those predicted clock errors when it is necessary for a clock to free-run following a period of normal operation during which calibration procedures are applied. Successful application of this algorithm could permit the use of lower cost clocks at some locations, or improvement in operation during a free-running period, or both. Studies for use of this last algorithm and the integration of it with other algorithms are still to be completed. Whether this last algorithm is implemented or not, it is practical to use the other algorithms to provide a very survivable, accurate, timing capability for nearly slip-free operation of a worldwide switched digital defense communications system.

PLANNERS PANEL

Panel Member: Dr. Thomas Goblick, Lincoln Laboratories

I have a few remarks I'd like to make from the system designer's point of view, and have some view graphs. I'd still like to use them if I can set up the machine.

From my position in viewing a number of large scale systems with many hundreds and thousands of users in the tactical environment, these are some of the key applications of precise timing and timing measurement. We know what the classical position location problems, two-way ranging radars, but currently we see more of the trend to one-way ranging. Deriving the position of users in a communication system where the users are tightly synchronized, passive multi-lateration systems are of great interest where time differences of arrival measurements at remotely located points are important to bistatic radar. Synchronization of communication systems is also a very important aspect. The time to enter a community of communications users depends on how far off the new users clock is, signal acquisition time and that also is directly related to the amount of processing that must be done to acquire a signal in the net and that depends on the time of uncertainties. Time division multiple access systems divide the time line precisely and the more precisely it can be divided without guard intervals the more capacity one might be able to get. In all these intercommunication systems relate to just how much overhead the communication system must provide, must carry out in order to maintain time synchronization to get users in the system and to keep their processors from being overloaded.

The tighter the time synchronization the simpler the system can be, and the less transmission can occur or need occur just for the purposes of synchronization and this leads to tighter transmission control and this is a very important factor in a tactical environment.

The last item I have is security. We talk of encrypting messages and we must insist that it is function of time as the position doesn't change for a very long time, conceivably an enemy could intercept one of the transmissions and use it for his purposes.

And so, for an active exploitation type of mode. Let me discuss, a little bit here, the one-way ranging problem which is more stringent than the two-way. I have plotted here the fractional timing error required as a function of the synchronization interval, of the users' clock and the upper right curve one-way ranging to an accuracy of 10 microseconds. This is the curve I'd like to talk about.

This curve is a trade-off curve, in my view, for a one-way ranging system which would provide an accuracy of 10 microseconds. My approach would be to take the approach that JATIDS (Joint Tactical Information Distribution System) took and design a system architecture around a set of protocols that pass time around constantly within the system.

So that a user can enter the system with a poorly synchronized clock and eventually synchronize that clock and then be a full participating user and if his clock is a very good one, he in turn may have time accuracy eventually good enough to pass on to someone else.

The synchronization interval in a system like JATIDS is a fraction of a second. And for this level or even the one microsecond level of one-way ranging accuracy you see the clock demands for that kind of JATIDS terminal are pretty miniscule. But the system has paid in terms of complexity and in terms of extra time to do the processing and in terms of the use of the system, how much transmission takes place.

On the other hand one could take the other approach that one had a really stable clock. One wanted to simplify the system, one could say, I'd like to synchronize the clock at the beginning of a mission and then not have to worry about the clock from then on.

That would say, that a several hour mission would lengthen the synchronization interval to something like 10^4 seconds. And now the clock requirements get to be considerably more. So, if in a tactical environment that sort of a clock is available, the system can be simplified. The multi-lateration systems are more demanding because of the geometric dilution of precision in locating users and their requirements are such that they have no possibility of doing very accurate location of targets without constantly resynchronizing the clock during the course of the mission.

And system designers take this into account, as I illustrated in the JATIDS case there is a trade-off. One can trade system complexity for the clock quality or one can try to build a good clock into the system to simplify the design.

I'd like to talk a little bit about Identification Friend or Foe (IFF). IFF is the system in which an encrypted interrogation is sent to a target which then if its a friendly target can send an encrypted reply back. It is essentially an electronic password system.

These are some of the uses of IFF equipment ranging from an airborne surveillance system which is very important on a very large platform to a sophisticated but a very densely packed fighter aircraft which provides a particular type of physical environment, to a roaming land vehicles to provide air defense support, to some other very sophisticated radars and missile systems and even man portable systems. Now, the kind of clock one would put on an AWACS aircraft is very different from the kind of clock we would put on this ground vehicle or on that man portable unit.

I'd like to just illustrate that latter case, a little bit more clearly. This is a photo of the stinger weapons system with IFF interrogator. Now the airplane is a cartoon, but this soldier person, I'm not sure of the gender, has the weapon in the tube on his or her shoulder aiming through the visual

sight here, the optical sight, and these elements are two YAGI elements of the IFF interrogator, they are the antenna. The IFF electronics are in this box and via this cable, connect into the handgrip, which has the control switches.

The IFF system is a fairly potent weapon system and an IFF system that maintains time synchronization so that encryption can be changed as a function of time very quickly must contain this kind of constraint. Where this soldier can't have very much of a fancy clock. He must power it by battery also carried by the same person. It cannot be resynchronized by a time distribution system using satellites or some other sophisticated network; probably has to go at least 24 hours without resynchronization.

If this terminal needs one millisecond accuracy through the course of the day that's a fairly demanding requirement that the clock occupy a small part of the electronic box and be powered by batteries all of that time, even if the rest of the electronics are shut off.

That could well be the driving clock requirement in an IFF system, not the AWACS requirement or the fighter plane requirement. So, clock stability is one aspect in tactical systems, but there are others.

I just want to emphasize that, precise timing, of rubidium and cesium clocks they are fine and they are needed in a system, perhaps, in the time distribution system but they don't make a large difference to this particular weapons system.

This weapons system has to get by another way. In fact the IFF system may have to be designed to provide him updates via the radio links.

So, in summary, I'd like to readdress the question of why don't we hear system designers screaming for many orders of magnitude improvement in clocks? In the tactical business, system designers like their jobs. They like to be employed. And, therefore, they're going to design systems around the kind of hardware they can get their hands on. And, they're not going to design a system with 30,000 terminals, and design it around unproven clock technology. So, you don't hear that kind of push on clocks that have to be resynchronized as often as you should.

There are other aspects too and I'd like to point them out today. There's another answer, answer B, and this is that you see good systems designers can make do with what's available.

In terms of meeting the environmental spec as well as meeting the stability and performance spec. They will design the system to operate with existing clocks and keep the timing accuracy to the level required by provision within the system of passing time around and resynchronizing clocks. In the case of JATIDS, a great deal of the architecture is laid out to do just this function. Then as we get a little bit smarter, there is another level of answers where you find really good systems designers will make provision for improvement in clocks such that when a clock that is an order of magnitude or two better comes along, a module can be replaced. If the system was properly designed

the overhead that was paid in the beginning operation of the system to use a poorer clock, can be taken advantage of by dropping the overhead of synchronizing and gaining some other asset for the system, such as perhaps increased capacity or increased performance. I can't point to any real systems like this, so maybe we really don't have any really good systems designers.

But, I must say that, very seldom is the question asked that the system has to be designed that way. As a postscript, I would like to add that, of course, in order of magnitude or two is always appreciated; that the tactical environment also has other specifications that are difficult to meet and as I pointed out in the Stinger application.

I guess that's about all the remarks that I have. We can get into questions on what I have said later on.

PLANNERS PANEL

Panel Member: Dr. Michael Garvey, Frequency and Time Systems, Inc.

I'd like to make some comments this morning from the industry point of view. I haven't coordinated with my colleagues in industry, so what I'm saying might prompt some discussion from them.

I'm trying to draw obvious conclusions. I would like to address the topics of technology advances which we see; which we might predict. Mechanisms for accomplishing this and different forms that the advancement may take.

I'd also like to address some issues, which I think have been pointed out in previous discussions even this morning of the industrial implementation of clocks and clock systems, in a timely and affordable way.

I think to look into the future is a dangerous task to do that, one needs a crystal ball which might be looked at with the same sort of task in mind of introducing a new crystal cut.

In this case, it might be a spherical resonator. But to try and make some predications anyway, I think that it's safe to say that progress is the result of hard work, it is based on existing technologies and experience.

It's based on the applications of new technologies for the most part existing concepts and systems. I think if we look at new ideas in time and frequency, one might advance that there is nothing truly earth shaking ready to appear on the marketplace.

I think there are some very interesting ideas in the laboratory at the moment and examples there might be the ion storage work at NBS, some optical pumping work which I think has very interesting potential to enhance not only reliability but performance of frequency standards.

I think some of the concepts of cryogenic and passive crystal resonators that have been explored in the laboratory also offer some promise.

However, these are I think, still in the laboratory stage and that's the way everything starts after all. If we look at the technology of cesium, we have come 30 years to obtain the current status of being able to launch a cesium standard on a satellite if you like.

To ask how technology proceeds, I think that there are three ways that technology may go forward. Technology may go as it is pushed. By that I mean that technology may be pushed to exploit some new issue in the marketplace and take advantage of some new need or some new system requirement.

It may also be pushed by the market and I think this is particularly germane to the audience in discussion of this conference because it's, I think, unique to military system and DoD procurement activities where the marketplace pushes the technology in a particular direction.

There is, of course, the requirement in that respect for smaller, lighter, more rugged devices. I think the example of the Stinger System was a very good one.

You can envision that this system has to run rain, shine, night, day, snow, heat, etc. In these tactical applications I think are probably very significant technological challenges for the clock designer.

On the other hand, from sort of the other side of the coin, as technology makes advance when we look for enhanced performance and primarily there are non-tactical applications.

A few comments to say about that later. I think tie in a very interesting way the system design concepts, which were discussed in the last view graph.

The second way that I think that the technology can be pushed forward, is that there are obvious advances in technology in other realms of electronics, of physics, of optics, of communications, if you like which can be very conveniently applied and in an available basis.

These are logical, they occur because of their logic. They are self-justifying, usually enhancing cost, performance, size, weight, etc. Examples there might be the integrated circuit, hybrids, more recently, microprocessors, which are becoming so prevalent, easy to use and cost effective.

The third area where technology may be advanced are technological changes which are focused primarily at increase in performance. Some examples there might be the BVA resonator, BVA oscillator concept which has been explored. Optical pumping and beam devices and a few of the other laboratory applications which I discussed earlier. I think all of these techniques are appropriate at times, sometimes the techniques go astray.

I think it's worthwhile to now interlace this idea a bit with procurement aspects because I think that's a very crucial interface between the system designer who configures the system, who creates a concept around which the system will evolve and, ultimately, its realization in the industry from the people who are going to have to create, build, test and maintain the hardware.

One should be always beware of the repackaging in the guise of technology improvement. I think this is a fallacy which is perhaps only realized with difficulty that merely changing dimensions of an object may necessitate complete redesign of the instrument.

I would implore the system designers to realize that clocks themselves are systems, that few systems are created without learning curves and I think the learning curve for many of the clocks we have today has been a long one.

I think it's a very solid one and based upon a lot of experience we shouldn't neglect the opportunity to exploit that. Particularly when total system performance depends intimately on clock performance. It is crucial that the system designers be sensitive to the realization that use of proven clock designers will result in a system with a basis on which good performance can result. System designers would ideally make efforts to accommodate the system to the complexity of the frequency standards and I think to support the last view graph to anticipate improvements which will occur in clock systems and to allow these improvements to be employed within the system. To focus a bit on financial aspects of this, as I'm sure everyone realizes, any coherent program probably has a life span of longer than a year, and I think funding programs often neglect the realization that the planning and recruitment and assignment of key personnel to development projects cannot proceed in time frames of less than a year. It is very disruptive to industrial, I think in general, activities to anticipate that you can reassign key personnel to different programs in time frames shorter than a year.

To focus a little bit on the third type of technological change which I discussed before, that is technological change for enhancement of performance. I think there's an increasing realization and implementation of the idea that both government and industry can work in a cooperative mode to accomplish this sort of an advancement. An example has been demonstrated numerous times with the cooperative programs with the Bureau of Standards in the parallel effort of development of concept, demonstration of feasibility and a transfer of technology from the laboratory into the industrial marketplace.

One, I think very important aspect of this, is that the efforts must proceed in parallel not necessarily from the initial stage in both fields, but to say that a design can be presented in the industrial marketplace as a stack of schematics and parts list, I think is naive.

The industrial mode of operation has people who are keyed to parts acquisition to testing. There is an available labor force to buy, build, to complete in-process testing. There are procedures available to support these and the design has to be sensitive to these requirements.

I think the obvious advantage of these parallel efforts is that there is an allocation of talent and resources where they exist. Puts tasks where they belong. Importantly, it provides a rather quick mechanism to produce statistical hardware. By that I mean, that it's very difficult to talk about a design until you have built 10 of something or 100 of something, depending on a little bit upon its complexity.

So we face now the question of how, and who in order to approach this solution to technological advancement. I think the answers to those questions are revolutionary, perhaps, a different approach may be taken, depending upon the task.

I think there's a front-end need for planning and funding for the whole project and not just on the short time or time available basis. A commitment of resources, of personnel planning would wind up and wind down activities.

These are particularly crucial to us, as I mentioned in the application of key personnel.

To address the issues of affordability, I think the suggestion of standard components is probably a good one. That's not really however a task which I think industry can undertake and impose upon the DoD procurement activity. I think industry is very willing to respond to that sort of a design concept and it has, I think, some very good advantages particularly with respect to affordability.

It's I think not realized by people who have not had intimate contact with how costly and expensive it can be, merely to support the documentation to add or move a single connector. So some sensitivity to these concepts, I think is important.

In terms of deployment at the systems level, I think the integration of proven and existing clock designs is a valid and defensible design technique. I think that the time and frequency reference needs to be integrated into the system not necessarily as given at the beginning, but the advantages which can be accrued from such a technique, are I think very clear.

Thank you.

PLANNERS PANEL

Panel Chairman: John C. Cittadino, Director, Theater and Tactical C³,
Office of Secretary of Defense

We'll take a few minutes for any questions, or perhaps before we take any questions, I might ask if any other pannelist have any questions or cross talk they might like to get involved in. Okay, are there any questions from the floor? There's one way back there.

QUESTION FROM THE AUDIENCE: I was under the impression there is a new directive from DoD for P³I on all new systems?

MR. CITTADINO: I wouldn't say that P³I is a requirement on all systems. It's certainly is something that is being considered for all systems that come through the development cycle. It is one of the alternate approaches in the development of the system. I think perhaps I missed some of the beginning of your questions, so if I'm not quite getting at the heart of it, please repeat it.

But if the question is, "Is P³I a requirement on the development of all systems within DoD?", it is not a hard fast requirement.

Well, P³I is a management technique that each development activity is being asked to consider as to whether or not it applies to the development of that individual system based on the requirement that is coming along.

And there are numerous factors that would come in to play. For instance, numerous requirements can be satisfied with just off-the-shelf type hardware.

And when you've got that type of situation and you fully can satisfy the requirement at a reasonable cost. Then, in that particular case, there's no need to consider P³I. But, when you've got a situation where you have a need for a particular system, and is utilizing such technology where there is a recognition that improvements would be coming down the pike as the system evolves, then it makes sense to build the system in various increments. Getting the usable capability as soon as possible and building the system for growth or evolution as the case may be and I think that's certainly the way I interpret that policy. I don't know, others might give you a different story.

DR. WINKLER: We have a few more minutes. I think that if we continue the discussion for 10 more minutes, it may be useful. I have found in each of your comments something which I find exceedingly important; of course affordability one always looks at the total system costs; meaning not only acquisition, but logistics, training required, life time and incidental operational costs, which in the case of atomic clocks can be much larger than the initial acquisition cost of an atomic clock.

And if we talk about improvements coming down the pike in industry, something struck me and that is, that in our present system we really do not pay enough attention to the building of capable teams and maintaining these teams. Our start/stop kind of contractual operation is really a disaster when it comes to maintaining capability in high technology. As Mike Garvey mentioned, it is not possible to move these key people around more quickly than at most I would say once a year and even that is a disaster.

So that the question of new developments and what is really critical today is really exceedingly complex. Let me mention another point which occurred to me, when I listened to Dr. Goblick's excellent presentation of the three types of systems designers. I think one has to distinguish between tactical clocks, particularly crystal clocks, which is one group by itself and the atomic clocks. Because they have their own individual and different problems. For tactical clocks, it is really weight, power consumption and this kind of thing and costs, because usually they are procured in greatest numbers. When it comes to atomic clocks exactly the opposite problem exists, cost here is less of a problem as compared to reliability. And it appears to me despite everything that you hear about new technology that that is the major problem still, because clocks operate somewhere inbetween our digital equipment and other more mundane things as power supplies, batteries, generators and so on. They contain after all, atomic clocks contain a physics package. The physics package contains analog circuits still. These are exceeding complex, in fact atomic clocks, I think, are those kinds of systems which should place the greatest requirements on subsystem performance. And for that reason some systems such as power supplies, phase detectors and so on have to be custom designed. And then of course that brings in immediately the reliability problem, because you can never, when there is an order of 10 or 20 or 50 units, go through the debugging and through a really high reliability procurement. So there are quite a few things which one, I think, has to keep separate.

Where finally something struck me when I listened to Stover's 12th commandment. The Good Lord had only Ten. Well, I think he said 11 principles. These principles are undoubtedly exceedingly important, they have been discussed before. We have heard them discussed here in previous meetings. As I see the systems being developed; they will not be implemented all at once. I think, there is one requirement which has been left out, and this is the gradual evolutionary development of more complicated systems.

After all we are not going to turn off our present operations on one day, and start the new ones the next day. In the meantime, we will have an agonizing transition period. In fact, I think, we are in that transition period right now. And it may preclude the adoption of all these sound principles of which I have mentioned. I wonder if you have any thoughts of that?

What are we going to do in the meantime?

DR. STOVER: As you said we are going to start out with only part of the timing capability that we need for a digital system and progress toward adding the rest. But, as you do that (this is where the last attribute comes in); you have to look to the future and prepare the road starting now, so that you can

provide all of the needed attributes when the time comes -- when you have the ability to do it, and when the need for them is even more demanding. Obviously we cannot afford to put it all in at one time. We can't afford to go out there and completely replace an existing communication system.

DR. WINKLER: What I was aiming at was the fact, in a moment, a number of systems come into use. In fact, the one which I mentioned, the Army systems, which right now, are procuring or thinking about procurement of large numbers of atomic clocks, and how are they going to be interfaced with existing operations. These are digital systems. Can you say something about that?

DR. STOVER: Of course the interfacing with existing systems is where I put the emphasis on UTC, to cause everything to come to a common standard. That way, we can use the Navigation Systems as a reference temporarily. In our first implementations we are now using and plan to make further use of LORAN-C. But LORAN-C is not a real survivable system. We need a much better system for a wartime digital communication system.

DR. WINKLER: Well maybe, could you paraphrase that and say that affordability and a smooth transition period will be assured if we learn to use all of our resources, whether they are in our own bailiwick or available someplace else. Such as, for instance electronic navigation systems, to be used as time reference by communications systems and others. Of course, in coming back to your initial comments about the astronomers, when we look at managers of the future, there is one thing quite certain. We'll want to have more done, at less expense. And when it come to military systems, we'll not only want to have them not only less expensive and more reliable, but also less vulnerable to jamming, to interference of all kinds, and to outages in certain areas.

This is, I think the real reason behind the push for more clock use in electronic systems. The main benefits which they give is that they make systems less vulnerable. They provide a greater access capability, at less signal-to-noise, if you narrow the time window; for instance, for an acquisition of a PRN system. So this brings me back to a comment that one always will welcome greater performance, because a well designed system will be able to utilize greater performance and offer payoffs that I haven't had too often in my contacts with system designs, yet. I am very grateful that you have made that point.

MR. CITTADINO: I just like to elaborate on one point that Dr. Winkler made, and that is with respect to the continuity of keeping teams together and having the clock technologist -- I find that the system development activities these days, system designers who are very pressured to meet milestones to design systems to prove that the system will work and there may be alternatives to designing very sophisticated systems but it may take resources that would have to be allocated to the development or refinement of clock designs.

When that comes to the systems designers' desk, most of the time the clock development is relegated to a few phone calls to find out what is available and then they put the money on the matched filters, transmitters, antennas and things of that sort.

I have seen this, and although systems designers could do a lot with better clocks, there is a very weak linkage between those people designing systems in full-scale engineering development to milestones that they have agreed to, and the technology community in general. That's too bad, because it seems the systems designers wind up making phone calls to companies and clock experts and I have to do this, too? I'd call up Nick Yannoni regularly with these kinds of questions, and to get a list of contacts. And similarly with the clock community.

I have the same kind of feelers coming to me saying, what kind of clock would you like in the future? But it isn't promoted in some centralized way, the government funds the clock technology, the government funds the systems development. But, I guess that's disturbing to me that you don't find systems designers screaming to the clock community: "Immediately I need this and I'm willing to pay you for it, and I want you to develop it on this time table."

The bulk of that kind of money and development sweat and effort will go into the basic system.

DR. WINKLER: Yes, and thank you, I'd like to mention that one of the nice features of the proceedings of this conference is a list of all participants and we hope that the main benefit of the conference will be to enable you to establish these contacts.

DR. KELLOGG: Is there any payoff in the transition in looking at an ensemble of existing mechanisms versus the hope for the future?

DR. WINKLER: You're the system expert.

MR. CITTADINO: I'm not sure I understand the question, could he say that one again?

DR. KELLOGG: If one rubidium clock doesn't work very well, the possibility of trading in an ensemble or a slightly higher reliability of 10 versus the hydrogen maser which is still breaking down in the laboratory.

DR. WINKLER: This is a very pointed question of course, my answer would be a very definite "yes". There is a tradeoff, in fact, that is precisely the policy which we at the Naval Observatory have adopted since many, many years.

Our time scale is based on the very large ensemble and the combined benefits of a very high reliability provided the clocks are in individually separated locations, with the benefit of a superior long-time performance.

I would say definitely, "yes". The only qualifying statement is that of course you buy additional troubles also because you must have a system controller, you can not do it really with just 3 or 4 in order to have any benefits. You would have to look at 6 or more of these clocks.

Rubidiums may not really be a simple thing because they have drift and it is easier to use groups of cesiums, in which I have a little bit more experience than groups of rubidiums.

TWO-WAY SATELLITE TIME TRANSFER USING LOW POWER CW TONES

C.C. Costain, H. Daams and J.-S. Boulanger
National Research Council of Canada
Ottawa, Canada

ABSTRACT

In the search for an economical means of precise time transfer, the NRC Time Laboratory decided to adapt, for time transfer, the techniques used by radio astronomers in an experiment to compare the phases of the local oscillators at widely separated VLBI stations. The objective is to design a system which would use commercial satellites, and which would be of reasonable cost for the ground stations and for operations.

Two satellite ground stations have been installed at NRC about 100 m from the Time Laboratory. The antennas are 3 m in diameter, and the transmitter power is 1W. For the preliminary experiment, a channel on the Anik A1 6/4 GHz satellite was made available by Telesat Canada.

Two tones were transmitted ± 16 MHz from the suppressed carrier. The difference frequency of 32 MHz was recovered using narrow band receivers. A low level 1 MHz phase modulation was added to identify the 32 MHz cycle, giving 1 μ s ambiguity in the time transfer. With less than $\frac{1}{4}$ W in each tone, the EIRP is 43 dB below that of a normal TV earth station, and no frequency dispersion is required.

The measurements taken each second for the 32 MHz have an rms scatter of 1 ns. The transponder of the failing Anik A1 (now out of service) was 15 dB down on normal performance, so that much better results are expected on the Anik A3 later this year.

It is three years since I reported here, in 1979, on the two-way satellite time transfer between NRC/NBS, NRC/USNO and USNO/NBS using the Hermes CTS satellite, and the NRC/LPTF transfer using the Symphonie satellite. The Hermes experiment ended July 1, 1979 after one year, and the Symphonie experiment ended July 1, 1982 after four years.

The PTB in Braunschweig joined the Symphonie experiment in February 1980, and I would like to make a brief report on the results of the past two years, because the results are relevant.

The primary interest in the time transfer between NRC and PTB was to compare the frequencies of the NRC primary clock CsV with the PTB primary clock Cs1. The results are shown in Figure 1.

CsV was evaluated at MJD 44512, with a resulting increase in frequency of 4×10^{-14} . There was little change in the frequency of CsV at MJD 44865 for the next evaluation in September 1981. The regular variations, over the central period, we attributed to the reversal of the beam of Cs1, about every 35 days, because there appeared to be a correlation between the reversal dates and the change frequency of the order of 5×10^{-14} . However the PTB assures us that from their internal evaluation this could not occur, so it must be attributed to noise.

This curve, and the fact that the curve for the previous three years also lies in this $2 \mu\text{s}$ interval, gives a long term agreement between the PTB and NRC standards of 2×10^{-14} . Measurement of frequency differences to 1×10^{-14} on a monthly basis was achieved, except for the last year, where for two periods there were numerous equipment failures and changes in the CRC terminal used by the NRC.

Except for these periods, transfers between the three stations normally gave closures of $\pm 2\text{ns} - 10\text{ns}$. The 10 ns bias resulted from the change in frequency and the satellite transponder which was necessary for the LPTF/PTB transfer. Because the three transfers were run consecutively over a period of an hour, it was also necessary to determine the relative rates of the station clocks and extrapolate to a common time.

These results of 1 or 2 parts in 10^{14} are in marked contrast to the seasonal variations of 3×10^{-13} which are evident in comparing our frequency to that of the USNO via Loran C. While Loran C has been, and remains, very useful to us, it has been obvious for some time that we need a better system for precise time dissemination, and that need is reflected in many of the papers to be presented at this meeting.

It has also been obvious from the first that both the Hermes and Symphonie satellite time transfer experiments had a limited lifetime. In searching for a reasonably economic means to achieve precise time transfer, we decided to experiment with methods used by the radio astronomers to establish phase coherent links between VLBI stations at the Naval Research Laboratories, Washington, Algonquin Park, Ontario and Penticton, British Columbia¹. In this experiment two CW tones were exchanged over each path, and the beat notes recorded at each station were subsequently compared to determine the relative phases of the local oscillators at the three stations. They recently achieved an rms noise of 25 ps for 0.1 s averaging time.

For the NRC time transfer experiment, and we hope for ultimate operational use, we have set up two transmit-receive satellite ground stations about 100 meters from the Time Laboratory, with several triax cables connected directly to the Time Laboratory facilities. The antennas are 3 m in

diameter, and the transmitter power 1 W. For the preliminary experiment, a channel on the Anik A1 6/4 GHz satellite was made available by Telesat Canada. The EIRP of our stations is about 40 dB below that of a normal TV ground station, and so frequency dispersion is not required. A 120 K low noise preamplifier preceded the narrow band receiver.

In our experiment the initial CW tones were ± 16 MHz from the carrier frequency, with the carrier suppressed 35 dB below the tones. In the receiver, with 70 MHz IF, the frequency of 54 MHz was recovered first, with a 1 MHz bandwidth filter, and a 54 MHz VCO with a ramp search and 15 Hz bandwidth in the acquisition loop. The ramp search was necessary to accommodate a possible 20 kHz offset arising from the satellite transponder, the Doppler shift and the receiver local oscillator. For the received 54 MHz, the signal to noise was -37 dB for 1 MHz bandwidth or 23 dB Hz. The 32 MHz was recovered from the 86-54 signal with a crystal oscillator in the loop, because only a Doppler shift of 1 to 2 Hz is to be expected.

For cycle identification of the 32 MHz, two methods were tried. In the first, the ± 16 MHz tones were switched to ± 16.5 MHz at a 10 kHz rate, and 33 MHz was recovered as well as the 32 MHz as above. This gave a 1 MHz signal with $1\mu\text{s}$ ambiguity in the time transfer. In the second method, a 1 MHz signal was used to phase modulate the 16 MHz at a low modulation index, and the 1 MHz was recovered directly. The results obtained are shown in Figure 2. The upper dots are the measurements taken each second of the 1 MHz locked signal. The middle section gives the measurements of the 32 MHz signal, and the lower set of measurements are from a Canada/France transfer using the Symphonie satellite. It can be seen that the quality of the CW tone transfer is not as good as the Symphonie results, but it should be mentioned that the performance of the Anik A1 satellite was 15 dB below normal.

In Figure 3, the results of another run are presented, with a line giving the 10 point moving average. The 1 MHz results are adequate to identify a cycle of the 32 MHz, and the 32 MHz results show that sub-nanosecond precision was obtained.

The feasibility of using 3 m terminals with 1 W power for sub-nanosecond time transfer has therefore been demonstrated. However, we are not now so certain of the practicality of the system. One difficulty arises from the fact that commercial up-converters and down-converters have too much FM noise for the narrow band system, and direct synthesis for frequency agile units becomes complex and expensive.

A more serious difficulty is the cycle ambiguity. While the present $1\mu\text{s}$ ambiguity could be reduced to $10\mu\text{s}$ or $100\mu\text{s}$, power is lost with each additional modulation frequency. The complexity also makes it more difficult to achieve a fully automated system.

We are now planning to make tests with a pseudo random noise code with our low power terminals. This method has been proved out by the RRL in Japan², and much earlier between RRL and NASA, but at a rather higher S/N than we will have available.

I would like to suggest that an effort should be made to agree on a standard PRN modulator and demodulator that could be used on any time transfer experiment, geostationary satellites, GPS, STIFT, etc. The goal should be sub-nanosecond precision and accuracy, and economy.

We would like to thank Telesat Canada for making the experiment possible in giving us access to the Anik A1 satellite, and for the very helpful assistance and advice of their staff in the course of the experiment.

¹ S.H. Knowles et al "Time Transfer via Satellite-Link Radio Interferometry", Proc of the 11th Annual PTTI Meeting, p. 471, Nov. 27-29, 1979, NASA CP 2129.

² M. Imae et al "Time-Comparison Experiments with a Small K-Band Antenna SSRA System via a Domestic Geostationary Satellite", CPEM 1982, page M-5.

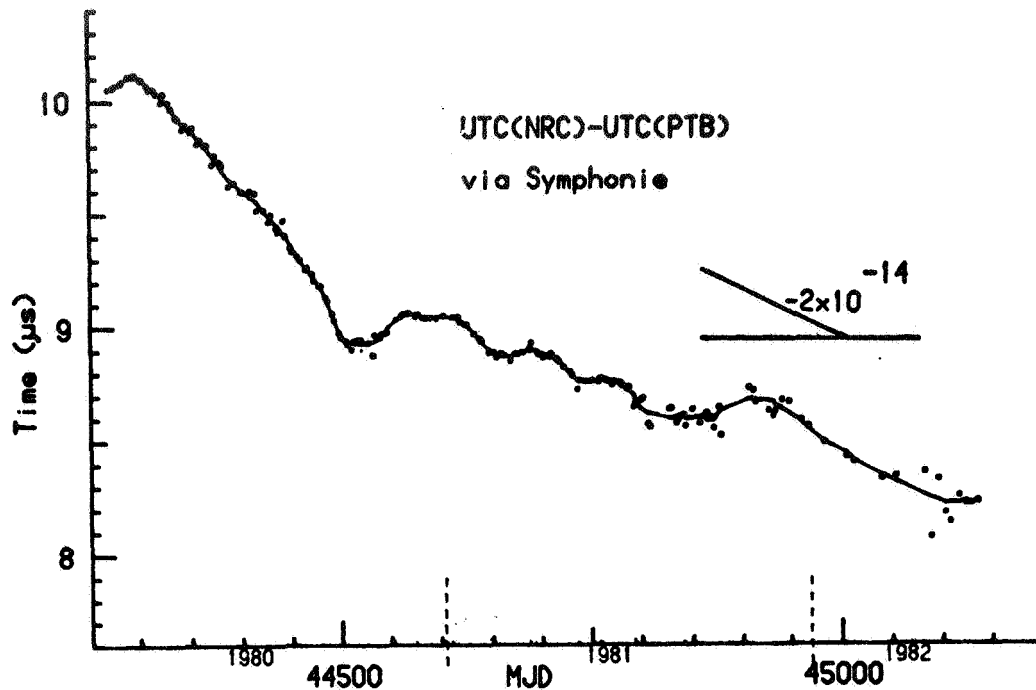


Fig. 1 - The absolute time difference UTC(NRC) - UTC(PTB) via the Symphonie satellite.

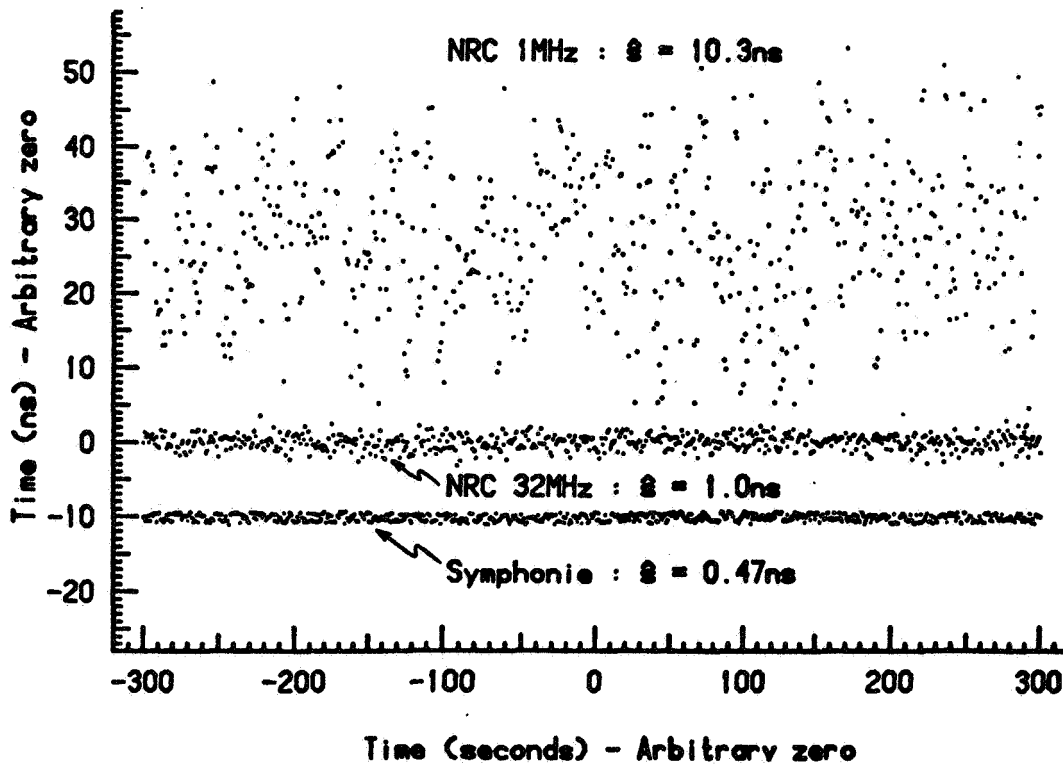


Fig. 2 - A comparison of the results using CW tones via Anik A1 with the results using a 6 MHz video band via Symphonie.

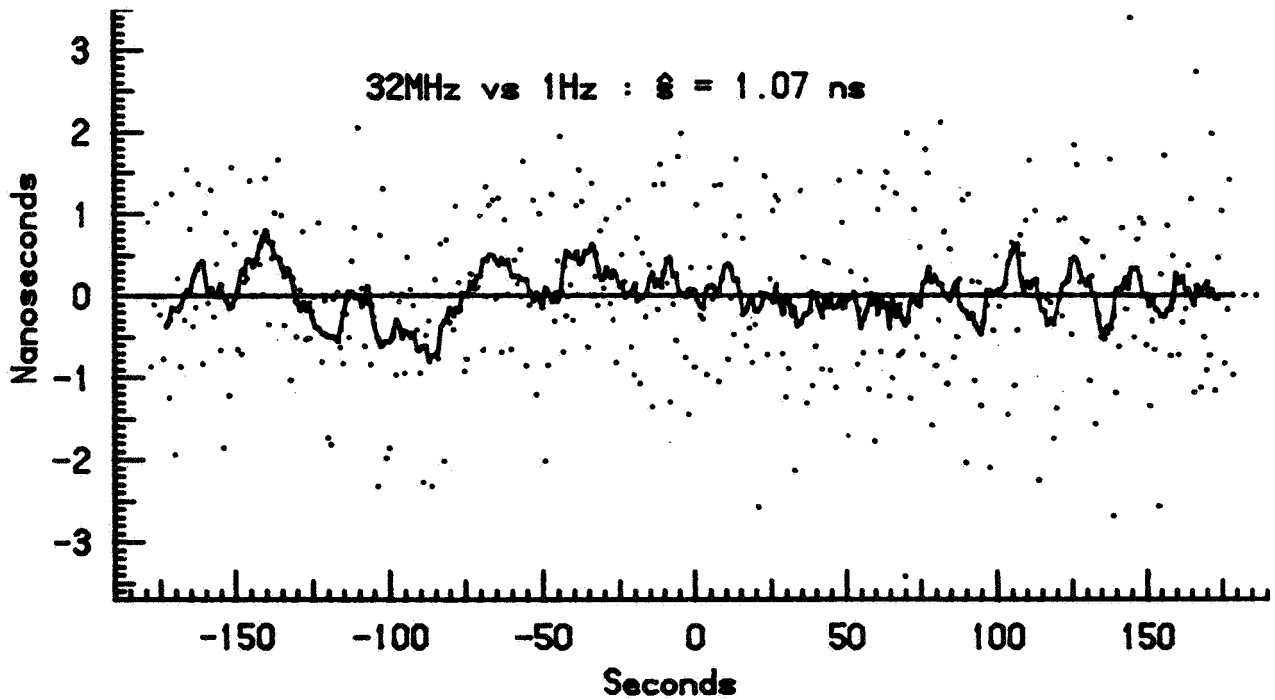
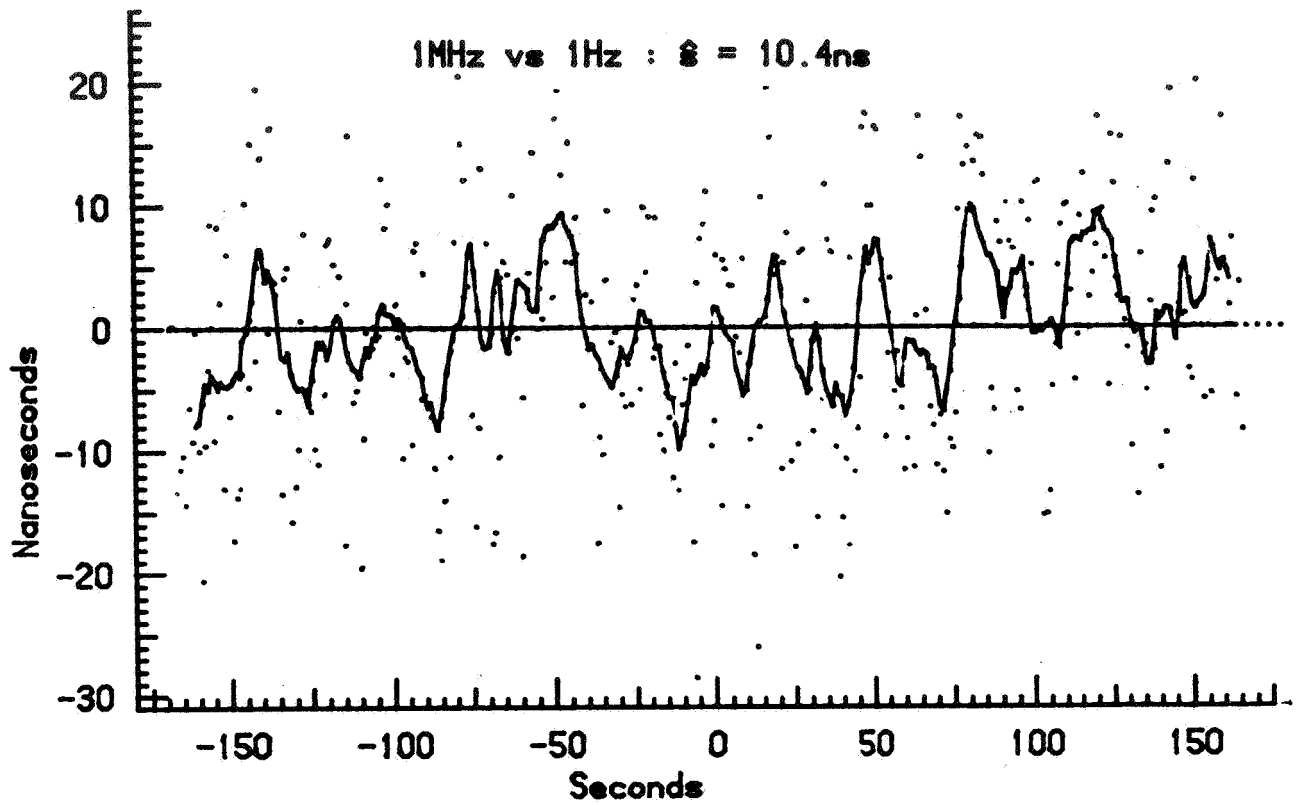


Fig. 3 - The 10 point running average and standard deviation of the recovered 1 MHz and 32 MHz signals via Anik A1.

QUESTIONS AND ANSWERS

MR. L. J. RUEGER, JHU/APL

Have you obtained permission to use active transmitter links to the satellites in other countries?

DR. COSTAIN:

Yes, I should qualify my statements by the fact that we now have an experimental license to use a commercial satellite. There is probably rather a bigger step to get a commercial license to operate a ground station when it is an active station transmit/receive. In Canada we might be able to do this by giving title of the station to TELESAT, who are the only ones allowed operate. And I think in some countries it is even more difficult.

I think that we could probably accommodate on this continent with the motherhood that we have for systems, it might be a little more difficult in Europe. But if we can keep the EIRP 40 dB down, in fact you really can't be detected except by the compatible system. And one of the virtues is that we cannot interfere with other systems, which makes it a little more practical to get licensed.

DR. WINKLER:

I may add the important thing seems to be as Dr. Costain said, low power but the second one, I believe, it is easier to obtain licenses if you can stick to a fixed schedule of 5 or 10 minutes a day; the same time, because then the primary user of such a frequency assignment can notify you if he needs to pre-empt. In this case, it seems to be easier to obtain licenses. And we have had no difficulty to obtain an experimental license for a peak power of ten watts, for the anticipated LASSO experiment, which unfortunately did not materialize.

DR. COSTAIN:

Yes, also, this is one reason why we have very simple programming really in this type of experiment and one reason I want fully automated outfits so that we could do it at 3 o'clock in the morning, and I don't have to be in the laboratory.

TIME MAINTENANCE OF USER CLOCKS VIA THE
TRACKING AND DATA RELAY SATELLITE SYSTEM

Gary Whitworth, J. W. McIntyre, and R. E. Downs
The Johns Hopkins University Applied Physics Laboratory
Laurel, Maryland

ABSTRACT

During the 1980's, all NASA-supported low earth orbital spacecraft will be supported by the Tracking Data and Relay Satellite System (TDRSS). User spacecraft will have the capability of time-tagging science and house-keeping data on board the spacecraft. This activity requires that the on-board time scale be relatable to a standard time scale such as Universal Time Coordinated (UTC). A system is described which uses the TDRSS itself to compare the user satellite clock with a clock at the White Sands station that is referenced to UTC. No command of the spacecraft by the system is required, and actual on-board clock corrections are made by the spacecraft control center at its discretion.

Computer models were constructed using basic orbital parameters for user and TDRS satellites. With only first-order corrections and simple averaging techniques for constant clock rates, error measurement precision of better than one microsecond was obtained. More sophisticated computations should allow considerable improvement over this.

NASA supported spacecraft in the future will require on board time tagging and operational timing requirements in the microsecond and sub-microsecond range. Such precision is not achievable using ground based clocks. It can only be obtained by having high quality clocks on board the spacecraft and a means of closely maintaining the spacecraft time scale to a universal standard such as UTC. These spacecraft will be supported by NASA's Tracking and Data Relay Satellite System (TDRSS), which is scheduled to become operational in 1984.

This paper describes a proposed system for high precision maintenance of user spacecraft clocks which is planned to be a service of the TDRSS. Detailed descriptions have been given in an earlier report (1). This timing system determines coarse and fine spacecraft clock error with

respect to UTC. Coarse error is determined from the spacecraft clock time code to one second resolution. Fine error is defined as the error in the once per second clock "tick."

To begin, a brief description of the TDRSS and its communications link to user satellites is in order. Figure 1 shows the basic geometry of the TDRS system. Here the communications paths between the single ground station at White Sands New Mexico and a low earth orbital user spacecraft via the geosynchronous Tracking and Data Relay (TDR) satellite are shown. The TDR satellite is transparent to data between ground station and user spacecraft. The command link to the user spacecraft is referred to as the "forward" link. Spacecraft telemetry returns to the ground station via the "return" link.

Three main elements make up the TDRS communications system, shown in Figure 2. A user spacecraft is commanded by and returns telemetry to a Project Operations Control Center (POCC), which is located remotely from the White Sands station. Command and telemetry data streams between the POCC and the TDRS ground station are carried over NASCOM (NASA Communications) circuits which may involve any of several private and commercial communications paths including communications satellites. (The resulting unpredictability of time delay renders virtually impossible the precise monitoring of a user spacecraft clock from the POCC.)

As the forward (command) and return (telemetry) data streams enter and depart the White Sands station, they are monitored for quality. Capability exists for passively and noninterruptively monitoring the data flow between any and all of the user POCC's and spacecraft.

The TDRS ground terminal accepts command data as it enters from a POCC, modulates it on an S- or Ku-band RF link, and transmits it to the user spacecraft via the TDR satellite. Likewise, telemetry returned from the spacecraft via the TDR satellite is demodulated and routed to the POCC.

A prime function of the TDRS system is to measure the radio range of the user spacecraft from the White Sands station via the TDR satellite. This is done by means of a pseudo-random noise (PRN) code which is modulated on the forward RF link along with the command data. At the user spacecraft, the third element of the communication system, the PRN code is received along with command data in a transponding receiver.

A second PRN code, exactly like that received from the ground in length and chip rate but different in bit pattern, is modulated on the return RF link along with telemetry by the user spacecraft transponder. The code epoch, i.e., the defined "starting" point of the return code, is made to occur either simultaneously or in very precisely controlled synchronism with the received code epoch.

When the return code is received at the White Sands station, the round trip delay and thereby an estimate of one-way range to the user spacecraft may be determined by measuring the delay between the forward and return link code epochs. Although ranging may not be performed continuously on a user spacecraft during support periods, the forward and return PRN codes will still be present.

In addition to a TDRS compatible transponder, a user spacecraft will have command and telemetry processing equipment. Also, since this discussion assumes the presence of a relatively stable oscillator and clock on board the user spacecraft, these are included in Figure 2.

The ready-made PRN code provides the TDRSS with the built-in capability for precise time monitoring of a user spacecraft. The high bit rate of these codes (bit period equal to approximately 325 nanoseconds) provide the wide frequency bandwidth required to observe small increments of time. The high autocorrelation function of the codes, performed by the ground and spacecraft receivers, provide the high signal-to-noise ratios required to make precise measurements.

The basic time error calculation to be performed is that typical of all PRN time transfer systems. Figure 3 shows the timing relationships involved, in an oversimplified form. The ground clock once per second tick is indicated as the characteristic short pulse. The once per second mark of the user spacecraft clock, with error ϵ , is shown as the transition of the 2⁰ (i.e., unit) second bit in the spacecraft parallel time code. Measurements at both ground and spacecraft begin with a clock one second mark and end with a code epoch. Repeating code epochs are represented by a series of short pulses, one PRN chip wide. The primary TDRSS code period is approximately 85 milliseconds.

The time interval between the ground clock one second tick and a particular code epoch, indicated by the dot, is measured as Δ_1 . The dotted epoch propagates to the user spacecraft via the forward link and its time of arrival measured as Δ_2 . The coherently transponded code epoch is transported to the ground via the return link where its time of arrival is measured as Δ_3 .

To a first approximation, the forward path delay t_f is equal to the return path delay t_r . This approximation permits the simplest clock fine error calculation to be

$$= \frac{(\Delta_1 + \Delta_3)}{2} - \Delta_2.$$

It can be seen that there must be timing system equipment on both the spacecraft and at the ground station in order to perform the measurements and calculations. This equipment fits into the existing TDRS communications system as shown in Figure 4. The minicomputer-controlled ground station Time Transfer Unit (TTU) will have access to the return telemetry stream by way of the data quality monitoring equipment. As with the latter equipment, the TTU only passively observes the data. It is particularly important to note that the TTU at no time interferes with or takes control of the command data.

To minimize the burden to the spacecraft, all mathematical manipulations are performed in the ground station TTU. The spacecraft TTU is required only to measure Δ_2 and perform certain other logic operations necessary to compensate for real world complications not included in the simple model shown (such as how to identify the dotted epoch). Additionally, the spacecraft equipment must provide these measurements and logic results to the spacecraft telemetry system.

In addition to the telemetry data, the ground TTU also receives the ground station transmitted and received code epochs related to the spacecraft whose clock is being monitored. These code epochs at this point are precision digital signals. The delays between the TDRS and TTU are precisely known to within a predictable tolerance within the TTU. The TTU uses these epochs to ultimately determine Δ_1 and Δ_3 .

The ground TTU then unravels the practical complications involved, corrects for known biases throughout the entire system, and determines the error between the spacecraft clock and the ground station clock which is maintained with respect to UTC. This operation can be performed as frequently as once per second. Averaging and curve fitting techniques are then used on a set of such data to refine the determination of clock error and clock error rates. Error prediction calculations can also be performed. This information is then time tagged and sent to the spacecraft POCC over NASCOM lines by the TTU. At its discretion, the POCC may simply note the clock error or send corrective commands to the spacecraft immediately or at some future time.

We now examine the two TTU's in functional form. The ground station TTU, Figure 5, is under operational control of the Computer and Controller to which all hardware is connected by a standard data and control bus. A bus extender provides for communications with the POCC via NASCOM. The Telemetry and Command Monitor is able to monitor data of all spacecraft, which may vary widely in bit rate, frame length and format. Command data is monitored only to observe POCC commands for enabling the spacecraft TTU.

Gating and Counting Logic in the ground TTU controls both the time interval measurements and performs the necessary manipulations of timing

information in telemetry, to determine clock error. The Time Code Buffer supplies the ground station clock time code in proper format to the computer and controller for determining coarse time error.

The spacecraft TTU, shown in Figure 6 consists basically of Gating and Logic Circuitry and a holding register. The arrival of a received code epoch loads the holding register with the contents of a timing counter driven by the spacecraft clock. The contents of the holding register, which is reset to zero by the transition of the 2⁰ second bit of the spacecraft time code constitutes a measure of Δ_2 , and this is entered into the telemetry stream.

Note that the resolution of the Δ_2 measurement depends on the frequency of the spacecraft oscillator. As shown in Figure 6 the spacecraft time code has a resolution of only microseconds and thus is driven at 1/10 the oscillator frequency, while the Δ_2 measurement resolution is 0.1 microsecond. If the time code and Δ_2 measurement resolutions are the same, the timing counter could be eliminated and the time code read directly into the holding register.

It is necessary that the spacecraft time code for unit (2⁰) seconds and above be entered into telemetry to monitor coarse time.

In general, the code epoch timing, telemetry data and frame rates, and the clock one second tick will be asynchronous. The timing system has been designed with this in mind, but this in no way precludes the use of synchronous timing aboard the spacecraft.

Also of course, the real world is not as simple as the pictures just discussed. One of the major complications is differential delay between return link code and telemetry data. This problem arises because reference marks in the telemetry are used to identify the particular epoch (i.e., the dotted epoch of Figure 3) to which Δ_2 was measured. Differential delay occurs at the ground station due to delays in decoding the telemetry which has been convolutionally encoded on the spacecraft (a TDRSS requirement). This differential delay can confuse the ground TTU unless a sufficient number of logic cues are provided in the telemetry. Supplying these cues is the major function of the spacecraft Gating and Logic circuitry.

A second major complication is doppler frequency shift which necessitates modification of the basic propagation time calculation. It also alters the period of the PRN code, T_c , which is important in the resolution of range ambiguity caused by the short code length. These complications are all worked out by the ground based TTU.

Without exploring further the equipment or processing involved, the precision to be expected from this system is now considered. It is expected that all TDRSS equipment and transmission delays will be known to

within a tolerance sufficient to meet the specified TDRSS ranging error of ± 50 nanoseconds. User spacecraft delays should be determined to equal tolerance. These uncertainties will result in systematic errors which will vary from one service interval to the next due to equipment switching and spacecraft location.

Random errors will be caused primarily by RF system noise-induced jitter on the code epochs. This error, which will generally be filtered by the averaging of many measurements, is estimated to be a few percent of the code bit period of 325 nanoseconds.

The remaining errors are those caused by the degree of refinement of the measurements and calculations. To obtain information on the performance to be expected, a computer simulation was performed. In this simulation, asynchronous counters were run to simulate ground and spacecraft clocks, code period, and telemetry frame rate. Also, delay parameters which mimic the differential delays were incorporated. Time interval measurements were made to one-quarter microsecond resolution. The positions of the White Sands station, the TDR Satellite, and the user spacecraft as a function of time were simulated by describing the satellite orbits with standard Kepler parameters in an earth centered inertial coordinate system. The ground station was modeled as a fixed point on a slightly oblate spheroid with a rotation period equal to one sidereal day.

Two sets of results of this simulation, which used only simple first order calculations to determine clock error are presented here. The first, Figure 7 shows the results when the user clock rate was set to zero, and the error estimate calculated by averaging a set of individual measurements over a 10 second interval (10 individual measurements). On the left are shown the results with no correction made for doppler shift for cases of user spacecraft approaching and retreating from the TDR satellite at maximum doppler shift, and for minimum doppler shift. The dot is the average error and the extremes are maximum excursions of individual measurements.

The results on the right are for the same conditions but with a simple first-order doppler correction added. The doppler correction was obtained from successive differences in the round trip range estimates ($\Delta_3 - \Delta_1$). Maximum deviations with doppler corrections are seen to be within 0.1 microseconds.

The second simulation result is shown in Figure 1. Here the user clock rate was set to a fixed rate with some initial error, and the capability for error prediction examined. The simulation program gathered two small sets of individual error measurements separated by minutes or hours. A line fit to this data was made and the time error projected to 5 minutes past the last data point. Data are shown for relatively high

and low rates of the user clock. It may be seen that comparable results are obtained when more time is taken to determine the smaller rate.

The results indicate that the system will be able to predict short-term clock error to within one microsecond. With no measurement procedure changes, more sophisticated computations should permit even better performance.

Although the timing system is primarily intended to service earth orbital spacecraft, service to surface or airborne vehicles is also possible. Indeed time transfer to fixed locations using this system could provide precision comparable to results achieved in earlier ground-to-ground PRN timing experiments (2). One such application is the maintenance of the ground station clock itself by links through the TDRSS with USNO or NBS.

This work was sponsored by NASA Goddard Space Flight Center.

REFERENCES

1. McIntyre, J.W., G. G. Whitworth, and R. E. Downs, Time Correction For User Satellite Clocks Via the Tracking and Data Relay Satellite System, S3C-1-113 (JHU/APL), Feb. 1, 1982.
2. Chi, A.R. and E. Byron, Two Way Time Transfer Experiment Using a Synchronous Satellite. Proceedings of the Seventh Annual Precise Time and Time Interval Planning Meeting, pp. 357-377.

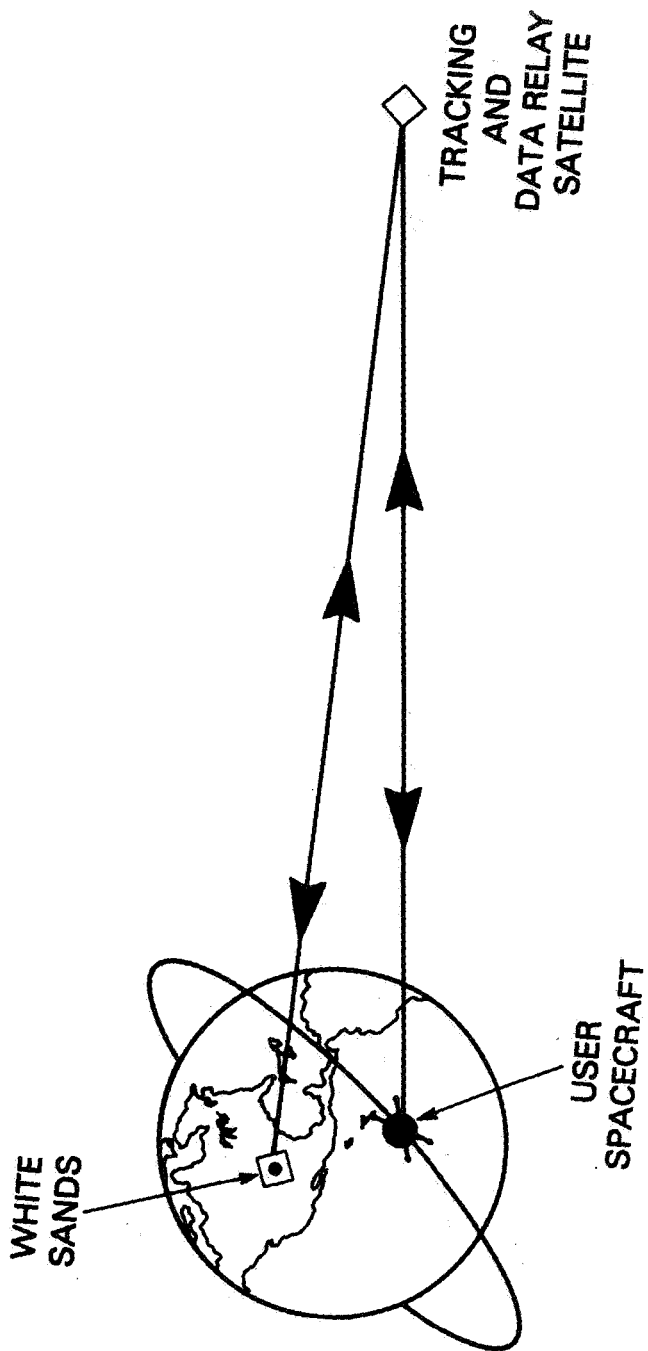


FIGURE 1
USER/TDRS RELAY

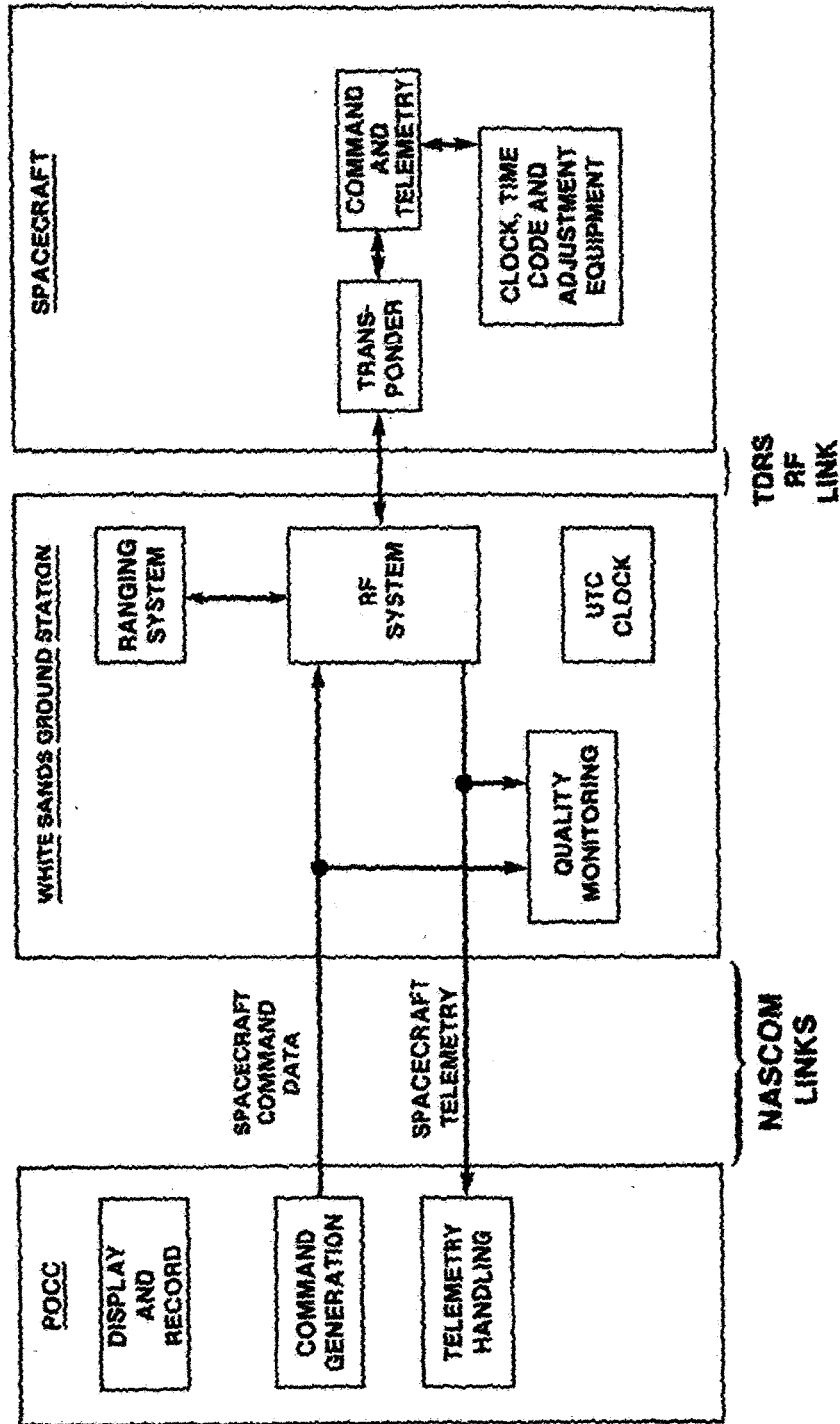


FIGURE 2
TDRS COMMUNICATIONS SYSTEM
MAJOR SYSTEM ELEMENTS

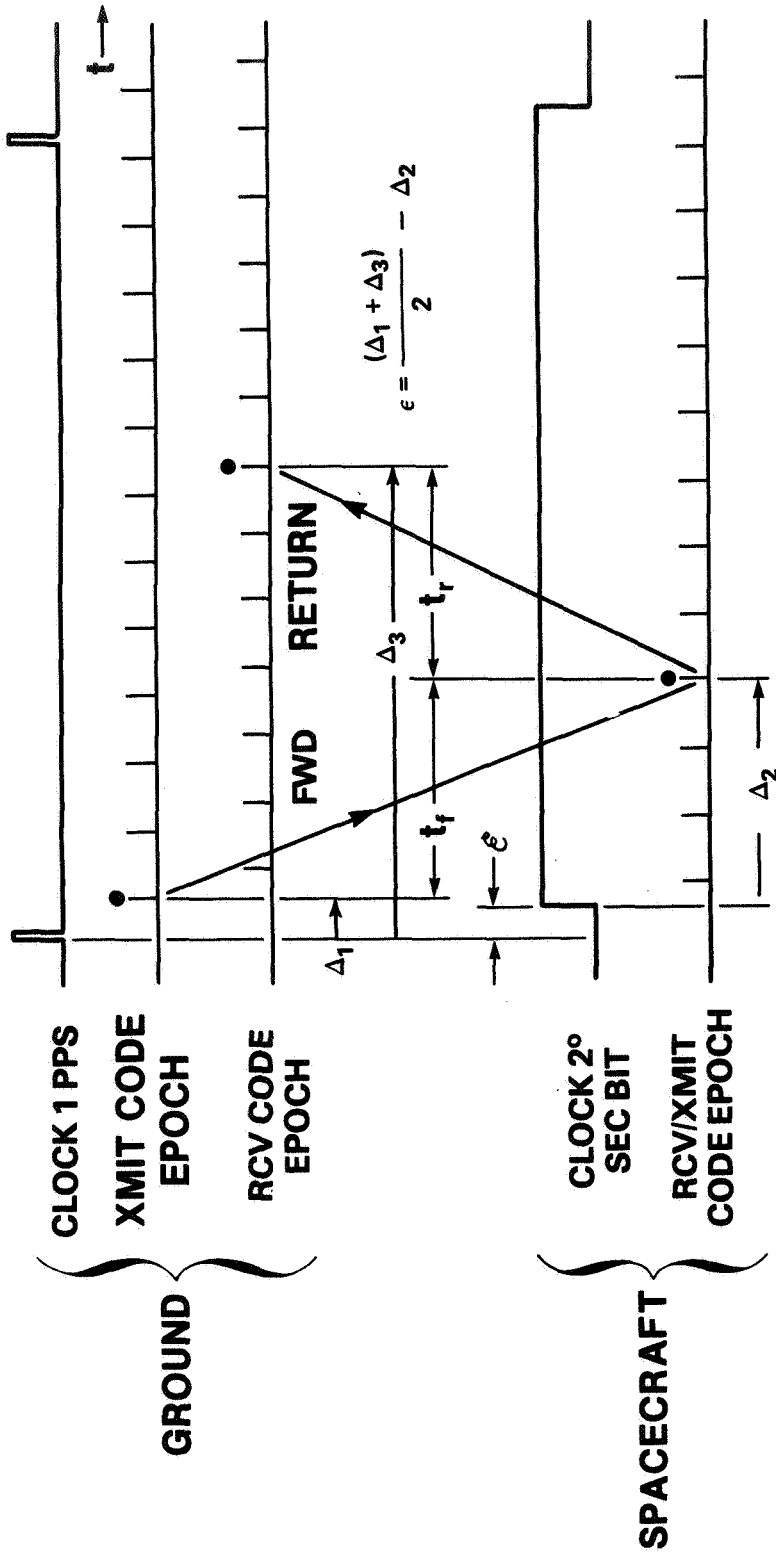
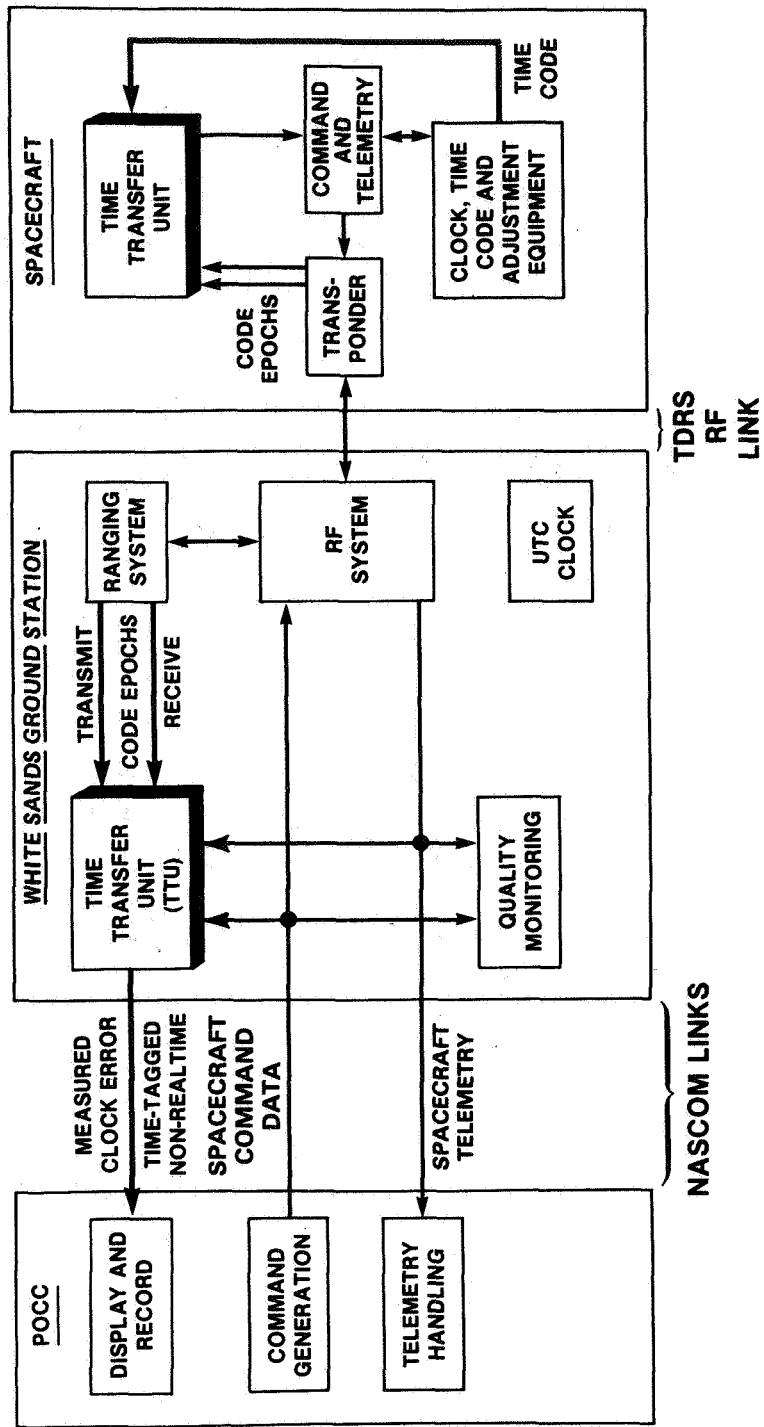


FIGURE 3
BASIC TIMING RELATIONSHIPS



*TIME TRANSFER COMPONENTS INDICATED IN RELIEF

FIGURE 4
TDRS TIMING SYSTEM CONCEPT—
MAJOR SYSTEM ELEMENTS

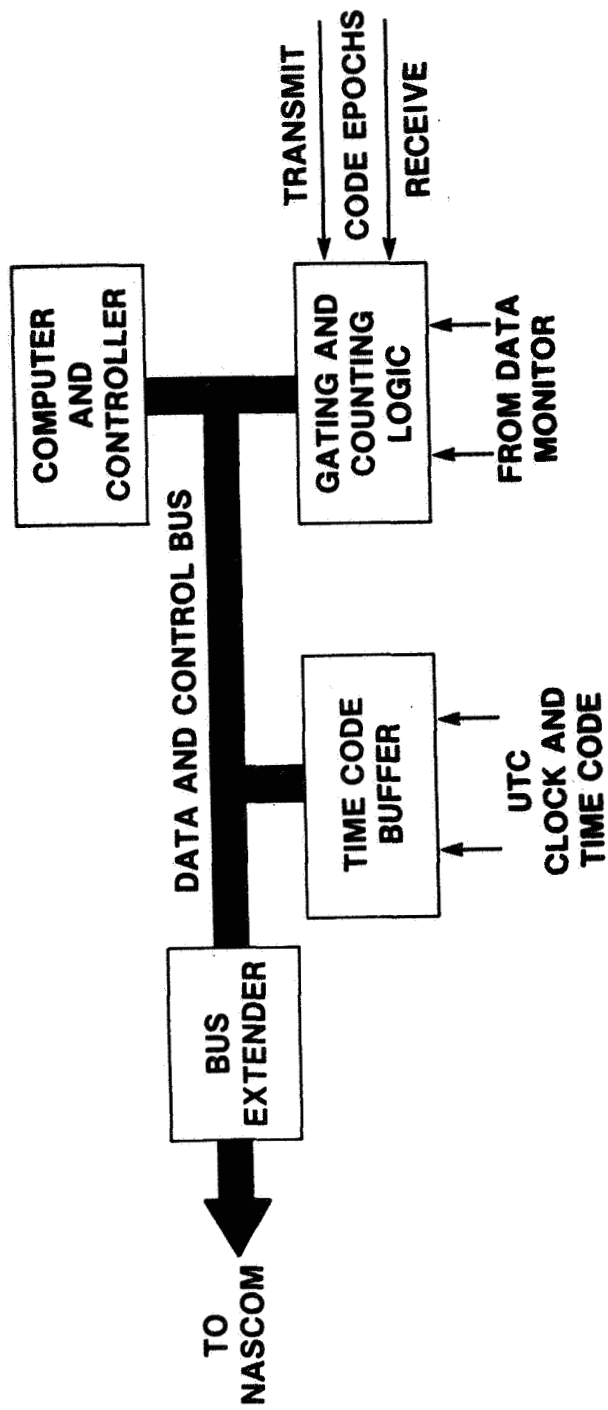


FIGURE 5
GROUND STATION TIME TRANSFER UNIT

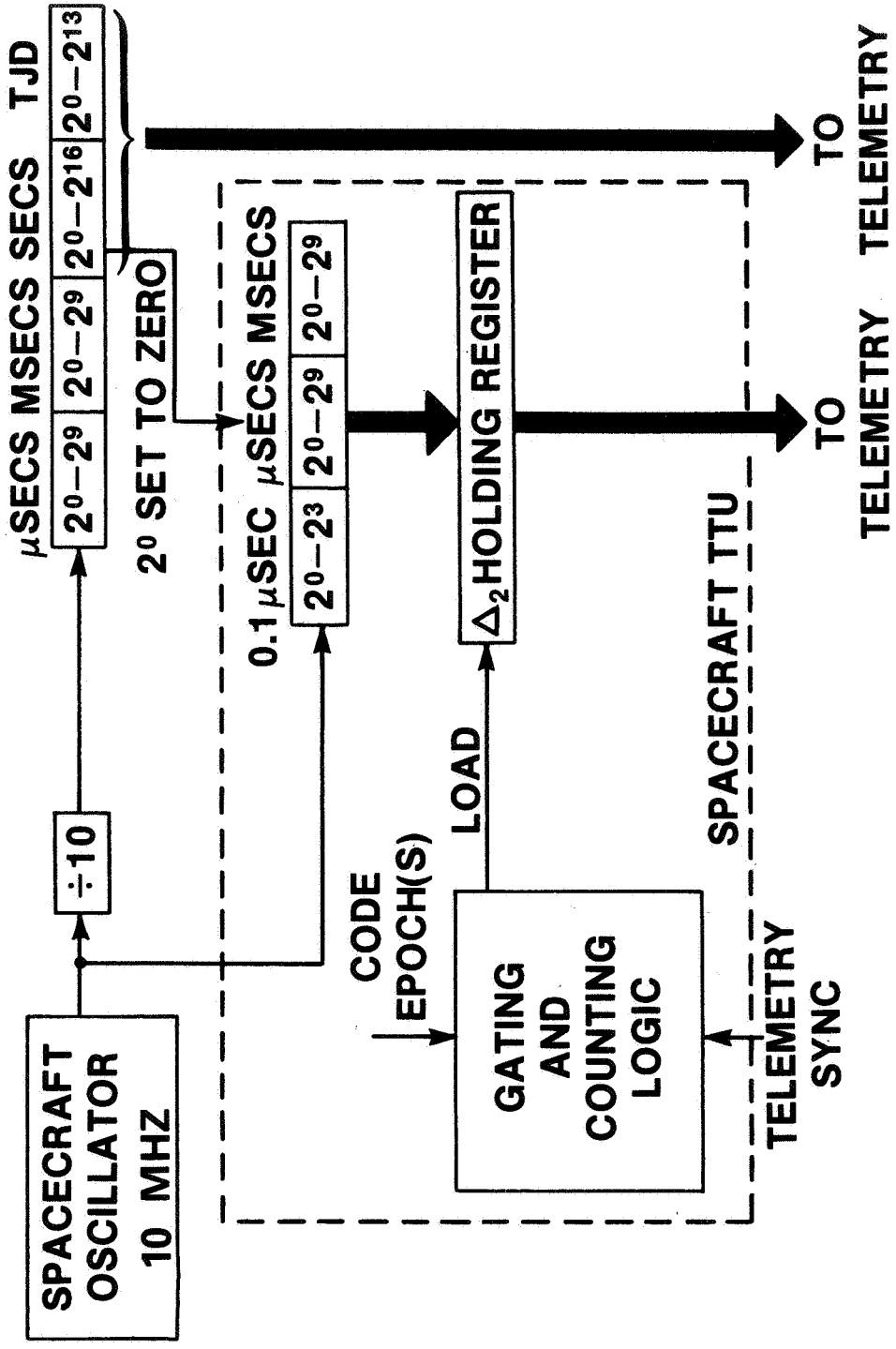


FIGURE 6
SPACECRAFT TIMING EQUIPMENT

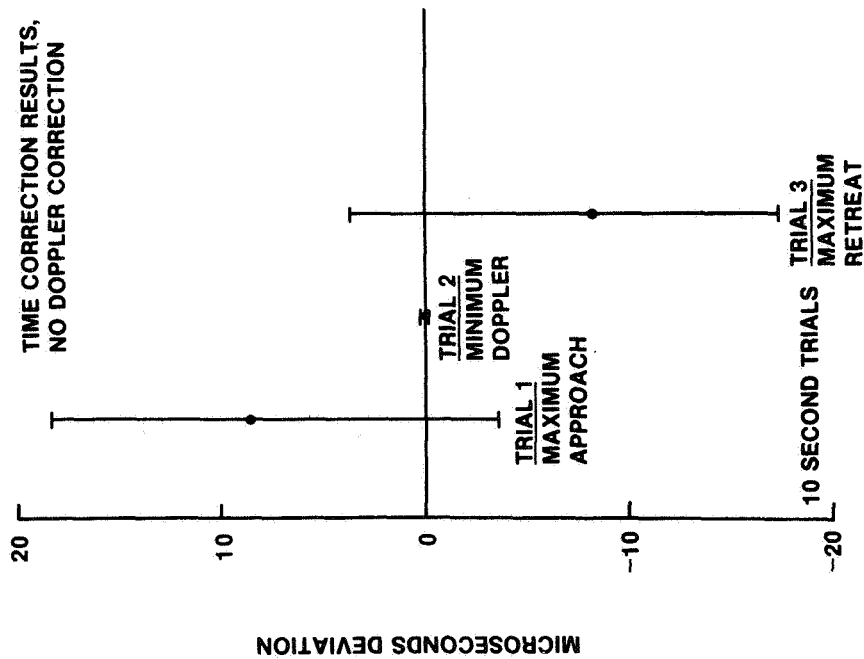
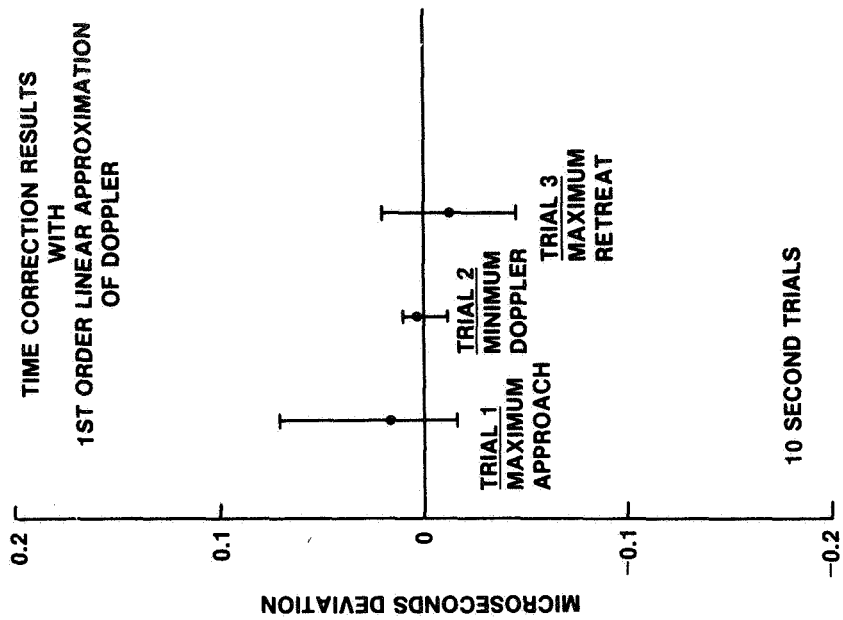


FIGURE 7
SIMULATION RESULTS

	TRIAL 1	TRIAL 2
CLOCK ERROR RATE	1 MICROSECOND/SECOND	0.1 NANOSECOND/SECOND
INITIAL CLOCK ERROR	1 MICROSECOND	-2.5 MICROSECOND
NO POINTS PER DATA SET	3	5
TIME BETWEEN DATA SETS	5 MINUTES	ONE ORBIT
ERROR FOR 5 MINUTE PROJECTION	0.158 MICROSECOND	0.273 MICROSECOND

TABLE 1
SIMULATION RESULTS SPACECRAFT CLOCK
MODELED WITH CONSTANT DRIFT RATE
(TWO DATA SET LINE FIT)

QUESTIONS AND ANSWERS

MR. PETER WOOD, Goddard Space Flight Center

If one would make a comparison and trade off between the GPS systems for time transfer versus the TDRS, what are the criteria and how does your proposed system compare in performance and other factors?

MR. GARY WHITWORTH, JHU/APL

I'm not sure I can comment directly on how they would compare in performance when one of the major differences would be expense of course. The TDRS user has already invested money in a standard transponder. The time transfer unit that we've described here would probably be a very inexpensive option on that transponder. And essentially since this is a TDS service it would be essentially very small additional cost to the user. I would think that at this point that performance with the refinement that can take place in the processing of the TDRS timing system, performance can be achieved to be quite comparable.

DR. WINKLER:

Two way, one way?

MR. GARY WHITWORTH:

Yes, this is a two-way system and as I've pointed out before, it can achieve that type of accuracy, certainly for fixed users, in this case if compensated for properly, the orbital user can achieve that same accuracy.

DR. WINKLER:

I would like to ask you a question concerning the last slide. On the last slide the comparison was between the two clocks, where the clock which was 10,000 times better at the rate of only a tenth of a nano-second per second, 10^{-10} , yet for a 90 minute calibration interval you end up with an error in the prediction twice as large as the other one. Is that mainly due to greater data rate on the first clock?

MR. GARY WHITWORTH:

No, I think that probably the answer to that is that you are using to determine a very small break, it is very difficult to do to start with; one needs to --

DR. WINKLER:

Well the clock rate is much smaller, alright, but the prediction error ought to be smaller also commensurate I would guess. It is somewhat paradoxically, the result, and I was wondering whether----

MR. GARY WHITWORTH:

Yes, this has been pointed out before. The only thing I can say in this case that this is a result of very simple corrections to the algorithms and I think for that sort of rate, probably one would need to extrapolate over several orbits.

This is just a first cut result and we were shooting to demonstrate one microsecond capability and we haven't proceeded further than that.

GOES SATELLITE TIME CODE DISSEMINATION

R. E. Beehler, Time and Frequency Division, National
Bureau of Standards, Boulder, CO 80303

ABSTRACT

The National Bureau of Standards, in cooperation with the National Oceanic and Atmospheric Administration (NOAA), has been disseminating a time code referenced to UTC(NBS) via two of NOAA's geostationary GOES satellites since 1975. A review of the GOES time code system, the performance achieved to date, and some potential improvements in the future will be discussed.

The disseminated time code is originated from a triply redundant set of atomic standards, time code generators and related equipment maintained by NBS at NOAA's Wallops Island, VA satellite control facility. It is relayed by two GOES satellites located at 75°W and 135°W longitude on a continuous basis to users within North and South America (with overlapping coverage) and well out into the Atlantic and Pacific ocean areas. Downlink frequencies are near 468 MHz. The signals from both satellites are monitored and controlled from the NBS labs at Boulder, CO with additional monitoring input from geographically separated receivers in Washington, DC and Hawaii. Received time code accuracies are typically better than 1 ms if the user only applies a constant correction to compensate approximately for his geographical location or better than 100 μ s if manual or automatic corrections are applied for path delay using satellite position data encoded into the GOES time code signals.

Performance experience with the received time codes for periods ranging from several years to one day is discussed. Results are also presented for simultaneous, common-view reception by co-located receivers and by receivers separated by several thousand kilometers.

Based on the general acceptance of the GOES time code, NBS and NOAA have recently extended their formal Memorandum-of-Agreement to continue the GOES time code operations for at least an additional five-year period.

INTRODUCTION

In 1975 the National Bureau of Standards (NBS) began regular dissemination

of an NBS-referenced time code via two geostationary GOES satellites (Geostationary Operational Environmental Satellites) operated by NOAA (National Oceanic and Atmospheric Administration). The primary mission of the GOES satellites and associated support systems is to gather a variety of environmental data from various sources, including large numbers of remotely located sensing platforms throughout the Western hemisphere, relay the information via the satellites to a central processing facility, and make the processed information available to the World Meteorological Organization and other interested users. The NBS time code is interleaved into the data collection platform interrogation channel, providing a continuously available accurate time-of-day reference both for internal NOAA data handling operations and for more general time and frequency applications throughout much of the Western hemisphere. Commercial time code receivers are readily available for a few thousand dollars that can provide received timing accuracies of better than 100 μ s over averaging periods of hours, months, or years.

The cooperative NBS/NOAA program to provide and disseminate the NBS time code via the operational GOES satellites was formalized for a five-year period in May, 1977 by an NBS/NOAA Memorandum-of-Agreement, which was extended by both organizations in May, 1982 for an additional five-year period. Since 1975, significant improvements have been made in the NBS time code generation and control equipment at the GOES Satellite Control Facility at Wallops Island, VA; the time code control and monitoring procedures used by NBS to assure overall system accuracy and reliability; and in the newer generations of the GOES satellites themselves. In the remainder of this paper the overall GOES time code system will be described, including some recent improvements. Performance of the system during the past four years will be discussed based on reception of the time code at NBS/Boulder, the U.S. Naval Observatory in Washington, DC, and at NBS radio station WWVH in Hawaii. Finally, some potential future improvements will be described briefly.

GOES SYSTEM DESCRIPTION

The GOES time code system consists of an NBS-owned time code generation, monitoring, and control system at NOAA's Wallops Island site; the satellite uplink facilities at Wallops Island; the East and West operational GOES satellites located at 75°W and 135°W longitude, respectively; monitoring, computing, and data storage facilities at NBS/Boulder; a two-way dial-up data communication link between Boulder and Wallops Island; and support operations such as NOAA's satellite tracking operations. The triply-redundant time-code-generation system is based on three atomic standards, presently consisting of two cesium standards and one rubidium device. The time code used is specially designed for compatibility with the GOES Data Collection System and has been described in previous publications.⁽¹⁾ The code as transmitted via the two GOES satellites includes complete time-of-year information; DUT1 values -- i.e., estimates of the current difference between the UT1 and UTC time scales; and satellite position information for computing path delays. The

NBS equipment at Wallops Island also includes capabilities for measuring and storing various time difference data, fault detection and alarm circuitry, provisions for monitoring Loran-C transmissions as an independent timing reference, memory for storing 10 days worth of position prediction data for each of the two operational satellites, and modems for use with the Boulder-Wallops Island data link.

The time code is continuously transmitted from this system to the east and west GOES satellites at S-band and is then downlinked on two slightly different frequencies near 468 MHz in one of the meteorological satellite allocated bands. This constraint to use meteorological satellite frequency allocations for the GOES/East and GOES/West downlinks may result in interference in receiving the time code transmissions in some urban areas, since these allocations are shared with the very large and very active land-mobile service. Furthermore, the land-mobile use is designated as the "primary" one within the U.S. while the meteorological satellite use is "secondary." In practical terms this means that if interference to the time code is experienced from land-mobile transmissions, it must be tolerated. Fortunately, time code receivers can be designed to effectively ignore much of this type of interference when necessary. In general, the time code as received from GOES/East is less affected by interference than that from GOES/West because one of the land-mobile channels exactly coincides with the GOES/West frequency while the closest one to the GOES/ East frequency is somewhat offset.

The satellite position information included in the time code format is generated from a sophisticated, very large orbit prediction program run on a large computer at NBS/Boulder. Data inputs for this program include the satellite orbital elements which are determined from satellite tracking data obtained by NOAA and/or NASA. The computer program generates position predictions for each satellite for each hour during the next ten-day period and these are further processed by the microprocessor-based time code generation equipment at Wallops Island to generate updated values each four minutes that are then encoded along with the time information. Users then have the option to simply decode the received time information achieving accuracies of about 1 ms or to also use the position data to compute a path delay from Wallops Island to the user's particular location that is updated each four minutes to compensate for movements of the satellites. In the latter case, timing accuracies of better than 100 μ s can be achieved. GOES timing accuracy as transmitted from Wallops Island is maintained to within at least 10 μ s by continuous monitoring relative to Loran-C and by occasional portable clock trips.

Reception of the GOES time code is possible on a continuous basis throughout much of the Western hemisphere as shown by the coverage maps for both satellites in Figure 1. Overlapping coverage is provided within the continental U.S. and certain other areas. While there are also operational satellites in the European (METEOSAT) and Japanese (GMS) regions that are part of the same worldwide meteorological satellite system as GOES, these satellites do not currently include an identical or similar time code in their broadcast formats. Several forms of commercial GOES

time code receivers are currently available which feature automatic operation with small antennas. Prices range from about \$2800 to \$4000, depending on the accuracy level provided.

As the GOES time code system and operational procedures have evolved during the past few years, several improvements have been incorporated. A second-generation system has been installed at Wallops Island that provides increased reliability through triple redundancy, more elaborate diagnostic information available remotely to NBS/Boulder personnel, and the replacement of two rubidium standards with more stable (in long term) cesium devices. The information transmitted to users has been expanded to include higher-resolution satellite position data and UT1 time scale information. Monitoring has also been expanded by placing receivers at the U.S. Naval Observatory in Washington, DC and at radio station WWVH in Hawaii to provide better geographical coverage and by acquiring dedicated backup receivers for the NBS/Boulder system. GOES status information is now available to interested users via the monthly NBS Time and Frequency Bulletin⁽²⁾ and, on a more current basis, from the USNO Automated Data Service. The USNO system can be accessed using a variety of terminals at either 300 or 1200 baud with even parity. Telephone access numbers are: (202) 653-1079 (commercial); 653-1079 (FTS); and 294-1079 (Autovon). After responding to the prompt asking for identification, the GOES status information is obtained by requesting the file "NBSGO" with the command "@NBSGO" followed by a carriage return. These status reports are designed to report interruptions in service, temporary perturbations in operations which result in reduced reception accuracies or other problems, and accomplished or projected changes that affect the GOES time code. Possible additional future improvements are discussed at the end of this paper.

OBSERVED TIME CODE PERFORMANCE

In general there are three different modes in which the GOES time code can be used:

- 1) Uncorrected. In this mode the received time signal is simply decoded and used without using the position information in the signal to compute and compensate for path delays as they change due to satellite motion. The transmitted time code is advanced by a fixed 260,000 μ s. The received signals nevertheless arrive at any point within the coverage area within ± 16 ms of UTC(NBS). Furthermore, a fixed-location user can compensate for most of this fixed bias by applying a fixed correction which depends on his specific location to all received data. If this procedure is followed, the received time signal will provide an accurate local UTC reference that varies less than 1 ms in long term due to uncompensated satellite motion. In the discussions of time code performance that follow, the term "uncorrected" will refer to this mode of reception;

- 2) Corrected. In this mode either the user or the automatic receiver uses the satellite position data in the received timing signal and the known geographical locations of his site and the Wallops Island origination point to compute a specific path delay that can be updated each four minutes as the satellite position varies. When these corrections are applied to the received time code, either manually or automatically, a local version of UTC(NBS) is provided, generally accurate to within $\pm 100 \mu\text{s}$. This received accuracy at the user's site is deteriorated relative to the "as-transmitted" accuracy of about $10 \mu\text{s}$ because the satellite position predictions used to compute path delays contain some uncertainties. Also, uncertainties and instabilities in the receiver delays can contribute to the usable accuracy as received. In the following discussions of received data this mode will be referred to as "corrected"; and
- 3) Common-view. In this mode multiple users at separated sites within the coverage area of the same satellite can compare their local clocks with one another by making simultaneous measurements of the received time code at each site. Simple subtraction of the results between two sites yields clock differences that to some degree are insensitive to the actual satellite position and any time errors that may exist between UTC and the transmitted code. In this case the received timing signal functions only as a "transfer standard" to compare two or more clocks.

Observed Performance in "Uncorrected" Mode

Figures 2-5 show some of the results of monitoring the uncorrected GOES/East and GOES/West time codes at NBS/Boulder. In all cases the Y-axis is (UTC(NBS) - the received time code) in microseconds with no correction being applied for Boulder's fixed location. Figures 2 and 3 show typical results (for GOES/East and GOES/West, respectively) over a period of several weeks where each plotted point is an hourly measurement of (UTC(NBS) - received signal). The obvious variations within each day are due to satellite motion which varies the path delay. For GOES/East during this period the maximum peak-to-peak variation was less than $200 \mu\text{s}$. The GOES/West hourly data in Figure 3 show somewhat larger daily variations of about $250 \mu\text{s}$ during part of the period and a definite change on day #19 when a GOES/West satellite station-keeping maneuver was executed. Figures 3 and 4 show the longer term variations in the received "uncorrected" time codes over a period of nearly four years. In these plots the points up to 5/1/81 (day number 852) are actually single measurements made once each day, while after 5/1/81 an average of 24 hourly measurements is plotted for each day. The somewhat-more-erratic values prior to 5/1/81 are due mainly to the greater sensitivity of single measurements to temporary perturbations from such causes as land-mobile interference. The many points where abrupt changes occur, producing the "scalloped" appearance, correspond to days on which satellite station-keeping maneuvers took place. Note especially in Figure 4 how the station-keeping on GOES/East has improved since the shift to a new GOES/East satellite (GOES-5) at about day #970 on the plot. The important

point, however, is that during the entire four-year period both satellites provided a UTC time reference that varied by less than ± 1 ms with respect to a fixed offset due to Boulder's geographical location.

Observed Performance in "Corrected" Mode

Figures 6-9 show received data obtained with commercial receivers that automatically use the satellite position data to compute updated path delays and adjust the output 1pps pulse accordingly. In each plot the Y-axis runs from $-200 \mu\text{s}$ to $+200 \mu\text{s}$ with respect to UTC(NBS). Figure 6 shows the relatively short-term performance for both satellites by plotting hourly measurements over a typical 1-month period. The peak-to-peak variations within each day, ranging from about 10 to 35 μs during this period, are apparently due to small imperfections in the tracking data, orbital-element generation, or the computer program used to generate the satellite position predictions. Abrupt changes in the peak-to-peak amplitude of the daily variations are sometimes observed when a new set of orbital elements is processed (about once per week). Also, a general increase in the amplitude sometimes occurs as the time increases since the last "fresh" set of orbital elements -- e.g., note the first eight days of GOES/West data in Figure 6. Based on years of monitoring at NBS the typical peak-to-peak daily variation is about 20 μs , although there have been occasional periods due to lower-quality orbital elements when values of greater than 100 μs were observed.

Figure 7 shows corresponding data over a longer period of $4\frac{1}{2}$ months where an average of 24 hourly measurements is plotted each day. The step change of about 40 μs that occurred in GOES/West early in August, 1982 has no apparent explanation. The more temporary large excursions of up to 150 μs in GOES/West that occurred during a two-week period around day #90 resulted from two consecutive sets of orbital elements that were of poor quality.

Figures 8 and 9 show the long-term performance over nearly four years of the GOES/East and GOES/West time codes, respectively, as received at NBS/Boulder. Each point prior to May 1, 1981 (day number 852) is a single measurement per day while each point after that time is a daily average of hourly measurements. Considering the entire period of more than 1400 days, the received time codes from both satellites, averaged over a day, have generally remained within $\pm 100 \mu\text{s}$ of UTC(NBS) with the exception of occasional brief periods of 1-15 days.

Based on the experience at NBS during 1982 (325 days), a GOES/East time code user would have observed daily averages within $\pm 25 \mu\text{s}$ of the mean value 95% of the time and no values greater than 50 μs from the mean. A corresponding GOES/West user, however, would have observed only about 65% of the values falling within $\pm 25 \mu\text{s}$ of the mean, although 93% of them would be within $\pm 50 \mu\text{s}$.

Observed Performance in "Common-view" Mode

Figures 10-12 summarize the relatively short-term performance over about a 1-month period when the GOES time code is used in the "common-view" mode. In Figure 10, the hourly measurements of GOES/East are plotted from two co-located receivers at NBS/Boulder along with the hourly differences in the values. Although the output of each receiver has time code variations of several tens of microseconds, the differences between the simultaneous hourly measurements remain generally stable to within a few microseconds with occasional jumps of 5-10 μ s.

Figures 11 and 12 show similar data for receivers which are separated thousands of kilometers. Figure 11 applies to the simultaneous reception of GOES/East at NBS/Boulder and the USNO in Washington, DC while Figure 12 applies to reception of GOES/West in Boulder and Hawaii. Although the Boulder/Washington differences are not much worse than for the co-located receivers, the Boulder/Hawaii differences show larger variations and a relatively large step change at about day #25 on the plot. The Boulder/Hawaii data may be adversely affected by the greater sensitivity of the GOES/West downlink frequency to land-mobile interference and by the fact that the Hawaii receiver is an older model, not containing some improvements incorporated into the later versions used in Boulder and Washington.

Figure 13 presents all of the NBS/USNO common-view data currently available, but in this case, using daily averages of the hourly measurements at each site. At present it is not clear why the results seemed to improve since early October, 1982. Finally, all the available Boulder/Hawaii common-view differences based on daily averages are shown in Figure 14. The data gap in mid 1982 results from a failure in the receiver at WWVH. The observed common-view performance with GOES/West during this period is clearly inferior to the NBS/USNO comparisons via GOES/East. Further testing will be necessary in order to identify the specific cause or causes.

Based on the available data to date it appears that the common-view approach with GOES should not be depended on for comparisons of separated clocks to better than 10 μ s. Such a result is probably not too surprising in view of the constraints imposed by the 400-Hertz bandwidth limitation on the GOES time code channel.

SOME POTENTIAL FUTURE IMPROVEMENTS

- 1) NBS Access to More Current Position Data. Under present operating procedures, there sometimes are substantial delays between the creation of a revised set of satellite orbital elements by NOAA or NASA and the time at which new position predictions based on them can be inserted into the time code transmissions. The current procedure requires distribution of the orbital elements from NOAA to NASA and then to NBS, the running of a large computer program in Boulder to generate the revised position data, and the transmittal of

these predictions to the Wallops Island equipment. The delays involved may be particularly significant at times when satellite maneuvers are implemented. Efforts are now in progress to streamline this process by developing direct access by NBS to the most current satellite data residing in NOAA's computer at Suitland, MD. It may also prove feasible to generate improved position predictions more quickly and more efficiently directly from the GOES tracking data obtained approximately every four hours for each satellite.

- 2) Accuracy Indicators in Time Code. Suggestions to include in the time code format some indicator of when the usable accuracy is degraded due to various reasons are under consideration. Unused code bits are available for this purpose and receiver manufacturers have indicated willingness to provide a corresponding visible or other form of alert at the user's receiver as appropriate.
- 3) Automatic Compensation for Eclipse Periods. Due to GOES spacecraft limitations the time code transmissions are shifted to an in-orbit spare satellite at 106°W longitude for scheduled 2-hour periods each day during eclipse periods (March 1-April 15 and Sept. 1-Oct 15). During these 2-hour periods the satellite position data cannot at present be revised to reflect the spare satellite's position. Changes to the GOES time code system software at Wallops Island are being considered to alleviate this problem.
- 4) Automatic Delay Monitoring at Wallops Island. At present equipment delays through the Wallops Island transmission channel processing equipment are not monitored directly and could introduce uncompensated changes in path delay when subsystems are replaced or modified. Capabilities for monitoring such station delays may be incorporated in the future.
- 5) Use of GOES Trilateration System for Higher Accuracy Time Transfer. Some of the current limitations in GOES timing accuracy are related to the limited 400-Hz interrogation-channel bandwidth available and uncertainties in the satellite position predictions. NBS plans to investigate the possibility of removing or reducing these limitations through the use of the GOES trilateration ranging system for time transfer. Ranging signals are transmitted at about 1.6 GHz approximately every four hours. With sidetones as high as 200 kHz, these ranging signals could provide timing resolution in the 1 ns range. Furthermore, since the satellite positions are determined accurately during each of the ranging operations, time transfers should be possible at these times with both higher precision and higher accuracy. Benefits may be realizable in both a general dissemination mode and a higher accuracy common-view comparison mode.

ACKNOWLEDGEMENT

NBS would like to acknowledge the assistance of Arbiter Systems, Inc. and

the U. S. Naval Observatory in making possible the additional GOES/East monitoring capability in Washington, DC and also USNO's provision of its Automated Data Service facilities for the GOES status reports.

REFERENCES

- (1) D.W. Hanson, D.D. Davis, and J.V. Cateora. NBS time to the western hemisphere by satellite. Radio Science, vol. 14, No. 4, p. 731-740 (July-August 1979).
- (2) NBS Time and Frequency Bulletin. Available upon request to Time and Frequency Division, National Bureau of Standards, 325 Broadway, Boulder, CO 80303.

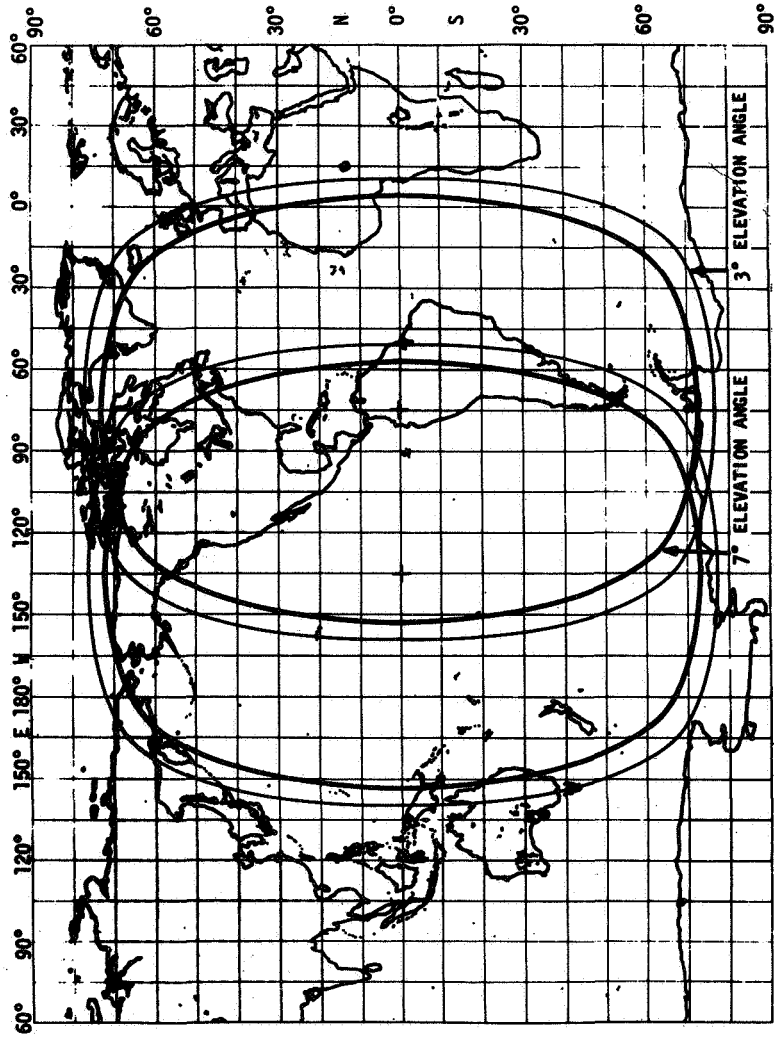


Figure 1. GOES/East and GOES/West coverage areas.

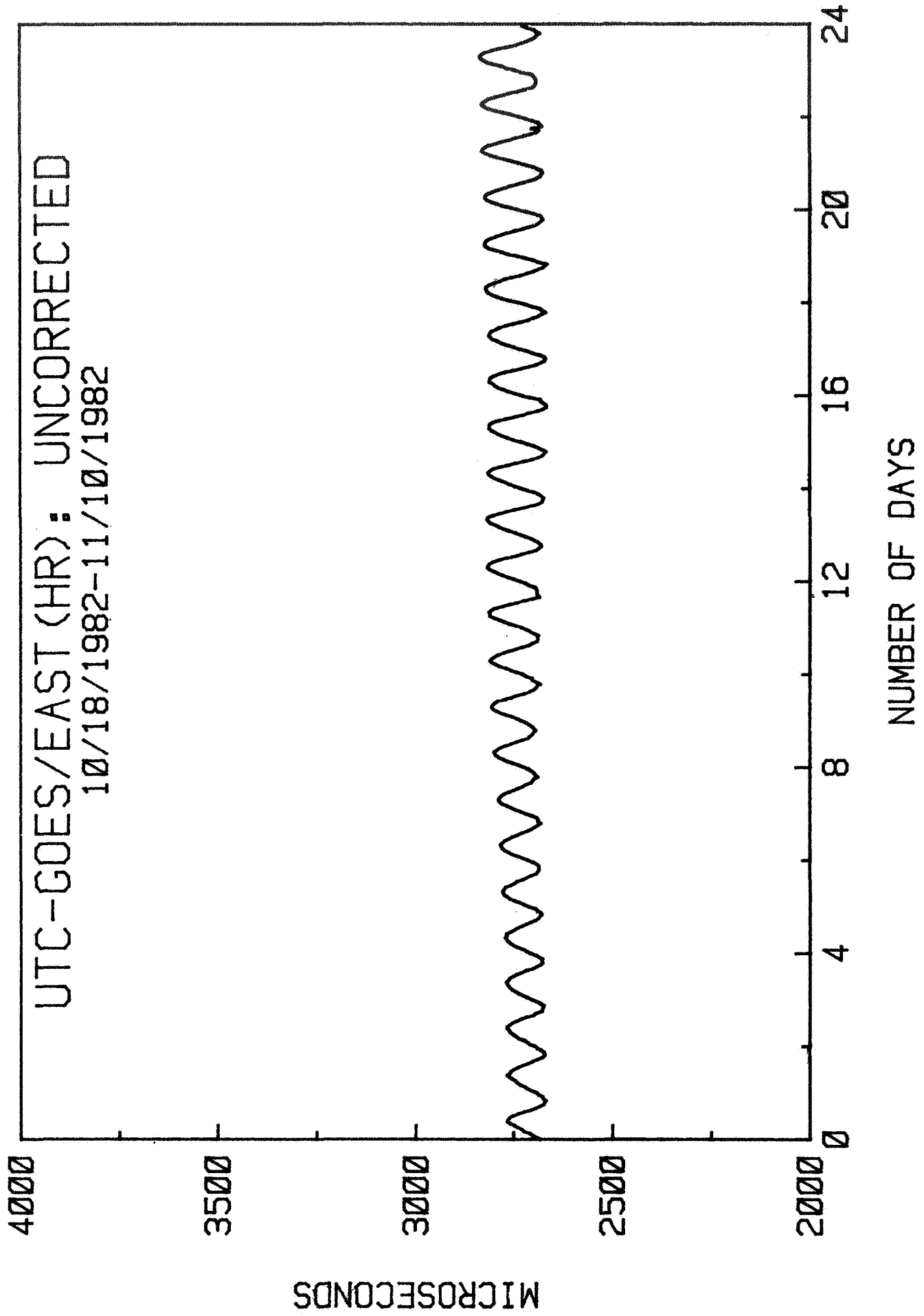


Figure 2

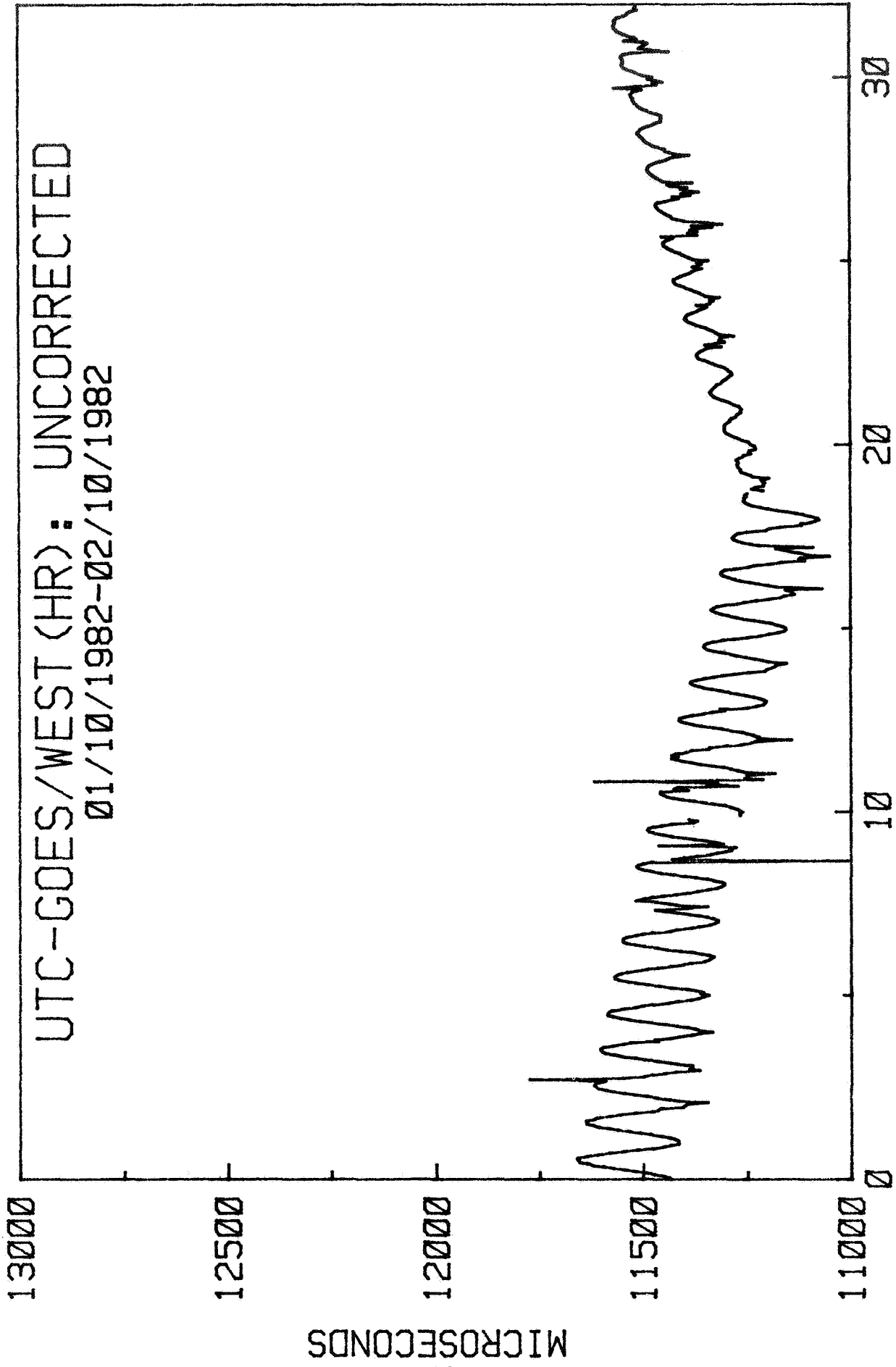


Figure 3

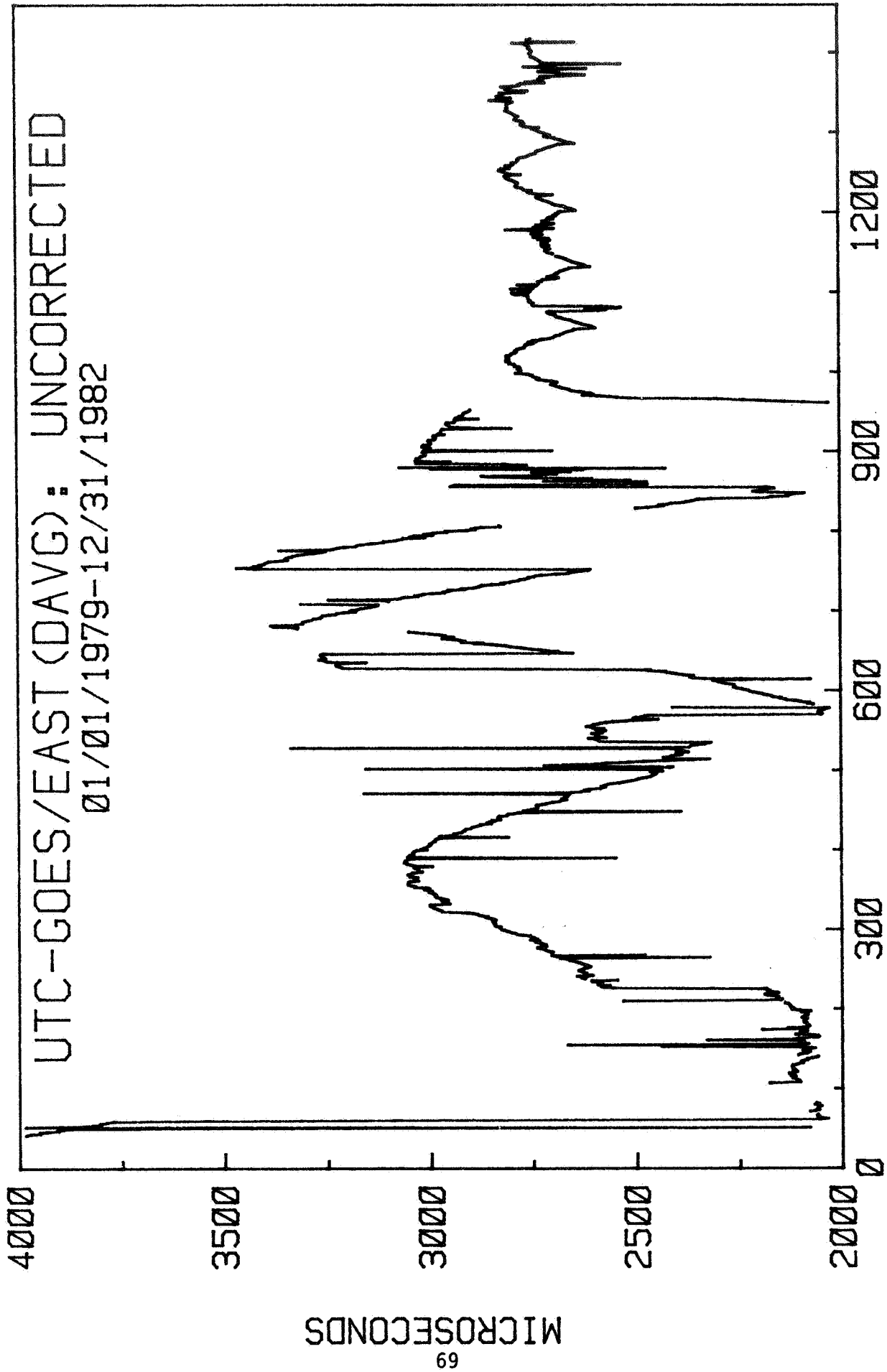


Figure 4

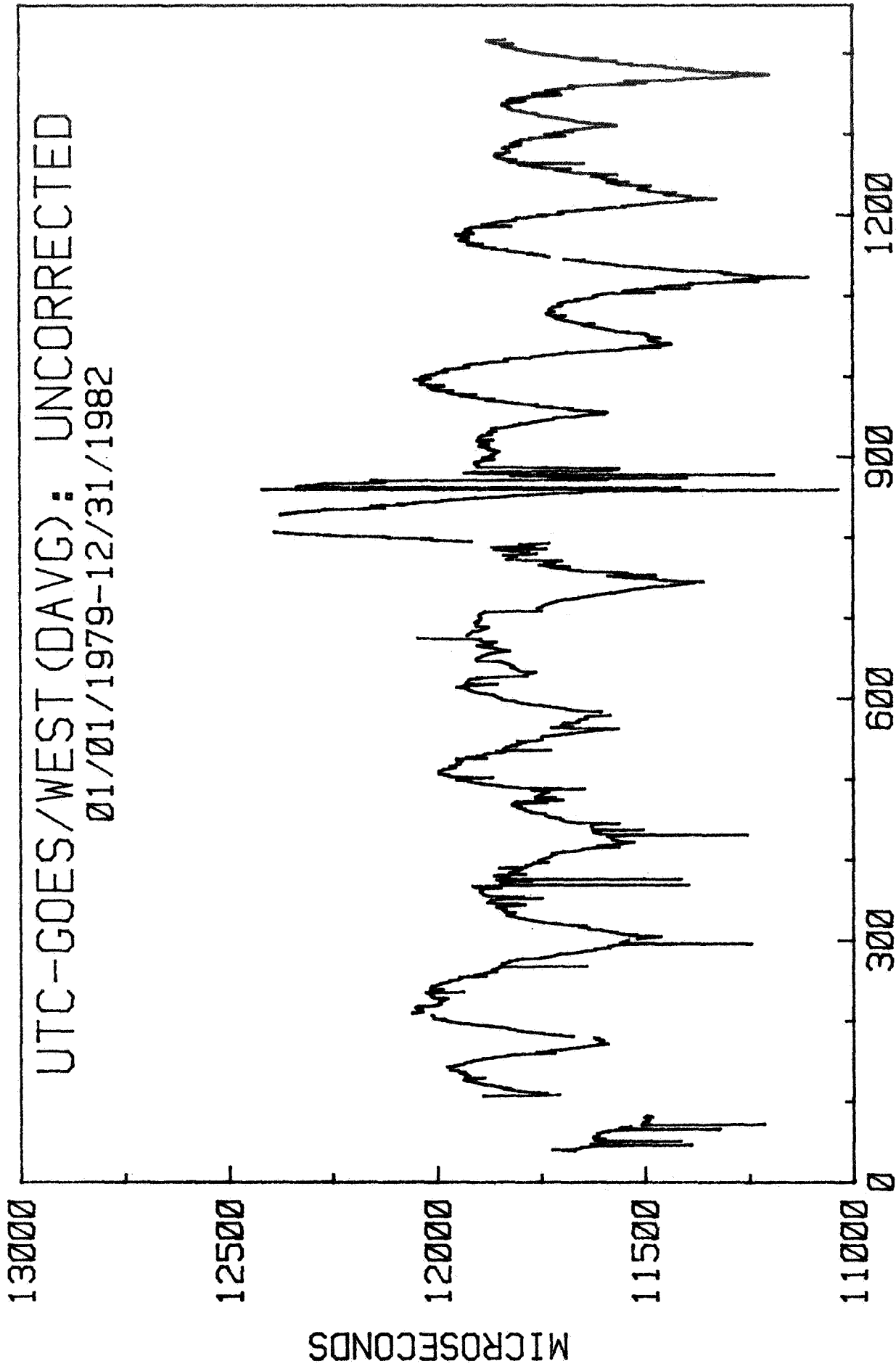


Figure 5

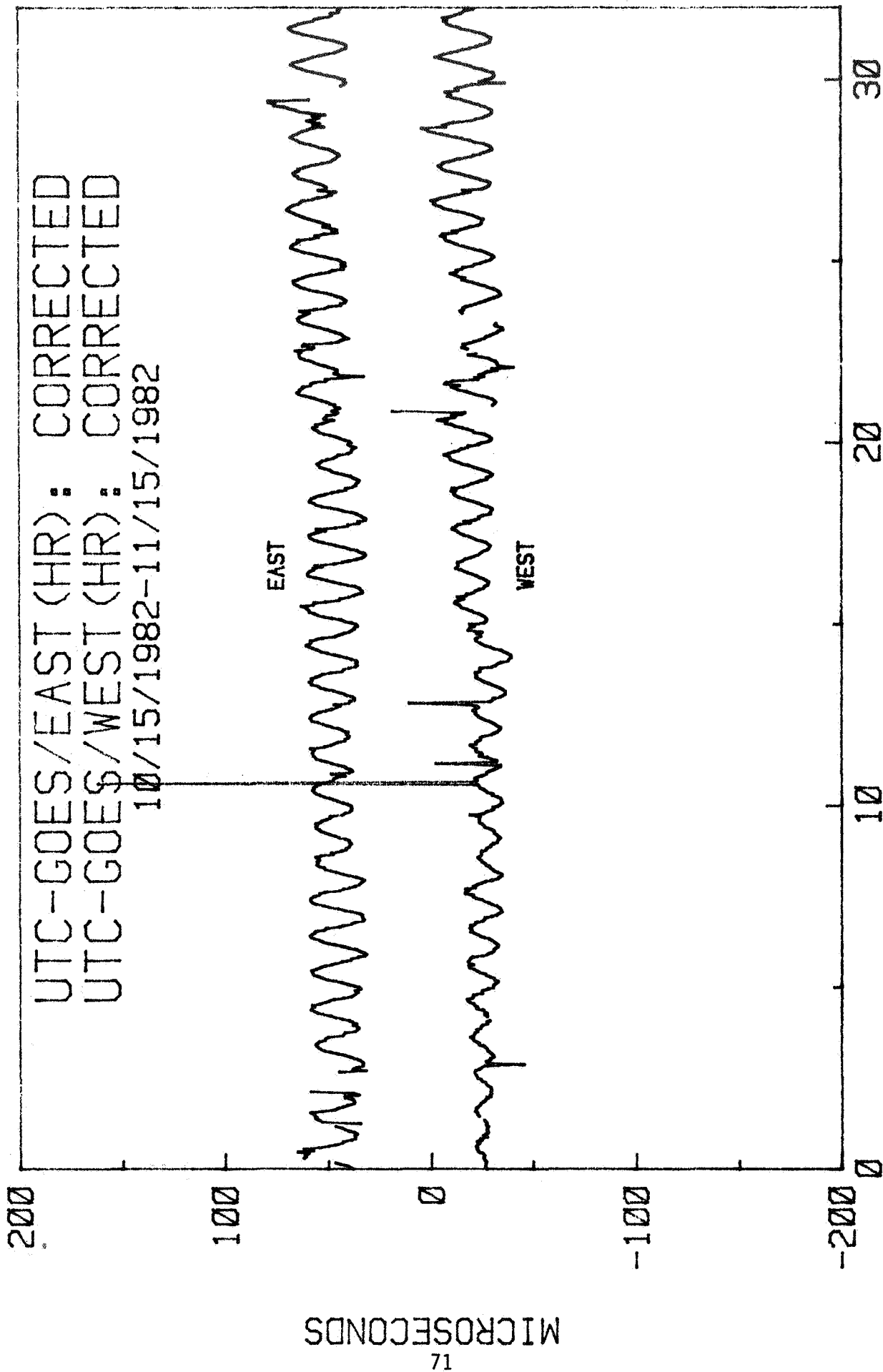
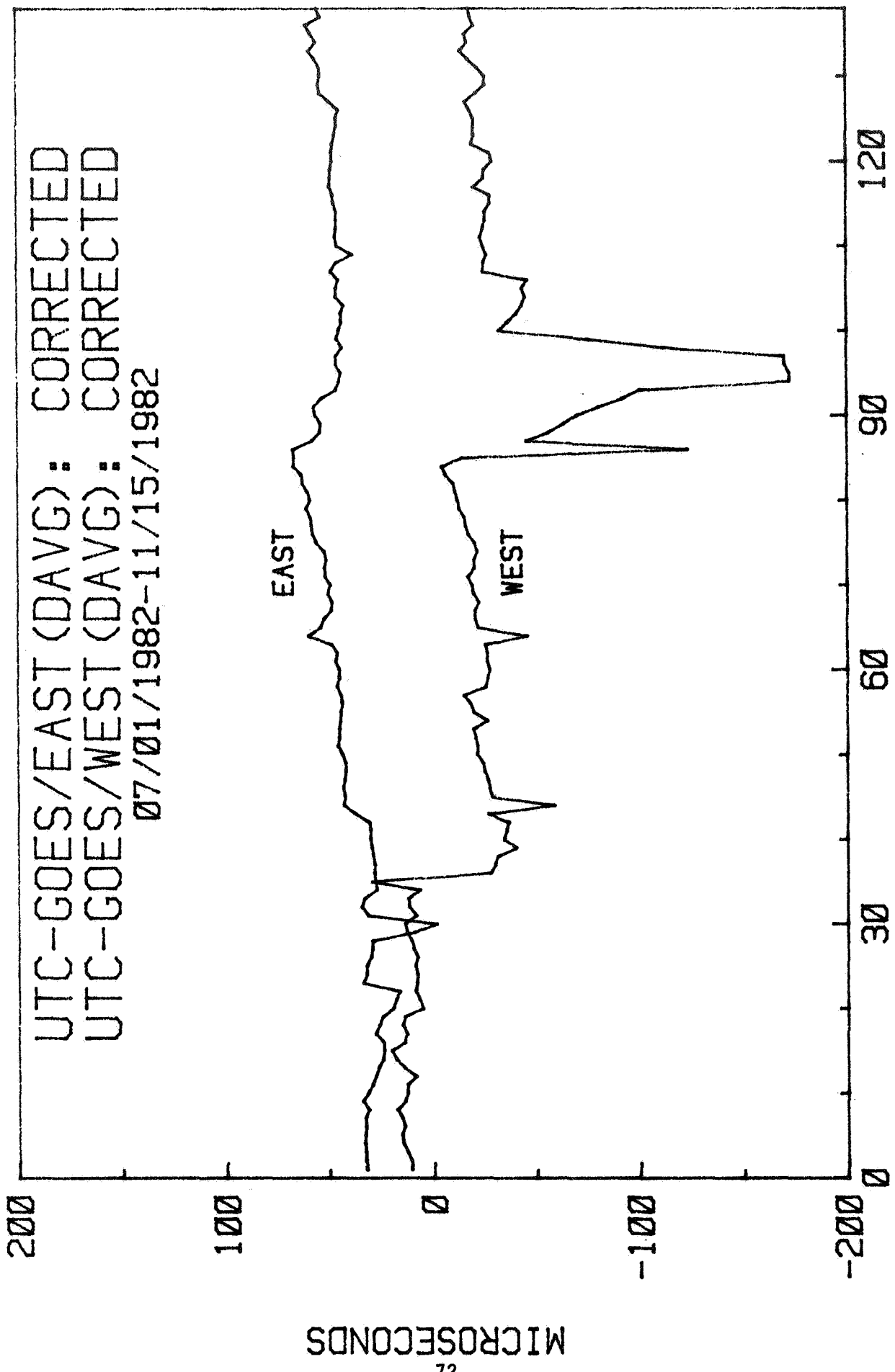


Figure 6



NUMBER OF DAYS

Figure 7

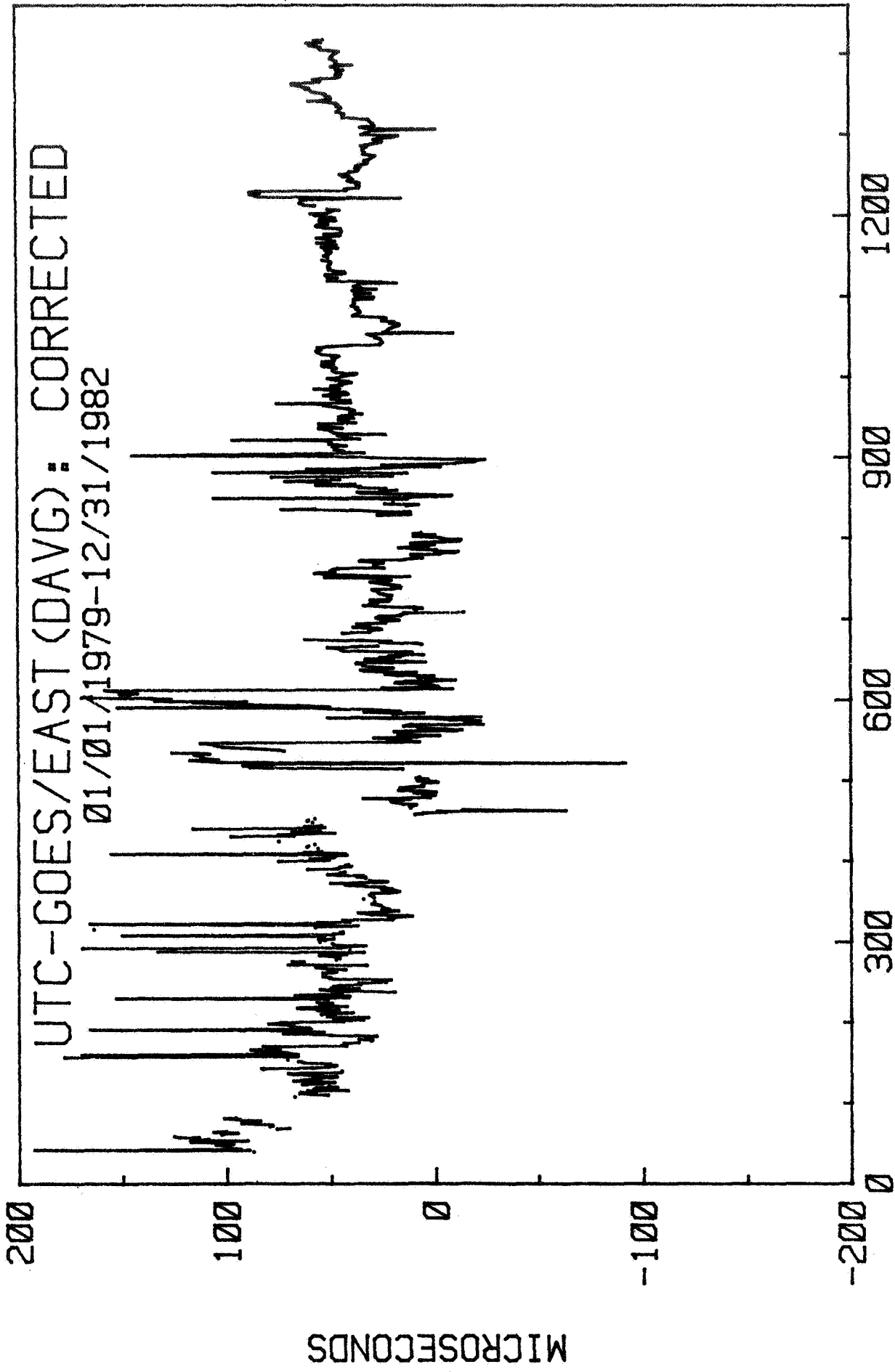


Figure 8

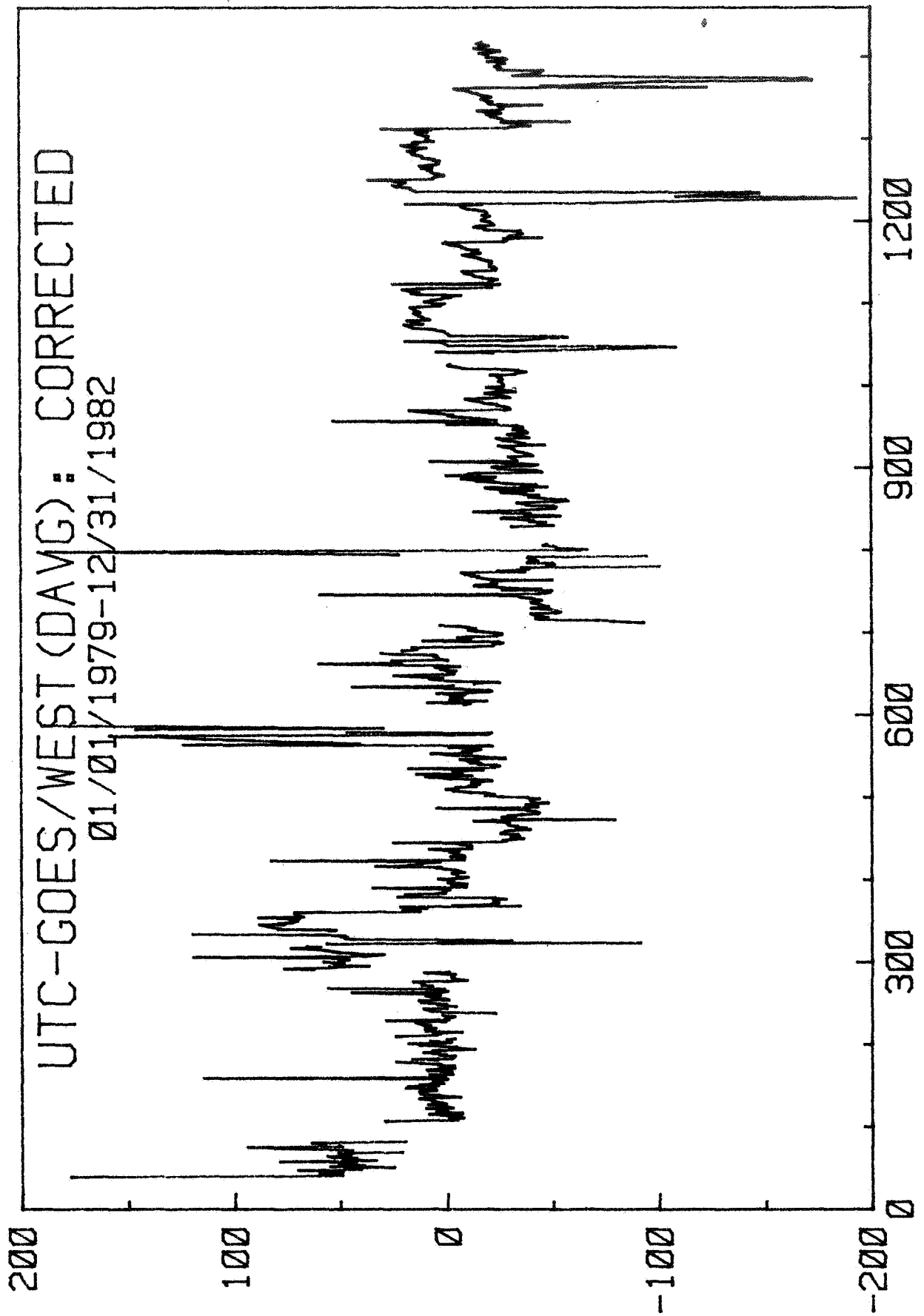


Figure 9

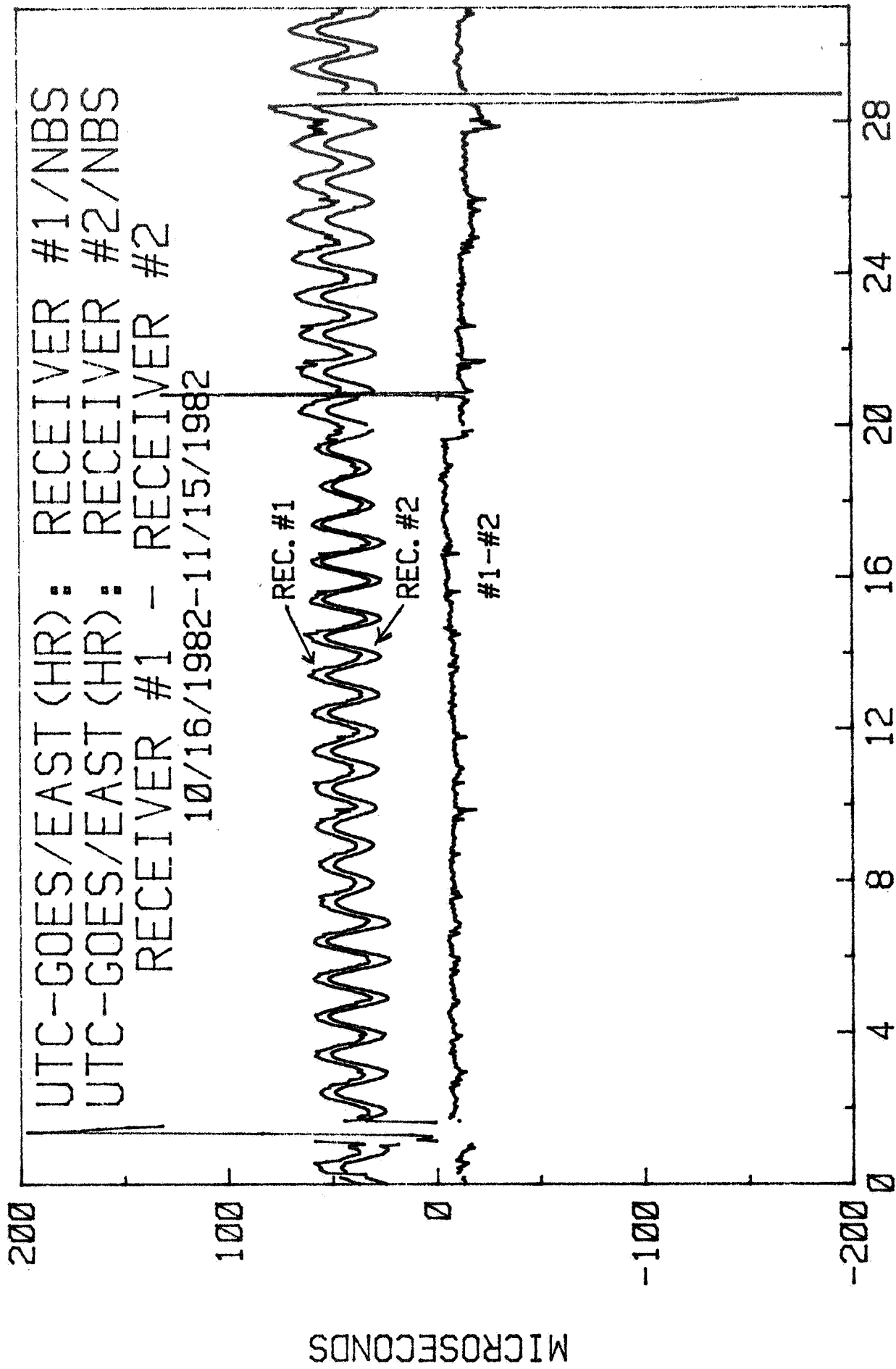


Figure 10

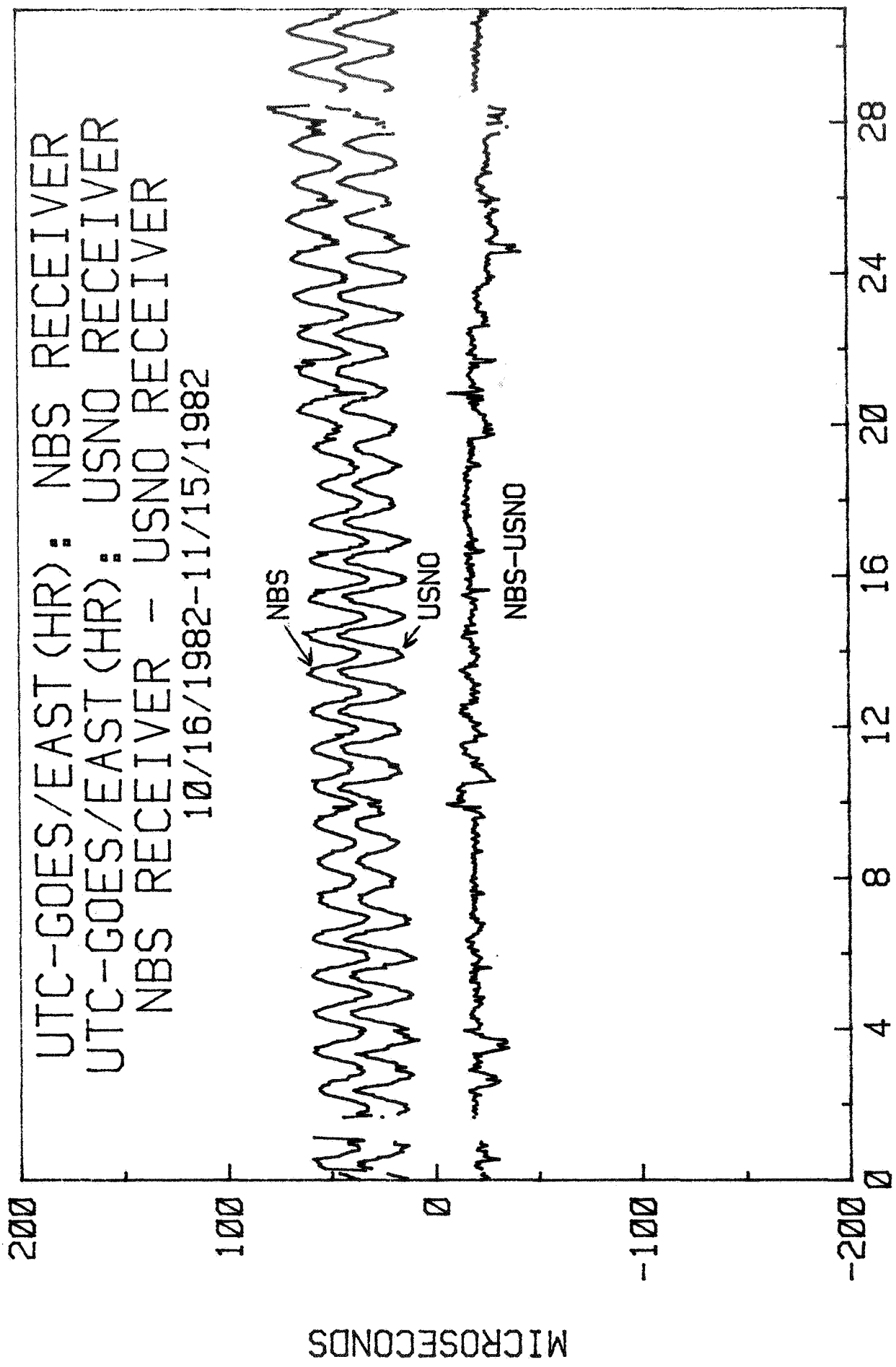
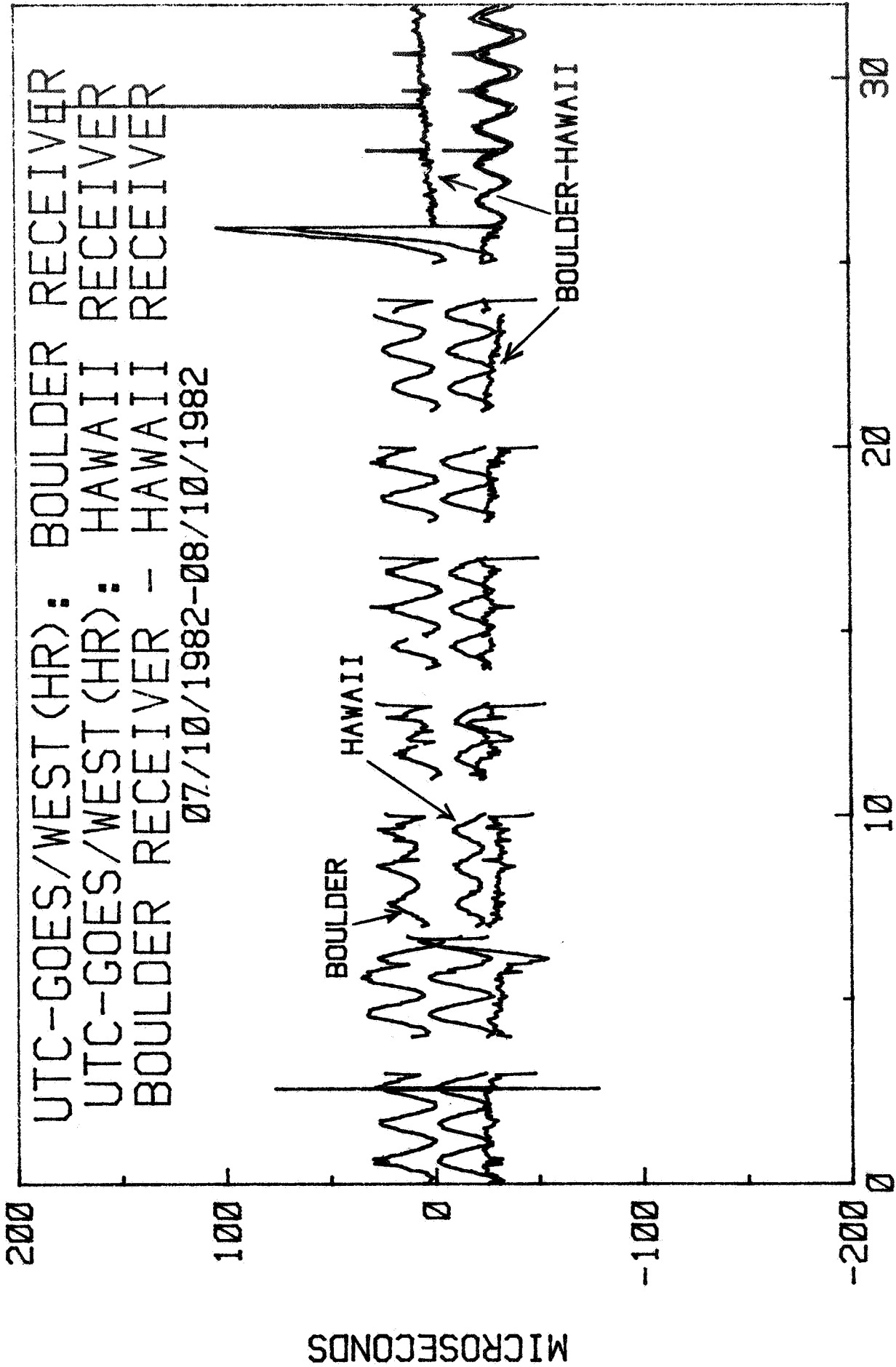


Figure 11



NUMBER OF DAYS

Figure 12

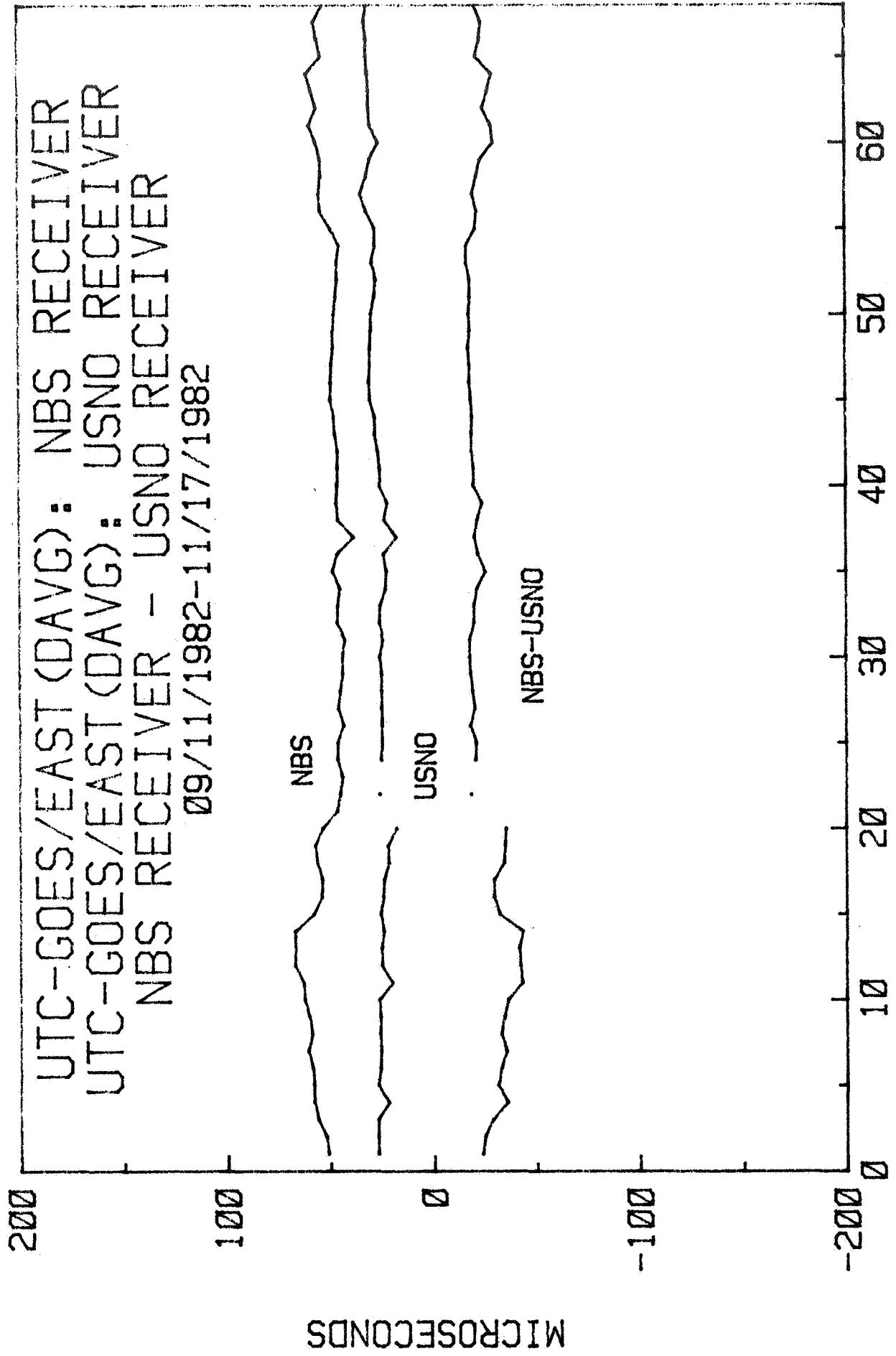


Figure 13

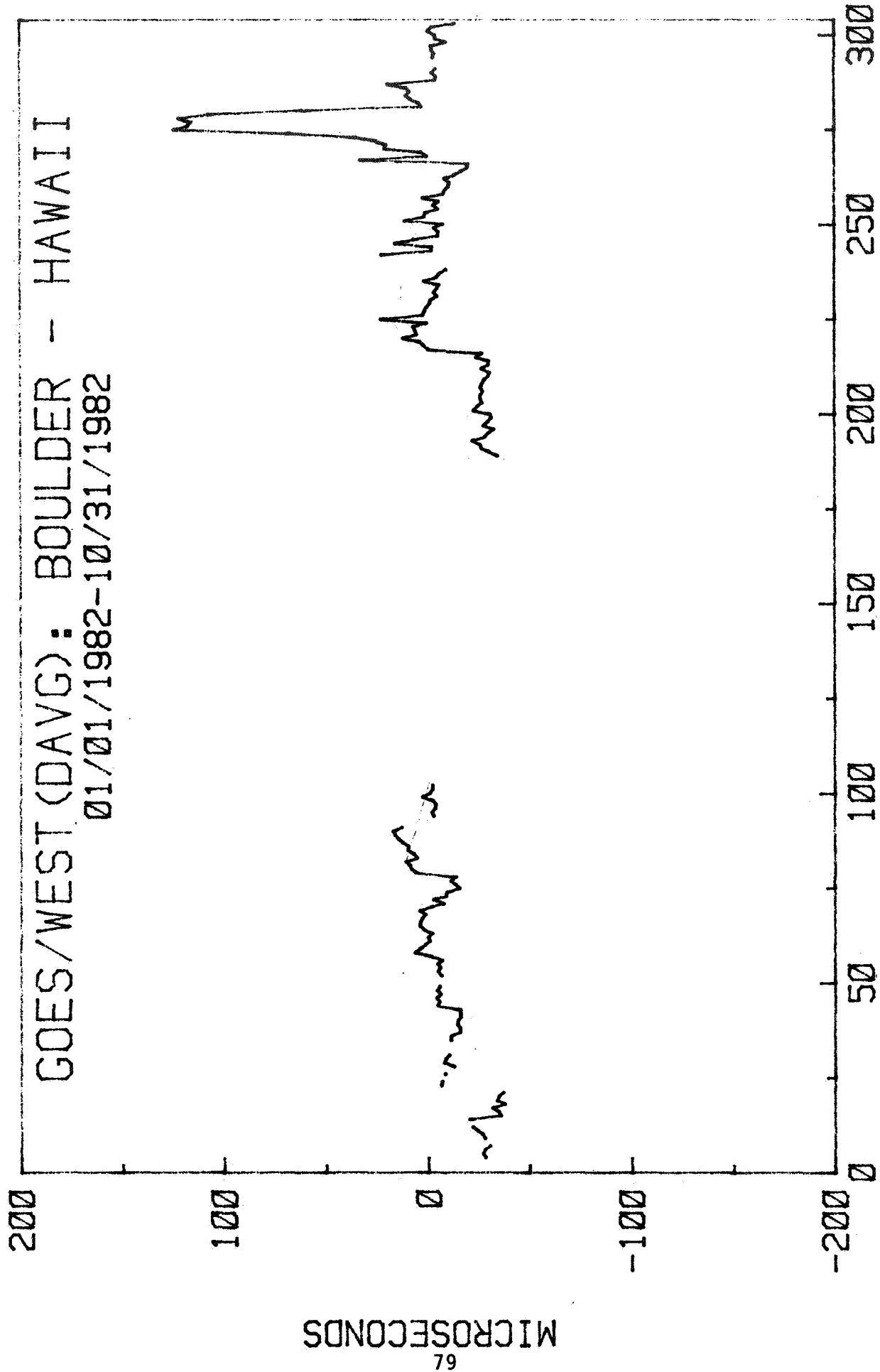


Figure 14

QUESTIONS AND ANSWERS

MR. ANDREW C. JOHNSON, USNO

Is there any possibility of expanding an area of coverage to other governments?

MR. BEEHLER:

The U.S. GOES satellites are part of an international system which include the MEDISAT Satellites in the European area and GMS Satellites in the Japanese area. There have been some continuing discussions relative to providing the code that we provide here, or something similar on those satellites to make it into pretty much an international system.

At present, I understand that the decision of the Japanese government is not to include the time code and the European Space Agency still has under consideration, including it on the European System. But, at present there are no definite plans.

AUDIENCE:

I have a question concerning your Wallops Island set-up, the 3 cesium standards, are they configured as an ensemble or a simple redundancy?

MR. BEEHLER:

They're configured now just for simple redundancy.

DR. KELLOGG:

Last year, Allan talked to us a little bit about another development in Boulder using the GPS Satellite between Boulder and the US Naval Observatory. In the longer range future, will both of these co-exist or will you choose the better of the two or if not?

MR. BEEHLER:

Well, I think for the foreseeable future we would say that they're both going to co-exist. I think you want to keep in mind, first of all, that we're really dealing with different accuracy capabilities here. At least with the time code constraints as we reported here today, your really confined to something at the 50 to 100 microsecond level, with GPS on the other hand the measurements have shown that you're able to do better than 100 nanoseconds. So they are not really competing systems.

I think, especially at the moment and if the tri-lateration were on the GOES system, would eventually look favorable at the one to ten nanosecond range, then I think one just simply has to look at probability of the GPS signals continuing to be available and the trade-off involved, the cost and so on before making any long-term decision.

DR. KELLOGG:

That raises another question, may I please? Do you have an idea of the relative size of the two bodies of customers for the different precision signals?

MR. BEEHLER:

Well, I think there's no question that the larger number of users of course are for the more modest accuracy needs. If you look at, for example, the users of WWV, they probably number in the hundreds of thousands.

When you get down to the GOES region where you're talking about perhaps fifty to 100 microseconds the users of that service are probably numbering between 500 and a 1,000 at the present time.

When you get down to the GPS capabilities of better than 100 nanoseconds I really can't answer except I'm sure it's a much smaller number.

DR. WINKLER:

That is true, I'd like to share also here in this discussion what we have observed, however, that a system when it becomes very reliable then the greatest capability system will carry the day.

In other words, people will buy receivers for the one system which can satisfy all requirements. That brings me, of course, back to a question which we just had before, a comparison between the different systems, essentially has to be made, I believe on the basis of one-way versus two-way operation. In the case of the two-way operation, the system determines the propagation delay for you, or by transmission and reception, the propagation problem simply goes away. And, therefore, a two-way system, at the expense of transmitting at the site, which may not always be possible or practical, but it does provide for essentially a much less expensive capability down to the nanosecond region.

In favor of the one-way system, one can only repeat that it doesn't require transmissions; it can be set up anywhere on earth; but, because you have to compute the propagation delays very carefully it is essentially a more expensive solution.

I can see the future, both of them co-exists. Where the one-way systems will, eventually be the counsel of despair for all the users who cannot transmit and I think that they are the large majority of the users. Where as the two-way comparisons will be used mainly by those who have an easy access or are nearby a communication terminal or communications center where the transmission problem really does not exist.

I think you will see in the future, both of these methods to co-exist and a question whether those can be pushed to that kind of a precision or not, will have to be seen.

DR. KELLOGG:

You added UT-1, to the capability to the signal, was this as an experiment or as a responsive to a demand?

MR. BEEHLER:

Well, I'd say it's in response to a small demand. The particular user that was interested in this is involved with electric power system timing. And, the reason for needing it, it's kind of a strange application you might think, but the reason goes back to historical arguments. They simply have a large number of older receivers in the system, which at one point in time were configured in a hardware sense to use UT-1, and if they cannot continue to reference to UT-1 and they switched to UTC as a reference then they would have to modify in a hardware sense many of the older equipment. So they would prefer to let that go until the equipment just naturally phases out.

DR. WINKLER:

One more point, by using UT-1 you don't have the leap seconds.

SESSION II

RUBIDIUM FREQUENCY STANDARDS

**Alfred Kahan, Chairman
Rome Air Development Center**

AFTERNOON SESSION

MR. ALFRED KAHAN, Rome Air Development Center

This afternoon session considers improved timing devices, namely Rubidium Frequency Standards, and a continuation of a topic of Synchronization.

Several years ago, I think it was in 1978, according to the proceedings of this conference, I made some remarks, during one of the panel sessions regarding the lack of research and development in rubidium frequency standards. And even the possible obsolescence of the standard.

Clark oscillators promise quantum improvements and cesium standards were suppose to become smaller and cheaper, and rubidium was being squeezed in the middle. At that time, and since then I have received severe reaction to those comments, and I think in this same spirit the organizing committee considered it poetic justice that I should chair this session on R&D and Rubidium Frequency Standards.

Before I call the first paper, I would like to relate to you an incident I had this weekend. I was over at some friend's house and she showed me a collector's bound volume of the illustrative London News from 1871, which was a beautiful copy of a combination of life and time type of thing of today. Today it has a little bit of times, a little bit of sports, and has everything else. In that one it was related that, in the June 3rd issue of 1871 that was called clocks and photographs. And evidently Mr. Norman Lockyer, who I'm told by Dr. Winkler is a known astronomer, gave his sixth lecture on instrumentation using modern astronomy, that was devoted to clocks and photographs, as such. And he went on to review the history of the development of clocks starting with Archimedes and the wheels moved by weight. And then he mentioned that the first clock in England was in Court Place Yard in Westminster in 1268. And then he started with the further development in 1639 by Galileo, who discovered the isochronal properties of oscillating bodies suspended by equal strings and hope that would apply in 1658 by Huygens to the suspended pendulum and things like that. And then he recalled the further developments of Hooke, Clemens, Grayham and Harrison.

Let us just continue then, Mr. Lockyer by 8 of diagram explained this successive improvement and then proceeded to exhibit in action a splended modern astronomical clock, loaned to him by Colonel Strange stating that the principles now demanded in such clocks are that the weight shall be small, and the pendulum heavy, and that there shall be as solid a connection between the two as possible. A word to the precautions necessary to be observed to preserve the pendulum from the action of temperature as much as possible in order to take advantage of the compensated pendulum. Then he went on to say, Mr. Lockyer then referred to Sir Charlie Whitstone's patent in 1840 to apply the electro-magnetic force to record a very minute section of time and thought that

a tenth of a second or less they could do it that way. Then Mr. Lockyer concluded by demonstrating the great importance of photographs in that the determination of the longitude of distance places, such as Washington.

This was 111 years ago. I just wonder if anyone 111 years from to-day will read our proceedings; What's their opinions of our world, one hundred and eleven years from now?

INFLUENCE OF MODULATION FREQUENCY IN
RUBIDIUM CELL FREQUENCY STANDARDS

C. AUDOIN and J. VIENNET
Laboratoire de l'Horloge Atomique
Equipe de Recherche du CNRS,
associée à l'Université Paris-Sud
Bât. 221 - Université Paris-Sud
91405 Orsay - France

and

N. CYR and J. VANIER
Laboratoire de Recherches sur les
Oscillateurs et les Systèmes
Département de Génie Electrique
Université Laval
Québec G1K7P4 - Canada

ABSTRACT

The error signal which is used to control the frequency of the quartz crystal oscillator of a passive rubidium cell frequency standard is considered. The value of the slope of this signal, for an interrogation frequency close to the atomic transition frequency is calculated and measured for various phase (or frequency) modulation waveforms, and for several values of the modulation frequency. A theoretical analysis is made using a model which applies to a system in which the optical pumping rate, the relaxation rates and the r.f. field are homogeneous*. Results are given for sine-wave phase modulation, square-wave frequency modulation and square-wave phase modulation. The influence of the modulation frequency on the slope of the error signal is specified. It is shown that the modulation frequency can be chosen as large as twice the non-saturated

*) A typical experimental situation satisfying approximately these conditions is that of a small cell placed in the center of a TE_{011} cavity.

full-width at half-maximum without a drastic loss of the sensitivity to an offset of the interrogation frequency from line center, provided that the power saturation factor and the amplitude of modulation are properly adjusted. The interest of square-wave phase modulation is pointed out for large modulation frequencies.

Experimental data has been obtained on a laboratory set-up in which a rubidium cell fills a TE_{111} microwave cavity.

Experimental results achieved with this configuration are in excellent agreement with the predictions of the given model.

1. INTRODUCTION

In passive frequency standards, such as the rubidium cell frequency standard, frequency control requires that the microwave interrogation signal is phase (or frequency) modulated. An error signal is obtained, which is proportional to the offset of the interrogation frequency from the line center, if this offset is small enough. The error signal drives the frequency control loop. The slope of this error signal has to be optimized in order to achieve the best frequency stability of the controlled quartz crystal oscillator. In practice, the modulation frequency should be large enough, i) to allow amplification of the modulated atomic cell response in a frequency range where shot noise dominates flicker noise and ii) to enable a reduction of the attack time of the frequency control loop, in order to ensure a better attenuation of the effect of perturbations, such as acceleration, which might affect the frequency of the quartz crystal oscillator.

Although investigation of frequency modulation effects has been performed by several authors in the framework of magnetic resonance experiments, very few analysis of frequency modulation has been given, which are directly applicable to the field of atomic frequency standards [1-4]. Furthermore, previous results are of limited practical interest because r.f. power saturation effects were not taken into consideration.

In this paper we give :

i) analytical expressions for the slope of the error signal assuming, at first, that the modulation is slow. Optimum values of the saturation factor and of the modulation depth are specified for sine-wave phase modulation and square-wave frequency modulation. The achieved results are used as a basis for further comparison with results derived when the dynamical behaviour of the atomic medium has to be taken into consideration i.e. when the modulation frequency is not small compared to the atomic line-width.

ii) analytical expressions for the slope of the error signal, for arbitrary values of the modulation depth and of the modulation frequency, but for weak saturation. We show that the results derived by Andres et al [1] and which were the only available for a long time are not exact.

iii) computed values of the slope of the error signal, for a large range of values of the saturation factor, the modulation depth and the modulation frequency. Sine-wave phase modulation, square-wave frequency modulation and square-wave phase modulation are considered. The influence of the value of the modulation frequency on the slope of the error signal is specified. The values of the saturation factor and of the modulation depth which maximizes the slope of the error signal are given.

iv) experimental values of the slope of the error signal for a rubidium cell filling a TE_{111} microwave cavity. Results are obtained for the three considered modulation waveforms. They confirm that the reduction of the error signal is small at modulation frequencies up to twice the non-saturated atomic line width.

2. THE MODEL USED FOR THE THEORETICAL ANALYSIS

In order to point out the results of major interest, we will consider a model in which the following simplifying assumptions are made.

i) the properties of the rubidium cell are homogeneous. This means that any effect related to the progressive absorption of light inside the atomic cell is neglected and that the light intensity is a constant across the light beam cross-section. In particular, the longitudinal and transverse relaxation times T_1 and T_2 , respectively, will be assumed constant over the cell volume. Motional averaging in a coated cell without buffer gas would yield homogeneous values of T_1 and T_2 .

ii) the microwave field is uniform over the rubidium cell volume. This condition is approximately verified close to the center of a microwave cavity in which the TE_{011} mode is excited. On the contrary, the amplitude of the microwave field varies largely over the volume of a rubidium cell filling the entire volume of a TE_{111} cavity, an arrangement which is used widely in practice, in order to reduce the size of the frequency standard. However, we show in Section 7, that the experimental results are in very satisfactory agreement with the theoretical predictions and that, consequently, the model chosen is adequate.

iii) rubidium atoms behave as a two-level quantum system in which optical pumping has created the necessary population difference.

The given results are valid for passive frequency standards in which the atomic resonance is probed via a measure of the population difference between the two involved atomic levels. This measure consists either in the monitoring of the absorption of the pumping light, as in the passive rubidium cell frequency standard, or of the fluorescence of the optically pumped medium, as in the mass 199 mercury ion device.

Throughout this paper, we will assume that the following condition is fulfilled :

$$\omega_i - \omega_0 \ll W \quad (1)$$

where ω_i is the interrogation angular frequency*, ω_0 is the atomic transition angular frequency and W is the full-width at half-maximum of the atomic resonance line (expressed in angular frequency unit).

The modulation depth will be characterized by a dimensionless parameter, u_2 , defined as :

$$u_2 = T_2 \omega_m \quad (2)$$

where ω_m is the amplitude of the periodic angular frequency deviation. Similarly, we will introduce the normalized modulation frequency v_2 defined as :

$$v_2 = T_2 \omega_M \quad (3)$$

where ω_M is the modulation angular frequency.

We will assume that synchronous detection consists in the multiplication of the fundamental component of the periodically modulated cell response by a demodulation function $g'(t)$ such as :

$$g'(t) = \begin{cases} + 1 & \text{for } 0 < t < T_M/2 \\ - 1 & \text{for } T_M/2 < t < T_M \end{cases} \quad (4)$$

3. THE STATIC LINE SHAPE

It may be shown that the intensity I of the light transmitted by the rubidium cell is given by :

$$I = I_b + I_0 \left[1 - \frac{S}{1 + S + T_2^2 (\omega - \omega_0)^2} \right] \quad (5)$$

where I_b is a background component, I_0 depends on the atomic density in the cell and on the properties of the light flux emitted by the rubidium lamp. The quantity S is the saturation factor defined as :

$$S = T_1 T_2 b^2 \quad (6)$$

where T_1 and T_2 are the longitudinal and transverse relaxation times, respectively and b^2 is a measure of the microwave field applied to rubidium atoms.

Equation (5) describes the resonance line as a lorentzian function of the difference between the angular frequency ω of the microwave field and the angular transition frequency ω_0 . The full-width-half-maximum of the line, W , is given by :

*) The interrogation frequency is the mean value of the modulated instantaneous frequency. Therefore, equation (1) does not mean that we restrict ourselves to small time dependent frequency deviations. On the contrary, we will consider frequency excursions which are of the order of magnitude of the atomic line-width.

$$W = \frac{2}{T_2} \sqrt{1+S} \quad (7)$$

and the height of the resonance line is I_ℓ such as :

$$I_\ell = - I_0 \frac{S}{1+S} \quad (8)$$

where the minus sign indicates that the resonance appears as a dip in the transmission profile of the resonance cell. For very large values of S , we have $I_\ell = - I_0$.

4. THE NORMALIZED SLOPE OF THE ERROR SIGNAL

The error signal, which is useful for frequency control of the quartz crystal oscillator is proportional to the low-pass component of the synchronous detector output. Under the condition given by equation (1), it is proportional to the angular frequency offset of the interrogation frequency from the line center. We then define the following normalized slopes of the error signal for

$$(\omega_i - \omega_0) \ll W : \quad \text{i) } p = \frac{\overline{I_p(t)g'(t)}}{I_0 T_2(\omega_i - \omega_0)} \quad (9)$$

where $I_p(t)$ is the component of the fundamental of the cell response which is in phase with the modulation waveform. The bar means time average.

$$\text{ii) } q = \frac{\overline{I_q(t)g'(t)}}{I_0 T_2(\omega_i - \omega_0)} \quad (10)$$

where $I_q(t)$ is the component of the fundamental of the cell response which is in quadrature with the modulation waveform.

$$\text{iii) } a = (p^2 + q^2)^{1/2} \quad (11)$$

This is the slope of the error signal when the phase of the fundamental of the cell response and of the demodulation signal are matched.

5. SLOW FREQUENCY MODULATION

In the condition of slow frequency modulation, the period $T_M = 2\pi/\omega_M$ of the frequency modulation is large compared to the atomic longitudinal and transverse relaxation times. We then have :

$$v_2 \approx 0 \quad (12)$$

In this quasi static approximation, the atomic medium is assumed to reach a steady state for every value of the angular frequency ω of the applied microwave field. Equation (5) is then valid, with ω depending on time.

5.1. Square-wave frequency modulation

The instantaneous angular frequency $\omega(t)$ is given by :

$$\omega(t) = \omega_i + \omega_m g(t) \quad (13)$$

where $g(t)$ is the modulation function which describes the frequency modulation waveform. For square-wave frequency modulation, it is given by :

$$g(t) = \begin{cases} +1 & 0 < t < T_M/2 \\ -1 & T_M/2 < t < T_M \end{cases} \quad (14)$$

It can easily be seen that under condition (1), the fundamental component of the modulated light intensity, which is transmitted by the rubidium cell is in phase with the frequency modulation waveform.

We have :

$$I_p(t) = \frac{8}{\pi} I_0 \frac{S u_2 T_2 (\omega_i - \omega_0)}{(1+S+u_2^2)^2} \sin \omega_M t \quad (15)$$

The fundamental component of the demodulation waveform $g'(t)$ being $(4/\pi)\sin \omega_M t$, the normalized slope a of the error signal is given by :

$$a = \frac{16}{\pi^2} \frac{S u_2}{(1+S+u_2^2)^2} \quad (16)$$

It can easily be shown that the maximum value of $a = 0.203$ occurs for $S = 2$ and $u_2 = 1$. These values define the optimum operating conditions for applied microwave power and modulation depth. Figure 1a shows the variation of a versus the quantity u_2 for different values of S .

5.2. Sine-wave frequency modulation

The frequency modulation waveform function $g(t)$ of equation (13) is now :

$$g(t) = \sin \omega_M t \quad (17)$$

The fundamental component of the transmitted light intensity can be either derived directly thanks to standard techniques of calculation of the coefficients of the Fourier series expansion of the response, or using general results obtained by Arndt [5] who has analyzed the quasi-static sine-wave frequency modulation of a Lorentzian line.

The fundamental of the cell response is in phase with the frequency modulation waveform, and we have :

$$a = \frac{4}{\pi} \frac{S u_2}{(1+S)^{1/2} (1+S+u_2^2)^{3/2}} \quad (18)$$

The maximum value of $a = 0.189$ is achieved for $S = 2$, as in the previous case, but for $u_2 = 1.22$. Figure 1b shows the variation of a versus the quantity u_2 for different values of S .

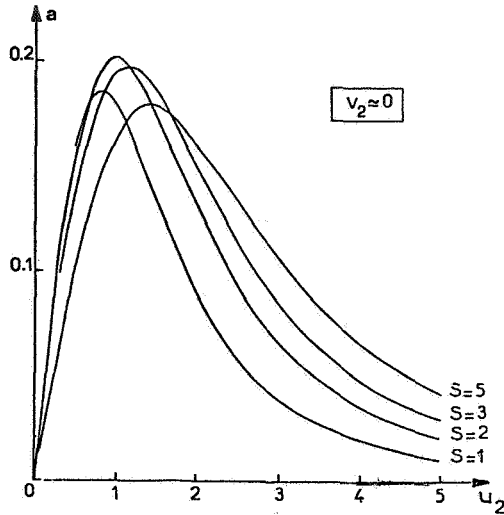


Fig. 1a

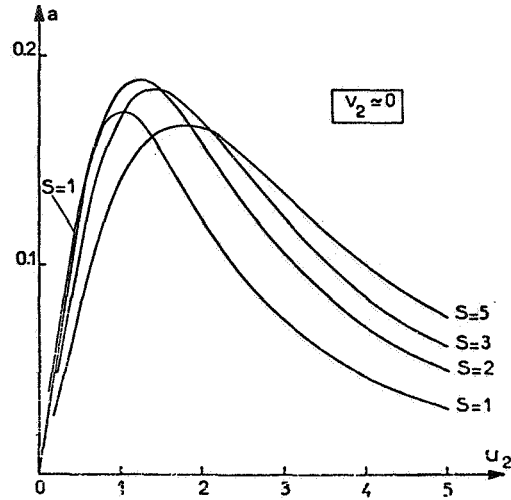


Fig. 1b

Fig. 1. Quasi static approximation. Variation of the normalized slope a of the error signal versus the normalized modulation depth $u_2 = T_2 \omega_m$ for different values of the saturation factor S , in the quasi-static approximation.

- a) square-wave frequency modulation with narrow band filtering of the response, at the modulation frequency.
- b) sine-wave frequency modulation with narrow band filtering of the response, at the modulation frequency.

6. INFLUENCE OF THE MODULATION FREQUENCY ON THE SLOPE OF THE ERROR SIGNAL

6.1. Bloch equation of the modulation problem

In general, the behaviour of any two level quantum system which follows assumptions i) to iii) of Section 2 can be described by Bloch equations [6]. For a $\Delta F = 1$, $\Delta m_F = 0$ transition, as used in an atomic frequency standard, those equations are best expressed in terms of the so-called coherence of the atomic medium, $a(t)$, and of the population difference between the two atomic levels, $a_3(t)$. The quantity $a(t)$ is a complex one, and we set $a(t) = a_1(t) + ia_2(t)$.

It can be shown that, in the presence of modulation, the Bloch equations of the considered problem are the following :

$$\begin{aligned}
T_2 \dot{a}_1 + a_1 + T_2(\omega_i - \omega_0) a_2 &= T_2 b a_3 \sin \Psi \\
T_2 \dot{a}_2 + a_2 - T_2(\omega_i - \omega_0) a_1 &= T_2 b a_3 \cos \Psi \\
T_1 \dot{a}_3 + a_3 &= \lambda T_1 - T_1 b (a_1 \sin \Psi + a_2 \cos \Psi)
\end{aligned}
\tag{19}$$

where the dot means time derivative. The quantity λ is the creation rate of the population difference which in the present case is obtained by optical pumping. The time dependent quantity Ψ is the instantaneous phase of the microwave interrogation signal, and the instantaneous angular frequency is :

$$\omega(t) = \omega_i + \dot{\Psi} \tag{20}$$

The quantity of interest to us is the population difference $a_3(t)$ merely because the transmitted light intensity changes are proportional to $a_3(t)$. We will consider the fundamental component of $a_3(t)$ in the presence of specified phase modulation waveforms. From now on, the in phase and in quadrature components of the fundamental of the cell response will be referred to the *phase* modulation waveform rather than to the *frequency* modulation waveform.

A look at equations (19) shows the following :

- i) they are coupled to a degree which depends on the microwave field amplitude b , and thus of the saturation factor S
- ii) the driving terms in their right hand sides are periodic functions of time which need to be represented by Fourier series with in general an infinite number of terms. Equations (19) then generate, in general, an infinite set of coupled equations.

Consequently, it is not tractable to derive analytical solutions for the quantity a_3 , unless simplifying assumptions are made. One of them is the weak saturation assumption which will be considered in Section 6.2. Equations (19) have also been analytically solved for arbitrary saturation, but under the assumption of fast modulation, for which the spectrum of the cell response can be limited to frequencies $-\omega_M$, 0 and $+\omega_M$. The related results will be published elsewhere.

For operating conditions prevailing in rubidium cell frequency standards, equations (19) must be solved by numerical techniques. The results are given in Section 6.3.

6.2. Analytical solution for weak saturation

As it will be shown later, operating conditions are optimized for saturation factors larger than unity. However, we wish to consider weak saturation (i.e. $S \ll 1$) at first with the purpose of pointing out that one should not rely on previously published results [1] established under this assumption.

In quantum electronics, it is usual practice to expand the quantities such as a_1 , a_2 and a_3 in increasing powers of the field amplitude, and to derive solutions for components of a given degree. However, the equations obtained are more and more intricaded as the degree of the considered component increases.

We will limit the expansion to degree two of field amplitude, i.e. to degree one of saturation factor. The validity of the results is then limited to small values of S , i.e. $S \ll 1$.

This perturbation expansion has been considered for sine-wave phase modulation, square-wave frequency modulation and square-wave phase modulation [4]. We will focus here on sine-wave phase modulation.

We define the slopes $p^{(2)}$ and $q^{(2)}$ of the error signal when the fundamental of the cell response is observed in phase or in quadrature with respect to the phase modulation waveform. The superscript means that results are valid to order two of field amplitude only. It comes :

$$\frac{1}{S} p^{(2)} = \frac{v_1}{1+v_1^2} \alpha'_1 + \frac{1}{1+v_1^2} \alpha'_2 \quad (21a)$$

$$\frac{1}{S} q^{(2)} = \frac{1}{1+v_1^2} \alpha'_1 - \frac{v_1}{1+v_1^2} \alpha'_2 \quad (21b)$$

where we have $v_1 = T_1 \omega_M$ and where the quantities α'_1 and α'_2 are given by the following equations :

$$\alpha'_1 = \frac{8}{\pi} \sum_{\ell=1}^{\infty} \frac{\ell v_2}{(1+\ell^2 v_2^2)^2} [J_{\ell+1}(m) + J_{\ell-1}(m)] J_{\ell}(m) \quad (22a)$$

$$\alpha'_2 = \frac{4}{\pi} \left\{ J_0(m) J_1(m) + \sum_{\ell=1}^{\infty} \frac{1-\ell^2 v_2^2}{(1+\ell^2 v_2^2)^2} [J_{\ell+1}(m) - J_{\ell-1}(m)] J_{\ell}(m) \right\} \quad (22b)$$

J_{ℓ} is Bessel function of order ℓ . The quantity m is the phase modulation index such as $m = \omega/\omega_M$. ℓ is an integer.

In practice relaxation times T_1 and T_2 have values which are very close together, in the considered atomic medium. In order to derive general information on the slope of the error signal, we set :

$$T_1 = T_2 = T \quad (23)$$

in equations 21 and 22.

We then have : $v_1 = v_2 = v = T\omega_M$ and $u_2 = u = T\omega_m$. The phase modulation index is $m = u/v$.

Figures 2a and b show the variations of $p^{(2)}$ and $q^{(2)}$, respectively, versus the normalized modulation frequency v for different values of the normalized modulation depth u . These sets of curves differ significantly from that given by Andres et al [1]. An examination of their derivation shows that the longitudinal relaxation was not properly accounted for. In figures 2a and b, the undulations are related to additional resonance features which occurs at frequencies $\omega_0 \pm \ell\omega_M$, in the presence of periodic phase modulation.

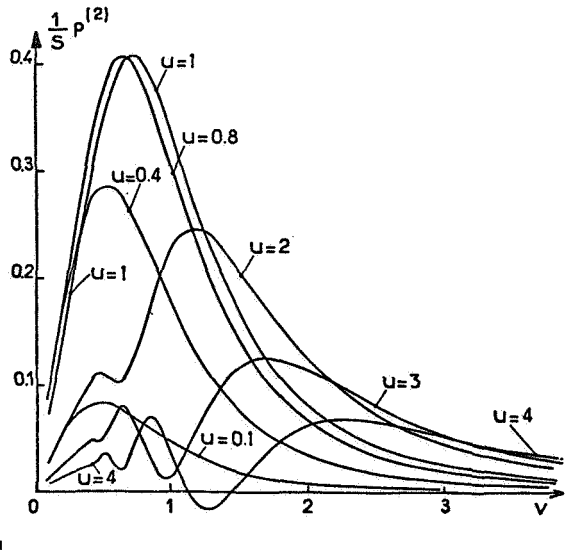


Fig. 2a

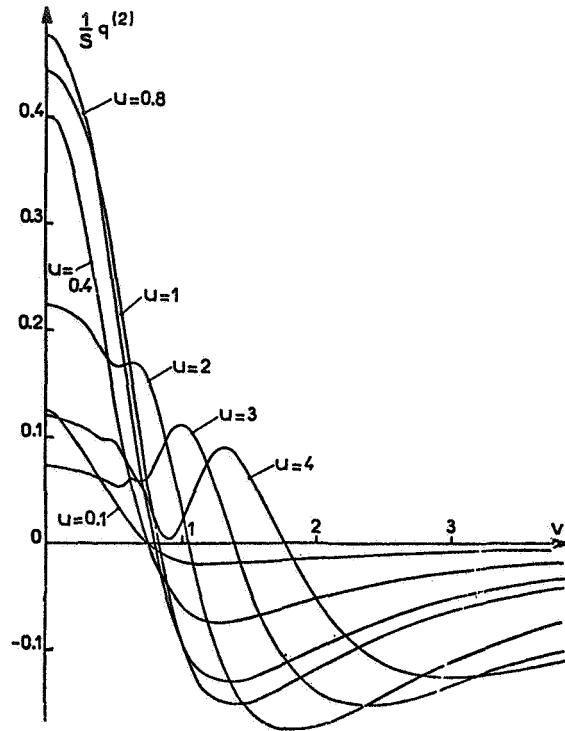


Fig. 2b

- Fig. 2. Sine-wave phase modulation and weak saturation ($S \ll 1$). The curves show the variation of the slope of the error signal versus the normalized modulation angular frequency $v = T\omega_m$ and for different values of the normalized modulation depth $u = T\omega_m$.
- the fundamental of the cell response is observed in phase with the phase modulation waveform.
 - the fundamental of the cell response is observed in quadrature with the phase modulation waveform.

6.3. Computed results for values of the modulation frequency of the modulation depth and of the saturation factor in ranges of practical interest

The set of equations (19) has been integrated numerically, assuming $T_1 = T_2 = T$ for sine-wave phase modulation, square-wave frequency modulation and square-wave phase modulation. The quantity $(\omega_i - \omega_0)$ has been fixed to a value which equals 1/10 of the half-width at half-maximum of the non-saturated resonance line (i.e. $T_2(\omega_i - \omega_0) = 0.1$). It has been checked that this offset is small enough that it allows a precise enough calculation of the slope of the error signal, and of the phase of the fundamental of the cell response, for $\omega_i = \omega_0$. Physically sound initial conditions have been chosen and the numerical integration has been performed until transient

effects vanish. The components of the fundamental of the population difference change which are in phase and in quadrature with the modulation waveform are extracted using standard techniques of Fourier coefficients computation. The values of the slopes p and q are then derived. Physically, they are obtained when the fundamental of the cell response is observed in phase or in quadrature with respect to the phase modulation waveform.

In the following we will give the values of the slope a , defined by equation (11), which is obtained when the reference signal applied to the synchronous detector is delayed in order to match its phase to that of the fundamental component of the cell response. The phase of this fundamental, relative to the phase modulation waveform is ϕ given by :

$$\tan \phi = \frac{q}{p} \quad (24)$$

Double precision computation techniques have been used to derive numerical results. Furthermore, it has been checked that the computed results agree with analytical ones, in the limits of weak saturation, or fast frequency modulation, for the three considered types of phase modulation.

6.3.1. Results for sine-wave phase modulation

Figures 3a to 3e show the computed variation of the slope a of the error signal and of the phase ϕ of the fundamental of the population difference change versus the normalized modulation depth $u = T\omega$ for different values of the saturation parameter $S = T_1 T_2 b^2$, which is proportional to the microwave power. Figures differ by the ν value of the normalized modulation frequency $\nu = T\omega_M$.

On figure 3a established for a relatively slow frequency modulation such as $\nu = 0.1$, the circles represent values calculated under the quasi-static approximation i.e. for $\nu = 0$, according to equation(18). For $\nu \approx 0$, the fundamental of the population difference change is in quadrature with the phase modulation of the interrogation microwave field. One sees that the validity of the quasi-static approximation is extremely good for $\nu = 0.1$.

Figures 3a to 3e are for increasing values of the modulation frequency. The origin of the undulations is the same as in figures 2a and 2b.

Table 1 gives, for specified values of the normalized modulation frequency ν , the values of the saturation factor S and of the normalized modulation depth u for which the slope a of the error signal is a maximum. It shows off the main result : the slope of the error signal does not depend strongly on the modulation frequency provided that the saturation factor and the modulation depth are properly increased as the modulation frequency takes larger values. For instance, for $\nu = 1.9$, i.e. for a modulation frequency almost equal to the non-saturated full-width- at half-maximum, the slope a may be made equal to its value for slow frequency modulation. It may also be noticed that the loss in the value of the slope remains small for $\nu \approx 4$.

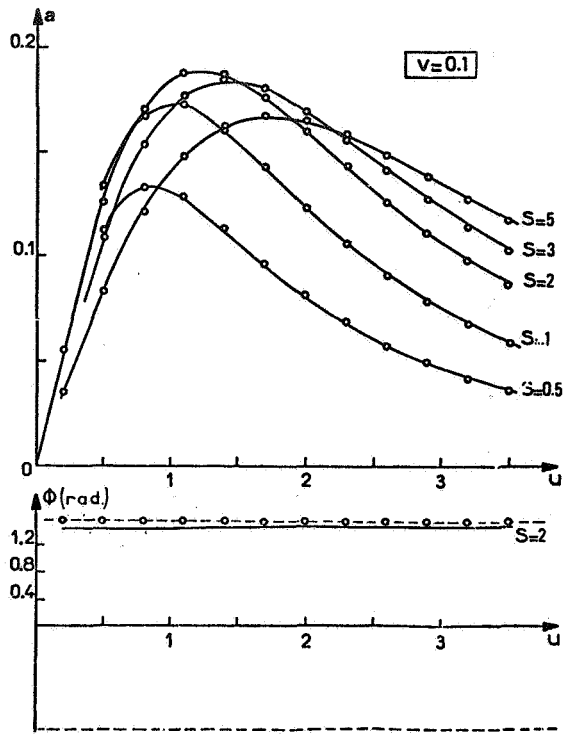


Fig. 3a

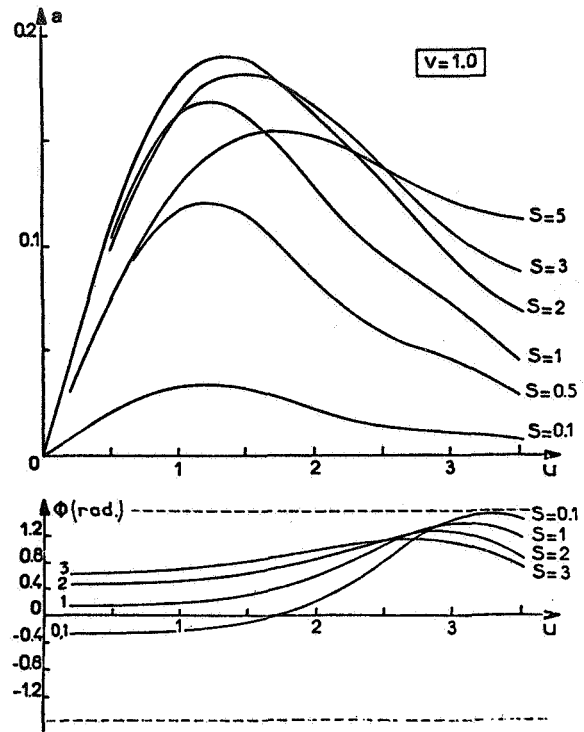


Fig. 3b

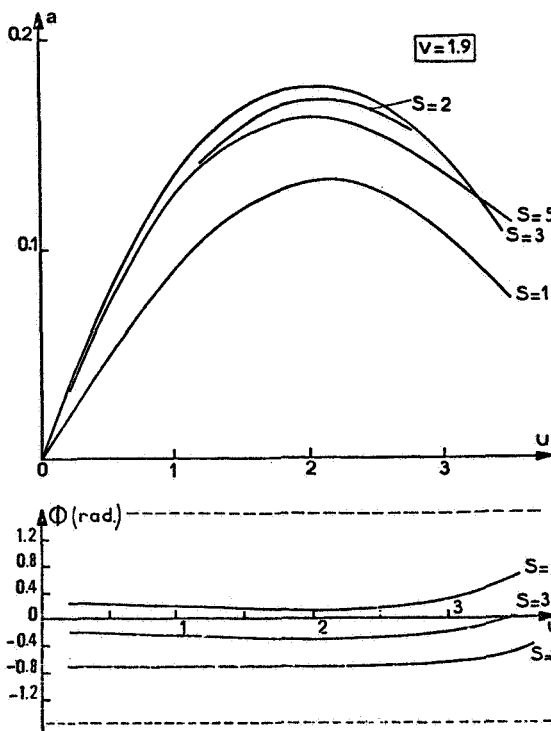


Fig. 3c

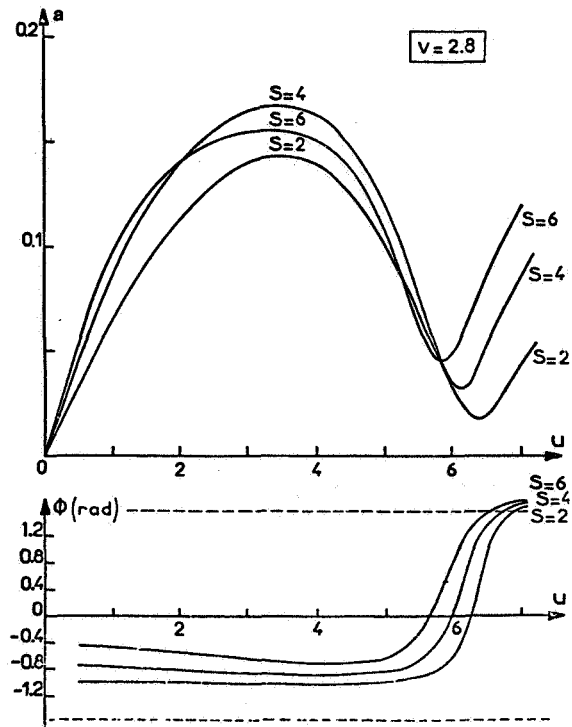


Fig. 3d

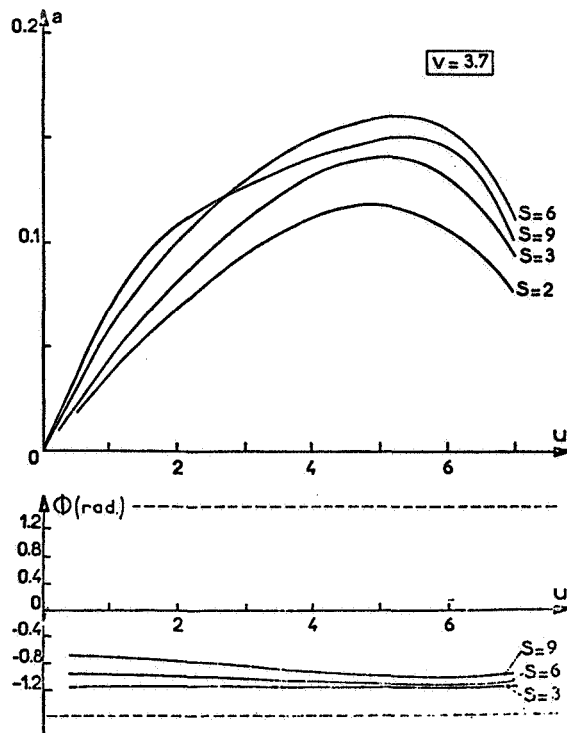


Fig. 3e

Fig. 3. Sine-wave phase modulation *computed results*. Variation of the slope of the error signal and of the phase ϕ , versus the normalized modulation depth u and for different values of the saturation factor S .

- a) $v = 0.1$. Circles represent the values calculated under the quasi static approximation, according to equation (18).
- b) $v = 1.0$
- c) $v = 1.9$
- d) $v = 2.8$
- e) $v = 3.7$

v	S	u	a	ϕ
0	2.0	1.22	0.189	1.57
0.1	2 (± 1)	1.1 (± 0.3)	0.187	1.47
1.0	2 (± 1)	1.4 (± 0.3)	0.190	0.60
1.9	3 (± 1)	2.0 (± 0.3)	0.189	- 0.30
2.8	4 (± 1)	3.5 (± 0.5)	0.166	- 0.87
3.7	6 (± 1)	5.5 (± 0.5)	0.160	- 1.10

Table 1. Sine-wave phase modulation *computed values*. For a given value of the normalized modulation frequency v , the slope a of the error signal shows a maximum for the specified values of the saturation factor S and of the normalized modulation depth u . For $v = 0$, results are derived from the quasi-static approximation. The quoted uncertainties on S and u are equal to the step of change of these parameters in the computations made. The phase ϕ is expressed in radian.

6.3.2. Results for square-wave frequency modulation

Figure 4 shows an example of the computed variation of the slope a of the error signal and of the phase ϕ of the fundamental of the population difference change versus the normalized modulation depth u , for different values of the saturation parameter S .

Table 2 gives, for specified values of the normalized modulation frequency v , the values of the saturation factor S and of the normalized modulation depth u for which the slope a of the error signal shows a maximum.

For $v = 0.1$, the computed results are closely identical to the results obtained under the quasi-static approximation, and given by equation (16). The same sort of remarks and conclusions which have been made for sine-wave phase modulation apply for square-wave frequency modulation.

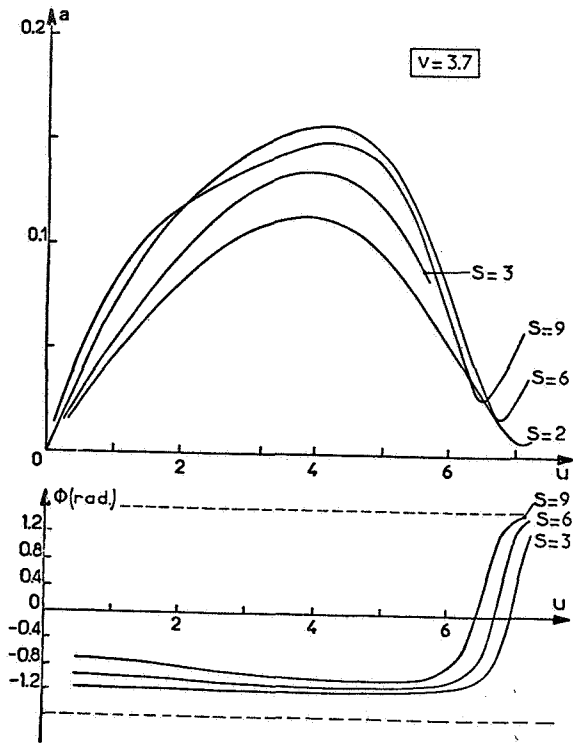


Fig. 4. Square-wave frequency modulation *computed results*. Variations of the slope a of the error signal and of the phase ϕ , for $v = 3.7$, versus the normalized modulation depth u and for different values of the saturation factor S .

v	S	u	a	ϕ
0	2.0	1.0	0.203	1.57
0.1	2 (± 1)	1.1 (± 0.3)	0.201	1.47
1.0	2 (± 1)	1.1 (± 0.3)	0.197	0.59
1.9	3 (± 1)	1.7 (± 0.3)	0.178	- 0.30
2.8	4 (± 1)	2.5 (± 0.5)	0.163	- 0.85
3.7	6 (± 1)	4.0 (± 0.5)	0.157	- 1.09

Table 2. Square-wave frequency modulation *computed values*. For a given value of the normalized modulation frequency v , the slope a of the error signal shows a maximum for the specified values of the saturation factor S and of the normalized modulation depth u . For $v = 0$, results are derived from the quasi-static approximation. The quoted uncertainties on S and u are equal to the step of change of these parameters in the computations made. The phase ϕ is expressed in radian.

6.3.3. Results for square-wave phase modulation

For square-wave phase modulation, the atomic medium response is entirely founded on transient effects which occur after phase jumps. In that case, the quasi-static approximation is then meaningless, because the first harmonic content of the cell response vanishes for $\nu \approx 0$. Intuitively, one might think that the cell response is significant when the modulation frequency is of the order of the atomic line-width. This is verified, in order of magnitude, by quantitative results.

Figures 5a to 5d show the computed variations of the slope a of the error signal and of the phase ϕ of the fundamental of the population difference change versus the amplitude of the phase deviation φ_m , for different values of the saturation parameter S (it should be noticed that the phase steps amount to $2\varphi_m$). Figures differ by the value of the normalized modulation frequency ν .

Table 3 summarizes the important results. It gives for the specified values of the normalized modulation frequency ν , the values of the saturation factor and of the amplitude of the phase change φ_m for which the slope a of the error signal shows a maximum. The optimum value of φ_m is close to $\pi/4$. This slope decreases only very slightly from $\nu = 1.9$ to 3.7 , in the explored range, when the saturation factor S and the phase change φ_m are adjusted to their increasing optimum values.

ν	S	φ_m	a	ϕ
1.0	2 (± 1)	0.8 (± 0.1)	0.148	0.44
1.9	3 (± 1)	0.8 (± 0.1)	0.171	- 0.42
2.8	4 (± 1)	1.0 (± 0.1)	0.170	- 0.97
3.7	7 (± 1)	1.1 (± 0.1)	0.169	- 1.15

Table 3. Square-wave phase modulation *computed values*. For a given value of the normalized modulation frequency ν , the slope a of the error signal shows a maximum for the specified values of the saturation factor S and of the amplitude of phase deviation φ_m . The quoted uncertainties on the values of these parameters are equal to their step of change in the computations made. The phases φ_m and ϕ are expressed in radian.

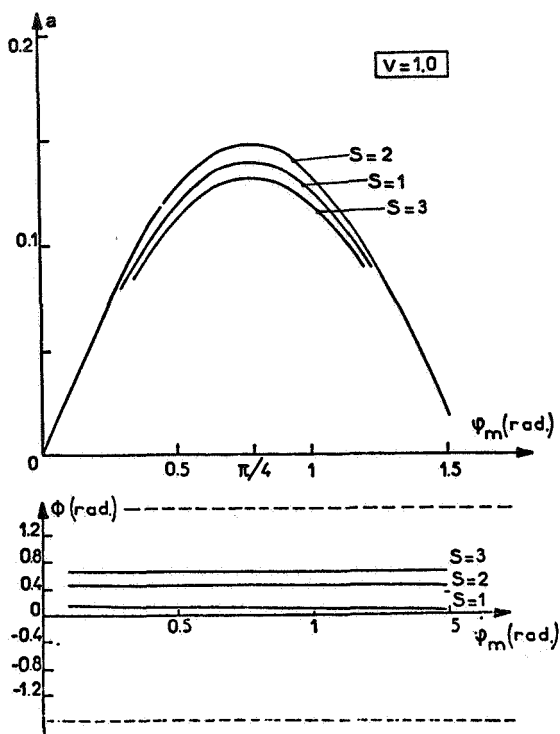


Fig. 5a

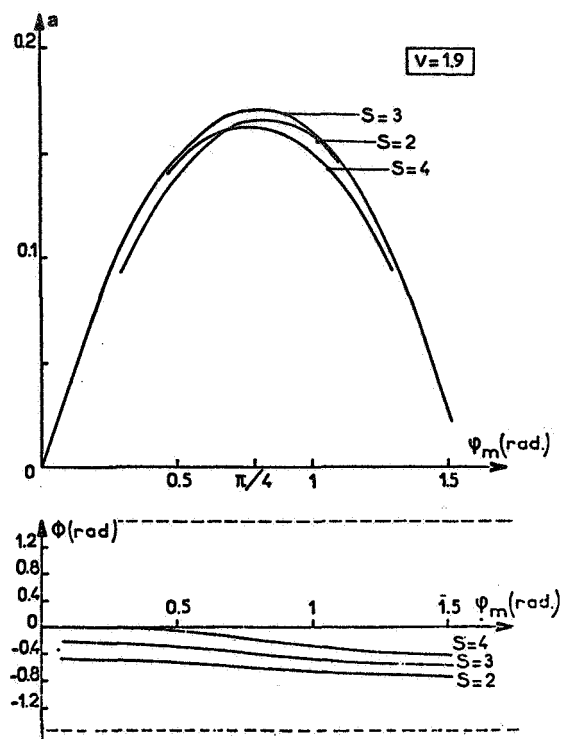


Fig. 5b

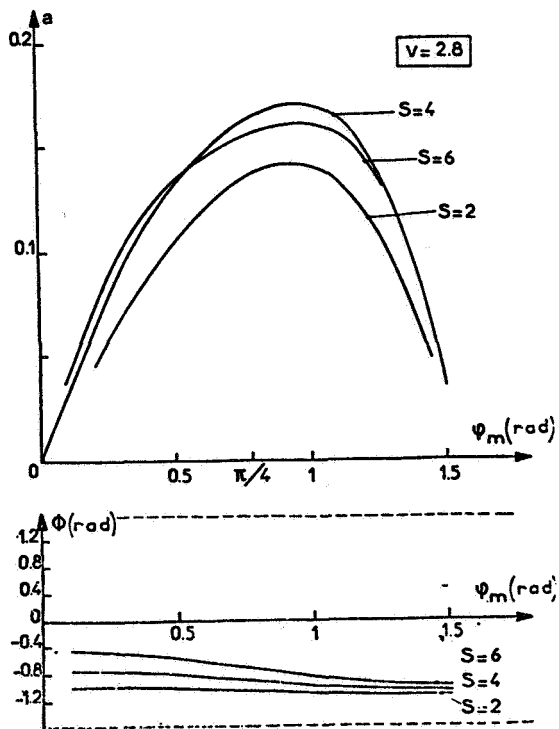


Fig. 5c

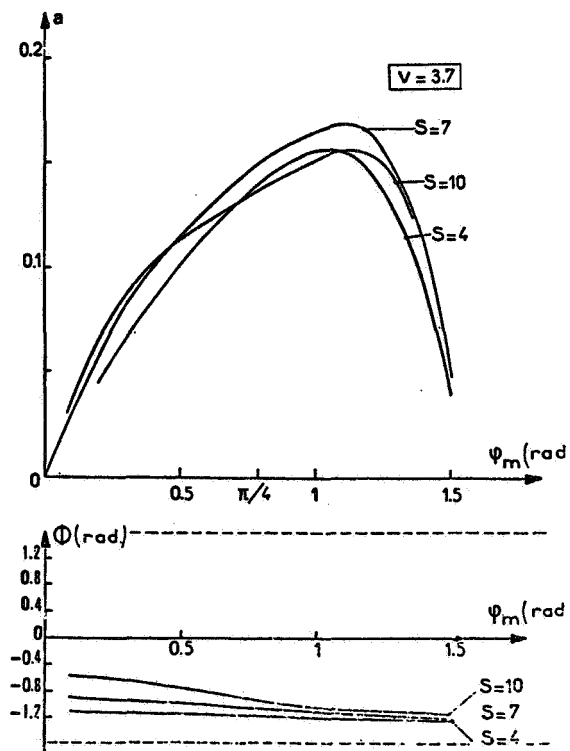


Fig. 5d

Fig. 5. Square-wave phase modulation *computed results*.
 Variation of the slope a of the error signal and
 of the phase ϕ , versus the amplitude of the phase
 change ψ_m and for different values of the satura-
 tion factor S .
 a) $v = 1.0$
 b) $v = 1.9$
 c) $v = 2.8$
 d) $v = 3.7$

7. EXPERIMENTAL RESULTS

Experimental results have been obtained with a set-up having a widely used⁸⁷ configuration. An isotopic filter, with 80 Torrs of argon is used. The Rb cell containing 20 Torrs of nitrogen is operated at 60° C. It fills almost entirely a cylindrical microwave cavity operated in the TE₁₁₁ mode. In this experimental arrangement, optical pumping and relaxation are not homogeneous in the cell. In addition the microwave magnetic field amplitude shows large variations over the cell volume. The experimental results can then be used to check the ability of our model to predict the influence of the modulation frequency on a practical device.

An average saturation factor S' is defined from the dip of the transmitted light at microwave resonance. We have, from equation (8) :

$$S' = - I_l / (I_0 + I_l) \quad (25)$$

The value of the transverse relaxation time T_2 is measured by extrapolating the atomic line-width to zero microwave power.² It is found that the full-width at half maximum W varies as follows :

$$W^2 = W_0^2 (1 + \alpha S') \quad (26)$$

where $W_0 = 2/T_2$ is the non-saturated linewidth. Experimentally, one has $\alpha = 5.2^0$ and

$$T_2 = 1.77 \pm 0.18 \text{ ms}$$

It can be shown that the value of α depends on the microwave field configuration, the light intensity, the length of the cell, the temperature and also on the area of the photo cell exposed to the transmitted light.

The value of the longitudinal relaxation time is measured by observing the exponential variation of the transmitted light intensity after the microwave power has been switched off. We have

$$T_1 = 1.82 \pm 0.04 \text{ ms}$$

Thus it turns out that the condition $T_1 = T_2$ which has been assumed in Section 6.3. is fulfilled quite satisfactorily.²

The slope of the error signal is measured as follows. A quartz crystal oscillator is frequency locked to the rubidium cell, but with a voltage added to the synchronous detector output. The frequency of the quartz crystal oscillator is measured for two opposite values of the voltage, and the normalized slope of the error signal is obtained. It has been checked that the offset of the interrogation frequency from the resonance frequency remained smaller than 1/10 of the full-width at half-maximum. The phase of the fundamental component of the light intensity changes shows an extremum for $\omega_i = \omega_0$, so that its measurement was precise enough with the stated experimental procedure.

Sine-wave phase modulation, square-wave frequency modulation and square-wave phase modulation have been applied to the microwave signal.

Figures 6a to 6d show the results for sine-wave phase modulation. The value of the measured slope is smaller than the value calculated from the model, and the optimum occurs for smaller values of the saturation factor (for $v = 0.1$ the optimum value of S' is 1.3). However, for a given value of v , the shape of the computed and of the measured variations is quite similar. Table 4 summarizes the experimental results. It shows that the optimum value of a does not depend drastically on the value of the modulation frequency.

v	S'	u	$a \times 10^2$	ϕ
0.11	$1(\pm 0.5)$	1.3 ± 0.1	9.3	1.48
1	$1(\pm 0.5)$	1.5 ± 0.15	8.6	0.58
2.9	$1.5(\pm 0.5)$	3.5 ± 0.25	5.6	- 0.51
3.7	$2(\pm 0.5)$	4.2 ± 0.25	5.1	- 0.72

Table 4. Sine-wave modulation. *Experimental values.* For a given value of the normalized modulation frequency v , the slope a of the error signal shows a maximum for the specified values of the saturation factor S' and of the normalized modulation depth u . The quoted uncertainties on S' and u are equal to the step of change of these parameters in the measurements made. The phase ϕ is expressed in radian.

Figure 7 shows an example of measured results for square-wave frequency modulation with $v = 3.7$ and Table 5 gives the main results, with the same general conclusions as for sine-wave phase modulation.

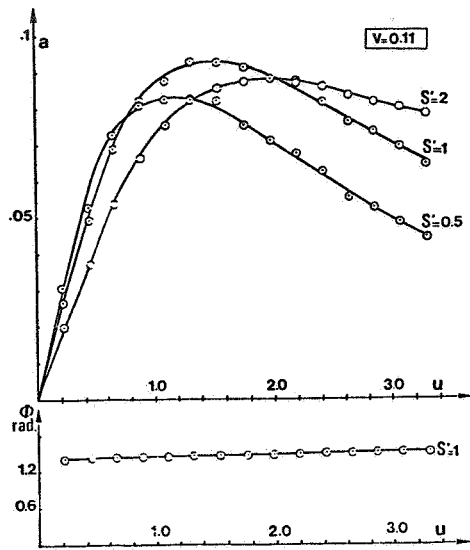


Fig. 6a

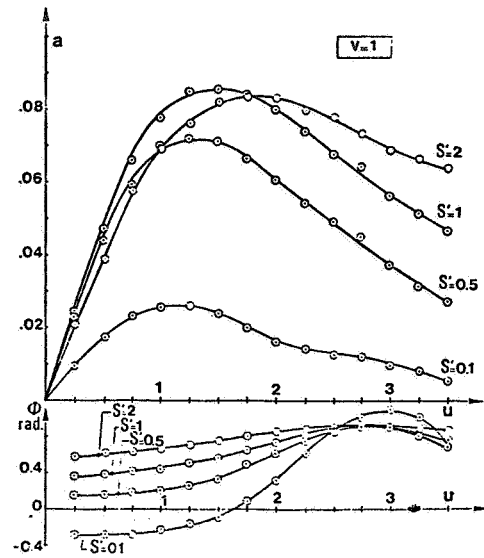


Fig. 6b

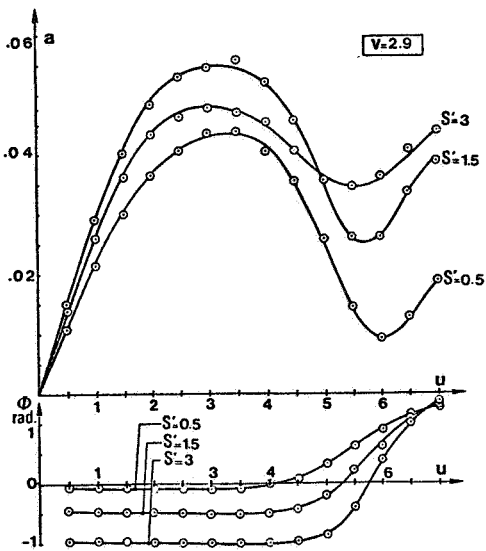


Fig. 6c

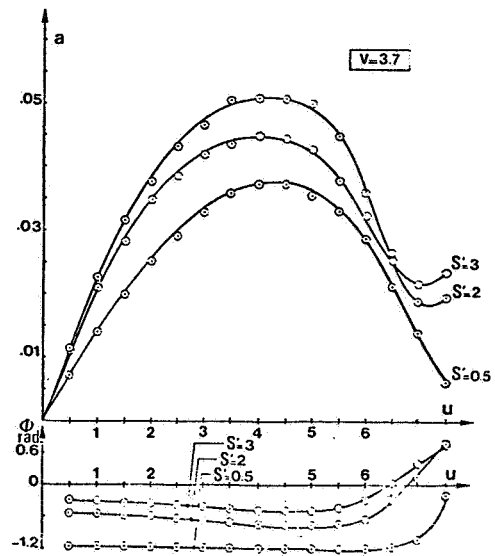


Fig. 6d

Fig. 6. Sine-wave phase modulation. *Experimental results.*
 Variation of the slope a of the error signal and of the phase ϕ , versus the normalized modulation depth u and for different values of the saturation factor S' . Circles represent the experimental points.
 a) $v = 0.11$ b) $v = 1.0$
 c) $v = 2.9$ d) $v = 3.7$

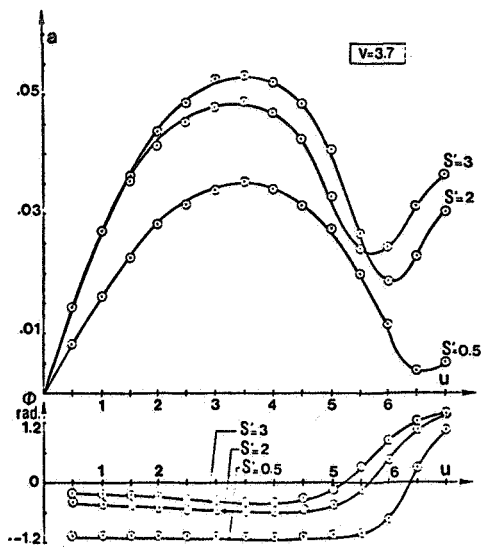


Fig. 7. Square-wave frequency modulation. *Experimental results.* Variation of the slope a of the error signal and of the phase ϕ , for $\nu = 3.7$, versus the normalized modulation depth u and for different values of the saturation factor S' . Circles represent the experimental points.

ν	S'	u	$a \times 10^2$	ϕ
0.2	1 (+0.5)	1.1 \pm 0.15	10.0	1.52
1	1 (+0.5)	1.25 \pm 0.15	8.6	0.79
2.9	1.5(+0.5)	2.5 \pm 0.25	5.9	- 0.38
3.7	2 (+0.5)	3.5 \pm 0.25	5.3	- 0.60

Table 5. Square-wave frequency modulation. *Experimental values.* For a given value of the normalized modulation frequency ν , the slope a of the error signal shows a maximum for the specified values of the saturation factor S' and of the normalized modulation depth u . The quoted uncertainties on S' and u are equal to the step of change of these parameters in the measurements made. The phase ϕ is expressed in radian.

Figures 8a to 8c show the variation of the normalized slope a in the case of square-wave phase modulation as a function of the amplitude of the phase deviation φ_m for different values of the saturation factor S' and of the normalized modulation frequency ν . Again, the shapes agree quite satisfactorily, but with smaller values of a and S' . Table 6 shows that the optimum values of φ_m agree closely with the computed ones.

Comparison of Tables 4 to 6 shows that square-wave phase modulation yields an optimum value of the slope a which is even larger than with the two other types of modulation for $\nu \approx 4$.

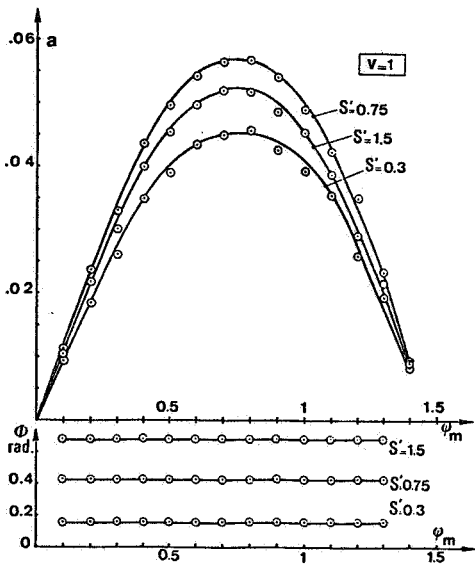


Fig. 8a

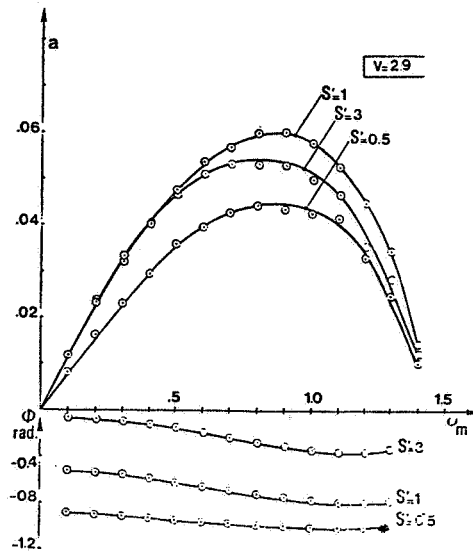


Fig. 8b

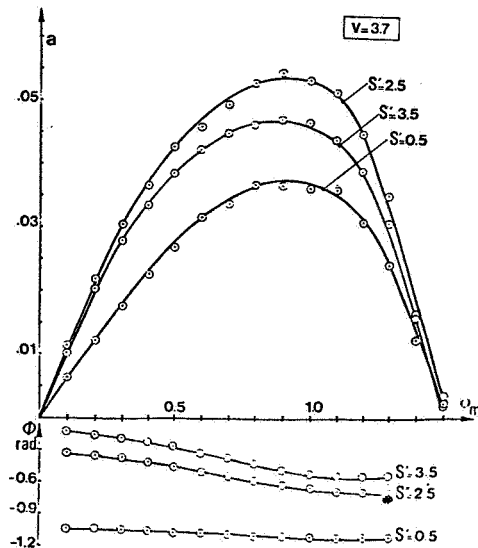


Fig. 8c

Fig. 8. Square-wave phase modulation. Experimental results. Variation of the slope a of the error signal and of the phase ϕ , versus the normalized modulation depth u and for different values of the saturation factor S' . Circles represent the experimental points.

- a) $\nu = 1.0$
- b) $\nu = 2.9$
- c) $\nu = 3.7$

ν	S'	φ_m	$a \times 10^2$	ϕ
1	0.75 (± 0.5)	0.8 ± 0.5	5.7	0.44
2.9	1 (± 0.5)	0.9 ± 0.5	6.0	- 0.75
3.7	2.5 (± 0.5)	0.95 ± 0.5	5.5	- 0.63

TABLE 6. Square-wave phase modulation. *Experimental values.* For a given value of the normalized modulation frequency ν , the slope a of the error signal shows a maximum for the specified values of the saturation factor S' and of the amplitude of phase deviation φ_m . The quoted uncertainty on the values of these parameters are equal to their step of change in the computations made. The phases φ_m and ϕ are expressed in radian.

8. CONCLUSIONS

Our theoretical analysis has been made with the assumption that optical pumping, relaxation and the r.f. field are homogeneous over the rubidium cell. Our experimental data has been obtained with a rubidium cell in a TE_{111} cavity and those conditions are not satisfied. However, these results agree satisfactorily with the theoretical predictions. Consequently, we may conclude the following :

i) for sine-wave phase modulation and square-wave frequency modulation, the results of the quasi-static approximation can be used up to $\nu \approx 1$, as far as the slope a of the error signal is concerned. It yields a satisfactory estimate of the values of the saturation factor and of the normalized modulation depth for which this slope is maximum.

ii) for sine-wave phase modulation and for square-wave frequency modulation, the slope a of the error signal decreases only slightly if the modulation frequency is increased up to a value such as $\nu \approx 4$, provided that the saturation factor and the modulation depth are adjusted to increasing optimum values specified in Tables 1 and 2. One sees that when the modulation frequency increases, the line must be power broadened in order that the linewidth tends to follow the value of the modulation frequency. Similarly, the frequency excursion around the interrogation frequency has to be increased.

iii) for square-wave phase modulation, the optimum modulation frequency is such as $\nu \approx 2$ and the slope a falls off very slightly for $\nu > 2$ when the values of the saturation factor and of the amplitude of the periodic phase change are adjusted to the values given in Tables 3 or 6.

iv) for large modulation frequency such as $\nu \approx 4$, the slope a becomes a little larger for square-wave phase modulation than for the two other sorts of modulation which have been considered. Square-wave phase modulation might then be the best modulation method in applications where fast

frequency modulation is required. In addition, it has other known specific advantages such as ease of implementation and excellent immunity to non-linear distortion of the phase modulator.

REFERENCES

- [1] J.M. Andres, D.J. Farmer and G.T. Inouye, IRE Trans. on Military Electronics 3 (1959) p. 178-183
- [2] R.P. Kenschaft, Ph. D. (1970)University of Pennsylvania
- [3] G. Missout and J. Vanier, Canadian Journal of Physics 53 (1975) p. 1030-1043
- [4] P. Thomann and G. Busca, Journal de Physique. Supplément au n° 12. Colloque C8 (1981) p. C8-189 - C8-197
- [5] R. Arndt, Journal of Applied Physics 36 (1965) p. 2522-2524
- [6] A. Abragam, Principles of Nuclear Magnetism, Clarendon Press (1962)

QUESTIONS AND ANSWERS

(Signals inadequate for transcription for Paper #4.)

LASER INDUCED ASYMMETRY AND INHOMOGENEOUS BROADENING
OF THE MICROWAVE LINESHAPE OF A GAS CELL
ATOMIC FREQUENCY STANDARD

J.C. Camparo, R.P. Frueholz and C.H. Volk
Chemistry and Physics Laboratory
The Aerospace Corporation
P.O. Box 92957, Los Angeles, CA 90009

ABSTRACT

Recently, there has been interest in the possibility of replacing the rf discharge lamp in a rubidium gas cell clock with a single mode laser diode. Since the short term stability of the rubidium frequency standard is limited by the shot noise of the photodetector, an increased signal-to-noise ratio due to more efficient laser diode optical pumping might improve the short term performance. Because the emission wavelength of the laser diode can be tuned, improved long term performance could be gained through the control of the light shift effect. However, due to the nature of the gas cell frequency standard, various physical phenomena are strongly coupled in their effect on the frequency output, and thus careful consideration must be given to any change in one parameter because of its interrelation with other parameters. We report here some investigations concerning the coupled effect of the optical and microwave fields in the rubidium atomic clock. We show that this type of coupling is an important consideration for any attempt to incorporate a laser diode into a gas cell clock.

INTRODUCTION

Laser diodes have been proposed for use in atomic frequency standards because of the potential for improved clock performance.¹⁻⁶ In particular, in the gas cell frequency standard, the use of a laser diode in place of the conventional rf discharge lamp should increase the signal-to-noise ratio and thus produce better short term stability, while drastically reducing the detrimental effects due to the light shift.^{1,3,4} These projections of laser pumped clock performance must be tempered by the possibility of new effects that could arise due to the intense optical pumping provided by lasers. We report here our investigations into laser induced asymmetries and broadening of the rubidium microwave lineshape. These effects are important both in determining and understanding the optimum conditions for laser optical pumping.

A schematic diagram of a typical gas cell clock is shown in Figure 1. Some of the more important elements in the physics package of this device include: i). the source of optical pumping radiation; ii). the light filter; iii). the absorption cell; iv). the microwave cavity; and, v). the externally applied axial magnetic field.

Traditionally, an rf discharge lamp has been used as the optical pumping source. The limitations in these lamps include: stability,⁷ reliability,^{7,8} tunability and limited light intensity due to size constraints. Additionally, light from a discharge lamp must be filtered to achieve optimum optical pumping, and this filtering necessitates either a separate filter cell,⁹ mixed isotopes in the absorption cell,¹⁰ a lamp filter combination,¹¹ or magnetic tuning.¹² Conversely, a laser diode can provide an intense tunable light beam which, because of its narrow spectral linewidth, would eliminate the need for light filtering. Also, the tunable nature of the laser diode would allow for the possibility of either eliminating or controlling light induced frequency shifts that arise from a spectral offset between the pumping radiation and the absorption lines.

The microwave lineshape, which controls the clock's performance, has complex dependencies on various physical phenomena that occur in the absorption cell. The optical pumping radiation, the buffer gas, the microwave power and distribution in the cavity, the magnetic field and the thermal environment all affect the size and the shape of the microwave line. As a result of the inhomogeneous nature of the microwave line, the effects of various parameters on the clock performance are coupled.¹³ Thus, a change in one parameter, e.g. the pumping light intensity, designed to improve performance could result in degraded performance due to an incomplete understanding of the way these parameters affect the microwave lineshape and center frequency. In this present study we consider the coupled effect of the optical and microwave fields on the incorporation of a laser diode in a gas cell frequency standard.

EXPERIMENTAL

The experimental apparatus is shown schematically in Figure 2. The absorption cell of an Efratom FRK-L rubidium frequency standard¹⁴ is illuminated by the emission from a single mode diode laser, Mitsubishi ML-4001, which is tuned to one of the ⁸⁷Rb D₁ hyperfine resonance lines (794.7 nm). We measure the lineshape by ramping the frequency of a VCXO through the hyperfine resonance and monitoring the light transmitted through the absorption cell. The VCXO is linear and carefully calibrated which allows us to convert VCXO voltage directly to frequency. The microwave field is chopped with a diode switch at a few Hz, and a lock-in amplifier is used to enhance signal-to-noise on each sweep. Typically, sixteen repetitive scans, taking about two minutes each, are averaged with the aid of an HP 9825 computer. We estimate about 5 Hz accuracy in the lineshapes with this method.

We do not have a direct measure of the strength of the microwave field in the cavity. Multiplication up to the microwave frequency from the nominal VCXO frequency is accomplished using a 'step-recovery' diode. Ideally, the microwave power in the Nth harmonic is expected to be:¹⁵

$$P_N = P_0/N \quad (1)$$

where P_0 is the input power to the step-recovery diode. However, the coupling coefficients between the diode and the cavity antenna, and the cavity antenna

and the cavity, will modify Eq. (1). We believe that a reasonable estimate of the microwave power in the cavity is on the order of $10 \mu\text{W}$.

The spectral linewidth of the ML 4001 diode laser, measured with a Fabry-Perot interferometer, was found to be about 100 MHz. The laser's wavelength could be tuned to either of the Doppler broadened hyperfine absorption lines, $\Delta\nu_D \sim 500$ MHz, by varying either the diode temperature or injection current. The diode laser is heat sunk into a copper block whose temperature is stabilized and controlled by a thermistor in one leg of a bridge circuit, which controls the current through a solid-state thermoelectric device. In this manner, the diode laser's center frequency can be held to less than 100 MHz of the center of the hyperfine absorption line for about 30 minutes without active stabilization of the laser diode.

Typically, the laser is tuned by first adjusting the temperature so that the lasing wavelength is near the Rb D_1 line at 794.7 nm. The injection current is then used as a fine control to tune the laser over the hyperfine absorption spectrum, and as long as lasing mode hops do not occur, the injection current can be calibrated to the lasing frequency. This is found to be approximately 16 GHz/mA. Since the laser's single mode output power is a function of the injection current, the laser power will vary as the laser is tuned. However, the fractional change in power is found to be only about 1% as the laser is tuned over several GHz, and thus the variations in laser power are neglected for these measurements. The typical total laser power in the single mode line is found to be about 3 mW in a Gaussian beam diameter of ~ 0.45 cm.

RESULTS

In Figure 3 we present representative samples of our microwave lineshape measurements. The upper lineshapes correspond to low incident laser intensity, $\sim 0.5 \text{ mW/cm}^2$, for several different detunings of the laser frequency. From left to right these are -420 MHz, 0 and +420 MHz. The lower curves were observed with full laser intensity, $\sim 10 \text{ mW/cm}^2$. The frequency axis indicates the total scan of the microwaves from some arbitrary start frequency, and $\Delta\nu_{\text{hfs}}$ denotes the shift of the center frequency of the microwave line from that found for zero laser detuning, shown in both the upper and lower center scans. From the figure it is apparent that for higher laser intensities the microwave lineshape is asymmetric when the laser is tuned off resonance, and that this asymmetry has the same sign as the light shift. Furthermore, this asymmetry is correlated to the recently observed non-linearity of the clock's light shift.¹⁶ In Figure 4 we have plotted the microwave frequencies corresponding to a lineshape's peak and first moment as a function of laser intensity (the laser detuning was ~ -400 MHz). The difference between these two frequencies can be considered as a measure of the asymmetry of the line. It should be noted that the asymmetry and non-linearity become significant for the same light intensity levels. This is more than coincidental; it is the result of both effects being due to light induced inhomogeneous broadening, and in this type of broadening the light intensity and microwave field strength act together to produce the shape and center frequency of the observed resonance line.

DISCUSSION

We have recently developed a lineshape model for the gas cell clock which describes optical pumping with a spectrally narrow, low intensity laser source (i.e. low with respect to the intensity necessary to saturate the optical transition).¹⁶ Since the typical gas cell clock uses a buffer gas in the absorption cell, we consider the atoms in our model as being essentially frozen in place due to the presence of this buffer. Atoms in different regions of the cell experience different local light intensities and different local microwave field strengths. The observed lineshape, and thus the shape that controls clock performance, is a superposition of regional transmission signals which are determined by the local parameters. The local light intensity and magnetic field strength determine the local resonance frequency through the light shift effect and second order magnetic field dependence, respectively; the combined effect of the local light intensity and the local Rabi frequency, determined by the microwave field strength, determines the amplitude of the regional transmission signal. In Figure 5 we present the calculated microwave lineshape in a TE₁₁₁ cavity for both low and high laser intensity, off-resonance pumping. In Figure 6 we show the calculated inhomogeneous light shift for several values of laser detuning. The close agreement between the theoretical model and our experimental results demonstrates the significance of light induced inhomogeneous broadening on the clock signal.

In practice the calculation of the clock lineshape is performed numerically by summing all the regional transmission signals as a function of microwave frequency. Though this is an accurate and straightforward procedure for obtaining the lineshape, it does not readily lend itself to an intuitive understanding of the relationships among the parameters in the problem. In this context we therefore consider the effect of the local parameters on the homogeneous lineshape.

It is quite easy to show that the amplitude of a regional transmission signal can be written approximately as:

$$S = I_{\text{trans}}(\Delta\omega=\infty) - I_{\text{trans}}(\Delta\omega=0) \sim \frac{\Gamma/2}{\Gamma+\gamma} \left[\frac{\omega_1^2}{(\Gamma + \gamma)^2 + \omega_1^2} \right] \quad (2)$$

where some constants have been omitted for clarity.¹⁷ In the above

- I_{trans} = the transmitted light intensity,
- $\Delta\omega$ = microwave frequency detuning from the hyperfine resonance,
- Γ = optical pumping rate,
- γ = relaxation rate (we assume the longitudinal rate is equal to the transverse rate), and
- ω_1 = microwave Rabi frequency.

The regional behavior of S is reflected in the fact that both Γ and ω_1 have spatial dependencies.

It is important to realize that the complexity of the problem in obtaining the total transmitted intensity is not due to the form of Eq. (2), but to the fact

that the pumping rate, and hence the light shift, in the n^{th} region of the cell depends on the transmission from the $n-1$ previous regions:

$$S_n(r, \theta) = f(S_1(r, \theta), S_2(r, \theta), \dots, S_{n-1}(r, \theta)) \quad (3)$$

However, we can gain qualitative information on the processes that determine the total transmission signal by considering the regional transmission signals at a particular axial position.

In Figure 7 we have plotted the regional transmission signal S as a function of (Γ/ω_1) for several different values of (γ/ω_1) . If we consider for example the case where $\gamma = 0.1\omega_1$, we see that the maximum transmission signal will occur for $\Gamma \sim 0.4\omega_1$, (i.e. not for arbitrarily large Γ). This implies that an increased pumping rate does not immediately guarantee larger signal amplitude and thus improved signal-to-noise. Rather, it is the ratio of Γ to ω_1 that is the important parameter. Furthermore, since the peak of the inhomogeneous lineshape corresponds to the largest amplitude homogeneous lineshape, and since this in turn is a function of both Γ and ω_1 , it follows that the inhomogeneous light shift is a function of Γ and ω_1 .

Let's now consider the radial dependence of Γ and ω_1 explicitly; we assume a Gaussian laser beam, and a TE_{111} microwave cavity:

$$I(r) = I_p \exp(-4 \ln^2(r/a)^2), \quad (4a)$$

$$\Gamma(r) = \Gamma_p \exp(-4 \ln^2(r/a)^2), \quad (4b)$$

$$\omega_1(r) = \omega_{1p} \lambda J_1(1.841(r/R)), \quad (4c)$$

where I is the light intensity, r is the radial position in the cell, a is the laser beam diameter, R is the cavity radius, λ is a normalizing factor and all quantities are related to their peak values, denoted by the subscript p . Substituting these expressions into Eq. (2), we have plotted the normalized transmission signal amplitude as a function of radial position within the cavity in Figure 8. The three different curves correspond to three different values of (Γ/ω_{1p}) assuming that $\gamma = 0.1\omega_{1p}$ and $(R/a)=2$. As we would have expected from Figure 7 if we consider Γ_p as fixed, then as ω_{1p} varies the radial position giving the maximum signal amplitude changes. Since these radial positions correspond to different light intensity levels, we have the so called position shift effect.¹³ Thus, the position shift effect is just one consequence of the coupled effect of Γ and ω_1 when light induced inhomogeneous broadening determines the clock lineshape.

It should now be understood that it is both Γ and ω_1 that determine the asymmetry observed in the present experiments. The distribution in Γ determines the distribution of homogeneous lineshapes; the ratio of Γ to ω_1 determines the envelope. It should be noted that even though no asymmetry was observed for on-resonance pumping, an asymmetry may be present due to the hyperfine splitting in the excited state of ^{87}Rb . Since the excited state hyperfine splitting is on the order of the Doppler linewidth, the absorption lines partially overlap and off-resonance pumping to some degree is unavoidable.

Operating on-resonance, moreover, increases the slope of the light shift forcing tighter constraints on the frequency control of the laser diode.³

SUMMARY AND CONCLUSIONS

We have observed a gross asymmetry in the microwave lineshape of a gas cell clock when pumping off resonance with a laser diode. This asymmetry, along with the non-linearity of the clock's light shift and the position shift effect, can be explained by a model based on light induced inhomogeneous broadening of the hyperfine transition.

In this model the light intensity and microwave field strength cannot be regarded as acting independently in their effect on the observed lineshape. Thus, the anticipated changes in clock performance on changing either of these parameters must be tempered by an appraisal of their combined effect. The significance of the asymmetry on actual clock performance, and the constraints it will place on laser optical pumping schemes is still unclear. However, its observation and interpretation lead to some rather important considerations. Since the inhomogeneous microwave lineshape has a center frequency and amplitude which depend both on the light intensity and microwave field strength, this could imply that many of the advantages of laser diode pumping may not be fully realized with the standard clock design. If this is the case, it might be advantageous to design a laser diode pumped clock with a bufferless wall coated cell, most likely a cesium cell in a TE_{011} cavity,¹⁸ which would have a homogeneous microwave line. However, with a bufferless cell one would have the additional complication of radiation trapping. Finally, since light induced inhomogeneous broadening is so significant in laser diode pumping, and since there is reason to believe that it is also important for the standard lamp pumping;¹³ it may be possible to extrapolate results from these laser diode studies to the regime of the lamp, and thus gain a better understanding of the mechanisms which limit the standard gas cell clock's performance.

REFERENCES

1. F.L. Walls, "Prospects for Advances in Microwave Atomic Frequency Standards," Proceedings of the 11th Annual Precise Time and Time Interval Applications and Planning Meeting; Greenbelt, Maryland; p. 619 (1979).
2. M. Arditi and J.L. Picque, "A Cesium Beam Atomic Clock Using Laser Optical Pumping. Preliminary Tests." J. de Phys. Lett. 41, L370 (1980).
3. L.L. Lewis and M. Feldman, "Optical Pumping by Lasers in Atomic Frequency Standards," Proceedings, 35th Annual Symposium on Frequency Control, US Army Electronics Command, Ft. Monmouth, N.J. pp. 612-624, (1981).
4. C.H. Volk, J.C. Camparo and R.P. Frueholz, "Investigations of Laser Pumped Gas Cell Atomic Frequency Standard," Proceedings of the 13th Annual Precise Time and Time Interval Applications and Planning Meeting; Greenbelt, Maryland; p. 631 (1981).
5. M. Arditi, "Microwave Ramsey Pattern in a Laser Pumped Cesium Beam, Application to Velocity Distribution and 2nd Order Doppler-Shift in Frequency Standard," J. de Phys. Colloque C-8, 42, 261 (1981).
6. L.L. Lewis, M. Feldman and J.C. Berquist, "Impact of Lasers on Primary Frequency Standards and Precision Spectroscopy," J. de Phys. Colloque C-8, 42, 271 (1981).
7. H. Oyamada, K. Takahashi, Y. Sato and H. Uchida, "A Consideration of Rubidium Lamp Stability for Rubidium Frequency Standard," Proceedings 28th Annual Frequency Control Symposium, US Army Electronics Command, Ft. Monmouth, N.J. pp. 340-343 (1974).
8. R.P. Frueholz, M. Wun-Fogle, H.U. Eckert, C.H. Volk and P.F. Jones, "Lamp Reliability Studies for Improved Satellite Rubidium Frequency Standard," Proceedings of the 13th Annual Precise Time and Time Interval Applications and Planning Meeting; Greenbelt, Maryland (1981).
9. M.E. Packard and B.E. Swartz, "The Optically Pumped Rubidium Vapor Frequency Standard," IRE Trans. on Instr. I-22, 215 (1962).
10. E. Jechart, "Miniature Rubidium Gas Cell Frequency Standard," Proceedings, 27th Annual Symposium on Frequency Control, US Army Electronics Command, Ft. Monmouth, N.J., p. 387 (1973).
11. N. Kuramochi, S. Naritsuka and N. Oura, "Composite-Type ^{87}Rb Optical-Pumping Light Source," Opt. Lett. 6, 73 (1981).
12. G. Rovera, A. De Marchi and J. Vanier, "The Optically Pumped Passive Cesium Frequency Standard: Basic Theory and Experimental Results on Buffer Gas Frequency Shifts," IEEE Trans. Instr. and Meas. IM-25, 203 (1976).

13. A. Risley and G. Busca, "Effect of Line Inhomogeneity on the Frequency of Passive Rb⁸⁷ Frequency Standards," Proceedings, 32nd Annual Symposium on Frequency Control, US Army Electronics Command, Ft. Monmouth, N.J. pp. 506-513 (1978).
14. Manufactured by Efratom California, Inc.
15. Hewlett-Packard Application Note, #913, "Step Recovery Diode Frequency Multiplier Design."
16. J.C. Camparo, R.P. Frueholz and C.H. Volk, "The Inhomogeneous Light Shift in Alkali Atoms," (submitted for publication in Phys. Rev.).
17. L.C. Balling, "Optical Pumping," Advances in Quantum Electronics, (Academic Press, N.Y., 1975).
18. A. Risley, S. Jarvis and J. Vanier, "The Dependence of Frequency Upon Microwave Power of Wall-Coated and Buffer-Gas-Filled Gas Cell Rb⁸⁷ Frequency Standards," J. Appl. Phys. 51, 4571 (1980); H.G. Robinson and C.E. Johnson, "Narrow ⁸⁷Rb Hyperfine-Structure Resonances in an Evacuated Wall-Coated Cell," Appl. Phys. Lett. 40, 771 (1982); R.P. Frueholz, C.H. Volk and J.C. Camparo, "The Use of Wall Coated Cells in Atomic Frequency Standards" (submitted for publication in J. Appl. Phys.).

FIGURE CAPTIONS

- 1) Schematic diagram of a typical gas cell clock. B_0 represents the externally applied magnetic field, with its direction indicated by the arrow.
- 2) Experimental set up for determining clock lineshape.
- 3) Experimental results of the clock's lineshape when pumping with a laser diode. The top row of lineshapes correspond to low laser intensity ($\sim 0.5 \text{ mW/cm}^2$), the bottom row to high laser intensity ($\sim 10 \text{ mW/cm}^2$). The frequency axis indicates the total scan of the microwaves from some arbitrary start frequency, and $\Delta\nu_{\text{hfs}}$ denotes the shift of the center frequency of the microwave line from that found for zero laser detuning.
- 4) Frequency of the peak and first moment of the laser pumped clock lineshape for a laser detuning of $\sim -400 \text{ MHz}$. The difference between these two curves is a measure of the lineshape's asymmetry; the change in the frequency of the lineshape's peak corresponds to the clock's light shift.
- 5) Calculated clock lineshapes for low and high laser intensity, laser detuning of -411 MHz .
- 6) Calculated clock light shift for several detunings of the laser. From top to bottom these are -411 MHz , -201 MHz and $+219 \text{ MHz}$.
- 7) Relative transmission signal amplitude for a homogeneous region in the absorption cell as a function of (Γ/ω_1) for several values of (γ/ω_1) . Γ is the optical pumping rate, ω_1 is the microwave Rabi frequency, and γ is the hyperfine spin relaxation rate.
- 8) Relative transmission signal amplitude at a particular axial position in the absorption cell as a function of radial position within the cavity. Curves for several different values of (Γ/ω_{1D}) are shown. Γ_D and ω_{1D} are the peak values of the optical pumping rate and the microwave Rabi frequency, respectively.

Schematic Diagram of Typical Gas Cell Frequency Standard

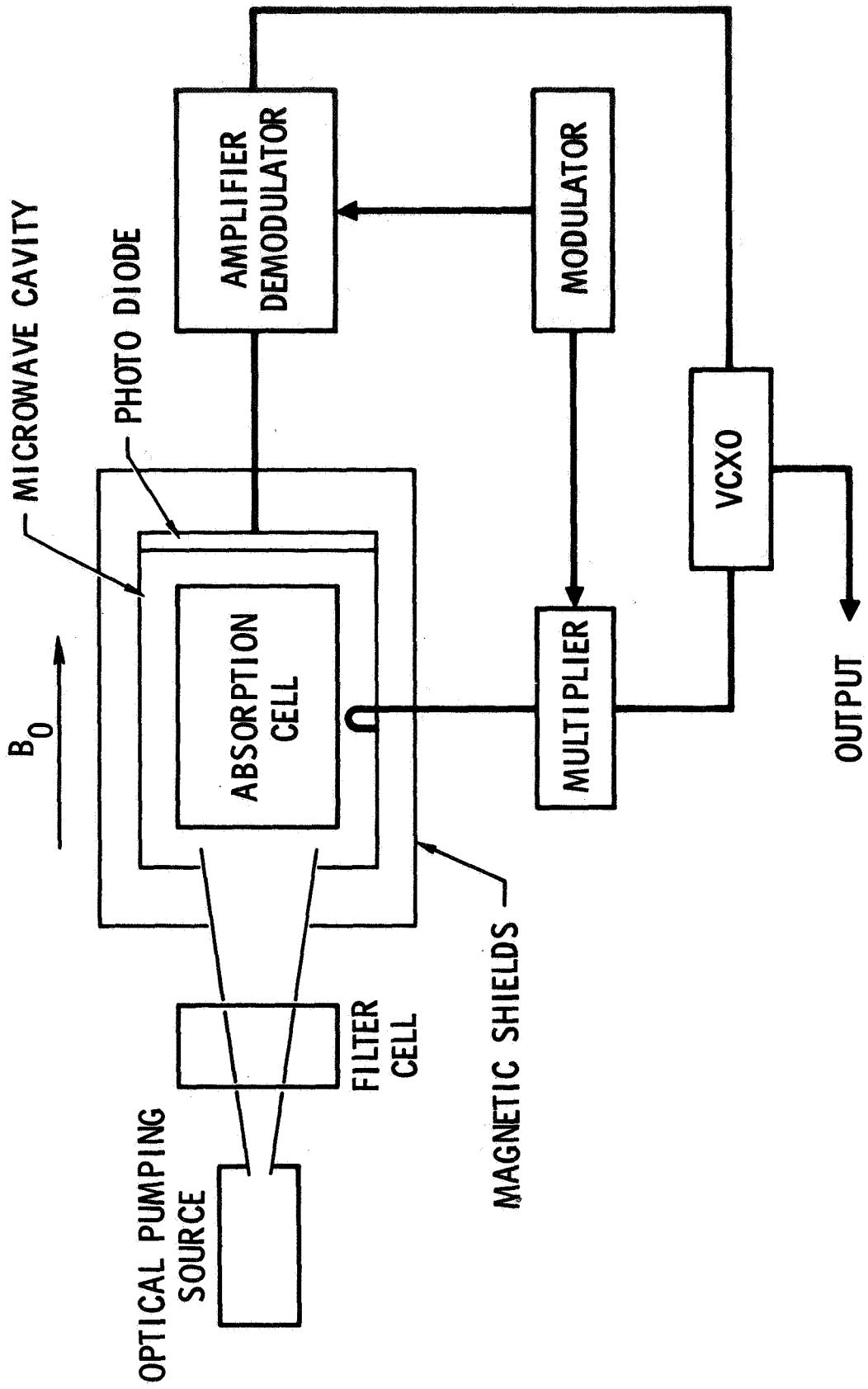


Figure 1



Apparatus for Lineshape Measurements

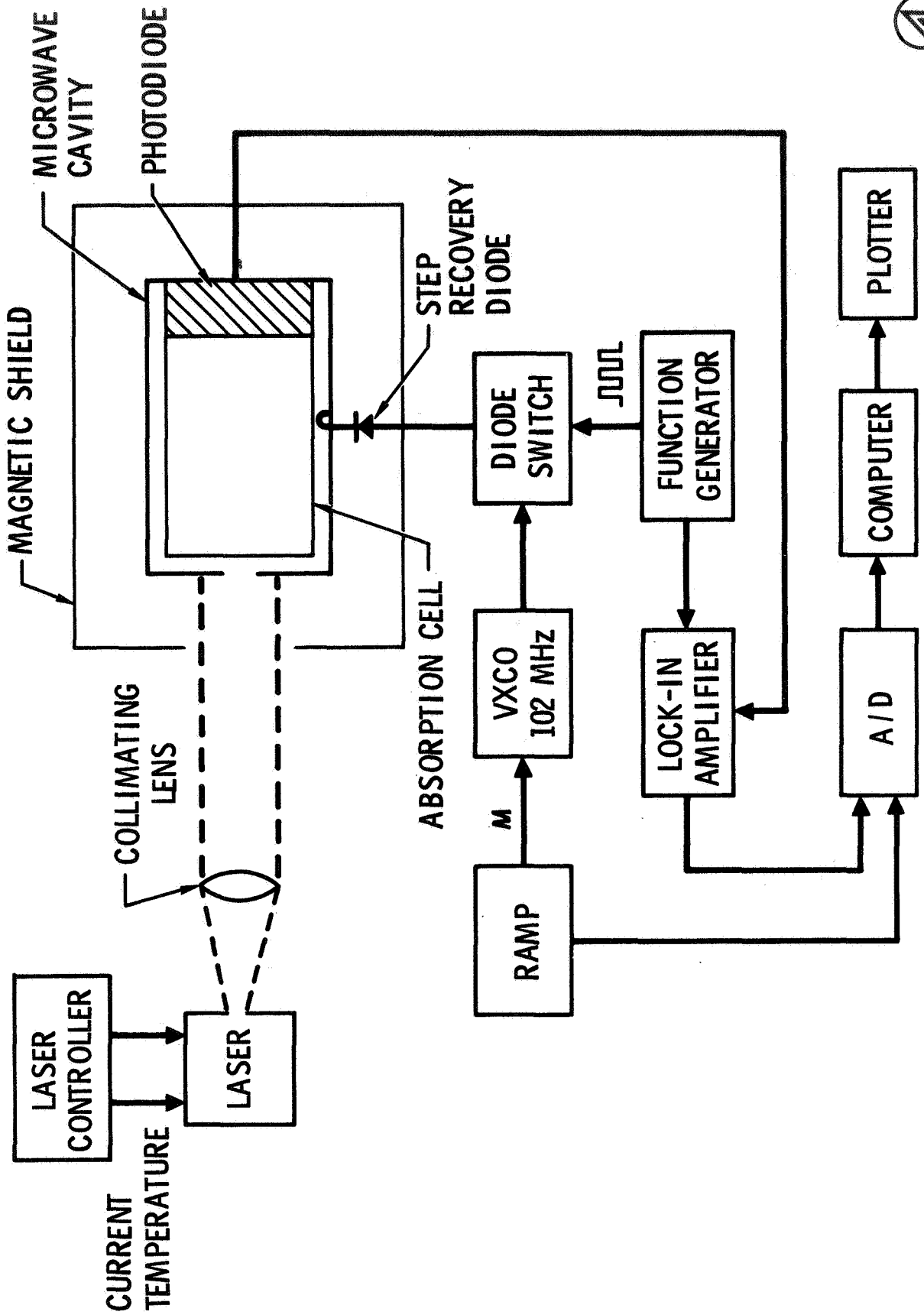


Figure 2



Observed Clock Lineshapes

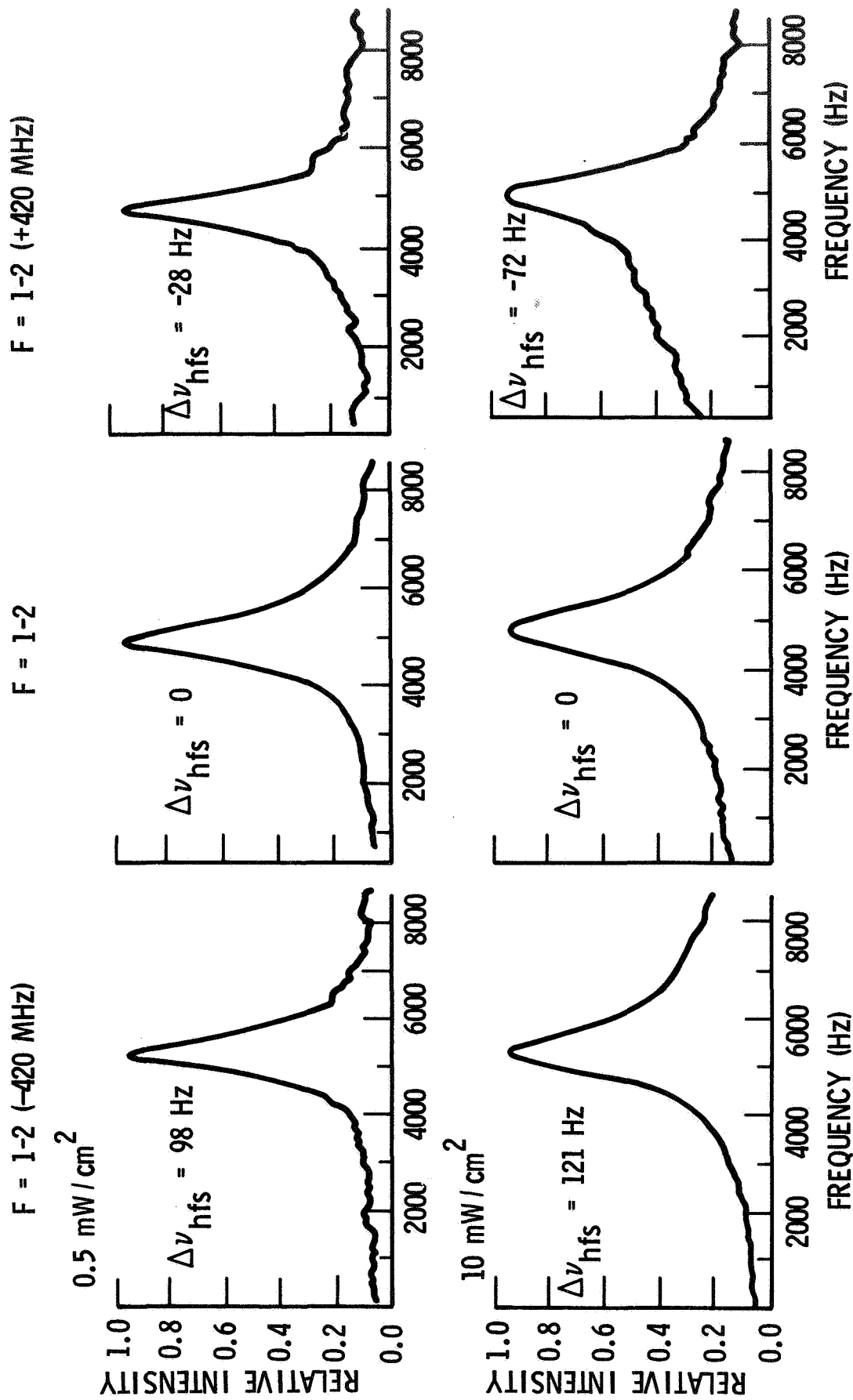


Figure 3



Observed Lineshape's Peak and First Moment vs Laser Intensity

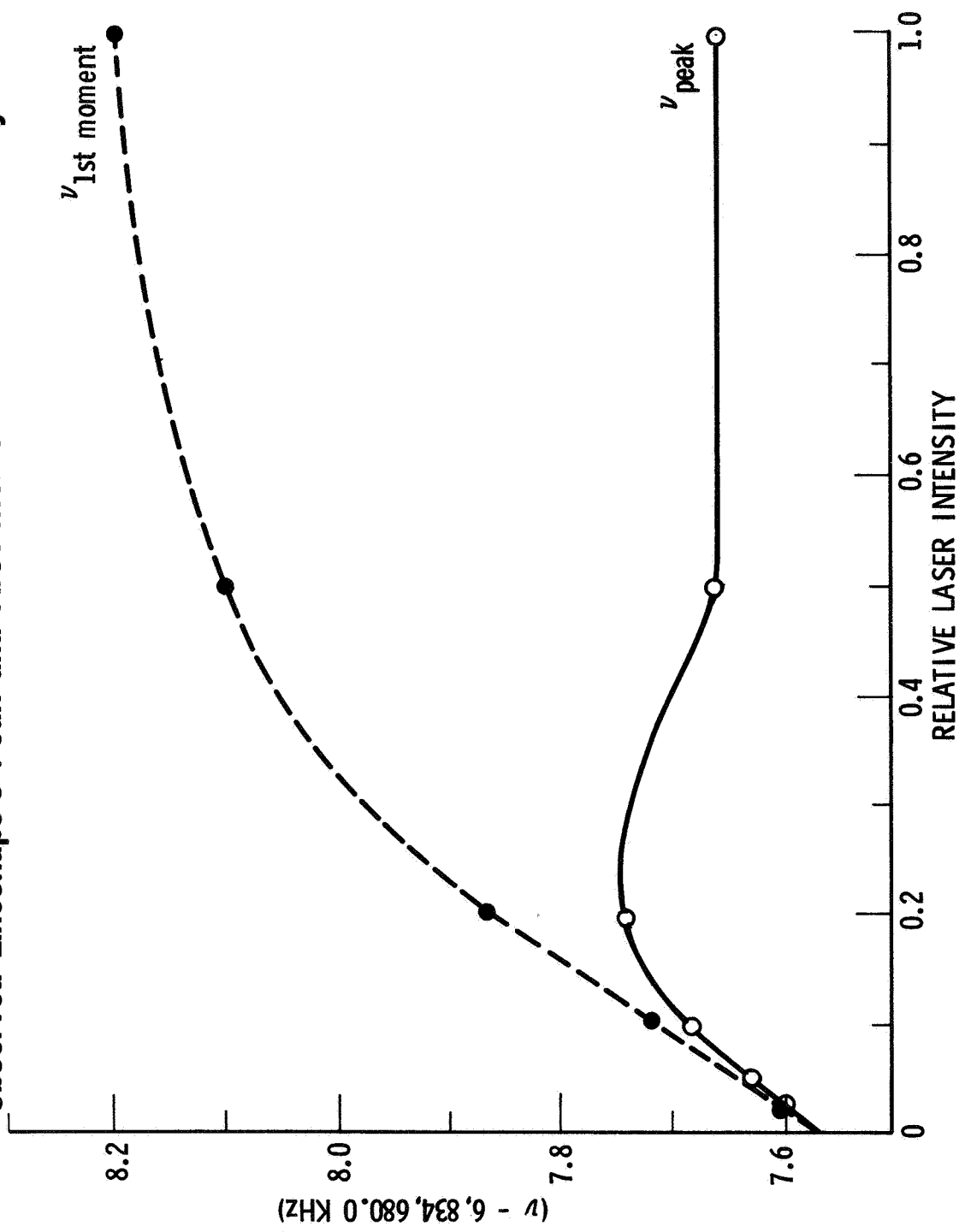


Figure 4

Calculated Inhomogeneous Light Shift

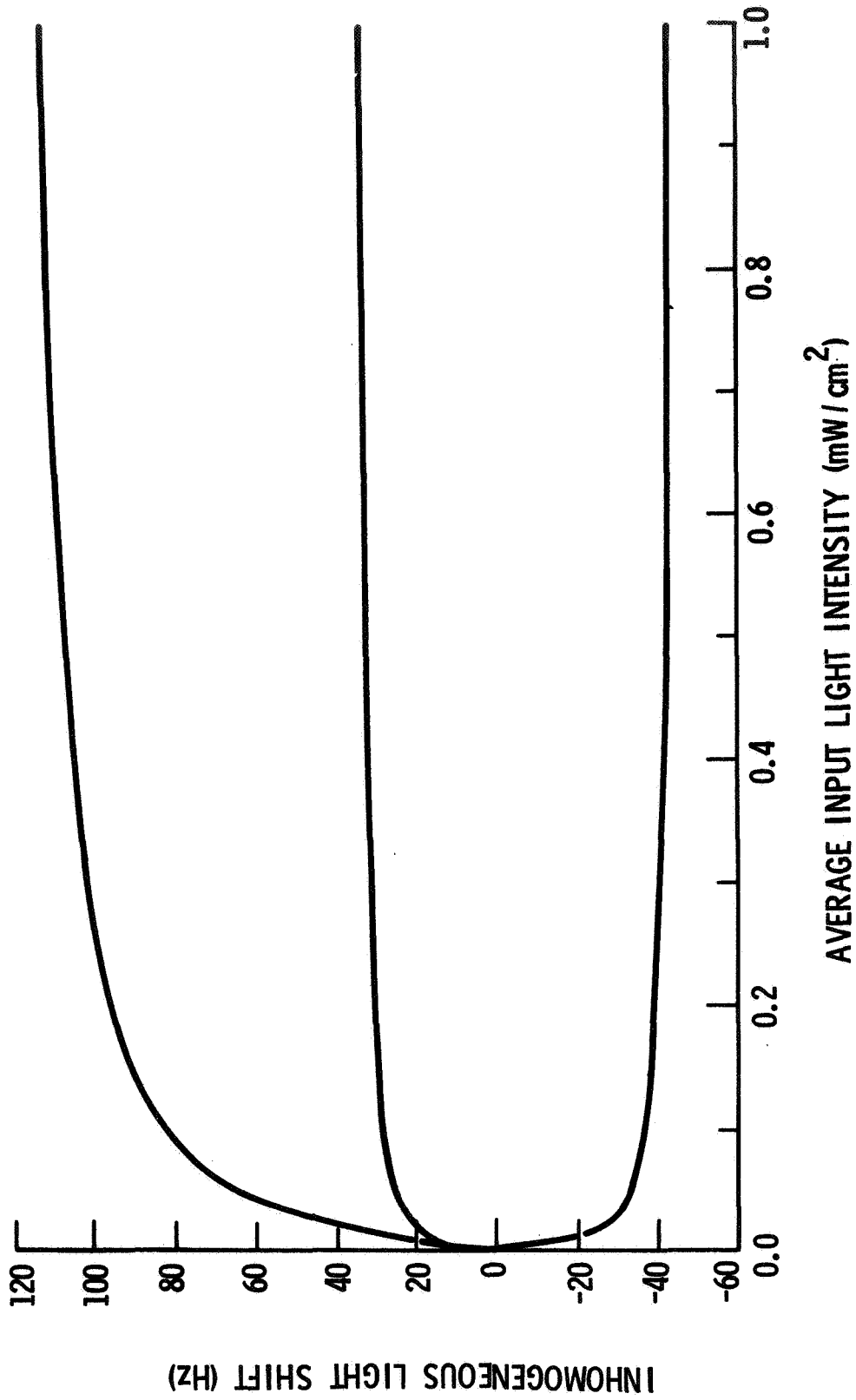


Figure 5



Calculated Lineshapes

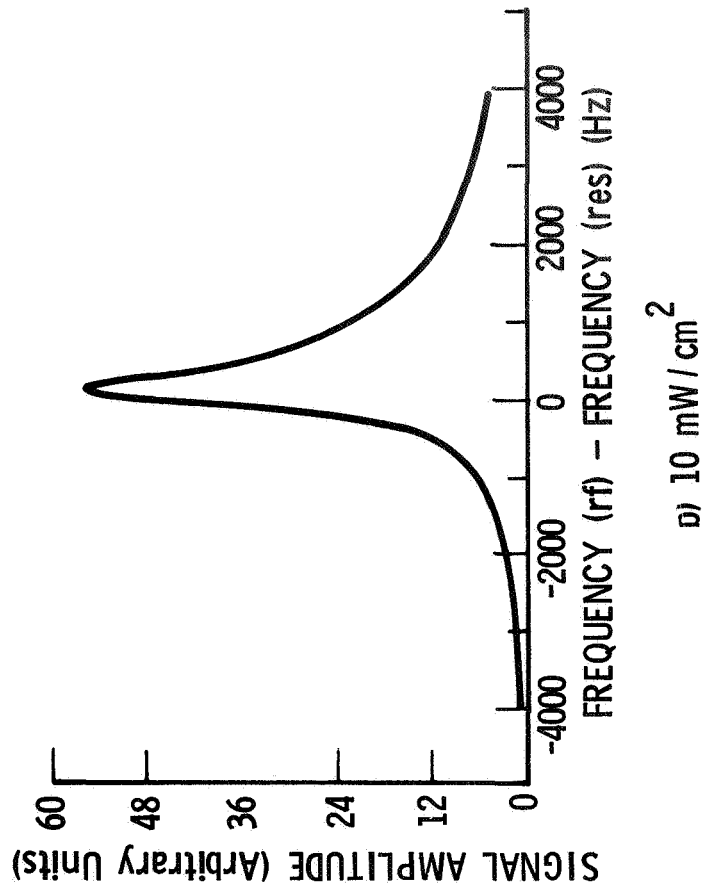
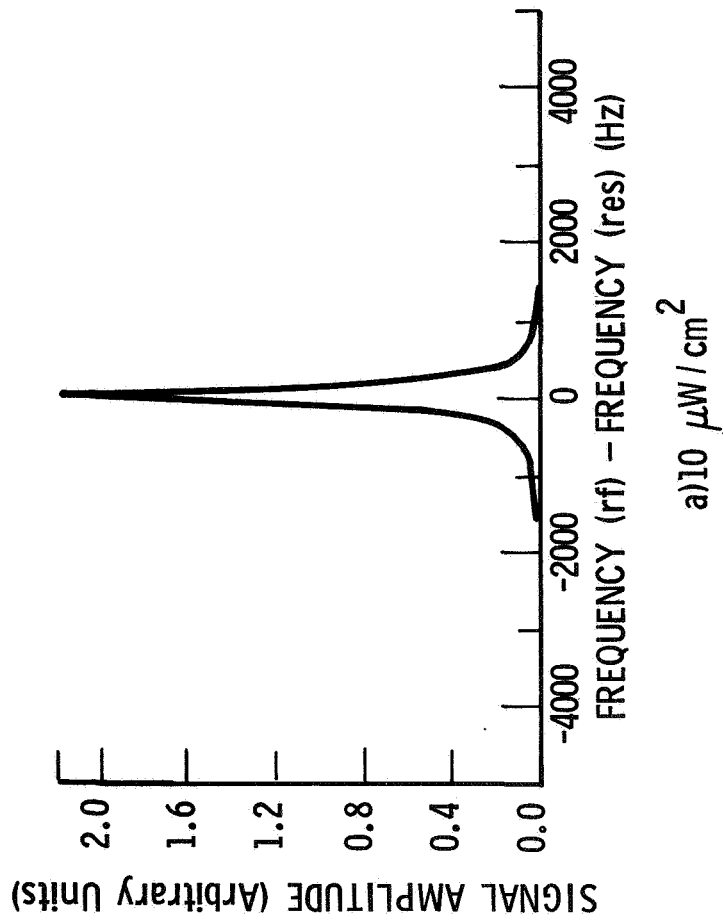


Figure 6

Transmission Signal Amplitude as a Function of (Γ/ω_1)

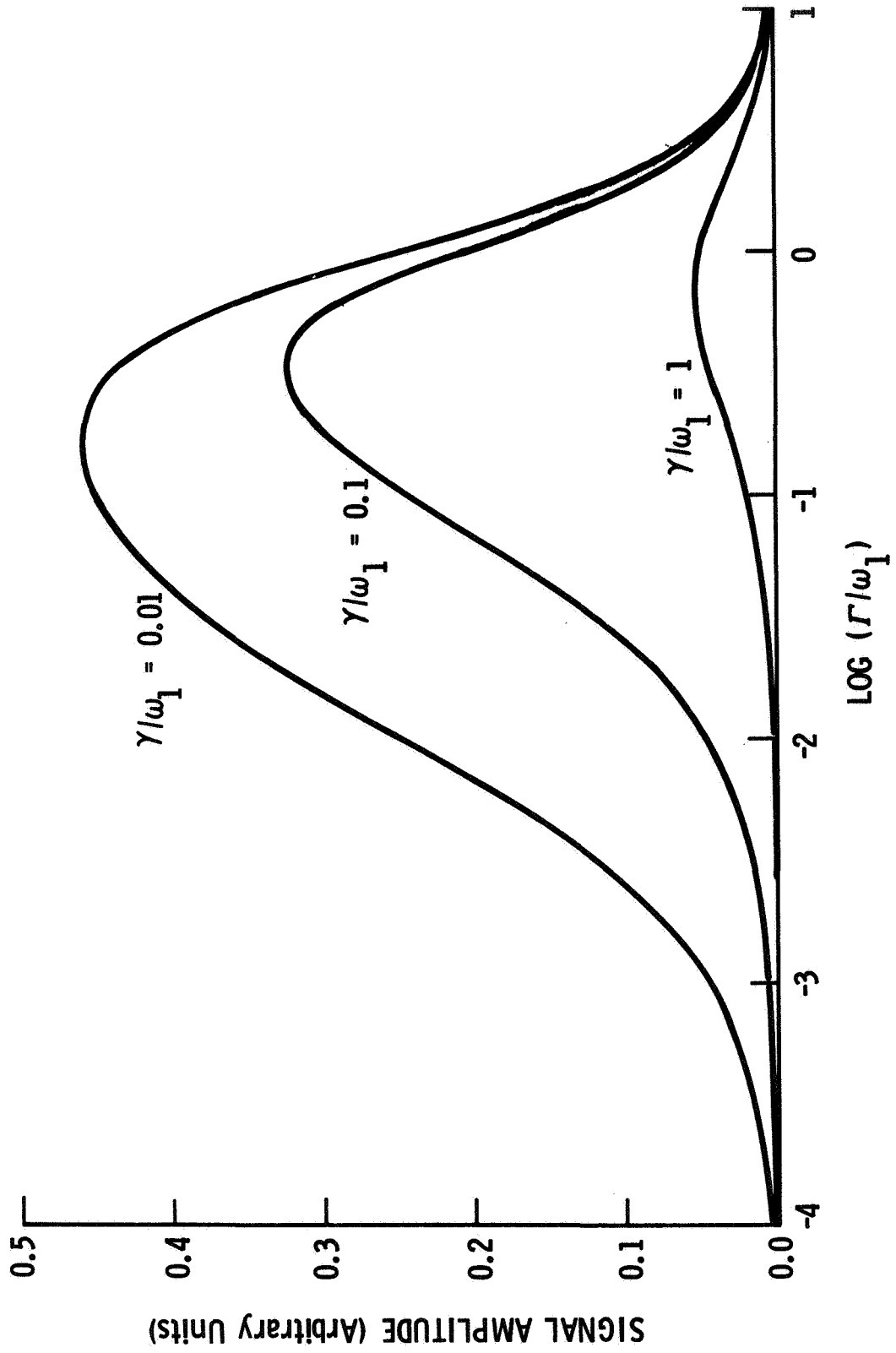


Figure 7



Transmission Signal Amplitude as a Function of Radial Position in the TE₁₁₁ Cavity

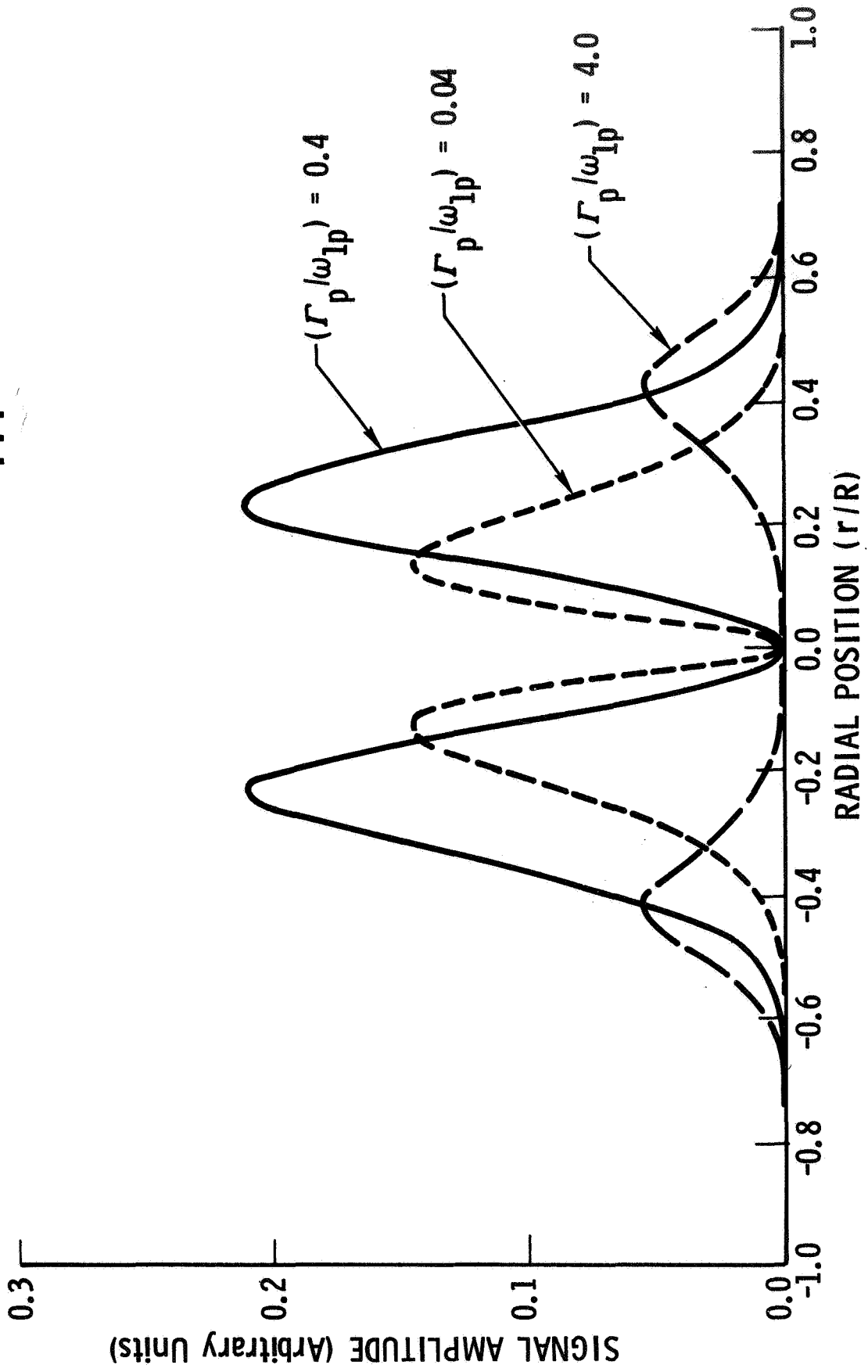


Figure 8

QUESTIONS AND ANSWERS

MR. DEHMELT:

Why does one want such a high intensity at all?

After all, the light goes up proportional to the power and the signal-to-noise goes only up by the square root of the power, so one doesn't want much power.

MR. VOLK:

Well, I think our computer model is showing that you have to reach optimum trade-off between that, that's certainly true.

You start broadening as soon as you start pumping but you must reach some degree of polarization before you can have a signal.

MR. DEHMELT:

I was under the impression this can be reached with ordinary lamps?

MR. VOLK:

The optimum? I'm not sure.

MR. DEHMELT:

Comment on it.

MR. VOLK:

I think even if you could reach that there would be advantages of replacing the lamp with the laser diode. And so, I think one must look at the ramifications of doing that.

MR. DEHMELT:

I can see that you couldn't see your maximum for diagnostic purposes.

MR. VOLK:

I'm sorry, I couldn't hear that last comment.

MR. DEHMELT:

For diagnostic purposes it's probably fine to use a laser.

MR. VOLK:

Yes, I agree with that.

DR. WINKLER:

Since you do have so much power, much more than you need, wouldn't it be advisable since you want to use the diode for other reasons to deliver this spread out the power over the total line width by noise modulating the laser, laser frequency. And then you would get away from these troubles of generating asymmetry by an unbalanced power distribution along the wavelength.

MR. VOLK:

I really think that's a good point.

STUDY OF MULTIPLE OPTICAL TRANSITIONS IN ^{87}Rb USING LASER DIODES

C.L.J. Newton and H.G. Robinson
Physics Department, Duke University, Durham, N.C. 27706

ABSTRACT

Recent work with laser diodes has indicated their potential usefulness in optically pumping atomic frequency standards. We consider various optical pumping schemes for ^{87}Rb incorporating such light sources at two D1 frequencies for experimental situations of either evacuated wall-coated cells or atomic beams. Numerical integration of rate equations governing the level populations with arbitrary pumping light choices of intensity, D1 hyperfine transition(s), and polarization and subsequent calculation of scattered light provide a simplified 0-0 hyperfine signal analysis. By frequency modulating one laser diode, we have excited two optical transitions in an evacuated wall-coated cell and observed a large $\Delta m_F = 1$ hf signal.

INTRODUCTION

The demonstration of ^{87}Rb hyperfine transitions as narrow as 10 Hz (FWHM) in an evacuated wall-coated cell¹ led to our interest in various schemes for optically pumping and detecting the $(F, m_F) = (2, 0) \leftrightarrow (1, 0)$ hyperfine "clock" transition. Recent work with laser diodes has indicated their potential usefulness in optically pumping frequency standards.^{2,3} The spectral width obtainable from such diodes can be considerably less than the Doppler width of the D1 transition for room temperature ^{87}Rb , and initially we model this light source as a delta function in frequency which can be tuned to any of these optical transitions. In the case of an evacuated cell, the primary light-atom interaction is in the cell volume. This is a free-space interaction so that no mixing in the excited $2p_{1/2}$ state occurs. In this sense, the atomic beam and evacuated wall-coated cell are quite similar. This is in contrast to the case of the buffer gas filled cell where mixing does occur in the excited state. The wall-coating reduces relaxation at the wall so that an atom may suffer many wall collisions before having its quantum state severely perturbed. As a result, the atom can undergo an optical pumping process (i.e., a redistribution of ground state level populations by scattering light of specific polarizations and frequencies) extending over many wall collisions.

RATE EQUATION CALCULATIONS

Rate equations are written for the populations of the eight m_F sublevels of the $2s_{1/2}$ electronic ground state of ^{87}Rb using electric dipole transition

matrix elements to describe the various leaving and entering rates. Such equations are well-known from early optical pumping experiments⁴ and have recently been used in the analysis of 0-0 hyperfine transitions in atomic beams of Cs and Rb.^{5,6} Our specific interest at present deals with ⁸⁷Rb D1 optical transitions. The rate equations are put in a general matrix formalism which allows use of any combination of intensities and polarizations of the four hyperfine components of the D1 transitions. (These transitions are labeled as (F-F')=(1-1'), (1-2'), (2-1'), and (2-2') where the primed number indicates the ²P_{1/2} state F-value and the unprimed number, the corresponding value for the ²S_{1/2} state. Thus pumping using various frequencies and Δm_F selection rules can be investigated. The limiting case of no T₁ relaxation is treated. It is a reasonable approximation in view of the long relaxation time attained in the wall-coated cell and the relatively high intensity available from the laser diode. Numerical integration by computer gives the time evolution of the level populations. The starting distribution assumes equal populations in each of the eight m_F-sublevels.

When a microwave-induced hf transition is present, the rate equations are modified by adding a term to the affected levels equal to a fixed fraction of the 0-0 level population difference. The "resonant signal" is taken as the difference between the total scattered photon flux under conditions of level population equilibrium when the mw power is on and the flux when the mw power is off. Other detection schemes are possible; we have chosen this method mainly for its simplicity and ease in making a relative comparison between several pumping cases. No attempt is made to consider optimal adjustment of mw power. A weak mw perturbation is used to avoid saturation effects. The choice of intensities of the various pumping components affects the scattered light at population equilibrium and hence, affects the 0-0 signal size. Thus intercomparison of pumping/detection schemes is dependent on the relative intensities used. In this paper, we choose equal relative intensities for each applied primary pumping component, σ^+ , σ^- or π . In an experimental situation, different effective intensities of the components could be produced.

The simple procedure outlined above permits a comparison of pumping schemes with regards to level populations and scattered light intensity changes as the "signal." However it does not address the issue of the 0-0 resonance resolution obtained for various pumping schemes. For this we would need a resonance lineshape calculation including linewidths and saturation effects as well as signal amplitude and background flux.

Large population differences are attainable using two appropriate optical frequencies for pumping. For example, with circularly polarized light directed along the magnetic field axis ($\Delta m_F=+1$), at frequencies (2-2') and (1-2'), all population is pumped into the (F,m_F)=(2,2) ground state level. By frequency modulating one laser diode with a square-wave current, we were able to excite these two transitions and to demonstrate a large hf signal for the (2,2) \leftrightarrow (1,1) transition in a 1.5G magnetic field.⁷

Three of the best pumping schemes investigated for observing the 0-0 hf transition are now presented. Figure 1a shows the time development of level populations for the case of two resolved optical frequency transitions driven simultaneously by 1) linearly polarized σ -light at the (2-2') frequency and 2) linearly polarized π -light at the (1-1') frequency. The first causes $\Delta m_F = \pm 1$ transitions, while the second, $\Delta m_F = 0$ transitions with $0 \rightarrow 0'$ excluded. In equilibrium, all population has been driven into the (1,0) level. This achieves one of the desirable conditions for efficient pumping/detection: namely, large difference of population between the levels specified by the mw transition.

If the laser source has a finite frequency width and the cell has the real Doppler width for the D1 transitions, then optical transitions to the $F'=1$ and 2 states of the $^2P_{1/2}$ state from a common F-value in the ground $^2S_{1/2}$ are not completely resolved. For example, the tail of the (2-1') transition overlaps the (2-2') transition center. The unintentional excitation of (2-1') when exciting (2-2') provides a depumping mechanism which reduces the 0-0 level population difference. An estimate of optical resonance overlap was made for an optically thin cell by taking the absorption lineshape to be Gaussian with Doppler width of 500 MHz and the laser lineshape to be Lorentzian with width 300 MHz. The convolution of these two functions gives an absorption curve which has a ratio of tail height to on-resonance height of $\sim 5\%$ when the tail frequency corresponds to the hf separation in the $^2P_{1/2}$ state (~ 818 MHz). Actually the laser linewidth is expected to be ≤ 100 MHz for which the tail-center overlap is $\leq 1\%$. However, the examples discussed will use a 5% overlap to emphasize the effect.

In Fig. 1b, the primary optical pumping transitions are the same as in Fig. 1a but now, in addition, light of 5% relative intensity is added at each of the (1-2') and (2-1') transitions. The relative 0-0 hf transition signals in these two cases are in the ratio $\sim 1.8:1$.

As shown in Fig. 2a, all population can be pumped into the (2,0) level by using transitions (2-2') π and (1-1') σ . The effect caused by addition of 5% relative intensities at (2-1') and (1-2') is shown in Fig. 2b. The ratio of 0-0 hf signals for these cases is $\sim 2.1:1$.

A third example uses (2-2') π and (1-2') π -pumping radiation. See Fig. 3a and 3b where again an additional 5% relative intensities have been used at the (2-1') and (1-1') transitions. The ratio of 0-0 hf signals for these cases is $\sim 2.1:1$.

An rf plasma excited Rb lamp with ^{85}Rb filtering is modeled by using unpolarized σ light with primary pumping transitions at (1-2') and (1-1') and secondary transitions (2-2') and (2-1') at 10% relative intensities. Figure 4a gives the level population history. In Fig. 4b we use linearly polarized π -radiation for pumping. The ratio of the respective 0-0 hf signals is $\sim 0.7:1$.

An intercomparison of the 0-0 signals for Figs. 1a, 2a, 3a, and 4a relative to Fig. 4a gives the ratios 20:22:30:1. Differences in the rate of approach to equilibrium are evident from the figures. The case presented in Fig. 3 is the simplest from an experimental viewpoint since only one polarization and direction of propagation of light is required.

Several pumping schemes have been considered which show the possibility of obtaining a large 0-0 population difference with relatively large hf transition signals. Doppler linewidth and laser linewidth were treated to show effective depumping resulting in a reduced population difference and a larger background of scattered light intensity. The atomic beam method can take advantage of the much reduced effective Doppler width to avoid depumping. For either beam or evacuated cell, substantial improvement over conventional Rb lamp pumping is expected for the parameters discussed. We are actively pursuing an experimental comparison with these calculations.

REFERENCES

1. H.G. Robinson and C.E. Johnson, *Appl. Phys. Lett.* 40, 771 (1982).
2. L.L. Lewis and M. Feldman, *Proc. 35th Ann. Symposium on Freq. Control, U.S. Army Electronics Command, Fort Monmouth, N.J.*, 612 (1981).
3. C.H. Volk, J.C. Camparo, and R.P. Frueholz, *Proceedings of the 13th Annual Precise Time and Time Interval (PTTI) Applications and Planning Meeting, Greenbelt, Maryland, December 1-3, 1981.*
4. W. Franzen and A.G. Emslie, *Phys. Rev.* 108, 1453 (1957).
5. P. Cerez and F. Hartmann, *IEEE J. Quantum Elec.* QE-13, 344 (1977).
6. M. Feldman, J.C. Bergquist, L.L. Lewis, and F.L. Walls, *Proc. 35th Ann. Symposium on Freq. Control, U.S. Army Electronics Command, Ft. Monmouth, N.J.*, 625 (1981).
7. The laser for this experiment was kindly supplied by L.L. Lewis, Time and Frequency Division, National Bureau of Standards.

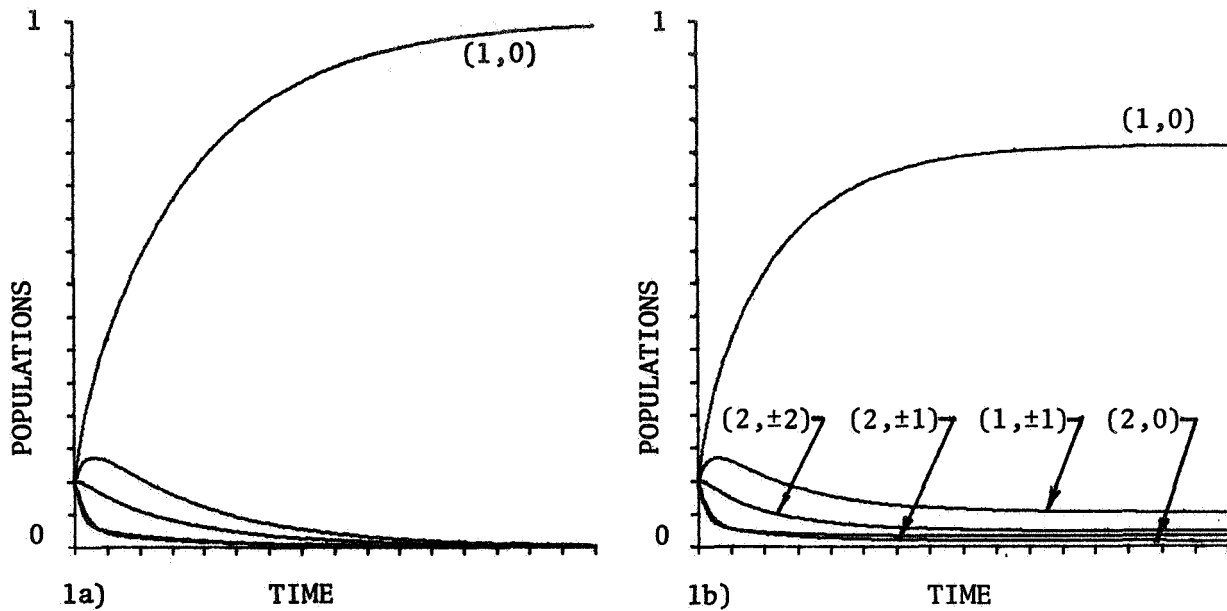


Figure 1. Level populations as a function of (arbitrary) time when pumping with $(2-2')$ σ -light and $(1-1')$ π -light. Completely resolved optical transitions are treated in a "a" while in "b", an additional 5% excitation is assumed for each of the $(2-1')$ and $(1-2')$ transitions.

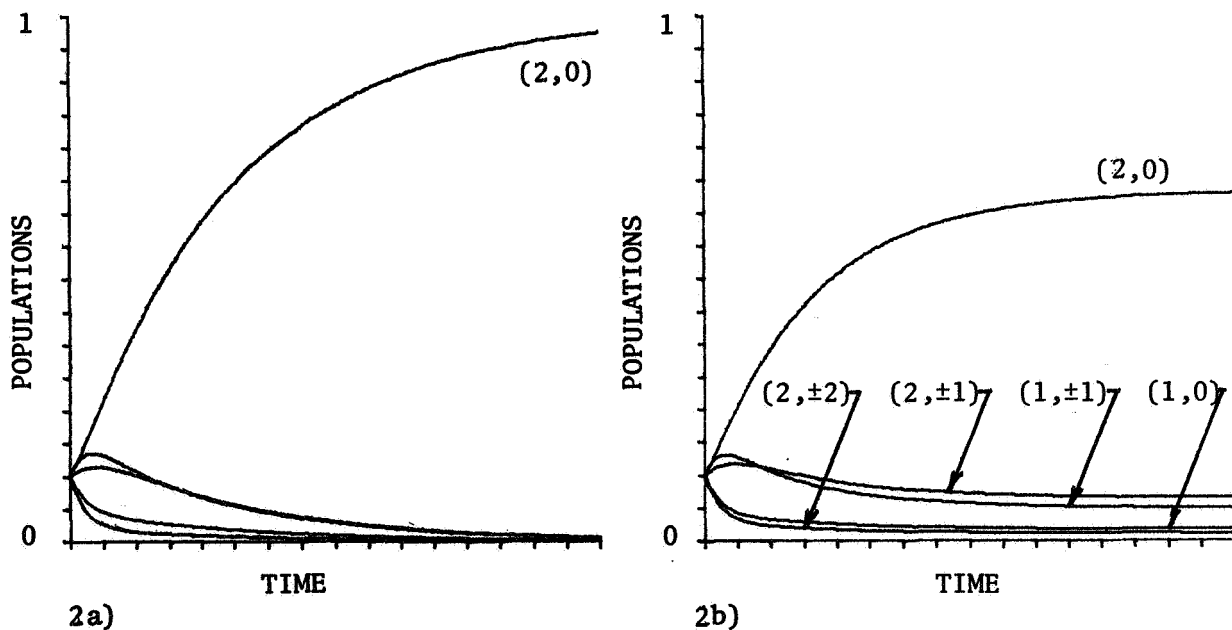


Figure 2. Time history of level populations when pumping with $(2-2')$ π -light and $(1-1')$ σ -light. In "b" an additional 5% excitation is assumed for each of the $(2-1')$ and $(1-2')$ transitions.

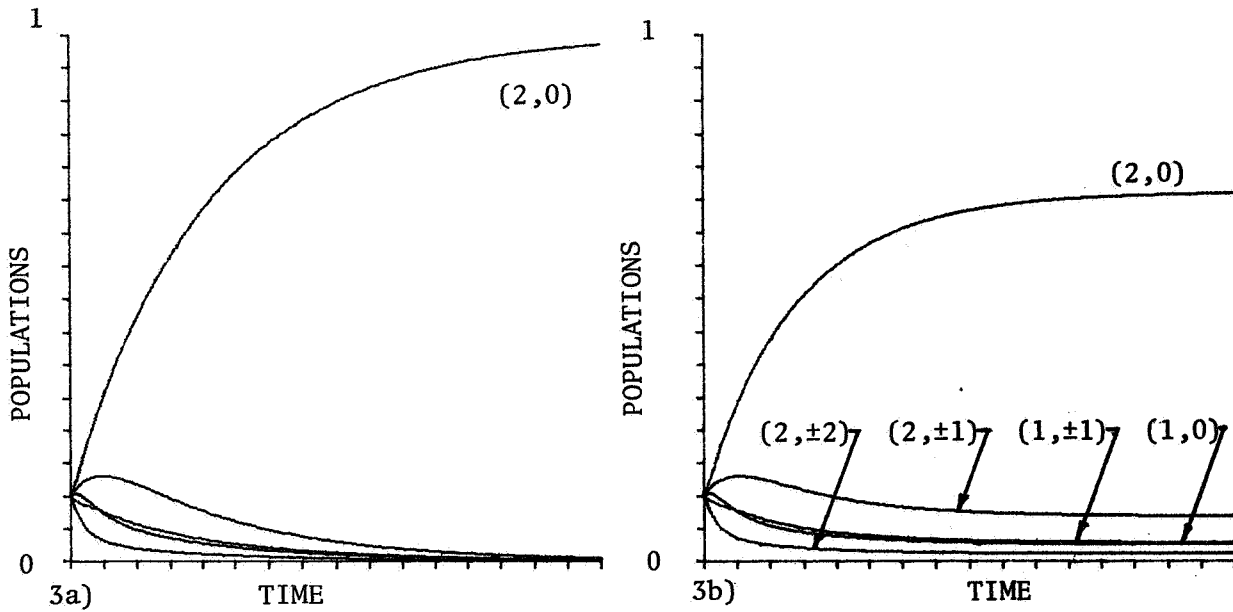


Figure 3. Time history of level populations when pumping with $(2-2')\pi$ light and $(1-2')$ π -light. In "b" an additional 5% excitation is assumed for each of the $(2-1')$ and $(1-1')$ transitions.

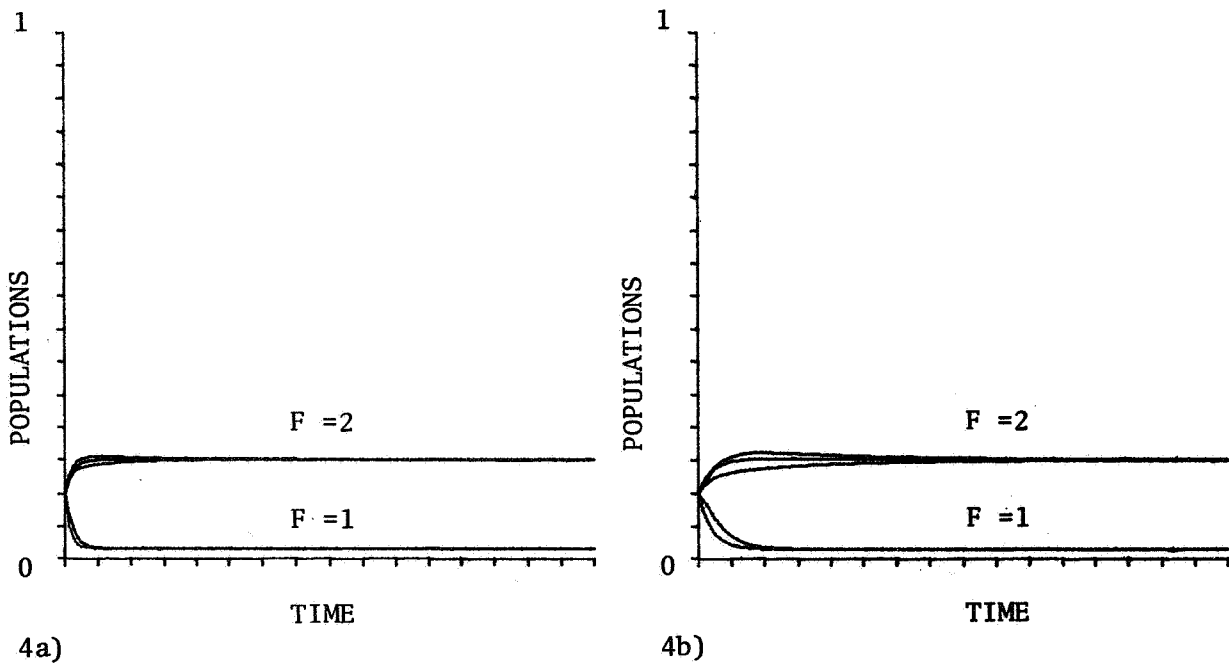


Figure 4. Time history of level populations when pumping with modeled Rb plasma lamp. Primary pumping is at $(1-2')$ and $(1-1')$ transitions with an additional 10% excitation at each of the $(2-1')$ and $(2-2')$ transitions. In "a" σ -light is used while in "b" π -light is used.

QUESTIONS AND ANSWERS

PROFESSOR ALLEY:

Could you tell us the state of the experiments please, Hugh?

MR. ROBINSON:

Yeah, Carroll. The experiments are in a state where we need some research funding. We have a laser which has been loaned to us by Lyndon Lewis and we are now in the act of trying to get a light system so we can put the light in at right angles to the field. The apparatus that we have, is built specifically for the Delta M plus one transition or minus one circular of polarized light.

And we are accustomed to looking at Zeeman transitions and getting the light in perpendicular to the access just requires a little bit of effort and we're now undertaking that. So we hope to go ahead and do these experiments that we would like to see is some comparison with this theory.

A RUBIDIUM CLOCK FOR SEEK-TALK

William J. Riley
EG&G, Inc., Frequency and Time Department
Salem, Massachusetts

ABSTRACT

The work at EG&G, Inc., on a miniature rubidium frequency standard for the SEEK-TALK program has now reached the prototype stage. This paper describes the design objectives and approach, the more important design features, and the results obtained thus far.

INTRODUCTION

EG&G, Inc., with support from the U.S. Air Force Electronic Systems Division, has developed a tactical rubidium frequency standard (TRFS) for the SEEK-TALK program. This effort, which is now entering the prototype stage, is directed toward the establishment of a production capability for miniature rubidium clocks of medium stability capable of fast warmup and extreme ruggedness for military avionics applications. The overall unit will consist of an ultra-miniature physics package and four plug-in circuit boards inside a 2½-inch square by 4-inch box. This size is achieved without the extensive use of hybrid microcircuitry, yet is believed to be the smallest atomic frequency standard yet developed. A mockup of the unit is shown in Figure 1.

The physics package is about the size and shape of a "D" flashlight battery. It combines the best features of the integrated and discrete filter cell approaches by using separate filter and absorption cells, both of which are inside the microwave cavity. Small size is achieved by dielectric loading of the cavity and by a unique electric field mode of lamp excitation. Performance is enhanced by excellent line homogeneity made possible by an optical design giving uniform light distribution, separate hyperfine filtration, and a uniform C-field. Low net temperature coefficient is achieved by cancellation of the individual filter and absorption cell coefficients. The discrete filter cell also allows zero light shift to be conveniently obtained by adjusting cavity temperature. The overall physics package assembly includes a low-noise photo-detector and microwave multiplier, as well as lamp exciter and VCXO circuits and a second magnetic shield.

The TRFS electronic block diagram has a single frequency lock loop that contains a wide bandwidth A/B PLL synthesizer as a subloop. A particularly simple rf chain is used that has no mixing and a few tuned circuits. The servo amplifier is a low-complexity cascade detector configuration and the power supply and temperature controller sections use efficient high frequency switching techniques.

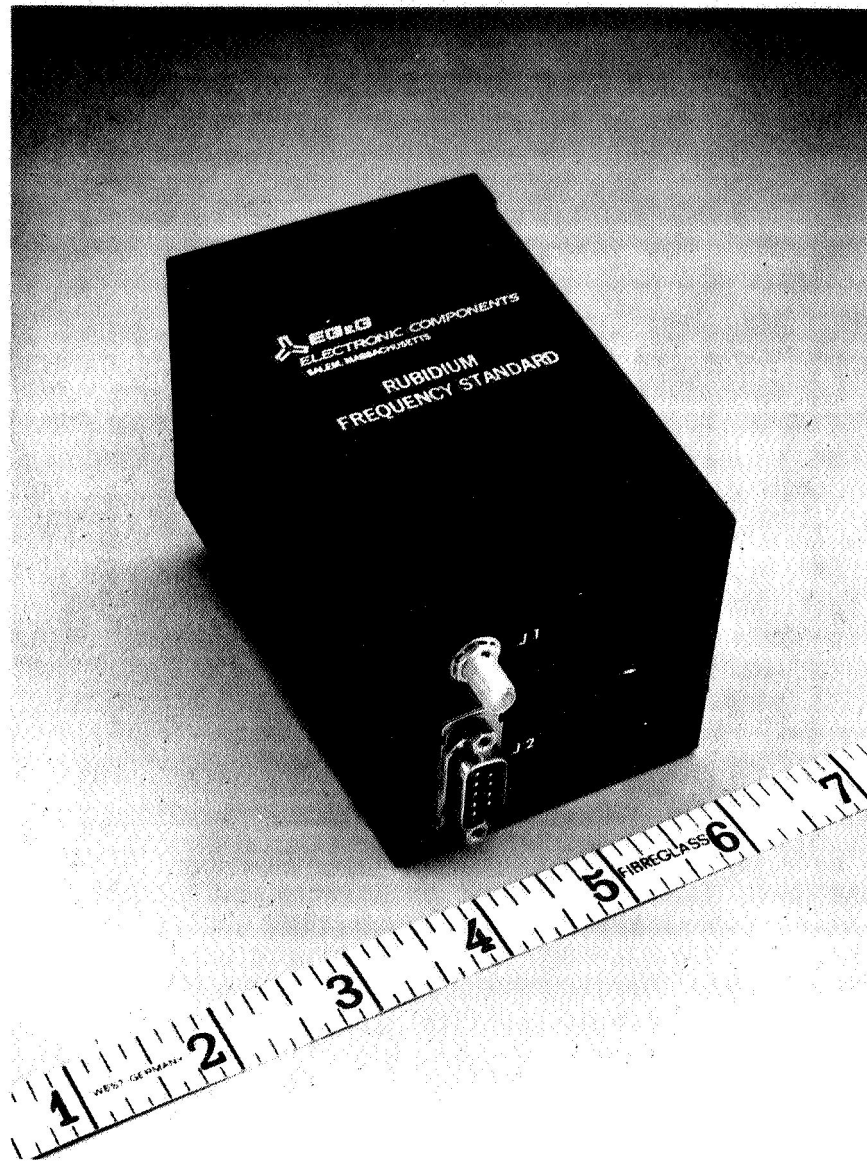


Figure 1. Photograph of TRFS Mockup Unit.

SPECIFICATIONS

The specifications for the TRFS are shown in Table 1 and are based on the general requirements of the SEEK-TALK program.

Table 1. TRFS condensed specifications.

Output Frequency, MHz	10
Output Level, V rms into 50 ohms	0.5
Harmonics, dBc	-30
Spurious components, dBc	-80
Phase Noise $\mathcal{L}(f)$, dBc/Hz	
f = 1 Hz	-80
f = 100 Hz	-120
f = 1 kHz	-135
DC Power, watts	
Steady State at 25°C	<13
Warmup	<70
DC Input Voltage, volts	22-32
Warmup, minutes	
from 25°C	1.5
from -55°C	4
Drift	
per month	<5 x 10 ⁻¹¹
per year	<5 x 10 ⁻¹⁰
Short Term Frequency Stability	
1 sec	<4 x 10 ⁻¹¹
10 sec	<1 x 10 ⁻¹¹
100 sec	<4 x 10 ⁻¹²
Trim Range	≥3 x 10 ⁻⁹
Voltage Coefficient	<1 x 10 ⁻¹¹ /10%
Temperature Coefficient, -54 to +71°C	<3 x 10 ⁻¹⁰
Retrace	≤3 x 10 ⁻¹¹
Storage Temperature, °C	-62 to +85°C
Magnetic Susceptibility, (worst axis)	<2 x 10 ⁻¹¹ /Gauss
Altitude from SL to 50,000 feet	<1 x 10 ⁻¹³ /mbar
Humidity, %	100
Shock	30 g peak
Acceleration	<4 x 10 ⁻¹¹ /10 g
Sinusoidal Vibration	4 g peak
Random Vibration	0.04 g ² /Hz
Reliability, airborne inhabited, hours	≥20,000
Size, inches	2½ x 2½ x 4
Weight, pounds	<2.0

BLOCK DIAGRAM

A block diagram of the TRFS is shown in Figure 2. This block diagram combines high performance, simplicity, and manufacturability. The major sections are:

- a. The physics package which acts as a frequency discriminator to produce an error signal which indicates the magnitude and sense of the difference in frequency between the applied rf excitation and the rubidium atomic resonance.
- b. A servo amplifier which processes the error signal to produce a control voltage for a voltage controlled crystal oscillator (VCXO).
- c. A VCXO section which contains the locked crystal oscillator, circuits to produce the desired (5 or 10 MHz) output, and one divider portion of the synthesizer.
- d. A VHF section which contains the rest of the synthesizer that converts the standard output frequency into a direct submultiple of the rubidium resonance.
- e. A power section which provides supply voltages to the circuitry and has temperature controllers for the two physics package ovens.

PHYSICS PACKAGE

The heart of the TRFS unit is, of course, the physics package. EG&G began this project with the internally sponsored development of a rubidium physics package that combines good performance with ultra-miniature size. The features include a new concept in lamp excitation and a dielectrically loaded cavity that contains separate filter and absorption cells. The basic physics package structure is shown in Figure 3.

Extreme miniaturization of the lamp assembly was accomplished by eliminating the usual rf coil surrounding the rubidium lamp. An electric field structure was developed for starting and maintaining the lamp plasma. Fabry-Perot studies confirmed the proper spectral output from this structure, which is approximately half the overall diameter of an equivalent coil arrangement since no spacing is required between the lamp and oven wall. The lamp is excited by a conventional Colpitts rf power oscillator which will be located inside the physics package.

Miniaturization of the microwave cavity was obtained, paradoxically, by putting more into it. It was decided to use a discrete filter cell for best performance. This allows independent nulling of the light shift and gives good spatial homogeneity in the absorption cell that results in a low rf power coefficient. It was further decided to locate the filter cell inside the cavity to avoid the volume of an additional oven. The common thermal environment also allows cancellation of the filter cell temperature coefficient by that of the absorption cell, since the latter is adjustable by its binary buffer gas mix ratio. The

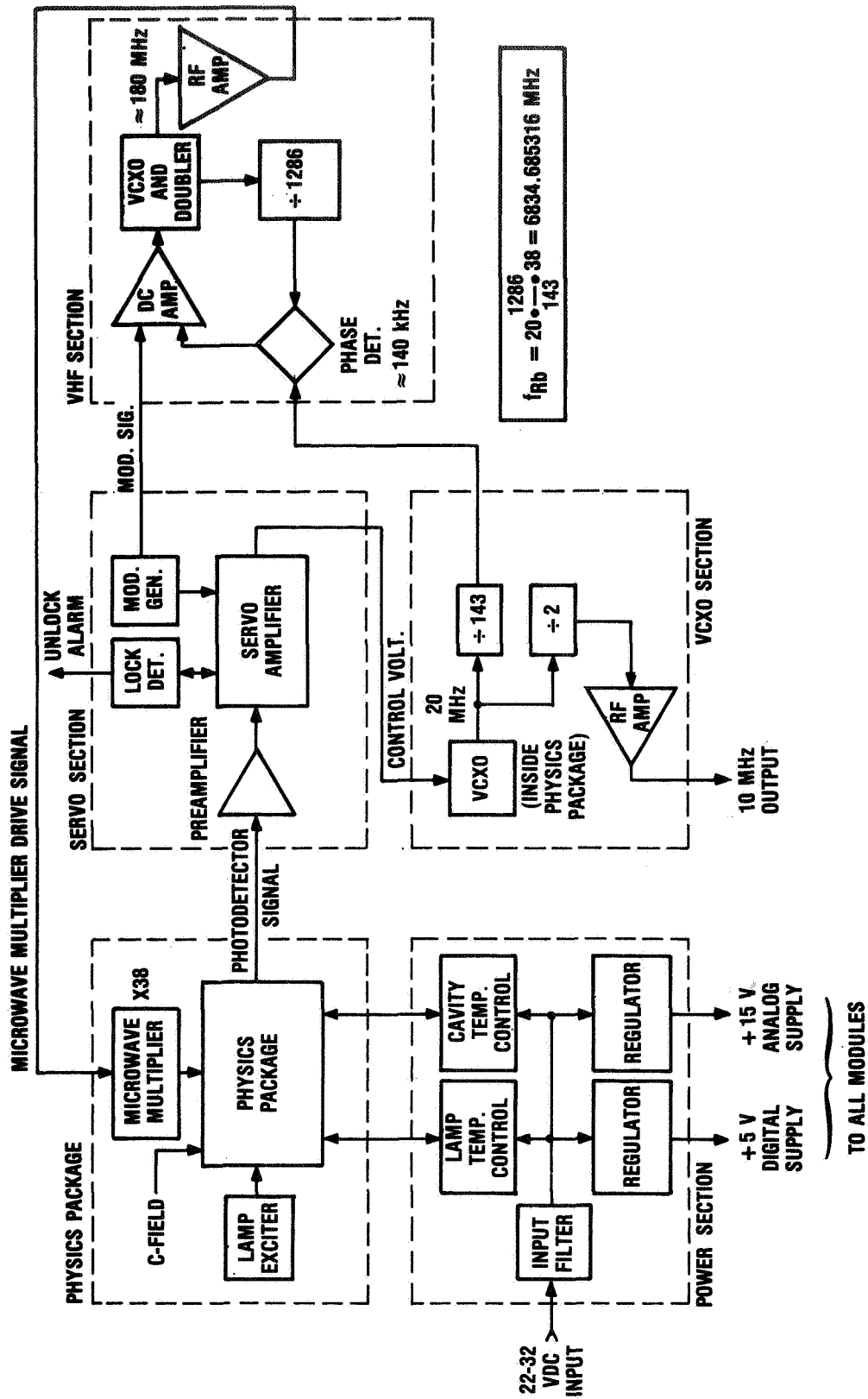


Figure 2. TRFS Block Diagram.

resulting increase in the amount of glass dielectric in the TE₁₁₁ cavity also reduces its size.

A further advantage is that the filter and absorption cells become shorter, which is desirable for optimum signal at a high operating temperature.

The physics package includes two lenses in the optical path. The first, located in front of the absorption cell, collimates the lamp output to give a uniform light intensity distribution. The second lens, located behind the absorption cell, focuses the light on the $\approx 1 \text{ cm}^2$ photodetector to give good collection efficiency.

Two C-field coils are used to provide $\pm 1\%$ C-field uniformity, which helps to ensure good line homogeneity and minimizes rf power sensitivity.

A nonmetallic conical spacer rigidly connects the lamp and cavity ovens for ruggedness and low vibration sensitivity with low heat transfer between the ovens.

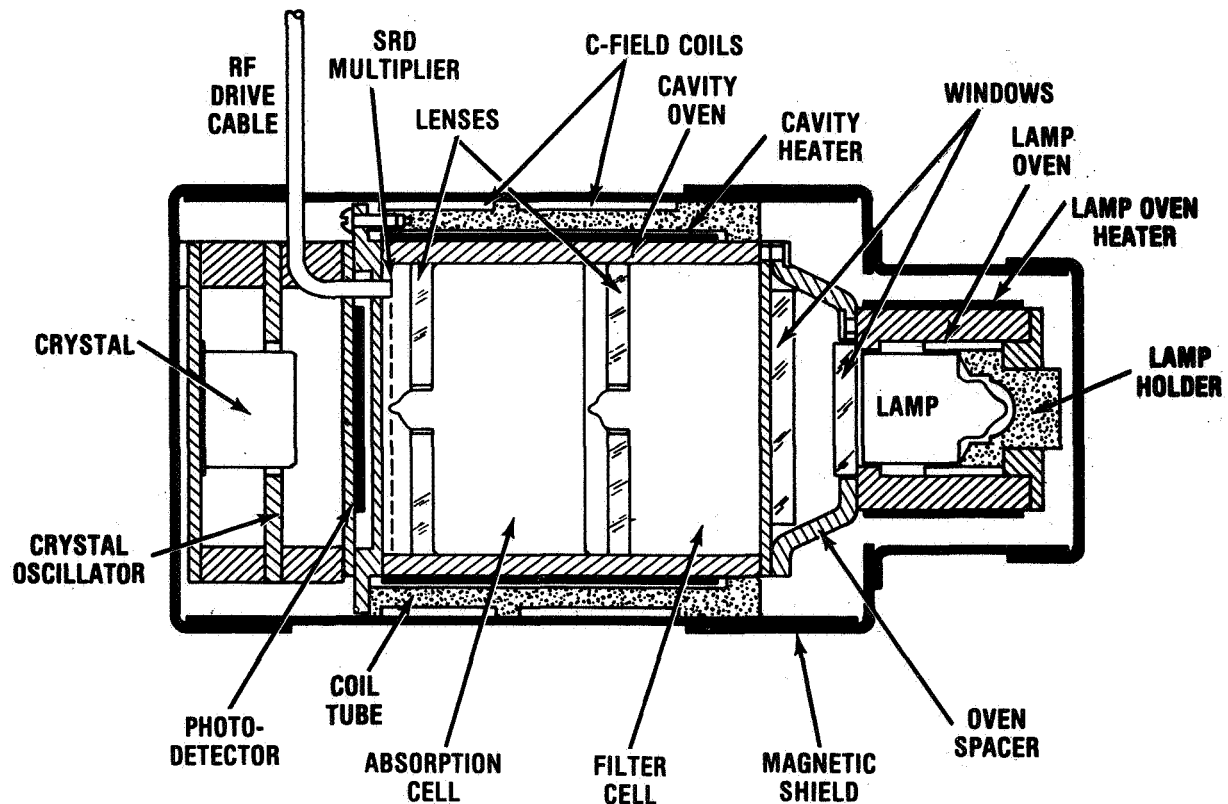


Figure 3. Layout of Miniaturized Physics Package.

The SRD microwave multiplier is incorporated into the temperature-controlled cavity. Its design is both simple and efficient since it works as a straight X38 multiplier.

Table 2 lists some of the physics package parameters and Figure 4 shows the major parts. The synthesizer ratio results in a buffer gas offset that is ideal for such considerations as linewidth, fill tolerance, and barometric coefficient.

Table 2. Physics package parameters.

Parameter	Value
Lamp Size	0.31 in. dia. x 0.45 in. long
Lamp Fill	$\approx 100 \mu\text{gram Rb}^{87} + 7 \text{ torr Kr}$
Lamp Oven Temperature	115°C
Filter Cell Size	0.81 in. dia. x 0.25 in. inside length
Filter Cell Fill	$\approx 100 \mu\text{gram Rb}^{85} + 120 \text{ torr Ar}$
Absorption Cell Size	0.81 in. dia. x 0.30 in. inside length
Absorption Cell Fill (for ≈ 0 Cavity TC and +2.7 kHz offset)	$\approx 100 \mu\text{gram Rb}^{87} + 8.4 \text{ torr}$ N ₂ /Ar mixture
Cavity Temperature (for 0 lamp oven TC)	80°C
DC Photodetector Current	$\approx 100 \mu\text{A}$
Linewidth (full width between inflection points at normal rf)	$\approx 600 \text{ Hz}$
Maximum Fundamental Photodetector Signal (at $f_{\text{mod}} = 235 \text{ Hz}$)	$\approx 20 \text{ nA rms}$
Discriminator Slope at Photodetector	$\approx 80 \text{ pA per } 1 \times 10^{-10}$
Lamp Oven TC	$< \pm 4 \times 10^{-11}/^\circ\text{C}$
Cavity TC	$< \pm 1 \times 10^{-10}/^\circ\text{C}$
RF Power Sensitivity	$< \pm 1 \times 10^{-11}/\text{dB}$
Frequency Stability (1 sec $\leq \tau \leq 1000 \text{ sec}$)	$2 \times 10^{-11} \tau^{-\frac{1}{2}}$

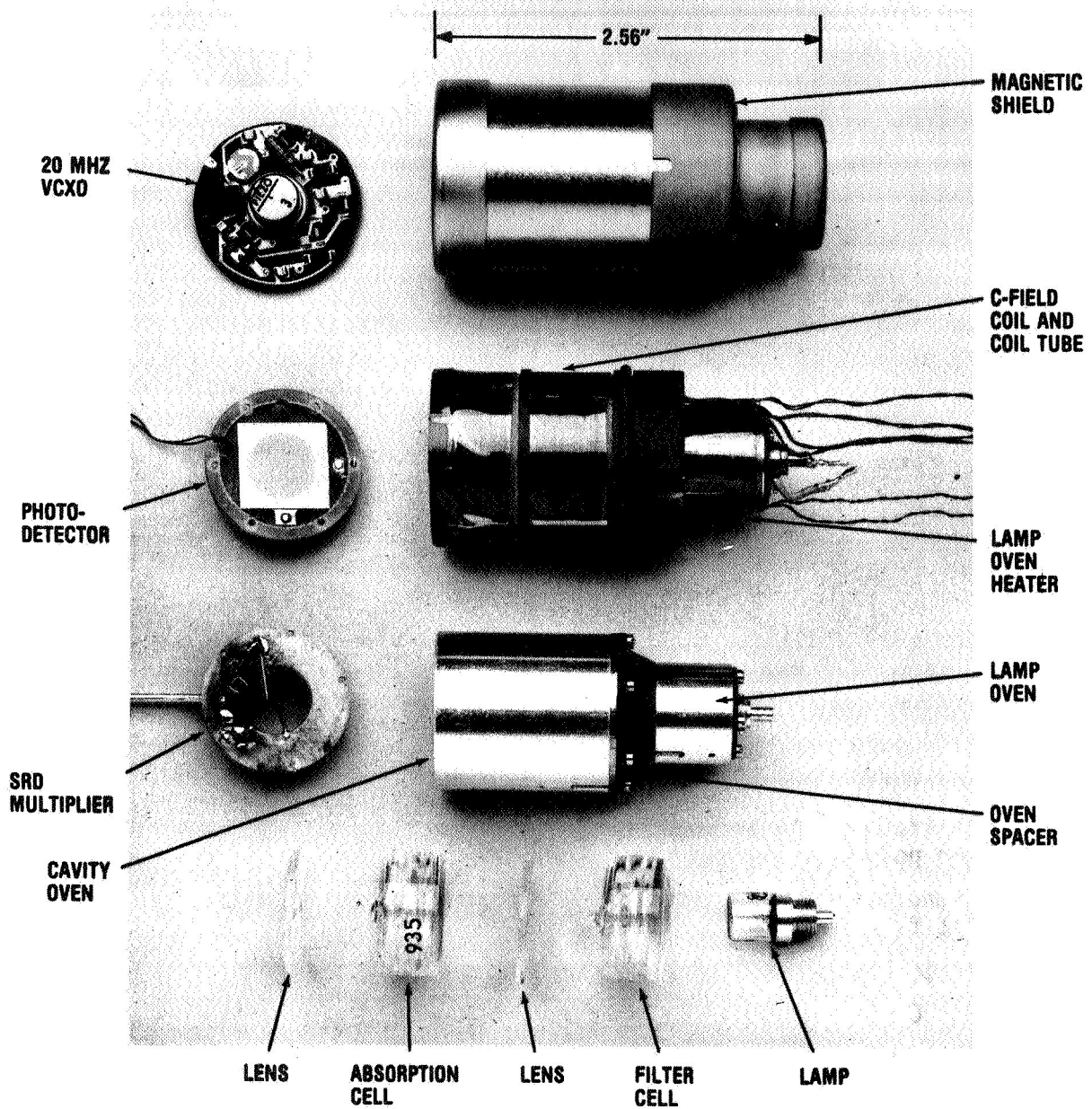


Figure 4. Physics Package Parts.

SERVO AMPLIFIER

The function of the servo amplifier is to process the error signal from the physics package so as to lock the frequency of the 20 MHz crystal oscillator to the stable rubidium atomic resonance. The major blocks are: (1) a preamplifier that converts the photodetector current to a voltage, (2) a synchronous detector that converts the fundamental ac error signal to a dc voltage, (3) an integrator that develops the control voltage for the crystal oscillator, (4) a second harmonic detector that indicates lock, (5) a sweep circuit that aids lock acquisition, and (6) a modulation rate generator that produces reference signals for the synchronous detectors and phase-modulates the cavity excitation.

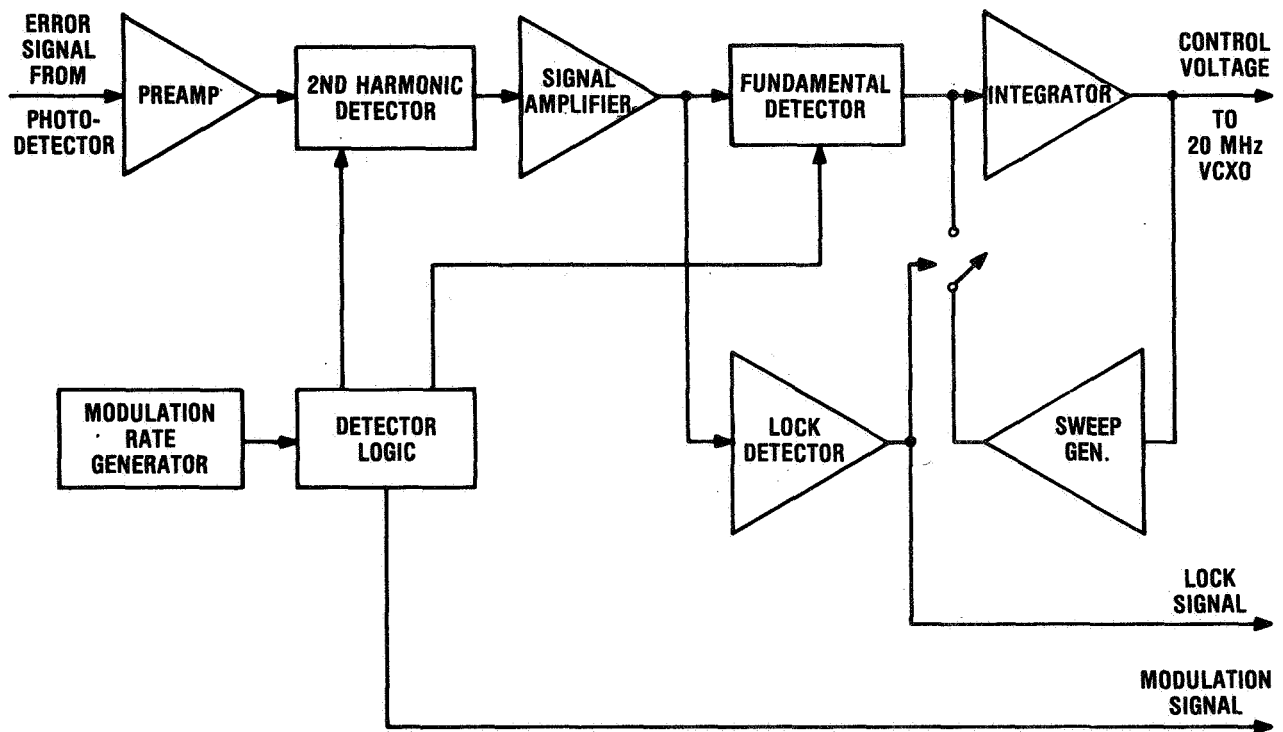


Figure 5. Servo Amplifier Block Diagram.

The TRFS servo amplifier, shown in Figure 5, uses a cascaded detector arrangement wherein the fundamental error signal passes through the second harmonic detector before reaching the fundamental detector. This has the advantage of requiring less hardware. The op amp associated with the second harmonic detector also provides gain for the fundamental signal. The large amplitude second harmonic signal is shifted to the fourth harmonic ahead of the fundamental detector, making it possible to obtain sufficient dynamic range without a bulky notch filter.

VCXO SECTION

The VCXO section consists of a 20 MHz crystal oscillator, frequency dividers to 10 MHz and ≈ 140 kHz, and a tuned amplifier to produce the 10 MHz output.

The voltage controlled crystal oscillator uses a 20 MHz third overtone SC-cut crystal in an HC35/U style holder operated at $\approx 80^\circ\text{C}$ in the cavity oven. This crystal type is chosen for its small size, ruggedness, fast warmup, and low vibration sensitivity. The VCXO is followed by a high speed comparator to provide isolation and conversion to TTL levels. Straightforward TTL logic divides the 20 MHz by 2 and 143 for the output and synthesizer, respectively. The output amplifier is a differential configuration using a single tuned circuit. Another binary divider section is available to produce 5 MHz as an optional output.

VHF SECTION

The VHF section generates a signal at ≈ 180 MHz that is a direct submultiple (1/38) of the rubidium resonance. This frequency is produced by a phase-locked loop (PLL) that operates as a X1286 multiplier from the ≈ 140 kHz reference from the VCXO section. The PLL also serves as the means to apply phase modulation. This approach is hardware efficient and avoids bulky and critical tuned circuits. The rf circuitry consists of a ≈ 90 MHz VCXO, a diode doubler, and an rf power amplifier. The PLL consists of an ECL divider, a TTL phase detector, and a loop amplifier/filter. The loop has sufficient bandwidth for vibration immunity and servo modulation.

POWER SECTION

The power section of the TRFS consists of input filters, temperature controllers for the lamp and cavity ovens, and +5V and +15V power supplies.

The lamp and cavity ovens are supplied directly from the input bus and are controlled by high frequency switching controllers. These controllers provide both warmup and running power and are simple, efficient, operate over a wide dynamic range, and maintain constant thermal gain as the oven power changes. Each controller consists of only one active device and a few discrete components.

All TRFS electronic circuits are powered from +5V and +15V supplies which also use switching regulators. Provision is made for a separate "no-break" input to maintain operation during an interruption in heater power.

PACKAGING

The overall TRFS packaging is shown in Figure 6. The physics package (including cylindrical inner magnetic shield, VCXO, SRD multiplier, and lamp exciter) is located in the center. It is supported inside the square second magnetic shield by resilient material that provides shock and vibration isolation. The four main electronic circuit boards surround the physics package and plug into a mother board. The electronic components face outward for good access. An L-shaped member provides overall support, while power filters and connectors are mounted to the mother board.

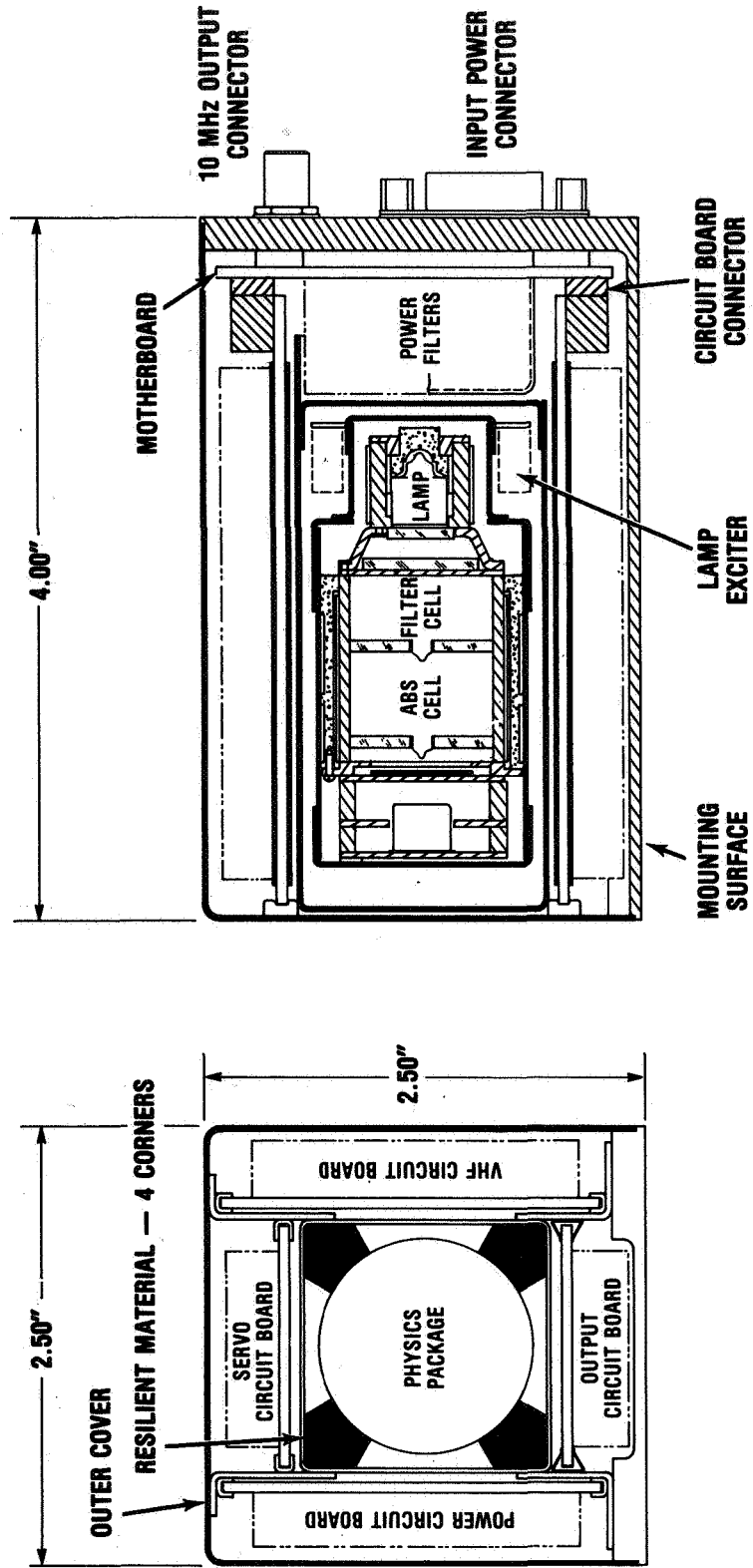


Figure 6. TRFS Packaging Layout.

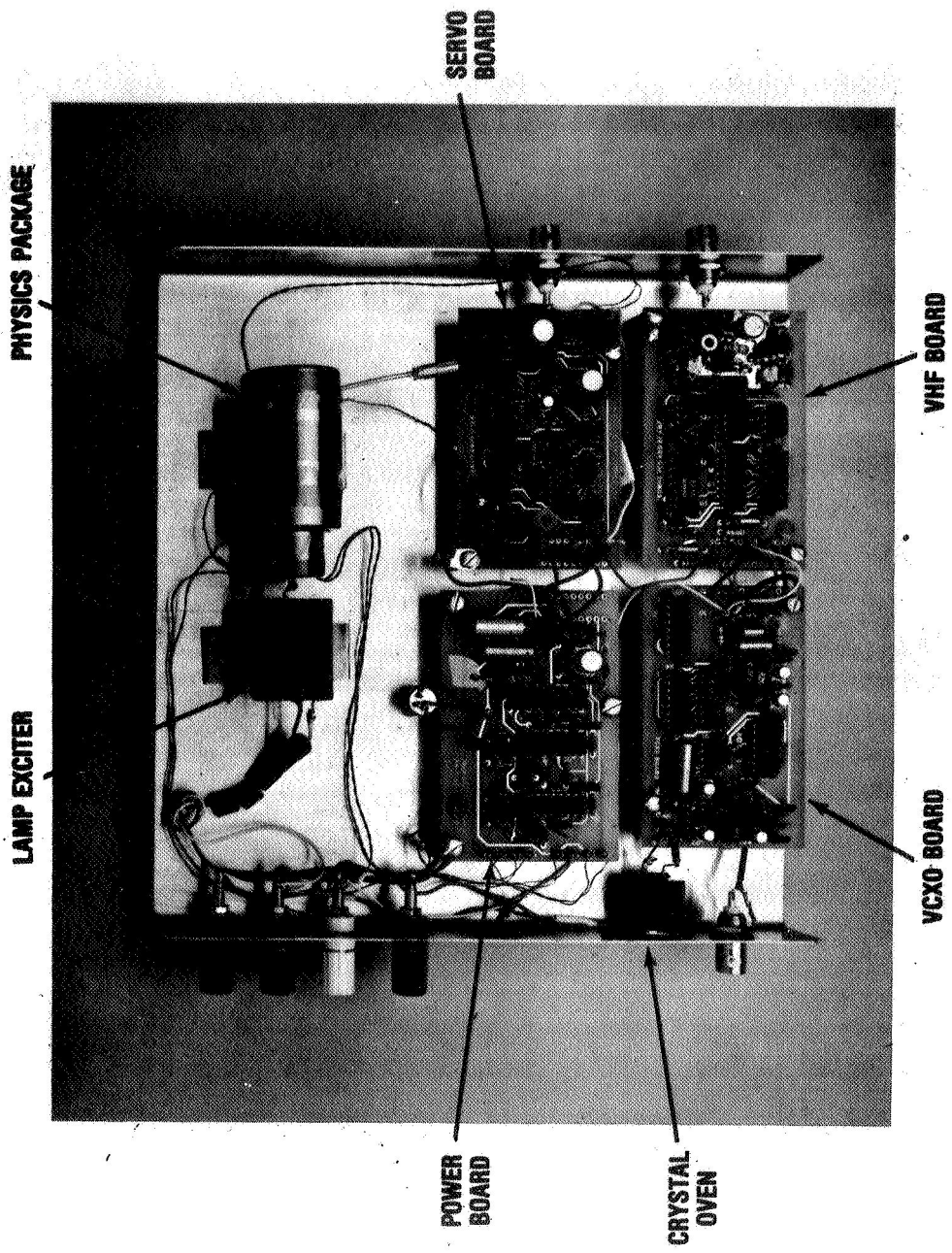


Figure 7. Photograph of TRFS Bench Model 1.

PROGRAM STATUS

The TRFS program began with the development and test of the ultraminiature physics package. This was followed by the design of the complete unit. Fabrication and test of a bench model was then accomplished with Air Force funding.

The bench model TRFS consists of the ultraminiature physics package and four circuit boards mounted flat on a 9-inch square pallet as shown in Figure 7. This configuration is well suited for developmental testing.

The physics package is complete out to the first magnetic shield, including a custom low-noise EG&G silicon photodetector and the SRD microwave multiplier. The lamp exciter is housed separately in a small shield box and the VCXO circuit is on one of the main boards with the crystal in a small separate component oven.

Test results on this unit have confirmed the validity of the overall design concept. The program has now advanced through a prototype redesign stage where detailed design has been done for a packaged prototype.

ACKNOWLEDGMENTS

Support for the TRFS development program has been provided by the U.S. Air Force Electronic Systems Division. At EG&G, Mr. S. Goldberg was responsible for overall scientific direction, and valuable engineering contributions were made by F. Chang, T. Lynch, J. Kirby, K. Lyon, J. McDonald, and E. Sullivan.

QUESTIONS AND ANSWERS

DR. VESSOT:

I would like to comment that in the 1950's when Bob Dickey, Tom Carver and I were doing some of the early work on hyperfine section and rubidium, we had a room full of equipment and we used to joke that there's no reason you couldn't put this in a match box.

So, we were happy to see progress towards that end.

MR. RILEY:

Well, I never really believed. I heard some comments about putting it into a beer can one time. And I never really believed it for many years, but this is really smaller.

A NEW CALIBRATION METHOD FOR TIME DELAY STANDARD AND
ITS APPLICATION

Bing-Wei Su and Su-Xiu Song

Beijing Institute of Radio Metrology & Measurement
Beijing, CHINA

ABSTRACT

This paper presents a new method which is used to measure time delay accurately by using a Type 900-LB Slotted Line. The accuracy for calibrating time delay of a precision coaxial air line Type 900-L is about $\pm(0.4-0.6)$ ps, and for coaxial cables with VSWR less than 1.5 and time delay t less than 50ns is about $\pm(3-5)$ ps.

Theoretical analysis and mathematical derivation of microwave networks in cascade are given in this paper. Methods to eliminate the errors which are caused by the discontinuities and the error analysis of the measuring system are presented.

In the last part of this paper, skin effect analysis of the transient characteristic of coaxial transmission line are discussed in detail. Methods to eliminate the errors which are resulted from using the calibrated time delay standard to calibrate time interval measurement instruments are presented. The estimation of errors and formulae for correction of those errors are described.

1. INTRODUCTION

Owing to the rapid growth of the requirement of measuring time delay accurately nowadays, a lot of commercial precision electronic instruments such as time delay generators with an accuracy ± 1 ns, electronic counters for time interval measurement with an accuracy of ± 100 ps, and coaxial time delay standard with

an accuracy of ± 50 ps have been developed and manufactured. Since frequency f is the reciprocal of period T and there is no difficulty to set a frequency within the accuracy of $\pm 1 \times 10^{-9}$, it is possible to measure the time delay of a coaxial transmission line accurately by means of frequency domain measurement method. By using the method described in this paper a coaxial cable with VSWR less than 1.5 and time delay t less than 50ns has been measured. The accuracy of measuring the time delay of that cable is about $\pm(3-5)$ ps. Skin effect analysis of the transient characteristic of coaxial transmission line have been discussed in detail. The effect of the inductive component and resistive component of the coaxial line on pulse transient characteristic have been analyzed and estimated also. This paper indicates how to correct the error which is caused by skin effect, in this consequence measuring and transfer accuracy has been increased. When the calibrated time delay standard is used to calibrate a precision time measurement counter, the total calibration uncertainty is about ± 10 ps.

II Principle and Method of Measurement

2.1 The principle of measurement is based on the method of measuring the displacement of the minimum of the standing wave pattern as shown in Fig.1.

When the device under test (DUT) is disconnected and connected between the Slotted Line and Short, the displacement of the minimum of the standing wave pattern is Δd . The time delay t of the device under test at measuring frequency is known as

$$t = \frac{n}{2} \frac{1}{f} \pm \frac{\Delta d}{c} \quad (1)$$

Where c is the velocity of the electromagnetic wave and n is any positive integer.

2.2 Method of Measurement

There are two methods to measure the time delay of coaxial transmission line accurately by using a Type 900-LB Slotted Line.

They are the periodic and the nonperiodic method.

Periodic Method

When the time delay of the DUT is exactly $n/2$ multiples of the period of the measuring frequency, the Δd in eq.(1) equals zero. Through properly adjusting the measuring frequency the displacement of the minimum of the standing wave pattern Δd should approach zero, when the DUT is disconnected and connected between the Slotted Line and Short. Then the time delay of the DUT at measuring frequency is

$$t = \frac{n}{2} \frac{1}{f}$$

This method is called "Periodic Method". It is suitable to measure the time delay of two port devices with small VSWR.

If S_{11} , S_{22} and S_{21} are the scattering parameters of the reversible two ports DUT then the maximum measured phase and time delay errors can be represented as

$$\begin{aligned} \Delta \phi &\approx \pm \sin^{-1} \left(\frac{|S_{11}| + |S_{21}|^2 |S_{22}|}{|S_{21}|^2} \right) \quad (\text{degree}) \\ \Delta t &= \frac{\Delta \phi}{720} \cdot \frac{1}{f_{GHz}} \quad (ns) \end{aligned} \quad (2)$$

Nonperiodic Method

If the VSWR of the DUT is rather large, the measured phase error $\Delta \phi$ in eq.(2) will be quite large and it is difficult to adjust the measuring frequency properly to make the displacement of minimum of the standing wave pattern Δd approach zero, so that the measured time delay error Δt would be rather large. In such condition it is impossible to acquire an accurate time delay measurement by making measurement at one frequency only; the nonperiodic method which makes time delay measurement with a series of measuring frequencies is required.

2.3 Example of measurement

Use the nonperiodic method to measure the time delay of a piece of coaxial cable with N connectors.

In order that the coaxial cable can be inserted into the Type

900-LB Slotted Line system, the coaxial cable with Type N connectors has to be connected with the Type 900-QNJ adaptors as shown in Fig. 2.

The system of connection is as in Fig. 1. When the DUT is inserted in system at terminal 1-1, the minimum of the standing wave pattern would shift. The method, which evaluate the time delay of the DUT by means of measuring the displacements of minimum and the measuring frequencies, is called nonperiodic method, and eq. (1) is suitable for this method to calculate the time delay.

The measurement procedure is as follows.

1. According to a certain test frequency f_1 , there is a corresponding displacement of minimum Δd_1 , and the time delay (including the two Type 900-QNJ adaptors in this example) can be evaluated.
2. Repeat a series of time delay measurement by changing the test frequency in fixed frequency intervals, and obtain a set of time delay data which would be changing periodically with frequency.
3. As shown in Fig.2. the measuring terminal is changed owing to the adding of Type 900-QNJ adaptors. They are shifted from terminals T_1 and T_2 to terminals 1-1 and 2-2 respectively. There would be discontinuities at terminal T_1 , and T_2 owing to the mismatch between the coaxial cable and Type N connectors. In general the VSWR of conventional coaxial cables are about 1.3 to 1.5 and the VSWR of Type 900-QNJ adaptors are 1.1016 at 3 GHz so that it can be neglected as compared with the coaxial cable.

There are rapid periodic variations in the time delay data, owing to the discontinuity at T_1 , and the error of measurement can be minimized by taking the arithmetical mean value of the maximum and minimum time delay values in the frequency range of interest. But the discontinuity at T_2 would introduce unnoticed systematic error if the terminal T_2 is connected directly to the Short Type 900-WNC. In our experimental system terminal T_2 is connected through a Type 900-QNJ adaptor to the Short Type 900-WNC. The electric length of the Type 900-QNJ adaptor is 5cm, so that there are slow periodic variations (about 3000MHZ) superimposed on the

rapid periodic variations in the time delay data. In order to increase the electric length a piece of Type 900-L30 Air Line is added between terminal 2-2 and the Type 900-WNC Short, then the frequency of slow periodic variation becomes 428.6 MHz and it is acceptable in this experiment. By using the method described above, a set of time delay data with two kinds of periodic variations would be present; take the arithmetical mean value of the maximum and minimum time delay values in the frequency range of interest as the required time delay datum. Then the systematic error owing to the discontinuities at Terminal T₁ and T₂ can be eliminated.

4. Why are there two kinds of periodic variation in the time delay data? There is a $e^{-j2\beta(l+l_{20})}$ term in eq.(4) (section III), which is introduced by the reflection at the M network in Fig 3. Let $l_1 = l + l_{20}$, then $e^{-j2\beta(l+l_{20})}$ changes into $e^{-j2\beta l_1}$. The condition for producing a periodic variation is $2\beta l = 2n\pi$, therefore the frequency interval for a rapid periodic variation is

$$\Delta f = \frac{c}{2l_1} \quad (3)$$

For example $l_1 = l + (l_{20} + l_{30}) = l + l'_{20} = 267.5 \text{ cm}$

l --electric length of the coaxial cable with Type N connectors

l_{20} --electric length of Type 900-QNJ Adaptor

l_{30} --electric length of Type 900-L30 Air Line

l'_{20} --electric length of Type 900-QNJ Adaptor and 900-L30 Air Line.

put the value of l_1 into eq. (3) and obtain $\Delta f_1 = 56 \text{ MHz}$

In the same way the slow periodic variation which is caused by the reflections at N network in Fig 3. can be analyzed.

If the Type 900-L30 Air Line is connected in the measuring system the frequency interval for it would become

$$\Delta f_2 = 428.6 \text{ MHz}$$

The calculated values of Δf_1 and Δf_2 are well matched with the experimental curve shown in Fig. 6.

5. Evaluate the time delay of the coaxial cable under test.

In this paper a Type N connector coaxial cable with a Type 900-QNJ

adaptor at each end is used as a device under test (DUT). Take the arithmetical mean value of the maximum and minimum time delay value to obtain the accurate time delay value of the DUT.

$$t = \frac{1}{2} (t_{\max} + t_{\min}) = 8209.6 \text{ ps.}$$

The time delay of the air line has been discounted from this value.

III Theoretical Analysis of Microwave Networks in Cascade

Let l represent the electric length of the coaxial cable, l_{10} and l_{20} the electric length of Type 900-QNJ adaptors, l'_{20} is the electric length of Type 900-QNJ adaptor and Type 900-L30 Air Line as shown in Fig.3. Terminal 1-1 is connected to the output terminal of the 900-LB Slotted Line and Terminal 2-2 (or 2'-2') is connected to the Type 900-WNC Short.

Use m_{11} , m_{21} , m_{12} and m_{22} to represent the scattering matrix elements of the connector pair M and n_{11} , n_{21} , n_{12} and n_{22} to represent the scattering matrix elements of the connector pair N. Use S_{11} , S_{21} , S_{12} and S_{22} to represent the scattering matrix elements of the network between the terminals T_1 and T_2 and S'_{11} , S'_{21} , S'_{12} and S'_{22} to represent the scattering matrix elements of the network between the terminals 1-1 and 2-2 (or 2'-2').

When terminal 2-2 (or 2'-2'), is connected to the Type 900-WNC Short, the reflection coefficient Γ'_1 at terminal 1-1 can be represented as (see appendix I)

$$\Gamma'_1 \simeq -m_{12}n_{12}m_{21}n_{21}e^{-j2\beta(l+l_{10}+l_{20})}(1+2\delta)\left[1 - \frac{m_{11}e^{j2\beta(l+l_{20})}}{m_{21}m_{12}n_{12}n_{21}}(1-2\delta) - \frac{n_{11}e^{j2\beta l_{20}}}{n_{12}n_{21}}(1-\delta) - n_{22}e^{-j2\beta l_{20}} - n_{12}n_{21}m_{22}e^{-j2\beta(l+l_{20})}(1+\delta)\right] \quad (4)$$

The $m_{12}n_{12}m_{21}n_{21}e^{-j2\beta(l+l_{10}+l_{20})}$ term in eq.(4) represents the required quantity for the time delay measurement of the DUT, and the other four terms in the bracket represent the rapid and slow periodic variations of the time delay measurement data. If there is no l_{20} , n_{11} and n_{22} would introduce an unnoticed systematic error. If l_{20} is very short, the frequency of the slow periodic variation would be very high (as described in Section II it is 3000MHZ). After adding

a 30 Cm precision air line the frequency decreases to 428.6MHZ. In the point of view of our experiment it is acceptable and easy to be realized.

The phase angle $\beta(l+l_{10}+l'_{20})$ in eq.(4) corresponds to the time delay between terminals 1-1 and 2'-2', from which the time delay of the DUT can be evaluated by subtracting 1.0012 ns, the time delay of the precision air line Type 900-L30.. If the time delay of the two 900-QNJ adaptors are subtracted, the time delay of the coaxial cable with Type N connector can be obtained.

It doesn't introduce systematic error in time delay measurement when the DUT has loss, but it increases the random error as the sharpness of the minimum of the standing wave pattern decreases.

Proceed the error analysis according to eq.(4) as follows

1. Let the VSWR of the DUT be 1.5, then $|S_{11}| = |S_{22}| = 0.2$, $|m_{22}| = |n_{11}| = 0.1$ so that $|\delta| = 0.01$. Under the worst phase combination it corresponds to a phase angle of 1.15° . When the measuring frequency is 4 GHz, it just introduces an error of 0.4 ps.

2. The effect of m_{12} n_{12} m_{21} n_{21} .

Evaluate m_{12} m_{21} as shown in Fig. 4.

Evaluate n_{12} n_{21} by the same way.

If the transmission line has an impedance discontinuity at a certain interface, we use network M to represent this discontinuity and let m_{11} , m_{21} , m_{12} and m_{22} represent the elements of the M matrix. For convenience use normalized impedance in Z_1 and Z_2 . Let $Z_1 = 1$, $Z_2 = 1+x+jy$ There is the following relation

$$m_{12}m_{21} = \frac{1}{1 + \frac{(x+jy)^2}{4(1+x+jy)}} = 1 + \delta' \quad \text{where } \delta' = \frac{-(x+jy)^2}{4(1+x+jy)}$$

since $|S_{11}| = |S_{22}| = 0.2$ $x = 0.1$, $y = 0.1$ so that $\delta' \leq 0.01$ In the same way n_{12} $n_{21} = 1 + \delta'$ then m_{12} m_{21} n_{12} $n_{21} \approx 1 + 2\delta'$ (5)

From eq.(5) it introduces a 0.4 ps time delay uncertainty, but in precision time delay measurement, this uncertainty can be eliminated by interchanging the input and output of the DUT in two measurements and taking the mean value.

3. Analysis about the effects of the other four terms in the bracket

Consider the $\frac{m_{11} e^{j2\beta(l+l_{20})}}{m_{12} m_{21} n_{12} n_{21}} (1-2\delta)$ term and $n_{12} n_{21} m_{22} e^{-j2\beta(l+l_{20})} (1+\delta)$

term first. Neglect δ as a small quantity, and assume the M matrix is lossless, then the extrema of the expression

$$1 - \frac{m_{11} e^{j2\beta(l+l_{20})}}{m_{12} m_{21} n_{12} n_{21}} - n_{12} n_{21} m_{22} e^{-j2\beta(l+l_{20})} \quad (6)$$

are $1+g+jh$ and $1-g-jh$, they correspond to the phase angles

$$\theta_1 = \tan^{-1} \frac{h}{1+g}, \quad \theta_2 = \tan^{-1} \frac{-h}{1-g} \quad (7)$$

Then the expression for the phase error $\Delta\theta$, while taking the mean value of the extrema as the time delay, is

$$\Delta\theta \approx \frac{1}{2} \tan^{-1} (-2gh) \quad (8)$$

In the same way, the effect of the two terms $\frac{n_{11} e^{j2\beta l_{20}}}{n_{12} n_{21}} (1-\delta)$

and $n_{22} e^{-j2\beta l_{20}}$ can be considered.

Since $|S_{11}| = |S_{22}| = 0.2$, $g \leq 0.14$ $h \leq 0.14$

then $\Delta\theta/2 = 35'$ it corresponds to a 0.4ps time delay uncertainty.

When taking the mean value of the extrema as the time delay of the DUT, the four terms in the bracket would introduce an uncertainty of $2 \times 0.4ps$.

IV Measurement Errors

There are eight kinds of errors source for the time delay measurements of two ports DUT in the Type 900 system.

1. The frequency instability of the signal generator introduce the error Δt_1

$$\Delta t_1 = \frac{\Delta f}{f} \cdot t$$

in example above $\Delta t_1 = \pm 0.4ps$.

2. The inaccuracy of the slotted line scale introduces the error Δt_2 . The inaccuracy of the slotted line scale is 0.1mm, (with the micrometer it can be decreased to 0.01 mm).

so that $\Delta t_2 = \pm 0.33 ps$.

3. The Type 900-L30 precision Air Line introduces time delay error Δt_3 . In the measuring system, a Type 900-L30 Precision Air Line is added to increase the electric length of λ_{20} , and its time delay is 1001.2 ± 0.4 ps, so that it introduces the error Δt_3 .

$$\Delta t_3 = \pm 0.4 \text{ ps.}$$

4. The M and N networks of the connector pairs would introduce the error Δt_4 .

This error comes from the δ term in eq. (4) and it has been described in part III

$$\Delta t_4 = \pm 0.4 \text{ ps.}$$

5. The test frequency interval can't be infinitesimal, it would introduce the error Δt_5 .

Since a series of measured time delay data of the required measuring frequencies are required to obtain the extrema, the smaller the measuring frequency interval, the more accurate extrema can be obtained. In the example described in Part II, the measuring frequency interval is 10MHZ, and a frequency interval of two to three MHZ can be used in the neighborhood of the extrema. According to the data analysis, the error Δt_5 is less than 1ps.

6. The reflection of the Type 900-BT connector would introduce the error Δt_6 .

Type 900-BT connectors are used in both the terminal 1-1 and 2-2 of the measuring system, and the time delay error introduced by them is less than 0.8 ps.

7. While taking the mean value of the extrema to evaluate the time delay it would introduce the error Δt_7 and Δt_8 .

As described in part III, $\Delta t_7 = \pm 0.4$ ps. $\Delta t_8 = \pm 0.4$ ps.

From Δt_1 to Δt_8 the total r.m.s. error is about 1.6 ps.

V Skin Effect Analysis of the Transient Characteristic of Coaxial Transmission Line.

The time delay of a coaxial transmission line changes with frequency. Since the series inductance changes with frequency owing to skin effect. For example if the time delay of a piece of coaxial cable

is 4996.64 ps at 1000MHZ it would change to 5000 ps at 3000MHZ. So that, when it is operated in a pulse condition, the risetime of the output pulse would be degenerated owing to the frequency response of time delay. If an input pulse with 1ns risetime is passing through a coaxial cable with 50ns time delay the rise time of the output pulse would change to 1.14ns. On the other hand the changing of series resistance owing to skin effect degenerates the risetime of the output pulse too. The magnitude of degeneration is a function of the attenuation of the coaxial cable and the risetime of the input pulse. If an input pulse with 1ns risetime is passing through a coaxial cable with 0.4 dB attenuation, the risetime of the output pulse would change to 1.03ns.

5.1 The relation between the frequency response of the series inductance and the pulse time delay and transient characteristic. As described above, the series inductive component increases as the frequency decreases so that the wave propagation speed through the cable decreases and the time delay increases. For this reason the calibrated time delay standard should be used at the calibrated frequency. If it is used on the other frequencies, correction should be taken. According to the relation between the electromagnetic wave propagation velocity and the inductive component, the formula of time delay as a function of frequency can be derived. (see appendix II)

$$t = t_0 \left(1 + \frac{b}{\sqrt{f_{GHz}}} \% \right) \text{ ns.} \quad (9)$$

As the existence of skin effect, the phase frequency characteristic is no longer linear. When working in a pulse condition, since the time delays are different for each of the harmonic components of the pulse, the resultant output waveform would change and the risetime degenerates as shown on Fig. 5.

This means, the frequency response of the inductive component would also degenerate the pulse output waveform besides the frequency response of the resistive component but, when using the calibrated time delay standard to calibrate time measurement in-

struments the effect of the inductive component is very small and can be neglected, provided the calibrating frequency of the time delay standard and the bias voltage of the calibrated equipment are properly selected.

$$\text{Let } U_1(t) = \frac{E}{2} + \frac{2E}{\pi} \sum_{\nu=0}^{\nu=\infty} \frac{\sin(2\nu+1)\Omega t}{2\nu+1} \quad (10)$$

where $\Omega = \frac{2\pi}{T}$ — fundamental angular frequency

E -- pulse (or square wave) amplitude

If the coaxial transmission line has ideal linear phase frequency characteristic and the module of the transmission coefficient is constant throughout the passband and equal to zero outside the passband, then the output can be represented as

$$U_2(t) = \frac{KE}{2} + \frac{2KE}{\pi} \sum_{\nu=0}^{\nu=\nu_m} \frac{\sin(2\nu+1)\Omega(t-t_c)}{2\nu+1} \quad (11)$$

where K -- the module of transmission coefficient

t_c -- delay time

Since the phase frequency characteristic is nonlinear owing to skin effect, the delay time is no longer constant and should be expressed as

$$t_x = t_0 \left(1 + \frac{b}{\sqrt{f_x \epsilon_h}} \right) \quad (12)$$

where t_0 -- delay time of zero depth of penetration

t_x -- delay time at frequency $f_x = x \cdot f$

f -- the highest harmonic frequency of the input pulse

$f \approx 0.35/d_0$

b -- correction coefficient

under this condition eq. (11) should change to

$$U_2(t) = \frac{KE}{2} + \frac{2KE}{\pi} \sum_{\nu=0}^{\nu=\nu_m} \frac{\sin(2\nu+1)\Omega(t-t_x)}{2\nu+1} \quad (13)$$

When the bias voltage equals to $KE/2$, there is a delay time, $t=t_A$ which satisfies the following formula (14)

$$\sum_{\nu=0}^{\nu=\nu_m} \frac{\sin(2\nu+1)\Omega(t_A-t_x)}{2\nu+1} = 0 \quad (14)$$

$$t_A - t_x = t_0 b \left(\frac{1}{\sqrt{A}} - \frac{1}{\sqrt{X}} \right) \frac{1}{\sqrt{f_0 \text{ GHz}}} \% \quad (15)$$

$$f_A = A \cdot f_0 \quad (16)$$

Substituting formulae (15) and (16) into formula (14) and taking integrating we get

$$A \approx 0.3 \quad (17)$$

so that
$$t_A = t_0 \left(1 + \frac{b}{\sqrt{0.3 f_0 \text{ GHz}}} \% \right) \quad (18)$$

According to the preceding analysis, when $KE/2$ is used as the bias voltage, $0.3 f_0$ should be taken as the calibrating frequency for the time delay standard. For example, if the input pulse $E=0.5V$ and the pulse risetime $\bar{\sigma}_0=0.1ns$, then $f_0=3.5GHZ$. When use $0.25V$ as the bias voltage, the time delay data should be taken at the measuring frequency $f=1.05GHZ$ as the standard time delay value for this specified condition.

Besides, from eq. (12) and Fig. 5. it is evident that the time of the lower part of the leading edge of the delayed pulse corresponds to delay time of its higher harmonics. So that, when the risetime and the amplitude of the input pulse are rather large $KE/10$ (or smaller) may be used as the bias voltage, and f_0 is taken as the calibrating frequency for the time delay standard. When using the calibrated time delay standard to calibrate time measurement instruments the error which is caused by the frequency response of the inductive component, can be eliminated by using the method described above.

5.2 The distortion of pulse transient characteristic owing to the skin effect of resistive component.

When a pulse passes through a coaxial cable, the output waveform would be degenerated owing to the changing of the high frequency loss of the coaxial cable. But in general the dielectric loss is much smaller than the resistive loss.

1. The expression of resistive component in coaxial cable may be expressed as

$$R = \frac{\rho_b}{2\pi\delta_b b_o} + \frac{\rho_a}{2\pi\delta_a a_o} \quad (19)$$

where δ_b , δ_a are the skin depths of the inner and outer conductors ρ_b , ρ_a are the resistivities of the materials of the inner and outer conductors.

b_o , a_o are the radius of the inner and outer conductors

It shows that the changing of the resistive component owing to skin effect of the coaxial cable increases with frequency. It doesn't introduce time delay measurement error when the standard is calibrated at a single frequency but it would degenerate the output pulse. Since the higher harmonics have larger attenuation so the risetime of the output pulse would increase. If the bias voltage used is not zero, time delay measurement error is introduced. The larger the bias voltage used, the larger the time delay measurement error that would be introduced, but by using the correction formula (22) given below, this error term can be reduced by a factor of 10.

2. Correction formula for reducing the time delay measurement error owing to the resistive component

Considering the resistive loss of the coaxial cable, the increment of the risetime can be evaluated as (see appendix IV)

$$\Delta\sigma' = \delta_o a_s$$

where
$$a_s = \frac{2}{3}\alpha_{f_o} - \frac{1}{4}(\alpha_{f_o})^2 + \frac{1}{15}(\alpha_{f_o})^3 - \dots \quad (20)$$

α_{f_o} -- the attenuation nB at the highest frequency $f_o = 0.35/\delta_o$

δ_o -- the risetime of the input pulse

As described above if 0.1KE or 0.5KE is used as bias voltage the correction value should be

$$\begin{aligned} \Delta\sigma_1 &= 0.1\delta_o a_s && \text{for 0.1KE bias voltage} \\ \Delta\sigma_2 &= 0.5\delta_o a_s && \text{for 0.5KE bias voltage} \end{aligned} \quad (21)$$

So that in a pulse condition the effective standard delay time of the calibrated time delay standard should be

$$\begin{aligned}
 t_s &= t_h + 0.1 \delta_0 a_s \approx t_h + \frac{\alpha_{fs}}{15} \delta_0 \\
 t'_s &= t'_h + 0.5 \delta_0 a_s \approx t'_h + \frac{\alpha_{fs}}{3} \delta_0
 \end{aligned}
 \tag{22}$$

where t_s --effective standard delay time of the calibrated time delay standard, when the input pulse risetime is δ_0 and the bias voltage is 0.1KE.

t'_s -- the same as t_s , except 0.5KE is used as bias voltage

t_h --delay time of the calibrated time delay standard at frequency f_0 .

t'_h -- the same as t_h , except it is at frequency $0.3 f_0$.

δ_0 -- the risetime of the input pulse

α_{fs} -- the attenuation in neper of the time delay standard at frequency f_0 .

VI Conclusion

1. This paper presents a new method to calibrate the time delay standard (coaxial cable). The accuracy of calibration is $\pm(3-5)$ ps.
2. When we use the calibrated time delay standard to calibrate precision time measurement instruments, we must use formula (22) to evaluate effective standard delay time for correcting the errors owing to skin effect.
3. When we use the calibrated time delay standard to calibrate precision time measurement instruments, two additional errors should be considered as follows.
 - a. The evaluation of the highest limiting frequency may have a tolerance of 10%, and it introduces an error $\Delta t'_1$.

$$\Delta t'_1 = 0.054 \frac{t_0 b}{\sqrt{f_0 \epsilon H_0}}$$

when $f_0 = 0.35$ GHZ, $b = 0.0816$, $t_0 = 8200$ ps, $\Delta t'_1 = 0.61$ ps

when $f_0 = 0.35$ GHZ $b = 0.0816$, $t_0 = 50.000$ ps $\Delta t'_1 = 3.72$ ps

It is evident the higher the f_0 , the smaller the $\Delta t'_1$.

b. 10% tolerance of the bias voltage used may introduce an error $\Delta t_2'$.

$$\Delta t_2' = 0.0067 \alpha_f \delta_0 \quad \text{for } 0.1\text{KE bias voltage}$$

$$\Delta t_2' = 0.033 \alpha_f \delta_0 \quad \text{for } 0.5\text{KE bias voltage}$$

Since α_f is proportion to $\sqrt{f_0}$, and $\delta_0 \approx 0.35/f_0$, then $\Delta t_2'$ decreases as δ_0 decreases in the rate of $\sqrt{f_0}$.

In general, for an input pulse with $E \geq 2\text{V}$, $\delta_0 \leq 1\text{ns}$ or $E \geq 0.5\text{V}$, $\delta_0 \leq 0.1\text{ns}$, using the calibrated time delay standard to calibrate time measurement instruments, the additional error owing to skin effect is less than $\pm 5\text{ps}$.

So that, when the calibrated time delay standard is used to calibrate a precision time measurement instrument (counter), the total calibration uncertainty is less than $\pm 10\text{ps}$.

Appendix I

Formula derivation for the reflection coefficient at the input terminal of the microwave networks in cascade.

As shown in Fig. 3. the microwave networks has the following relation

$$\begin{aligned} b_1 &= m_{11} a_1 + m_{12} A_2 \\ B_2 &= m_{21} a_1 + m_{22} A_2 \end{aligned} \quad (1)$$

and

$$\begin{aligned} A_1 &= B_2 e^{-j\beta l} \\ A_2 &= B_1 e^{-j\beta l} \end{aligned} \quad (2)$$

$$\begin{aligned} B_1 &= n_{11} A_1 + n_{12} a_2 \\ b_2 &= n_{21} A_1 + n_{22} a_2 \end{aligned} \quad (3)$$

where β --phase constant, thus

$$\begin{aligned} S_{11} &= m_{11} + \frac{m_{12} m_{21} n_{11} e^{-j2\beta l}}{1 - m_{22} n_{11} e^{-j2\beta l}} \\ S_{22} &= n_{22} + \frac{n_{12} n_{21} m_{22} e^{j2\beta l}}{1 - m_{22} n_{11} e^{-j2\beta l}} \\ S_{21} &= \frac{m_{21} n_{21} e^{-j\beta l}}{1 - m_{22} n_{11} e^{-j2\beta l}} \\ S_{12} &= \frac{n_{12} m_{12} e^{-j\beta l}}{1 - m_{22} n_{11} e^{-j2\beta l}} \end{aligned} \quad (4)$$

Since the Type 900-QNJ Adaptors have electric length the S' matrix of the network between terminal 1-1 and 2-2

becomes

$$\begin{aligned} S'_{11} &= S_{11} e^{-j2\beta l_{10}} \\ S'_{22} &= S_{22} e^{-j2\beta l_{20}} \\ S'_{12} &= S_{12} e^{-j\beta(l_{10} + l_{20})} \\ S'_{21} &= S_{21} e^{-j\beta(l_{10} + l_{20})} \end{aligned} \quad (5)$$

Let $\delta = m_{22} n_{11} e^{-j2\beta l}$, eq. (5) can be rewritten as

$$\begin{aligned} S'_{11} &\approx m_{11} e^{-j2\beta l_{10}} + m_{12} m_{21} n_{11} e^{-j2\beta(l + l_{10})} (1 + \delta) \\ S'_{22} &\approx n_{22} e^{-j2\beta l_{20}} - n_{12} n_{21} m_{22} e^{-j2\beta(l + l_{20})} (1 + \delta) \\ S'_{12} &\approx n_{12} m_{12} e^{-j\beta(l + l_{10} + l_{20})} (1 + \delta) \\ S'_{21} &\approx m_{21} n_{21} e^{-j\beta(l + l_{10} + l_{20})} (1 + \delta) \end{aligned} \quad (6)$$

According to theory of the network analysis, the expression for the reflection coefficient at the input terminal of the S' network is

$$\Gamma' = S'_{11} + \frac{S'_{12} S'_{21} \Gamma_L}{1 - S'_{22} \Gamma_L}$$

where Γ_L is the reflection coefficient of the termination of the network. When this S' network is terminated a Short, $\Gamma_L = -1$

$$\Gamma' = S'_{11} - \frac{S'_{12} S'_{21}}{1 + S'_{22}} \quad (7)$$

Substituting eq. (6) into eq. (7) and neglecting δ^2 and higher order terms of the small quantities the expression for the reflection coefficient at terminal 1-1 becomes

$$\begin{aligned} \Gamma'_1 = & -m_{12} n_{12} m_{21} n_{21} e^{-j2\beta(l+l_{20})} (1+2\delta) \left[1 - \frac{m_{11} e^{j2\beta(l+l_{20})}}{m_{12} m_{21} n_{12} n_{21}} (1-2\delta) - \frac{n_{11} e^{j2\beta l_{20}}}{n_{12} n_{21}} (1-\delta) - \right. \\ & \left. - n_{12} n_{21} m_{22} e^{-j2\beta(l+l_{20})} (1+\delta) - n_{22} e^{-j2\beta l_{20}} \right] \quad (8) \end{aligned}$$

This is the eq. (4) in this paper.

Appendix II

Formula derivation for the relation between delay time and measuring frequency.

In lossless coaxial transmission line the propagation velocity of the electromagnetic wave is

$$V = \frac{1}{\sqrt{LC}} \quad (9)$$

where L --inductance per unit length

C --capacitance per unit length

The delay time for a piece of transmission line is inversely proportional to the propagation velocity

$$t \propto \frac{1}{V} \quad (10)$$

$$\text{Thus } t \propto \sqrt{L} \quad (11)$$

the expression of inductance for zero skin depth is

$$L_0 = 2 \ln \frac{D_0}{d_0} \times 10^{-9} \text{ H/cm} \quad (12)$$

where D_0, d_0 --the inner diameter of the outer conductor and the outer diameter of the inner conductor respectively.

In those frequencies, where skin effect can not be neglected, the effective diameters of the inner and outer conductors of the coaxial transmission line are no longer their mechanical dimensions d_0 and D_0 . In this case, the effective diameter of the outer conductor increases with the amount of skin depth, on the contrary, the effective diameter of the inner conductor decreases with the amount of the skin depth. So that, the value of inductance is no longer expressed as eq. (12) it should change to

$$L = 2 \ln \frac{D}{d} \times 10^{-9} \text{ H/cm} \quad (13)$$

where D, d --the effective diameters of the outer and inner conductors considering the skin effect.

From eq. (11), (12) and (13) we get

$$\frac{\Delta t}{t_0} = \frac{\sqrt{L} - \sqrt{L_0}}{\sqrt{L_0}} \% \quad (14)$$

From eq. (14) we can express the time delay as the function of measuring frequency

$$t = t_0 \left(1 + \frac{b}{\sqrt{f_{GHz}}} \% \right) \quad (15)$$

where b -- correction coefficient for the inductive component variation owing to skin effect.

Coefficient b is the function of the diameter of the coaxial transmission line, and the resistivity of the conductors. Here are some examples for the Type 900-LZ Reference Air Line b is 0.0284, and for the Type SYV-50-5 and SYV-50-2-2 coaxial cables made in China b is 0.0816 and 0.1711 respectively.

Appendix III

The relation between the risetime of the output pulse and the bandwidth.

Let the expression for input pulse (square wave)

$$\text{as } U_1(t) = \frac{E}{2} + \frac{2E}{\pi} \sum_{\nu=0}^{\nu=\infty} \frac{\sin(2\nu+1)\Omega t}{2\nu+1} \quad (16)$$

where $\Omega = \frac{2\pi}{T}$ — fundamental angular frequency

E -- amplitude of the input pulse (square wave)

When the input pulse has passed through an ideal network which has linear phase frequency characteristic and constant transmission coefficient inside the pass band and zero transmission coefficient outside the pass band, the output pulse becomes

$$U_2(t) = \frac{KE}{2} + \frac{2KE}{\pi} \sum_{\nu=0}^{\nu=\mu_m} \frac{\sin(2\nu+1)\Omega(t-t_c)}{2\nu+1} \quad (17)$$

where K -- transmission coefficient

t_c -- delay time

μ_m -- the maximum value which depends on the highest order $(2\mu_m+1)$ of harmonics which can pass through the network.

$$\text{It is evident that } (2\mu_m+1)\Omega \leq \omega_0 \quad (18)$$

where ω_0 -- the highest angular frequency of the passband.

Differentiate with respect to eq. (17)

$$\frac{dU_2(t)}{dt} = \frac{2KE\Omega}{\pi} \sum_{\nu=0}^{\nu=\mu_m} \cos((2\nu+1)\Omega(t-t_c)) \quad (19)$$

$$\text{when } t = t_c, \quad \left[\frac{dU_2(t)}{dt} \right]_{\max} = 2KEf_0 \quad (20)$$

where f_0 -- the highest frequency of the passband.

So that the risetime of the output pulse can be expressed

$$\text{as } \delta_0 = \frac{KE}{\left[\frac{dU_2(t)}{dt} \right]_{\max}} = \frac{0.5}{f_0} \quad (21)$$

In practice, when $\omega > \omega_0$, the transmission coefficient is not zero, but it decreases rapidly as the frequency increases. So that in general the following formula is used instead of (21)

$$\delta_0 \approx \frac{0.35}{f_0} \quad (22)$$

Appendix IV

Formula derivation for the output pulse risetime increment owing to the variation of coaxial transmission line loss.

Assume that the coaxial transmission line has linear phase frequency characteristic, When an input pulse expressed as eq. (16) passes through a piece of coaxial transmission line with loss, the amplitude frequency characteristic of the output pulse can be expressed as

$$U_2(t) = \frac{E}{2} + \frac{2E}{\pi} \sum_{\nu=0}^{\nu=\nu_m} \frac{\sin(2\nu+1)\Omega(t-t_c)}{2\nu+1} e^{-\alpha} \quad (23)$$

where α --attenuation of coaxial transmission line in neper

$$\alpha = \frac{\alpha'}{8.68} l \quad (\text{Neper}) \quad (24)$$

For conventional coaxial cable

$$\alpha' = 2.98 \times 10^{-9} \sqrt{f} \frac{1}{a_o} \left(\frac{a_o}{b_o} + 1 \right) \frac{\sqrt{\epsilon_r}}{\ln \frac{a_o}{b_o}} \quad (\text{dB/cm}) \quad (25)$$

Where b_o , a_o --the radius of the inner and outer conductors respectively

ϵ_r --relative dielectric constant of the dielectric medium

f -- frequency

According to eq. (25), can rewrite eq. (24) to

$$\alpha = K \sqrt{f} \quad (26)$$

Differentiate with respect to eq. (23)

$$\frac{dU_2(t)}{dt} = \frac{2E\Omega}{\pi} \sum_{\nu=0}^{\nu=\nu_m} \cos(2\nu+1)\Omega(t-t_c) e^{-\alpha(f)} \quad (27)$$

since $\alpha_{f_x} = \sqrt{x} \alpha_{f_o}$, make transformation $x = \nu/\nu_m$ and integrate when $t=t_c$ (assumed t_c is constant), there is

$$\left[\frac{dU_2(t)}{dt} \right]_{\max} = \frac{E\omega_o}{\pi} \left(1 - \frac{2}{3} \alpha_{f_o} + \frac{1}{4} (\alpha_{f_o})^2 - \frac{1}{15} (\alpha_{f_o})^3 + \dots \right) = 2E f_o a \quad (28)$$

$$\begin{aligned}
 a &= 1 - \frac{2}{3}\alpha_f + \frac{1}{4}(\alpha_f)^2 - \frac{1}{15}(\alpha_f)^3 + \dots \\
 a_s &= 1 - a = \frac{2}{3}\alpha_f - \frac{1}{4}(\alpha_f)^2 + \frac{1}{15}(\alpha_f)^3 - \dots
 \end{aligned}
 \tag{28}$$

where α_f --attenuation in neper at the highest frequency f ,
 f , -- the highest harmonic frequency of the input pulse

take $f_s = 0.35/\delta_s$

δ_s --risetime of the input pulse

thus, the increment of the output pulse risetime can be obtained

$$\Delta\delta' = \delta_s a_s
 \tag{29}$$

Reference

1. "Type 900 Reference Coaxial Air Line", General Radio Company, U.S.A.
2. R.L. WIGINGTON AND N.S. NAHMAN "Transient Analysis of Coaxial Cables Considering Skin Effect" PIRE, Vol. 45, February 1957. p.166.
3. "Type 900-LB Precision Slotted Line", General Radio Company, U.S.A.
4. Gerhard Megla, "Dezimeterwell entechnik. "Fachbuchverlag Leipzig 1954.
5. S. Ramo and J.R. Whinnery, "Fields and Waves in Modern Radio," 3rd ed., 1946.
6. David M. kerns, "Definitions of u,i,z,y,a,b, Γ and S," Proc. IEEE, Vol. 55, pp. 892--900, June 1967.

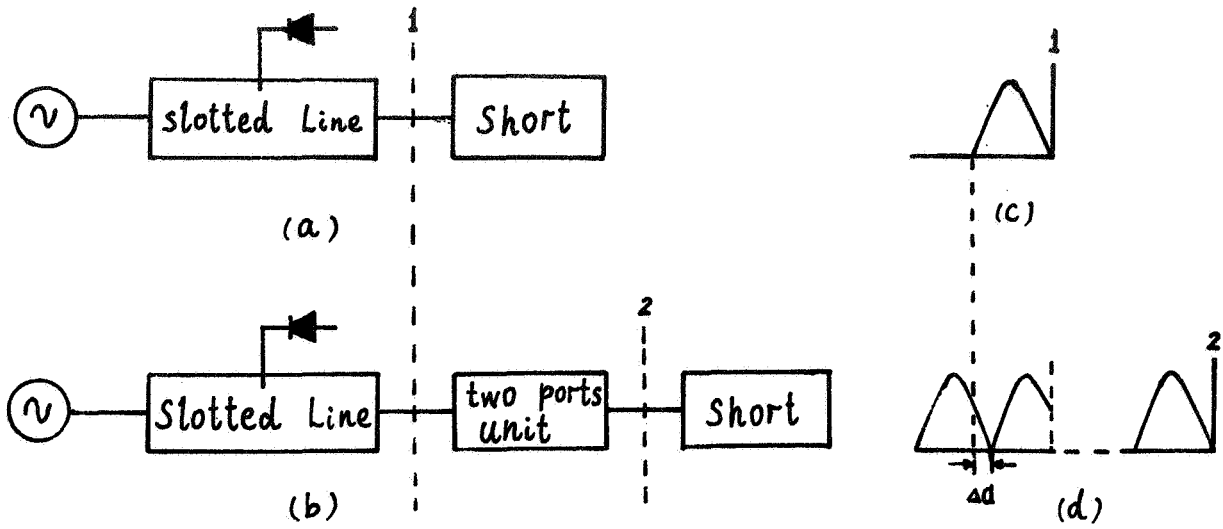


Fig.1 principle diagram for time delay measurement with microwave system

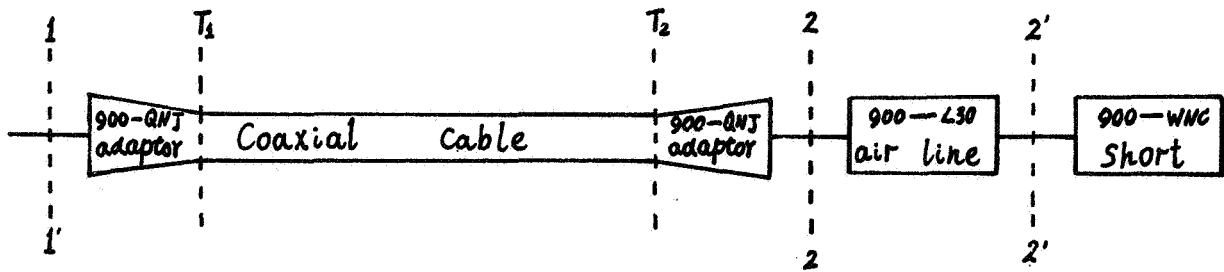


Fig.2 Using the nonperiodic method to measure coaxial cables with Type N connectors

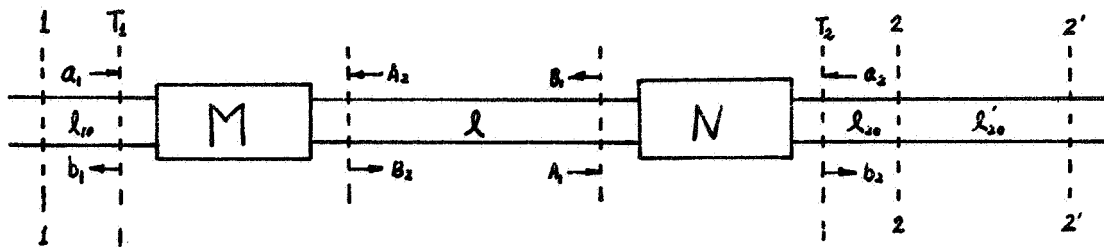


Fig.3 Theoretical analysis of microwave networks
in cascade



Fig. 4

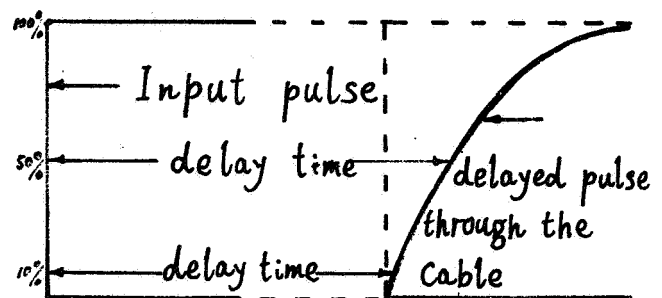


Fig. 5

Fig.4 Analysis at the discontinuity of network M

Fig.5 Step response distortion owing to non-linear phase
frequency characteristic of skin effect

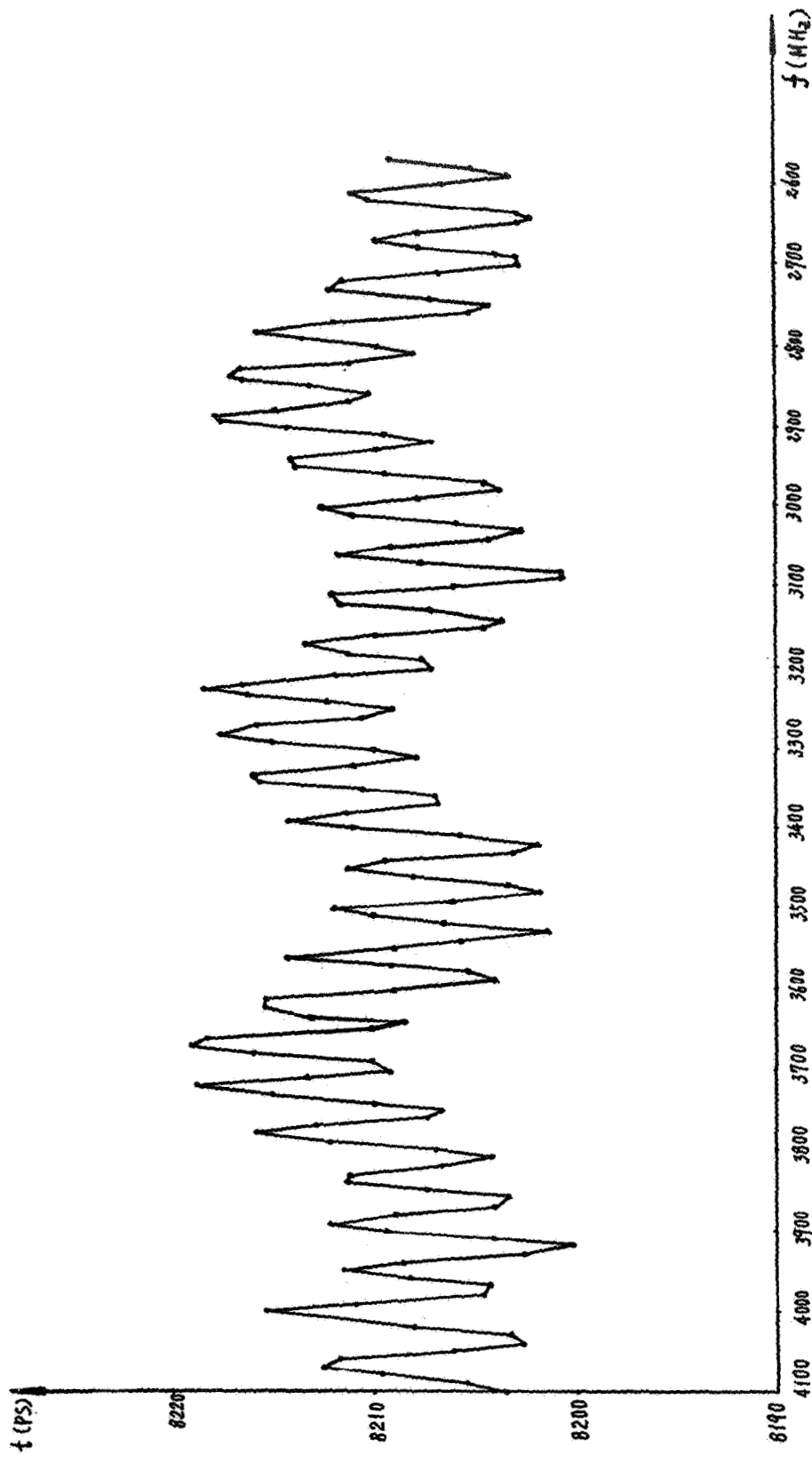


Fig. 6 Delay Time Versus frequency

QUESTIONS AND ANSWERS

None for Paper #8

NAVEX - A SPACE SHUTTLE EXPERIMENT
WITH ATOMIC CLOCKS

S. Starker, H. Nau, J. Hammesfahr (DFVLR *)
H. Tschiesche (SEL **), F.R. Germany

ABSTRACT

NAVEX is a navigation- and time transfer experiment. It will be flown within the payload of the first German Spacelab mission D-1, scheduled in June 1985. The objectives of the experiment are to synchronize distant ground stations with an accuracy of better than 10 nsec and to demonstrate one way ranging with an accuracy of better than 30 m. Spread spectrum signals will be used and the related technique will be tested. On board a Cs and a Rb clock will be used. The relativistic effect of these clocks will be about -25 μ sec per day. On the ground at least two receiving stations and one transmitting-receiving station will be installed. The synchronization of the ground clocks by Shuttle signals will be compared to those achieved with clock transportations and with GPS measurements. The paper gives a system description of this experiment, containing details on the technical concept, the hardware and the planned data evaluation. The present state of the preparatory work is briefly reviewed.

INTRODUCTION

The recent successful mission of the Space Shuttle Columbia was not only a considerable success for NASA; it was also a step forward for all those experimenters who make preparations for future investigations with the Shuttle.

Such preparations are also running in Europe on the basis of an agreement from 1973 between the United States and nine European countries who contribute to the European Space Agency (ESA). This agreement provides cooperation in the development and utilization of the new Space Transportation System (STS).

*) DFVLR = Deutsche Forschungs- und Versuchsanstalt für Luft- und Raumfahrt, Oberpfaffenhofen

***) SEL = Standard Elektrik Lorenz, Stuttgart

The work is sponsored by the 'Bundesministerium für Forschung und Technologie' (BMFT) of the Federal Republic of Germany.

The European contribution to the development of the STS comprises the development of a SPACELAB which houses astronautes and equipment in a terrestrial atmosphere, and the development of pallets and special structures which carry experiment equipment outside of the lab in the cargo bay of the Shuttle.

A special arrangement of SPACELAB and a unique support structure (USS) with some experimental equipment is shown in Fig. 1. This arrangement will be used on Shuttle Mission STS 26 which we call D-1-Mission, because it is the first flight booked by the Federal Republic of Germany. The SPACELAB and the pallet structure will have been space proved in earlier flights STS 9 and STS 19.

The pallet structure shown in Fig. 1 is also known under the name SPAS (Shuttle Pallet Satellite) and will be flown for the first time in spring 1983. During the D-1 Mission it will carry equipment for experiments NAVEX and MEA. MEA is a Material Experiment Assembly from the United States. NAVEX is an experiment of the Federal Republic of Germany with the aim to investigate future possible applications of space borne atomic clocks. It will be the first European step in this direction. Therefore the experiment will be confined to a few basic questions in this field: the investigation of a microwave link for comparison of on-board and ground based clocks and some test measurements for one way positioning. In both cases spread spectrum techniques with pseudo noise codes will be applied. In the following some more information on this experiment is given.

GENERAL VIEW

The Shuttle experiment NAVEX is part of the German SPACELAB utilization program. It arose from two proposals made by SEL and by DFVLR. The first concerned one-way ranging, the second time transfer with space borne clocks. During the succeeding study phase, both proposals were combined in a single experiment with the focal point on navigation; because of that the name NAVEX (= NAVIGATION EXperiment) was chosen.

Table I shows the main stages of the experiment evolution from proposals to the Shuttle Mission 1985. From 1977 until 1979 an engineering model was built and preliminary field measurements were performed.

Fig. 2 shows the configuration of field measurements. A Cs-clock on an airplane was compared with another on the ground by a two way microwave link. Additional range information for data analysis were received from simultaneous ranging with radar. The results were encouraging. A precision of $\sigma_t < 10$ nsec could be demonstrated (Fig. 3). Afterwards a time lag occurred because of funding problems and by the lack of a flight opportunity. In mid 1981 the decision was made for NAVEX participation in the D-1 mission. For that some conceptual and technical modifications and reductions had to be accepted.

The modified concept and the main objectives of the experiment are shown in Fig. 4. The two way clock comparison will be accomplished by L-Band signals. Simultaneous ranging with a C-band radar will allow the determination of the propagation effects of ionosphere and the true range between Shuttle and the ground control station. By additional receiving of the L-Band Shuttle signals at two ground receiving stations the Shuttle positions during the short visible arc can be determined. For this purpose the ground stations have to be equipped with atomic clocks, which must be synchronized by additional means. After the Shuttle positions and the true ranges to the different ground stations are known with an accuracy of $\sigma_r < 10$ m, the one way positioning of a ground receiving station can be tested.

In Fig. 5 the experiment configuration is shown with the main functions of the participating installations. For the coordination of several ground stations, a central operation control is provided. The station operation control requires orbit and attitude predictions of the Shuttle from the Payload Operation Control Center (POCC) at Houston. These data will be received via the German Payload Operation Center (GPOC). NAVEX housekeeping data transfer will occur via TDRSS. During ground station contacts the on-board measurement data will be transmitted to the ground by digital modulation of the L-Band carrier.

The synchronization of the ground station clocks will be done by clock transportation and by an additional microwave link. Concerning the latter, time transfer investigations with GPS and with a communication satellite are presently going on.

At the launch site the on-board clocks will have to be checked before and after the mission. For an accurate determination of the clock frequency difference on-board and on the ground, a frequency transfer from the launch site to the control station will be necessary. We think that GPS could be a good solution for this task. Finally, after all data and time transfer, the measurement results will have to be gathered, preprocessed and recorded for the off line data evaluation.

After this rough survey some details may be outlined.

EXPERIMENT EQUIPMENT

The NAVEX specific hardware consists of the on-board station, of one ground control station and two receiving stations; it has to be completed by an AN/MPS-36 radar and by additional equipment for tests, for data handling and for ground clock synchronization and frequency transfer.

The on-board equipment is mounted on three GAS-containers. (GAS = get away specials). These containers were chosen because they will be available and already space proved from another experimental program. These three containers and three antennas are mounted on a SPAS structure (Fig. 6). The accommodation in the cargo bay of the Shuttle is shown in Fig. 7. The geometry is such that cable lengths between containers and the Spacelab sub-

systems are minimized, that good antenna viewing angles are achieved and that optimal environmental conditions are obtained. Fig. 8 shows the functional assemblies of the on-board station and the main signal flow with the RF- and Base Band (BB) signal interfaces: Container # 1 contains the onboard time reference assembly (OTR) with a Cs- and a Rb-frequency standard, a phase comparator, a divider and synthesizer, clock interface, power supply, redundancy switch and a battery. Container # 2 includes the receiver assembly, the measurement assembly with code modulator and demodulator and a time interval measurement unit, a processor assembly with the data acquisition control system (DACS 11-N), with a memory module and with I/O-modules for operation control, and a second power supply. Finally container # 3 contains the L-band transmitter with PSK-modulator, preamplifier and a 25 W RF-power amplifier, the C-band radar transponder and a third power supply.

Fig. 9 shows the ground control station, which contains very similar functional assemblies as the onboard station without the radar transponder. The receiver station (Fig. 10) is identical to the control station without the transmitting equipment.

The main technical parameters concerning the RF-links between Shuttle and ground stations are given in Table II.

As for the additional equipment, only that for synchronization of the ground stations and for frequency transfer should be mentioned here. The basis for synchronization will be clock transportations. In cooperation with our national time institute 'Physikalisch-Technische Bundesanstalt' (PTB) several clock transportations over a distance of 700 km between PTB and DFVLR have been carried out with an accuracy of + 5 nsec. Moreover GPS-signals should be received at the different groundstations and used for synchronization according to the 'Common View Technique' [12]. For preliminary investigations of this opportunity an experimental GPS receiver was built and C/A code signals from several satellites were received. Fig. 11 shows the fluctuation of single point measurements. The difference between the NAVEX-master clock and GPS time was taken every two seconds. The RMS of these single samples was $\sigma = 54$ nsec. By averaging on 300 samples, received during 10 minutes observation time, the RMS could be reduced to $\sigma = 3$ nsec. With these more precise mean values a frequency comparison between GPS- and the NAVEX master clock could be made during more than 10 days. The results received with NAVSTAR SV # 6 are shown in Fig. 12. As the frequency difference between USNO-masterclock and GPS time is known from USNO-Time Service for the same period, the frequency difference between USNO-MC and NAVEX-MC could be calculated. The results let us anticipate that slowly varying systematic errors will be small enough for a frequency transfer with sufficient accuracy. These measurements will have to be continued.

EXPERIMENT OPERATIONS

The D-1 mission will have a duration of 7 days. The operating time of the

NAVEX onboard equipment will be about 150 hours. An overall timeline of the onboard operations is given in Fig. 13.

The equipment of container # 1, these are mainly the clocks, will be running all the time. The equipment of containers # 2 und # 3 will be switched on only when passing the ground stations because of power constraints. Every day 6 successive passes will occur during a time span of 8 hours.

The timeline during each pass is shown in Fig. 14. The activation of transmitters will occur before the Shuttle appears at the horizon of the ground stations. The duration of each contact to the ground stations will be 5 to 8 minutes. After that the transmitters and other equipment of containers # 2 and # 3 will be switched off again. The changing power consumption of the NAVEX onboard equipment is shown in Fig. 15.

The data links between the Shuttle and the ground stations and the ground data net are shown in Fig. 16. Besides a data and voice link via TDRSS and POCC to the GPOC, a direct data transfer of 250 bit/sec is provided from the Shuttle to the NAVEX ground stations. Between the ground stations and the NAVEX operation control center, the data transfer will be executed by a 1.2 k bit/sec data link, by telex, by telephone and by magnetic tapes. The data exchange between GPOC and NAVEX operation control needs no special equipment, because both will be housed in the German Satellite Operation Center (GSOC) at DFVLR Oberpfaffenhofen and because the same data system will be used by both.

DATA EVALUATION

The raw data coming from the Shuttle via POCC, from the ground stations and from auxiliary measurement devices, as for instance refractometers, have to be preprocessed for two different purposes (Fig. 17): one is the near real time evaluation, necessary for antenna pointing, Doppler frequency predictions and for data monitoring; the other is the production of an experiment tape for the off-line data evaluation. The main points of the off-line evaluation are given by the experiment objectives in Fig. 4.

The principle of two way clock comparison between on-board and ground based clocks is illustrated by Fig. 18. The time difference ΔT between both can be calculated from time interval measurements onboard and on the ground. Transmitter and receiver delays have to be determined before the mission and will be controlled before and after each pass. The upward and downward propagation delays will be somewhat different because of the relative motion between Shuttle and ground station and because of the different ionospheric influence on the two signal frequencies. Taking this into consideration, ΔT can be determined by the formula

$$(1) \quad \Delta T = T_G - \frac{1}{2} T_S + \frac{1}{2} \left[(\tau_{TG} - \tau_{TS}) + (\tau_{RS} - \tau_{RG}) + (\tau_{L2} - \tau_{L1}) \right]$$

T_G = time difference measured at ground station

T_S = time difference measured onboard

τ_{TG} = delay time of ground transmitter

τ_{TS} = delay time of onboard transmitter

τ_{RG} = delay time of ground receiver

τ_{RS} = delay time of onboard receiver

τ_{L1} = delay time of downward signal

τ_{L2} = delay time of upward signal

Because of the relativistic effect a frequency deviation of the onboard clocks relative to the ground master clock is expected. This causes an increasing time difference Δt between both clocks according to the formula

$$(2) \quad \Delta t = \frac{1}{c^2} \int_0^t \left[\frac{1}{2} (v_s^2 - v_{gr}^2) - (\phi_s - \phi_{gr}) \right] d\tau$$

v_s = Shuttle velocity

v_{gr} = velocity of ground station

ϕ_s = gravity potential at the Shuttle

ϕ_{gr} = gravity potential at the ground

c = velocity of light

Fig. 19 illustrates the increase of the expected time difference during one revolution of the Shuttle for orbit eccentricities $e = 0$ and $e = 0,01$.

For the determination of the ionospheric propagation effect, the range rate dr/dt between control station and Shuttle has to be taken into account in a similar way as for the two way time transfer

$$(3) \quad \Delta r = \int_{\tau_{TS}}^{\tau_{RS}} \frac{dr}{dt}(t) d\tau \approx c \cdot \Delta\tau_{L2}$$

$c = \text{velocity of light.}$

The frequency dependence of the ionospheric refractive index N_I can be described in the frequency range from 1 to 6 GHz by the relationship

$$(4) \quad N_I = - \frac{40,3 \cdot 10^6 N_e}{f^2}$$

$N_I = (n_I - 1) \cdot 10^6 = \text{modified refractive index of ionosphere}$
 $N_e = \text{electron density in electrons/m}^3$
 $f = \text{signal frequency in Hz}$

as was verified by [10].

From this the integral ionospheric effect $\Delta\tau_I$ can be calculated by integration of N_I along the ray path between Shuttle and ground control station

$$(5) \quad \Delta\tau_I(f) = \frac{10^{-6}}{c} \int_{s_c(\text{Control Station})}^{s(\text{Shuttle})} N_I(s) ds \approx \frac{40,3}{c \cdot f^2} \int_{s_c(\text{Control Station})}^{s(\text{Shuttle})} N_e(s) ds.$$

The integral on the electron density on the right side of the above equation is called electron content along the ray path. Its value can be determined by delay time measurements at different frequencies. For the special case of NAVEX this electron content can be determined from corrected delaytime measurements in L-band ($\tau_{L1} + \tau_{L2}$) and in C-band ($\tau_{C1} + \tau_{C2}$) using the formula

$$(6) \quad (\tau_{L1} + \tau_{L2}) - (\tau_{C1} + \tau_{C2}) = (\Delta\tau_{IL1} + \Delta\tau_{IL2}) - (\tau_{C1} + \tau_{C2})$$

$$\approx \frac{-40,3}{c} \int_{s_c(\text{Control Station})}^{s(\text{Shuttle})} N_e(s) ds \cdot \left[\frac{1}{f_{L1}^2} + \frac{1}{f_{L2}^2} - \frac{1}{f_{C1}^2} - \frac{1}{f_{C2}^2} \right].$$

$\Delta\tau_{IL1}, \Delta\tau_{IL2}$ = ionospheric delays in the L-band

$\Delta\tau_{IC1}, \Delta\tau_{IC2}$ = ionospheric delays in the C-band

The influence of the troposphere is assumed to be independent of frequency. It can be determined by integration on the known profile of tropospheric refractive index N_{TR}

$$(7) \quad \Delta\tau_{TR} = \frac{10^{-6}}{c} \int_{s \text{ (Troposphere)}} N_{TR}(s) ds,$$

when the height of the ground station and the refractive index at the ground station are known.

For accurate Shuttle position determination, corrections have to be derived from control station measurements for the receiving station one-way measurements. For this purpose a simple ionospheric model may be sufficient for estimating the electron content along the ray path from the Shuttle to the receiving stations [9].

$$(8) \quad \int_{s_C \text{ (Control Station)}}^{s \text{ (Shuttle)}} N_e(s) ds \xrightarrow[\text{model}]{\text{ionospheric}} \int_{s_R \text{ (receiving Station)}}^{s \text{ (Shuttle)}} N_e(s) ds$$

The determination of ground station positions relative to each other has been carried out by TRANSIT measurements in cooperation with the 'Institut für Angewandte Geodäsie' (IFAG) Frankfurt. An accuracy of $\Delta x, \Delta y, \Delta z < 1$ m has been achieved.

Finally the accuracy of one way pseudo range measurements for a ground station position determination may be evaluated by using the relation

$$(9) \quad (x_G - x_i)^2 + (y_G - y_i)^2 + (z_G - z_i)^2 = r_i^2 = c^2 \cdot (\tau_i - \Delta T)^2$$

$i = 1, 2, 3, 4$

x_G, y_G, z_G = coordinates of ground receiving station

x_i, y_i, z_i = coordinates of the Shuttle at four different points of time

τ_i = propagation delay times after ionospheric and tropospheric corrections.

This procedure is well known from GPS and need not be explained any more. The ionospheric and tropospheric corrections will be made as mentioned before.

EXPERIMENT ORGANIZATION

The implementation of the experiment will be supported by several organizations with different activities:

DFVLR-PT/Köln:	Project D-1 and NAVEX management
SEL/Stuttgart:	Hardware development, manufacturing and receiving station operation
DFVLR-NE and WT: Oberpfaffenhofen	Operation control and data evaluation Ground control station and radar Synchronization of groundstations Frequency transfer German Payload Operation Center
PTB/Braunschweig:	Receiving station and primary clock
BMFT/Bonn:	Funding support
USNO/Washington:	Support for frequency transfer.

The main funds come from the Bundesministerium für Forschung und Technologie (BMFT) and from DFVLR.

The time schedule is shown in Fig. 20.

The main events will be the delivery of the NAVEX onboard equipment in spring 1984 and the Shuttle mission D-1 in mid-1985.

Concerning the D-1 mission a special agreement was signed by NASA and by DFVLR in September 1982, in which NASA assured the necessary support.

ACKNOWLEDGEMENT

The authors are indebted to their colleagues at DFVLR and SEL, who contributed to the results presented here. Particularly mentioned should be Mr. K. Friedel and R. Schimmel, who contributed Figures 16 and 19.

LITERATURE

- [1] Studie zur Definition von Spacelab Experimenten auf dem Gebiet der Kommunikation und Navigation. BMFT, RV-V 59/74-KA-50.
- [2] Durchführbarkeitsstudie Zeitsynchronisation und Einwegentfernungsmessung, BMFT, O1QV 165 A-V 22-WRT 1075-2.19.

- [3] Rother, D.: "Ein Spacelab-Experiment zur Zeitsynchronisation und Einwegentfernungsmessung"
Nachrichtentechnische Zeitschrift 29 (1976) H. 9, S. 673-677.
- [4] Tschiesche, H.: Experiment zur "Synchronisation und Einwegentfernungsmessung" für Spacelab-Missionen.
Kleinheubacher Berichte, Band Nr. 20, 1977;
edited by F.T.Z. Darmstadt.
- [5] Starker, S.: "Spacelab Experiments with Atomic Clocks".
ESA SP-137, Proceedings of a European Workshop;
Schloß Elmau 16 - 21 January 1978.
- [6] S. Starker, D. Rother, "A Spacelab Experiment on
Clock Synchronization and One-Way Ranging".
Ortung und Navigation, I/1979; Vierteljahresmitteilung
der Deutschen Gesellschaft für Ortung und Navigation
(DGON), pp. 35 - 53.
- [7] R. Decher, D.W. Allan, C.O. Alley, R.F.C. Vessot and
G.M.R. Winkler, "A Space System for High-Accuracy Global
Time and Frequency Comparison of Clocks". Proceedings of
the Twelfth Annual Precise Time and Time Interval (PTTI)
Applications and Planning Meeting. December 1980.
- [8] S. Starker, H. Nau, "Atomuhrenexperiment NAVEX, Status
und Planung 1981-1985."
Interner DFVLR-Bericht Nr. 551-80/16, Oktober 1980.
- [9] V. Stein, "Modelle der ionosphärischen Elektronendichte-
verteilung zur Korrektur von Ausbreitungsfehlern elektro-
magnetischer Wellen". DFVLR-Mitteilung 82-03.
- [10] P.E. Schmid, et al. "NASA-GSFC Ionospheric Corrections to
Satellite Tracking Data"
NASA-Report X-591-73-281.
- [11] D. Rother, H. Tschiesche, H. Kallerhoff, "GPS und NAVEX
für die satellitengestützte Navigation"
NTZ September 1982, Band 35, Heft 9, pp. 582-587.
- [12] D. Allan, M. Weiss, "Accurate Time and Frequency Transfer
During Common View of a GPS Satellite".
Proc. 34th Annual Symposium on Frequency Control (SFC), 1980.

**UNIQUE SUPPORT STRUCTURE (USS)
with NAVEX**

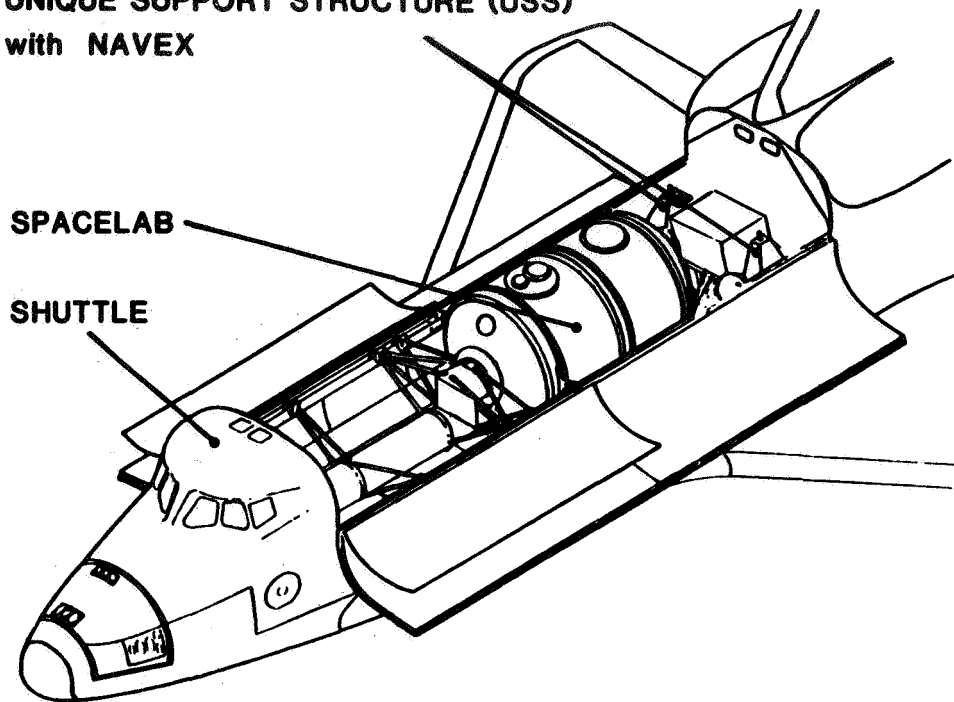


Fig. 1 - Payload of Spacelabmission D1

1974	PROPOSAL ON ONE WAY RANGING	PROPOSAL ON TIME TRANSFER
1975	SPACELAB-UTILIZATION STUDY	
1976	NAVEX-FEASIBILITY STUDY	
77/78	ENGINEERING MODEL DEVELOPMENT	
78/79	PRELIMINARY MEASUREMENTS	
80/81	SEARCH FOR A FLIGHT OPPORTUNITY	
1981	DECISION FOR D-1 PARTICIPATION CONCEPT MODIFICATIONS	
1982 1984	HARDWARE DEVELOPMENT EXPERIMENT PREPARATIONS AND TESTS	
1985	SHUTTLE MISSION D-1 (STS 26)	
1986	DATA EVALUATION	

Table I - The NAVEX-Story

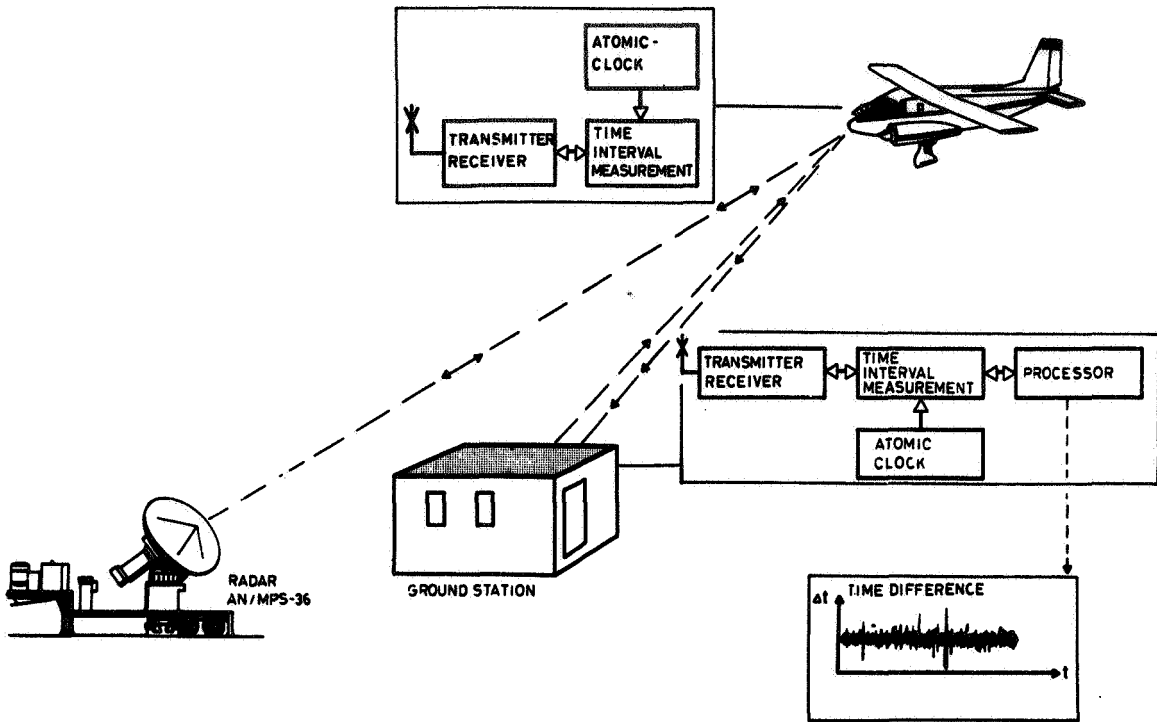


Fig. 2 - Comparison of on-board and ground based clocks by a two-way microwave link

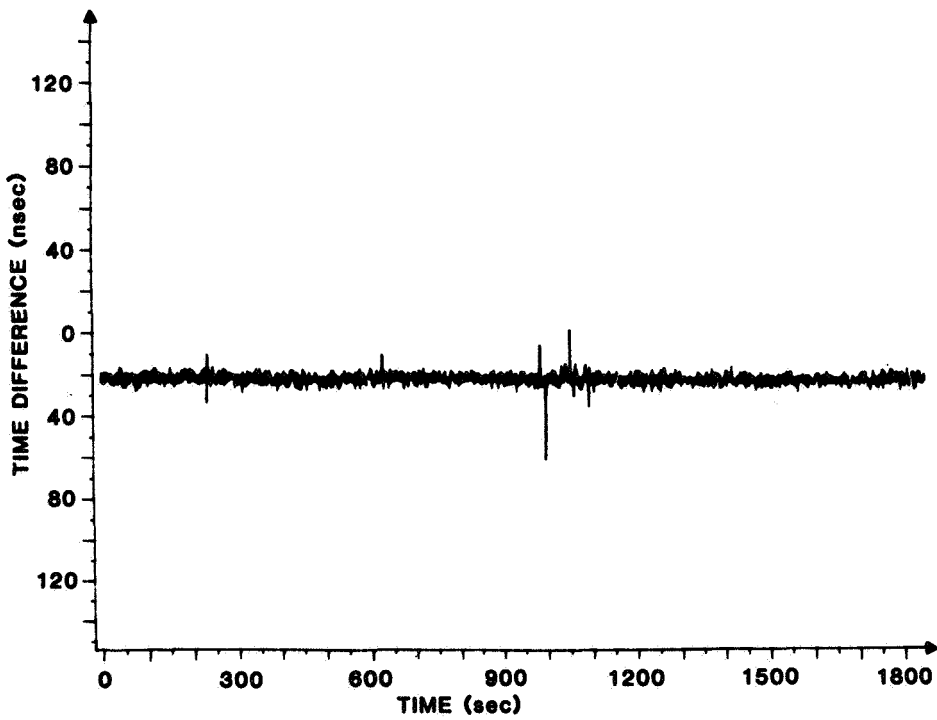


Fig. 3 - Result of a preliminary experiment with aircraft

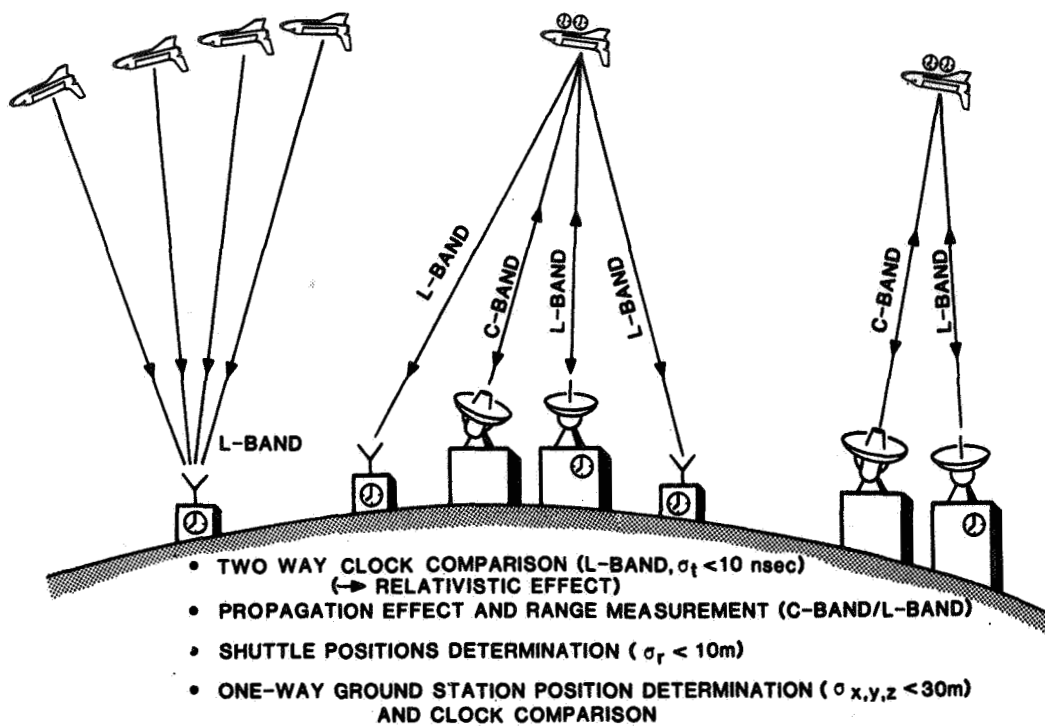


Fig. 4 - NAVEX - Objectives

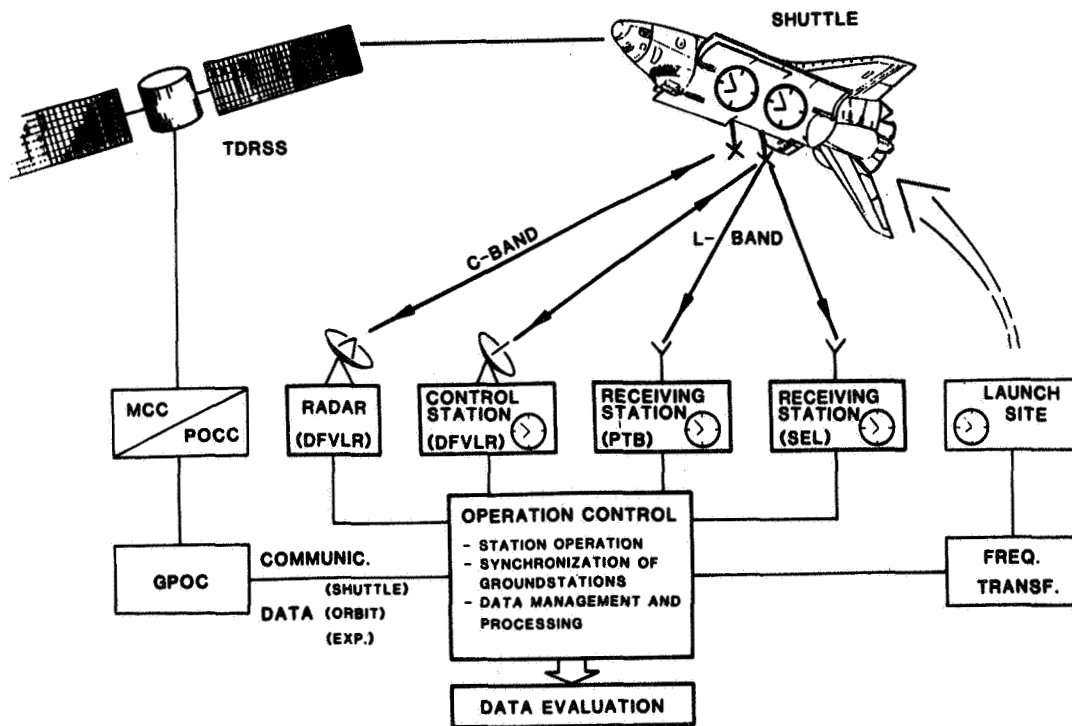


Fig. 5 - NAVEX - Experiment Configuration

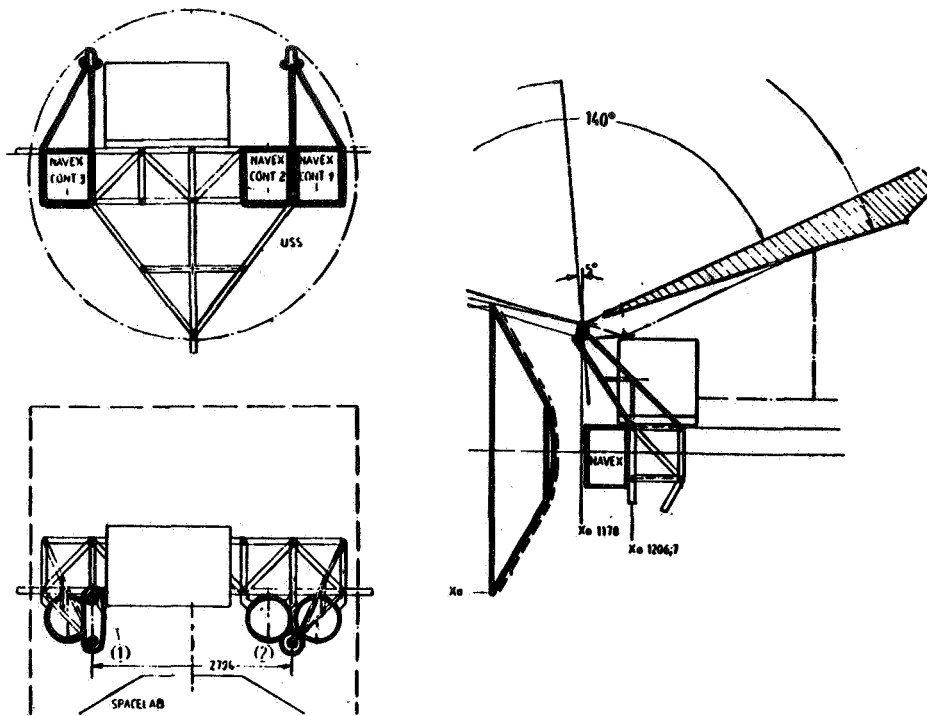


Fig. 6 - Accomodation of on-board station

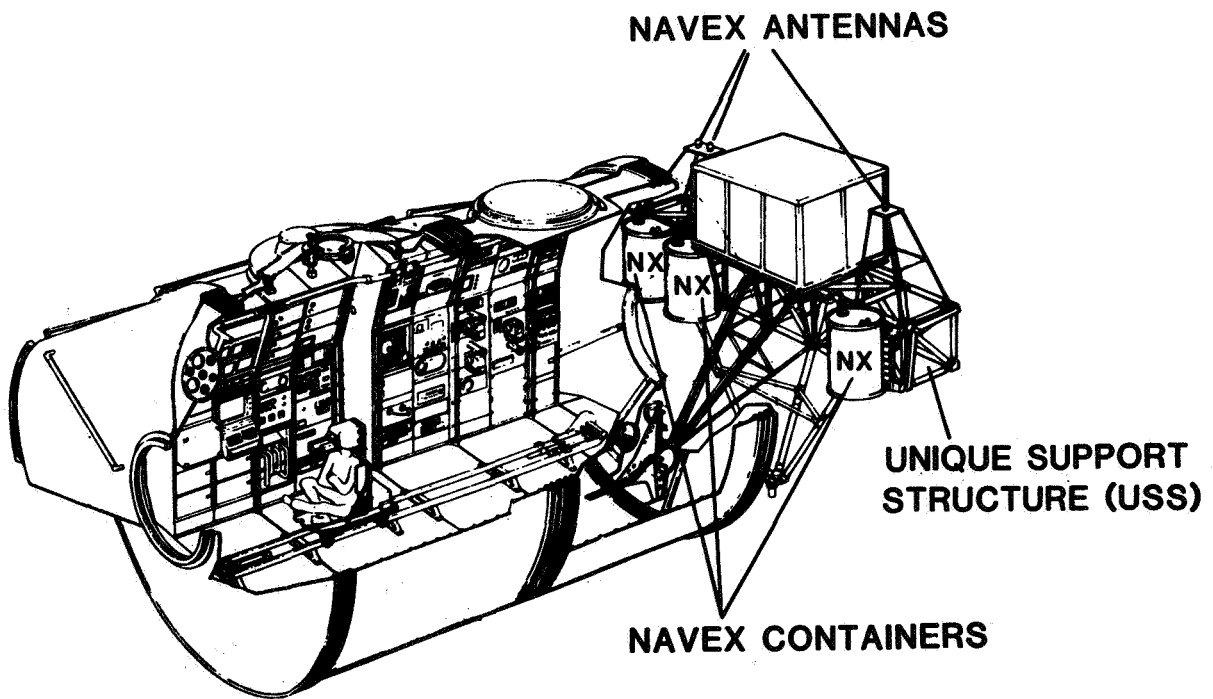


Fig. 7 - Configuration of on-board equipment

Interfaces to Ground

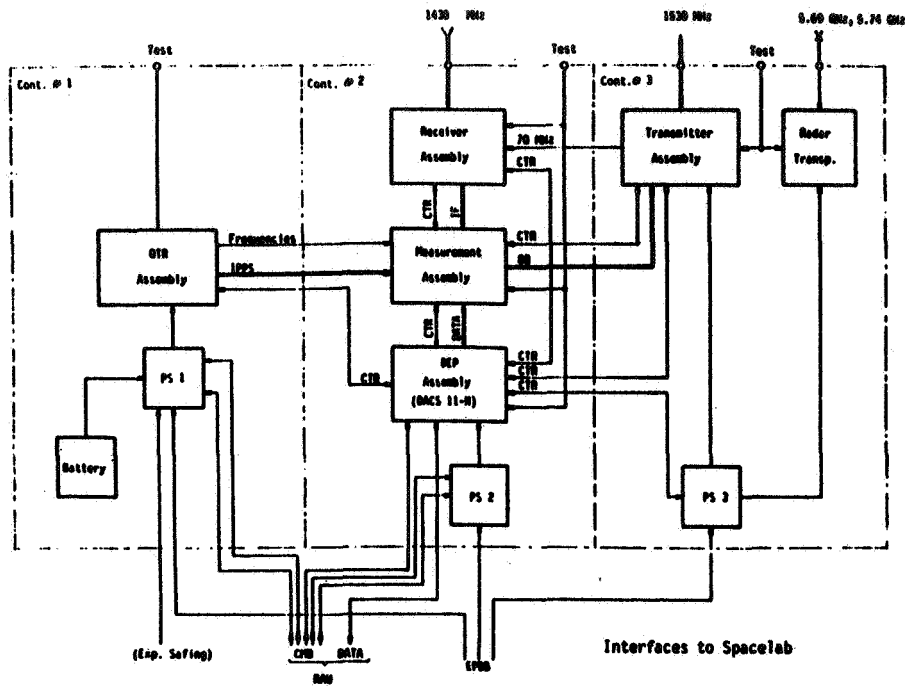


Fig. 8 - Onboard Station

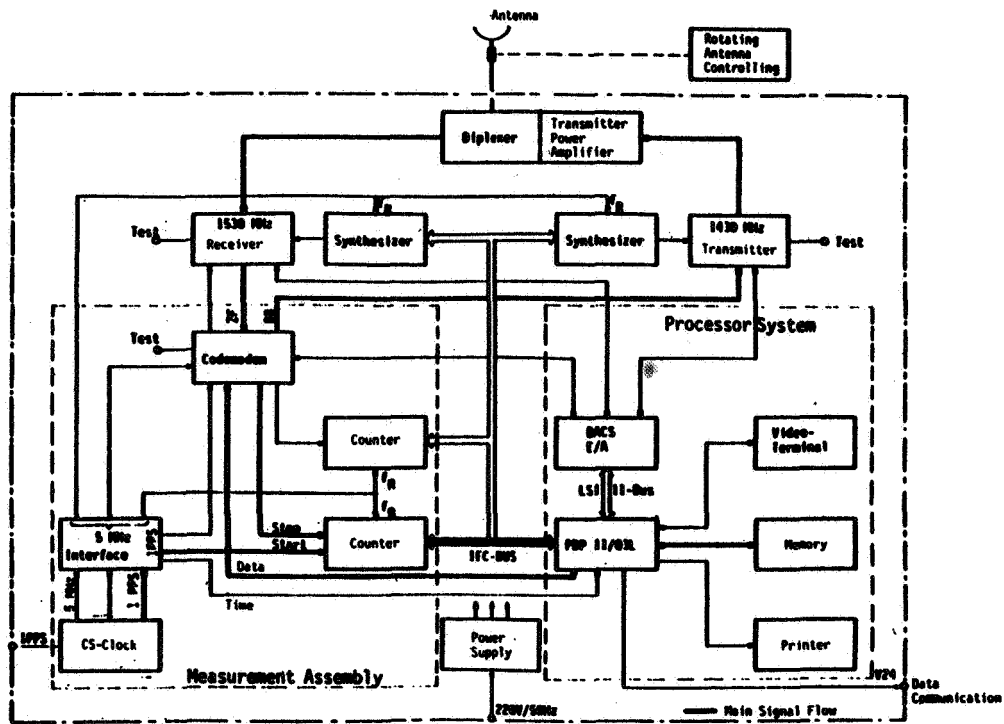


Fig. 9 - Ground Control Station

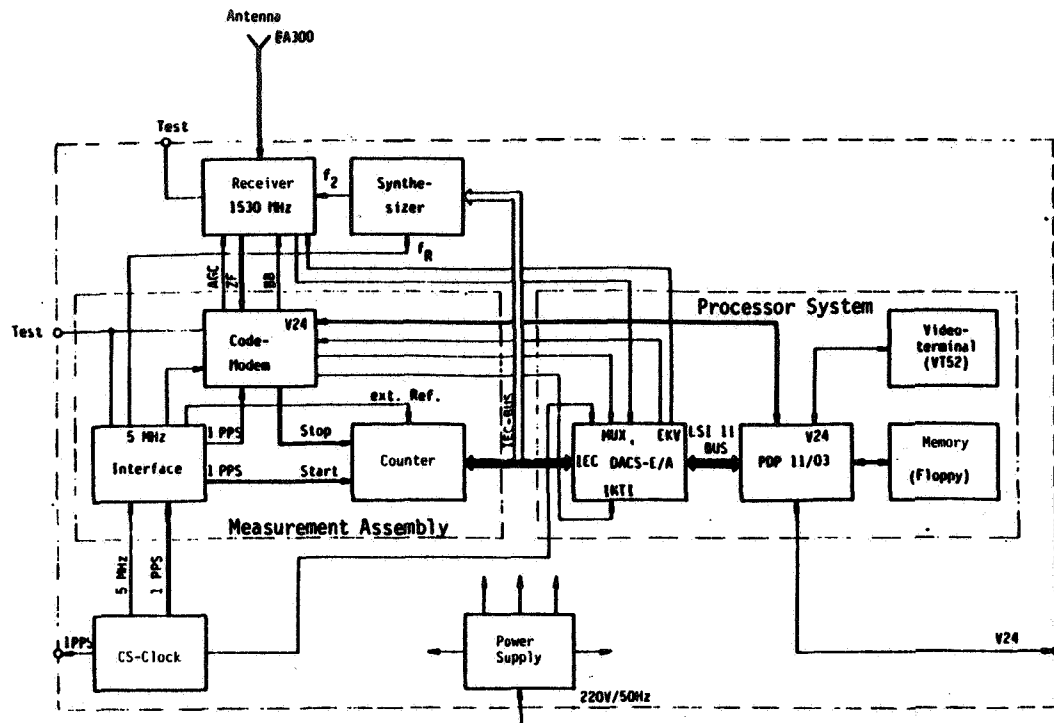


Fig. 10 - Receiver Station

SIGNAL PARAMETERS	ONBOARD STATION	GROUND CONTROL STATION	RECEIVER STATION
TRANSMIT FREQUENCY	1.53 GHz	1.43 GHz	--
RECEIVING FREQUENCY	1.43 GHz	1.53 GHz	1.53 GHz
RF-POWER	25 W	25 W	--
ANTENNA GAIN	-1 ± 5 dB	24 dB	-1 ± 5 dB
RECEIVING LEVEL	-79...-99 dBm	-83...-101 dBm	-99...-125 dBm
SIGNAL TO NOISE RATIO (S/N AT B=2MHz)	+28...+8 dB	+24...+6 dB	+7...-19 dB
DOPPLER SHIFT	--	± 37 kHz	± 37 kHz
CODE CLOCK FREQUENCY	1023 kHz	DTO.	DTO.
NUMBER OF CODEBITS	1023	DTO.	DTO.
CODE PERIOD	1 ms	DTO.	DTO.
DATA RATE	250 BIT/s	DTO.	DTO.
MODULATION	2 - PSK	DTO.	DTO.
BANDWIDTH	CA. 2 MHz	DTO.	DTO.
ACQUISITION TIME	15 s	15 s	20 s

Table II - NAVEX - Signal Parameters

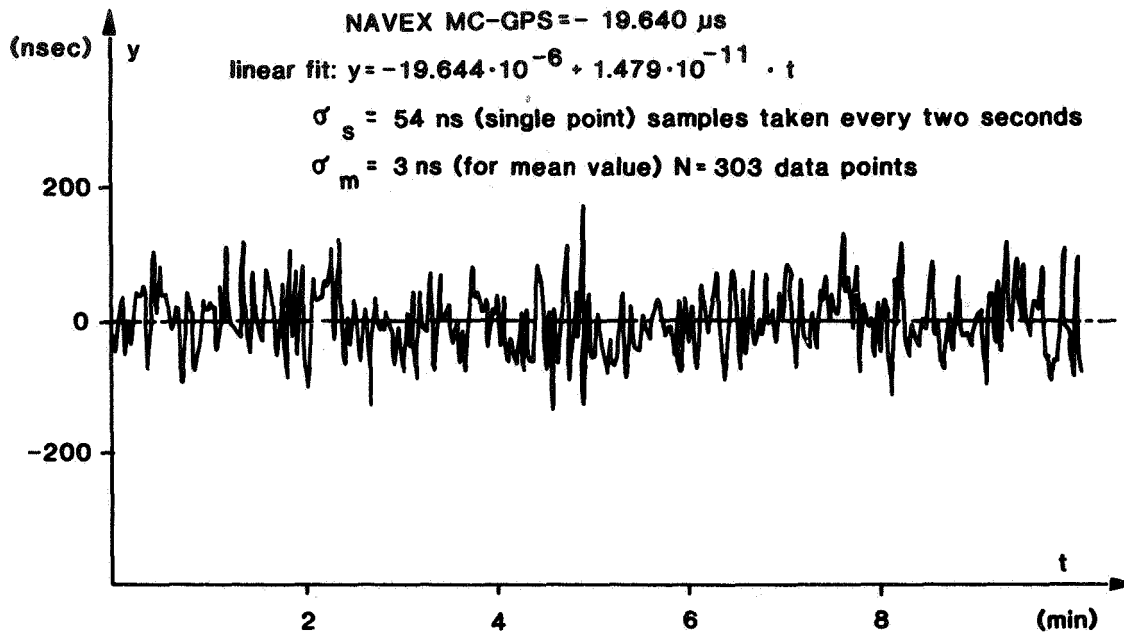


Fig. 11 - Time comparison with GPS NAVSTAR SV # 6

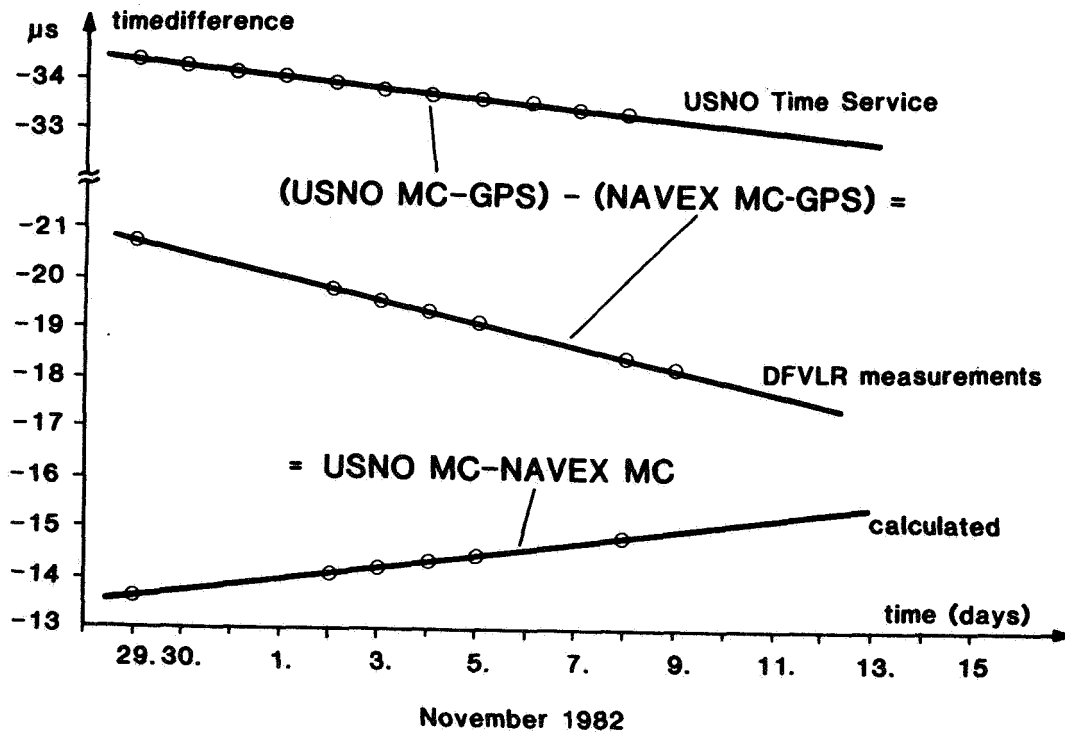


Fig. 12 - Frequency comparison between USNO MC and NAVEX MC with GPS NAVSTAR SV # 6

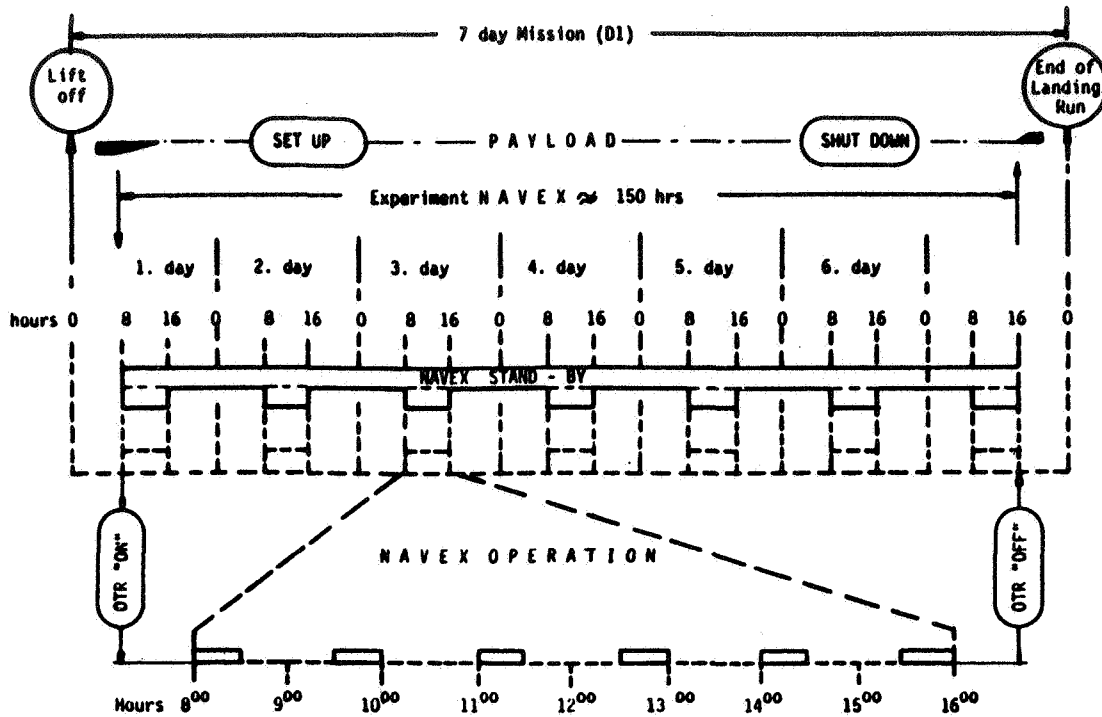


Fig. 13 - Timeline of PLE-NAVEX operations

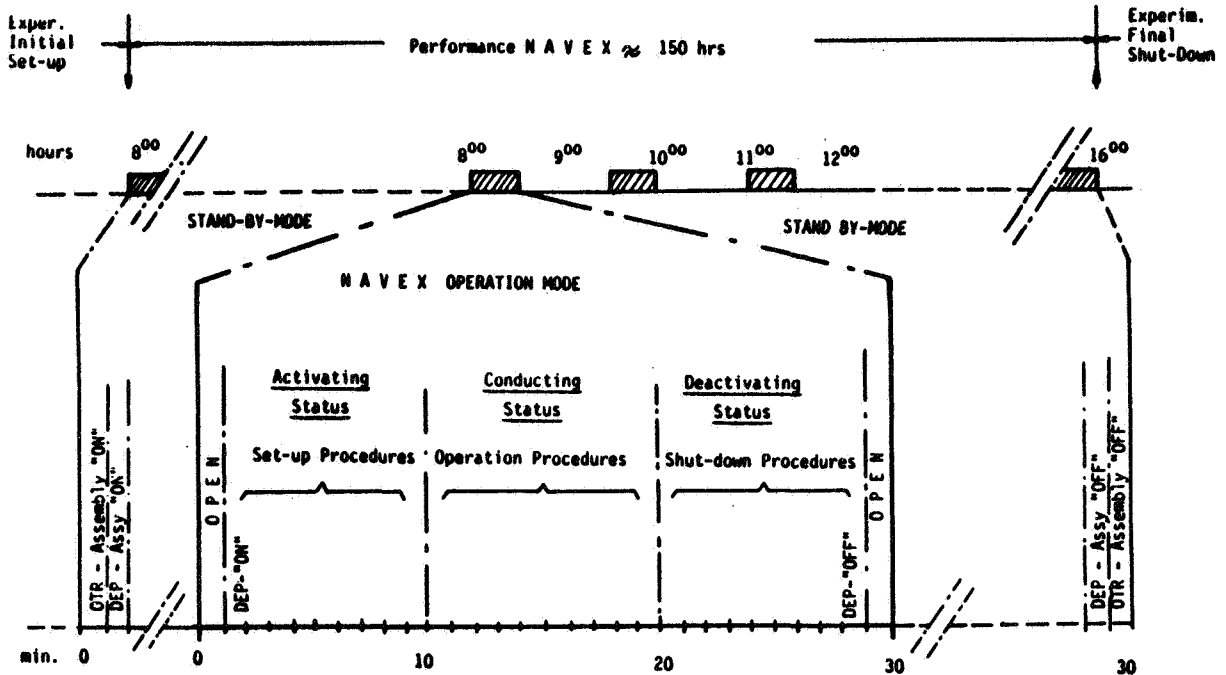


Fig. 14 - Timeline of element operation

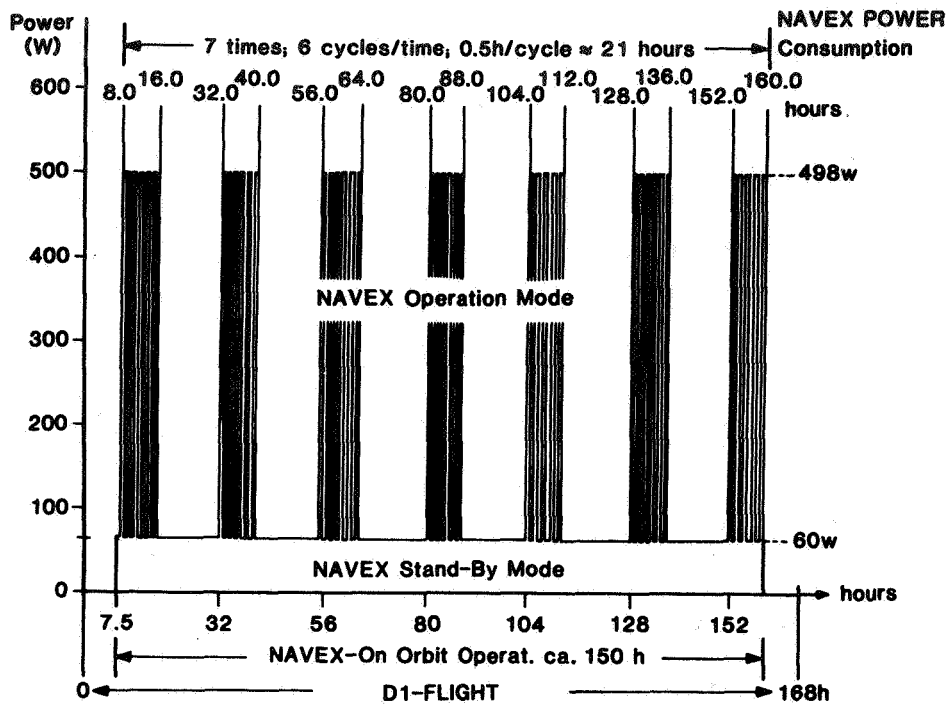


Fig. 15 - Typical power load modes

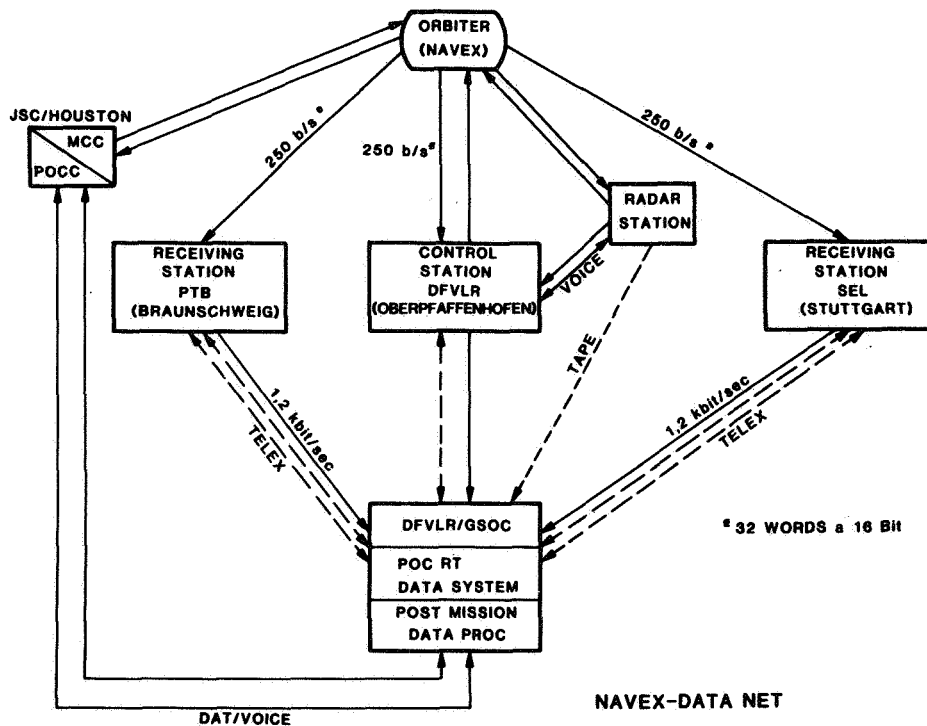


Fig. 16 - NAVEX-Data net

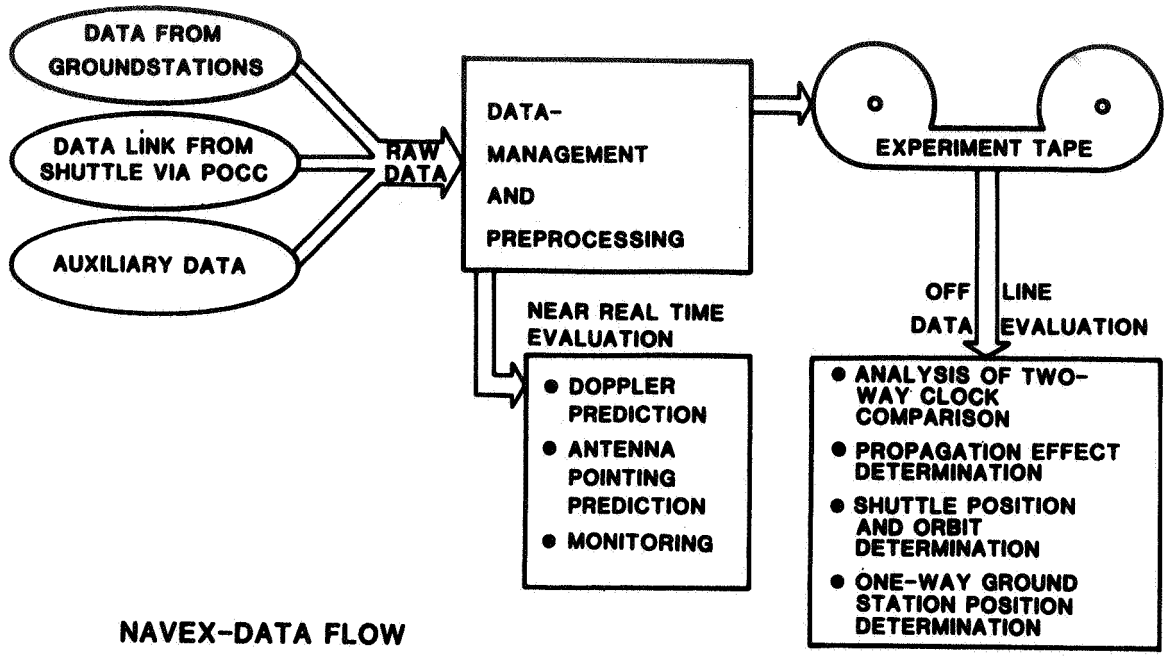


Fig. 17 - NAVEX-Data flow

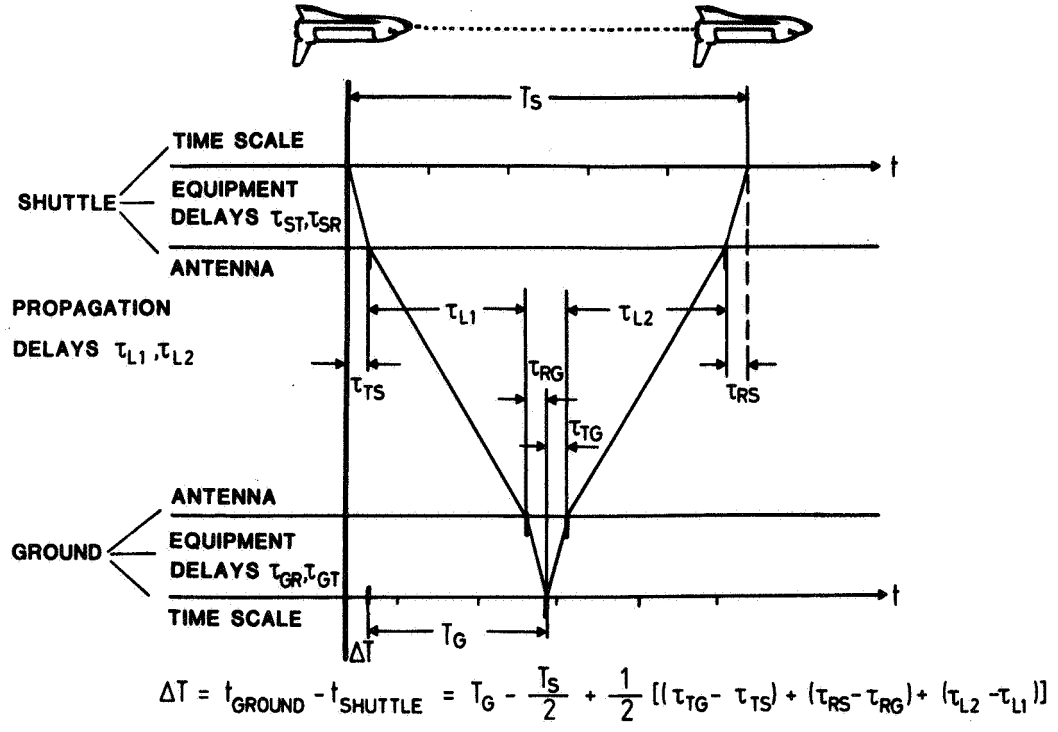
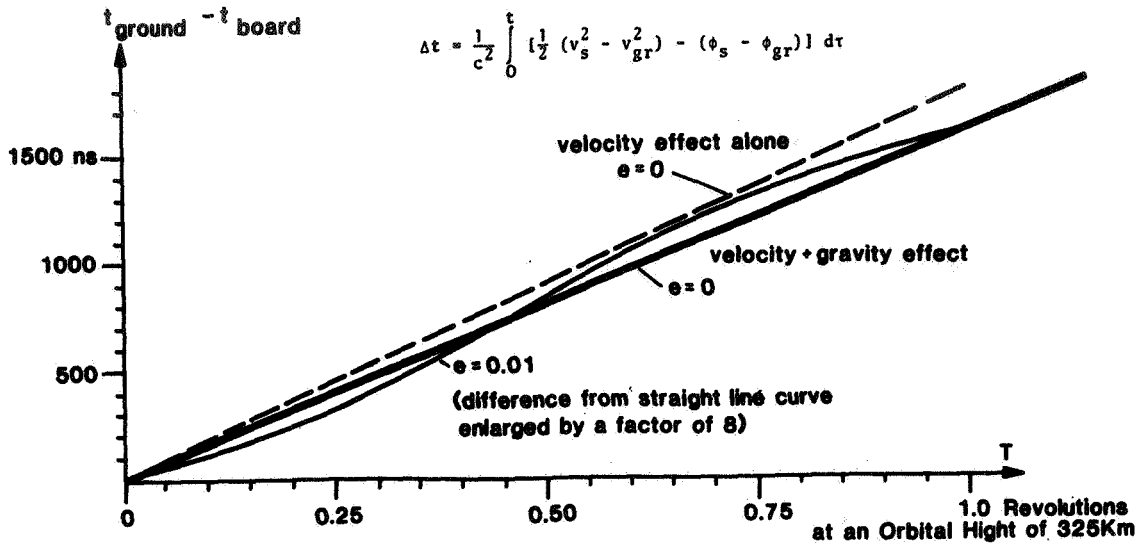


Fig. 18 - Principle of two-way clock comparison



EXPECTED RELATIVISTIC TIME DIFFERENCE BETWEEN IDEAL CLOCKS ON THE SHUTTLE (H=325 KM, E=0 AND E=0.01) AND ON THE GROUND (H=0.58 KM ABOVE SEA LEVEL FOR AN OBLATE EARTH).

Fig. 19 - Relativistic-effect

WORK PACKAGES	81	82	83	84	85	86
ON-BOARD EQUIPMENT						
- DEVELOPMENT	██████████					
- MANUFACTURING		██████████				
- INTEGRATION/D-1 INTEGR.			██████████	██████████		
- TESTS				██████████	██████████	
- CONTROL MEASUREMENTS						██████████
GROUND STATIONS (C.ST.,R.ST.)						
- DEVELOPMENT	██████████	██████████	██████████			
- MANUFACTURING		██████████	██████████			
- INTEGRATION			██████████	██████████		
- TESTS				██████████	██████████	
- MAINTENANCE						██████████
SYNCHRONIZATION EQUIPMENT						
- PRELIMINARY TRIALS						██████████
- MANUFACTURING			██████████	██████████		
- INSTALLATIONS				██████████		
- TESTS					██████████	
DATA-NET AND MONITORING						
- INSTALLATION				██████████		
- TESTS					██████████	
GROUND OPERATIONS						
- PREPARATIONS AND TRAINING					██████████	
- D-1-MISSION						██████████
- DATA COLLECTION						██████████
- CONTROL MEASUREMENTS						██████████
DATA-EVALUATION						
- PREPAR. + TEST OF COMP. PROGR.						██████████
- EVAL. OF TESTRESULTS			██████████	██████████	██████████	██████████
- EVAL. OF D-1-MISSION DATA						██████████

Fig. 20 - NAVEX-Time Schedule

QUESTIONS AND ANSWERS

DR. WINKLER:

Can it be in 10 parts? There has been such smorgasbord of interesting details that I think there are several questions.

Number one, what kind of a clock do you use now? In, yes, your master clock?

MR. STARKER:

We have a cesium clock from Hewlett-Packard.

DR. WINKLER:

Regular or high performance?

MR. STARKER:

High performance tube.

DR. WINKLER:

And in your interesting straight-line comparison between our clock and yours, over ten days, what have been the residuals?

MR. STARKER:

We could only measure the precision, our receiver is not calibrated. And the other is, that we are not sure if this is correct. If it's smaller than 5 nanoseconds, this signal, but over ten days we cannot save a good tape ---

DR. WINKLER:

From the graph, it look like 10 nanoseconds or 15, which is excellent, of course.

MR. STARKER:

Excuse me, my co-author is here, Mr. Nau, who had made these measurements. Perhaps he knows a more exact value.

MR. NAU:

If taken for ten days, we have a one sigma value for a single point for less than twenty nanoseconds.

PROFESSOR ALLEY:

Do you intend to fly the Hewlett-Packard cesium standards?

MR. STARKER:

No, this will be another clock. A cesium clock and a rubidium clock. We hope to get it from the United States, and from a company which has experience with phase one clocks.

PROFESSOR ALLEY:

Do you intend to keep the clocks running during the launch and landing?

MR. STARKER:

At first we intended to do so but Nau did not agree and we must switch it on, we are sorry.

PROFESSOR ALLEY:

So am I. Thank you.

MR. STARKER:

Thank you very much.

HIGH-ACCURACY GLOBAL TIME AND FREQUENCY TRANSFER WITH A SPACE-BORNE HYDROGEN MASER CLOCK

R. Decher (NASA), D. W. Allan (NBS), C. O. Alley
(U. of Maryland), C. Baugher (NASA), B. J. Duncan
(NASA), R.F.C. Vessot (SAO), and G.M.R. Winkler (USNO)

ABSTRACT

This paper describes a proposed system for high-accuracy global time and frequency transfer using a hydrogen maser clock in a space vehicle. Direct frequency transfer with an accuracy of 10^{-14} and time transfer with an estimated accuracy of 1 nsec are provided by a 3-link microwave system. A short pulse laser system is included for subnanosecond time transfer and system calibration. The basic concept of such a system was discussed at the 1980 PTTI Meeting. This paper presents the results of further studies including operational aspects, error sources, data flow, system configuration, and implementation requirements for an initial demonstration experiment using the Space Shuttle.

INTRODUCTION

NASA's Office of Space Science and Applications has supported a study of a space system for high-accuracy global time and frequency transfer which uses a hydrogen maser in a space vehicle. The concept of this system was presented at the Twelfth Annual PTTI meeting in 1980 and elsewhere (1). The present paper discusses the results of recent studies concerned with the implementation of a Space Shuttle demonstration experiment. The Shuttle experiment would be the first step toward a later operational system which would provide high-accuracy global time and frequency transfer on a more permanent basis.

The idea of the Space Time and Frequency Transfer (STIFT) system evolved from two earlier experiments performed several years ago to measure relativistic effects on clocks. In 1976, Gravitational Probe A (GP-A), a joint project of the Marshall Space Flight Center and the Smithsonian Astrophysical Observatory, carried a hydrogen maser clock into space to measure the gravitational redshift effect (2). The frequencies of the hydrogen maser clock in space and a ground-based hydrogen maser clock were compared with an accuracy of 10^{-14} using a specially developed microwave system which provided automatic cancellation of the first-order Doppler effect (3). The technology and the system concepts demonstrated in this experiment are the basis for the STIFT microwave time and frequency transfer system.

In 1975 and 1976, the University of Maryland with support from the U.S. Navy carried out several airplane experiments to

measure relativistic effects on clocks by employing a short-pulse laser technique (4). The time comparison of the airborne and ground based clocks by laser pulses was accurate to about 0.2 ns. The same technique would be applied for the laser part of the STIFT system.

The STIFT concept combines the two proven techniques to provide a space clock facility for high accuracy global time and frequency transfer. Such a system could be implemented on a space station or with a satellite. A Space Shuttle experiment is proposed as the first phase of such a program to test and demonstrate system performance capabilities. With this goal a study of the operational aspects, accommodation and implementation requirements, and error sources for a Shuttle experiment has been performed. The results are summarized in this paper.

Systems Description

The concept of the system is illustrated in Figure 1. Two widely separated clocks, A and B, are compared in time and frequency by means of an orbiting hydrogen maser clock which serves as a transfer standard. STIFT is composed of two independent systems, a microwave system which provides both time and frequency transfer and a short-pulse laser system for time transfer.

The microwave time and frequency transfer requires a ground terminal which receives signals from and transmits signals to the spacecraft. As the space clock passes over ground clock A, the two clocks are compared by microwave transmissions. The process is repeated when the space clock passes over ground clock B. Combination of the two measurements yields a comparison of clock A and B. The microwave system, which is similar to the system used with GP-A, provides automatic cancellation of the first-order Doppler effect and of propagation disturbances in the atmosphere. This technique permits very accurate direct frequency comparison which is a unique feature of the proposed system. Simultaneously with the frequency comparison, microwave time transfer is accomplished with PRN code modulation of the carrier frequencies and correlation techniques. The (1σ) accuracy of the frequency comparison ($\Delta f/f$) is known to be at least 10^{-14} for 100-second measurement intervals, and the accuracy (Δt) of the time transfer is estimated to be better than 1 nanosecond.

A simplified block diagram of the microwave system including the onboard system and the ground terminal is shown in Figure 2. The system transmits three CW, phase-coherent carrier signals at S-band. The frequencies shown are those used with GP-A and not necessarily the ones to be used in the proposed Shuttle experiment. A single antenna with a triplexer is used for all three frequencies.

The frequency comparison utilizes the phase information of the CW carrier signals. The onboard clock frequency (≈ 1420 MHz) is converted to S-band (frequency ratio 76/49) and transmitted to the ground terminal. This clock downlink frequency experiences a one-way Doppler shift and phase changes due to propagation disturbances. The ground clock signal is first transmitted to the space vehicle and returned to the ground terminal by the onboard transponder to obtain a measurement of the two-way Doppler and propagation effects. Dividing the two-way frequency shifts by 2 and subtracting the result from the one-way clock downlink cancels the first-order Doppler and most of the propagation disturbances before the two clock frequencies are compared. The various frequency conversion ratios indicated in the diagram of Figure 2 are compatible with an existing commercial transponder design and are chosen to eliminate ionospheric dispersion encountered by the use of different carrier frequencies. The resulting difference frequency Δf between ground clock and space clock contains relativistic frequency shifts (second-order Doppler and gravitational redshift) which are accounted for by calculations utilizing orbit data.

Time transfer is accomplished by the shaded functional blocks in the diagram (Figure 2) which represent an addition to the original GP-A system concept. The time code of the space clock is modulated on the clock downlink carrier using PRN phase modulation (5). The space clock time code received at the ground terminal is correlated with the ground clock time code to measure the time difference Δt which contains the one-way propagation delay. A range code modulation of the transponder link provides a two-way propagation delay measurement which is used to eliminate the one-way propagation delay.

The microwave system is relatively insensitive to adverse weather conditions (which can affect the laser system) and is therefore the primary mode of time and frequency transfer for an operational STIFT system. The user of such a system will require a comparatively inexpensive ground terminal which fits into a standard size instrument rack to interface with his clock. A microwave antenna with hemispherical coverage is part of the ground terminal.

The STIFT system can also perform time transfer using short-pulse laser techniques. The laser time transfer, which is independent of the microwave system, will be used with existing laser stations around the world. A block diagram of the laser time transfer method is shown in Figure 3. The onboard system is comprised of a corner-cube reflector array equipped with fast photodiode detectors and an event timer interfacing with the hydrogen maser clock. The laser pulse signal is returned to the ground station by the reflector array and is detected on board simultaneously by photo detectors. The event timer measures the

arrival time T_2 of the laser pulse at the space vehicle in the time frame of the onboard clock. This information is transmitted to the ground station by telemetry. The ground station determines the round trip time of the laser pulse and the midpoint time $(T_3 - T_1)/2$ between transmitted and received pulse. The difference between this midpoint and the time T_2 gives the time difference between ground clock and space clock. Relativistic corrections must also be applied to laser time transfer.

The short-pulse laser technique is the most accurate method of time transfer available. It provides an important extension of the capabilities of the microwave system and will be valuable for calibration of the microwave system (6). Simultaneous use of microwave and laser time transfer will provide a comparative evaluation of the two different techniques.

Space Shuttle Experiment

The ultimate application of the proposed STIFT technique is an operational space system which serves a global user community. A Space Shuttle experiment is proposed as a first step toward this goal. The Shuttle experiment will demonstrate and verify the performance of the system and provide the opportunity to optimize the system design for a later operational use. The experiment can be reflown, and, with relocation of ground terminals, increased user participation is possible. The Shuttle experiment could serve also as a test bed for testing atomic clocks intended for space applications.

Figure 4 illustrates the concept of packaging for the experiment flight instrument. All components are integrated into a modularized, self-contained assembly with minimal interfaces to the spacecraft. The dome on top of the assembly shows one of several antenna concepts consisting of a phased array of S-band elements combined with an interspersed array of corner-cube reflectors for the laser link. The assembly is mounted on a pallet in the Shuttle payload bay and deployed by the manipulator arm during operation. Deployment away from the space vehicle is desired to minimize interference and reflected signals from the vehicle structure (multipath propagation). Proven designs exist for the mechanical release and re-berthing mechanisms, and for the grapple fixture for use with the remote manipulator. This type of packaging and hardware design has been used already on early Shuttle missions with the Induced Environmental Contamination Monitor (IECM) which was deployed by the manipulator arm. The experiment container has an active closed-loop, thermal control system and includes batteries for operation of the maser clock during ground handling prior to launch. Otherwise, experiment power will be obtained from the utility Shuttle system. A minimum interface with the Space Shuttle systems makes the experiment compatible with a broader

range of complementary payloads and, thereby, increases flight opportunities.

Most Shuttle missions are flown in rather low earth orbits which allow for a short time interval between station contacts but give relatively short periods of visibility for individual ground stations. An orbital altitude of 360 km with 57° inclination has been assumed for the study. Figure 5 shows the ground tracks of the space vehicle and the radio horizon for some assumed locations of ground terminals. This pattern of orbital ground tracks is repeated every 24 hours. Time between over-flights and elevation angles for several stations is shown in Figure 6. Included are only those contacts in which the spacecraft remains visible from the ground for more than 6 minutes above 5 degrees elevation. The maximum time of visibility (contact with the spacecraft) above 5 degrees elevation is approximately 7 to 8 minutes. This visibility period is sufficient to perform time and frequency transfer. The above conditions, which are typical for a low-orbit Shuttle experiment, can be modified to some extent by selecting a Shuttle mission with different orbit parameters.

The accuracy capabilities of the STIFT system are such, that relativistic effects have to be taken into account. To correct for these effects requires accurate orbit data. The gravitational redshift effect depends on orbital altitude, and the relativistic Doppler effect (time dilatation) depends on the relative motion of the ground station and space vehicle. In the case of the Shuttle experiment, some special effort is needed to obtain orbit information of the required accuracy since Shuttle orbits are not as predictable as those of a free-flying satellite primarily because of space vehicle maneuvers executed during the mission. However, there are ways to overcome this difficulty.

In principle, accurate orbit data are needed only for those arcs during which the experiment operates during time and frequency transfer. Microwave two-way Doppler and range measurements made as part of the STIFT experiment can be used to improve orbit data available from the Mission Control Center. The laser ground stations also provide range measurements, accurate to a few centimeters and range rate measurements accurate to perhaps millimeters/second as well as angular position. These data, together with Shuttle operational navigation data, can be used with a standard orbit determination program to improve the accuracy of available orbit information. Another, and completely independent method, is the use of a Global Positioning System (GPS) receiver as part of the onboard experiment system. The GPS receiver can provide navigation data of required accuracy.

The number and locations of ground terminals for the Shuttle experiment is completely open at this time. To illustrate experiment operation during the Shuttle flight, a station configuration composed of two microwave terminals and two laser stations was assumed for analysis. Figure 7 shows two pairs of stations, each pair consisting of a microwave terminal and a laser station located close to each other to permit simultaneous operation of the microwave and laser systems. Each of the four stations is equipped with a hydrogen maser clock. The data output of the microwave terminals is the measured code shift $\Delta t'$ and measured beat frequency $\Delta f'$. Relativistic corrections are applied to obtain the true difference in epochs, Δt , and the true frequency difference, Δf , between space clock and ground clock. These data are recorded on magnetic tape together with the telemetry housekeeping data from the onboard and ground systems. The relativistic corrections to be applied to the time and frequency differences are computed from orbit information generated by the orbit update program which receives a variety of inputs, including coarse orbit data from the Mission Control Center in Houston and range and range rate measurements from the microwave terminal and the laser station. The laser station can also provide direction cosine information. Other tracking data could be obtained including tracking data from mobile laser stations, onboard Shuttle navigation data received by telemetry, and navigation data from an experimental GPS receiver included in the STIFT onboard system.

The laser station will be equipped with an S-band telemetry receiver to obtain the onboard measurement of the laser pulse arrival time T_2 which is required to determine the epoch difference T . Again relativistic corrections are applied to obtain the true difference in the epochs. Predicted pointing information for the laser telescope is derived from the orbit data received from the Mission Control Center. If an onboard GPS receiver is used, orbit determination and relativistic corrections could be accomplished in the Shuttle, and the resulting information could be distributed to ground stations by telemetry.

The same considerations apply to the remote station pair. All ground stations/terminals will be connected by data and voice link to the Mission Control Center for scheduling of station operations and distribution of operational information. In addition, the data links between ground stations/terminals can be used to exchange processed data of time and frequency transfer for evaluation of experiment performance during the Shuttle mission.

System Performance

There are two aspects concerning the accuracy of time and frequency transfer, namely the transfer between space clock and ground clock and the transfer between clocks on the ground using the space clock as a transfer standard.

In the Shuttle experiment the following accuracies can be expected for the space-to-ground transfer during a typical contact with a ground station: Microwave frequency transfer $\Delta f/f=10^{-14}$, microwave time transfer $\Delta t=1$ nanosecond or better and laser time transfer $\Delta t=0.1$ nanosecond. These accuracy goals are based on the results obtained from earlier experiments (GP-A and aircraft laser experiments). Advances in technology in recent years should make it possible to achieve further improvements in accuracy for the Shuttle experiment.

Figure 8 shows the recent improvements in clock performance. In the 1976 Redshift Test the microwave system demonstrated stability performance at the 10^{-14} level for 100 second averaging; this was the limit set by the then available hydrogen maser. The STIFT clock will benefit from advancements in maser technology which are reflected by the stability curve for the 1979 hydrogen maser. It is, therefore, reasonable to assume that the accuracy of the STIFT system will approach the several parts in 10^{15} level for the 4 to 5 minutes of observing (averaging) time available during typical ground station contacts.

Figure 8 also shows why the hydrogen maser is the obvious choice for the STIFT flight clock. It provides the highest degree of stability not only for the station contact intervals, but also for time intervals between station contacts (typically up to a few hours; see Figure 6).

A particularly important finding of the previous microwave and laser experiments was that the transfer systems did not introduce detectable errors into the time and frequency transfers. Since the Shuttle experiment represents a substantially different type of operation it is appropriate to examine its limits. Two relativistic effects, the gravitational redshift and the relativistic (second order) Doppler effect cause a shift in the frequency of the space clock oscillator as measured on the ground. The resulting effect in the frequency transfer and in the time keeping between the flight clock and ground stations must be accounted for. These relativistic effects are removed from the comparison data by analytical means using tracking data.

For the frequency transfer the present goal is to account for relativistic effects within a fractional frequency error of 1×10^{-15} . This requires accuracies of 10 meters in orbital altitude and about 1 centimeter per second in relative velocity.

Updating orbital data, as outlined earlier, should provide the necessary accuracy in orbit parameters for the short orbital arcs of experiment operation.

To assess the influence of relativistic effects on time transfer between stations one has to consider orbit prediction for periods between station contacts. For a circular orbit both relativistic effects depend only on spacecraft altitude as shown by the following expression:

$$\frac{\Delta T}{T} \approx \frac{GM}{2C^2 R_e} \left[1 - \frac{3h}{R_e} \right]$$

and

$$\delta \left(\frac{\Delta T}{T} \right) \approx \frac{3GM}{2C^2 R_e^2} \delta h$$

where

h is the altitude

R_e is the radius of the earth

From this one obtains $\delta \left(\frac{\Delta T}{T} \right) = 5.9 \times 10^{-4} \left(\frac{\text{ns}}{\text{hour}} \right) / \text{meter}$.

Therefore, if station-to-station contacts are arranged to be separated by only a few hours (see Figure 6), fairly large intra-station errors in altitude can be tolerated. For time transfer contacts separated by intervals of the order of 1 orbital period (90 minutes) even a kilometer error in the spacecraft altitude would impart only about a nanosecond error.

Differential phase changes between the individual microwave carrier links are a potential error source in the RF system. The Doppler cancellation system eliminates phase perturbations that apply uniformly to all three microwave links. In designing the RF system special attention must be given to minimize differential phase changes in those parts of the system, where the carrier signal paths are separated, by selecting components and units which have a low phase/temperature coefficient. The necessary phase stability can be achieved by providing temperature control for critical subsystems as was demonstrated with the GP-A system. For example, the GP-A flight transponder exhibited a phase/temperature coefficient of 13 degrees/°C, which was compensated for by temperature control. If the same transponder were used for STIFT, temperature control of 0.25°C/hour would reduce its error contribution in the frequency transfer to the part in 10^{15} level. This temperature stability is well within the state-of-the-art. In addition, it is always possible to calibrate the phase versus temperature behavior and to apply appropriate corrections derived from telemetry data.

Another potential source of phase perturbations is the flight antenna. Even though all three carrier signals use the same antenna, care must be taken to provide approximately equal phase characteristic for all three frequencies over a large

portion of the antenna pattern to minimize differential phase changes in the RF loops as the aspect angle between ground terminal and spacecraft changes during a contact.

The first order atmospheric and ionospheric refraction effects are eliminated by the Doppler cancellation system. The former because atmospheric refraction enters all three links uniformly and the latter because of the careful selection of frequencies used in the transfer (see Figure 2). The exact frequency selection for the ionospheric cancellation is based on the very good approximation that at S-band frequencies the ionosphere behaves like a dispersive medium whose refractive index is inversely proportional to the square of the frequency. With this approximation it is possible to start with the maser signal in Figure 2 and follow the frequency multiplication paths to show that if the relation

$$\left[\frac{\text{Ground Maser Uplink Frequency}}{\text{Flight Maser Downlink Frequency}} \right]^2 = \frac{1}{2} \left[1 + \frac{1}{(\text{Transponder Factor})^2} \right]$$

is satisfied, then ionospheric effects cancel.

Otherwise, only rare propagation anomalies may affect the operation of the experiment. There are occasions when ionospheric or atmospheric conditions can limit the experiment, particularly for operations attempted at very low elevation angles. In this study an operational limit of five degrees above the horizon has been used for planning purposes. Anomalous atmospheric refraction or unusual ionospheric scattering could drive the limit higher on occasion. In general these effects will impose no limit at all and the experiment can be operated essentially to the line-of-the sight cut-off. The foregoing discussions on performance deal specifically with a Shuttle demonstration experiment and somewhat different considerations apply to an operational STIFT system. For example, a more predictable, higher altitude orbit would be selected for such a system. Overall, the performance of an optimized operational system should be better than what can be achieved with the Shuttle experiment.

Conclusions

With continuing advancements in the performance of time and frequency standards the need for a higher accuracy global clock comparison system ever increases. The needs within the navigation, communication, and electric power technologies also continue to push for higher and higher synchronization accuracies among remote clocks. Figure 9 shows the improvements in the accuracy of NBS laboratory frequency standards over time together with the performance of clock comparison methods. Clock accuracy increased by a factor of 10 approximately every 7

years since 1950 (8), (9), (10). There are reliable indications that this trend will continue in the future, at least at the same rate, as shown by the projected accuracy of an improved cesium standard and a mercury standard using laser cooled ion storage techniques. Historically the accuracy of long distance (international) clock comparison methods, as measured over 24 hours, has always been lower than the accuracy of existing standards and this situation persists today with GPS currently being the most accurate generally available method. The proposed STIFT concept represents a major step in performance improvement and is the most accurate method for global time and frequency transfer conceived so far. The system would be able to satisfy growing accuracy needs of the future.

References

- (1) Allan, D.W., C.O. Alley, Jr., R. Decher, R.F.C. Vessot, and G.M.R. Winkler, "Shuttle Experiment to Demonstrate High-Accuracy Global Time and Frequency Transfer," IEEE Trans. Geo. and Remote Sensing, GE-20, 3, 321-325, 1982.
- (2) Vessot, R.F.C., M.W. Levine, E.M. Mattison, E. L. Blomberg, T. E. Hoffman, G. V. Nystrom, B.F. Farrel, R. Decher, P. B. Eby, C. R. Baugher, J. W. Watts, D. L. Teuber, and F. D. Wills, "Test of Relativistic Gravitation with a Space-borne Hydrogen Maser," Phys. Rev. Lett., 45, 2081, 1980.
- (3) Vessot, R.F.C. and M. W. Levine, "A Test of the Equivalence Principle Using a Spaceborne Clock," General Relativity and Gravitation, 10, 181-204, 1979.
- (4) Alley, C.O., "Relativity and Clocks," in Proc. 33rd Annual Frequency Control Symposium. (Atlantic City, NJ) pp.4-39, May 1979.
- (5) Penfield, H., E. Imbier, and R.F.C. Vessot, "Design of the STIFT Time and Frequency Microwave Ground Terminal," in Proc. 14th Annual PTTI Planning Meeting (NASA Goddard Space Flight Center, Greenbelt, Md., November 30-December 2, 1982) (in press).
- (6) Alley, C.O., J. D. Ragner, C.L. Steggerda, J.V. Mullendore, L. Small, and S. Wagner, "Time Transfer Between the Goddard Optical Research Facility and the U.S. Naval Observatory using 100 picosecond Laser Pulses," in Proc. 14th Annual PTTI Planning Meeting (NASA Goddard Space Flight Center, Greenbelt, Md., November 30-December 2, 1982) (in press).
- (7) Vessot, R.F.C., "Relativity Experiments with Clocks," Radio Science, 14, No. 4, pp. 629-647, 1979.

- (8) H. Lyons, Ann. N.Y. Academy of Science, No. 55, 831, 1952, Ann. Sci. America 196, 71, Feb. 1957.
- (9) Atomic Clock and Atomic Standard of Frequency and Time, NBS Technical News Bulletin, Vol. 33, No. 2, pp 17-24, February 1949.
- (10) Beehler, R. E., Cesium Atomic Beam Frequency Standard: A survey of laboratory standards developed from 1949-1971, Proc. 25th Annual Symposium on Frequency Control, p. 297, 1971.
- (11) Beehler, R. E., A Historical Review of Atomic Frequency Standards, Proc. IEEE, 55, p. 792, 1967.
- (12) Beehler, R. E., R. C. Mockler, and J. M. Richardson, Metrologia, 1, p. 114, 1965.
- (13) Glaze, D. J., Helmut Hellwig, Steve Jarvis, Jr., A. E. Wainwright, and D. W. Allan, Recent Progress on the NBS Primary Frequency Standard, Proc. 27th Annual Symposium on Frequency Control, p. 334, 1973.

STIFT CONCEPT

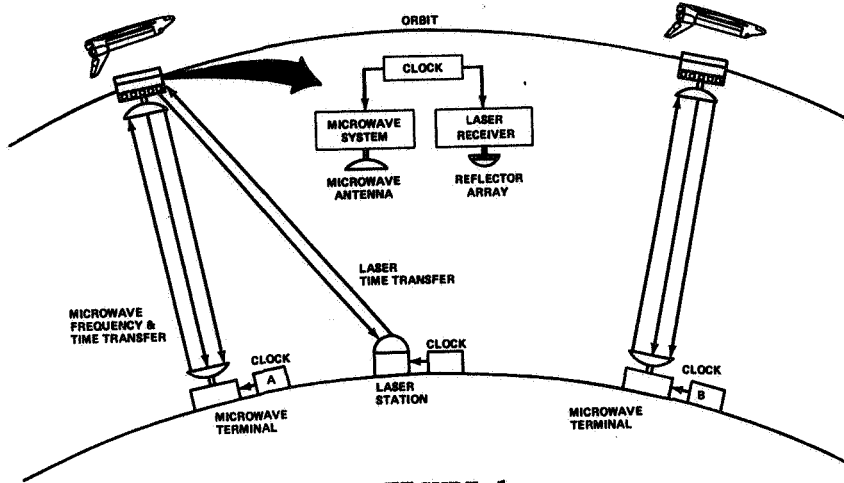


FIGURE 1

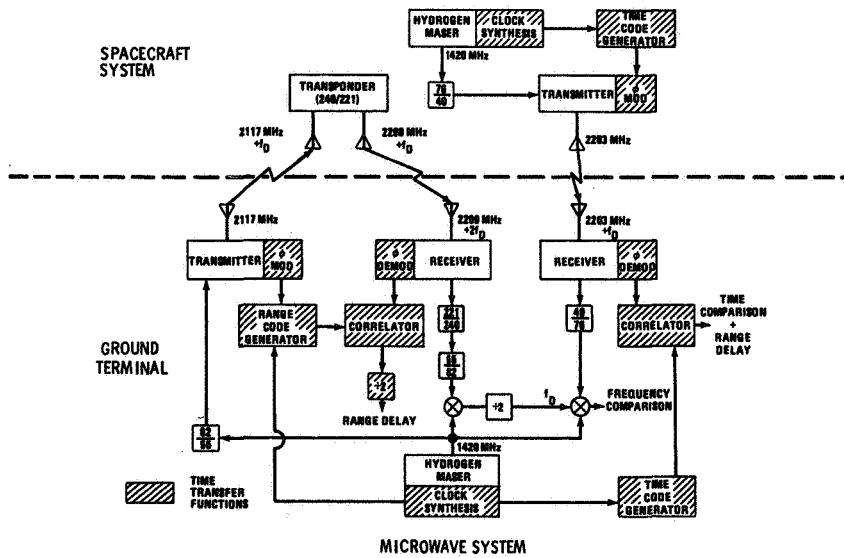
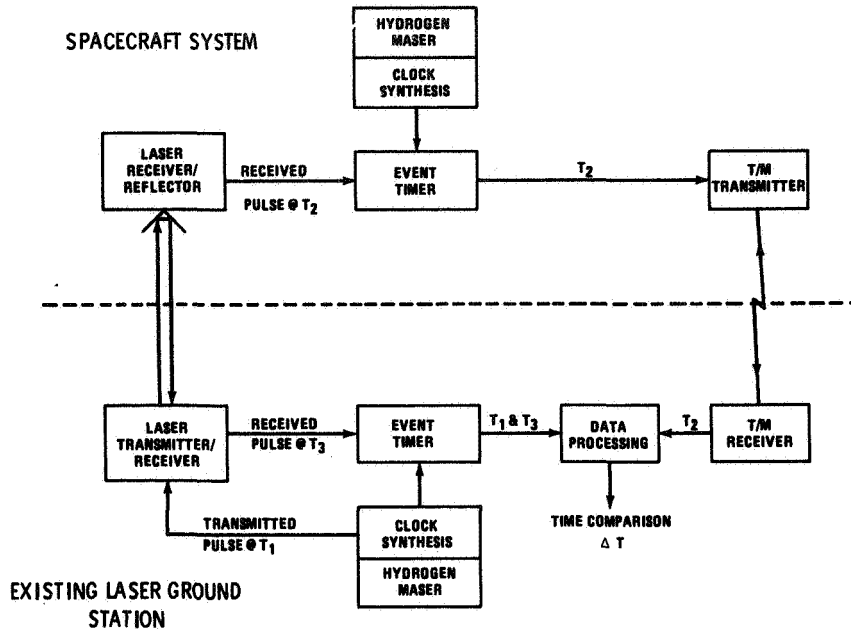


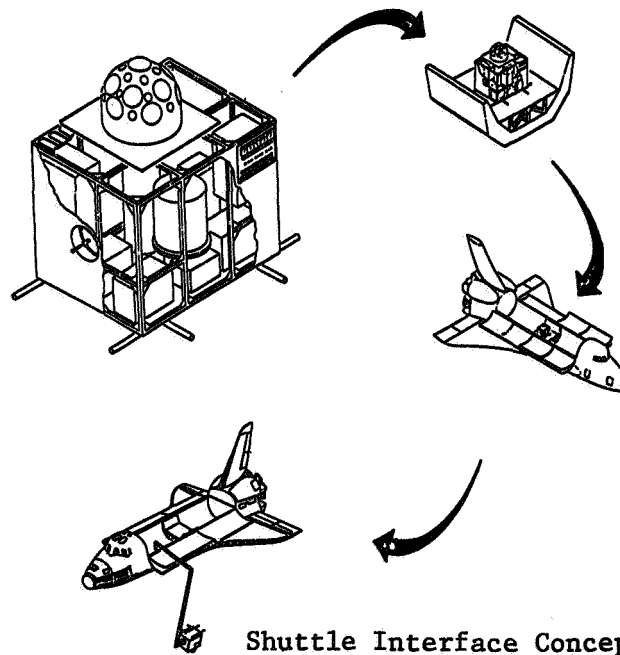
FIGURE 2



Laser Transfer System

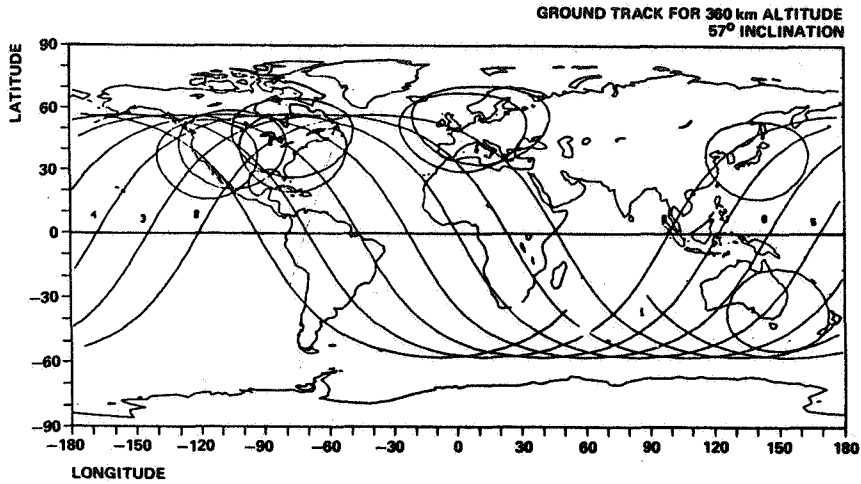
FIGURE 3

STIFT EXPERIMENT
(SHUTTLE TIME AND FREQUENCY TRANSFER)



Shuttle Interface Concept

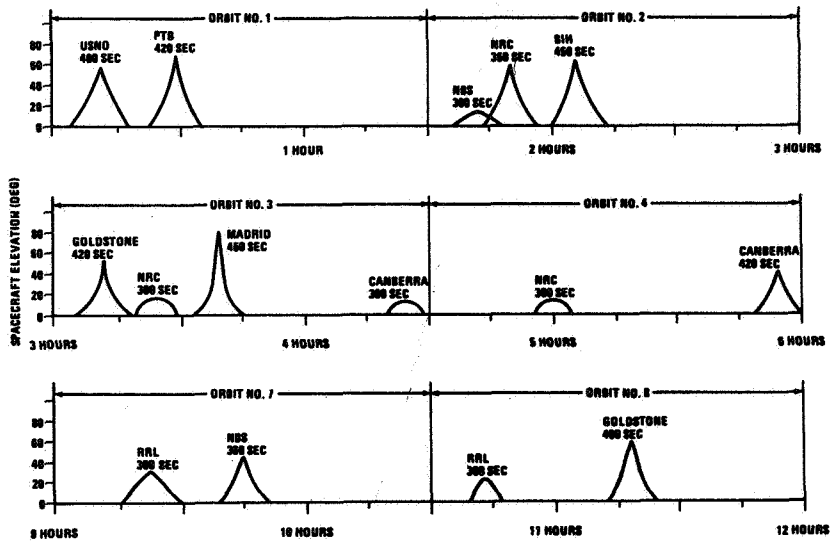
FIGURE 4



POTENTIAL LOCATION FOR MICROWAVE GROUND TERMINALS

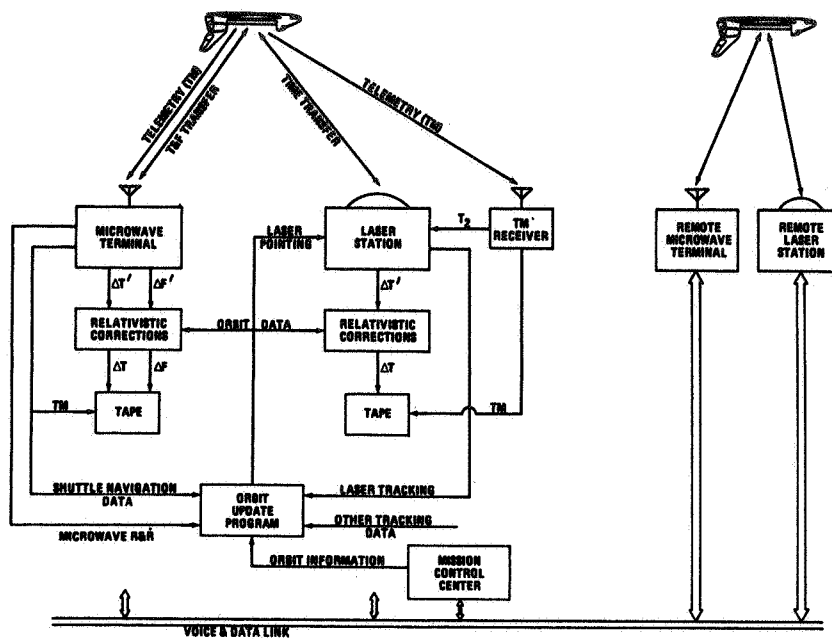
<u>DSN</u>	<u>NATIONAL STANDARD LABS.</u>	<u>TIME SERVICES</u>
GOLDSTONE	NBS - U. S.	USNO - U. S.
MADRID	NRC - CANADA	BIH - FRANCE
CANBERRA	PTB - W. GERMANY	
	RRL - JAPAN	

FIGURE 5



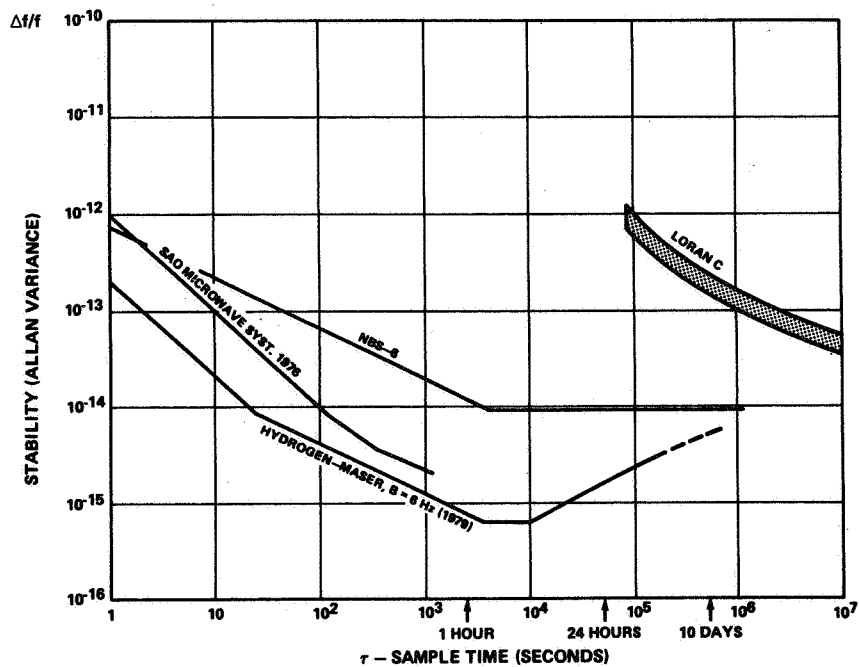
STIFT Elevation at Ground Stations

FIGURE 6



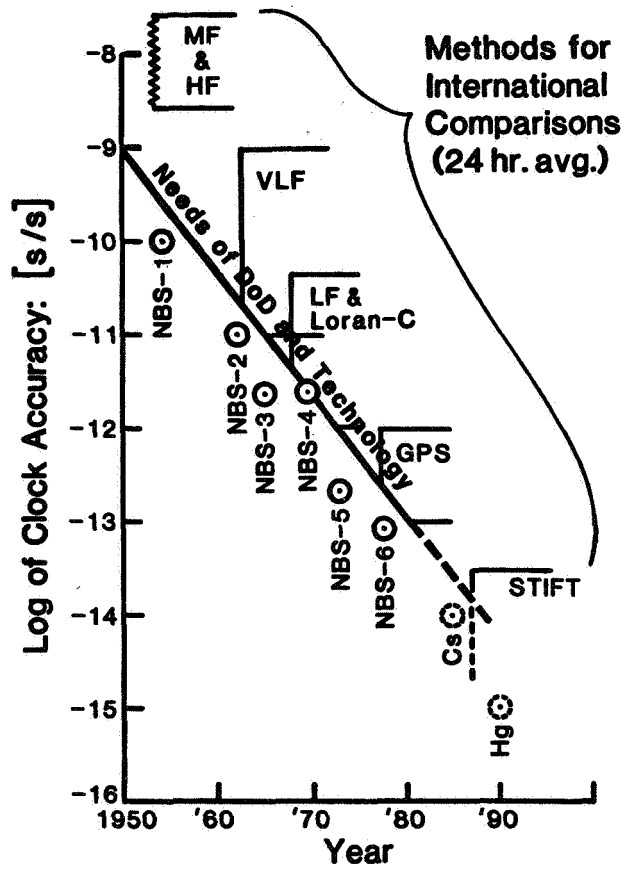
Data System and Interstation Communications

FIGURE 7



Advances in Start-of-the-art Masers

FIGURE 8



Historical Progress in Clock Accuracy Requirements

FIGURE 9

QUESTIONS AND ANSWERS

None for Paper #10.

DESIGN OF THE STIFT TIME AND FREQUENCY
TRANSFER MICROWAVE GROUND TERMINAL

H. Penfield*, E. Imbier⁺, R.F.C. Vessot⁺
Center for Astrophysics, Cambridge, MA

*Harvard College Observatory

⁺Smithsonian Astrophysical Observatory

ABSTRACT

The Satellite Time and Frequency Transfer System (STIFT) is intended to provide, simultaneously, global time comparisons at the subnanosecond level and frequency comparisons to better than 1 part in 10^{14} . It utilizes an orbiting hydrogen maser clock and frequency standard that communicates, via microwave links, time and frequency information to earth terminals operated by hydrogen masers controlling local clocks. A two-way microwave link, to and from the space vehicle provides Doppler information used to cancel the Doppler shifts in a one-way link from the spaceborne oscillator. Pseudo-random noise (PRN) modulation in the two-way link also provides range information to cancel the range delay in the PRN time transfer between space and earth. The pseudo-random noise modulation system for time difference measurement and its incorporation in the Doppler cancellation system for frequency comparison is explained. The particular PRN code sequence selected and an analysis of the system is discussed.

BACKGROUND

The ongoing development of atomic frequency standards presently provides us with stability better than 1 part in 10^{15} over hourly averaging intervals and ever increasing accuracy. This now poses a serious challenge to current techniques that transfer time and frequency on a global scale so that the precision of transfer is commensurate with the performance of these clocks. Today, the most commonly used time transfer technique is the transportable clock. However, this method has significant disadvantages. It is prohibitively costly, if carried out on a continuous basis, and the process is generally limited to an uncertainty of the order of 100 nanoseconds owing to environmental conditions during transport. The Global Positioning System (GPS) offers an alternative with an accuracy level of the order of 10 nanoseconds, but it does not have the capability of transferring frequency. However, the concept of a transportable clock, moving from one site to another as a means for coordinating time and frequency on a global scale can be logically extended to a clock orbiting the earth in a satellite. The hydrogen maser, with its frequency stability of the order of 6 parts in 10^{16} , for 1 hour averaging interval, is ideal for such an orbiting time transfer clock and oscillator to provide time and frequency difference measurements of 1 nanosecond and 1 part in 10^{14} respectively with stations anywhere in sight of the orbiting system.

Relation to GP-A

Experience already exists in the practical application of hydrogen maser technology to the space environment. In June 1976, SAO participated with NASA in the Gravitational Probe A (GP-A) experiment. This experiment was designed to probe the Earth's gravity field in a nearly vertical trajectory to an altitude of 10,000 KM. The hydrogen maser used in GP-A required highly specialized design to cope with the traumatic changes in thermal, magnetic and gravitational environment without allowing time for thermal stabilization or magnetic readjustment. Even though the maser operating life in space on GP-A was limited to about two hours, the maser was designed for continuous operation throughout many months of testing. The experience gained in designing and operating the space maser on GP-A is directly applicable to the orbiting transfer clock. In addition to the space maser technology, GP-A also provided important experience in the use of microwave links to compare space and ground clocks. The feasibility of cancelling propagation effects in the troposphere and ionosphere and of removing Doppler shifts was demonstrated successfully by the GP-A experiment.

Choice of Frequencies

The microwave frequencies used in the GP-A experiment were chosen to be compatible with the Unified S Band (USB) System and this same choice is to be carried through the Satellite Time and Frequency Transfer Experiment. The STIFT system requires both a 2-way up/down link and a 1-way down link between the orbiting clock and the ground clock. The frequencies in this system are selected to cancel the first order ionospheric dispersion. Thus, the 2-way link utilizes 2,117 MHz for the up transmission to the orbiting clock and 2,299 MHz for the transponded down transmission to the ground clock. The 1-way link transmits down from the orbiting clock on a frequency of 2,203 MHz. With this selection of frequencies, the combined ionospheric dispersion for the 2-way link is just twice that of the 1-way link and may be cancelled in subsequent frequency difference processing in the STIFT ground terminal.

SYSTEM DESCRIPTION

The STIFT system is designed to provide simultaneous precision measurement of time difference and frequency difference between a ground clock and the orbiting space clock. Figure 1 illustrates the overall STIFT system design including the Space Terminal, Microwave Ground Terminal and Laser Ground Terminal. The discussion that follows deals primarily with the Microwave Ground Terminal and the other sections of the system are shown in Figure 1 only to give some perspective to the role of the Microwave Ground Terminal.

2-way Link

The 2-way microwave link between the space terminal and the ground terminal serves three major functions. First, it measures the path delay between the two terminals; second, it provides the reference for first order Doppler cancellation and third, it compensates for ionospheric dispersion through selection of link operating frequencies relative to the 1-way link frequency.

The up-link transmit frequency is derived from the atomic hydrogen maser oscillator by a coherent frequency translation process. In Figure 1, the atomic hydrogen maser oscillator is shown as the ground clock and the 2,117 MHz up-link transmit carrier frequency is obtained by an 82/55 translation of the L-Band maser output. A part of the 2,117 MHz carrier is utilized as coherent local oscillator drive in the first heterodyne mixers of both the 2-way and 1-way receivers in the ground terminal.

Prior to being transmitted, the 2,117 MHz signal passes through a phase modulator which impresses a 90 degree phase shift on the carrier under the control of a pseudo-random noise (PRN) generator. This PRN phase modulated signal is then amplified to approximately ten watts and coupled through a ferrite circulator to the ground terminal antenna. This single antenna is a common element for both the 2-way and 1-way links and consists of a small (1 meter) steerable parabolic dish with a gain of about 25db and a half-power beamwidth of 9.5 degrees at the S-band operating frequencies.

The 2,117 MHz ground terminal transmit signal is received by a broad beam, circularly polarized antenna at the space terminal and is coupled through a triplex filter to the input of a phase coherent transponder. The transponder strips the phase modulation from the received signal, coherently translates the 2,117 MHz carrier by the ratio 240/221 and reapplies the phase modulation to form a 2,299 MHz transponder output signal. This 2,299 MHz signal is coupled through the triplex filter to the space terminal antenna and transmitted toward the ground terminal.

The received 2,299 MHz signal, at the ground terminal, is picked up by the parabolic antenna and coupled through the ferrite circulator to a diplex filter that separates the 2-way and 1-way received signals and provides high rejection to the 2,117 MHz transmit signal. The low-noise amplifier, at the output of the diplex filter, feeds the 2,299 MHz signal to a mixer where it is heterodyned with the 2,117 MHz local oscillator signal to form a 182 MHz IF signal. The carrier component of the IF signal is extracted by a carrier phase-lock loop and is used in subsequent processing to cancel first order Doppler in the frequency difference determination.

The 182 MHz IF signal (full band) and extracted IF carrier component also are fundamental input signals for the 2-way Time Discriminator. A digitally delayed PRN code generator (with the identical code sequence used to modulate the 2,117 MHz transmit signal) is coupled in a closed-loop tracking configuration with the Time Discriminator to automatically lock-on and track the path delay in the 2-way link. This 2-way path delay, in digital form, is divided by two and used in conjunction with the 1-way receiver output to determine time difference between the space clock and ground clock.

1-way Link

The 1-way microwave link between the space terminal and the ground terminal operates on a carrier frequency of 2,203 MHz. This signal is derived from the L-Band hydrogen maser coupled to a 76/49 frequency translator. A PRN

code generator, with the identical code sequence used by the PRN generators in the ground terminal, controls the phase modulation (90 degrees) that is impressed on the 2,203 MHz carrier prior to transmission from the space terminal. The triplex filter couples the 1-way link transmission to the common space terminal antenna used for both the 2-way and 1-way links.

The received 2,203 MHz signal, at the ground terminal, is coupled from the parabolic antenna through the ferrite circulator to the diplex filter in the same fashion as the 2,299 MHz 2-way link signal. The 2,203 MHz signal is split off separately by the diplex filter and fed through a low-noise amplifier to a mixer where it is heterodyned with the 2,117 MHz local oscillator to form an 85 MHz IF signal. The carrier component of this IF signal is extracted by a carrier phase lock loop and after frequency translation, is compared with the processed 2-way IF carrier to establish the frequency difference between the space clock and the ground clock.

The 85 MHz IF signal (full band) and extracted IF carrier component are coupled to the 1-way Time Discriminator. A PRN code sequence (identical to the other PRN code sequences used in the ground and space terminals) is digitally delayed and automatically locks-on and tracks the 1-way path delay plus the time difference between the ground clock and the space clock. Path delay is cancelled by subtracting half of the 2-way path delay leaving a direct, real time output of the apparent time difference between the two clocks. True clock difference is obtained from post-real time data reduction in which relativistic and gravitational effects are removed.

TIME DIFFERENCE MEASUREMENT

The STIFT microwave ground terminal is designed to provide time difference measurements between a space clock and a ground clock to an accuracy of 1 nanosecond. This time difference measurement is implemented through the use of a periodic pseudo-random noise (PRN) code that is phase modulated on the 2-way and 1-way microwave links. Simultaneous measurement of time delay in both the up/down (2-way) and down (1-way) receivers in the ground terminal allows cancellation of propagation delay between the space terminal and ground terminal.

Figure 2 is a detailed block diagram of the time delay tracking loops for both the 2-way and 1-way receivers.

PRN Time Discriminator Tracking Loop

The operation of the delay tracking loops is based on a time discriminator circuit that senses time coincidence between the PRN code modulation on the received signal and a PRN code that is precisely shifted relative to the received code.

When two similar periodic time functions, such as the two PRN code sequences, are shifted in time relative to each other and then multiplied together and averaged over one period, the result has the form of the autocorrelation

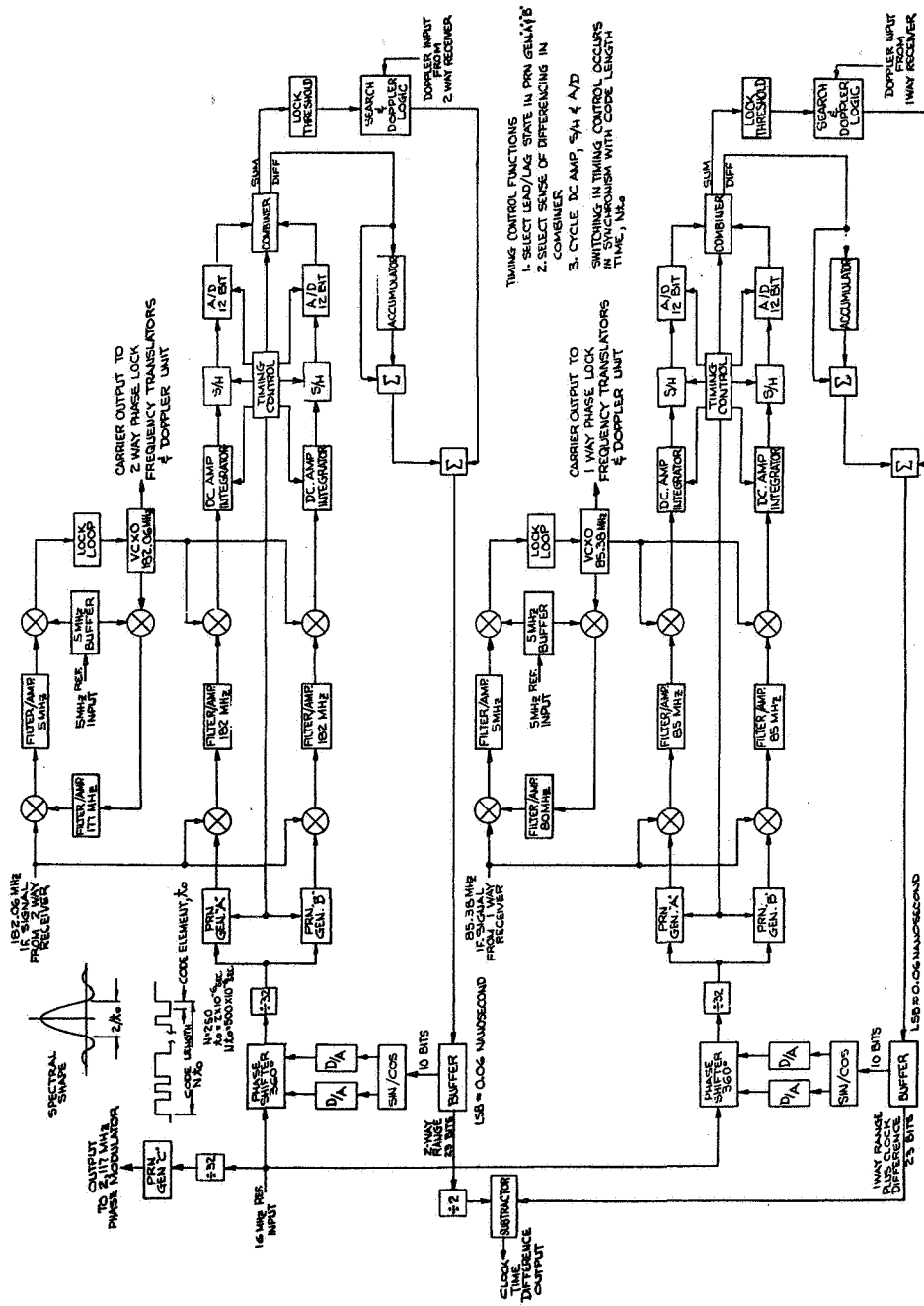


Figure 2. STIFT Microwave Ground Terminal Time Delay Tracking Loops

function of the original time function. Periodic autocorrelation functions are characterized by a maximum value that occurs when the relative time shift is zero or some integer multiple of the time function period. As the relative time shift increases (or decreases), the autocorrelation function drops to a lower value. The rate at which the autocorrelation function decreases either side of maximum is proportional to the spectral width (bandwidth) of the time function. The magnitude of the "hash" level between maximum points is determined by several factors including the product of the spectral width and time function period (time-bandwidth product) and the detailed shape of the time function. The PRN code sequence represents a time function that can be optimized to have an "ideal" autocorrelation function in which the "hash" level is uniform with a magnitude, relative to the maximum, that is equal to the reciprocal of one half the time-bandwidth product.

The PRN code is a binary sequence composed of "N" code elements in each period. Individual code elements have a duration of " t_0 " and may be either "1" (+) or "0" (-) as determined by the code sequence. Figure 2 gives a pictorial representation of the autocorrelation for a 31 element PRN code. Two different cases are illustrated; the first with an offset or delay (i.e., non-aligned codes) and the second without any offset (i.e., aligned codes). In each case, the output obtained by integrating the product of the codes over a complete period (Nt_0) is shown below the codes. Note that when there is no delay between codes, the integrated output builds up linearly over the period whereas in the case of an offset, the integrated output fluctuates back and forth about zero during the period.

The time discriminator utilizes two correlation circuits that are driven by separate PRN code generators operating with a fixed offset in time, relative to each other, equal to one code element, t_0 . Figure 4 is an expanded picture of the correlation process as a received code moves in delay relative to the two PRN codes, A and B. The code sequence in this figure is the same as that used in Figure 3. The A and B codes are displaced relative to each other by t_0 and are symmetrically displaced about the nominal zero delay point by $t_0/2$. Thus, the maxima in the A and B correlation outputs are displaced symmetrically either side of zero delay. When the A and B outputs are added together, the result is a flat topped signal with a half amplitude duration of $2 t_0$. When the B output is subtracted from the A output, the result is a time discriminator signal with a linear slope of $2/t_0$ times the amplitude of the maxima and passing through zero at the zero delay point. This time discriminator signal is utilized as the time error signal in the closed loop time tracking sections of both the 2-way and 1-way receivers of the STIFT microwave ground terminal.

Figure 5 shows a block diagram of the time discriminator and delay tracking loop. The circuit requires three inputs:

1. Signal (full band receiver IF),
2. Carrier (receiver IF carrier), and,
3. Clock drive for PRN generators,

and provides a digital output representing the delay between the received signal modulation code and the nominal zero delay point of the A and B PRN generators.

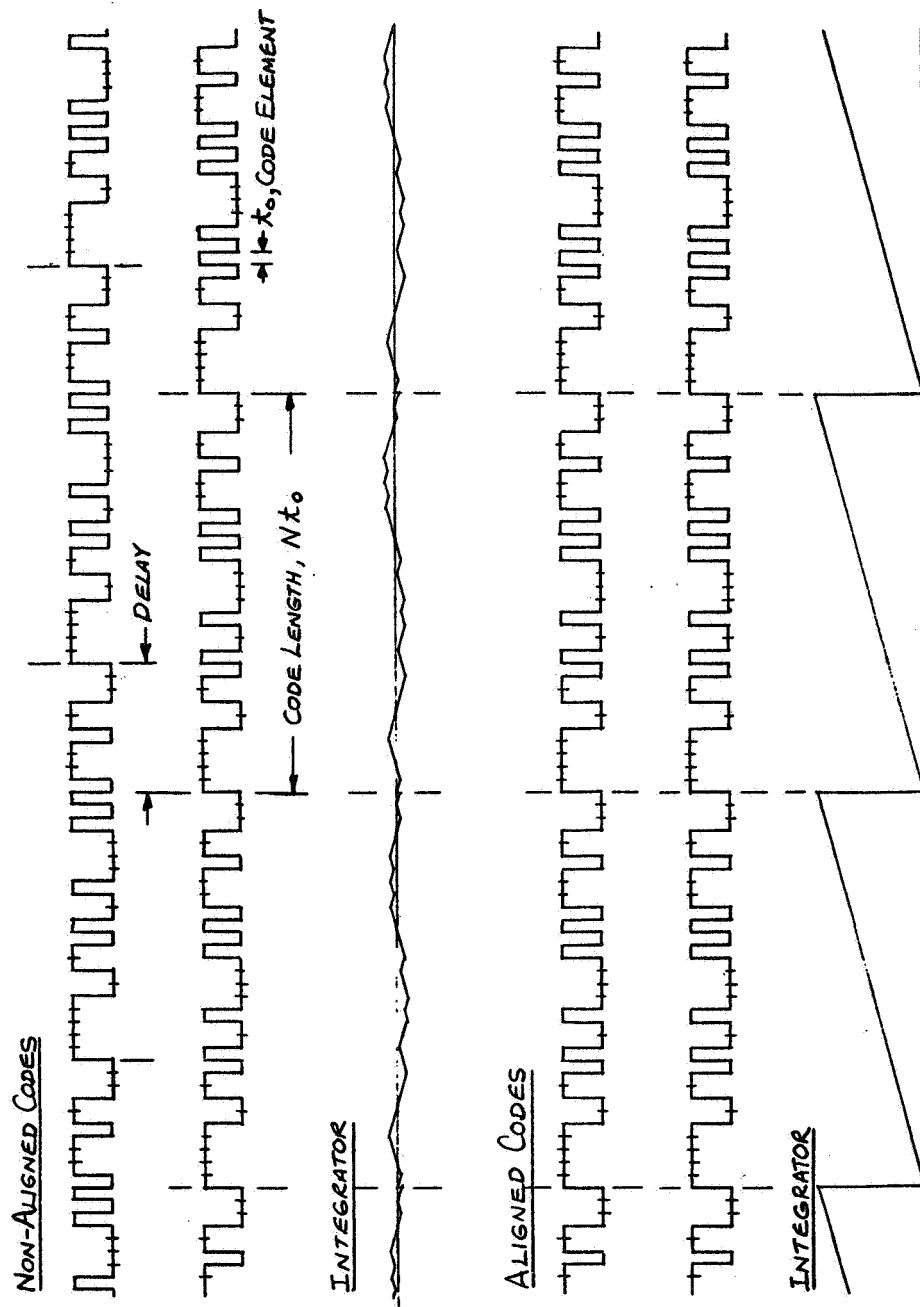


Figure 3. Non-aligned and Aligned Correlation of 31 Element Code

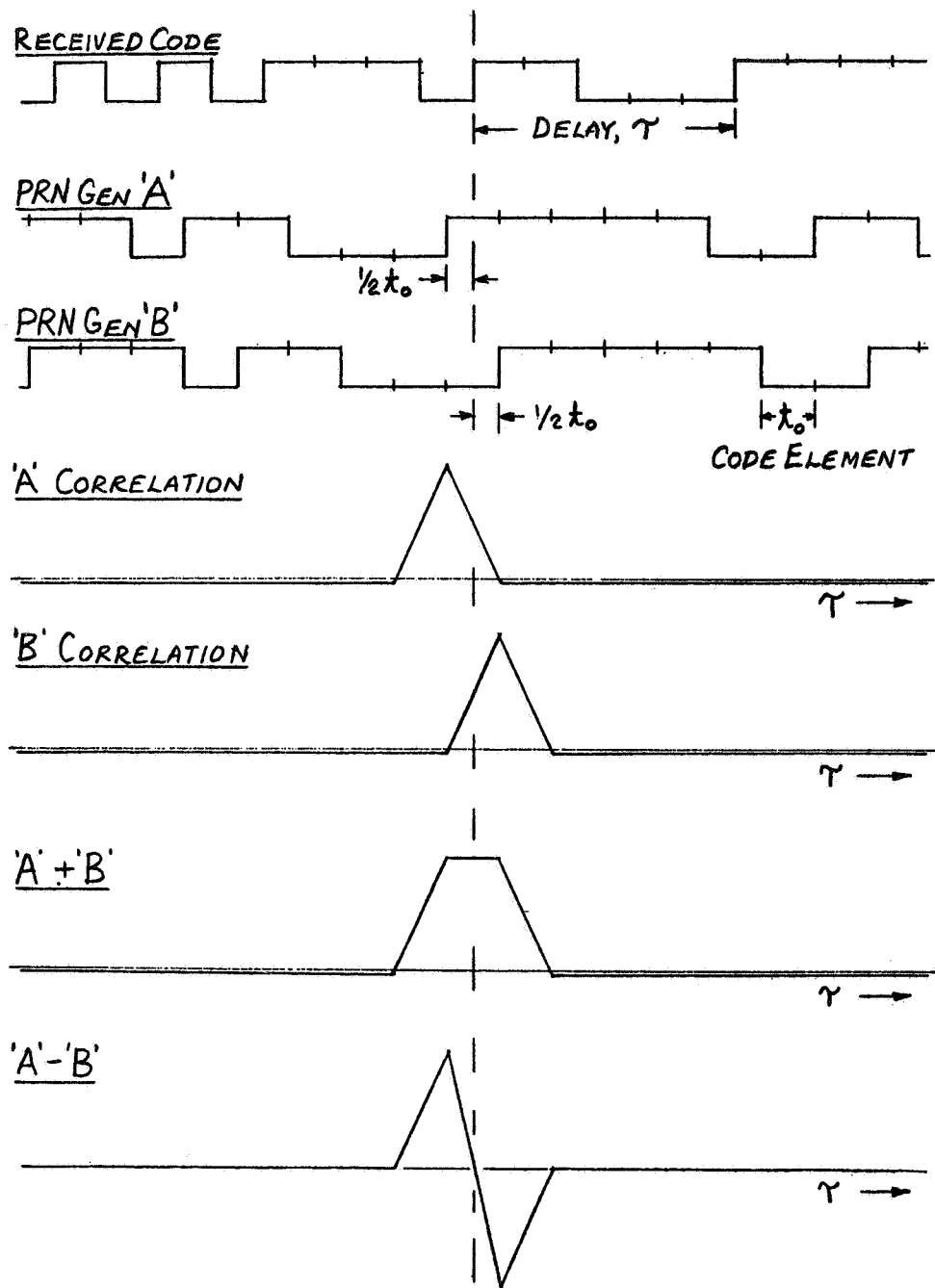


Figure 4. Time Discriminator Autocorrelation and Sum and Difference Outputs for 31 Element Code

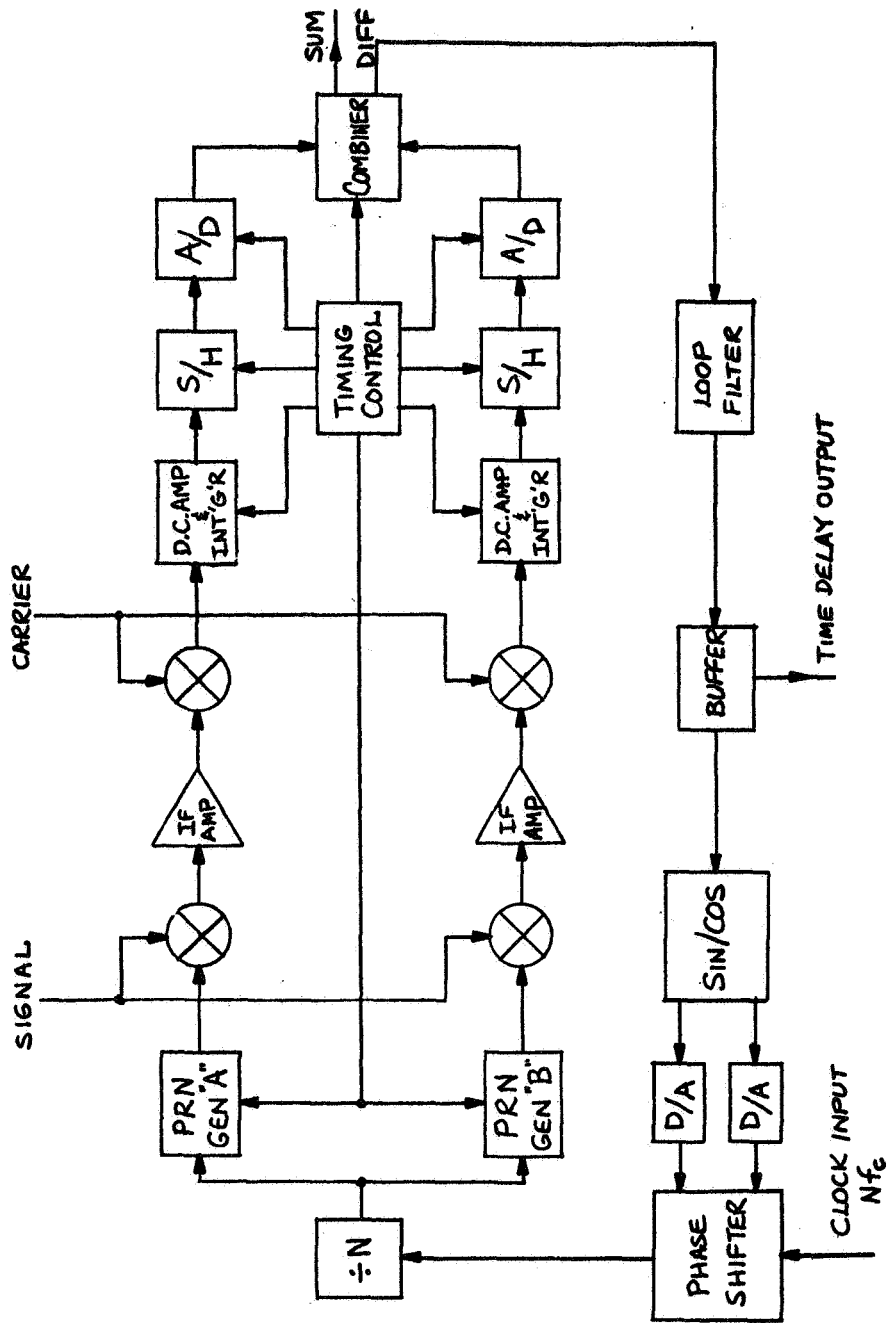


Figure 5. Block Diagram of Time Discriminator and Delay Tracking Loop

Precise control of the delay of the A and B PRN generators is obtained by passing the clock input through a phase shifter followed by a divider. The phase shifter is essentially a single sideband modulator that is driven by the digital error output from the time discriminator. The lower ten bits of the error output are converted to sine and cosine terms and these are then converted to quadrature analog signals by digital-to-analog (D/A) converters that drive the single sideband modulator. The full range of ten bits (1024) represents one complete cycle of phase shift at the clock input frequency. The phase shifted clock frequency drives a digital divider circuit to reduce the clock frequency to the $1/t_0$ rate required to drive the A and B PRN generators.

In the STIFT system, the value of t_0 is 2 microseconds (500 KHz clock rate) and the digital divider factor is 32. Hence, the clock input frequency to the phase shifter is 16 MHz. The time resolution of the time discriminator in terms of the time delay represented by 1 bit in the error signal is $1/(1024 \times 16 \times 10^6)$ or 0.06 nanoseconds. Relating this to the slope of the time discriminator response yields a total of 32,768 bits (32 complete cycles of the phase shifter) over the linear slope region between the maximum and minimum points. The period of the PRN code is 500 microseconds (250 code elements) thus, the total number of bits for one period is 8,192,000 (8,000 complete cycles of the phase shifter). In order to accommodate this full range of delays, the digital output from the tracking loop will be a 23 bit binary number. Since the period in terms of bits is less than the maximum numerical value of the 23 bit binary number (8,388,607) the loop output will be reset to zero when it tries to exceed 8,191,999.

The operation of the time discriminator and delay tracking loop illustrated in Figure 5 starts with the injection of the full band receiver IF signal into balanced demodulators (mixers) in both the A and B channels of the time discriminator. The A and B PRN generators provide the other input to these demodulators. The output from each demodulator (still at the IF level) is amplified and coupled to a second mixer where it is heterodyned with the IF carrier. The output from each of the second mixers is a fluctuating dc level representing the correlation voltage. This dc level is then amplified and integrated over the duration of one period of the PRN code. At the end of the integration cycle, the integrator output is sampled and held and converted to a 12 bit binary number. The separate digital outputs from the A and B channels are combined to form both sum and difference output numbers. The cycle timing for the integrators, sample/hold circuits and Analog-to-Digital converters is generated by a timing control circuit. This circuit also reverses the relative delay "sense" of A and B PRN generators and combiner differencing polarity at the end of each period in order to cancel drifts and voltage or current offsets in the A and B channels of the time discriminator. Thus, two complete periods of the PRN generator (1 millisecond) is the time required to obtain a valid error signal (difference output at the combiner). The digital error signal is coupled to a loop filter (accumulator) and then through a buffer to the sine/cosine unit to complete the tracking feedback loop.

The time delay output in the form of a 23 bit binary number is taken from the buffer. The update rate on this output is 1KHz.

PRN Code Sequence

There is no unique PRN code sequence that is optimum for the time difference measurement in STIFT. Several guidelines that were followed in establishing the parameters for the code are listed below:

1. The code length, or period, should be sufficient to allow easy resolution of any ambiguity.
2. The code length should be such that it can be conveniently used to time-tag the clocks.
3. The code element duration should be selected to give reasonable time discrimination characteristics and also to be compatible with the USB transponder bandwidth of approximately 800 KHz.
4. The code element duration should be compatible with the code length in the sense that the code length must be an exact integer multiple of the code element duration.
5. The code element duration should allow a clock rate that is easily derived from standard frequencies.

After consideration of the various tradeoffs involved in satisfying these guidelines, the choice of 500 microsecond code length with 250 code elements of 2 microseconds duration was made.

The STIFT system requires a total of six PRN generators, all of which may* provide identical code sequences. A convenient means of generating these codes is to utilize a digital shift register with feedback from two or more stages through Exclusive Or (XOR) logic gates to the input stage. With proper feedback connections, these shift register code generators provide a code that repeats every $2^n - 1$ shifts (elements) where "n" is the number of stages in the shift register. This special class of codes, known as "Maximal Linear Codes", have the characteristic of containing all possible sequences of length "n" except for the sequence of all zeros. These Maximal Linear Codes also exhibit a very special autocorrelation function in which the hash level between maxima remains "flat" with a magnitude of $1/(2^n - 1)$ relative to the maximum value.

A PRN code generator utilizing an eight stage shift register will yield a code sequence that contains 255 elements. The required length of 250 may be obtained by truncating this 255 element code. The truncation is implemented either by counting clock pulses and parallel loading the initial state in the shift register each time 250 pulses are counted or by sensing the particular state corresponding to the 250th shift and parallel loading at that point.

The truncation of a maximal linear code sequence destroys the flat hash level and replaces it with a noise-like fluctuation.

The behavior of the hash level in truncated maximal linear codes for eight stage shift registers has been investigated to determine if there is any particular feedback configuration that gives the lowest hash level. The results of this investigation are summarized in Table 1.

*The 2-way and 1-way link codes may use different sequences.

Table 1. Truncated Maximal Linear Code Hash Level

Stages Tapped for Feedback	Peak	Hash Level	
		Ave.	Rms
2,3,4,8	22	7.4	5.1
2,5,6,8	22	8.0	6.0
1,3,5,8	22	7.2	5.5
3,5,6,8	26	7.8	6.0
1,6,7,8	30	7.2	5.4

There is no great difference among the five feedback configurations that were studied, except for the higher peak hash values found with the last two configurations. In general, the hash level for all configurations remained low (peak less than 6) for at least 16 code element delays either side of the zero delay maximum. The 1,3,5,8 feedback configuration showed the lowest hash level for the greatest delay either side of zero delay so, for this reason plus its good performance in terms of overall average and rms hash level, it has been selected for the STIFT system. Figure 6 shows *one-half* cycle of the autocorrelation function for the PRN code sequence generated by the 8-stage shift register with feedback taps from stages 1,3,5 and 8.

FREQUENCY DIFFERENCE MEASUREMENT

The STIFT microwave ground terminal is designed to provide frequency difference measurement between a space clock and a ground clock to an accuracy of 1 part in 10^{14} . The realization of this level of accuracy is made possible through a first order Doppler cancellation scheme that was utilized in the GP-A experiment in 1976. The key to the first order Doppler cancellation is the use of phase-locked frequency translators in the 2-way and 1-way receivers to reference the 2-way IF carrier to the ground maser frequency and the 1-way IF carrier to the space maser frequency.

Frequency Translation

The ground maser frequency undergoes two coherent frequency translations prior to being received by the ground terminal 2-way receiver. A translation of 82/55 is applied prior to transmission toward the space terminal and a 240/221 translation occurs in the space terminal transponder. Both of these translations are then counteracted by 221/240 and 55/82 translations in the 2-way receiver. The space maser is translated in frequency by the ratio 76/49 prior to being transmitted toward the ground terminal and this translation is counteracted by a 49/76 translation in the 1-way receiver.

The effects of frequency translations and Doppler on the 2-way link are analyzed as follows:

Carrier transmitted to space terminal, f_1

$$f_1 = f_0 (82/55) \quad (1)$$

where f_0 = ground maser frequency.

PRN CODE AUTOCORRELATION ($1/2$ CYCLE)

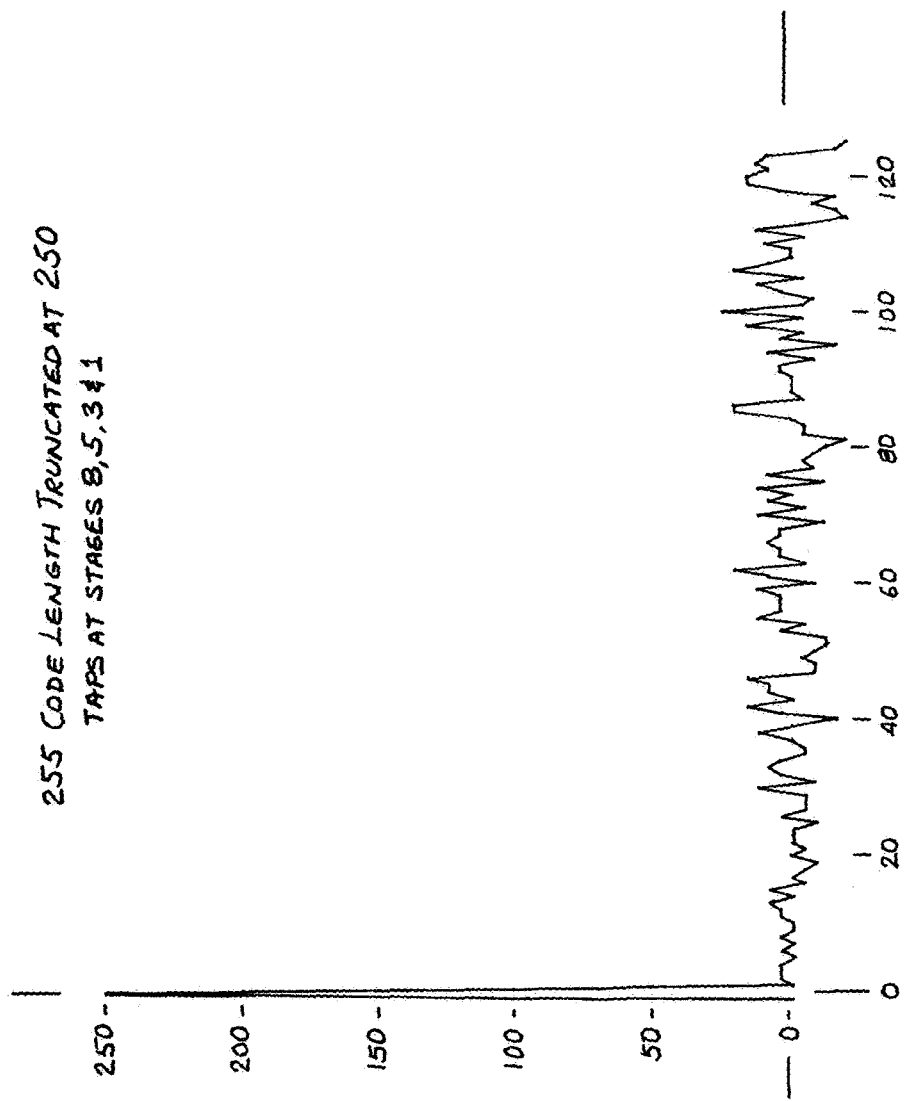


Figure 6. One-half Cycle of Autocorrelation for Truncated Eight Stage Shift Register PRN Code

Carrier received at space terminal,

$$f_1 (1 + v/c) \quad (2)$$

where v = radial velocity of space terminal relative to the ground terminal

c = velocity of propagation

Carrier transponded from space terminal,

$$f_1 (1 + v/c) (240/221) \quad (3)$$

Carrier received at ground terminal

$$f_1 (1 + 2 v/c) (240/221) \quad (4)$$

First IF carrier in 2-way receiver

$$f_1 (1 + 2 v/c) (240/221) - f_1 \quad (5)$$

2-way IF carrier after 221/240 and 55/82 translation

$$f_1 (1 + 2 v/c)(55/82) - f_1 (221/240)(55/82)$$

or by substituting $f_0 (82/55)$ for f_1

$$f_0 (1 + 2 v/c) - f_0 (221/240) \quad (6)$$

This last expression, (6), is the 2-way IF carrier output reference to the the ground maser frequency. Note that only first order Doppler is shown in the expression above. Relativistic and gravitational effects are discussed in the section below on Doppler cancellation.

The effects of frequency translations and Doppler on the 1-way link are analyzed as follows:

Carrier transmitted from space terminal, f_2

$$f_2 = f'_0 (76/49) \quad (7)$$

where f'_0 = space maser frequency.

Carrier received at ground terminal,

$$f_2 (1 + v/c) \quad (8)$$

First IF carrier in 1-way receiver,

$$f_2 (1 + v/c) - f_1 \quad (9)$$

1-way IF carrier after 49/76 translation
or by substituting for f_2 and f_1

$$f'_0 (1 + v/c) - f_0 (49/76)(82/55) \quad (10)$$

Expression (10) is the 1-way IF carrier output referenced to the ground maser frequency f_0 , and the space maser frequency, f'_0 .

Doppler Cancellation

First order Doppler cancellation is achieved by dividing the 2-way IF carrier output, (6), by 2 and taking the difference between that and the 1-way IF carrier output (10).

The desired end result in this process is to obtain a direct measure of Δf , the frequency difference between the ground maser and the space maser.

$$\Delta f = f_0 - f'_0 \quad (11)$$

Carrying through the Doppler cancellation and the substitution of Δf for $f_0 - f'_0$, the following result is obtained:

$$\Delta f + f_0 (83/100320) + (f_0/c^2) \left[(\vec{r}_{sp} \cdot \vec{\alpha}_e) - 1/2 (\vec{v}_{sp} \cdot \vec{v}_e)^2 + \Delta\theta \right] \quad (12)$$

In addition to the desired frequency difference, Δf , the output of the Doppler cancellation process contains; 1) a constant term, $f_0(83/100320)$, 2) an uncancelled Doppler term, $(f_0/c^2)(\vec{r}_{sp} \cdot \vec{\alpha}_e)$ where \vec{r}_{sp} is the line-of-sight vector and $\vec{\alpha}_e$ is the ground terminal acceleration due to Earth rotation, 3) a second

order Doppler term $(f/2c^2)(\vec{v}_{sp}-\vec{v}_e)^2$ where \vec{v}_{sp} and \vec{v}_e are the space and ground terminal velocity vectors and 4) a redshift term $(f_0/c^2)\Delta\phi$, where $\Delta\phi$ is the Newtonian potential difference between Earth and space. The constant term is removed by heterodyning the Doppler cancellation output with a synthesized frequency equal to τ_0 (83/100320), approximately 1.1751621 MHz. The uncanceled Doppler term, second order Doppler and redshift terms are removed by post-real time processing based on the position and velocity information computed from the satellite flight profile relative to the ground terminal.

ACCURACY ANALYSIS

The accuracy expected from the STIFT microwave ground terminal is calculated using the following system parameters:

Microwave Ground Terminal

Transmit Power (2-way uplink)	10 watts
Peak-to-Peak Phase Excursion	90 degrees
Receiver Noise Figure (includes input losses)	5 db
Antenna Gain (1 meter, 55% efficiency)	25 db
Polarization	Linear
PRN Code Element Duration	2 microseconds
PRN Code Sequence Length	250 elements

Space Terminal

Transmit Power (2-way down link)	250 milliwatt
Transmit Power (1-way link)	250 milliwatt
Peak-to-Peak Phase Excursion	90 degrees
Receiver Noise Figure (2-way uplink)	13 db
Antenna Gain	3 db
Polarization	Circular
PRN Code Element Duration	2 microseconds
PRN Code Sequence Length	250 elements

Propagation Path (2 cases)

Zenith Angle (ground terminal)	0 degrees	80 degrees
Range	437 km	1536 km
Path Loss	125 db	163 db
Atmospheric Loss	0 db	0.4 db

Link Noise Margins

Utilizing the system parameters listed above, the signal-to-noise ratios in a 1 MHz bandwidth at the receiver inputs are as follows

Ground Terminal Zenith Angle	0 degrees	80 degrees
S/N 2-way up link	13.8 db	2.8 db
S/N 2-way down link	6.1 db	-4.9 db
S/N 1-way down link	6.1 db	-4.9 db

If the space terminal transmit channels are increased to a 10 watt power output, the situation is improved as follows:

Ground Terminal Zenith Angle	0 degrees	80 degrees
S/N 2-way up link	13.8 db	2.8 db
S/N 2-way down link	22.1 db	11.1 db
S/N 1-way down link	22.1 db	11.1 db

When the carrier is phase modulated by a square wave type signal such as the PRN code, the fraction of carrier component in the output is given by:

$$(2/\pi\beta) \sin (\pi\beta/2) \quad (13)$$

where, β is the modulation index. For the case of 90 degree modulation (i.e., ± 45 degrees) β is unity and the carrier component, following phase modulation, has an amplitude of $2/\pi$ relative to the unmodulated carrier. Thus, in the 90 degree PRN phase modulated signal, 40.5 percent of the energy is in the carrier and 59.5 percent is in the modulation sidebands.

Time Difference Uncertainty

The uncertainty in time difference measurement is computed by proceeding step-wise through the time discriminator and delay tracking loop. For the case of a 250 milliwatt space terminal transmit power and the 80 degree zenith angle, the full band signal-to-noise ratio in 1 MHz is -4.9 db. Since 59.5 percent of the signal power is in the modulation sidebands, the effective signal-to-noise ratio at the signal input of the time discriminator is -7.2 db. The demodulation and integration process in the time discriminator provides coherent enhancement to the signal-to-noise ratio, under locked conditions, that is equal to the number of code elements in one period of the code sequence. Thus, the signal-to-noise ratio at the output of the integrator for the STIFT code sequence of 250 elements is 40.8 db. When the A and B channels of the time discriminator are combined to form the difference (loop error) output, this signal-to-noise ratio is reduced to 37.8 db. Further reduction in noise occurs in the loop filter where 64 of the difference outputs are accumulated to provide a resultant signal-to-noise ratio of about 46.8 db. In terms of time uncertainty, this represents an rms value of about 4.6 nanoseconds as determined from the slope of the time discriminator response.

When the 2-way and 1-way time tracking loop outputs are subtracted to get the time difference, the overall uncertainty is about 6.4 nanoseconds. Further improvement of this uncertainty to a subnanosecond level will occur through averaging of the difference output and improved IF signal-to-noise obtained at lesser zenith angles and/or increased transmit power.

Frequency Difference Uncertainty

The frequency difference uncertainty is computed for the case of a phase-lock tracking bandwidth of 50 Hz. Taking the 40.5 percent of signal power in the carrier and the case of 250 milliwatt space terminal transmit power and 80 degree zenith angle, the effective signal-to-noise ratio for the carrier in the

full IF band is -8.8 db. Applying the reduction in bandwidth to this ratio yields a signal-to-noise of 34.2 in the 50 Hz tracking bandwidth. Combining the 2-way and 1-way receiver signals in the Doppler cancellation process reduces the signal-to-noise ratio to 31.2 db.

When the Doppler cancellation output is converted to a zero frequency base band, through heterodyning with a 1.17517621 MHz signal followed by low-pass filtering, the maximum anticipated frequency is the order of 1 Hz. Assuming a 100 second averaging time to measure this frequency difference, the uncertainty is about 5 parts in 10^{14} for the 250 milliwatt transmit power at 80 degree zenith angle. When the transmit power is increased to 10 watts in the space terminal, the calculated uncertainty improves to well below 1 part in 10^{14} .

SUMMARY

The design study of the STIFT system shows that, with the current state of the art in atomic hydrogen maser oscillators and with existing time and frequency measurement techniques, it is reasonable to expect accuracy levels of 1 nano-second or less in time difference and 1 part in 10^{14} or better in frequency difference. The application of the STIFT system to time metrology on a global scale and to potential users such as the Deep Space Network, the Orbiting Space Station and the Very Long Baseline Interferometer stations would provide 1 to 2 orders of magnitude improvement over the present accuracy level.

ACKNOWLEDGMENT

The STIFT microwave ground terminal design has been supported thorough NASA grant NAG-8006.

REFERENCES

1. Dixon, R.C. "Spread Spectrum Systems". John Wiley & Sons, N.Y., 1976.
2. "Reference Data for Radio Engineers" H. W. Sams & Co./ITT, Chapter 23, Sixth Edition, Second Printing 1977.

QUESTIONS AND ANSWERS

None for Paper #11.

TIME TRANSFER BETWEEN THE GODDARD OPTICAL RESEARCH FACILITY
AND THE U.S. NAVAL OBSERVATORY USING 100 PICOSECOND LASER PULSES*

C. O. Alley, J. D. Rayner, C. A. Steggerda, J. V. Mullendore, L. Small
and S. Wagner

Department of Physics and Astronomy
University of Maryland
College Park, Maryland 20742

ABSTRACT

A horizontal two-way time comparison link in air between the University of Maryland laser ranging and time transfer equipment at the Goddard Optical Research Facility (GORF) 1.2 m telescope and the Time Services Division of the U.S. Naval Observatory (USNO) has been established. Flat mirrors of 25 cm and 30 cm diameter respectively have been placed on top of the Washington Cathedral and on a water tower at the Beltsville Agricultural Research Center since direct line of sight transmission is not possible. The bent path has a one-way distance of 26 km. Two optical corner reflectors at the USNO, identical to those placed on the Moon during the Apollo program, reflect the laser pulses back to the GORF.

Light pulses of 100 ps duration and an energy of several hundred microjoules from a neodymium-YAG laser, frequency-doubled to a wavelength of 532 nm (green) are sent at a rate of 10 pulses per second. The detection at the USNO is by means of an RCA C30902E avalanche photodiode and the timing is accomplished by an HP 5370A computing counter and an HP 1000 computer with respect to a 10 pps pulse train from the Master Clock.

The reflected light is detected back at the 1.2 m telescope at the single photoelectron level and the epoch of reception is recorded by a University of Maryland designed event timer attached to a NOVA 2/10 minicomputer. About 100 detection events are recorded for 1000 pulses transmitted. The outgoing pulses have their epoch of transmission recorded by the same event timer, which is driven by an HP cesium beam frequency standard.

* This work has been supported by the U.S. Naval Observatory and the Office of Naval Research under contract N000 14-78-C-0338. The following members of the Time Services Division of the USNO have participated actively in the experiments: G.M.R. Winkler, W. Klepczynski, K. Putkovich, A. Kubik, P. Wheeler and D. Chalmers.

The Einstein prescription is used to relate the epoch of the received event at the USNO to the midpoint between the transmitted and received events at the GORF. This procedure is independent of the delays introduced by the atmosphere. The standard deviation for 100 comparisons is typically 200 to 400 ps. The corresponding standard deviation of the mean is 20 to 40 ps. We are still working on the calibration accuracy which at present is 1 to 2 ns, established by a portable clock trip.

The link was to have been a near real time connection with the USNO during our planned participation in the LASSO experiment. The link is also serving to provide experience for the high accuracy short pulse laser time transfer part of the Space Time and Frequency Transfer (STIFT) experiment to be discussed at this PTTI meeting.

INTRODUCTION

There have been two major purposes for the experiments described in this paper.

1) To gain additional practical experience with the short laser light pulse technique of time comparison between remote clocks. The method was pioneered in atomic clock experiments with aircraft which measured the effect of gravitational potential on time.¹ It will be used in both the Laser Synchronization from Stationary Orbit (LASSO)² and the Space Time and Frequency Transfer (STIFT)³ experiments, if these are carried out. The technique offers the most accurate practical means of remote time comparison.

2) To provide a link to the USNO from the GORF 1.2 meter telescope to facilitate time comparison with Western Europe during the LASSO experiment. The failure on 20 September 1982 of the third stage of the ARIANE rocket carrying the SIRIO-2 satellite with the LASSO instrumentation has prevented this experiment from being performed. The LASSO participants have been informed by P. Berlin, the project manager for the SIRIO-2 satellite, and B.

¹ C. O. Alley, "Relativity and Clocks", Proceedings of the 33rd Annual Symposium on Frequency Control, U.S. Army Electronic Research and Development Command, Fort Monmouth, NJ, pp. 4-39A (1979). Copies available from Electronic Industries Association, 2001 Eye Street, N. W. Washington, D. C. 20006.

² B.E.H. Serene, "Progress of the LASSO Experiment," Proceedings of the Twelfth Annual Precise Time and Time Interval (PTTI) Applications and Planning Meeting; NASA Conference Publication 2175. pp 307-327, December 2-4, 1980.

³ R. Decher, D.W. Allan, C.O. Alley, C. Baugher, B.J. Duncan, R.F.C. Vessot, and G.M.R. Winkler, "High-Accuracy Global Time and Frequency Transfer with a Space-Borne Hydrogen Maser Clock", Proceedings of the Fourteenth Annual Precise Time and Time Interval (PTTI) Applications and Planning Meeting, November 30 - December 2, 1982. To be published as a NASA Conference Publication.

Serene, the project manager for LASSO, that there is active consideration now being given within the European Space Agency to flying a new SIRIO-2B satellite with LASSO instrumentation, using existing engineering test equipment. If the decision is favorable, and another ARIANE launch can be arranged, perhaps the LASSO experiment can be performed in about two years.

THE SHORT LIGHT PULSE TIME TRANSFER TECHNIQUE

Einstein's Prescription

The idea of using short light pulses to compare the readings of separated clocks is one of the conceptual foundations of relativity contained in Einstein's original paper.⁴ It is remarkable that the advent of lasers with their ability to produce very short pulses of light has allowed the method to be implemented as perhaps the most accurate means of remote time comparison.

The method is illustrated in the spacetime diagram of Figure 1. In an inertial system in the absence of an atmosphere, the speed of light is

$$c \approx 2.9979 \times 10^8 \text{ m/s} \approx 30 \text{ cm/ns}, \quad (1)$$

so that for the units shown, the light lines have a slope of 45° for an outgoing pulse and -45° for an incoming pulse, representing the same velocity in each direction.* If a pulse is sent out at time t_1 , reflected from a distant point at time t , and received back at time t_3 , then t_2 , the midpoint in time between t_1 and t_3 , is to be identified with t , according to Einstein:

$$t_2 = t_1 + (t_3 - t_1)/2 = (t_1 + t_3)/2 = t. \quad (2)$$

Also, the distance x is given by the radar equation from the difference between measured epochs t_1 and t_3 :

$$x = (t_3 - t_1) c/2. \quad (3)$$

The effect of the atmosphere is to reduce the speed of light from c to c/n , where n is the index of refraction. (The detailed physics leading to this result is rather complex and not widely known, but will not be discussed here.) The value of n depends on the frequency of the light, the atmospheric pressure, the temperature, and the composition of the atmosphere, including

⁴ A. Einstein, "Zur Elektrodynamik Bewegter Körper," *Annalen der Physik*, 17, 1905. A translation into English is available: "On the Electrodynamics of Moving Bodies," in The Principle of Relativity, a Collection of Original Papers on the Special and General Theory of Relativity, translated by W. Perrett and G. B. Jefferey, Dover Publications, Inc., New York, 1952.

* In a coordinate system attached to the surface of our rotating Earth, which is not an inertial system, the speed in the East-West direction differs from that in the West-East direction by about 3×10^{-6} at the equator. In the present experiment, the effect might be barely detectable as the calibration is refined.

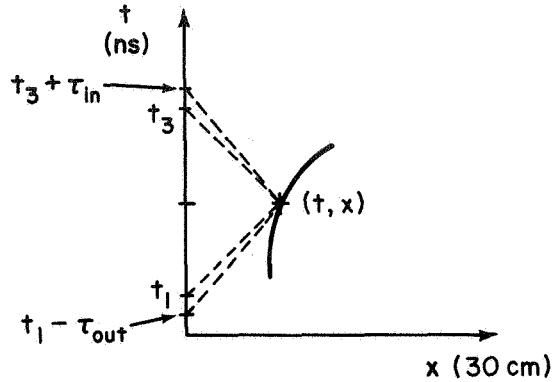


Fig. 1. The Einstein Prescription.

the partial pressure of water vapor. (The dependence on water vapor is far smaller for optical frequencies than for microwave and radio frequencies.) The atmosphere thus produces an additional time delay for the light pulse on the way out, τ_{out} , and a corresponding delay on the way in, τ_{in} , as shown in Figure 1. The Einstein prescriptions for determining the coordinates (t, x) of the reflection event as expressed in equations (2) and (3) now become

$$t = [(t_1 - \tau_{out}) + (t_3 + \tau_{in})] / 2 = (t_1 + t_3) / 2 + (\tau_{in} - \tau_{out}) / 2 \quad (4)$$

nearly cancel

$$x = [(t_3 + \tau_{in}) - (t_1 - \tau_{out}) - (\tau_{in} + \tau_{out})] c / 2 \quad (5)$$

measured round trip time additive

Note that for the time determination in equation (4), the atmospheric delays, τ_{out} and τ_{in} , occur as a difference. They are essentially the same and will nearly cancel. The Einstein prescription for determining the time of a distant event by the midpoint in time between the emitted and the received (reflected) pulse is essentially unaffected by the atmosphere.

This is to be contrasted with the effect of the atmosphere on the distance determination, equation (5), in which the sum of the delays τ_{out} and τ_{in} must be subtracted. An accurate distance measurement requires that the atmospheric delays be known.

An added advantage of the light pulse method of determining the time of a distant clock with respect to a local clock is that the motion of the distant clock does not have to be considered in the comparison between the local midpoint event and the distant reflection event. There are no Doppler effect complications.

However, if the distance between the clocks is not changing, one can use the radar delay to determine the one-way time difference. This is helpful when the returned light pulse is so weak that single photo-electron detection

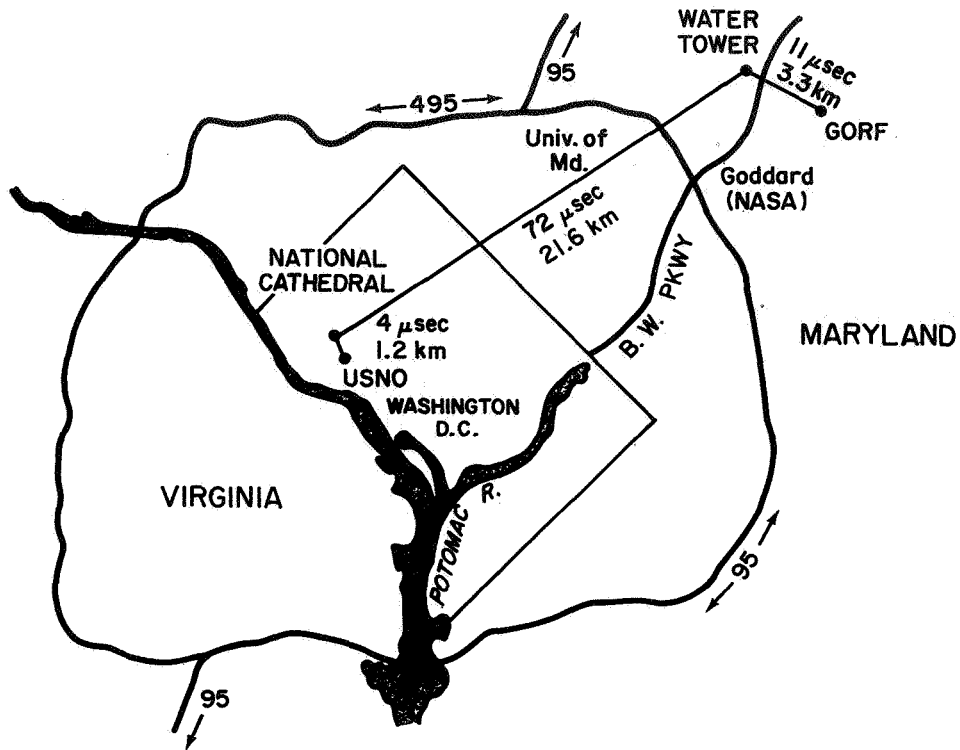


Fig. 2. The path of the laser beam across Washington.

is required. Under these circumstances the reflected pulse at t_3 will not be recorded for each shot, but only with a certain probability, perhaps one in ten. This will be discussed in the later section on the analysis of typical data.

Path Across Washington and Atmospheric Effects

The actual path of the light pulses from the 1.2 m telescope at the Goddard Optical Research Facility to the dome on the roof of the Time Services Building at the U.S. Naval Observatory where two lunar type corner reflectors and a detector are located is shown in Figure 2. A direct line of sight is not possible because of the topography of the Washington area, but a 30 cm flat mirror on a water tower at the Beltsville Agricultural Research Center and a 25 cm flat mirror on the top of the National Cathedral (the highest point in the Washington area) allow a connection. The approximate light travel times and distances for the several legs are given on the map. The total one-way light travel time is 87 microseconds corresponding to a total one-way distance of 26 km. The value of the atmospheric index of refraction⁵ for green light of 532 nm wavelength from the frequency-doubled neodymium YAG

⁵ C.W. Allen, Astrophysical Quantities, the University of London Athlone Press, London, Second Edition, 1955, pp 119f. This reference contains many useful tables and formulas for the optical index of refraction.

laser, for a pressure of 760 mm of Hg, for a temperature of 15° C, and for water vapor pressure of 4 mm of Hg is given by

$$n - 1 = 0.000277 \quad (6)$$

and produces a one-way atmospheric delay of 24 nanoseconds. This does not matter for the Einstein prescription, as discussed above. Other atmospheric effects do cause experimental troubles, however.

If the "visibility" as quoted for the Washington National Airport is less than five or six miles, we cannot detect reflected light over the 52 km round-trip path even at the single photo-electron detection sensitivity for our several hundred microjoule pulses of green light.

Instabilities in the atmosphere associated with a changing vertical temperature gradient, which often occur a cloudless cold night after a warm day, require frequent adjustment of the pointing of the 1.2 m telescope to keep the narrow laser beam on the water tower mirror. This bending of the light is similar to mirage effects. The laser beam is about 2 cm in diameter as it leaves the telescope, expanding to about 45 cm over the 3.3 km path to the water tower. At the cathedral the beam is 200 to 300 cm wide and scintillations are observed - a changing mottled pattern - caused by the non-uniformity of the atmosphere in the transverse dimension of the beam during the 21.6 km path to the cathedral. Changing vertical temperature gradients also require occasional angular adjustment of the water tower mirror to keep the beam on the cathedral mirror. At the USNO the laser beam has a horizontal extent of about 15 cm and a vertical extent of about 25 cm, the projected dimensions of the cathedral mirror as it intercepts the beam.

Methods of Aligning the Mirrors

It has proven necessary during a time transfer to have people at the various locations to make the initial mirror alignments and to maintain them: one person at the USNO, one person at the cathedral, and two persons at the water tower. Three persons are needed at the telescope to operate it, the laser, and the computer, and to coordinate all the activities. A telephone has been installed at each location and a conference call is arranged during each time transfer exercise to allow the necessary communications.

The most difficult adjustment is the initial alignment of the water tower and cathedral mirrors. A very elegant and fast method of accomplishing this was finally devised by D. G. Currie, J. V. Mullendore, C. A. Steggerda, and C. O. Alley, at the University of Maryland. The idea derives from methods used to direct narrow laser beams to a specific location on the Moon.⁶ The method uses a high quality 38 mm diameter circular corner reflector identical to

⁶ C.O. Alley, "Laser Ranging to Retro-Reflectors on the Moon as a Test of Theories of Gravity," in Quantum Optics, Experimental Gravitation, and Measurement Theory, edited by P. Meystre and M.O. Scully, Plenum Publishing Corporation, New York (1983).

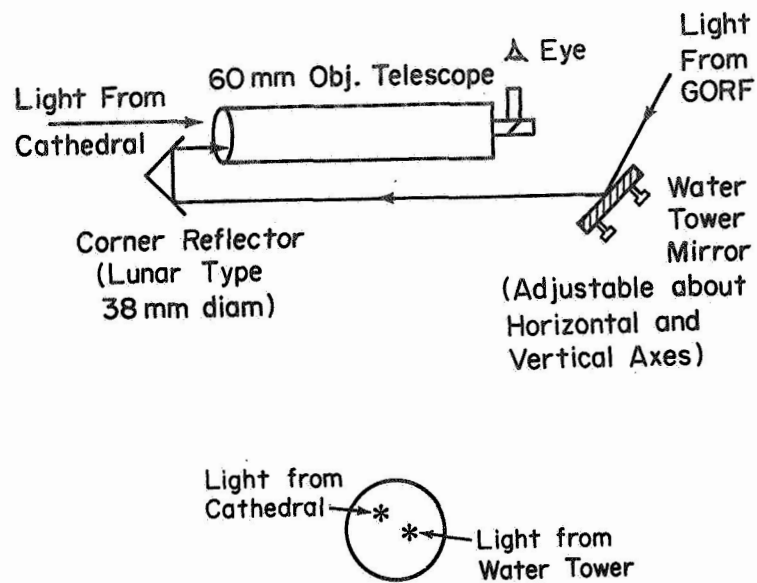


Fig. 3. Optical arrangement for the telescope which looks forward and backward at the same time.

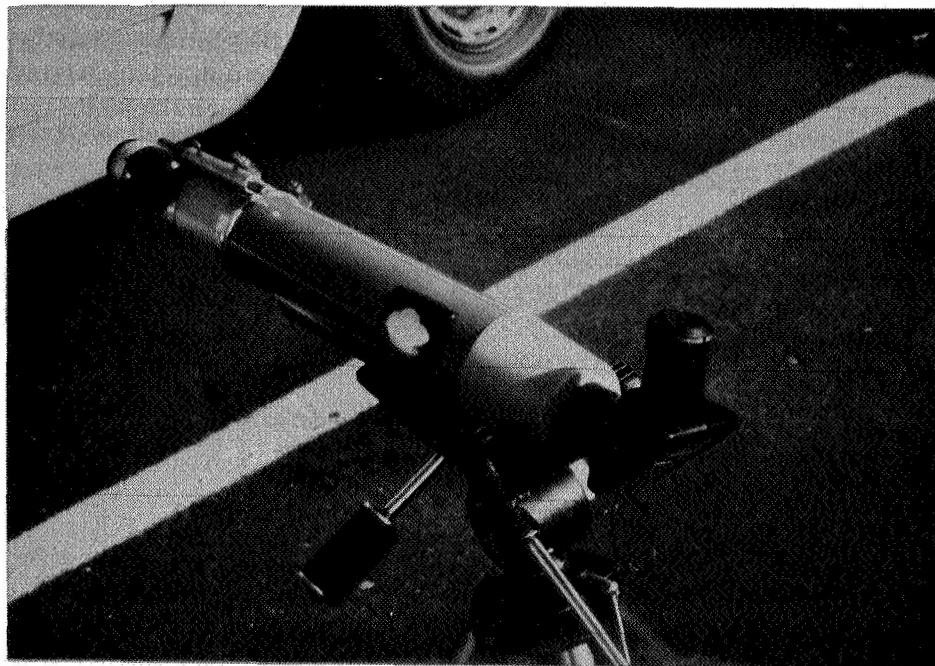


Fig. 4. Picture of the forward and backward looking telescope.

those placed on the Moon, together with an Edmund Scientific Company Celestial/Terrestrial 60 mm objective refracting telescope. Figure 3 shows the arrangement. It allows one to look forward and backward at the same time. A corner reflector has the property that an entering ray of light is reflected three times at three orthogonal mirrors, emerging at a diametrically opposed point with a reversed propagation vector. When the reflector is mounted as shown, halfway across the entrance pupil of the telescope, the view from behind is superposed on the normal field of view of the telescope. Coarse adjustment of the mirror is achieved by viewing the cathedral and the GORF telescope dome during daylight, bringing the telescope dome into coincidence with the corner of the cathedral spire. Fine adjustment is done at night by superposing the image of the attenuated laser beam on the image of an incandescent light placed at the cathedral mirror. Once this is done, the laser beam is guaranteed to hit the cathedral mirror. An even finer angular adjustment can now be accomplished by temporarily placing a corner reflector at the cathedral mirror and observing the reflection from it in the 60 mm telescope (after rotating its corner reflector out of the way) adjusting the water tower mirror to maximize the intensity. A picture of the forward and backward looking telescope is shown as Figure 4.

For the water tower mirror, this procedure with the two-way telescope and lights must be done before each time transfer exercise since the alignment does not stay constant. We believe that both the changing water level in the tank and the temperature changes in the structure cause the angular changes in the mirror. Carrying the equipment to the top of the tower, setting it up, and making the adjustments usually requires about a half-hour. For the cathedral mirror, the two-way telescope is used only rarely since the mounting of the mirror is very stable, and the optical "lever arm" to the USNO is only 1.2 km. Usually, an adjustment of only 30 to 60 cm in translation is needed. This is accomplished by observing the position of the green light from the laser on the back of the dome, and adjusting the cathedral mirror until the detector/reflector combination casts a shadow in the middle of the green spot. The propagation vector reversal of the corner reflectors adjacent to the detector at the USNO causes the reflected light to retrace the path back to the telescope at the GORF.

DESCRIPTION OF THE EQUIPMENT

Laser and Timing Instrumentation at the GORF

At the 1.2 m telescope a frequency doubled neodymium YAG laser produces 100 picosecond duration pulses of green light at 532 nm, each with an energy of about 0.5 millijoule. For the time transfer experiments the repetition rate is set at 10 pps to match the 10 pps master clock pulse train at the USNO, although the laser is capable of operating at 30 pps. This laser is described in detail in a recent paper⁷ and is the same one that was used in

⁷ C. O. Alley, "Proper Time Experiments in Gravitational Fields with Atomic Clocks, Aircraft, and Laser Light Pulses." in Quantum Optics, Experimental Gravitation, and Measurement Theory, edited by P. Meystre and M. O. Scully, Plenum Publishing Corporation, New York (1983).

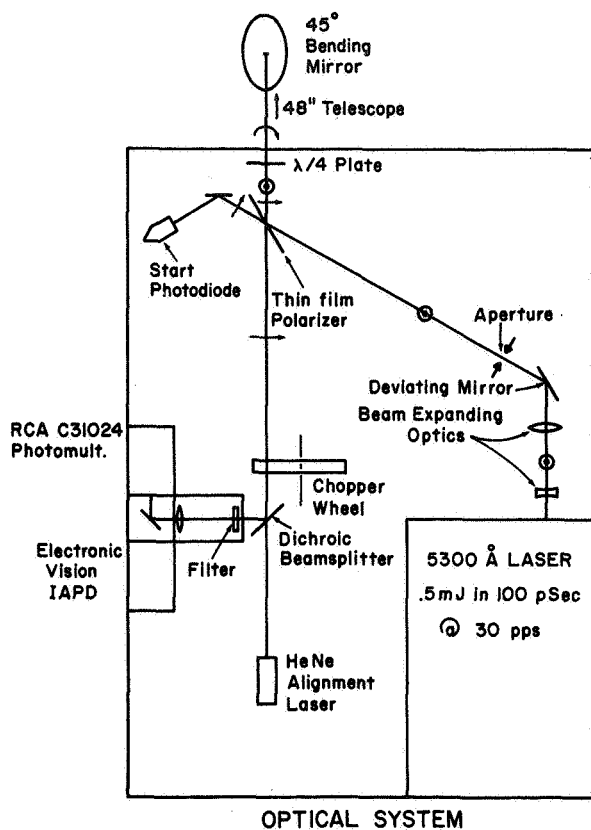


Fig. 5. Coupling of laser and detector to the telescope.

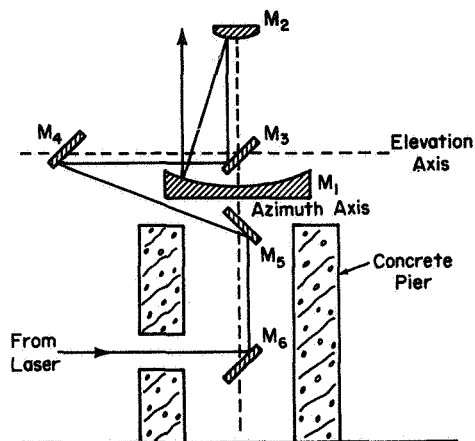


Fig. 6. Path of the laser beam through the telescope.

the aircraft atomic clock relativity experiments (reference 1). The optical system for coupling the laser to the telescope and for detecting the reflected light is shown in Figure 5. The pulse from the laser is linearly polarized with the electric vector vertical. It therefore reflects from the multi-layer thin film polarizer and passes through a quarter-wave plate which converts the linear polarization to circular polarization. The pulse is reflected off-center from a 45° bending mirror (M_6 in Figure 6), allowing it to proceed through the telescope optics as shown in Figure 6, emerging with a diameter of about 2 cm from the annular region between the edge of the primary mirror M_1 and the edge of the secondary mirror M_2 .

The returning light has suffered some depolarization, but is still mainly circularly polarized in the opposite sense. On passing through the quarter-wave plate the light becomes linearly polarized in the horizontal plane and therefore passes through the thin film polarizer. A rotating chopper wheel carries a vane which blocks the light which has been scattered back from the telescope optics and nearby atmosphere. The chopper wheel is phased to be open when the return light appears after the 174 micro-second round trip time. The light is reflected from a dichroic beam splitter through a 10 Å spectral filter and through neutral density filters (variable from zero

attenuation up to N.D. 12). The return light is then focussed to a small spot on the photocathode of an RCA 31024 photomultiplier tube. The neutral density filters allow the simulation of the single photo-electron detection which will be needed in the LASSO experiment (the satellite will be in synchronous orbit). They also allow the equipment to be checked at the single photoelectron level by ranging to a corner reflector located on the water tower. An excellent review article by S. K. Poultney gives many details on the techniques of accurate time measurements with single photoelectrons.⁸

The electronic timing equipment is shown in the block diagram of Figure 7. The start pulse is obtained from a fast photodiode responding to leakage light from the multilayer thin film polarizer. A standard NIM pulse is formed by an Ortec discriminator and passes through an 'or' circuit and a clean up discriminator to an event timer/computer combination which records the epoch of the outgoing pulse with a resolution of 50 ps. The single photoelectron pulse from the photomultiplier is amplified by two Hewlett-Packard wide band amplifiers and goes to an Ortec 473 constant fraction discriminator which minimizes the "walk" in time associated with amplitude fluctuations. A range gate is provided by an adjustable width pulse activated by an "alarm clock pulse" from the event timer/computer combination. The E G & G fast trigger is open only when activated by the adjustable width pulse. The return pulse then passes through the same 'or' circuit as the start pulse and on to the event timer where its epoch is recorded in the NOVA 2/10 computer. The equipment above the dashed line is located in the telescope dome and that below the dashed line is in a trailer adjacent to the dome.

The event timer is basically a clock which can be read with a resolution of 50 ps without stopping it. It can handle up to 100 pulses per second, a limit currently imposed by the associated computer. The operation of the event timer is illustrated schematically in Figure 8. A 5 MHz external reference frequency (currently an HP 5061 cesium standard; for the LASSO experiment a hydrogen maser was to have been used) is doubled to 10 MHz inside the event timer and operates a synchronous counter. An incoming NIM pulse latches the synchronous counter to provide the epoch to 100 ns. The 0.05 ns resolution is achieved by a dual slope integrator in which the pulse also starts a capacitor charging until it is stopped by an appropriate pulse in the 10 MHz train. The capacitor is then discharged in a time 250 times longer than the charging time, and the discharge time is measured with an 80 MHz oscillator to the nearest cycle. Details of the basic circuits are given in a University of Maryland Technical Report.⁹ (A new type of event timer is being developed at the University of Maryland by C.A. Steggerda with a resolution of 10 to 20 ps.)

⁸ S. K. Poultney, "Single Photon Detection and Timing: Experiments and Techniques," in Advances in Electronics and Electron Physics, vol. 31, edited by L. Marton. Academic Press, New York and London (1972).

⁹ C.A. Steggerda, "A Precision Event Timer for Lunar Ranging," University of Maryland Technical Report 74-038, November, 1973.

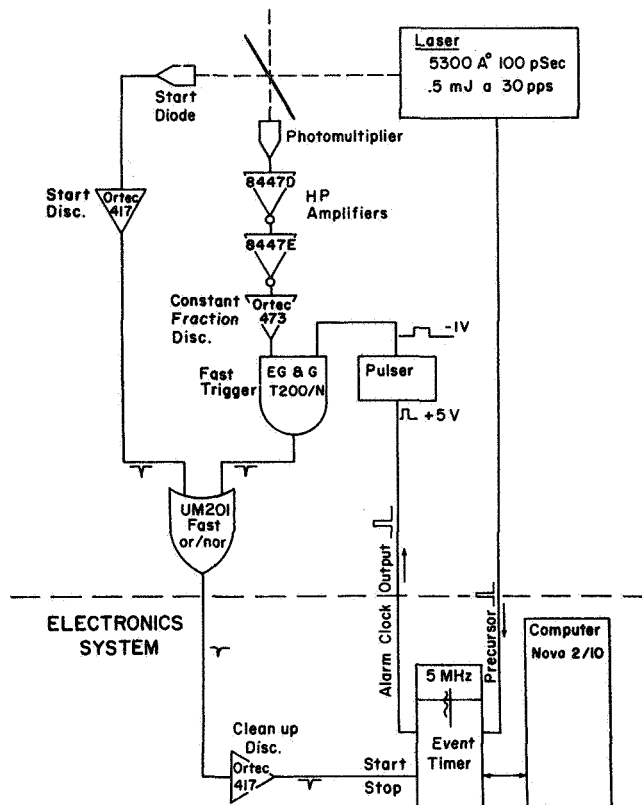


Fig. 7. Electronic timing equipment at the 1.2 m telescope.

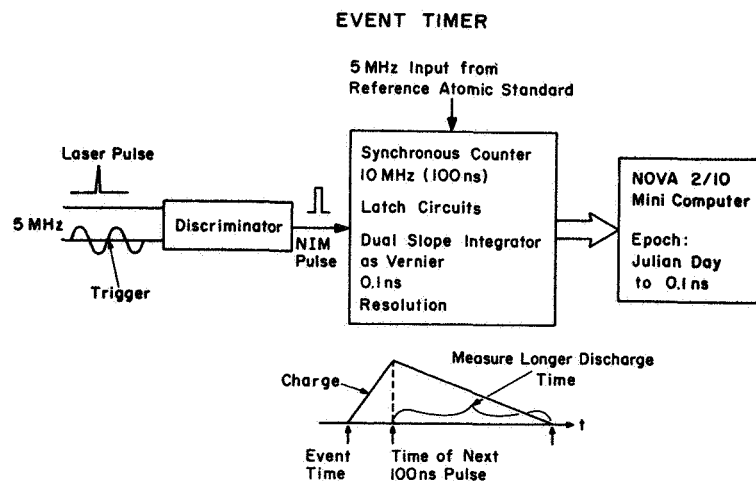


Fig. 8. Operation of the event timer.

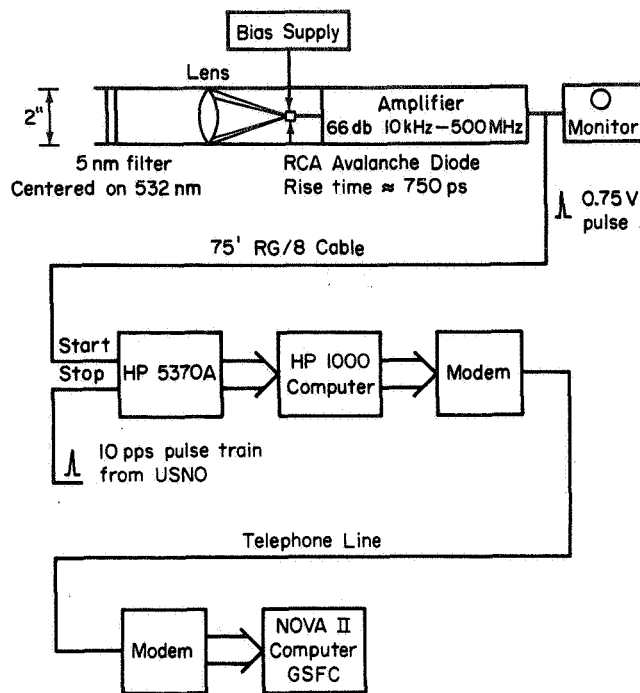


Fig. 9. Instrumentation at the USNO.

Instrumentation at the USNO

Figure 9 is a block diagram of the equipment installed at the Time Services Division of the USNO. The detector is an RCA C30902E silicon avalanche photodiode of the same type used in the LASSO instrumentation (reference 2). It has a rise time of 500 ps. We chose it rather than a faster detector in order to gain experience with the expected performance of the LASSO equipment. A 5 nm band pass spectral filter precedes a 2-inch diameter lens which focusses light on the diode. Provision is made for adding neutral density filters. The fluctuations in amplitude of the laser pulses reaching the detector are quite large due to scintillation effects in the 26 km air path across Washington. (It is interesting to note that in transmitting to space, the vertical scale height of the atmosphere is only 7 km). The wide band amplifier, similar to that in the LASSO equipment, produces a rise time of about 750 ps, and drives a typical 0.75 v pulse down 75 feet of low loss RG/8 cable to start a HP 5370A computing counter. The stop pulse for the counter comes from the 10 pps train of the USNO Master Clock. The measured arrival time of each laser produced pulse at the counter with respect to the Master Clock can be stored in an HP 1000 computer. This computer can be accessed by telephone connection from the NOVA computer at the GORF site and instructed to create a data file which is then transferred from the USNO. These are the times "t" to be compared with the times "t₁" and "t₃" defined above in the description of the Einstein Prescription. This analysis is done by the computer at the GORF site.

ANALYSIS OF TYPICAL DATA

The expected return from the LASSO retro-reflectors on the SIRIO-2 satellite in synchronous orbit was at the single photo-electron level. That is, not every firing of the laser would produce a detected return event, and one must treat the returns in a statistical way, there being only a probability of detection for each shot. To simulate this condition we are able to add neutral density filters in front of the photo-multiplier. This is necessary only when the visibility is very good -- on the order of 15 to 20 miles. For poorer visibility the single photoelectron detection must be used with zero attenuation. We try to simulate the LASSO return with a probability of about one detection in ten shots.

Under these conditions it is convenient to take advantage of the constant distance for the horizontal timing link. (The distance to a synchronous satellite is also approximately constant for short times; for longer times one could fit a smooth curve to the measured range). We measure first the two-way time delay (range) in a statistical way. Then one half of this value is taken as the one-way time delay and used to identify "matches" between the epoch t_1 of the sending event and the epoch t of the pulse arrival at the USNO. This allows a determination of the time difference between the clock at the GORF and the Master Clock at the USNO. A typical time transfer is carried out with 1000 transmitted pulses, requiring 100 seconds at the 10 pps firing rate. Midway into the run, the HP1000 computer is instructed to record epochs of arrival of pulses at the USNO for the next 100 transmitted pulses and to transmit these back to the NOVA computer, creating a data file. (Because of scintillations at the USNO detector, a few of the pulses are not detected.)

Some analyzed results from time transfers carried out 14 minutes apart during the evening of 2 July 1982 are shown in Figures 10 and 11 (draftsman's copies of the display on the Tektronix graphics terminal attached to the NOVA 2/10 computer). The top histogram in each figure shows the distribution of the round trip time measurements. In our earlier notation, the measured quantity is

$$(t_3 + \tau_{in}) - (t_1 - \tau_{out}).$$

The bottom histogram in each figure shows the distribution of the measured time difference between the USNO and the GORF. In our earlier notation, the measured quantity is

$$t - [(t_1 - \tau_{out}) + \langle (t_3 + \tau_{in}) - (t_1 - \tau_{out}) \rangle_{AV}].$$

For each of the time transfers, an attenuation of the returned signal by N.D. 3.5 (approximately 3×10^3) was imposed to obtain single photoelectron detection.

For the earlier time comparison of Figure 10, 55 returns were recorded out of 1000 shots yielding a measured round trip time of 174.3291 μ s with a standard deviation of 690 ps. The spread in the distribution is caused primarily by the jitter in the transit time in the photomultiplier detector

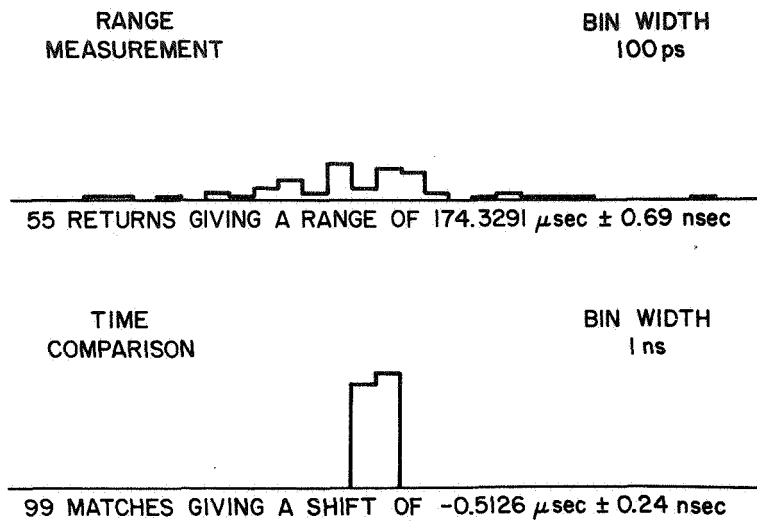


Fig. 10. Time Transfer on 2 July 1982 at 04:32 UTC.

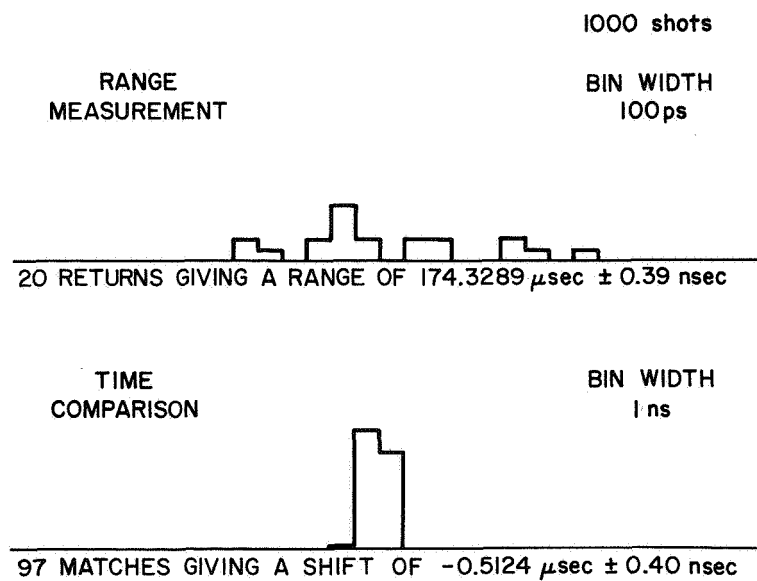


Fig. 11. Time Transfer on 2 July 1982 at 04:46 UTC.

operating at the single photoelectron level. The spread in the distribution of time comparisons is somewhat tighter since no single photoelectron detection is involved. For 99 matches, the standard deviation is 240 ps about a mean time difference of -512.6 ns.

For the later time transfer, shown in Figure 11, atmospheric conditions had deteriorated somewhat and only 20 returns were detected out of 1000 shots. The measured round trip time was 174.3289 μ s with a standard deviation of 390 ps. There were 97 time comparisons, giving a mean time difference of -512.4 ns with a standard deviation of 400 ps. The two measurements are consistent.

The standard deviations of the mean for the two time comparisons are 24 ps and 41 ps respectively. Most of the spread in the distributions is thought to be caused by the detector electronics at the USNO as influenced by the scintillation induced intensity fluctuations in the light pulses. We intend to install a faster detector and circuits whose delay is less sensitive to amplitude changes. Also in the future, we intend to replace the photomultiplier detector with another photomultiplier having faster response, less jitter, and higher quantum efficiency.

If the Einstein prescription for time comparison were used directly with the above data, only 55 comparisons in the first run and 20 in the second run would be possible. This would not matter if the measured distributions had very small dispersions, but with the present detectors the incorporation of the measured round trip time is desirable. In addition, use of the Einstein prescription would have required that the arrival times at the USNO be recorded for each of the 1000 transmitted pulses and sent back to the GORF instead of recording and sending back the 100 pulses in the middle of the sequence.

Calibration of the laser timing link has been accomplished so far only by a clock trip of about 30 minutes duration between the USNO and the GORF. The portable clock was compared directly with the USNO Master Clock at the HP5370A computing counter and by means of the event timer at the GORF with the HP cesium beam clock at that site. These are the basic reference points for the time comparison. The stability of the clock during the trip, estimated at 1 to 2 ns, gives the level of calibration. We plan to make measurements of the actual delays between the optical detectors and the basic reference points. It is hoped that these delays can be determined to 0.1 ns. The laser pulse link alone could then establish synchronization at this level which would require allowance for the East-West asymmetry in the speed of light mentioned earlier as a footnote to the discussion of the Einstein prescription for time comparison.

PHOTOGRAPHS OF THE EQUIPMENT

The details of experimental equipment are often best shown by actual photographs, which also convey impressions not achievable with words and drawings. The following series of pictures traces the path of a photon participating in the light pulse time transfer as the photon itself might

see it.

Figure 12 is a cutaway artist's drawing of the 48-inch (1.2 m) precision tracking telescope at the GORF.* The optical path through the telescope shown in Figure 6 can be better understood by comparing it with Figure 12. The computer controls for directing the telescope are in the room to the left. Our event timer and related equipment are located in a trailer parked adjacent to the dome on the right.

Figure 13 shows the Newport Research optical table on which the equipment of Figure 5 is located. The electronic equipment of Figure 7 is in the rack under the table. The enclosure on top of the table contains filtered air to protect the optics.

Figure 14 shows the water tower on the horizon 3.3 km from the telescope as seen through the dome opening.

Figure 15 is a picture of the water tower. The 30 cm mirror mount can be seen on the left inside the catwalk. The ladder for climbing the tower is hidden by the trees.

Figure 16 is a view of the water tower mirror mount with the front removed from the aluminum box which protects the mirror from the weather. The finely adjustable mirror mount was made by Aerotech. The micrometers for rotating about the horizontal and vertical axes can be seen at the bottom of the mount.

Figure 17 is a picture of the National Cathedral as seen on the horizon from the water tower. Because the cathedral is on a hill, the top of its tower is slightly higher than the Washington Monument.

Figure 18 is a picture of the cathedral tower taken from the ground showing the parapets between which the laser pulses enter and leave. The mirror mount cannot be seen from the ground.

Figure 19 shows the mirror mount on top of the brick stairwell enclosure. This is a very solid structure containing a spiral staircase. The adjustable mount for the mirror is identical to the one on the water tower but houses a 25 cm (10 inch) flat mirror. The reason for the difference in sizes is that these mirrors were available from the beam directing optics used in the aircraft relativity experiments with atomic clocks performed in 1975 and 1976, described in references 1 and 7, and also at the last PTTI meeting.¹⁰

* We are very grateful to Michael Fitzmaurice, John Degnan, and others of the Optical Instrumentation Branch of the Goddard Space Flight Center for kindly allowing us to use this excellent facility.

¹⁰ C.O. Alley, "Introduction to Some Fundamental Concepts of General Relativity and to Their Required Use in Some Modern Timekeeping Systems," Proceedings of the Thirteenth Annual Precise Time and Time Interval (PTTI) Applications and Planning Meeting; NASA Conference Publication 2220, pp. 687 - 724, December 1 - 3, 1981.

Figure 20 shows the domes of the USNO framed between parapets with the Kennedy Center and Potomac River in the background. The small dome in the center is on top of the Time Services Building and contains the detector and corner reflectors. Spectacular views of Washington are seen from the top of the cathedral.

Figure 21 shows the dome on the roof of the Time Serves building. The detector/reflector combination is mounted on an unused telescope mount in the center, as seen in Figure 22. The detector/amplifier assembly shown in Figure 9 is in the cylinder at the top left. The two corner reflectors are at the top right. They are the same ones used in the aircraft time transfer experiments described in references 1, 7 and 9 and are mounted in the housings constructed for the outside of the aircraft. The lower panel of reflectors was lent by the Marshall Space Flight Center as part of the studies for the STIFT experiment. It is not presently used.

Figure 23 shows the top of the cathedral above the trees as seen from the roof of the Time Services Building. The green laser flashes come from between two smaller parapets at the right.

Figure 24 looks toward the water tower from the top of the cathedral. Since the water tower does not project above the horizon it is not distinguishable at its distance of 21.6 km in this daytime photograph. However at night, when the laser beam is correctly pointed, the green flashes are by far the brightest light in the whole Washington area.

The final picture in the series, Figure 25, is a reflection in the water tower mirror of the many domes at the Goddard Optical Research Facility. The large dome on the right, just to the left of the dome on a tower, contains the telescope where the trip began, which is also the final destination for the photon.



Fig. 12. Transmit/Receive telescope at the GORF.

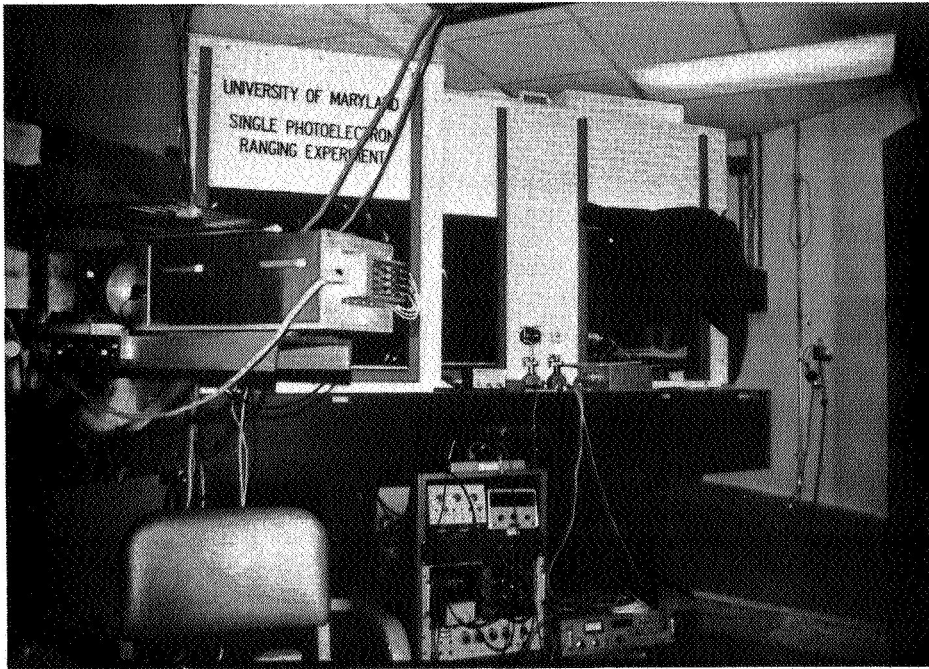


Fig. 13. Optical and electronic equipment for transmitting and receiving laser pulses.



Fig. 14. Water tower seen from the telescope.

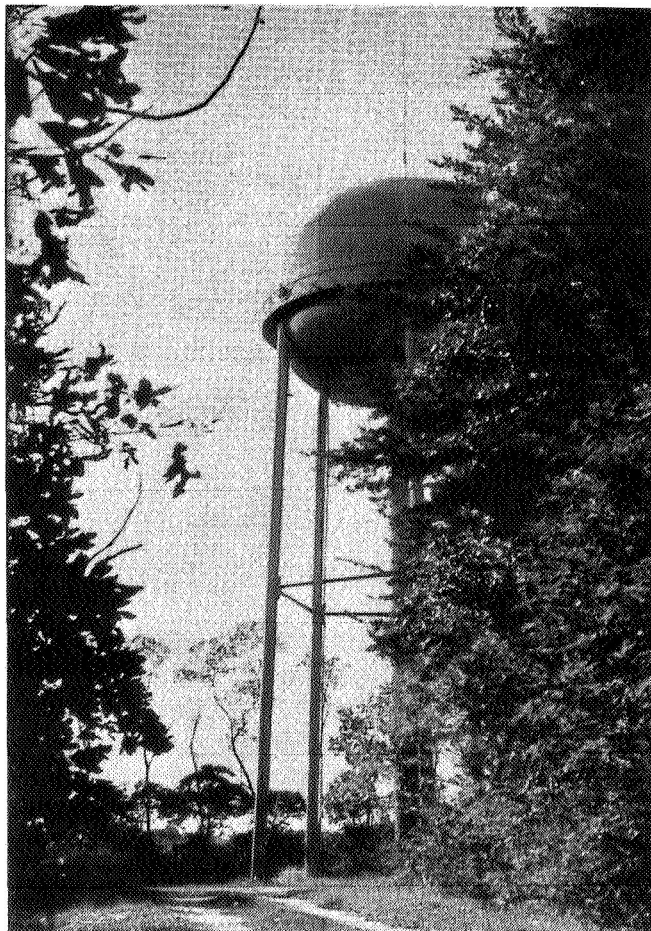


Fig. 15. Water tower seen from near its base.

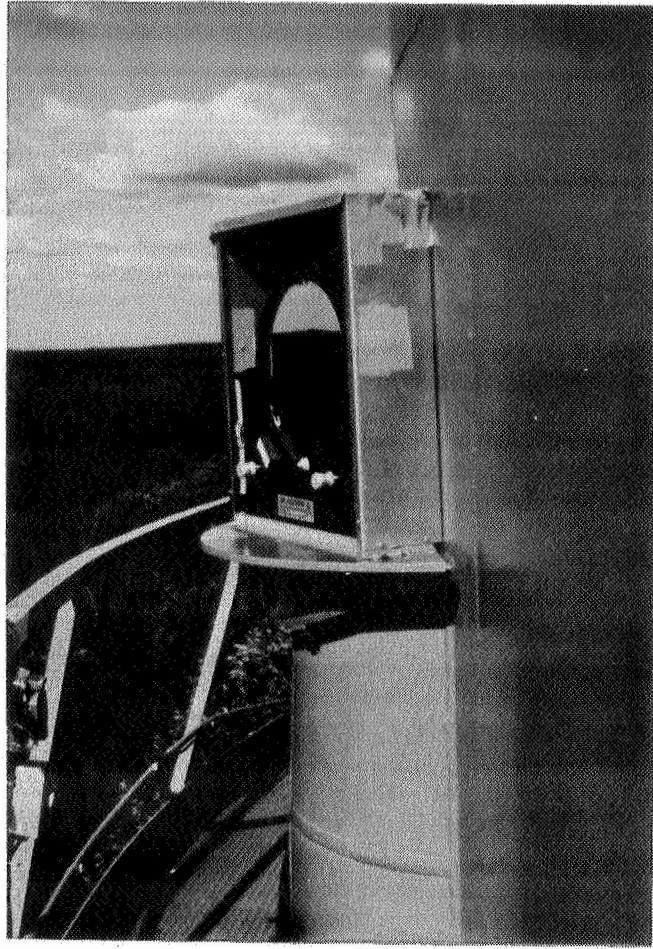


Fig. 16. 30 cm mirror on the water tower.

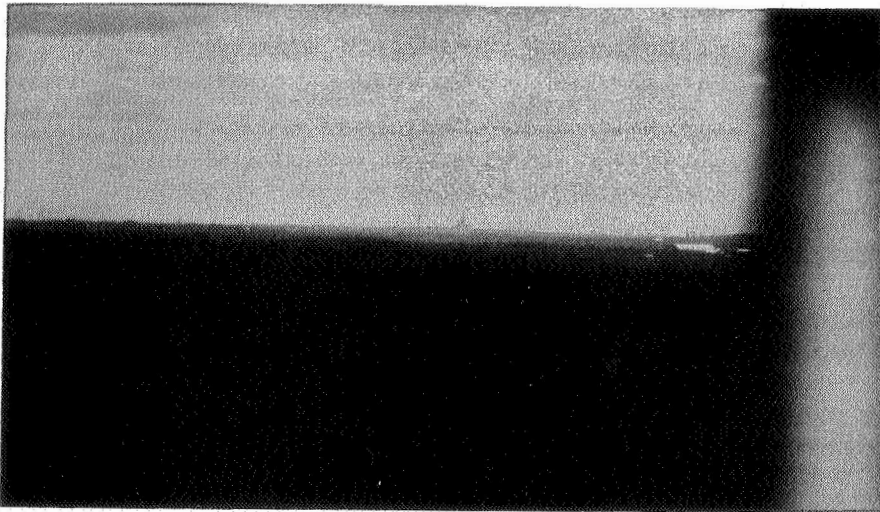


Fig. 17. National Cathedral on the horizon as seen from the water tower.

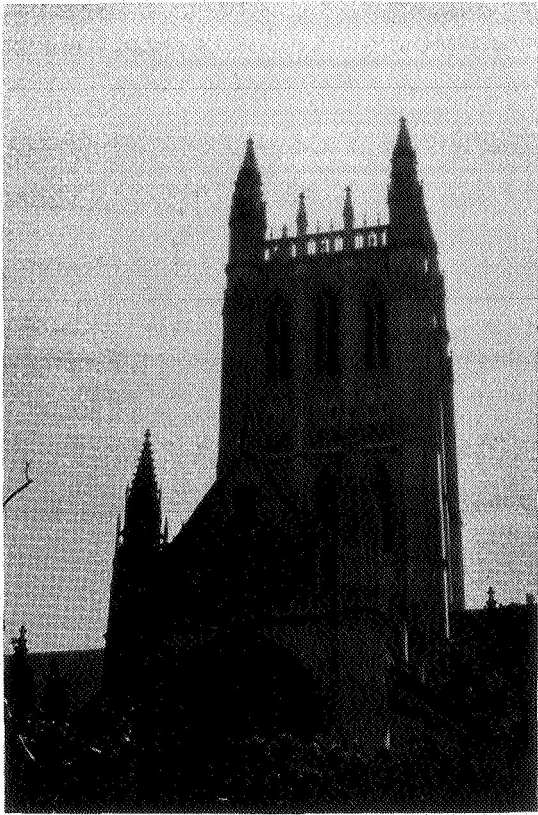


Fig. 18. Cathedral tower

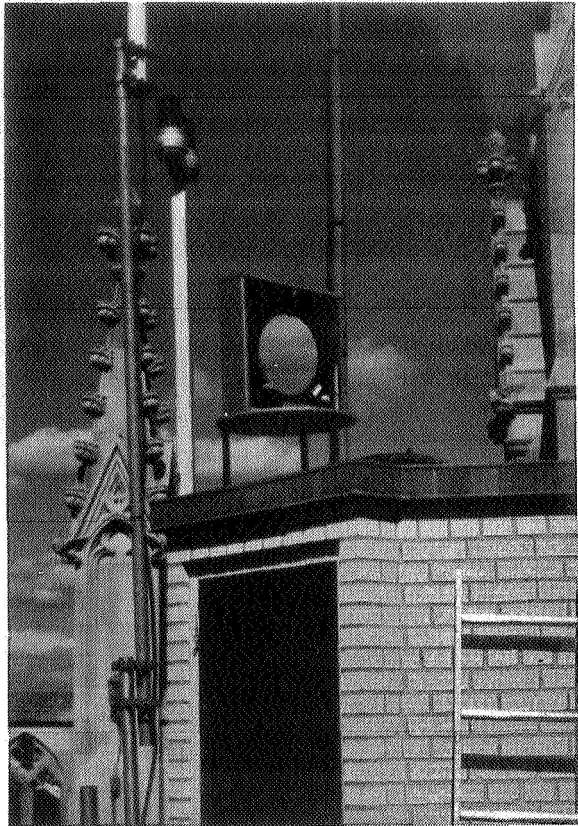


Fig. 19. Mirror on Cathedral tower.



Fig. 20. The USNO from the Cathedral tower.

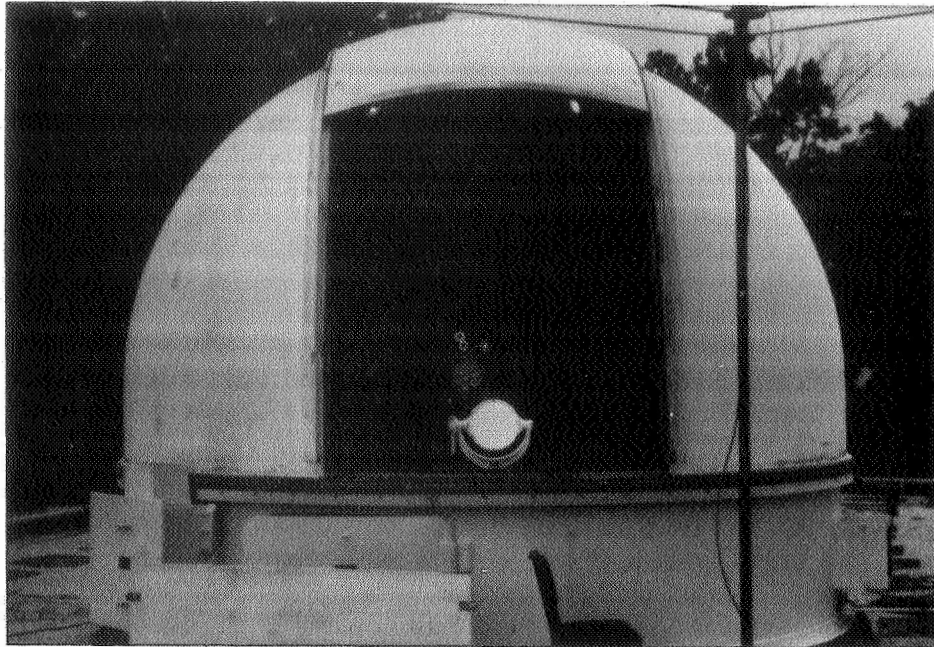


Fig. 21. Dome on the roof of the USNO Time Services Building.

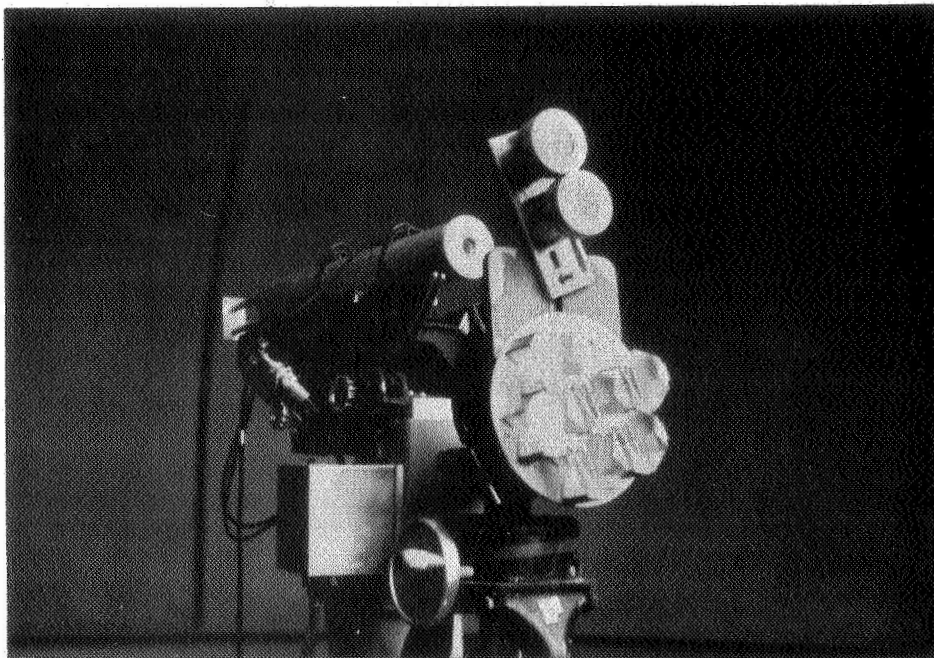


Fig. 22. Detector/reflector assembly at the USNO.

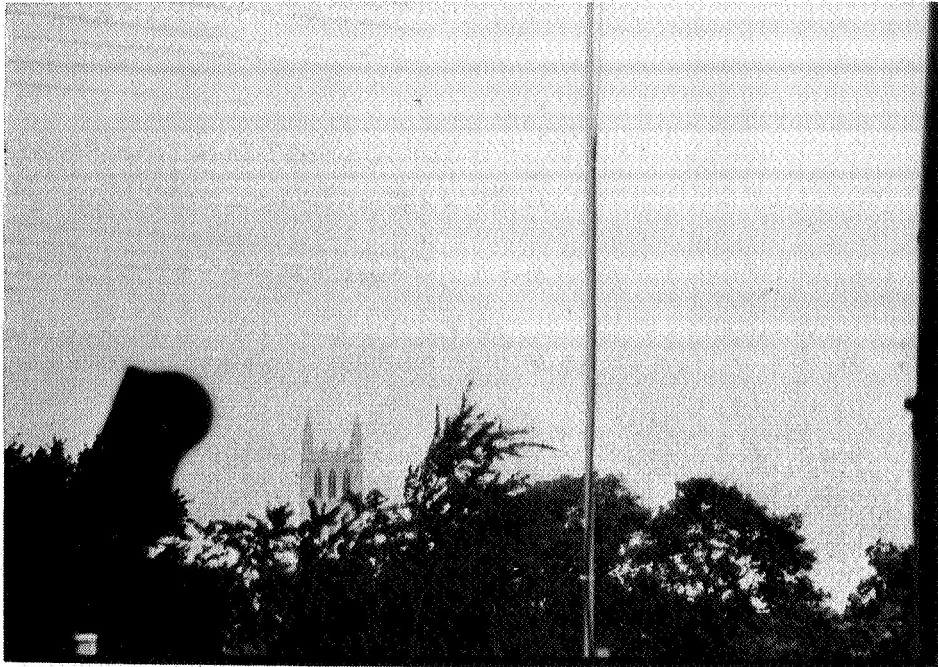


Fig. 23. Top of the Cathedral seen from the roof of the Time Services Building.



Fig. 24. Looking toward the water tower from the Cathedral.



Fig. 25. Domes of the Goddard Optical Research Facility reflected in the water tower mirror.

QUESTIONS AND ANSWERS

DR. KELLOGG:

What's the time constant for aligning the two mirrors that are at D?

PROFESSOR ALLEY:

Oh, No! Our electronics engineer, Mr. Steggerda is also an expert at lining that up and he can do it in a matter of 5 or 10 minutes, I guess. It takes a little longer than that to get all the equipment up on the water tower, and so on. But we typically can get a number of measurements done during an evening's run of several hours, provided the weather permits. We don't have to have freedom from cloud cover. In fact cloud cover is good because it stabilizes these vertical temperature gradients.

MR. KAHAN:

Can you work in rain?

PROFESSOR ALLEY:

No! No!

I should say that we checked with the airport forecasters -- visibility however they define it, and I don't know quite how they define it, but if it's less than 6 miles, we begin to get into trouble. We like to work with visibility of 15 to 20 miles but we can work with 5 or 6 miles. But we cannot work in rain or fog.

DISCUSSION ON GODDARD SATELLITE TIME TRANSFER

DR. WINKLER, The United States Naval Observatory

I think the discussion will take place. I should like to invite a few people here to join me at the table, certainly Dr. Decker, the project team leader of STIFT, and Mr. Starker, if he is willing to come up here. He has given us an excellent discussion of the German projects and could we ask somebody who's familiar with GPS time transfers to volunteer?

Nobody wants to volunteer? Yes, please, would you join us. I would also like to invite Professor Alley to come up and I think that we would have a little group and discuss the various aspects and summarize and ask questions. I would like the audience to be as active as possible.

Let me begin by giving you best regards from our European colleagues Dr. Bernard Serene; I talked with him yesterday morning to get some new information on the status of the LASSO project, and he regrets that he was unable to come, obviously, but on the news we received it appears as Professor Alley has already mentioned, that the LASSO is not dead.

In fact it's a very good chance that it might be a series of two successors, which will either be on a SERIES-2 type satellite, two experiments of course, or where it will be on METEORSAT as a piggyback effort. And then as mentioned by Professor Alley what we will expect, so that we will have to find out what is going to happen.

In looking over the papers which we have heard today and some of the papers which are still to come, and we have again the two classes of experiments of techniques: The one-way time transfers using a navigation system such as GPS, or such as TRANSIT and two-way transmission, using a communication satellite or using the ranging signals which are available on some of the other satellites, in the piggyback fashion.

I was very much intrigued by the slide shown by Mr. Starker today, about unscheduled and completely passive of comparison between Washington and PTB in Germany using completely different GPS receivers and achieving as we have heard a standard deviation of, something like 20 nanoseconds over a period of 10 days which includes all of the variations in the two clocks, in all the circuits and everything. And it includes the uncertainty of the GPS time transfer.

And just from that, but also when these experiences have been reported by David Allan and the NBS group and others. It is obvious that today we have the capability to synchronize any two clocks to about 20 nanoseconds wherever they are. Using the system which, in its original purpose, was far from being operational, but for a time transfer it is more than operational because we have five satellites which can be used and are being used.

Now, may I ask a couple of leading questions? We have heard today about the laser microwave time transfers and these super precision experiments and I would like to ask maybe anyone to answer here, how they see the future, and what role the laser is going to play in lets say 5 or 10 years from now, is it going to be a calibration tool or maybe it will become an operational tool?

PROFESSOR ALLEY:

The laser has the immediate disadvantage of not being able to go through clouds, at least in the powers available to civilian users. But, I think as a calibration technique it could play a very important part in the future.

I would think, for example, if we could calibrate using 1/10 nanoseconds laser pulses, the GOES positioning satellites are few, and the GOES positioning satellites were as they were tied directly to a master clock, for example, at the Naval Observatory then using the conventional readouts, one could improve on the global time transfer from the ten nanosecond level down to the precision of which the GPS is capable which is at the one nanosecond, or perhaps even better.

DR. WINKLER:

That is certainly an interesting comment, because we hear about developments of clocks which are capable of keeping time down to the 10th of a nanosecond and it is a question what utility they would have without a better readout capability. That question has been raised several times, and I think it has not been answered satisfactorily.

I would like to ask Dr. Decker about his estimate, I mean that may be an indiscrete question; but it is a planning meeting and we ought to discuss these things as candidly as possible.

What is your present assessment of this STIFT experiment?

DR. DECKER:

Well, at the present time, this is a study place, so it's not an approved colloquium. And it is rather difficult to start any new program today because all agencies are suffering from budgetary problems.

The system, as presently studied by NASA, would be of benefit to a large outside user group and in order to get something like this going, I think one needs the support or the expression of interest from outside users to NASA to support the start of such a program.

So, at the present time, we do not have any committed start or start of the development of this STIFT system.

DR. WINKLER:

And so it is a concept, essentially, which is still looking for sponsors for support?

DR. DECKER:

That's right.

DR. WINKLER:

And as I heard, Mr. Starker, today, your experiment is apparently going in full force, is that true?

MR. STARKER:

Yes, you are right. It is in full force and it can be, and there is no doubt that it is a decision of great determination.

And to your question about laser or microwave links, I come from a microwave Institute, and I think that microwave links will be the operational tool for time transfer and laser will be used as a calibration tool, perhaps. And for us, not the highest experiencing is our aim in this first experiment with dual links. We find that the experimental technique to use a computer and a noise code as time signals, is a very important thing which can be used with communication satellites or with low-orbiting satellites, as well. And this is our aim and we made some experiments to offer as proof and we got also precisions of smaller than 1 nanosecond.

DR. WINKLER:

Your presentation presented us with such a wealth of interesting information and interesting details, I really think you should look very carefully through your panel paper.

But it appears to me that in Europe the schedules-- that it may be very wise for ESA to establish much closer relationships with this European group and find out how we could possibly participate --- what possibilities still exists? As we have heard, one of the main driving objectives in the German experiment is to gain experience in using clocks in space.

DR. DECKER:

I have a question. Do you have any plans in the future for this particular experiment? You said it was the first one?

MR. STARKER:

We would like to do it, but we have no plans, up to now.

DR. WINKLER:

Well, we can change the subject, in that this panel member say something about whose point of view they have in GPS satellites and time transfers.

MR. TALLEY:

Well, I guess there's at least one comment with regard to the laser and that's probably contrary to Dr. Alley's interest, we have never had a lot of interest trying to do laser tracking of one of our satellites in order to separate the ephemeris from our clock information. We recognize that as data base line, and many of us who are involved in clocks, are involved in the ephemeris evaluation are interested in that.

There has been considerable reluctance on the part on the program officers to sponsors such an activity. And they are still working it they are interested in NRL doing that, and the groundwork has been laid, and I --- well it hasn't happened yet.

DR. WINKLER:

Right now, I think there are two aspects which I don't think have been sufficiently emphasized. One is that the laser propagation is, from a physics point of view, a cleaner one. That you do not have to be this unknown dispersion; there is no noticeable, or not as large in the texture coming from the tropospheric water vapor. And the same thing is true from any atmospherics. True in principle, that's very interesting.

But there is a second aspect which I think that we should not forget, that it is intrinsically an ultra secure way of accessing a well-known object. It is much more secure than any microwave system ever is going to be. And I think that the program office has not considered that aspect yet. But I think it would be a very powerful motive to investigate the use of lasers for special purposes, in conjunction with very high precision calibration.

MR. TALLEY:

Would you like to have some status for the general audience as to where our GPS clocks are?

DR. WINKLER:

I think that would be most useful.

MR. TALLEY:

We have six navigation developmental satellites in orbit and four of those actually have the atomic clocks all running, two of which have the rubidium clocks and two of them cesium clocks running. We have NAVSTAR 1 and 2 radiating in L Band controlled by a crystal clock. NAVSTAR 1 is still being tracked with the KALMAN filter and it is being updated and has a NAV message that can be tracked. We have several satellites that are ready to be launched and are only waiting for a stage vehicle to put them up.

We actually have three vehicles in storage and the fourth one going into thermal vac tests this week. The development of the satellites themselves are almost done as far as the contractor is concerned for the first demonstration phase.

We are about 18 months late in launching our next one. We had a rather drastic propulsion failure in December of last year, just about a year ago now, and so that was a significant setback in getting them on orbit and now we have a heavier version of the satellite with what we call the secondary payload and we have to have a new stage vehicle. And that stage vehicle has had difficulties in terms of its nozzle. If and when that is solved we will be launching, but not before June of '83. The data that was shown on GPS comparison was not from a cesium clock but from a rubidium clock, which was on NAVSTAR 3.

DR. WINKLER:

That is a very interesting comment. Just by looking at the observatory data, its clock is performing extremely well and if it were not for the need to re-set it frequently because it has such a large rate due to its aging but it can be modeled as a quadratic state extremely well and over 10 days has residuals less than 10 nanoseconds using a quadratic model.

Unfortunately, you can't do it longer for about 14 days because then you see the recycle 500,000 microseconds the other way and change the frequency and your model needs to be picked up again because you don't know what actually happened to that clock, but the rubidium has the capability in space, in that particular case to give extra ordinarily good service.

Well, maybe we should invite some questions from the audience. Yes sir, could you please give your name for the record.

DR. ROBERT VESSOT, Smithsonian

I don't think that in the past there has been as great a discrepancy or difference between the alleged accuracy of the atomic clocks and the means by which this accuracy can be conveyed about the world?

I have a suspicion that the technology of clocks are out running our means for comparison at a greater rate now than ever before. I wonder if you care to discuss this point and the fact that at some point in time some action is likely to be needed, what action can be taken?

DR. WINKLER:

Any comments?

MR. TALLEY:

I have one comment with regard to GPS in this area. As far as our observation in orbit is concerned, from the GPS program point of view, it is through KALMAN filter observations at the master control station and if we look at two of the clocks one of which has a temperature coefficient on the rubidium and one has a suspicion of a variation in beam current in the cesium, the KALMAN doesn't show the diurnal effect. Yet we are highly suspicious that the clocks have these variations.

I think that the ability to look at the clocks on the ground has deteriorated to some extent.

We are working to try to separate that.

DR. WINKLER:

I happen to completely agree with him on his comments, that this is true. That, in fact, years from now, we're not going to have any means to utilize much better clocks which we can expect to have. I think that there are definite gaps in our planning and development. We are talking about many experiments but now not one of them will be useful at the one nanosecond level with the possible exception of the GPS system, but this will require some doing.

Further discussion on the clocks?

MR. WHITWORTH, JHU/APL

I'd like to ask what determinations have been made as to what sort of timing accuracy can be delivered to user spacecraft by GPS?

MR. TALLEY:

Well, it's a little out of my field, but I'll attempt to comment. I assume that we can, with the proper equipment on board, that we can approach the units nanoseconds transfer capability.

I think that that will take some special equipment that's not presently on board in satellites but it seems to be within the capability range.

DR. WINKLER:

I would like to add to that that I completely agree that we have to remember that we're still in the developmental stage and the learning phase and the operators who make the adjustments to operate the system are making deliberate changes from time to time and in order to gain experience.

I think some operational changes will be required to reach that but in my opinion, it's entirely possible to obtain the one nanosecond.

PROFESSOR ALLEY:

I'd like to address a question to Mr. Talley in relation to the question from the audience. I've heard that the GPS is now considering spacecraft to spacecraft communication and synchronization. Is it possible, tell us more about this plan.

MR. TALLEY:

Well, you've heard right. There is a significant study in that area. It is not to improve the performance that we've been demonstrating in this phase one, it is addressing a survivability question, an autonomy out beyond 14 days; up to, like, 180 days. It is true that it is being worked and studied. It would require considerably more computational capability on board the spacecraft than is currently available but it does appear to be feasible in concept form.

PROFESSOR ALLEY:

Do the antennas permit this sort of thing or will new antennas be required?

MR. TALLEY:

I believe that the antennas would be satisfactory.

DR. WINKLER:

Are there any more questions?

MR. ALLAN:

Mr. Starker, I'd like to also congratulate him on an excellent paper but my one comment in regard to that is that between his site and PTB there's a very short baseline and using GPS in common view you could probably appreciate about one nanosecond because of the large removal of the ephemeris error and we would of course, be extremely interested in that tie. In the February time frame, we will loan one of the NBS type receivers to the PTB and you would be able to conduct such an experiment. This would give you a tie to PTB at the one nanosecond level.

DR. WINKLER:

Can I repeat? One of the results which you reported at the Frequency Control Symposium that over a period of 2 or 3 weeks the residuals in common view mode between NBS and Washington using precisely the same satellites, the time difference in data, was on the order of 2 nanoseconds.

MR. ALLAN:

That's correct.

MR. STARKER:

We would be very interested in such measurements and as soon as the PTB would have the GPS receiver, we would have also the possibility to calibrate our receiver which is delayed up to now.

PROFESSOR ALLEY:

I'd like to return to our earlier discussion, Mr. Starker. I don't want to leave the impression that the STIFT planners have not had that kind of mutual interest but they did not find anyone within the NASA organization.

DR. WINKLER:

Not up until now. Any more question, please? I would like to ask about GPS denial of access to time?

MR. TALLEY:

Well, again, this is not something that I worry about and talk about every day. But it does border on a classified type of discussion. I personally suspect that before the system goes operational there will be contamination of the GPS signal as we know it today. I think it will not be such that -- recognized users would still be able to decode it and make it available in a sense that it would still be useful.

DR. WINKLER:

Maybe we can shorten the discussion if we say -- I should have mentioned that the paper which was given, I believe one or two years ago, at this conference by somebody from the GPS Program Office. I think it was Capt. Tennant. I want to know whether any significant change has occurred?

MR. TALLEY:

I don't recall exactly his position, I was here when he gave the paper; gave his talk. I believe that he did give some assurance that the signal would not be contaminated and I believe that that is not correct and that is how things stand today.

I believe that Dave Allan is aware of the type of contamination that is expected and maybe he would care to comment on how civilian users would react to the contamination.

MR. ALLAN:

Basically, I think we cannot talk about these kinds of techniques, but the common view approach would eliminate some of the problems that would be encountered and I think this will allow us to still use the system even under some disturbed circumstances.

So, I think that the system will be continued.

DR. WINKLER:

Instinctively, I have a feeling that the system is of very great use right now.

On the other hand, we have to be prepared. Not one of the systems can be guaranteed to work when we need it and there is nothing more important in time systems than to have a common interface to allow us to get time from one of the other many coordinated systems.

That's the whole purpose of coordination.

Well, I think, Mr. Chairman, that we have finished now and I thank you very much.

MR. KAHAN:

I would like to thank all of these speakers this afternoon.

SESSION III

NOISE STUDIES AND ATOMIC STANDARDS

PANEL DISCUSSION ON APPLICATIONS

Dr. Samuel R. Stein, Chairman
National Bureau of Standards

THE FUNDAMENTAL STRUCTURE FUNCTION OF OSCILLATOR NOISE MODELS*

Charles A. Greenhall
Jet Propulsion Laboratory, Pasadena, California

ABSTRACT

Continuous-time models of oscillator phase noise $x(t)$ usually have stationary n th differences, for some n . The covariance structure of such a model can be characterized in the time domain by the structure function:

$$D_n(t; \tau_1, \tau_2) = E \Delta_{\tau_1}^n x(s+t) \Delta_{\tau_2}^n x(s) \quad (0)$$

Although formulas for the special case $D_2(0; \tau, \tau)$ (the Allan variance times $2\tau^2$) exist for power-law spectral models, certain estimation problems require a more complete knowledge of (0).

We exhibit a much simpler function of one time variable, $D(t)$, from which (0) can easily be obtained from the spectral density by uncomplicated integrations. Believing that $D(t)$ is the simplest function of time that holds the same information as (0), we call $D(t)$ the fundamental structure function.

We compute $D(t)$ for several power-law spectral models. Two examples are $D(t) = K|t|^3$ for random walk FM, $D(t) = Kt^2 \ln|t|$ for flicker FM. Then, to demonstrate its use, we exhibit a BASIC program that computes means and variances of two Allan variance estimators, one of which incorporates a method of frequency drift estimation and removal. Except for a one-line function definition of $D(t)$, the program is independent of the phase noise spectrum. The outputs were used for assigning confidence intervals to the results of recent hydrogen maser performance tests at JPL.

THE STRUCTURE FUNCTION

The purpose of this paper is to demonstrate an easy way of computing a class of time-domain oscillator stability measures known collectively as the structure function. Let the phase of an oscillator with nominal frequency ν_0 be modeled by

$$2\pi\nu_0(t + x(t)) ,$$

where $x(t)$ is a random process representing the "phase time" of the

*The research described in this paper was carried out by the Jet Propulsion Laboratory, California Institute of Technology, under contract with the National Aeronautics and Space Administration.

oscillator. The most restricted version of the structure function, discussed by Lindsey and Chie [1], is

$$D_n(\tau) = E[\Delta_\tau^n x(s)]^2, \quad (1)$$

where Δ_τ is the backwards difference operator defined by $\Delta_\tau f(t) = f(t) - f(t-\tau)$, and E denotes the mathematical expectation. It is to be understood that the n th difference process $\Delta_\tau^n x(t)$ is wide-sense stationary, so that (1) does not depend on s . For $n = 2$ we obtain the Allan variance as

$$\sigma_y^2(\tau) = \frac{1}{2\tau^2} D_2(\tau).$$

A more general version of the structure function is

$$D_n(t; \tau_1, \tau_2) = E \Delta_{\tau_1}^n x(s+t) \Delta_{\tau_2}^n x(s), \quad (2)$$

which was used by Yaglom [2] as a basis for a theory of processes with stationary n th differences. For the application to be given at the end of this paper, we shall need the yet more general version

$$D(t; \underline{a}, \underline{b}) = E \Delta_{\underline{a}} x(s+t) \Delta_{\underline{b}} x(s), \quad (3)$$

where

$$\underline{a} = (a_1, \dots, a_n), \quad \Delta_{\underline{a}} = \Delta_{a_1} \dots \Delta_{a_n},$$

and likewise for \underline{b} , $\Delta_{\underline{b}}$.

By using the transfer function $1 - e^{-i\omega\tau}$ of the operator Δ_τ , one can express all of these quantities as integrals involving the two-sided spectral density $S_x(\omega)$ of the process $x(t)$, which is assumed to have stationary n th differences for some n . For example, if the long-term frequency drift rate is zero, then

$$\begin{aligned} D_2(\tau) &= \int_{-\infty}^{\infty} |1 - e^{-i\omega\tau}|^4 S_x(\omega) \frac{d\omega}{2\pi} \\ &= 16 \int_{-\infty}^{\infty} \sin^4\left(\frac{1}{2}\omega\tau\right) S_x(\omega) \frac{d\omega}{2\pi}, \end{aligned} \quad (4)$$

$$\begin{aligned} D(t; a, b, c, d) &= E \Delta_a \Delta_b x(s+t) \Delta_c \Delta_d x(s) \\ &= \int_{-\infty}^{\infty} (1 - e^{-i\omega a})(1 - e^{-i\omega b})(1 - e^{i\omega c})(1 - e^{i\omega d}) e^{i\omega t} S_x(\omega) \frac{d\omega}{2\pi}. \end{aligned} \quad (5)$$

(This is (3) with $n = 2$.)

Because of the importance of the Allan variance as a stability measure, the integral (4) has been evaluated in closed form for power-law spectral models

$$S_x(\omega) = K_\alpha |\omega|^{\alpha-2}, \quad \alpha = -2, -1, 0, 1, 2,$$

with a high-frequency cutoff when $\alpha \geq 1$ ("PM" noises) [3]. The expressions (5) and (3) are more complex, yet we shall show how to compute any of these in two easy steps: 1) By means of simple integrations involving only the spectral density, evaluate a single function $D(t)$ of one time variable; 2) apply a certain difference operator of order $2n$ to $D(t)$. This function $D(t)$, depending only on the spectral density, will be called the fundamental structure function because, merely by taking linear combinations of values of $D(t)$, one can generate the entire covariance structure of the differences of $x(t)$.

STATIONARY PHASE

If $x(t)$ is stationary, then $D(t)$ turns out to be just the autocovariance function:

$$D(t) = \text{Cov}(x(s+t), x(s)) = \int_{-\infty}^{\infty} e^{i\omega t} S_x(\omega) \frac{d\omega}{2\pi}. \quad (6)$$

Indeed, by expanding the differences in the middle expression of (5), one can show directly that

$$D(t; a, b, c, d) = \Delta_a \Delta_b \Delta_{-c} \Delta_{-d} D(t). \quad (7)$$

It is just this form of expression that will be extended to the nonstationary situation, where $S_x(\omega)$ is not integrable near zero frequency.

THE FUNDAMENTAL STRUCTURE FUNCTION IN GENERAL

Let us be given a process $x(t)$ with stationary n th differences. It is known [2] that x has a spectral density $S_x(\omega)$ with the properties

$$\int_1^{\infty} S_x(\omega) d\omega < \infty, \quad (8)$$

$$\int_0^1 \omega^k S_x(\omega) d\omega < \infty,$$

for some integer k , $0 \leq k \leq 2n$. (We ignore the more general case of a spectral distribution function.) Here is one way to compute the fundamental structure function $D(t)$: Define the function

$$B(z) = \int_0^{\infty} e^{i\omega z} (i\omega)^k S_x(\omega) \frac{d\omega}{2\pi} \quad (9)$$

on the upper half-plane $\text{Im } z > 0$. Let $C(z)$ be any k th integral of $B(z)$, i.e., any function such that $C^{(k)}(z) = B(z)$ on $\text{Im } z > 0$. It will always be found that $C(z)$ can be extended to the real line by continuity. Then let

$$D(t) = 2 \text{ Re } C(t), \quad t \text{ real} \quad (10)$$

If $k > 0$, then $D(t)$ is not unique; any polynomial of degree $< k$ may be added to it. If x is stationary then $k = 0$, and $D(t)$ reduces to the covariance function (6).

RANDOM WALK FM

To see how easy it is to carry out the above procedure for power-law noise types, consider the spectral density $S_x(\omega) = \omega^{-4}$, and take $k = 4$. Then

$$B(z) = \int_0^\infty e^{i\omega z} \frac{d\omega}{2\pi} = -\frac{1}{2\pi i z} \quad (\text{Im } z > 0),$$

a fourth integral of which is

$$C(z) = -\frac{1}{2\pi i} \frac{z^3 \ln z}{6} \quad (\text{Im } z \geq 0).$$

(One can throw out a polynomial of degree less than 4.) Taking $\ln z = \ln|z| + i \text{ Arg } z$ for $\text{Im } z \geq 0$ gives

$$\begin{aligned} D(t) &= 2 \text{ Re } C(t) = 0 && (t > 0) \\ &= -t^3/6 && (t \leq 0). \end{aligned}$$

Adding $t^3/12$ to this gives the alternate form

$$D(t) = |t|^3/12.$$

OTHER POWER-LAW NOISE TYPES

We now give $D(t)$ for the power-law spectrum

$$S_x(\omega) = K_\alpha |\omega|^{\alpha-2}, \quad K_\alpha = \frac{h_\alpha}{2(2\pi)^\alpha}.$$

The forms for the constant K_α and the power of ω link the results to an accepted notation for the noise spectrum, namely

$$S_y(f) = h_\alpha f^\alpha$$

[3], where $y = dx/dt$, $f = \omega/(2\pi)$, and $S_y(f)$ is the one-sided spectral density of y . Fractional values of α are allowed. We can take k to be the integer part of $2 - \alpha$ (refer to (8)).

Case 1. $\alpha < 1$, not an odd integer.

$$D(t) = K_{\alpha} \frac{-|t|^{1-\alpha}}{2\Gamma(2-\alpha) \cos(\pi\alpha/2)} . \quad (11)$$

This case includes white FM ($\alpha = 0$) and random walk FM ($\alpha = -2$).

Case 2. $\alpha = -1, -3, -5, \dots$

$$D(t) = \frac{K_{\alpha}}{\pi} (-1)^{(3-\alpha)/2} \frac{t^{1-\alpha} \ln|t|}{(1-\alpha)!} . \quad (12)$$

This case, which includes flicker FM ($\alpha = -1$), is actually the easiest of all.

Case 3. $\alpha = 1$ (Flicker PM).

Here we use the spectrum

$$S_x(\omega) = K_1 |\omega|^{-1} \exp(-|\omega/\omega_h|) .$$

The exponential high-frequency cutoff yields the elementary result

$$D(t) = -\frac{K_1}{2\pi} \ln(t^2 + 1/\omega_h^2) , \quad (13)$$

whereas the usual rectangular cutoff yields a cosine integral.

Case 4. $\alpha > 1$.

This phase noise process (provided with a high-frequency cutoff) is stationary; thus $D(t)$ is just the autocovariance function of x .

DERIVING THE STRUCTURE FUNCTION FROM $D(t)$

Having the fundamental structure function $D(t)$ in hand, we now show how to use it. Let $x(t)$ be a noise with spectral density $S_x(\omega)$, k the smallest integer satisfying (8), and n_0 the smallest integer such that $2n_0 \geq k$. The differences of x of order n_0 and higher are stationary, and to simplify matters let us assume that they are ergodic and have mean zero. For $n_0 = 2$, this means that an oscillator with phase time $x(t)$ has no long-term average frequency drift. Our main result is the following formula for the general structure function (3) of order $n \geq n_0$:

$$D(t; \underline{a}, \underline{b}) = \Delta_{\underline{a}} \Delta_{-\underline{b}} D(t) . \quad (14)$$

The proof, which has appeared elsewhere [4], starts from the spectral integral

$$D(t; \underline{a}, \underline{b}) = \int_{-\infty}^{\infty} \Delta_{\underline{a}} \Delta_{-\underline{b}} e^{i\omega t} S_x(\omega) \frac{d\omega}{2\pi}, \quad (15)$$

in which the differences operate on $e^{i\omega t}$ as a function of t . (Refer to (5) for the case $n = 2$.) One cannot simply pull the difference operators outside the integral, for the Fourier transform integral of $S_x(\omega)$ diverges (unless $k = 0$) if the singularity at $\omega = 0$ is not neutralized. One way to do this is through the function $B(z)$ given in (9). Another embodiment of $D(t)$ is given directly by the formula

$$D(t) = \int_{-\infty}^{\infty} \left[\cos \omega t - \frac{1}{1 + \omega^{2n}} \sum_{j=0}^{n-1} \frac{(i\omega t)^{2j}}{(2j)!} \right] S_x(\omega) \frac{d\omega}{2\pi} \quad (16)$$

where $n \geq n_0$.

MOMENTS OF STABILITY ESTIMATORS

The remainder of this paper presents a nontrivial application of the preceding theory. Let the phase time $x(t)$ have a long-term frequency drift component:

$$x(t) = x_0(t) + \frac{1}{2}ct^2,$$

where c is the constant rate of frequency drift, and $x_0(t)$ is a Gaussian process whose 2nd differences are stationary, ergodic, and have mean zero. Observing $x(t)$ for $0 \leq t \leq T$, we wish to estimate c and the quantities

$$\sigma_y^2(\tau) = \frac{1}{2\tau^2} E [\Delta_{\tau}^2 x(t)]^2 \quad (\text{Gross Allan variance}),$$

$$\sigma_{y0}^2(\tau) = \frac{1}{2\tau^2} E [\Delta_{\tau}^2 x_0(t)]^2 \quad (\text{Net Allan variance}),$$

which are the theoretical Allan variances before and after removal of drift.

To define and manipulate the estimators, it is necessary to set up some notation as follows: Write

$$C(a, b, t) = \frac{1}{ab} \Delta_a \Delta_b x(t).$$

(This has nothing to do with (10).) Then $EC = c$ for any a, b, t . A particular one of these is used for estimating c , namely

$$\hat{c} = C(\tau_c, T - \tau_c, T) \quad (17)$$

where $\tau_c = T/6.29$, a value chosen to minimize the variance of \hat{c} in the presence of flicker FM noise [5]. The interpretation of (17) is that the estimated drift rate equals the average frequency near the end of the record, minus the average frequency near the beginning, divided by the intervening time $T - \tau_c$.

Let us introduce the additional quantities

$$c_j = C(\tau, \tau, j\tau), \quad c_\tau = C(\tau, T-\tau, T), \quad (18)$$

where j is an integer. To estimate $(2/\tau^2) \sigma_y^2(\tau)$, we use the unbiased statistic

$$v = \frac{1}{m-1} \sum_{j=2}^m c_j^2, \quad (19)$$

where it is now assumed that T/τ is an integer m . This is just the usual Allan variance estimator involving the sum of squares of adjacent second differences. (The unusual scale factor $2/\tau^2$ is convenient for these calculations.) To estimate $(2/\tau^2) \sigma_{y0}^2(\tau)$, we use

$$v_0 = \frac{1}{m-1} \sum_{j=2}^m (c_j - \hat{c})^2. \quad (20)$$

Since

$$\frac{1}{m-1} \sum_{j=2}^m c_j = c_\tau,$$

we have

$$v_0 = v - 2\hat{c}c_\tau + \hat{c}^2. \quad (21)$$

Our goal is to compute the mean and variance of V_0 , a biased estimator. First, we see that V_0 does not depend on the true drift rate c , and so for this purpose we can take $c = 0$. Then

$$EV = (2/\tau^2) \sigma_{y0}^2(\tau), \quad (22)$$

$$\text{Var } V = \frac{1}{(m-1)^2} \sum_j \sum_k \text{Cov}(c_j^2, c_k^2), \quad (23)$$

$$EV_0 = EV - 2E\hat{c}c_\tau + E\hat{c}^2, \quad (24)$$

$$\begin{aligned} \text{Var } V_0 = \text{Var } V + 4 \text{Var}(\hat{c}c_\tau) + \text{Var} \hat{c}^2 - 4 \text{Cov}(V, \hat{c}c_\tau) + 2 \text{Cov}(V, \hat{c}^2) \\ - 4 \text{Cov}(\hat{c}c_\tau, \hat{c}^2). \end{aligned} \quad (25)$$

Because $x(t)$ is Gaussian, the fourth moments in (25) are determined from the second moments of \hat{c} , c_j , c_τ , and the general formula

$$\text{Cov}(uv, xy) = Eux Evy + Euy Evx, \quad (26)$$

where u, v, x, y are zero-mean random variables with a joint Gaussian distribution. In turn, the required second moments are just special cases of the structure function formula (14), which here takes the form

$$E C(a, b, s + t) C(c, d, s) = \frac{1}{abcd} \Delta_a \Delta_b \Delta_{-c} \Delta_{-d} D(t), \quad (27)$$

where $D(t)$ is the fundamental structure function of the phase-time noise $x(t)$. This expression, when written out, is a sum of 16 terms involving D . (See line 1040 of the BASIC program in Fig. 1.)

A BASIC PROGRAM

The tedious but elementary task of computing (23) - (25) by means of (26) and (27) is carried out by the BASIC program shown in Fig. 1. The main point to observe about this program is that the whole algorithm is independent of the phase noise spectrum, which enters only through the one-line function definition of $D(t)$ in line 1030 (and the print statement 130). The only requirement on $S_x(\omega)$ is that the integer k in (8) be at most 4. This guarantees that $x(t)$ has stationary second differences. Because of the way the outputs are scaled, a multiplicative constant in $D(t)$ can be neglected; thus we can let $D(t) = |t|^3$ for random walk FM. For flicker FM, line 1030 becomes

$$\text{DEF DD}(T) = T*T*LOG(\text{ABS}(T) + (T=0)).$$

Line 1040 evaluates (27), and the subsequent definitions evaluate the required special cases. Note that the length of the test run is used as a unit of time. It must be admitted that computational efficiency has been sacrificed to gain ease of coding.

Figure 2 shows the output of the program for random walk FM. The column MEAN(NET) gives the expected value of $(\tau^2/2)V_0$ relative to the true net Allan

variance $\sigma_{y_0}^2(\tau)$. The variances of V and V_0 , the estimators of gross and net Allan variances, are presented in terms of "degrees of freedom" (DF), defined for a positive random variable X by

$$DF = \frac{2(EX)^2}{\text{Var } X},$$

as if X had a χ^2 distribution. The DF(GROSS) result is valid only if the true drift has been subtracted from the phase data. When $T/\tau = 1$, the gross and net DF are both 1, since both V and V_0 are squares of mean-zero Gaussians.

CONFIDENCE INTERVALS FOR ALLAN VARIANCES

Following Howe et al. [6], we use the results shown in Fig. 2 to assign confidence intervals based on the χ^2 distribution, usually with a fractional DF. The author has not estimated the error caused by pretending that V and V_0 are proportional to χ^2 variables. Random walk FM was used as a noise model for $\tau > 10^4$ s. Fig. 3 shows the estimates of gross Allan variance (before drift removal) and net Allan variance (after drift removal) for a 72-day test run of a pair of hydrogen masers at JPL.

Different drift estimators are used in Figs. 3a and 3b. In Fig. 3a, we use a value of drift measured by retuning the masers over a period much longer than the 72-day test run. Regarding this value as close to the "true" value c , and using it in (21) in place of \hat{c} , we can use the gross DF numbers from Fig. 2 to assign confidence intervals to net Allan variance. In Fig. 3b, the estimated value \hat{c} was used, so that one must use the net mean and DF numbers to compute the confidence intervals. The negative bias of V_0 pushes the confidence intervals up; in fact, for $T/\tau = 2$ (one sample of second phase difference), the bias is so great that the 90% confidence interval does not contain the estimate itself. This is pushing things too far, perhaps.

The basic problem is that one cannot remove estimated drift (via (21), for example) without also taking a bite out of the long-term random fluctuations. The outputs of the above computer program for $\omega^{\alpha-2}$ phase noise ($-2.5 \leq \alpha \leq 0$) support the conjecture that the bias of the net Allan variance estimator V_0 is always negative.

REFERENCES

- [1] W. C. Lindsey and C. M. Chie, "Theory of oscillator instability based upon structure functions," Proc. IEEE, Vol. 64, pp. 1652-1666, 1976.
- [2] A. M. Yaglom, "Correlation theory of processes with random stationary n th increments," Amer. Math. Soc. Translations, Ser. 2, Vol. 8, pp. 87-141, 1958.
- [3] J. A. Barnes et al., "Characterization of frequency stability," IEEE Trans. Instrum. Meas., Vol. IM-20, pp. 105-120, 1971.

- [4] C. A. Greenhall, "A structure function representation theorem with applications to frequency stability estimation," TDA Progress Report 42-70, pp. 37-46, Jet Propulsion Laboratory, 1982.
- [5] C. A. Greenhall, "Removal of drift from frequency stability measurements," TDA Progress Report 42-65, pp. 127-131, Jet Propulsion Laboratory, 1981.
- [6] D. A. Howe, D. W. Allan, and J. A. Barnes, "Properties of signal sources and measurement methods," Proc. 35th Ann. Symp. on Frequency Control, pp. A1-A47, USAERADCOM, Fort Monmouth, New Jersey, 1981.

```

100 !MOMENTS OF ALLAN VARIANCE ESTIMATORS
110 GOSUB 1000
120 MC=6.29
130 PRINT \'NOISE TYPE = RANDOM WALK FM\'
140 PRINT \'MEAN & D.F. FOR GROSS & NET A.V. \'\'
    \'T/TAU\',\'MEAN(NET)\',\'D.F.(GROSS)\',\'D.F.(NET)\'
150 FOR M=2 TO 9,10 TO 18 BY 2,20 TO 50 BY 5
160   GOSUB 1080
170   DF=2/VARV,DF0=2*EV0*EV0/VARV0
180   PRINT M,EV0,DF,DF0
190   NEXT M
200 STOP

1000 !DEFINITIONS
1030 DEF DD(T)=ABS(T*T*T)  !FUNDAMENTAL STRUCTURE FUNCTION
    !FOR RANDOM WALK FM
1040 DEF MM(A,B,C,D,T)=(DD(T)-DD(T-A)-DD(T-B)-DD(T+C)-DD(T+D)
    +DD(T-A-B)+DD(T-A+C)+DD(T-A+D)+DD(T-B+C)+DD(T-B+D)+DD(T+C+D)
    -DD(T-A-B+C)-DD(T-A-B+D)-DD(T-A+C+D)-DD(T-B+C+D)
    +DD(T-A-B+C+D))/(A*B*C*D)
1050 DEF FF(A,B)=MM(A,1-A,B,1-B,0)
1060 DEF GG(A,B,J)=MM(A,1-A,B,B,1-J*B)
1070 DEF HH(A,J)=MM(A,A,A,A,J*A)
1073 RETURN

1080 !COMPUTATION SUBROUTINE
    !INPUTS: M=T/TAU, MC=T/TAUC (=6.29)
    !OUTPUTS: EV0/A.V., VAR(V)/A.V.**2, VAR(V0)/A.V.**2
    EV0      VARV      VARV0
1090 U=1/M,UC=1/MC  !U STANDS FOR TAU
1100 FUU=FF(U,U),FCU=FF(UC,U),FCC=FF(UC,UC)
1110 HU0=HH(U,0),HU02=HU0*HU0  !HU0 IS SCALED ALLAN VARIANCE
1120 !
1130 EV0=HU0-2*FCU+FCC
1140 M1=M-1,X=0\ H=HH(U,J),X=X+(M1-J)*H*H FOR J=1 TO M-2\
    X=2*X+M1*HU02,VARV=X*2/(M1*M1)
1150 VARCU=FCC*FUU+FCU*FCU, VARCC=2*FCC*FCC
1160 X=0\ X=X+GG(UC,U,J)*GG(U,U,J) FOR J=2 TO M\ COVVCU=2*X/M1
1170 X=0\ G=GG(UC,U,J),X=X+G*G FOR J=2 TO M\ COVVCC=2*X/M1
1180 CVCUCC=2*FCC*FCU
1190 !
1200 VARV0=VARV+4*VARCU+VARCC-4*COVVCU+2*COVVCC-4*CVCUCC
1210 RETURN WHERE EV0=EV0/HU0,VARV=VARV/HU02,VARV0=VARV0/HU02

```

Figure 1. A BASIC program for computing mean and variance of an estimator of net Allan variance.

NOISE TYPE = RANDOM WALK FM
 MEAN & D.F. FOR GROSS & NET A.V.

T/TAU	MEAN(NET)	D.F. (GROSS)	D.F. (NET)
2	.11213718	1	1.0000011
3	.4131003	1.882353	1.2011257
4	.56608639	2.7692308	1.9797428
5	.65837896	3.6571431	2.8213698
6	.72007427	4.5454549	3.6927653
7	.76417726	5.4339623	4.5779951
8	.7970189	6.3225806	5.4662905
9	.82222714	7.2112679	6.3534235
10	.84209356	8.1000005	7.2390502
12	.87125838	9.8775517	9.0083684
14	.89153524	11.655173	10.777728
16	.90639572	13.432836	12.546251
18	.91772997	15.210527	14.314574
20	.92664775	16.988236	16.084209
25	.9423454	21.432559	20.511747
30	.95254386	25.876923	24.943548
35	.9596919	30.321313	29.378236
40	.96497606	34.765708	33.814985
45	.96903914	39.210128	38.253179
50	.97225997	43.654528	42.692561

Figure 2. Output of the program of Fig. 1 for random walk FM noise.

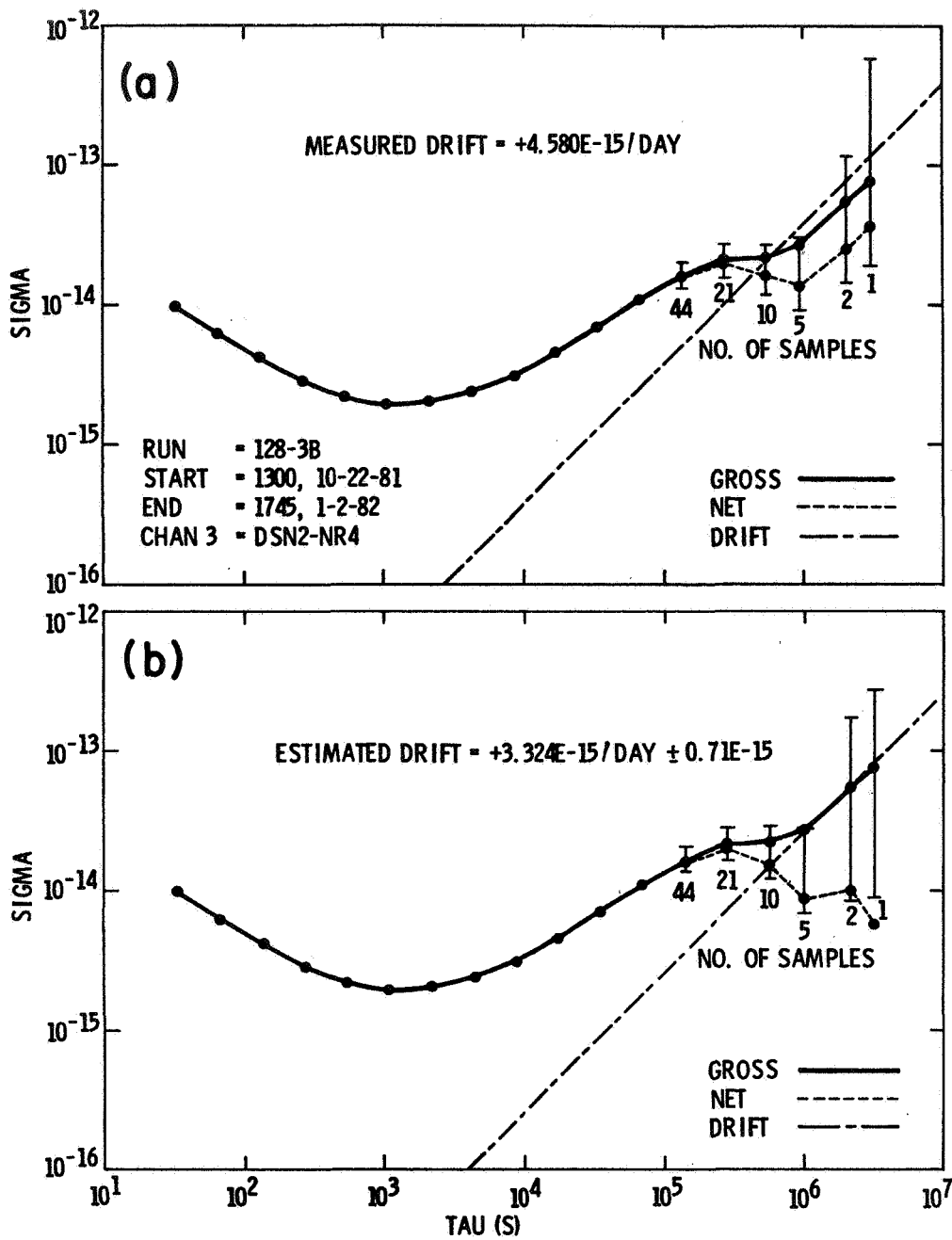


Figure 3. Allan variance of a pair of hydrogen masers (DSN2 and NR4) before and after removal of drift, with 90% confidence intervals for net Allan variance.

QUESTIONS AND ANSWERS

None for Paper #12

Stochastic Models for Atomic Clocks

J. A. Barnes, R. H. Jones, P. V. Tryon*, and D. W. Allan

ABSTRACT

Most workers in the field of atomic clocks encounter frequency and time instabilities which can be characterized (or modelled) as random fluctuations. These random fluctuations typically display a power spectral density which varies as a power-law over some significant range of (Fourier) frequencies (e.g., $S_y(f) = h_2 f^2$, where Y denotes the normalized, instantaneous frequency and f denotes the Fourier frequency). Typical oscillators and/or clocks may have regions where one specific power-law predominates and other regions where other power-laws predominate. In general, various combinations of five different power-laws seem to be adequate to describe almost all observed random behavior in atomic clocks. The five types are:

White phase modulation	$S_y(f) = h_2 f^2$
Flicker phase modulation	$S_y(f) = h_1 f^1$
White frequency modulation	$S_y(f) = h_0 f^0$
Flicker frequency modulation	$S_y(f) = h_{-1} f^{-1}$
Random Walk frequency modulation	$S_y(f) = h_{-2} f^{-2}$

In addition to the random components, oscillators and clocks often show systematic, (i.e., deterministic) trends such as offsets in frequency and time, as well as linear drifts in frequency.

For the atomic clocks used in the NBS Time Scales, an adequate model is the superposition of white FM, random walk FM, and linear frequency drift for times longer than about one minute. The model has been tested on several clocks using maximum likelihood techniques for parameter estimation and the residuals have been "acceptably random." Conventional diagnostics indicate that additional model elements contribute no significant improvement to the model even at the expense of the added model complexity.

I. INTRODUCTION

Many authors (1, 2, 3) have documented the fact that most precision oscillators and clocks exhibit both random and systematic variations in their output signals. The typical random parts may include white noise

*Deceased

phase modulation (PM), flicker noise PM, white noise frequency modulation (FM), flicker FM, and random walk FM. A subset of these five noises is usually adequate. In addition, most oscillators also exhibit a linear drift in frequency, which is often difficult to measure.

Experimenters often diagnose the various noises using the two-sample variance (or "Allan Variance") (4,5). On occasion, they will use an estimate of the power spectral density of the frequency fluctuations (4, 5). Of course, one cannot adequately observe the fluctuations of a single clock or oscillator by itself -- one must look at the difference between two clocks. The allocation of noise levels to individual clocks requires three or more clocks of comparable quality. This allocation process does not always provide reasonable results. In fact, often the process yields negative values for the variance -- an undesirable artifact of the estimation procedure.

The Allan Variance is defined (1) as the infinite time average of sample variances based on a sample size of only two adjacent values of frequency. That is,

$$\sigma_y^2(\tau) = \lim_{N \rightarrow \infty} \frac{1}{N} \sum_{n=1}^N \left(\frac{\bar{y}_n - \bar{y}_{n-1}}{2} \right)^2 \quad (1)$$

where \bar{y} is the average frequency departure from nominal, averaged over the time interval and divided by the nominal frequency. An equivalent form of Eq. (1) is:

$$\sigma_y^2(\tau) = \lim_{N \rightarrow \infty} \frac{1}{N} \sum_{n=1}^N \left(\frac{X_n - 2X_{n-1} + X_{n-2}}{2\tau} \right)^2 \quad (2)$$

where $x(t)$ and $y(t)$ are related by

$$y(t) = \frac{d}{dt} X(t) \quad (3)$$

and $X(t)$, the instantaneous time error, is related to the phase error of the oscillator by the relation:

$$X(t) = \frac{\phi(t)}{2\pi\nu_0} \quad (4)$$

where $\phi(t)$ is the phase error and ν_0 is the nominal frequency (e.g., 5MHz).

The Allan Variance is normally computed from finite data sets of the time difference, X_n , where

$$X_n = X(n\tau_0) \tag{5}$$

and the estimated Allan Variance is

$$\hat{\sigma}_y^2(\tau) = \frac{1}{N-2m} \sum_{n=1}^{N-2} \frac{(X_{n+2m} - 2X_{n+m} + X_n)^2}{2m^2\tau_0^2} \tag{6}$$

where $\tau = m\tau_0$.

Although Eq. (6) is very close in form to the definition of the Allan Variance (see Eq. (1)), it is NOT an optimum estimator of the "true" Allan Variance. That is, there are other statistical techniques which provide more precise estimates of the frequency variability. These improved techniques, however, are usually valid only for very specific clock models. Fortunately, commercial cesium beam atomic clocks have been studied extensively, and good models are well documented.

II. Optimum Estimates

In the introduction, we identified two problems:

- A. Statistically inefficient estimators of the level of oscillator noises and drift, and
- B. Difficulties in separating individual clock performances.

While these two problems cannot be totally eliminated, they are amenable to optimal estimation techniques. That is, we can minimize their effects.

The means of estimating these parameters has been developed by R.H. Jones and P.V. Tryon (6, 7). Basically, the technique is that of maximum likelihood estimation. The technique requires an ensemble of comparable clocks ($M > 2$) and time difference data between clocks covering a significant duration (e.g., a year). With the assumptions that the perturbing noises are both independent and Gaussian, and that the basic model is adequate, then it is possible to form the likelihood function as a function of the oscillator parameters. The likelihood function is obtained from a Kalman Filter algorithm applied to the clock ensemble data.

Using essentially the same notation as used by Gelb (8), the clock model

and measurements can be expressed as follows:

$$\begin{pmatrix} X_1 \\ Y_1 \\ X_2 \\ Y_2 \\ \vdots \\ \vdots \end{pmatrix} = \begin{pmatrix} 1 & 1 & 0 & 0 & \dots \\ 0 & 1 & 0 & 0 & \dots \\ 0 & 0 & 1 & 1 & \dots \\ 0 & 0 & 0 & 1 & \dots \\ \vdots & \vdots & \vdots & \vdots & \dots \\ \vdots & \vdots & \vdots & \vdots & \dots \end{pmatrix} \begin{pmatrix} X_1 \\ Y_1 \\ X_2 \\ Y_2 \\ \vdots \\ \vdots \end{pmatrix} + \begin{pmatrix} \varepsilon_1 \\ \eta_1 \\ \varepsilon_2 \\ \eta_2 \\ \vdots \\ \vdots \end{pmatrix} \quad (7)$$

where the subscripts on the matrices denote the recursion number (i.e., time).

$$Q = \begin{pmatrix} \sigma_{\varepsilon 1}^2 & 0 & 0 & 0 & \dots \\ 0 & \sigma_{\eta 1}^2 & 0 & 0 & \dots \\ 0 & 0 & 0 & \sigma_{\varepsilon 2}^2 & \dots \\ \vdots & \vdots & \vdots & \vdots & \dots \\ \vdots & \vdots & \vdots & \vdots & \dots \end{pmatrix} \quad (8)$$

$$H = \begin{pmatrix} 1 & 0 & -1 & 0 & 0 & 0 & \dots \\ 1 & 0 & 0 & 0 & -1 & 0 & \dots \\ \vdots & \vdots & \vdots & \vdots & \vdots & \vdots & \dots \\ \vdots & \vdots & \vdots & \vdots & \vdots & \vdots & \dots \end{pmatrix} \quad (9)$$

$$R = 0 \quad (10)$$

where the the number of clocks is M , the state vector, \underline{X} , is a $2M$ column vector, Φ and Q are $2M$ by $2M$ square matrices, and the measurement matrix, H , is $M-1$ by $2M$, since there are only $M-1$ independent clock differences.

In matrix form the equations become:

$$\underline{X}_n = \Phi \underline{X}_{n-1} + \underline{U}_n \quad (11)$$

and the measurements, \underline{z}_n , are:

$$\underline{z}_n = \underline{H} \cdot \underline{x}_n \quad (12)$$

The forecasts of \underline{x}_n and \underline{z}_n to step $n+1$ based on data up to and including step n are:

$$\hat{\underline{x}}_{n+1}^- = \underline{\phi} \cdot \underline{x}_n^+ \quad (13)$$

$$\hat{\underline{z}}_{n+1} = \underline{H} \cdot \hat{\underline{x}}_{n+1}^- \quad (14)$$

Of interest are the innovations at step $n+1$. The innovations are given by

$$\tilde{\underline{z}}_{n+1} = \underline{z}_{n+1} - \hat{\underline{z}}_{n+1} \quad (15)$$

with the covariance matrix \underline{V}_{n+1}

$$\underline{V}_{n+1} = \underline{H}' \cdot \underline{P}_{n+1}^- \cdot \underline{H} \quad (16)$$

where \underline{P}_{n+1}^- is the error covariance matrix for the state vector (see Appendix A for a brief summary of the Kalman filter relations).

Assuming that the driving noises, ε_n and η_n , are normal random deviates with zero mean, then the multivariate probability distribution can be written in the form

$$f(z_1, z_2, \dots) = [(2\pi)^m/2 \left| \underline{V} \right|^{1/2}]^{-1} \exp \left[-\frac{1}{2} \sum_{n=0}^N \tilde{\underline{z}}_n' \cdot \underline{V}_n^{-1} \cdot \tilde{\underline{z}}_n \right] \quad (17)$$

The function, ℓ , given by -2 times the log of the likelihood function, is

$$\ell = \sum_{n=1}^N \ln \left| \underline{V}_n \right| + \sum_{n=1}^N \tilde{\underline{z}}_n' \cdot \underline{V}_n^{-1} \cdot \tilde{\underline{z}}_n \quad (18)$$

Now, ℓ is an implicit function of the parameters σ^2 , because both the innovations and the error covariance matrix, \underline{P}_n^- , are dependent on these model parameters. The estimation procedure finds that set of parameters (σ^2 's) which minimizes ℓ (that is, maximizes the likelihood function). Unfortunately, ℓ is a non-linear function of the parameters and must be calculated by a complete pass through the data for each trial set of the $2M$ parameters. For example, if one has $M=10$ clocks and daily time difference data for a year, then one has $365 \times (M-1) = 3285$ independent measurements and $2M = 20$ parameters to adjust in order to maximize the likelihood function. There exist standard computer algorithms to perform such calculations.

Three additional concerns are (a) the estimates of confidence intervals for the parameters, (b) the diagnostics to test the adequacy of the basic model assumptions, and (c) the extension of the maximum likelihood estimates to include a frequency drift parameter for each clock (9). The model adequacy can be tested by testing of the residuals (\hat{Z}_n) for "whiteness" (i.e., randomness); and by comparing results to more complex model assumptions. References 6,7 include a discussion of the methods used to estimate the confidence intervals of the parameter estimates.

III. Experimental Results

For many years, the National Bureau of Standards (NBS) has accumulated large quantities of clock comparison data on the commercial cesium clocks used in the NBS time scale. We used a recent sample of time comparisons on a dozen clocks over about two months sampled every two hours. We also used another set of daily data on seven clocks over a period of one year.

The basic model assumption was that of white FM noise plus random walk FM noise plus linear frequency drift. Thus, for each clock in a data set we estimated σ_ε , σ_η , and D the drift parameter. Also estimated were the corresponding confidence intervals. The three parameters can be related to the more conventional Allan Variance through the equation (see Appendix B):

$$\hat{\sigma}_y^2(n\tau_0) = \frac{\sigma_\varepsilon^2}{n\tau_0^2} + \frac{\sigma_\eta^2(2n^2 + 1)}{6n\tau_0^2} + \frac{(Dn\tau_0)^2}{2} \quad (19)$$

Figure 1 displays plots of the Allan variance obtained from the use of Eq. 19, above and the estimated parameters. Figure 2 displays a cumulative periodogram of residuals for one of the clocks. A periodogram of pure "white" noise would fall within the boundaries shown 90% of the time. On the shorter data run, (~ 2 mos.) linear frequency drift was not statistically significant. In fact, even on the longer run (1 year), only infant clocks or older clocks approaching end of life showed significant drift. (Of course, the algorithm could only detect relative drifts between clocks, not a common drift shared by all clocks.) Tests were made using more complex models, but any improvement was found to be statistically insignificant.

IV. Conclusions

A viable clock model for commercial cesium beam clocks consists of three elements:

- (1) White FM
- (2) Random walk FM
- (3) Linear frequency drift

Maximum likelihood estimation techniques yield reasonable results and confidence intervals also. Conventional tests show the model to adequately describe observed clock behavior. Further, the technique allows one to estimate the individual performance of each clock. As pointed out by Jones, one can avoid the problem of negative variances by using a log transformation, $\gamma = \ln(\sigma^2)$.

Equation 19 allows one to express the results in the form of conventional Allan Variances.

The new NBS time scale algorithm (TA(NBS)) makes use of the parameter estimation routines covered in this paper. The technique is also used for NBS clock calibrations.

REFERENCES

1. Allan, D. W., "Statistics of Atomic Frequency Standards," Proc. IEEE 54, No. 2 pp. 221-236, February 1966.
2. Cutler, L. S., and Searle, C. L. "Some Aspects of the Theory and Measurement of Frequency Fluctuation in Frequency Standards," Proc. IEEE 54, No. 2 pp. 136-154, February 1966.
3. Barnes, J. A., et. al. "Characterization of Frequency Stability," IEEE Trans. on I + M Vol. IM-20, No. 2 pp. 105-120, May 1971 (Also published in NBS Tech. Note 394, April 1971).
4. Rutman, J., "Instabilité de Frequence des Oscillateurs," L'Onde Electrique 52, No. 11, pp. 480-487, Dec. 72.
5. Lesage, P., and Audoin, C., "Characterization and Measurement of Time and Frequency Stability," Radio Science, Vol. 14, No. 4 pp. 521-539, July-August, 1979.
6. Tryon, P. V. and Jones, R. H., "Estimation of Parameter in Models for Cesium Beam Atomic Clock," to be published in NBS Journal of Research, Vol. 88, 1983. Appears in the unofficial proceedings of the 2nd International Symposium on Atomic Time Scale Algorithms, National Bureau of Standards, Boulder, CO, 23-25 June 1982.
7. Jones, R. H., and Tryon, P. V., "Estimating Time from Atomic Clocks," to be published in NBS Journal of Research, Vol. 88, 1983. Appears in the unofficial proceedings of the 2nd International Symposium on Atomic Time Scale Algorithms, National Bureau of Standards, Boulder, CO, 23-25, June 1982.
8. Gelb, A., et. al., "Applied Optical Estimation," The MIT Press 1974.
9. Percival, D. B., "The U.S. Naval Observatory Clock Time Scales," IEEE Trans. on I + M, Vol. IM-27, No. 4, Dec. 1978.

APPENDIX A

SUMMARY OF DISCRETE KALMAN EQUATIONS

Model: $\underline{X}_n = \Phi \cdot \hat{\underline{X}}_{n-1} + \underline{U}_n$

Measurement: $\underline{Z}_n = \underline{H} \underline{X}_n + \underline{V}_n$

Forecast: $\hat{\underline{X}}_n = \underline{\Phi} \hat{\underline{X}}_{n-1}^+$

Error Covariance: $\underline{P}_n = \underline{\Phi} \cdot \underline{P}_{n-1}^+ \cdot \underline{\Phi}' + \underline{Q}$

Kalman Gain: $\underline{K}_n = \underline{P}_n \cdot \underline{H}' \cdot [\underline{H} \cdot \underline{P}_n \cdot \underline{H}' + \underline{R}]^{-1}$

Error Covariance: $\underline{P}_n^+ = \underline{P}_n - \underline{K}_n \cdot \underline{H} \cdot \underline{P}_n$

State Update: $\hat{\underline{X}}_n = \hat{\underline{X}}_n + \underline{K}_n \cdot [\underline{Z}_n - \underline{H} \cdot \hat{\underline{X}}_n]$

Allan Variance

$$\begin{aligned}
 \sigma_y^2(m\tau_0) &= E \left[\frac{(X_{n+m} - 2X_n + X_n)^2}{2m^2\tau_0^2} \right] \\
 &= E \left[\frac{\left[-\sum_{i=n+1}^{n+m} \eta_i + \sum_{i=n+m+1}^{n+2m} \eta_i \right]^2}{2m^2\tau_0^2} \right] \\
 &= \frac{\sigma_\eta^2}{2m^2\tau_0^2} \left[\sum_{i=1}^m (i-1)^2 + \sum_{i=1}^m (m-i+1)^2 \right] \\
 &= \frac{\sigma_\eta^2}{2m^2\tau_0^2} \left[2\sum_{i=0}^{m-1} (i)^2 + m \right] \\
 &= \frac{\sigma_\eta^2}{2m^2\tau_0^2} \cdot \left[\frac{m(2m^2 + 1)}{3} \right]
 \end{aligned}$$

Random Walk FM $\sigma_y^2(m\tau_0) = \sigma_\eta^2 \cdot \left(\frac{2m^2 + 1}{6m\tau_0^2} \right)$

Linear Frequency Drift

$$X_n = \frac{1}{2}D(n\tau_0)^2 \quad (\text{Deterministic})$$

Allan Variance

$$\sigma_y^2(m\tau_0) = \frac{(X_{n+2m} - 2X_{n+m} + X_n)^2}{2m^2\tau_0^2}$$

Allan Variance

$$\begin{aligned}\sigma^2(m\tau_0) &= \frac{\frac{1}{2}D\tau_0^2 [(n+2m)^2 - 2(n+m)^2 + n^2]}{2m^2\tau_0^2} \\ &= \frac{[\frac{1}{2}D\tau_0^2 \cdot (2m^2)]^2}{2m^2\tau_0^2} \\ &= \frac{1}{2}(Dm\tau_0)^2\end{aligned}$$

Composite: Assumes noises statistically independent.

$$\sigma_y^2(m\tau_0) = \frac{\sigma_\varepsilon^2}{m\tau_0^2} + \sigma_\eta^2 \frac{(2m^2 + 1)}{6m\tau_0^2} + \frac{1}{2}(Dm\tau_0)^2$$

If the time error, X_n , is sampled from a continuous process, then*

$$\sigma_y^2(m\tau_0) = \frac{\sigma_\varepsilon^2}{m\tau_0^2} + \frac{\sigma_\eta^2 m\tau_0}{3\tau_0^3} + \frac{1}{2}(Dm\tau_0)^2$$

* Private communication C. Greenhall.

QUESTIONS AND ANSWERS

DR. STEIN:

The model which you say seems to fit most of our clocks contains random walk frequency, no flicker frequency. Therefore, much much more pessimistic view of the clocks than we have usually adopted, and I was wondering if you could comment on, for instance, what happens if you include a flicker term, do the residuals get better, or, what is the reason for rejecting the flicker frequency model?

MR. BARNES:

OK. Everybody -- I guess from my reputation, if anybody used flicker noise it would have been me, but, if you had had flicker FM present, what would happen in these models would be that the minimum value would move up and tend to have a flatter region right in the center if you really had flicker noise.

I can't go and say that, unequivocally, there is no flicker noise in these clocks, but, I can say that if you looked at the residuals for the models without flicker noise and then added flicker noise, you would find that the improvement in the whiteness of the residuals was not statistically significant.

At least, that is our experience in this data.

We tried to test the model, to see if adding other noises would significantly reduce the magnitude of the residual, and for no other model did we find significant improvement. That doesn't mean that it does not exist, but it does mean that in this sample, we were unable to observe it.

DR. WINKLER:

I just want to take this beautiful opportunity to point out that your frequency standard is an excellent one for long-term.

MR. BARNES:

I guess that's what that things says, and it doesn't have error bars on this particular graph, but I would guess that this is not surprising, because the fact that it is so bad in short-term, means that it is harder to measure reliably the long-term performance, and hence, the confidence intervals along the random walk frequency, are so broad that it allows it to almost look too good. And that, I suspect, is an artifact of any kind of analysis. Thank you.

DR. STEIN:

In this case, I would have to say that our qualitative observations from many years indicate that this analysis is probably correct.

DR. WINKLER:

Nevertheless, I think that it is important to note that one should not use short-term stability parameters for rating of clocks long-term.

MR. ALLAN:

Johnson tried, independently, to assess the ability for the clock ensemble, and the assessment has been over a year period, and a year elapsed, and another year period, so there was a great deal of difference in the stream of data -- and the parameters on this particular clock were the same, two totally independent years.

NARROW ^{87}Rb and ^{133}Cs HYPERFINE TRANSITIONS IN EVACUATED WALL-COATED CELLS

H.G. Robinson
Physics Department, Duke University
Durham, North Carolina 27706

C.E. Johnson
Physics Department, North Carolina State University
Raleigh, North Carolina 27650

ABSTRACT

An extension of our work on wall-coated cells has been made to include observation by a triple resonance technique of the 0-0 hyperfine transitions in ^{87}Rb and ^{133}Cs . Conventional rf excited lamps were used. Interest in such cells is for possible application in atomic clocks. The Rb cell would appear to remain especially promising in this respect.

INTRODUCTION

We have previously reported¹ observation of ^{87}Rb $|\Delta m_F| = 1$ hyperfine transitions in a 200 cm^3 , evacuated wall-coated cell. The narrow Lorentzian component of the lineshape has a width of $\sim 11\text{ Hz}$, FWHM, giving a $Q \sim 0.65 \times 10^9$ for the resonance. Interest in the $(F, m_F) = (2, 0) \leftrightarrow (1, 0)$ hyperfine transition for potential use in Rb frequency standards has focused our attention toward exploring the characteristics of this "clock" transition.

EXPERIMENT AND RESULTS

The apparatus available uses a conventional rf plasma excited Rb lamp which, after filtering, produces circularly polarized D1 light. The cell is placed in a shielded solenoid producing a 1.5G magnetic field. The use of the $\sigma(+ \text{ or } -)$ radiation permits observation of $|\Delta m_F| = 1$ hyperfine transitions by monitoring the intensity of the transmitted light. This detection scheme relies on a change in $\langle S_z \rangle$, the z-component of the electron spin. Where the population is pumped toward the (2,2) level, the largest signals correspond to the $(2,2) \leftrightarrow (2,1)$ Zeeman transition and the $(2,2) \leftrightarrow (1,1)$ hyperfine transition. However, since the change in $\langle S_z \rangle$ is zero for the 0-0 hf transition, the method is not suited for direct observation of this resonance. Nevertheless, by exciting the Zeeman transitions $(2,2) \leftrightarrow (2,1)$ and $(2,1) \leftrightarrow (2,0)$, we can detect a change in the (2,0) population caused by a 0-0 transition. This triple resonance scheme was employed to obtain initial data on the clock transition in the sealed, evacuated wall-coated Rb cell.

Linewidths as narrow as 9 Hz FWHM are observed for the 0-0 resonance. Figure 1 displays such an observation having a 13 Hz linewidth with a Lorentzian lineshape function fitted to the data. The symmetry of the resonance is a sensitive function of the tuning of the two Zeeman resonance drives. The observed wall shift of the hyperfine frequency due to atom-wall interaction is - 52 Hz at 26 °C. Both width and wall shift are consistent with our previously reported¹ observations made on the $(2,|2\rangle) \leftrightarrow (1,|1\rangle)$ hf transitions.

A 100 cm³ sealed, evacuated wall-coated cell was also available for ¹³³Cs. We repeated the above procedure with the Cs cell using a conventional rf driven Cs lamp as the pumping source. The linewidth extrapolated to zero light and rf intensities is ~ 101 Hz. The wall shift observed is - 180 Hz at 26 °C. Upon cooling the Cs reservoir to 5.5 °C and heating the cell wall to 50 °C we obtained a wall shift of - 160 Hz for the $(4,|4\rangle) \leftrightarrow (3,|3\rangle)$ transitions.

These initial results leave unanswered questions of aging, retraceability, and whether substantially better evacuated wall-coated cells can be fabricated. However, the observation of ⁸⁷Rb hf resonance with $Q \sim 6.5 \times 10^8$ in a sealed, evacuated wall-coated cell shows a potential for use of this type of cell in an atomic frequency standard. We are pursuing pumping/detection schemes permitting efficient direct observation of the 0-0 transition using laser diodes.

REFERENCES

1. H.G. Robinson and C.E. Johnson, Appl. Phys. Lett. 40, 771 (1982).

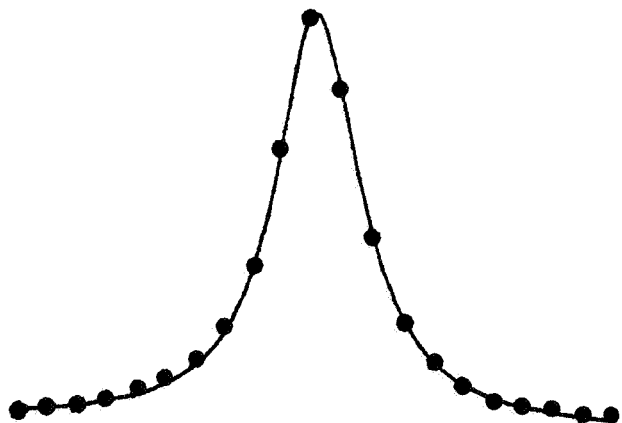


Figure 1. A 0-0 hf transition in ⁸⁷Rb with a linewidth of 13 Hz. The solid curve is a Lorentzian function fitted to the data points. Observation is by a triple resonance technique.

QUESTIONS AND ANSWERS

PROFESSOR JACQUES VANIER, Quebec, Canada

What kind of a coating material do you use in your cell?

MR. ROBINSON, Duke University

The material that's used here is, we believe, is TETROCONTAIN. These cells were built at a very chaotic time and the record keeping on these cells is not all it should be. But, we could tell, we could test that by taking the cell up to where we would melt the surface wax, find out unequivocally, but, we'd rather not do that, until we have played with the cells a little longer.

MR. DEHMELT:

Do you have an estimate of the optic frequency Zeeman for the transition in the rubidium cases? It varies -- more than I know.

MR. ROBINSON:

The line width of the zero-zero transition is very insensitive to the amount of power put on the Zeeman. The Zeeman line width is considerably in excess by broadening of RF, due to the transition due to the Zeeman transition power.

In other words, I would say the Rabi frequency is larger than 9 hertz for the Zeeman transition. We haven't understood that yet, but we have not worked with understanding it either, the experimental fact is that the zero-zero transition line is very insensitive to the amount of Zeeman power, you put on. The amplitude is sensitive. The amplitude is very sensitive, but the line -- it may be an Autler (?) -Townes situation.

AUDIENCE:

Yes. What do you think is the dominant contribution to the line width in these transitions you're seeing?

MR. ROBINSON:

The dominant contribution of the line width, we were able to, essentially, write a line width budget for the case of the Delta M-1 transition, and the dominant contribution, by far, is the effect on the wall. While it sits on the wall, there is a dispersion in the phase shift that you get. Each attack of the wall of the atom does not give you exactly the same phase shift as the random walk in phase. And it's that dispersion that is the dominant cause.

Out of that ten cycles for instance, at least six cycles worth of it is due to the random nature of this phase shift on the wall itself.

So, the wall is the dominant cause of the line width. The light intensity that we've used to take these resonances is on the order of, 1 1/2 microamps. That issue came up yesterday -- and I don't know how many microwatts per square centimeter that is, but that's the transmitted light intensity. It's a very, very low light intensity, so we don't get very much light broadening.

Now, we could go down a whole list of potential sources of line width, and they all reasonably add up. So, we have looked at that budget, but the dominant one by far is the wall itself.

DR. KELLOGG:

Do you have any plans to go the other way in the temperature spectrum? Maybe cooling the wall before you risk melting the wax?

MR. ROBINSON:

Well, theoretically, it looks like it's better to heat the wax. The lifetime, the time the atom sits on the wall, is related to the absorption energy.

What you want to do is to heat the wall up and, in fact, for the cesium case, we heated the wall up to about 55°C, and the line width narrows as you do this.

The wall shift decreases as you do this, or rather, the magnitude of the wall shift decreases. So, things get better as you heat the wall, until you reach a point where, perhaps, the wax begins to melt or change character, and then it turns around and goes the other way.

But, in fact, it looks like it's better to heat the wall in this particular case than, than to cool it.

These cells aren't expensive to produce. I don't know what -- how you count production costs, and whatnot, but there's just a trivial amount of wax involved in them, and glassblowing time and so forth, so the cost is not really significant, I think.

AUDIENCE:

I would like to ask one question, please. About the insensitivity to magnetic field gradient. I believe that is true if you use a high magnetic field, but like in a hydrogen maser, when you go to lower fields, that is when used for frequency standards, you start to have some trouble with the Zeeman frequency. If it is of the magnitude of the collision frequency of the atoms, then you start to lose signal and you have a shift in the frequency of the line. So the insensitivity to magnetic gradient is true only for high magnetic field and not for low field.

MR. ROBINSON:

I'm not sure I understood all that, but you're commenting on the fact that we have 1 1/2 gauss field and we did that in particular to resolve all the Zeeman transitions so that we could individually diagnose things, see what was going on.

The Zeeman line width is about 2 1/2 cycles in these cells. There's no reason why we couldn't reduce that field as far as we see. It's -- we understand how the averaging process for inhomogeneity occurs, and there should be no problem at all in reducing the field with respect to that particular parameter. So I don't see any, just offhand, any problem in going down to very small fields. There's no problem with optical pumping as I understand it and going to essentially zero fields as long as we have some direction for the Z direction for the system.

AUDIENCE:

What I mean is, is it possible to go to a lower field? Also what about the uniformity of the RF field?

(QUESTION NOT TRANSLATABLE IN THE RECORDING)

MR. ROBINSON:

The wall shift for the Delta M-1 transition was a much cleaner situation. And that was also -52 Hz. And we expect theoretically that the two wall shifts should be the same, to, within some small discrepancy. So the fact that we confirmed that by this very obtuse triple resonance technique I think is a good sign. It just means that we believe that result.

AUDIENCE:

Is there any plan to repeat the experiment with fresh cells?

MR. ROBINSON:

Yes, we need to do that. It's clear that there's some critical questions that arise as to how to get the cell to stabilize, will the wall shift itself drift forever, will it stabilize in a week or a month or two days, or just what. Same thing for the line width. Retractable if you heat and cool these things. What happens?

We'd like to do some of these things. It just takes research time that we haven't managed to get.

AUDIENCE:

Was there any data over this ten year period as to how much the wall shift changed?

MR. ROBINSON:

No, our initial experimental use of these cells was in shimming magnetic fields to look at magnetic moments. We have a history of looking at G factors in atoms, and in fact, we were just not interested in the hyper-fine transitions in these cells. So we never even looked at the hyper-fine transition when they were originally made. That was very unfortunate but that was the case.

They're extremely useful in tuning away magnetic field gradients, because the averaging process gives you a measure of the magnetic field at a point, mainly the very center of the sphere, so it's actually measuring the magnetic field literally over a volume in one sense, but the average is legitimately mathematically that of a point in the center of the cell.

And not only that, but it produces essentially a Lorentzian line shape, so that if you have magnetic field inhomogeneity shims which we have, you can tune each one and it uncouples them. So that essentially there's only one pass. It makes all of these knobs orthogonal. So this is our use for such cells and we just didn't have the foresight to look at these things.

It's clear that that needs to be done now. That is one of the main things if you look at the long-term drift of the wall shift.

AUDIENCE:

Do you know why the line width of the cesium was approximately ten times that for rubidium?

MR. ROBINSON:

There -- let's see, I think in principal from a theoretical point of view, you expect the cesium to be much worse because it has a higher polarizability. It's a much softer atom and we haven't put numbers into that. That would be a nice thing to do, to see if we could actually give a back of the envelope calculation to show that. Whether that's the factor that one would expect, I'm not certain. But that's certainly one reason.

A second thing is that we don't have enough cells to know whether the coatings that we get are reproducible. That is, from one thing to another. These are one of a kind cells, and it may be that the cesium cell just simply isn't as well coated.

The third thing is that the cesium has a much higher vapor pressure at room temperature, as you know. Some of our data here was taken with a 5°C cesium stem. We saw visible traces of cesium all over the external arms of the cell. That is, it had moved around over the time of the cell, so that it left its original reservoir and migrated through the cell and out into some of the other arms that we have on this cell.

And, it could be that that wall was damaged, or actually had some cesium sitting on it. We actually noticed an aging, or de-aging if you like, process over a period of maybe ten hours when we cooled the cesium cell. We didn't notice that for the rubidium.

But, we just don't know the answer to the question and there's some good theoretical reasons why it could have happened. And I will first go to this, to the polarized stability of the atom. I think that's the most likely thing.

CESIUM STANDARD FOR SATELLITE APPLICATION

M. Bloch, M. Meirs, I. Pascaru, B. Weinstein
Frequency Electronics, Inc., Mitchel Field, New York

ABSTRACT

This paper discusses a Cesium Frequency Standard that has been developed for satellite applications. It weighs 23 lbs. and uses 23.5 watts of power, achieves a stability of $1 \times 10^{-13}/10^5$ seconds, and is radiation hardened to meet GPS Phase II requirements. To achieve the weight and reliability requirements, both thick and thin film hybrid circuits were utilized. An SC-Cut crystal oscillator is used to improve short-term stability and performance on a moving platform.

INTRODUCTION

In order to meet GPS performances and weight requirements the Portable Real Time Clock [1] presently manufactured by Frequency Electronics, Inc. was redesigned. Hybrids were utilized for critical modules to increase the reliability and to lower the weight. A new air "C" field was used in the cesium resonator, in order to improve the frequency stability of the standard as a function of temperature. Radiation and thermal-vacuum operation were the prime factors in the mechanical design of this standard.

The chassis of the Standard is machined from a solid piece of aluminum to form a "shoe box" on which all the modules are mounted. A modular approach was taken to allow each subassembly to be individually tested to its performance requirements prior to integration in the system. A photograph of the Standard is shown in Figure 1. This shows the outside of the shoe box with the A6 Power Supply located on the extreme right-hand side. Adjacent to the power supply is the A4 high precision SC-cut oscillator. On the extreme left-hand side is an RF filter box through which all of the power and telemetry interface signals are filtered before entering the Cesium Standard. Also located under this cover are the two high voltage power supplies (A2 and A3) for the Vac Ion and Electron Multiplier, respectively. The Vac Ion Pump is also located under this enclosure.

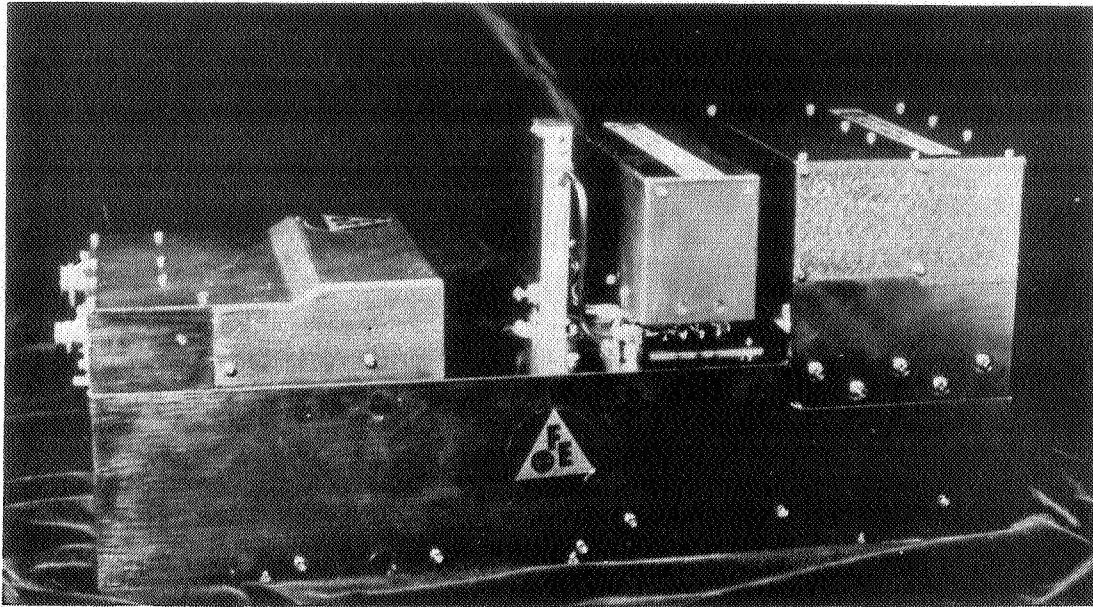


Figure 1 Portable Real Time Clock

Figure 2 is a photograph of the underside of the shoe box. The Cesium Beam Tube, A1, is located in the center of this area. The telemetry interface module, A8, is located directly above the tube. Below the tube are the A5 Modulator/Multiplier and A7 Synthesizer modules.

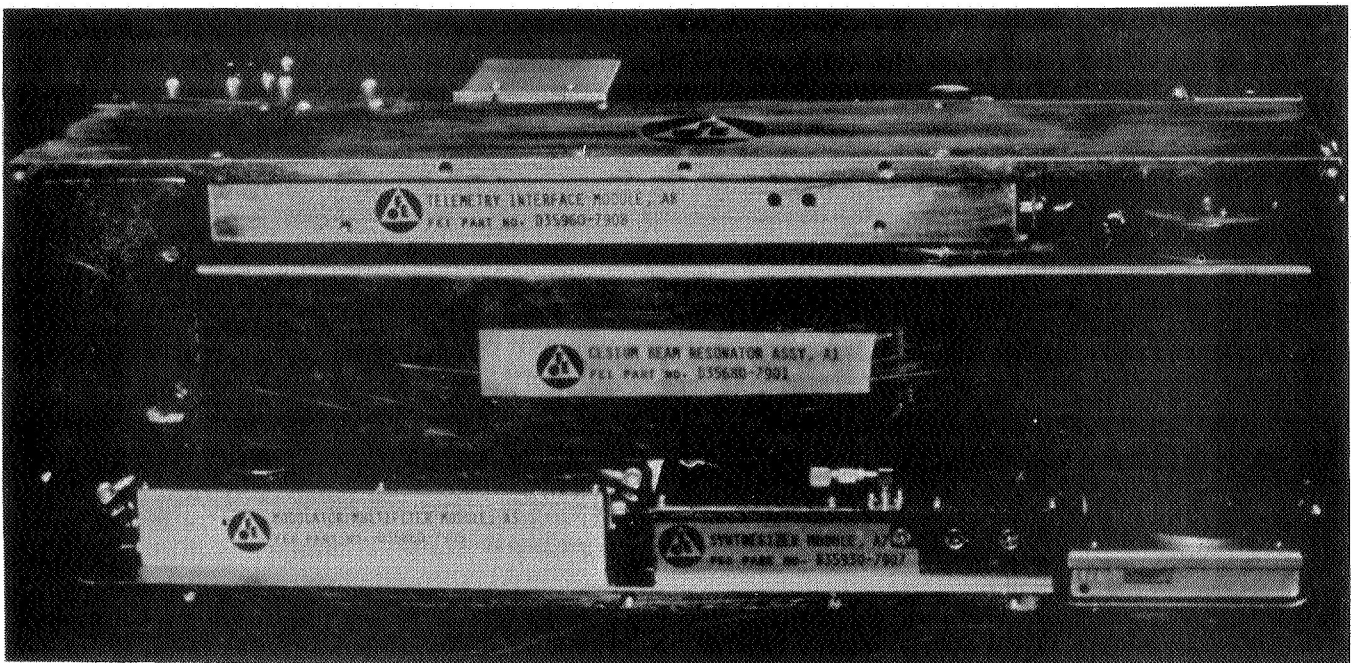


Figure 2 Portable Real Time Clock, Bottom View

SYSTEM DESCRIPTION

Figure 3 is a block diagram of the Cesium Standard. The 10.23 MHz output is taken from the A4 Oscillator Module. The 5.115 MHz oscillator frequency is split and drives the A5 Multiplier/Modulator and A7 Synthesizer. The multiplier/modulator phase modulates this frequency at an 83 Hz rate and then multiplies the signal by 1800 where it is mixed with a Synthesized 14.368 MHz beat frequency. This generates the 9.192+ GHz Cesium Transition Frequency which is fed into Cesium Beam Tube A1. Telemetry Interface Module A8 accepts discrete commands to direct the Cesium Standard and provides analog and digital monitors on the status of the Standard. Power supply A6 is the main DC to DC Converter that uses the 26.5 Vdc input to generate the necessary system voltages. Assemblies A2 and A3 are the High Voltage Power Supplies for the Vac Ion Pump and Electron Multiplier, respectively. These power supplies have been designed to be short-circuit-proof and to withstand the pressure environments from air to vacuum.

Figures 4 and 5 are photographs of the top and bottom of Multiplier/Modulator Module A5.

PERFORMANCE RESULTS

Tests have been performed on the prototype unit of the Spacecraft Cesium Clock, (SCC) with the following results. The Allan Variance was measured out to 10^5 seconds and showed a noise floor of 1×10^{-13} . This graph is shown in Figure 6. A phase deviation plot for a period of 4.63 days is shown in Figure 7. A summary of the specification requirements vs. the measured results is shown in Table 1. A thermal analysis was made on the SCC to determine the maximum temperature rise which will be seen in the vacuum environment. Figure 8 shows the location of the modules and test points. Figure 9 is the thermal equivalent circuit of the SCC from each module to the mounting plate. A maximum base plate temperature of 45°C was used. Table 2 summarizes the calculated temperatures with two of the actual measurement points that were made in thermal vacuum measurements. Relatively good correlation was obtained, especially when considering that the analysis used worst case conditions.

CONCLUSIONS

A Spacecraft Cesium Clock has been successfully designed and built that is capable of meeting the GPS Phase II requirements. As of this date, thermal analysis, thermal test and radiation testing have been completed with excellent results. Flight units are in fabrication and will be completed in mid 1983.

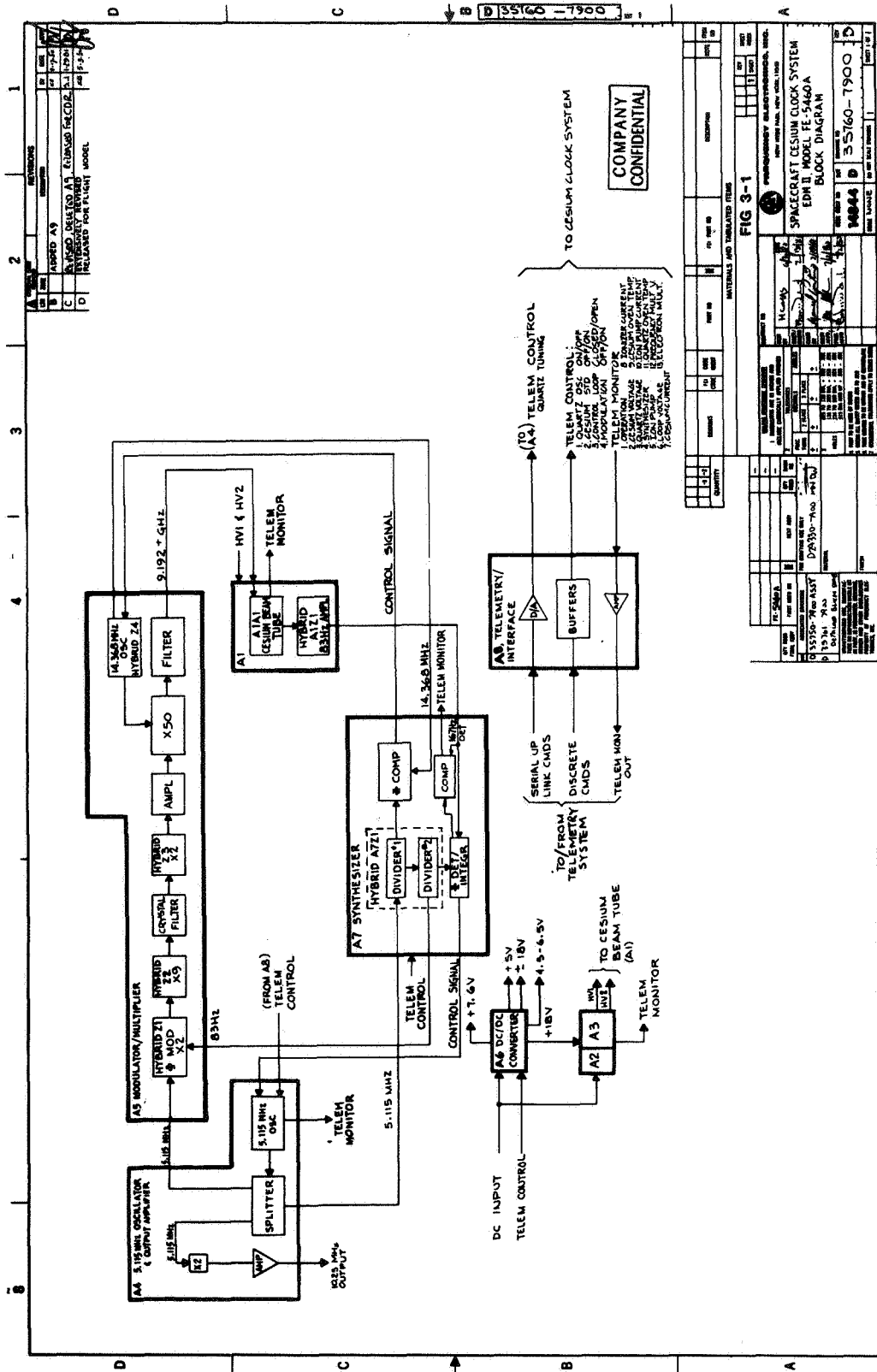


Figure 3 Spacecraft Cesium Clock System EDMII, Model FF-5460, Block Diagram

HYBRID 2X MULTIPLIER 5-10 MHZ HYBRID 9X MULTIPLIER 10-90 MHZ

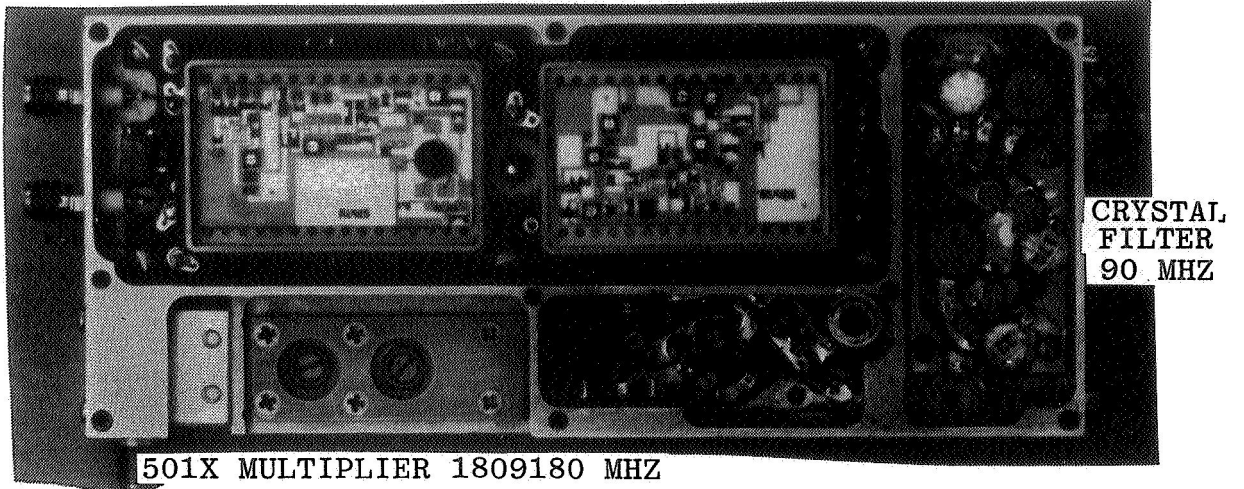


Figure 4 Modulator/Multiplier Module, A5

HYBRID OSCILLATOR 14 HZ DC FILTER/REGULATOR

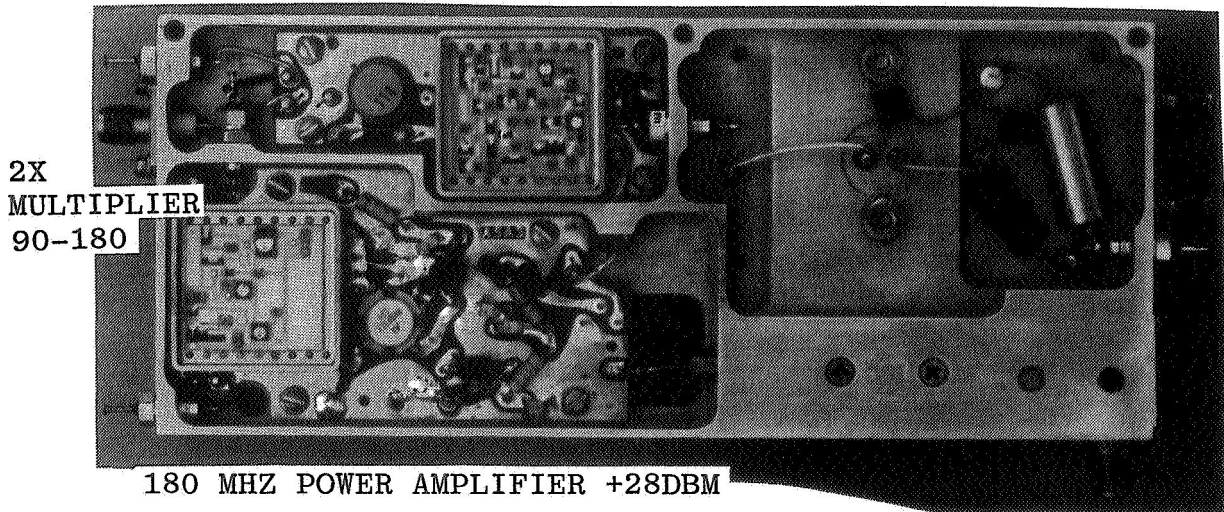
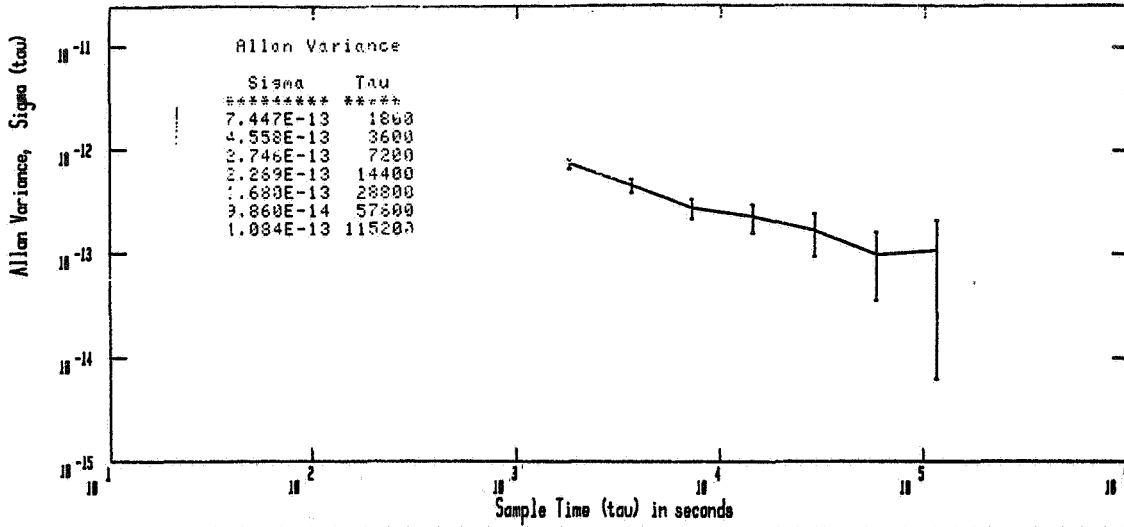


Figure 5 Modulator/Multiplier Module, A5



Date	Program	Data File Name	Points Found	Frequency	Measurement Interval	Counter Gate Time
10-05-82	Allan Variance	FE11	326	10.23 MHz	1800 secs	100 msec

Figure 6 Allan Variance, Spacecraft Cesium Clock, (SCC) FE-5460A

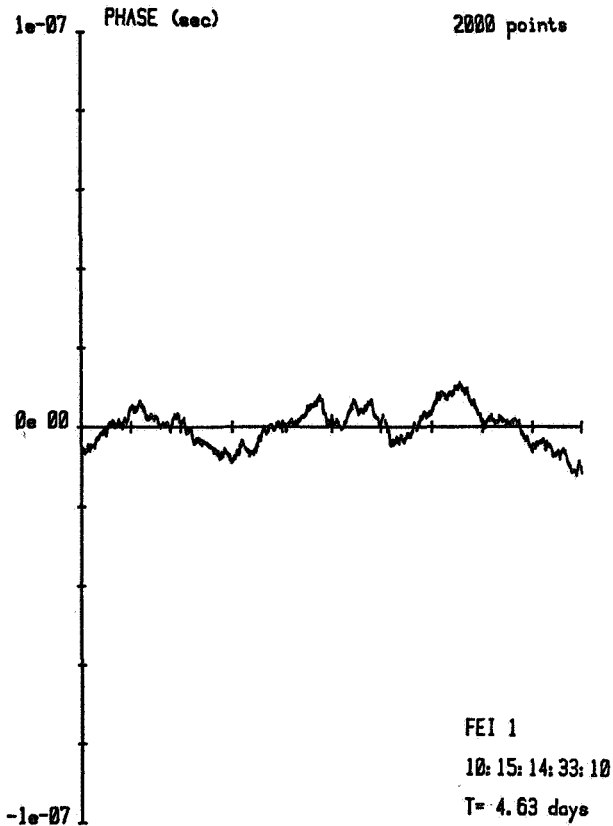


Figure 7 Phase Deviation, Spacecraft Cesium Clock(SCC) FE-5460A

TABLE I REQUIREMENTS VS. PERFORMANCE

PARAMETER	TECHNICAL REQUIREMENTS	MEASURED RESULTS PROTOTYPE
ACCURACY	$\leq \pm 1 \times 10^{-11}$	$\pm 5 \times 10^{-12}$
TEMPERATURE COEFFICIENT	$< 5 \times 10^{-14}/^{\circ}\text{C}$ goal of $\pm 1 \times 10^{-14}/^{\circ}\text{C}$	$8 \times 10^{-14}/^{\circ}\text{C}$ ($1.2 \times 10^{-14}/^{\circ}\text{C}$ on breadboard)
POWER		
WARM UP	$\leq 50\text{W}$	34.4W
OPERATING	$\leq 30\text{W}$	23.5W
WEIGHT	$\leq 28 \text{ lbs}$	23 lbs
WARM UP TIME (Lock)	60 min	<35 min

TABLE II SPACECRAFT CESIUM CLOCK
THERMAL ANALYSIS

MODULE	T(°C) CALCULATED	T(°C) MEASURED IN VACUUM
A1A7	58.7	
A1AB	58.7	
A1B	56.2	
A2	51.8	
A3	51.4	48.5
A4A	59.4	
A4B	59.4	
A5	56.4	
A6A	61.7	55.6
A6B	61.7	
A7	53.1	
A8	51.6	

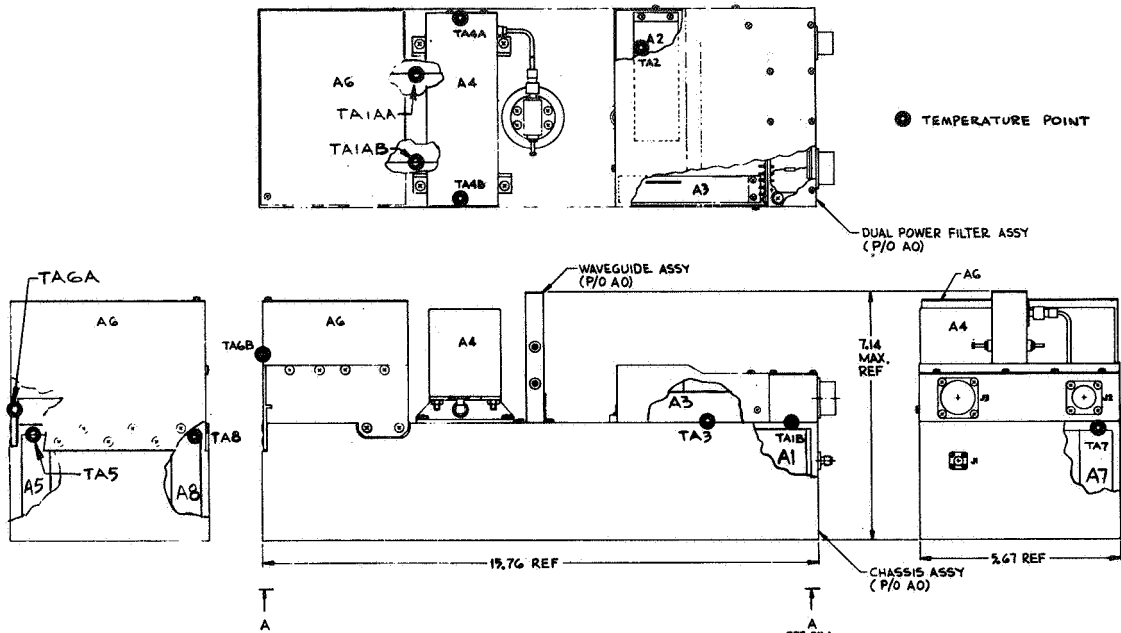


Figure 8 Thermal Measurements, Spacecraft Cesium Clock A6 Deck Mounted, Final Configuration

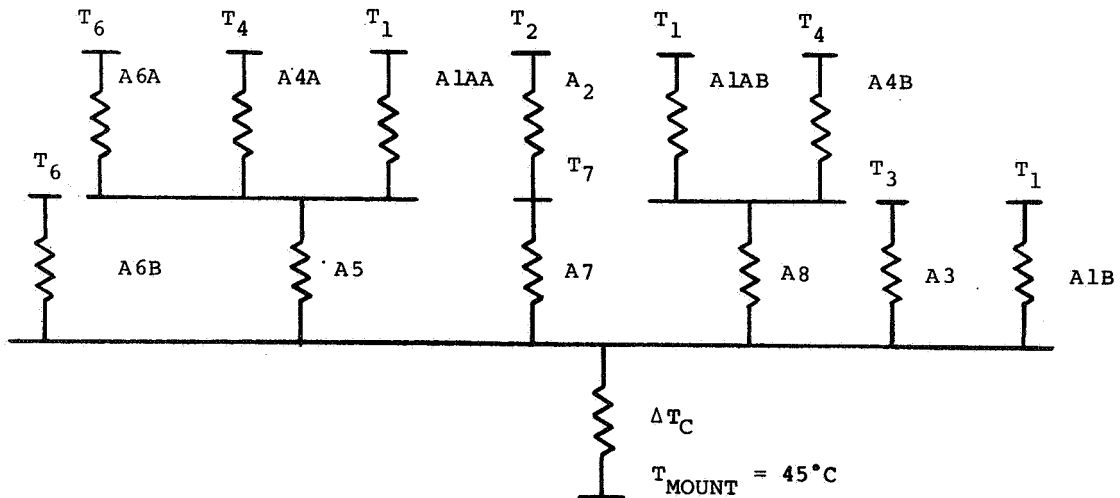


Figure 9 Thermal Schematic of Final Configuration

QUESTIONS AND ANSWERS

None for Paper #15

APPLICATIONS PANEL

Panel Chairman: Dr. Arthur O. McCoubrey, National Bureau of Standards

I'd like to welcome you to the panel discussion this morning. The panel this morning will focus upon the requirements for precise time and time interval technology from the viewpoint of the prospective users. Systems users and people who are responsible for the design of broad systems that depend on this technology.

As you recall, the panel discussion yesterday focused upon requirements from the perspective of planners. And I expect that there'll be a good deal of give and take between these two areas and the different perspectives.

As moderator, I'm not going to take any significant amount of time, what I would like to do is introduce the members of the panel and let them speak for themselves. We've asked each of them to speak for five or six minutes to identify their areas of interest as users, to identify the role or their corporations, or their organizations, and also to identify the areas of requirements as they see them from their perspectives.

I'll just introduce people now and I'll let each of them speak for themselves concerning the details of their involvement.

First, on my right is Bill Walker of Pan American Airways, and he represents that community of interests in the area of space vehicle test ranges.

Next is Ed Stein of Westinghouse in Baltimore. Ed's area of interest is communications. And on beyond Ed is David Clayton of Offshore Navigation, Incorporated. Ed's area of interest is navigation in a particular high frequency navigation. He'll have more to say about that.

Then next is Commander William May, the Commanding Officer of the United States Coast Guard, Omega Navigation Systems Operation Detail.

Next is John Illgen. John is a member of Kaman Sciences Corporation in Santa Barbara. John is also a member of the Board of Directors of the Wild Goose Association, an association of LORAN-C users.

Beyond John is Milton Boutte, also of Kaman Sciences, but in Albuquerque, and Milton's area of interest is communications.

And on the end of the table, opposite me, is Dr. Mohan Ananda, Aerospace Corporation. And Dr. Ananda is going to bear the torch for the Global Positioning System, NAVSTAR, and will reflect the perspective of the three segments of NAVSTAR: the Space Segment, the Users' Segment, and the Control Segment.

I'll be a little bit arbitrary about starting this off, and I'm going to ask Commander May to give his summary of his interest and involvement first.

APPLICATIONS PANEL

OMEGA NAVIGATION SYSTEM SYNCHRONIZATION

CDR William K. MAY, USCG

Commanding Officer,

OMEGA Navigation System Operations Detail

OMEGA

OMEGA is a long-range (10,000 nm), ground-based, very low frequency (VLF) navigation system which operates in the 10 to 14 kHz navigation band. Eight transmitting stations carefully sited throughout the world broadcast omni-directional, time-multiplexed 10 kW signals on 10.2, 11.05, 11.33, 13.6 kHz plus one frequency unique to each station. The timed transmissions allow easy identification of both station and phase. Phase measurements from three or more stations provide users with latitude and longitude to an accuracy of four nautical miles for 95% of the time. It is estimated that there are about 15,000 worldwide users of OMEGA. Early receivers were single-frequency, line of position (manual) instruments which required significant operator understanding and intervention in order to yield a position fix. However, today we have complex, multiple-frequency, state-of-the-art receivers (automatic) using microprocessors to convert OMEGA phase information directly into a latitude and longitude readout. Although marine user acceptance has been relatively slow due to early use of manual receivers coupled with an incomplete OMEGA system, the airborne community has dramatically increased its use of OMEGA within the last several years. Finally completed in August 1982 when Australia became operational, OMEGA is the most cost-effective, worldwide radionavigation system in existence today.

OMEGA STATIONS

Eight OMEGA transmitting stations are strategically located around the world. Each station has redundant timing and control equipment, two transmitters, and an antenna to ensure high operational availability. The antenna system is one of two types: A vertical tower approximately 1400 feet tall supporting 16 transmitting elements; or, a valley span antenna typically 10,000 feet in length. Each station radiates 10 kW on all transmitted frequencies. Station specifics are given in Table 1.

Table 1: OMEGA Transmitting Stations

Letter Designation	Location	Date Operational	Antenna Type
A	Aldra, Norway	DEC 1973	Valley Span
B	Monrovia, Liberia	FEB 1976	1400' gnd twr
C	Haiku, HI	JAN 1975	Valley Span
D	LaMoure, ND	OCT 1972	1400' hot twr
E	La Reunion Is. (FR)	MAR 1976	1400' gnd twr
F	Golfo Nuevo, Argentina	JUL 1976	1400' hot twr
G	Woodside, Australia	AUG 1982	1400' gnd twr
H	Tsushima Is., Japan	APR 1975	1500' hot twr

ONSOD

The OMEGA Navigation System Operations Detail (ONSOD) was established in 1971 in Washington, D.C. as a U.S. Coast Guard Headquarters Unit receiving technical direction from the Chief, Office of Navigation, U.S. Coast Guard. The mission of ONSOD is to provide worldwide coordination, day-to-day operation, and electronic maintenance support for the OMEGA System. The operational authority of ONSOD over OMEGA stations not on U.S. soil, but operated by partner nation agencies, is formalized in various Bilateral Agreements and supporting Technical Agreements between the governments of the partner nations and the United States.

ONSOD consists of 30 military and civilian personnel organized into three divisions. The Navigational Science Division is responsible for planning, organizing, directing and coordinating the acquisition and analysis of OMEGA data. It performs analytical investigation in such areas as semi-empirical signal modeling, improving propagation corrections, ionospheric modeling, and improving signal coverage diagrams. The Engineering side of the Engineering and Operations Division provides special maintenance and support of station electronics equipment, develops and installs field changes to station electronics equipment. Day-to-day control of station operations, navigational warning notices, and back-up synchronization control are the responsibility of the Operations side. The Comptroller Division performs the planning, programming and financial execution of ONSOD's annual \$5 million budget.

OMEGA SYSTEM SYNCHRONIZATION

One of ONSOD's principal missions is to ensure the OMEGA system is maintained within established timing tolerances. All OMEGA stations transmissions are synchronized, so that one station's signals do not interfere with signals from another station. Further, the accuracy of the system is dependent upon the stability at which phase-synchronized signals are transmitted. In order to ensure stability, the phase of each OMEGA transmission signal is controlled such that the phase relationship between signals from the eight stations does not deviate more than ± 2 us from the (estimated) system mean. The maintenance of this tolerance is called internal system synchronization.

Additionally, the OMEGA System is referenced to an external time standard: Coordinated Universal Time (UTC). To provide this synchronization, each station employs cesium frequency standards and considerable electronic circuitry within the Timing and Control Set. This circuitry provides and controls the proper timing signals to insure that each OMEGA station's synchronization (EPOCH) is correct relative to OMEGA standard time.

OMEGA standard time commenced on 1 January 1972 at 0000Z, when the phase of all OMEGA station transmissions were going through zero in the positive direction at all OMEGA transmitting antennas. At this instant OMEGA standard time was coincident with UTC. At present the OMEGA epoch leads UTC by integral number of seconds. Approximately once every year, UTC is retarded one second to compensate as atomic time and astronomical time are not congruent and also because of the continuing slow down in the earth's rotation. The OMEGA epoch is not retarded as this would cause navigation receivers to lose synchronization. The OMEGA epoch and UTC were coincident at 0000Z, 1JAN72. Since then 11 leap seconds have occurred, the last being on 1JUL82.

OMEGA EPOCH is defined as the beginning of each and every thirty second period from when OMEGA standard time commenced. OMEGA EPOCH occurs at the beginning of every third signal format at seconds 00 and 30 (on OMEGA standard time). The ten second transmission pattern, the OMEGA Navigation System signal transmission format, is held to within +5 us of UTC through comparison with LORAN-C signals (A, C, D & H), one-way OMEGA phase monitoring (OMEGA station D only), synchronized television signals (G), and periodic portable clock visits to the OMEGA Stations (OMSTAs). Future plans call for external time comparison with timing signals from the NAVSTAR Global Positioning System, with an anticipated accuracy of + 1 us using a low-cost, C/A only receiver.

System synchronization is purely a technical function performed by the Japanese Maritime Safety Agency (MSA) (since 17OCT77), and duplicated by ONSOD to provide a back-up capability. Each OMEGA station monitors the signals it receives from other stations in accordance with the assigned Station Operations Bill. Every Monday, this, plus other data, is provided to MSA and ONSOD by each station in their Weekly Station Data Message. Each Tuesday, ONSOD prepares and sends to MSA a message which lists Delta OMEGA corrections gathered from the four northern OMEGA stations (A, C, D, H) and four Loran-C chains plus one-way phase monitoring by U. S. Naval Observatory of Station D. Each Wednesday, ONSOD runs the SYNC2 Computer Program, compares results with the MSA Weekly Synchronization Message (also received Wednesday at ONSOD), investigates and resolves any discrepancies between the two SYNC2 results, and sends a message to MSA listing ONSOD SYNC2 results. Sending MSA the ONSOD SYNC2 results confirms to them our ability to function as a back-up, plus acts as a check to maintain system tolerance levels.

Further, each Wednesday MSA computes and sends each OMEGA station a Synchronization Directive listing ACCUM and CORRECTION values. This data is entered into the stations' cesium timing standards to maintain the transmitted phase to within + 2 us of mean epoch of the OMEGA System.

THE FUTURE OF OMEGA

Since the OMEGA System presently provides worldwide coverage, no expansion in the number of transmitting stations is expected. However, an expanded transmission format has been implemented. This expanded format involves the addition of a fourth navigation frequency (11.05 kHz) to further help resolve lane ambiguity, and the addition of a frequency unique to each station to provide positive station identification.

Differential OMEGA, still in the development stage in the United States, could provide another opportunity for improved OMEGA service. France, Canada, and the U.S. have all investigated the degree to which this technique can improve the accuracy of an OMEGA position fix. In fact, France already has over 15 differential OMEGA stations in operation today.

The Department of Defense has adopted OMEGA as an enroute navigation system for aircraft and ships. However, assuming NAVSTAR GPS becomes operational in 1987, the Army and Air Force plan to phase out OMEGA use by 1992. The Navy is presently evaluating continued use of OMEGA as a back-up to NAVSTAR GPS.

It is likely that OMEGA will be in operation at least until the year 2000. Six of the eight stations have been established on non-U.S. territory through Bilateral Agreements between the U.S. and partner nations. Because of the international character of the system and international user acceptance, operational decisions regarding the system must be coordinated with the partner nations. Thus, any disestablishment of the OMEGA system would be conditional upon international acceptance and in accordance with the applicable sections of the Bilateral Agreements.

APPLICATIONS PANEL

Panel Chairman: Dr. Arthur O. McCoubrey, National Bureau of Standards

Thanks very much Bill. I'll ask you to be thinking of the questions that you'll be wanting to ask these people after we've gone through the introductory statements, and I'm going to ask the panel for questions of each other, and then I'll be asking for questions from the audience, so, please make it clear to me when you have questions.

I'd like to call next on John Illgen to talk about the LORAN area.

APPLICATIONS PANEL

Panel Member: John D. Illgen, Kaman Science Corporation, Field Testing Technology Group

I work for Kaman Sciences Corporation, in the Field Testing and Technology group and we've been evaluating the potential accuracy of a number of navigation systems over the years. These have included both terrestrial and satellite systems.

I've been asked to focus on the LORAN-C system for this discussion today, and I'd like to discuss some of the improvements where we are with respect to LORAN-C.

Many of us have been using it for timing purposes. The potential of using LORAN-C for timing has been discussed in literature over the years. First of all, the LORAN-C system is a hyperbolic system. It certainly does have a textbook shape pulse. Any of you have ever monitored it know that when we monitor the 30 microseconds from the start to the first pulse, it's easily controlled.

The coverage for this particular system includes 20 million square miles. The CONUS is covered by approximately 80%, including Hawaii and Alaska, and the expansion of the system over the past few years has been enormous, and I've listed the countries that are either negotiating now, or have included LORAN-C over, just the past few years.

On the next view foil, I'd like to show what the present day coverage in fact looks like. The dark area on this particular view foil represents the ground wave coverage, and the outlining area represents the sky wave coverage, and, as we can see, a very large fraction of the earth's surface that is covered by this particular system.

A particular chain consists of a master and two or more secondaries. Over the years, the time synchronization, the system has been improved dramatically. Each, almost each, TRIAD has its own control monitor, which basically measures the time differences in real time from the master and secondary pairs, and compares those with established mean values at that monitor site.

The chains as we had found in tests and experiments is held to within 20-25-35 nanoseconds for the TD's. These are the RMS standard deviations that I am mentioning.

The cesium timer and transmitter variations are approximately 15-20 nanoseconds. That's a very quick rundown of where the LORAN-C system is now. I should mention that there have been some improvements as far as signal-to-noise ratio. The base lines of the system are shorter. Transmitters are going solid state. The geometry in many of the areas has been improved, there's been careful planning placed into these issues.

In recent years, we have discovered that 50 nanoseconds, or 50 foot accuracy, for this system is possible. And today, the system is being used in the Delaware Bay area for navigation purposes in some of the very tight channel areas just to give you a feel for the accuracy potential of the system.

And, there's a great deal of interest in the offshore industry with LORAN-C. I'm sure other gentlemen will be addressing that question.

APPLICATIONS PANEL

Panel Member: David A. Clayton, Offshore Navigation

I'm the key sea manager for Offshore Navigation. We've been in the radio positioning business for thirty-six years, so, we feel we do have a lot of experience. I feel it's a little humorous that we were not known in the PTTI community until someone discovered we had in excess of seventy cesium standards.

We presently have eighty-three.

Naturally, someone became a little curious as to what a company like ours was doing with all these cesiums. This led to the outcome where we're beginning to become familiar with the PTTI community, and it familiar with us, and the purpose of the community. I think we'll both benefit from this get-together. And for those who are not familiar with us, I'll explain briefly some of the functions we have for cesiums.

One of our main systems, we take a simple 1/2 to 2 megahertz hyperbolic phase comparisons radio positioning CW system and use it in the range-range mode. This is similar to the Coast Guard's LORAN-C chain. However, we work with much shorter base lines, and shorter ranges. Approximately 100 miles, this allows us to produce greater accuracies for the offshore oil industry and other people who require these accuracies.

Unlike the Coast Guard, we do not have sophisticated automatic time correction systems. We have a sort of clumsy monitoring system which detects clock drifts as they occur. When they fall out of tolerance, we dispatch a technician to each site who makes a C field correction. This is one of the most important problems we are faced with: how to keep these base stations synchronized at the lowest possible cost.

We're experimenting at the moment with microprocessor controlled micro-stepper connected to a modem, which in turn is connected through our land line. This land line is connected to a microprocessing control central monitoring station. The problem becomes a little more complex when we have to correct our cesium control transmitters which are installed in offshore platforms, which don't have the convenience of land lines.

We presently have six offshore platforms and thirteen on-site sites (on-shore sites we should say). The mobile tracking vessels offshore are passive, and their drift is determined by an on-board navigation computer, which is computing the ship's position from four simultaneously tracked ranges. The tracking of four stations also allows us to compute and correct the on-board clock drift. This assumes that the four stations are synchronized.

At the risk of sounding repetitive, to previous discussions, I feel our future requirements are the most obvious: one, that is stability; two, lower costs; three, less sensitivity to temperature changes; four, smaller physical dimensions; five, greater reliability; six, lower power consumption;

seven is an area I'm going to be cautious on. I'd like to see cesiums with built in microsteppers, but I believe someone is already doing that; and eight, more economical costs for replacement of parts: tubes, etc. We've found in the last ten years that replacement parts have skyrocketed for cesiums and it's something that's causing us a lot of concern.

One point that does need addressing, I feel, is the question of why cesium standards do not follow the trend of other electronic equipment that is: becoming less costly and more efficient with mass production. As far as the cesiums are concerned, they generally become more expensive to purchase and maintain with time.

We're also looking at other methods of keeping our transmitter clock synchronized, such as GPS, meteorburst, and other systems.

I would also like to mention that not only the HF system that I referred to, we do have a very, very large interest in the LORAN-C community, hyperbolic long range-range applications. And we feel that the requirement of cesium is going to be a long one in both our range-range and our hyperbolic systems.

Hopefully by the inventors, manufacturers and users getting together, such as at this meeting, we can look forward to an ever improving technology in the PTTI world.

Thank you.

APPLICATIONS PANEL

Panel Member: Dr. Mohan Ananda, Aerospace Corporation

As you all know, the Global Positioning System is currently in the concept and engineering system evaluation phase. We have six satellites up there, out of which four are in good health, and of the other two satellites, one of the satellites' clock is really bad, the other one is marginal.

We may have another satellite which will be launched early April or May. Also, the next phase, which is the operation phase, hopefully will begin late '85 or early '86. The Air Force office is currently negotiating with Rockwell International for the clock buy. It's planning to buy 28 satellites for the operational phase.

Now, each of the block two satellites will have two rubidium and two cesium clocks. In the future we may fly one hydrogen maser as an experimental clock.

Now, the performance of the space rubidium and cesium clocks have been extremely good. I have a chart to show. I have two.

The chart shows the clock prediction error for both NAVSTAR VI and NAVSTAR V, and NAVSTAR V has a rubidium clock and NAVSTAR VI has cesium. The dotted line is geared to the performance of 10^{-13} , the specification for the rubidium is 5×10^{-13} , whereas the cesium is 2×10^{-13} .

The performance exceeds the spec in both rubidium and cesium, if you're looking at a thirty days prediction. In fact the NAVSTAR VI shows somewhere around a five to eight times 10^{-14} , which is beyond expectations.

If you look at the next chart, the same thing predicted over a longer period for the bottom scale is ninety days -- The NAVSTAR V kind of drifts after forty or fifty days. NAVSTAR VI, still doing very well. So the manufacturers have built clocks of this type that are really very good.

Of course, the hydrogen maser technology, when it comes should provide better accuracy for a much longer period of time. As far as the space segment is concerned, there is quite a lot of interest in getting satellite autonomy or autonomous navigation where the two error sources are clock errors and errors in the ephemeris determination. Certainly, the clock error dominates after a long period of time.

There are two concepts we are pursuing. One of course would be a better clock. If a reliable better clock is available, that will be approached. If not, we are apparently thinking what's known as a cross-line communication concept which seems to provide a similar level of accuracy. We're still in an analysis phase.

What it consists of, there exists a cross-link capability for communication purposes, and we plan to modify the communications link to provide a ranging signal, and to generate range data between the satellites. Then if the clock synchronization can be achieved on board the satellite, the requirement for a long-term stable clock may not be that stringent.

Coming back to the clocks, the space segment is not the only user of the clock. We have two other segments, as you know. The control segment, which is responsible for computing the orbit parameters, as well as the clock parameters, which would be transferred to the satellite, and would be used by the user.

And obviously, we have to have a highly stable clock for the control segment monitor stations. And now their accuracy requirements are as stringent as the space vehicle clocks. However, there's really no weight or power limitation and the reliability requirement is not as stringent as in the cases of satellite clocks because we can always replace the parts or we can have redundant systems available to the ground stations.

There is a future set of users which may require stable clocks primarily because, from a navigation accuracy point of view, we don't need to depend upon four in-view satellites, if four in-view satellites are not available, you can still get the same accuracy if you have a stable clock on board the user and only 3 in-view satellites.

The satellite users, specifically surveillance satellites, which may require highly stable oscillators because if you want high accuracy the GPS antenna being limited to the earth pointing direction, the satellites above GPS have to look from the other side. So, the possibility of seeing several satellites is limited and you want 10 to 20 meter level of accuracy, you may need a, in fact, you do need a highly stable oscillator on board the satellite.

Of course, if you can live with 100 meter level of accuracy, then you don't really need the highest stability in the clock.

So, those are the three specific requirements from user control end and the space vehicle point of view.

Now, the most concern we have is the reliability of the on board satellite on clocks. Of course, lately we have had pretty good luck so far. We don't have a lot of experience, because we haven't flown that many cesium and rubidium clocks, so, hopefully, one of the problems the PTTI can solve is how to guarantee the reliability for a long period of time.

APPLICATIONS PANEL

Panel Member: L. Edward Stein, Westinghouse Electric Corporation, Defense and Electronics Center

Good Morning. Our corporation is an original equipment manufacturer and system design and integration company, principally for the DoD and for the other government agencies.

Most of the applications that I've had experience with personally, have been in the military strategic communications area. The environment is the usual military environment for the airborne or for the ground type application.

The particular area of communications is the VLF-LF, to some extent MF digital communications. The systems that we deal with are broadcast type of systems with a very limited number of transmitters and a large number of receivers used for the dissemination of information to various operational elements in the military.

The particular programs that we have done, or which are users for this type of equipment, are the 6168487L survivable low frequency communication system, the ARC-96, which is the airborne version of this survivable low frequency systems, the VERDAN, which is the Navy equivalent, the TACAMO, which is the Navy airborne version.

And then, all of these things interconnect into what is known as the minimum essential emergency communications network for the DoD, commonly called MEECOM. The communications technique is synchronous-coherent detection and direct sequence pseudo-random modulation is used in these systems.

That leads to the need for accurate time at the transmitters and receivers for system synchronization. Now, we use basically a correlator technique and the requirements that we have are much less stringent in terms of absolute time than the navigation requirement that I've been hearing today, here, this morning.

We have a requirement to know time at all the terminals in the network to an area that ranges from a few milliseconds in some systems, to tens and small numbers of hundreds of milliseconds in other systems, so that, in terms of absolute time, we thought we, we were pretty precise until I sat here this morning and listened to some of the navigation requirements. Now I don't feel very precise at all.

However, we do use cesium standards and we use cesium standards for several reasons. One is that we do want to maintain a systems standard at our transmitters which then can be used as reference for the rest of the system.

Also, we have the requirement, or certainly the desire, to maintain an accurate knowledge of time over a long period of time. Let's say a year or more, and the cesium standards provide the kind of accuracy that they can do that independent of periodic calibration. Also, the cesium standards provide a quite reliable, but redundant backup we use at the transmitting stations. Redundant timekeeping as you would expect for reliability, so we use a crystal standard and a cesium standard independently but, while they're not independent, they can be independent. They're normally connected together and monitor one another so that we have a way of determining if there is a time fault locally.

The area where we get into, perhaps, the driving thing for our technology right now then, is not so much absolute accuracy, but the types of problems that we face have to do with maintenance: the insertion, initial insertion and then the maintenance of time in the system. And, in the area of portability, particularly for airborne terminals, there is a requirement to be able to set time on board an airplane very simply.

The environment we're dealing in is a military user, where the people who are using the equipment are not people that are particularly trained in the techniques of precise time management. They're operational people, and what they want is to have something they can take in their hand and plug into a slot, push a button, and their system is going to work.

So, we find that we need equipment that is light, that is low power, that is highly reliable, it is very user tolerant, very user friendly (as they say in the computer business these days). Equipment that can be -- that does not hassle a man who's got many important responsibilities in serving time into his system being only one of them.

We also are finding currently, looking into the future, that our precision requirements are actually relaxing a little bit. Not a great deal, but somewhat, because we look to take advantage of the greatly increased processing capability that's coming along in terms of arithmetic processors, and high-speed, high capacity arithmetic processors. A high density low power, low cost memory that allows us to substitute a certain measure of processing for precise knowledge of time.

Sort of to sum up then, we are driven at the present time in the direction of low power, for portability, high reliability in terms of specific equipment such as cesium standards and crystal clocks which we use a great deal of. All of our receive stations are crystal clock controlled.

The other side of the coin is to find equipment which can be readily maintained and find techniques which we presently don't have, and which are some of the other things that are being discussed here today are relevant to that for inserting time into our system, both from a routine maintenance point of view, and from the point of view of recovering time in the event that some remote site loses real time.

Those are the areas that right now we are most concerned about, and we'd appreciate your comments and suggestions on it.

Thank you.

APPLICATIONS PANEL

Panel Member: Milton Boutte, Kaman Sciences Corporation

I work for Command Sciences Corporation in the Albuquerque office. My area of expertise is electronic warfare, and it's totally different from what you have heard thus far. I work as an independent test and evaluator, if you will, of tactical data links and navigation systems for the C³ environment.

As you all know, the heart of all data links and navigations system is precise time and timing intervals. That's how I'm getting involved. We do not actually look at the hardware in the way of precise timing from the standpoint of looking at the oscillator and cesium clock. We're more interested in being able to take and independently evaluate a particular data link or system in a battlefield environment with red forces, with blue forces, with all kinds of chad propagation from the electronic support countermeasure area, and be able to define to the user in the field what the capability of that data link navigation tactical system is, and what its limitations are.

From this standpoint, we do get involved in evaluating the timing requirement that the designer has put into the system. From the standpoint of the user in the field and what we've seen over the years, that the clock is not the problem that we're having.

The problem we're having is synchronization. And once we lose synch, we're having trouble locking back up, or the system's having trouble locking back up.

The other problem that is rapidly coming upon us is DoD's thrust towards GPS, where our systems are required to be compatible with the Global Positioning System. There's concern about the availability of GPS timing.

Thank you.

APPLICATIONS PANEL

Panel Member: William Walker, Pan American Airways

Pan American World Airways contracts with the Air Force for the operation and maintenance of the eastern test range. Responsibility includes the collection, reduction, analysis and publication of test data.

A directed responsibility also exist for PTTI engineering support to operations for planning, for specification, acquisition and installation and check out of new equipment as needed to meet changing program requirements.

The Eastern Test Range (ETR) is a 5,000 mile range extending from the launching facility at Cape Canaveral southeast, southeastward. The instrumentation and tracking platforms located on the Florida mainland sides, Grand Bahama, Grand Turk, Antigua and Ascension Islands, and on ships located in the Atlantic.

The range PTTI system provides services to both range users and range instrumentation systems, such as photo optics, range safety, command disrupt, communications, telemetry and radar.

The UTC time scale is employed and synchronization is maintained with respect to the DoD master clock located at the USNO. The interrange instrumentation group serial and parallel standard time group formats, are generated and distributed. Range count status information is also generated, distributed and displayed in the user areas.

The PTTI operating philosophy is to provide both range and range user systems, timing signals at the user site which are synchronized better than 50 microseconds.

In the past, this has been accomplished by direct synchronization to LORAN-C. The range is now in a modernization phase, which will upgrade synchronization to an accuracy of better than one microsecond with respect to the DoD master clock. Conversion will be accomplished sequentially by platform on an as needed basis. The Cape Canaveral master clock conversion is now in progress with completion expected in about six to nine months.

The Antigua platform is now operating on an interim basis to an accuracy of about five microseconds; better than five microseconds.

Complete range conversion is anticipated to take about three to four years, but it's dependent on yearly funding.

The PTTI operation philosophy employed at the ETR is to use a hierarchy of clocks, consisting of the range master clock located in the vault at Cape Canaveral, and synchronized to the USNO master clock to about one to two hundred nanoseconds.

The master clock consists of an ensemble of four or more cesium standards. A USNO, IEEE-488 Bus monitor system extends from Washington, D.C. to Cape Canaveral to monitor and verify the range master clock's synch status. Simultaneous time difference measurements between the USNO master clock and LORAN-C, and between the range clock at Cape Canaveral and LORAN-C, are the basis for the monitor system.

The same technique is applied in turn between the range master clock and station clocks located on each of the instrumentation platforms. When users are not co-located, the station clocks, site clocks, are installed at user sites. These clocks consist of synchronized time code generators with our local oscillators, operating in a discipline mode with memory.

This method assures PTTI integrity in the event of communication link failure between the station and site clocks. Timing signal input to the site clocks will be a modified IRIG serial time code, transmitted by a twenty-two gauge, or wide metal wire circuit, or by a microwave.

Correlation accuracy will be dependent upon transmission method used and will range from about one microsecond, to ten to twenty nanoseconds.

An ensemble of three or more cesium standards, frequency standards, is maintained at each station clock. The ensembles are steered continuously through the use of microphase steppers, the next higher level clock, with information obtained by portable clocks, and continuously verified by the monitor system.

As this system matures, control commands will be introduced via the bus from the Cape master clock to all station clocks to achieve a totally automated system with operator/technicians being required only for repairs or emergency manual control during periods of bus failure.

This technique minimizes direct dependence upon external PTTI dissemination systems at the expense of frequent clock trips. The technique is, however, flexible to place greater emphasis on external transfer systems as they become operational, portable and reliable.

PTTI dissemination system now used at ETR include LORAN-C, TRANSIT, GOES and WWV. The GPS receiver is under procurement with delivery expected by the end of 1983. We have noticed that a subtle change in the requirements from users numerous recent discussions concerning the need for timing signals which are active elements in ranging systems, rather than the more conventional use as a passive scaler for data tagging.

Requirements for a network synchronization of three to five ranging sites in the order of twenty to fifty nanoseconds have been discussed. We feel that these can be achieved through the use of the systems that I've described here.

APPLICATIONS PANEL

Panel Chairman: Dr. Arthur O. McCoubrey, National Bureau of Standards

That completes the statements by each of the panel members, and now we come to a period of discussion. I'd like to take advantage of my position as moderator and ask one question of one of the panel members to start it off.

As I listened to each of the presentations, I got a pretty good idea of where the requirements are, and where the most urgent requirements are. Yet, I may not have been listening hard enough, but there's one case where I didn't get the picture straight, and I'd like to be sure that we get it out, so I'll ask John Illgen a question.

John, if you had one wish, with one string attached, the string is that you've got to spend it on PTTI technology, briefly, what would it be?

MR. ILLGEN: I think presently, as far as the users' requirement is concerned for in the LORAN-C area, we've been, we have, the Coast Guard has installed cesium standards at each of the transmitters, and additionally, the control monitor that I referred to that is used to control the synchronization of the chain, of each chain, does have its own clock.

The computations to date, as I mentioned before, include cesium variations on the order of cesium variations and also transmitter fluctuations mixed in that we have measured at about fifteen nanoseconds.

Now, our receivers, our user receivers, the receiver noise is about twenty to twenty-five nanoseconds typically for time difference receivers. So, to really answer that question today, -- to do any better as far as synchronizing the chain from a high accuracy harbor standpoint, we're fine. But once the receiver, the onus today is on the receiver manufacturers to drive to reduce the error in the receivers.

And I think realistically, from a user standpoint, maybe what we're saying is, for harbor navigation we're not in too bad a shape.

DR. MCCOUBREY: OK. Thanks John.

Let me ask other panel members if they have some questions to ask of each other, or of the members of the audience to start the discussion here. Questions among the panel members?

DR. ANANDA: I have one. There was a concern about the availability of GPS timing.

DR. MCCOUBREY: Yes.

DR. ANANDA: Maybe explain what the concerns are?

MR. BOUTTE: The basic concern is that DoD is becoming extremely dependent on new systems for GPS, and I guess our concern is that we're going to be out in the field, and we're hoping that GPS is going to be there. And that's the basic concern. We need to track GPS and make sure that it gets there, because our systems are currently on schedule and we're worried.

DR. MCCOUBREY: Provide some assurances?

DR. ANANDA: As far as we know, we are also pretty close to schedule, unless something more happens.

MR. BOUTTE: Well, we're highly dependent on GPS and that's our concern. Without GPS we don't work.

DR. MCCOUBREY: John, perhaps you have a question?

MR. ILLGEN: Yes. From a user standpoint, what is the accuracy that will be provided to the civil community?

DR. ANANDA: As for the navigation accuracy, we have two modes, as probably everybody knows. One is for the military, or the classified community, and the other one for civil uses. However, the accuracy, full accuracy may be available to everybody. A decision to --

MR. ILLGEN: You're saying the precision code will be provided to the civilian and defense communities? That's a --

DR. ANANDA: Unless, there is a provision under which the security panel may choose not to make the precision code available to the user. All users. If that's the case, the navigation accuracy which will be around 200 meters. As far as the timing accuracy is concerned, it would be much better than that: 100 nanoseconds, or 150 or 200 nanoseconds. Just the time, that's only 1 parameter.

But if you want the full navigation accuracy, would like a circular probability on dimensions, then it's about 200 meters if the full accuracy is denied. Otherwise, the accuracy will be around fifteen meters in navigation, or better than ten nanoseconds in time.

MR. ILLGEN: There are many people that are using the systems for LORAN-C for timing, and a recent report that was issued by GAO recommends that LORAN-C be phased out in favor of GPS. That's one of the reasons why people, I think, are asking questions regarding the GPS schedule, and I guess the real concern is, currently the GPS system is in the conceptual stage, design stage, and in fact, production of the operational space segments, that has not started yet.

Is that true or false?

DR. ANANDA: The Operational satellites, what we call block two satellites; the prototype, which is the satellite twelve, already being built; thirteen through twenty-eight satellites, which we are going to buy, are funded and the contract is being negotiated. It's funded, that's the key, funded, at least for the next fiscal year.

Since the block buy is funded, we can hope that the missions will be there. The current schedule is, we will have in the beginning of '86, that there will be six satellites of block one, and subsequently we will start launching block two satellites at the rate of seven satellites per year.

So, by the end of '87, or the middle of '88, we'll have an eighteen satellite constellation there out, to be a mix of block one and block two. The block one satellites are in 63° inclination and the block two are fifty-five. However, as the time goes, one of the block one satellites will be phased out, and we will replenish and maintain an eighteen satellite constellation. --That's the correct one.

DR. MCCOUBREY: Ed, do you have a question?

MR. EDWARD STEIN: I'd like to raise a question in that same context. In the communications systems which we service, as I said before, time acquisition and maintenance is a problem for us and some different sites go at this in different ways. Different maintenance organizations.

But, people have used, or thought about using LORAN-C quite a bit. Television, line ten television synchronization has been discussed. I don't know that anybody is using it. I heard Omega mentioned -- By the way, all the systems that we're talking about are sufficiently accurate for our application, so I'm wondering, looking ahead, say, fifteen years from today, which systems would provide the most economical long-term approach.

If you were setting up a maintenance facility say, and one that would be responsible for the maintenance of time for a number of receiver sites, what way would you go? I'm asking anybody that would have an opinion on that in terms of utilization of Omega or LORAN-C, or, looking ahead to GPS.

DR. MCCOUBREY: Who wants to handle that?

MR. EDWARD STEIN: Would anyone like to comment on it?

DR. MCCOUBREY: Lets, ask Bill May to tackle it first and then, Mohan Ananda.

CMDR. MAY: I'd like to address that from the viewpoint of what radio navigation systems we have, and what the Federal government's planning forecasts are for these systems.

The Department of Defense, of course, runs some navigation systems, they run TRANSIT, they will run GPS. They run a number of aeronautical systems. The Department of Transportation, the two operating agencies in the Department of Transportation, the FAA and the U.S. Coast Guard, run the remainder of the government provided radio navigations systems for general use: the VOR/DME, the micro-wave, the ILS, LORAN-C, and Omega.

A number of years ago, it became apparent that there was not adequate coordination between DoD systems and DOT systems. So, we formed working groups in each of the Departments.

A navigation working group in DoD, and a navigation working group in DOT. These two groups talk to one another at least once a quarter and usually more frequently, to tell one another what they're doing.

Under mandate by Congress, we came out with an animal called the Federal Radio Navigation Plan, which is available through NTIS in Springfield. Unfortunately, at a fairly high cost. I think, \$30.00 to \$40.00.

This plan, now in its second revision, the second being March of 1982, details the long-range outlook for Federally provided radio navigation systems.

I'm only familiar with the marine segment, and I'll summarize what I know of it for you. For LORAN-C DoD has said their requirement will cease approximately five years after GPS becomes operational, or in late 1992.

So, we, the Coast Guard, are operating overseas LORAN-C to meet a DoD requirement.

I'll address TRANSIT, and GPS, and then Omega.

For LORAN-C, the Coast Guard operates the overseas LORAN-C chains. The current plans are that DoD requirements for overseas LORAN-C will end when GPS becomes operational.

DR. MCCOUBREY: Yeah, Alright. OK.

CMDR. MAY: I'm sorry. That means in 1992, the overseas chains will no longer be required by the DoD, and current plans are to phase out Coast Guard operation of these overseas chains.

There might possibly be host nations agreeable to taking over the stations and running them, but it's pure speculation at this point.

We foresee the CONUS chains, east coast, west coast, Gulf of Alaska, Hawaiian Islands as remaining on the air, continued to be operated by the Coast Guard to meet the needs of the United States coastal confluence zone.

TRANSIT is a Navy system. Always has been, and will be until it ends. Projected to end, again, in 1992, because the DoD requirement will transfer from TRANSIT to GPS.

There has been a lot of talk about a civilian consortium taking over operation of TRANSIT. To the best of my knowledge, there has been no active putting up of funds to take this over.

So, that is a DoD system which they have announced will end in 1992, about five years after GPS is operational. Omega, the system I'm most concerned with, is operated by the United States and six other partner nations. We're entirely a civilian system. We have 15,000 civilian users, more or less. Only 1,500 DoD users. We enjoy a fairly high degree of support from commercial civil aviation; somewhat less from civil maritime users.

Because we have so many partner nations involved and so much international acceptance, and a relatively low operating cost, it costs the U.S. Government approximately \$8,000,000.00 a year to operate Omega, and that's for a worldwide system. My personal feeling is that Omega will be around at least until the year 2,000.

The Federal radio navigation plan hedges on this. They say that the Navy is re-evaluating their requirement for Omega as a backup to GPS even if the Navy does not want GPS. I still project it will be required for many years to meet civilian needs.

DR. MCCOUBREY: Thanks, Bill.

I'd like to begin to ask for questions from the audience.

MR. SAMUEL WARD, JPL: My question is to Commander May. You presently have your Omega operation in Australia, and its traceability to UTC is being established, as you said through TV, to the Department of National Mapping, and to UTC by way of UTC Australia? Do you plan to furnish them with GPS receivers so that you lower that present uncertainty that you have by, maybe, an order of magnitude or two?

You stated the TV traceability was plus or minus half a microsecond. And with the GPS that could drop to fifty nanoseconds or less, and for the UTC traceability plus or minus five microseconds, that of course, that could drop two orders of magnitude.

CMDR. MAY: Right. The primary purpose of precise time for Omega is to synchronize our signals for navigational use. The larger the time error between the phase synchronized signals, the larger the navigational error. The traceability back to UTC is sort of a side light, an extra provided service.

Our requirement is to keep our signal, our signals from our eight stations to within two microseconds of the mean Omega system epoch. OK. In doing this, we -- Oh, by the way, -- tie this into UTC, the Australian horizontal TV synch pulse, which is directly traceable to USNO through tying our signal into the LORAN-C system at our four northern stations and through USNO monitoring of our North Dakota station, they monitor the signal here in Washington, D.C.

All these various inputs go into a fairly complex computer program that produces weekly corrections which are entered into our system to bring all signals to within two microseconds of our Omega epoch. And the Omega epoch is within five microseconds, usually better, but, almost always within five microseconds of UTC.

To directly answer your question, we are planning to procure, if we can get a reasonable cost, and I'll define that as somewhere in the area of 10 K, a standard accuracy (the old CA code accuracy), commercial grade GPS receiver when it eventually becomes available on the market.

I've budgeted funds in 1984 to procure one of these, for trial, and to procure a number of these in following years, depending on the results of the first one. We would put these GPS receivers first on the stations that are not tied to an external UTC reference. That being Argentina, Liberia and Reunion Island.

If we get the funding, yes, we do plan to put it on all the stations as an external timing source which would indeed improve the accuracy. It would improve the accuracy to roughly what we get from GPS, which, I'm told by some of the experts in the field, that using a low cost standard accuracy receiver, we should expect somewhere between a half a microsecond and a microsecond and a half accuracy from GPS.

This will be another external input because if Omega, in fact, is a backup to GPS, which is the current plans, we cannot rely entirely on GPS. We have to be independent. So it would be an extra link.

DR. MCCOUBREY: Others? Sam? Another question?

MR. WARD: My question had to do with tying your Omega station to, directly to National Mapping Service.

CMDR. MAY: I'm not familiar with that, sir.

MR. WARD: To use two receivers at the same time. One at the Omega location, and the second at the National Mapping facility in the Canberra district, and,
--

CMDR. MAY: You're talking about a differential GPS time recover?

MR. WARD: What'd you say?

CMDR. MAY: Are you referring to a differential GPS time recover system?

MR. WARD: Yes. That doesn't have to rely on the GPS clock. It would essentially provide real time synchronization.

CMDR. MAY: Again, our primary purpose is to synchronize our Omega signals in phase with one another using a satellite that happens to be synchronized to UTC. It will do us no good, the way our current synchronization program runs, to take only one station, Australia, and tie it down very closely to UTC. Because the other stations, then, could drift up to five microseconds from UTC and my synchronization program as written would tend to pull Australia away from being tied down to UTC.

What you're suggesting would only work if I could tap all of my stations down to the GPS time. Perhaps we could discuss it later, after the discussion.

DR. MCCOUBREY: Are there other questions from the audience? I have one over here.

DR. KELLOGG: I'm a aerospace representative, working for Lockheed. I have a question about why you're so confident that you have ephemerides under control? When one looks at other data sources of the on board clock performance, specifically from the U.S. Naval Observatory, I find it difficult to be as optimistic as you, if you know what the causes are.

DR. ANANDA: I'm not clear what you're referring to.

DR. KELLOGG: I'm mostly concerned about on board clocks' reliability, and I have a good feeling about the accuracy of ephemerides. I cannot agree with that statement. I'm wondering what your source of data is. Do you weight the U.S. Naval Observatory data very lowly? Do you include it, or what?

DR. ANANDA: No. Many predict the GPS orbits. The loss of accuracy if you do not receive the navigation message, daily, or whatever the time period is, there are two error sources existing; one is due to the stability of the on-board clock; the second is the inability to model the ephemeris to the required accuracy.

Now, if you compare these two error sources, the clock error dominates that. I'm not saying that the orbit errors are not there. Maybe I didn't quite understand what you're suggesting.

DR. KELLOGG: Before I predict anything, I'd like to know where I am. If I'm uncertain about that, I assert that influences my predictions since at the present moment, I will assert you have some difficulty in establishing or distinguishing between an ephemeris error and timing error with the way GPS is set up.

DR. ANANDA: We can estimate that orbit accuracy to a few meters which includes the clock, as far as the knowledge phase is concerned. Then you extrapolate and you predict. That's when the users start using. The current operational control segment, the concept is, we process the available data, and every eight hours, or every ten hours, we upload a NAV message which would be available to user, so the total time predicted is ten hours.

And, we maintain a user range error of six meters, which includes the clock, as well as the ephemeris part. We do not plan to separate, however, if you start predicting further down, the correlation between the clock and the ephemeris breaks down and the clock starts taking off, which becomes the dominant error source.

So when we're talking about clock synchronization, it applies to only, on an autonomous basis, or navigation over a long period of time. We do not absorb a clock error in say, for example, two months. Then, if you do not have some

kind of clock synchronization capability, you certainly cannot achieve that. You have to absorb the clock information more frequently.

So the ephemeris error comes from two sources. One is what we call the wide bias error, which is the misalignment of the solar panel, looking at the sun, which introduces a torque, and that contributes a radiation pressure effect on the satellite which is hard to model at present.

However, the concept which we are pursuing, which referred to using cross link ranging measurements, and a single ground station ranging signal measurement, we can estimate all those parameters and we can predict for a long period of time that doesn't contribute to the same level as the clock stability error. That's what I was referring to.

DR. KELLOGG: I don't wish to pursue that subject even further. I would like to ask a different question, if I may, sir.

DR. ANANDA: OK.

DR. KELLOGG: One of the other items, I believe, as I understand it in the GPS system, is that a search for users of time precision failed to unearth anybody who would ask for a precision greater than 100 nanoseconds and, consequently, the system accepts the fact that that's the floor. Will this decision be reviewed sometime between now and some sort of operational date?

DR. ANANDA: The timing accuracy as it stands in the program is 100 nanoseconds between USNO and GPS system time. That is, the maximum off-set between UTC and GPS system time would be 100 nanoseconds.

As far as validating the GPS system itself, there is no such requirement as 100 nanoseconds. You can actually do the time transfer to a level of ten nanoseconds or better. So 100 nanoseconds comes to the relationship between USNO and the GPS system time.

I do not believe there's any plan to improve upon that requirement unless there is a community which forces upon the GPS program to improve the accuracy, of the offset between the USNO and the GPS system time.

DR. MCCOURBEY: OK. It's getting close to the time now to conclude the session, but, I'd like to ask, is there one more question from the audience? Mr. Allan?

MR. ALLAN: I'd like to pursue a little bit more, if I may, the questions raised by Dr. Kellogg with respect to the GPS, to the Aerospace representative. You referred in your discussion to the desirability of getting much more highly stable clocks on board the GPS in order to allow for the projection during an autonomous period.

I'd like to just suggest that what was discussed on the panel yesterday a little bit, and what we discussed at some of these meetings before. In order to have a basis for projection, you've got to be able to read out the clocks with sufficient accuracy so that you have a projection base on which to go. And it seems to me, in all the discussions I've heard, that the Kalman filter readouts that are currently used, and presumably would be incorporated in these cross links and so on, do not have sufficient precision to accomplish the kind of data base that the projections would need.

DR. MCCOUBREY: OK. Just in winding up, I would like to observe that from the viewpoint of all the users I'm very much impressed with the need, the requirements for synchronization technology.

I'm also very much impressed that various system users are depending upon other people's systems in connection with synchronization. And, it does raise the question as to whether or not that interdependence among the systems, of one set of users depending on LORAN-C, and another set on Omega, GPS and so on, dependence which goes beyond the original intent of the system, perhaps, whether or not those requirements are getting into the planning at high enough levels.

In other words, are the planners at the very highest levels really listening to the users in these areas? Perhaps Dr. Winkler could comment on that.

DR. WINKLER: I do not know what the highest levels are doing.

DR. MCCOUBREY: You'd better do something.

DR. WINKLER: And moreover, we have all the indications that they change course every three years.

And, I want to remind you that the comment which was made by one of your panel members about the recent report that LORAN-C be phased out comes only six years after a major push for more LORAN-C as being instituted by the Department of Transportation, in which it was declared one of the two operational and reference systems for the coastal regions of the United States.

So you must expect that turbulence to continue. It is simply a fact of life. And, in regard to your question, is that good or bad if different systems depend on each other. I think it is a strength. It is in fact a big thing which PTTI, a coordinated system, has to offer.

That also, every single synchronized system ought to, as a matter of policy, be able to resynchronize itself from within the system. By having additional interfaces to other coordinated systems you gain a tremendous amount of redundancy, of insensitivity to disturbances of all kinds.

So, the question that you have asked is extremely difficult to answer, I think one must realize we have very great turbulence. Remember last year, the GPS system about which we are all concerned, it was whacked out by one of the Congressional subcommittees. Completely. It was restored later on, but that is how

that is. We are living in a turbulent state, and we cannot project, I think, for longer than a couple of years in the future for any individual system. That's why we have to be coordinated.

CMDR. MAY: Art, if I could, just one minor thing here?

DR. MCCOUBREY: Yes

CMDR. MAY: When the U.S. Coast Guard petitioned Congress, and Congress decided to phase out LORAN-A in favor of LORAN-C, this was for the coastal confluence zone of the United States.

The U.S. Coast Guard is planning on running LORAN-C even after GPS, within the United States coastal confluence zone. What I was talking about is the phasing out of our overseas LORAN-C chains which were initially established to meet the DoD requirements.

Once these requirements end, the U.S. Coast Guard has no statutory authority to maintain radio navigation systems outside of the use of the United States' fifty states.

The other thing is that you are very correct, the FRP (the Federal Radio Navigation Plan) is a long range planning document which projects the needs of U.S. radio navigation mix and needs to the year 2,000. Unfortunately, funding of all the systems, the operation of all systems, is on a year to year basis.

So what you have is: the FRP is revised yearly, and in some cases it doesn't make a whole heck of a lot of sense, in my personal opinion, to revise a twenty year plan document every year. Yet, that's the way our system is organized.

DR. MCCOUBREY: John Illgen, a short one?

MR. ILLGEN: I'll try and make this short.

But, one of the points that I would like to make, and I do, I think CMDR. May has partially answered the question that I'm about to raise, and that is for the LORAN-C system has been around since the late 1930's, and has taken many, many years to sort out and understand a lot of the error sources associated with the system.

And, what worries me when I hear dates like GPS being operational in 1988, or '89, and then we turn the switch in 1992, because we now have an operational satellite system. That concerns me a lot.

And I just-- one of the questions I was going to ask is how concrete is this Federal Radio Navigation Plan?

And I believe CMDR. May partially answered that in saying that it is revised every year. But a lot of people are taking the GPS system very seriously in the military communication area. And, it's needed in Europe. It's needed outside of the United States, GPS or LORAN-C for timing purposes, and I sure hope

that the high level authorities within our government understand that there had better be considerable overlap between the two systems until the problems are sorted out on GPS.

DR. WINKLER: We may not be able to depend on the understanding, but we can depend on the inertia.

DR. MCCOUBREY: Well, with that I'd like to thank each of the panel members for joining us this morning. It's been a very interesting session. I'll turn it back over to the session Chairman.

SESSION IV

HYDROGEN MASER TECHNOLOGY

Dr. Robert J. Coates, Chairman
NASA Goddard Space Flight Center

AFTERNOON SESSION

DR. ROBERT J. COATES, NASA/GSFC

While everyone is taking their seats, I'll introduce myself. I'm Bob Coates, the session Chairman this afternoon. The topic of this afternoon is Hydrogen Maser Technology. As you note from your papers, the topics covered go all the way from performance reports on existing hydrogen masers, to the progress on the science of new masers and even work on very much smaller and more economical hydrogen masers, so, I think we have a very interesting afternoon.

EVALUATION OF MODERN HYDROGEN MASERS*

Albert Kirk, Paul Kuhnle and Richard Sydnor
Jet Propulsion Laboratory
California Institute of Technology
Pasadena, California

ABSTRACT

During the last two years the Jet Propulsion Laboratory (JPL) has been conducting an evaluation of modern hydrogen masers in a program sponsored by the National Aeronautics and Space Administration (NASA). The goal was to perform a series of tests and evaluations which would be as complete, accurate and unbiased as possible. A board of nationally recognized experts in hydrogen masers and in frequency and time was selected to design the testing program, supervise the tests and release the final report. This board consisted of:

Hugh Fosque	NASA Headquarters	Chairman
Joel Smith	JPL	Convening Authority
Norman Ramsey	Harvard University	
Robert Vessot	Smithsonian Astrophysical Observatory (SAO)	
Victor Reinhardt	Goddard Space Flight Center (GSFC)	
Richard Sydnor	JPL	
James Barnes	National Bureau of Standards, Boulder (NBS)	
Gernot Winkler	United States Naval Observatory (USNO)	
Andrew Chi	GSFC	
Arthur Zygielbaum	JPL	Executive Secretary

The maser types tested were the SAO VLG-11B, the GSFC NR and, as a result of the testing process, the JPL DSN. The masers were tested for environmental sensitivities (magnetic field, temperature, barometric pressure) and long-term aging. Allan variance runs of 72 days were made in order to attain averaging times from several seconds to 10^6 seconds. Auto- and cross-correlation techniques were used to determine the effects of uncontrolled parameters such as humidity. Three-cornered-hat and other data reduction techniques were used to determine the characteristics of the individual masers.

*The research described in this paper was carried out by the Jet Propulsion Laboratory, California Institute of Technology, under contract with the National Aeronautics and Space Administration.

INTRODUCTION

The three maser types evaluated represent the newest models manufactured by the Jet Propulsion Laboratory (JPL), the Goddard Space Flight Center (GSFC) and the Smithsonian Institution Astrophysical Observatory (SAO). The characteristics that distinguish these from earlier laboratory models are: transportable for routine field operation anywhere in the world, highly reliable, well documented, ease of servicing, equipped with built in instrumentation for simplified verification of performance and diminished dependence on the operating environment.

The GSFC Hydrogen Maser is manufactured by Johns Hopkins University Applied Physics Laboratory (APL) as the model NR. GSFC and APL supplied serial number four (4), identified in this paper as NR-4. The Smithsonian Astrophysical Observatory supplied one model VLG 11B serial P14 which is identified as SAO 14. This test series was conducted in the Interim Frequency Standard Test Facility located at JPL in Pasadena, California. JPL designed and maintains two reference Hydrogen Masers in this facility. These two frequency standards are identified as DSN2 and DSN3.

A considerable amount of data was collected with the goal of assessing the current state of the art of active hydrogen maser technology and to gather information that will be used to evolve a development program for the next generation of atomic frequency standards used by NASA.

The data in this paper is a small but representative sample of all the data that was collected during the tests. An official JPL report will be published in three volumes under the heading "Hydrogen Maser Comparison Test." Volume I is an executive summary covering all aspects of the test but limited in detail and amount of data. Volume II contains detailed descriptions of all tests and a complete set of all but the raw data. Volume III consists of all raw data such as magnetic tapes, strip charts, terminal print outs and log books. Due to the bulk of Volume III data specific records should be requested by those interested.

TESTS PERFORMED

A list of this test series is shown in Table 1.

(1) Verification of Inputs, Outputs and Proper Functioning of Controls

After receiving the masers, all subsystems were checked to make sure they were functioning according to JPL's and the manufacturer's expectations. Some anomalies were found and corrected by JPL or the manufacturer. The information gained was that more thorough testing is essential prior to shipment. This operation guaranteed that all subsequent tests were done with properly operating masers and assured a fair comparison of performance with minimal interruptions.

(2) I.F. Meter Calibration

To allow correct interpretation of the data that was collected, certain conditions must be stated. Maser cavity output power is one of those. Since output power of a maser is normally indicated on a front panel display, which is derived from an I.F. power measurement, the display is calibrated with reference to the actual maser cavity output power by substituting a precisely known signal for that of the cavity output. The resulting calibration charts are shown in Figures 1 and 2.

(3) Pressure Control Setting Dependent Parameters

The operating point of a maser is a function of the hydrogen gas pressure setting. Output power, line Q, vacion current and hydrogen source dissociator efficiency are determined by this setting. All these variables were recorded for different pressure control settings and the data subsequently graphed. Of particular interest is the relationship of line Q vs. output power. Knowledge of this data is essential for diagnostic purposes. This "baseline" data was also used to determine the optimal operating conditions of each maser for all subsequent tests. The measurement results are shown in Figures 3, 4, 5 and 6.

(4) Environmental Tests

a. Output Frequency Vs. Input Voltage

The DC input voltage was stepped between 22 and 31V while the output frequency was monitored. Sufficient time was allowed between each voltage step for the maser frequency to shift and settle. This test sequence was repeated several times. The NR-4 showed no measurable frequency shift above the recorded noise level of 1×10^{-14} .

The SAO-14 indicated variations on the order of 5×10^{-15} . This value is at the level of the measurement uncertainty. The results shown are for the entire 22 to 31 VDC test range. Figure 7 shows the output frequency variations of NR-4 and a reference maser during the above test sequence.

b. Output Frequency Vs. Ambient Magnetic Field

A 90-inch diameter helmholtz coil was placed about the hydrogen maser under test to produce a DC magnetic field aligned with the maser's vertical axis. Initial testing was done by varying the magnetic field in small steps first in one direction up to a specified maximum value then back to zero and then continuing in small steps in the opposite direction up to the specified maximum value and again back to zero. Thus the test went around the "loop" once. Output frequency, Zeeman frequency and output power were measured and recorded at each step as shown in Figure 8. This test is difficult to perform since any overshoot in field variations causes hysteresis distortion. Repeatability was poor. It does however show the effects of hysteresis and the fact that the slope is influenced by the way the test is done.

All subsequent testing was done by stepping the magnetic field equally above and below the ambient field five times. The corresponding output frequency shifts were averaged and tabulated in Figures 9 and 10. Notice that in general the hydrogen maser output frequency is more sensitive to changes in the magnetic field when the maser is operated at a higher hydrogen flux setting and also when the ambient magnetic field is varied by smaller increments. It should be noted that the data shown is for homogeneous magnetic field variations applied to the hydrogen maser's vertical axis only.

c. Output Frequency Vs. Ambient Temperature

The maser was placed in the test chamber and two separate temperature tests were performed. For one test the maser was allowed to stabilize at approximately 23°C then the temperature was increased by 3 degrees centigrade and held within $\pm 1^\circ\text{C}$ of the setpoint until the hydrogen maser output frequency was stable. Due to random walk and aging of the test and reference hydrogen maser, the "stable frequency" is difficult to determine over a period of several hours. Hence a minimum of five thermal time constants was allowed before the temperature was decreased by 3°C. The second test was performed in a similar manner except the temperature was stepped between 21°C and 29°C. During this test as well as all others, environmental data such as temperature, humidity, atmospheric pressure and ambient magnetic field was continually recorded. It should be noted that during the temperature test the humidity inside the test chamber varied appreciably and in correlation with temperature. Since our test chamber is not equipped to control humidity, it is difficult to separate the influence that this parameter has on the hydrogen maser output frequency. The measurement results showed a coefficient $\Delta f/f/^\circ\text{C}$ of -7×10^{-15} for the SAO-14 and -1.4×10^{-14} for the NR-4. Temperature test results are shown in Figures 11 and 12. During this test the line Q of SAO-14 was 1.7×10^9 and that of NR-4 was 1.65×10^9 .

d. Output Frequency Vs. Barometric Pressure

The maser was placed in the test chamber and the temperature was held constant. Several tests were performed. The test chamber barometric pressure was varied $\pm 12'' \text{ H}_2\text{O}$ while the hydrogen maser output frequency was monitored. What distinguished one test from another was the rate at which the (barometric) pressure was changed and the dwell time. It was generally found that for fast pressure changes ($\Delta 24'' \text{ H}_2\text{O}$ in less than 30 minutes), the output frequency varied slightly more than for slow pressure changes ($\Delta 24'' \text{ H}_2\text{O}$ in greater than 30 minutes). It should be noted that the frequency change was of a transient nature, that is after an initial maximum deviation the frequency tended to return towards the original value. Since the frequency changes were generally small for the $\pm 12'' \text{ H}_2\text{O}$ pressure step, measurement uncertainty due to noise and random walk of the test and reference masers is quite significant and the uncertainty is dependent on dwell time. We found for a typical slow step that the barometric pressure coefficient $\Delta f/f/''\text{H}_g$ for the SAO-14 is $+5 \times 10^{-15} \pm 5 \times 10^{-15}$, and for the NR-4 is $+1 \times 10^{-14} \pm 5 \times 10^{-15}$. Figures 13 and 14 show some typical data recorded during the barometer pressure test.

e. Output Frequency Vs. Time

The output frequency of a hydrogen maser at any given time depends on its random behavior, its susceptibility to the environment and its aging mechanism. Random behavior as a function of measurement time can be predicted. A statistical technique of measuring this behavior is known as the Allan Variance which results in a sigma/tau plot of frequency stability vs. measurement time.^[1] This type of measurement was performed and will be discussed in the following section. It should be clearly understood however that when the systematic effects of the environment and aging on a masers output frequency dominate over its random behavior, which is usually the case for measurement times greater than a few thousand seconds, the Allan Variance plot ceases to convey random behavior and must be interpreted carefully. There are methods of removing long term drift but the degree of success depends on precise knowledge of this drift. The method we used to determine long term behavior of output frequency vs. time was to manually spin exchange tune the masers periodically and plot the resulting maser cavity frequency as a function of time. This was combined with measuring the relative frequency offset of the various masers involved at the time they were tuned to separate output frequency changes due to cavity aging from other effects. The resulting data clearly shows that cavity aging can be significant.

Figure 15 is a plot of cavity frequency vs. time for NR-4 over a 500 day period. The ordinate scale of the graph is the cavity register bit setting required for the maser to be tuned. Each dot represents a tuning event. We assumed the cavity Q to be constant. The line Q was periodically measured and found to be constant for a given operating point. Between days 200 and 500 the $\Delta f_o/f/cavity\ bit = 1.166 \times 10^{-16}$. The output frequency aging rate due to cavity pulling for this maser was thus determined to be $-1.35 \times 10^{-14}/day$ at a hydrogen flux pressure control setting of 450 and a hydrogen line Q of 1.64×10^9 . The frequency offset change near day 50 was probably due to mechanical shock since work was done on the maser during that period. Between 10-22-81 and 1-1-82 the masers output frequency was monitored continuously against 3 other masers and no sudden shifts in output frequency between NR-4 and the reference masers was found. Furthermore, Figure 15 data suggests that the cavity shifted more than expected during that period by about 3000 bits. Actual output frequency measurements however indicated that less of a frequency change took place. A possible explanation is that the atomic operating frequency increased by 3.5×10^{-13} during that period. A Zeeman frequency measurement showed no significant change.

Figure 16 is a plot of cavity frequency vs. time for SAO-14 covering an 800 day period. The ordinate scale of the graph is the cavity tuning varactor diode bias voltage setting required for the maser to be tuned. D = Drift per day and was calculated for consecutive time segments assuming a line Q of 1.84×10^9 and corrected for diode nonlinearity. The value of D is inversely proportional to operating point line Q. The large shifts shown on days 100, 150, 375 are due to experimental work that was performed with the cavity RF probe output coax cable. Unlike the NR-4 maser the cavity frequency of SAO-14 changed at a fairly high rate when the maser was new but

this aging or settling rate diminished steadily to about 5×10^{-15} /day in terms of output frequency near the end of the test.

5. Frequency Stability - Allan Variance

Figures 17 and 18 are two typical Allan Variance plots. These cover a total uninterrupted time period of approximately 72 days. All other Allan Variance test runs were of shorter duration. The dashed line with a fixed slope starting at the bottom of the graph represents the computer estimated drift between the maser pair.[2] The measured output drift (see previous section) for the 3 masers involved during the same time period are:

DSN-2 - 1.2×10^{-14} /Day @ Line Q = 6.7×10^8 , P.O. = -88.2 DBM
NR-4 - 8.6×10^{-15} /Day @ Line Q = 1.7×10^9 P.O. = -101.0 DBM
SAO-14 + 6.5×10^{-15} /Day @ Line Q = 1.65×10^9 , P.O. = -97.5 DBM

These masers reach a minimum noise level at about a 2000 second sampling period (τ). Systematic effects dominate at a τ of about 300,000 seconds. It appears that if a maser is used as a clock only, continuous flux gate tuning could be appropriate. The data shown in Figures 17 and 18 is for the pair sigma. Figures 19, 20, 21 show the Allan Variance for each maser of the set SAO-14, NR-4 and DSN-2. This data was obtained from pair data that resulted in comparing all of the above hydrogen masers with each other. "Three Corner Hat" analysis basically involves solving the three simultaneous equations given by the pair data for each maser. All the pair data must be measured at the same time to give satisfactory results and the number of samples should be large at each value of tau. The spreading of the calculated values at the higher taus is to be expected since the number of samples is lower and a well convergent value has not been reached.

6. Power Spectral Density of Phase

The masers were measured in pairs and the data for each individual maser was derived from the pair data. One maser in each pair was adjusted so that its output signal was in quadrature with respect to the other. These signals were mixed and analyzed with a fast fourier transform spectrum analyzer. Measurements were taken at the 5 and 100 MHz outputs. The noise as a function of offset from the carrier is plotted in Figures 22 and 23. Comparison of four masers with each other yields six sets of data, each maser appears as one of the pair in three of those sets. The best noise characteristic curve was selected from the three and arbitrarily assigned to the maser. This method is justified in that the standard technique of solving simultaneous equations yields calculation errors which grow enormously with the measurement errors and with the disparity in absolute noise level of the various sources. Although this method has its own intrinsic problems, it is considered to be reasonably conservative for this application.

7. Tuning Repeatability

In simplified terms, a maser is considered to be tuned when the cavity frequency is set equal to the atomic operating frequency. When the cavity frequency shifts it "pulls" the atomic line frequency to produce a maser output frequency that can be described by the following equation:

$$f_o - f_A = (f_c - f_A) \frac{Q_1}{Q_c}$$

where:

f_o is the maser output frequency

f_A is the atomic operating frequency

Q_1 and Q_c are the line Q and cavity Q of that particular maser

The tuning method which we employed consisted of measuring the change in output frequency that occurred when the masers line Q (Q_1) was changed from its normal value to an arbitrarily higher value. No change in output frequency indicates that the cavity frequency is properly set.

It can be shown that $f_e = |k \Delta f HL|$

where f_e is the output frequency offset due to cavity mistuning. ΔfHL is the change in output frequency due to change in line Q, and

$$k = \frac{r}{r-1}$$

where

$$r = \frac{\text{HIGH } Q_1}{\text{LOW } Q_1}$$

For a given maser, k can be easily determined and generally remains constant. It can be seen that the resolution of ΔfHL and the value of k determine the precision to which a maser can be tuned.

The following values of k were obtainable for the masers involved in this test.

NR-4 k = 12

DSN 2 k = 3.0

SAO-14 k = 5.5

DSN 3 k = 4.8

With a measurement resolution of $\pm 5 \times 10^{-15}$ the worst case frequency offset error due to cavity mistuning of the NR4 - SA014 maser pair is estimated to be $\pm 5 \times 10^{-15} (12 + 5.5) = 8.75 \times 10^{-14}$.

During a 48 day test period the masers were manually tuned four times while the frequency was continually monitored. Figure 24 is a plot of the frequency difference between NR-4 and SAO-14. The data was derived from daily phase measurements and no corrections or offset changes were made. After the masers were initially tuned they drifted apart at a rate which was determined earlier. (Refer to paragraph 4e) (Output frequency vs. Time). The masers were tuned 3 more times during the 48 day period as indicated by arrows at the top of the chart. The data shows that the measured tuning repeatability is better than predicted for this pair. One can see the clean time residuals and the characteristic parabolas for the pair of masers in Figure 25.

8. Absolute Calibration Against NBS

In order to continually track long term stability, we calibrated each maser with reference to NBS. Each hydrogen maser's output frequency can be arbitrarily set by means of the receiver synthesizer, cavity frequency and cavity magnetic field bias. For calibration purposes each maser cavity was tuned as precisely as possible. The typical output frequency uncertainty is $\pm 3 \times 10^{-14}$ due to cavity mistuning. The magnetic field bias was specified and the corresponding Zeeman frequency measured. Each maser receiver synthesizer was then set to a value that produced an output frequency equivalent to the national standard. The process involved maintaining a Cesium frequency standard ensemble as the local reference against which the masers were measured. The ensemble offset from NBS was determined by making several clock trips to NBS with a portable Cesium standard. At the test conclusion the "standard" synthesizer setting was thus determined for each maser. The particular synthesizer settings derived for the two test masers, given tuned cavities are:

<u>Maser</u>	<u>Synthesizer Setting</u>	<u>Zeeman Frequency</u>
NR-4	5751.689467 Hz	400 Hz
SAO-14	405751.68900 Hz	700 Hz

It should be noted however that when a maser physics unit is opened up and a new storage bulb or teflon coating is installed the calibration becomes void. Furthermore, there is evidence the maser output frequency changes without a corresponding change in cavity frequency or Zeeman frequency. Additionally we have found that when a maser is opened up for vacuum element replacement the maser's output frequency may or may not be affected due to some unknown mechanisms. A maser calibration, however useful over the short term, may be of limited value for long term purposes. The calibration uncertainty of this experiment is estimated to be $\pm 1 \times 10^{-13}$.

9. Correlation of Measured Parameters

In order to gain additional insight into the dependence of maser performance on environmental parameters, the auto and cross correlation matrices were computed for all possible combinations of data sets. This data was collected during the uninterrupted 72 day Allan Variance test. The most significant finding was a strong correlation between output frequency and dew point for two of the four masers (NR-4 and DSN-2) as shown in Figure 26.

Table 2 shows the four test masers dew point coefficient and the delay after change of dew point. From this table it can be determined that only DSN-2 and NR-4 had a significant response to dew point.

The cause of this correlation between humidity and output frequency has not been resolved at this time.

10. Reliability and Repairability

All problems and malfunctions were carefully logged during the test period. Most discrepancies were found during the initial verification tests. It seemed appropriate to categorize and separate the problems into two groups in order to gain some realistic insight into the reliability of these masers.

Table 3 summarizes the findings regarding maser reliability. It is expected that with the knowledge gained by this evaluation substantial testing will be performed before masers are released to the field and problems such as in Group I will have been corrected at the manufacturers facility. It is obvious that vacuum pump failures constituted the most serious problem affecting time out of service. Other than that, the masers promise to be quite reliable.

CONCLUSIONS

The extensive series of tests which were run as part of this program yield the most definitive set of data to date on performance and operability of the Hydrogen maser frequency standard. Based on the data, the experimenters conclude that the tested masers indicate that the state of the technology provides frequency stability of about 1×10^{-15} over 1000 to 2000 seconds under conditions of an extremely well controlled environment. As a frequency standard, the Hydrogen masers are a factor of 100 better than the best Cesium standards available for short term stability. In terms of long term stability, the tests indicate that the masers age at the rate on the order of 10^{-14} per day and are retunable to better than 10^{-13} .

Environmental factors can affect a maser output frequency by as much as a part in 10^{14} . This suggests that to obtain the ultimate performance available, the masers must be kept in an environment 10 times more stable than that of a normal office or laboratory. Additional work is needed to characterize and explain and then to correct the, as yet, mysterious dependence of frequency upon humidity.

Finally, the Hydrogen masers appear to be limited in reliability by their vacuum systems. The vacuum pumps proved to be a continuing problem. Nevertheless, when subjected to a very protected environment, the masers were surprisingly reliable, showing a "down-time" of less than 2.5%.

ACKNOWLEDGEMENTS

The authors wish to acknowledge the contribution of several individuals to this report. Roland Taylor and Donald Bodkin of JPL were involved in the testing of the masers and the operation of the entire test facility. JPL's Charles Greenhall, Roger Meyer, Earl Endsley, Philip Clements and Phuong Tu supported the effort with analysis, special tests and data processing.

REFERENCES

- [1] D. W. Allan, "Statistics of Atomic Frequency Standards," Proc. IEEE, vol. 54, pp. 221-230, February 1966.
- [2] C. A. Greenhall, "Removal of Drift from Frequency Stability Measurements," JPL-TDA Progress Report, 42-65, pp. 127-132, 1981.

Table 1. Tests Performed

1. VERIFICATION OF INPUTS, OUTPUTS, PROPER FUNCTIONING OF CONTROLS
2. I.F. METER CALIBRATION
3. PRESSURE CONTROL SETTING DEPENDENT PARAMETERS
BASELINE FOR RELATIONSHIP OF LINE-Q, POWER OUTPUT, PRESSURE
4. ENVIRONMENTAL TESTS:
 - a. OUTPUT FREQUENCY VS. AC/ DC INPUT VOLTAGE
 - b. OUTPUT FREQUENCY VS. AMBIENT MAGNETIC FIELD
 - c. OUTPUT FREQUENCY VS. AMBIENT TEMPERATURE
 - d. OUTPUT FREQUENCY VS. AMBIENT BAROMETRIC PRESSURE
 - e. OUTPUT FREQUENCY VS. TIME
5. FREQUENCY STABILITY - ALLAN VARIANCE $1s < \tau < 1 \times 10^6s$
6. POWER SPECTRAL DENSITY OF PHASE
7. TUNING REPEATABILITY
8. ABSOLUTE CALIBRATION AGAINST NBS
9. CORRELATION OF MEASURED PARAMETERS
10. RELIABILITY AND REPAIRABILITY ASSESSMENT

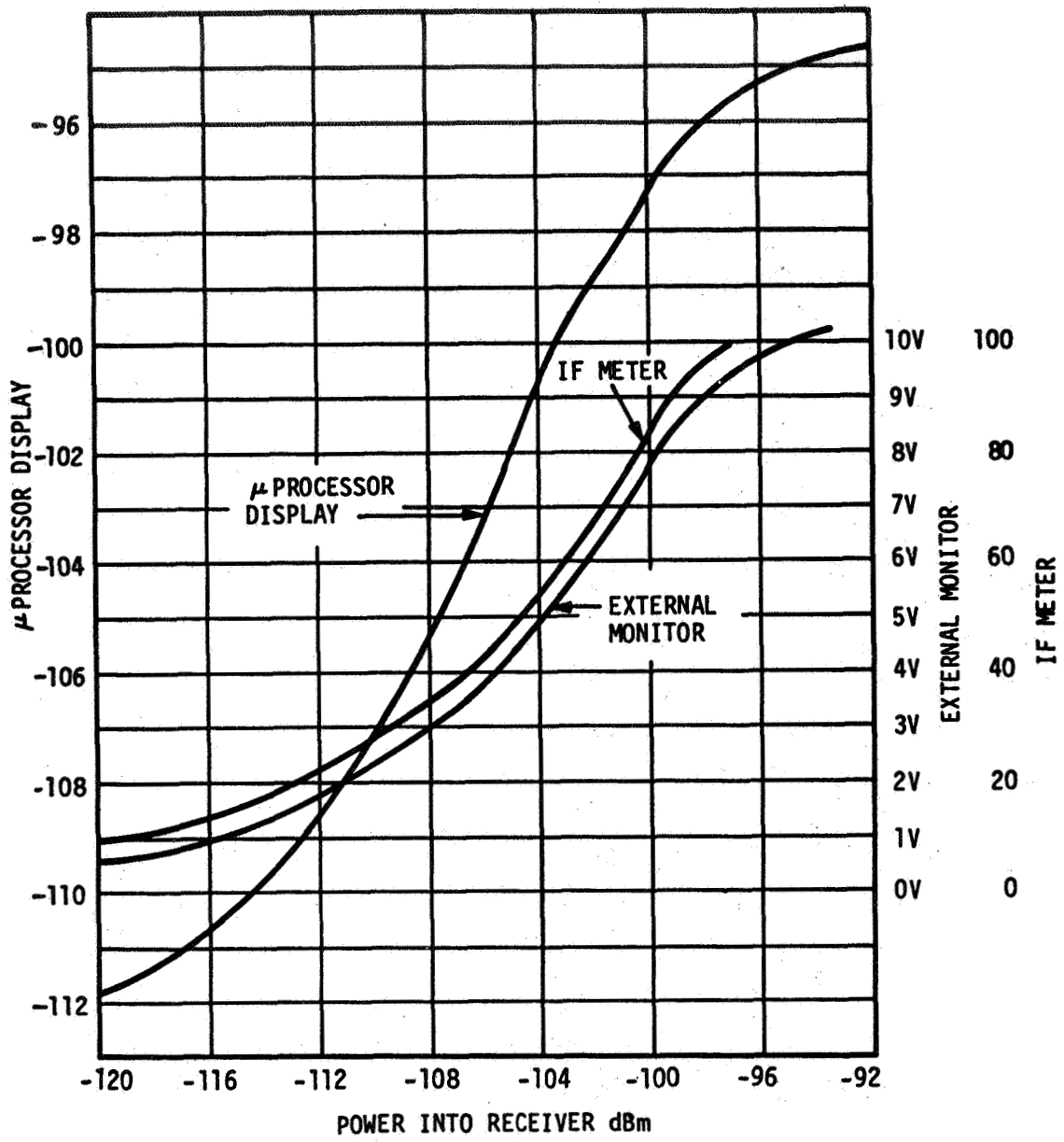


Figure 1. NR-4 Output Power Calibration

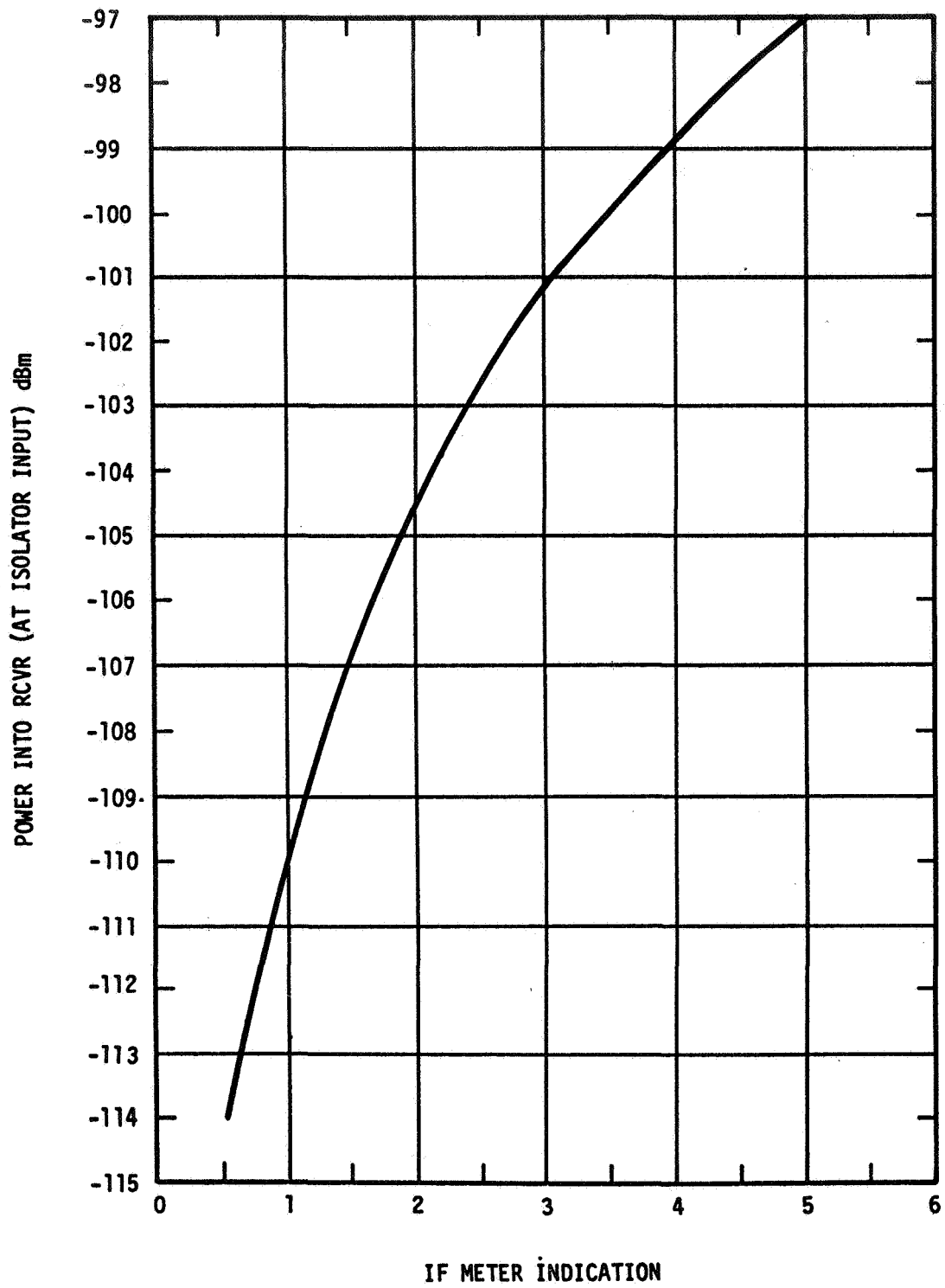


Figure 2. SAO-14 Output Power Calibration

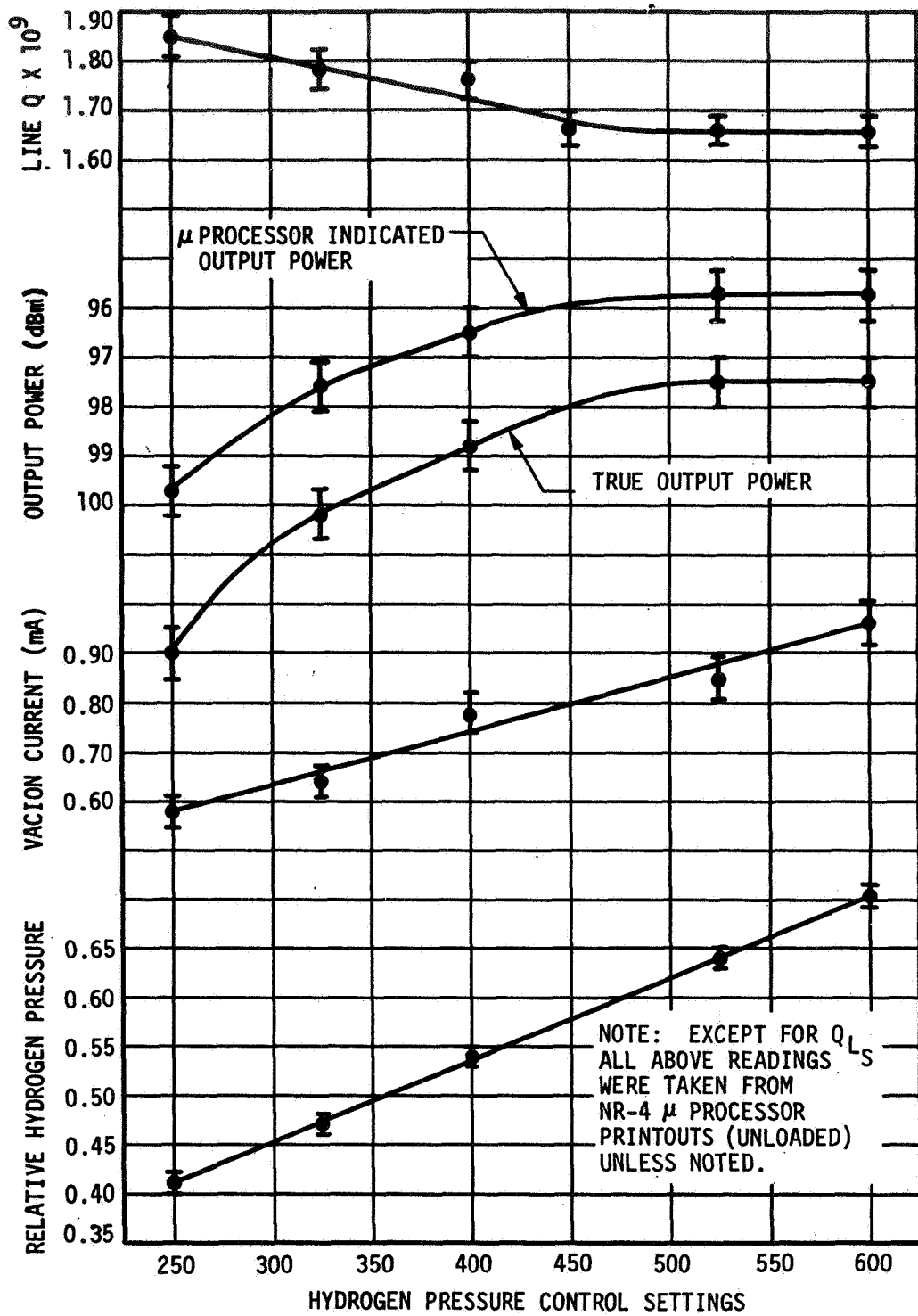


Figure 3. NR-4 Pressure Dependent Parameters

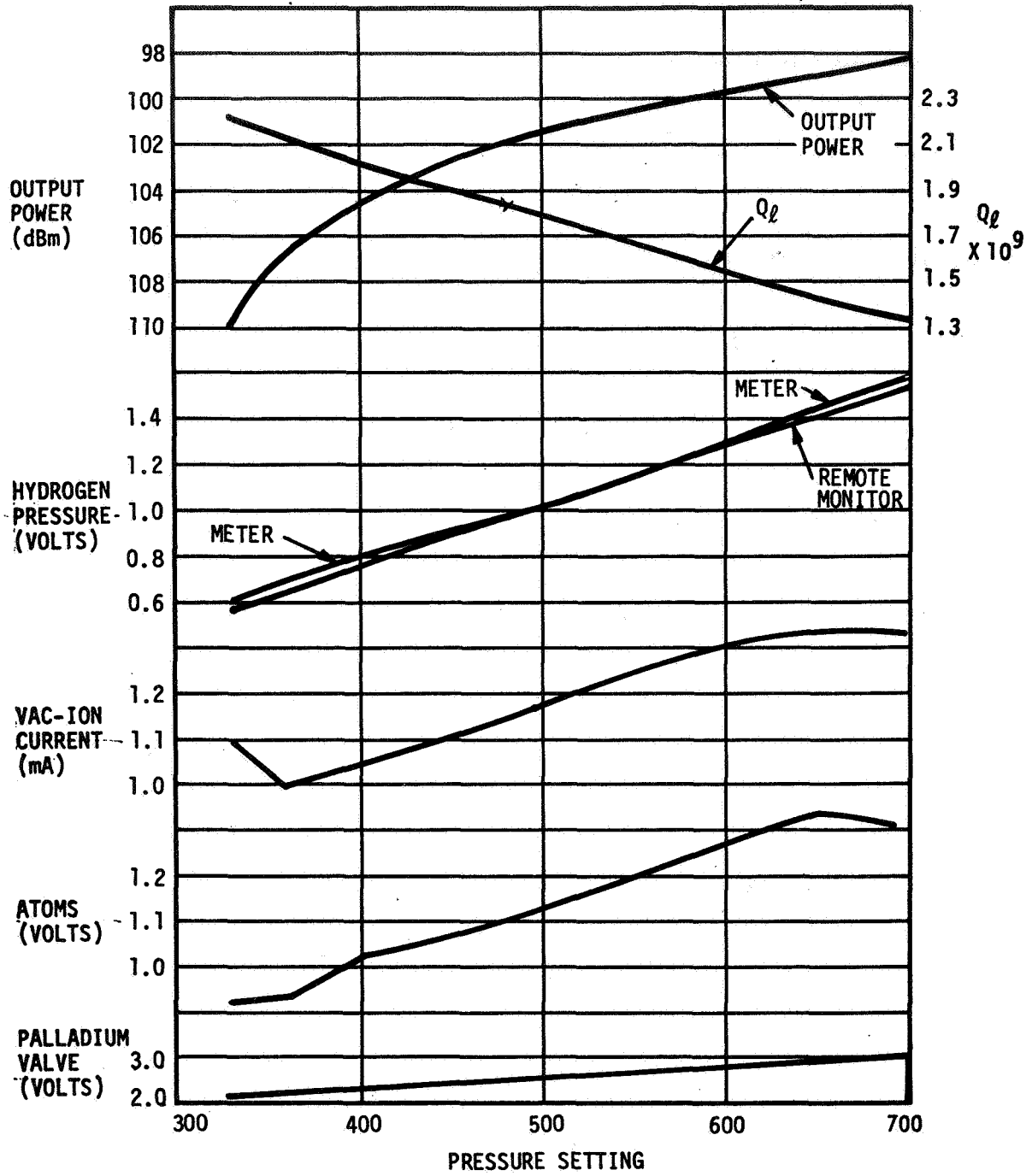


Figure 4. SAO-14 Pressure Dependent Parameters

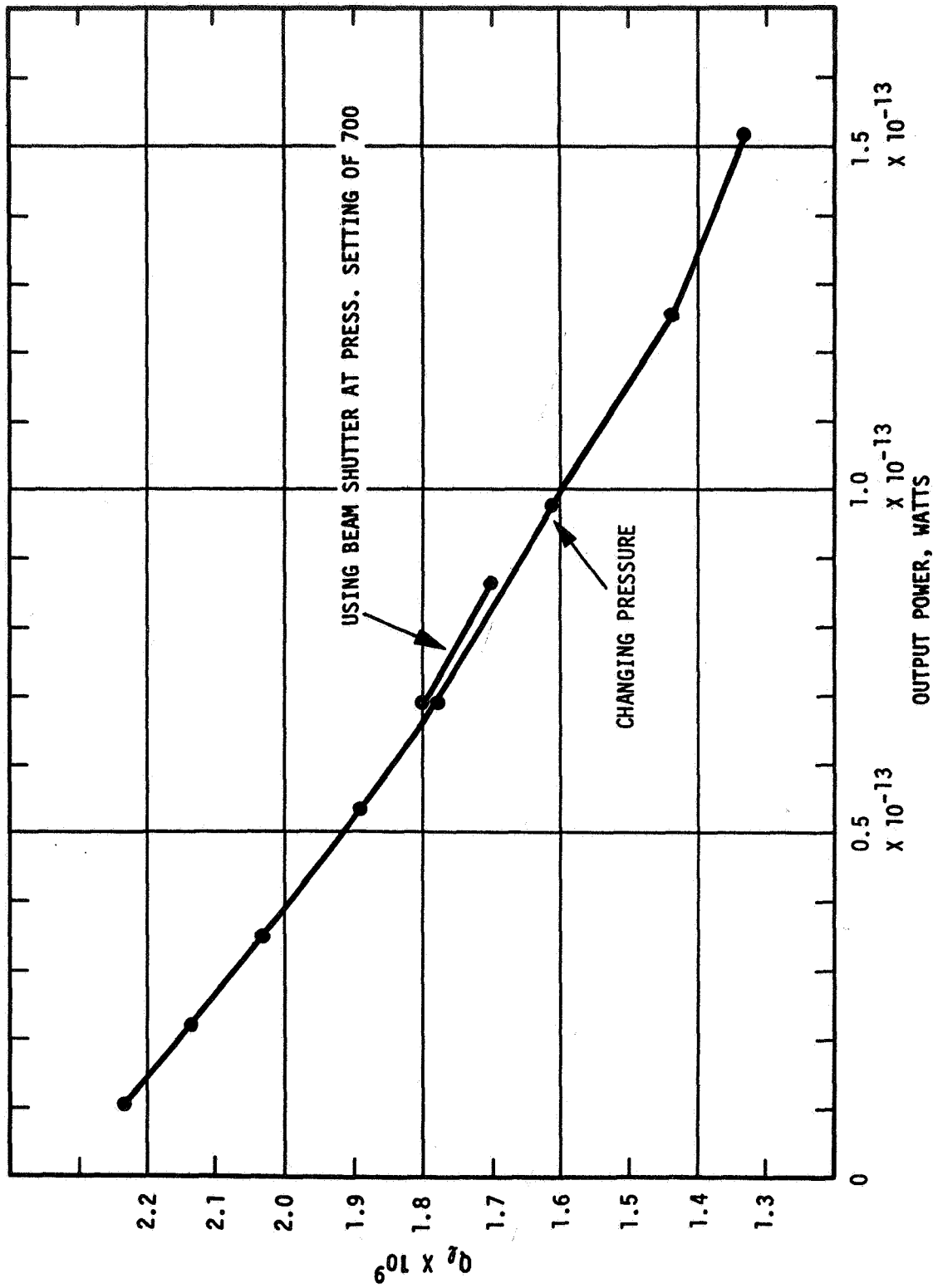


Figure 5. SAO-14 Line Q vs Output Power

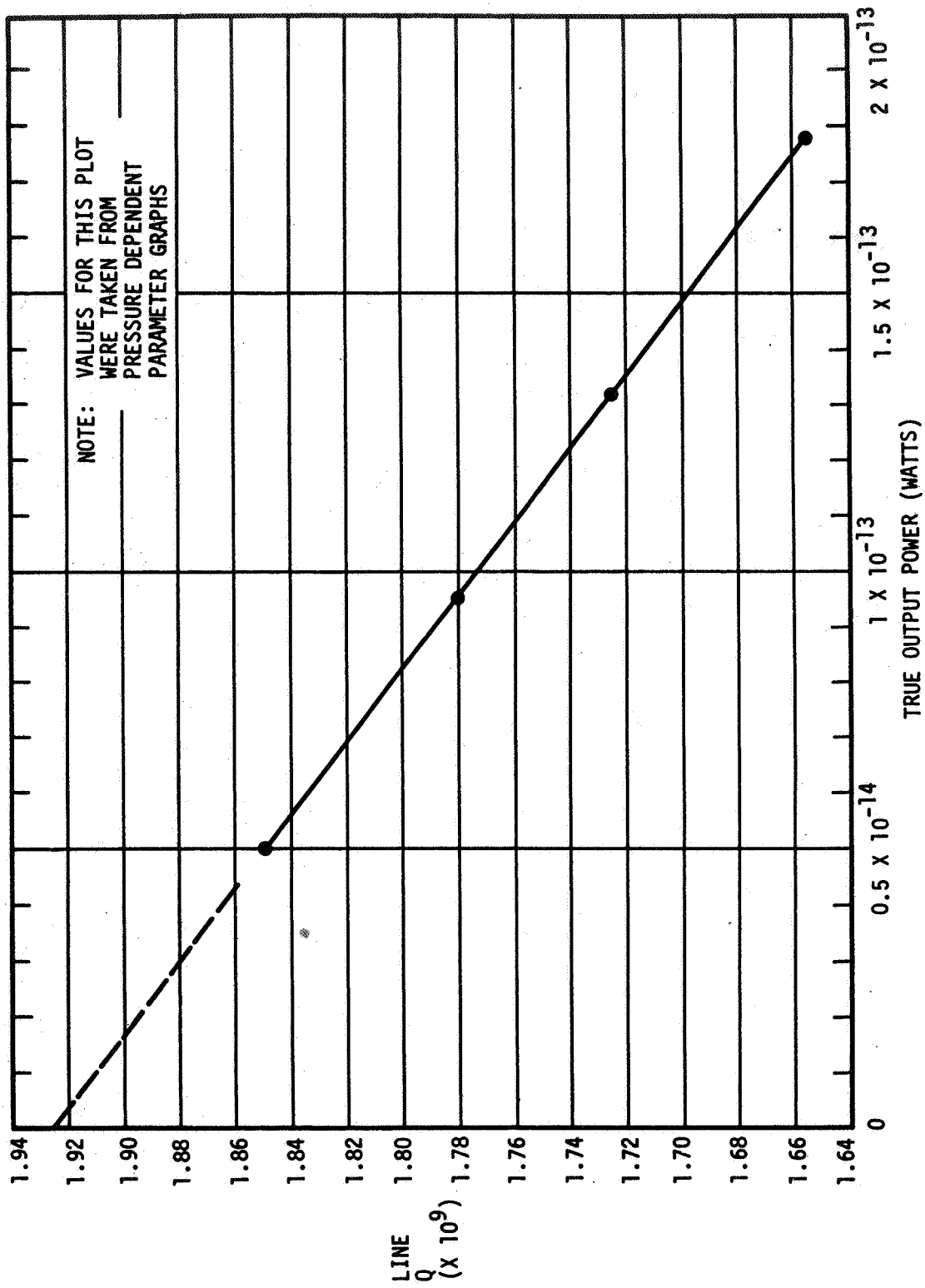


Figure 6. NR-4 Line Q vs Output Power

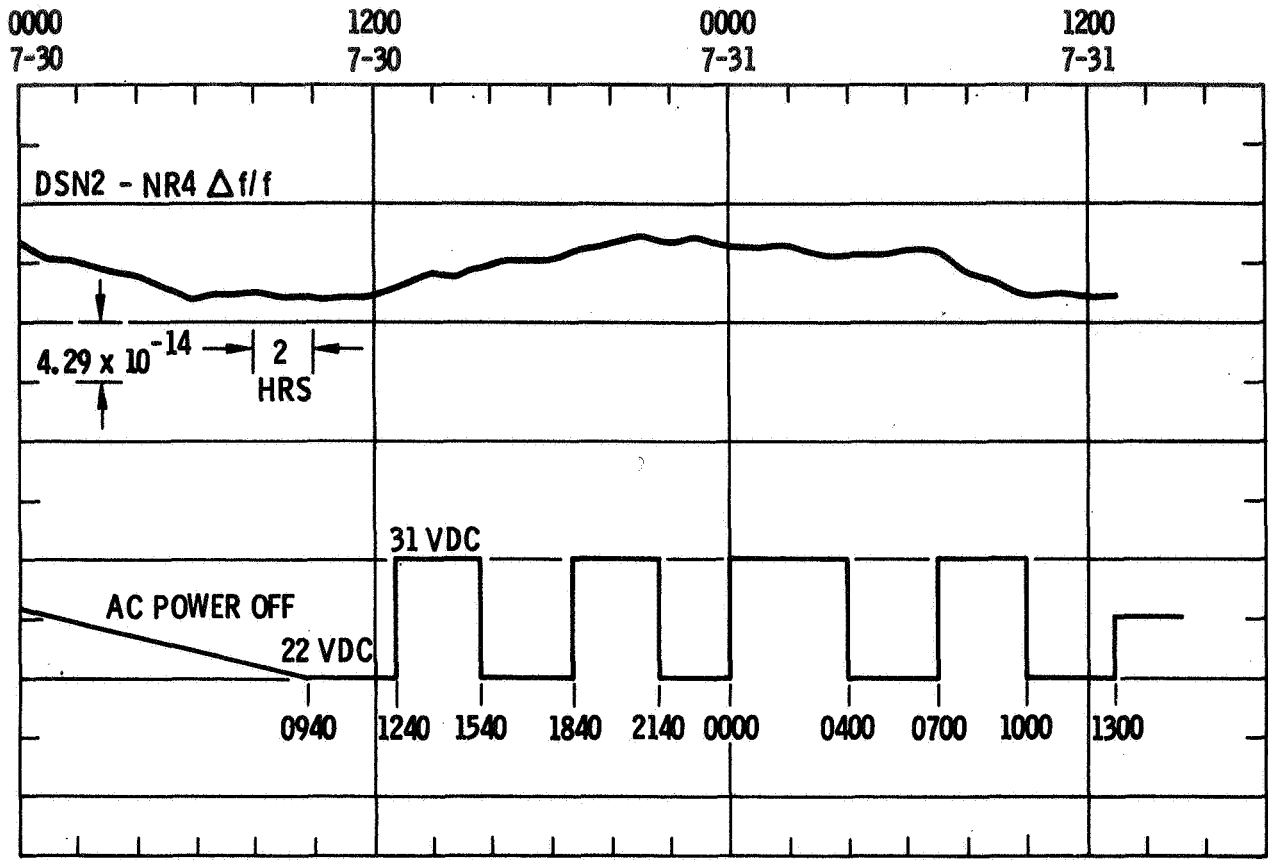


Figure 7. NR-4 Output Frequency Shift vs DC Input Voltage

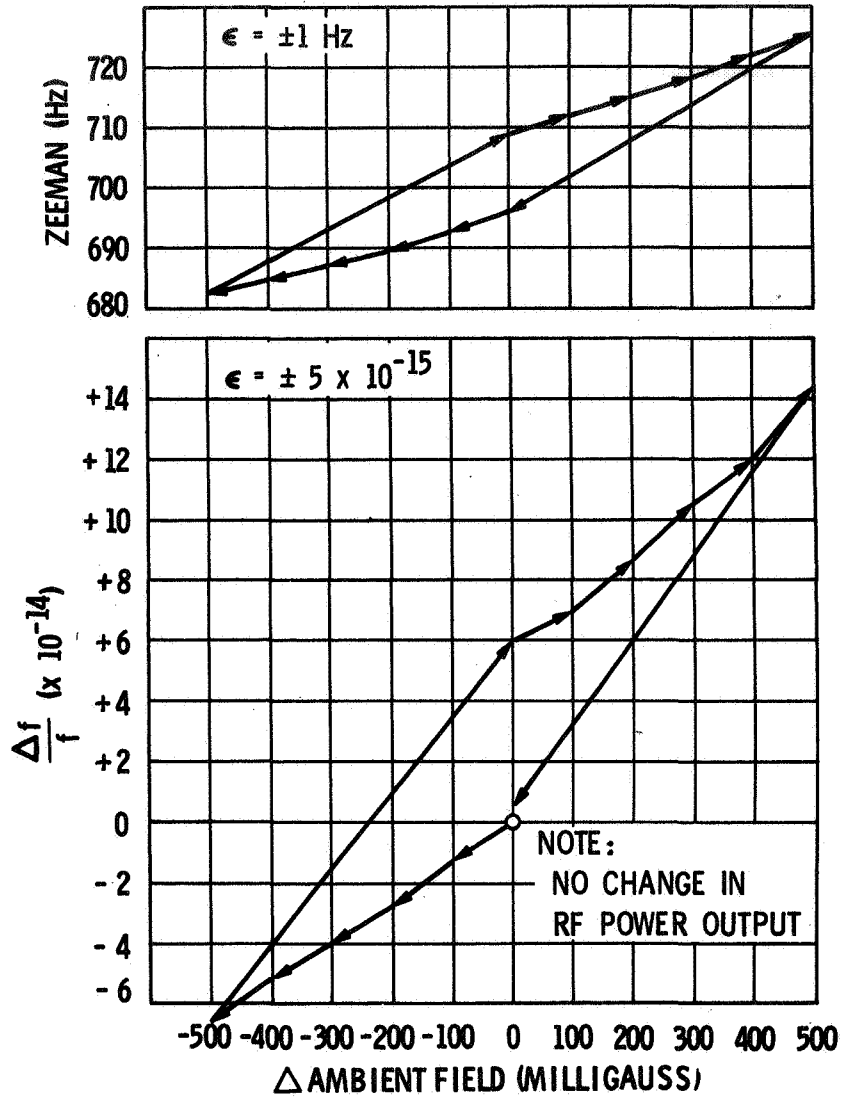


Figure 8. SAO-14 Magnetic Field Test - 1st Series

MAGNETIC FIELD	FRACTIONAL FREQ SHIFT PER GAUSS		
	HYDROGEN PRESSURE CONTROL SET TO 325, LOW FLUX	HYDROGEN PRESSURE CONTROL SET TO 525, NORMAL FLUX	HYDROGEN PRESSURE CONTROL SET TO 600, HIGH FLUX
200 mG PEAK TO PEAK	5.88×10^{-14}	8.01×10^{-14}	7.71×10^{-14}
600 mG PEAK TO PEAK	5.71×10^{-14}	5.53×10^{-14}	5.96×10^{-14}
1000 mG PEAK TO PEAK	4.49×10^{-14}	5.06×10^{-14}	4.77×10^{-14}

- NOTES: 1. ALL $\Delta f/f$ VALUES HAVE AN UNCERTAINTY FACTOR OF $\pm 5 \times 10^{-15}$
2. AMBIENT TEMPERATURE = 23°C
3. ZEEMAN FREQUENCY = 400 Hz
4. THE UNCERTAINTY OF ΔH IS ESTIMATED TO BE $\pm 5\%$
5. ALL MEASUREMENTS AVERAGE OF 5 STEPS

Figure 9. NR-4 Frequency Shift vs. Magnetic Field

MAGNETIC FIELD	FRACTIONAL FREQ SHIFT PER GAUSS	
	HYDROGEN PRESSURE CONTROL SET TO 360, LOW FLUX	HYDROGEN PRESSURE CONTROL SET TO 500, NORMAL FLUX
200 mG PEAK TO PEAK	1.87×10^{-13}	2.75×10^{-13}
600 mG PEAK TO PEAK	1.40×10^{-13}	2.17×10^{-13}
1000 mG PEAK TO PEAK	1.23×10^{-13}	1.88×10^{-13}

- NOTES: 1. ALL $\Delta f/f$ VALUES HAVE AN UNCERTAINTY FACTOR OF $\pm 5 \times 10^{-15}$
2. AMBIENT TEMPERATURE = 24°C
3. ZEEMAN FREQUENCY = 700 Hz
4. THE UNCERTAINTY OF ΔH IS ESTIMATED TO BE $\pm 5\%$
5. ALL MEASUREMENTS AVERAGE OF 5 STEPS

Figure 10. SA0-14 Frequency Shift vs. Magnetic Field

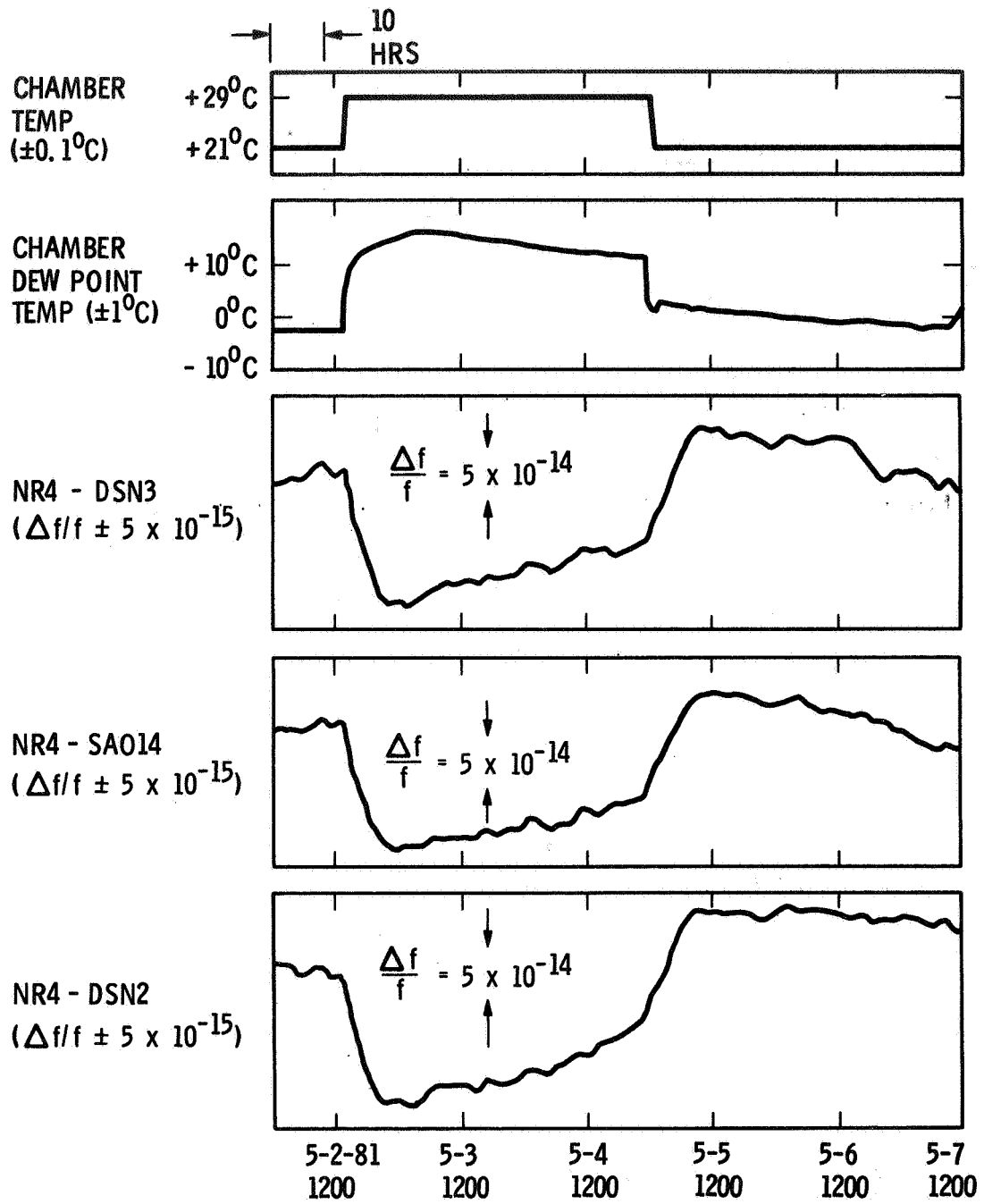


Figure 11. NR-4 Temperature Test

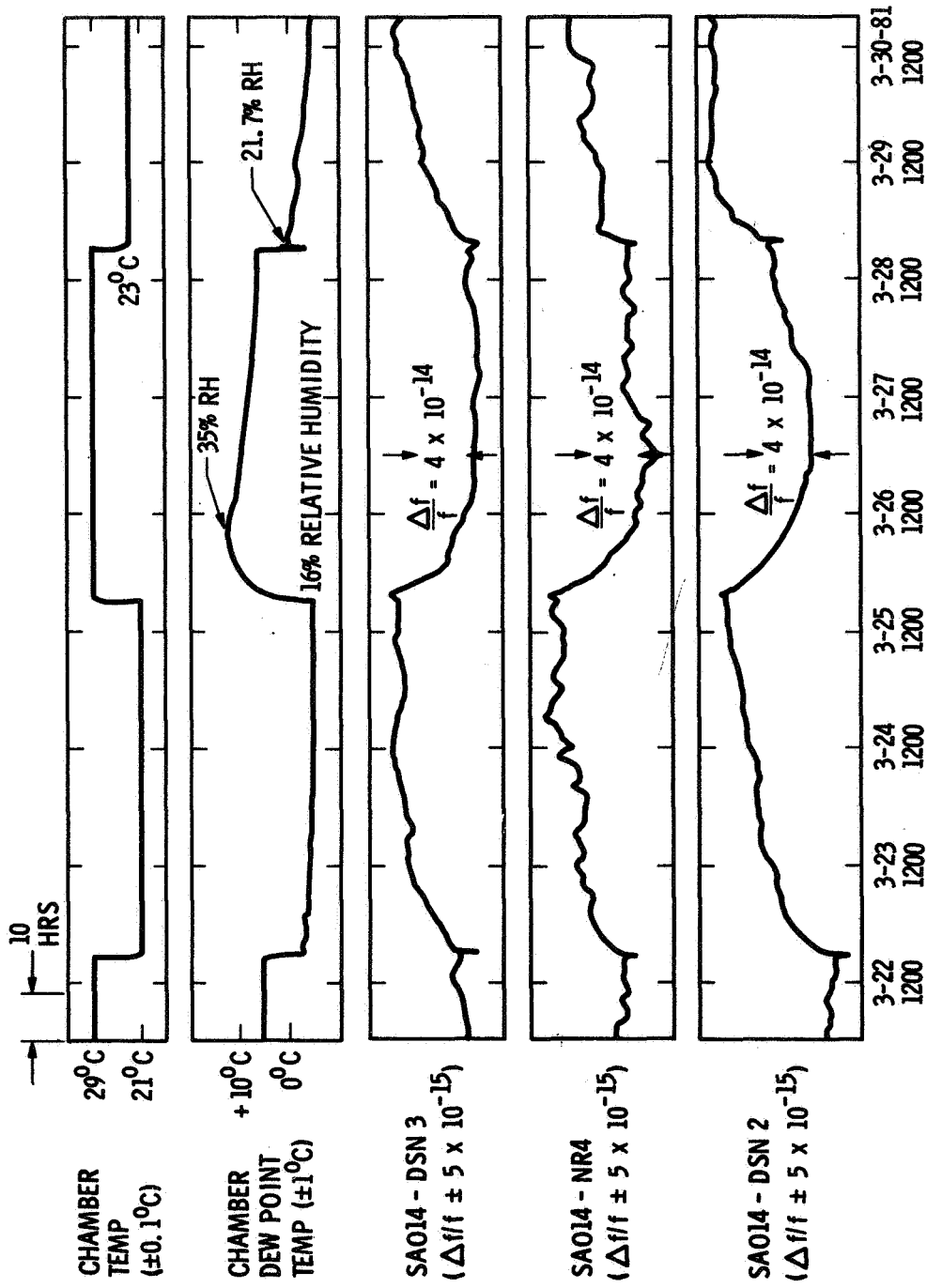


Figure 12. SAO-14 Temperature Test

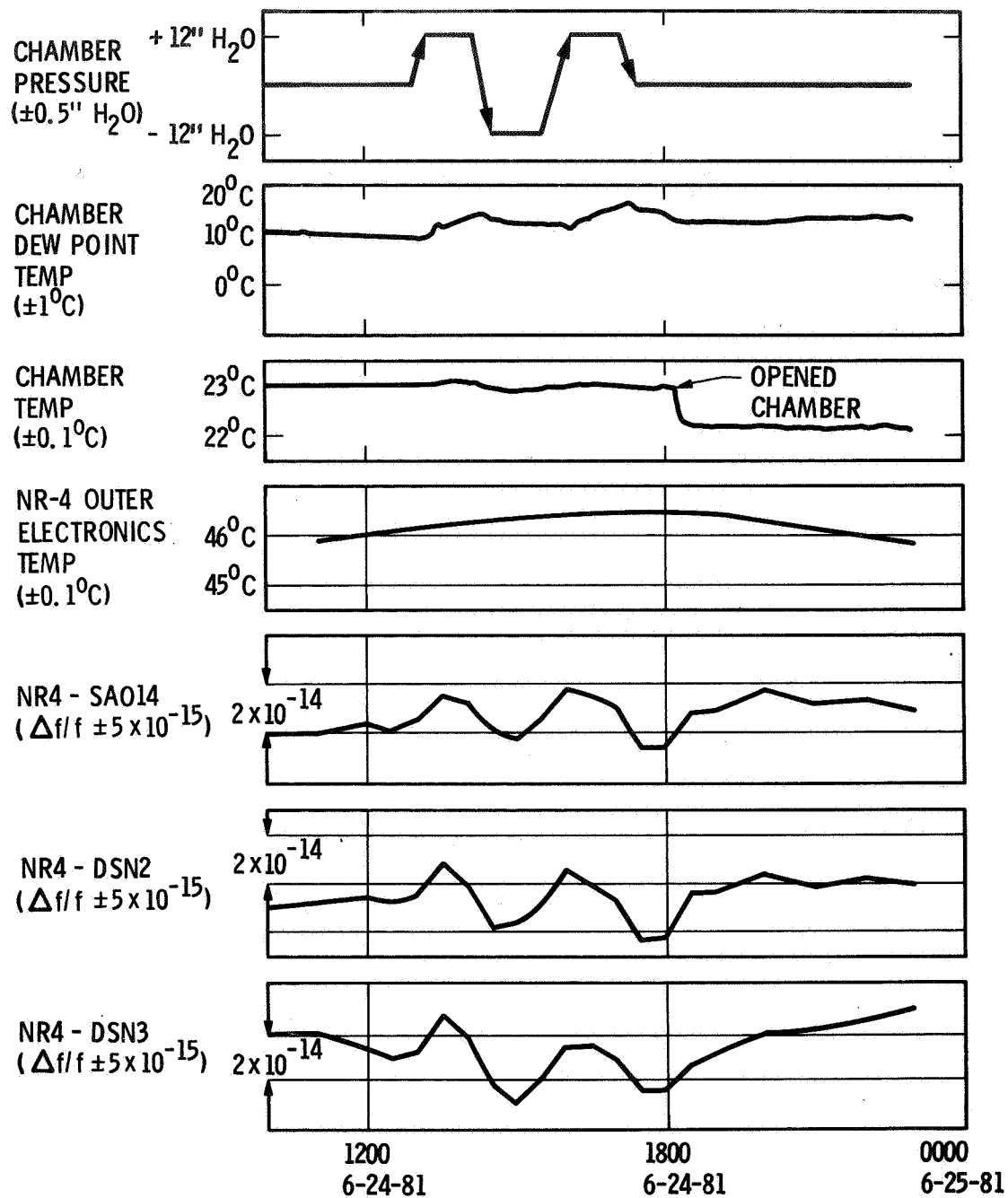


Figure 13. NR-4 Barometric Pressure Test

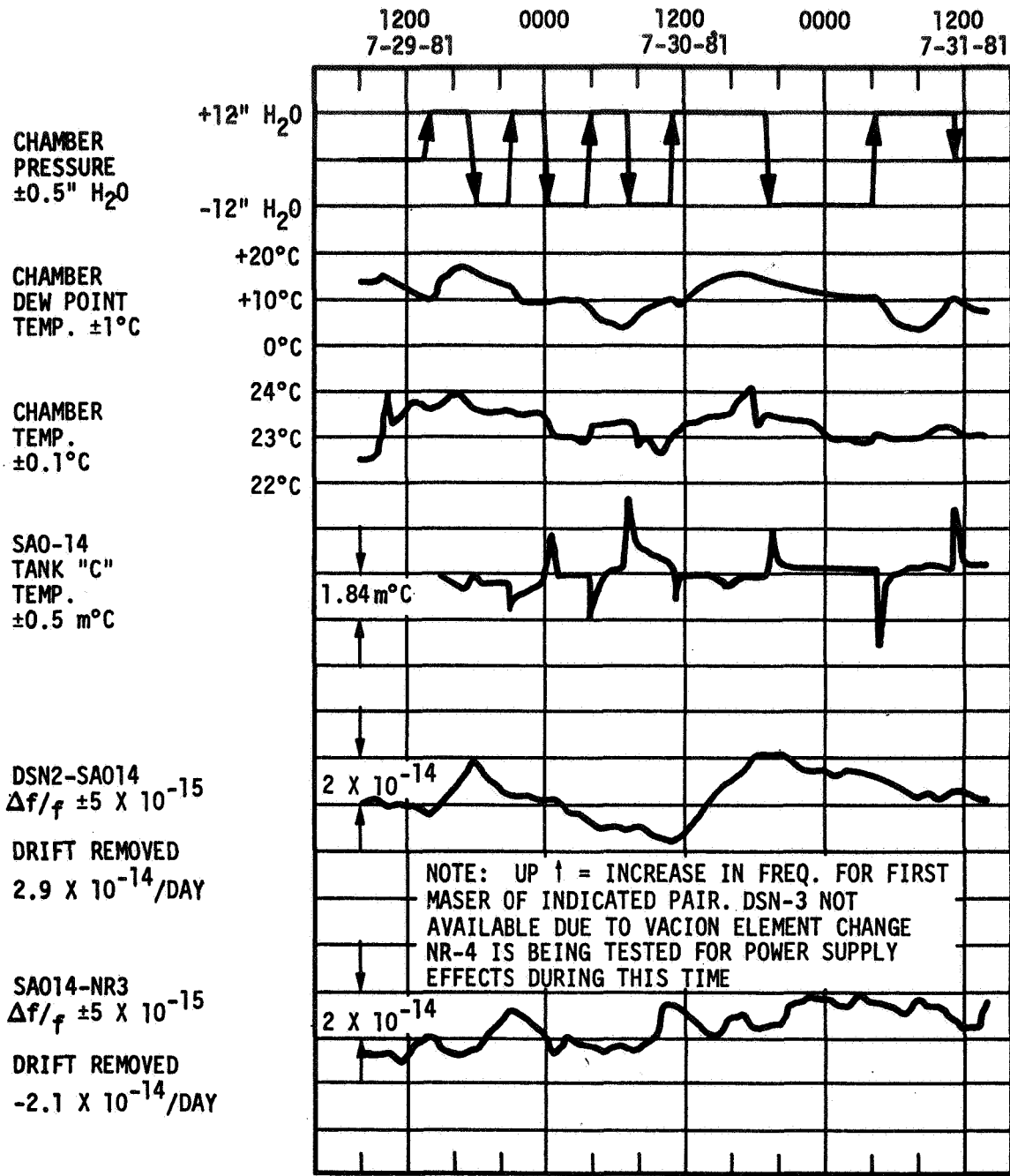


Figure 14. SAO-14 Barometric Pressure Test

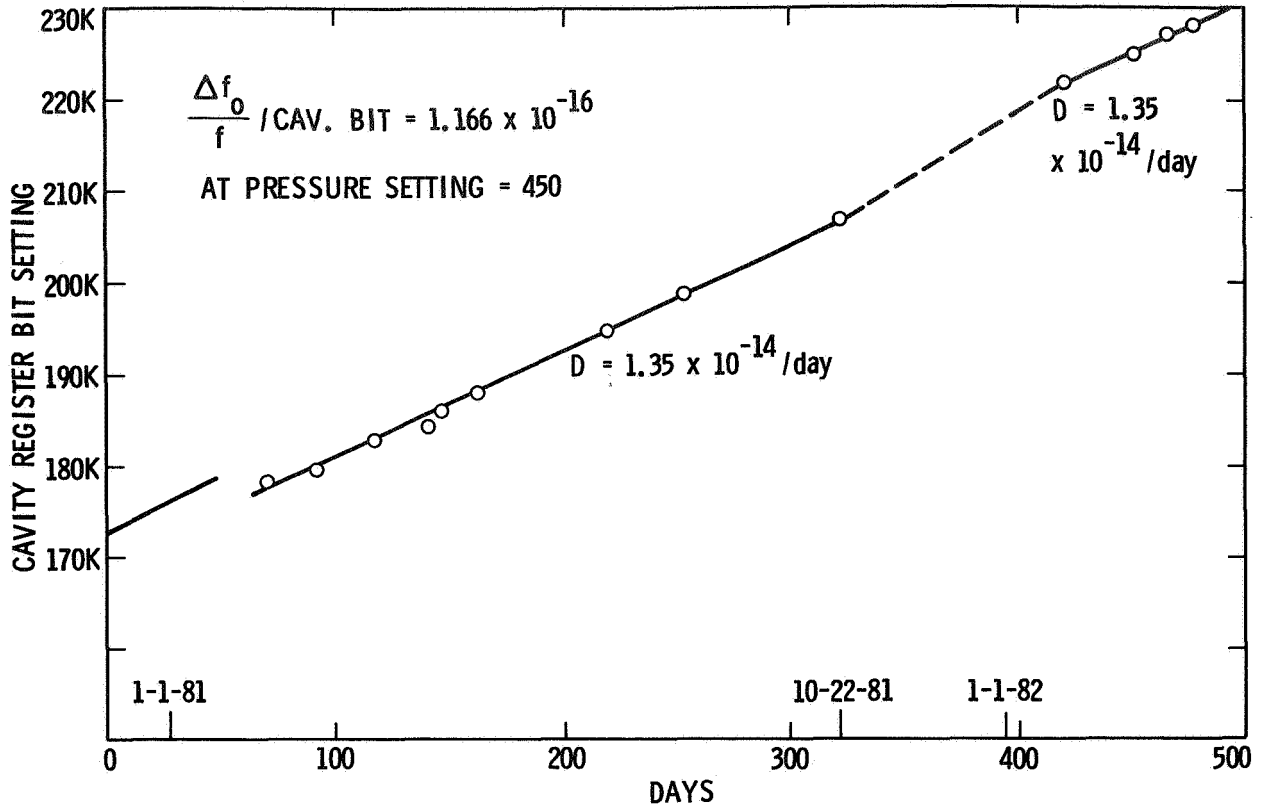


Figure 15. NR-4 Cavity Tuning

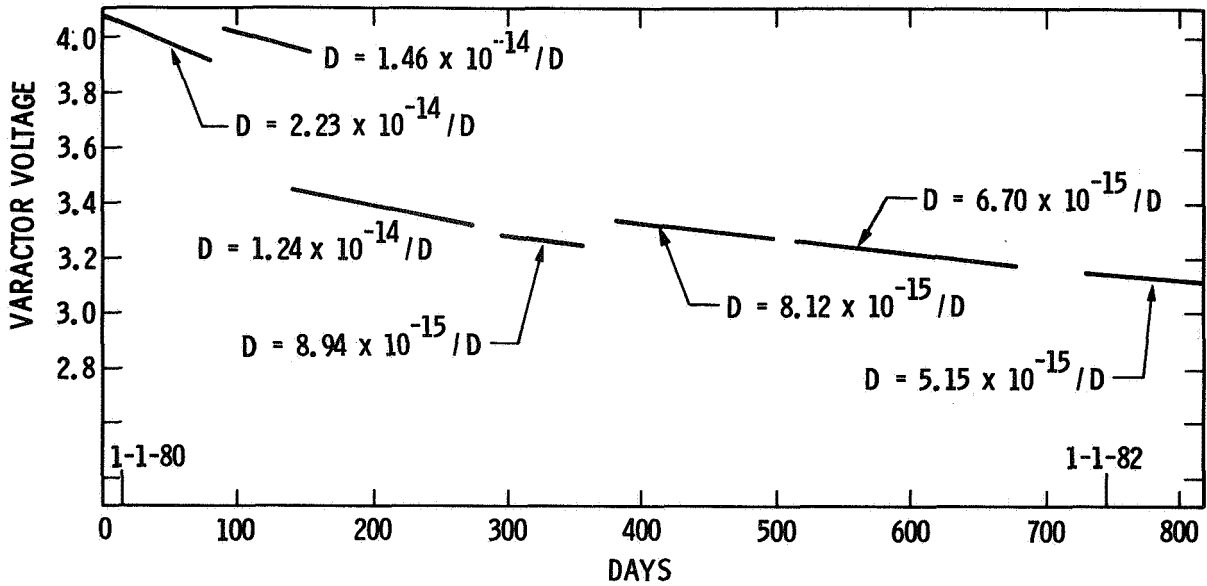


Figure 16. SAO-14 Cavity Tuning

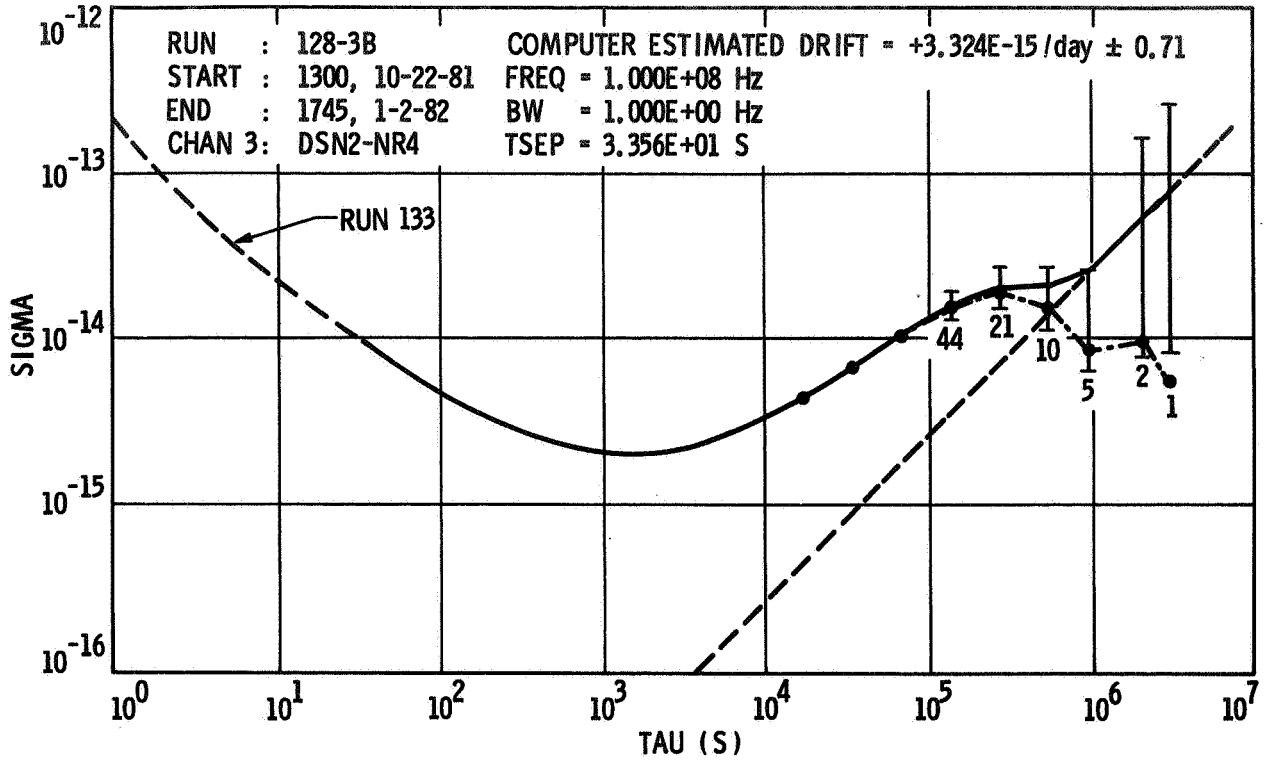


Figure 17. Allan Variance with Computed Drift Removed Between DSN-2 and NR-4

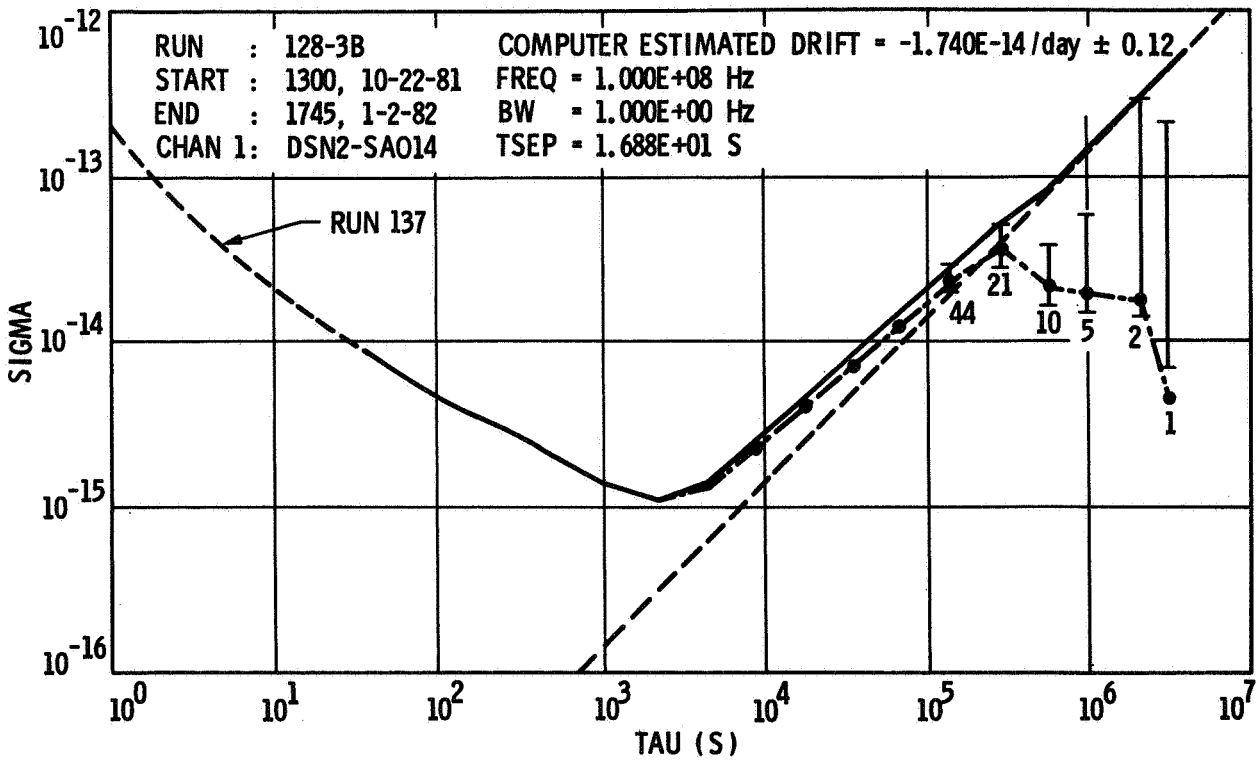


Figure 18. Allan Variance with Computed Drift Removed Between DSN-2 and SAO-14

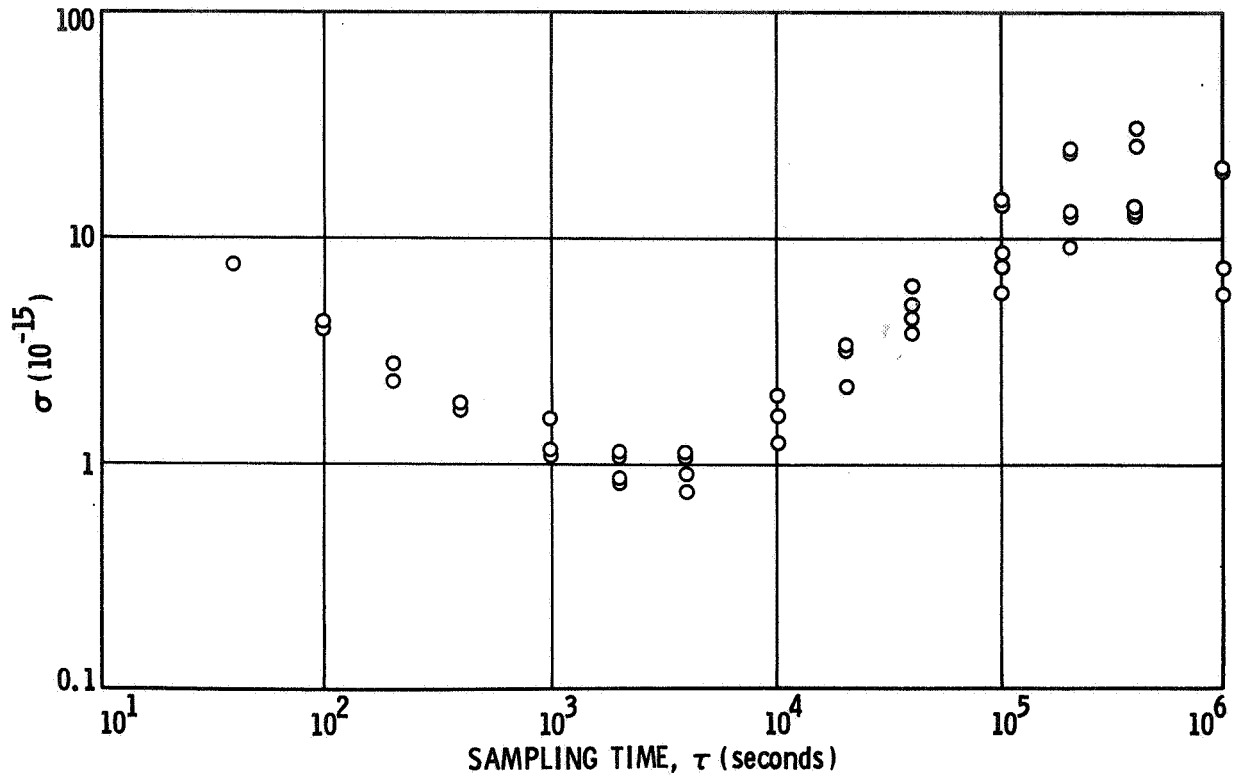


Figure 19. SAO-14 Three Corner Hat Analysis

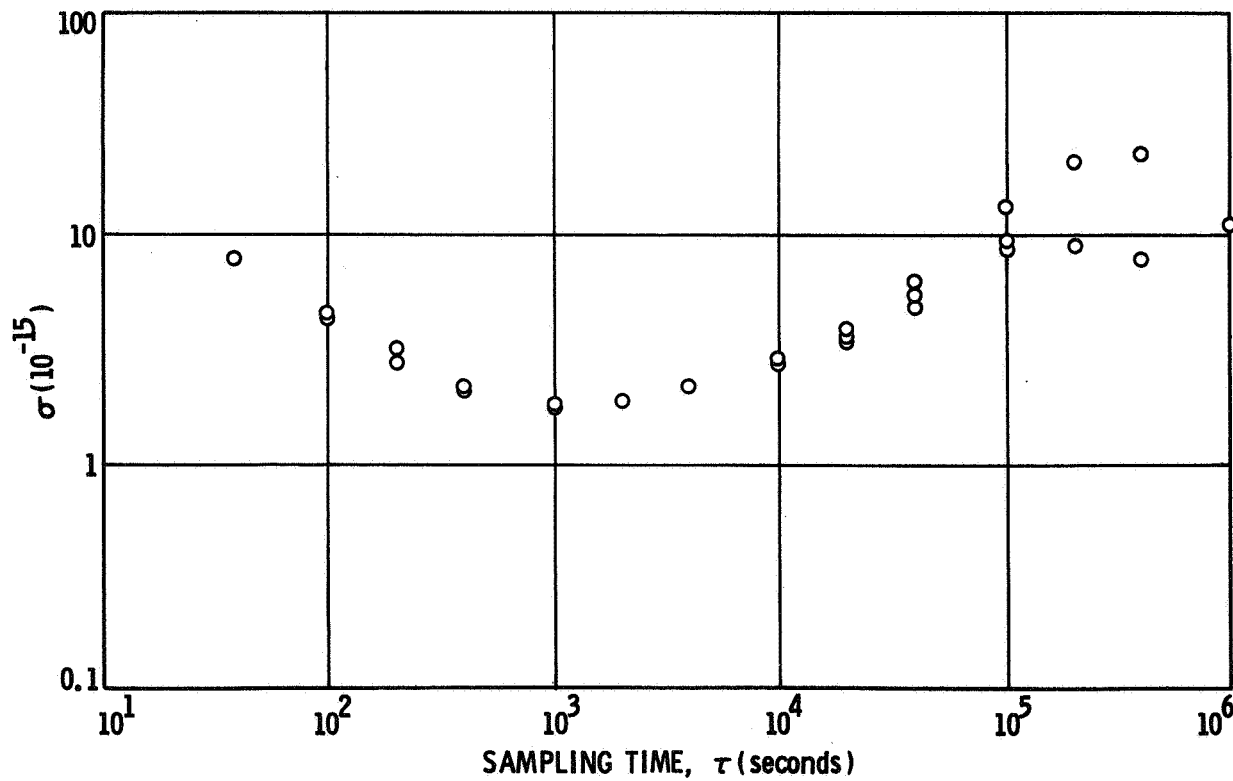


Figure 20. NR-4 Three Corner Hat Analysis

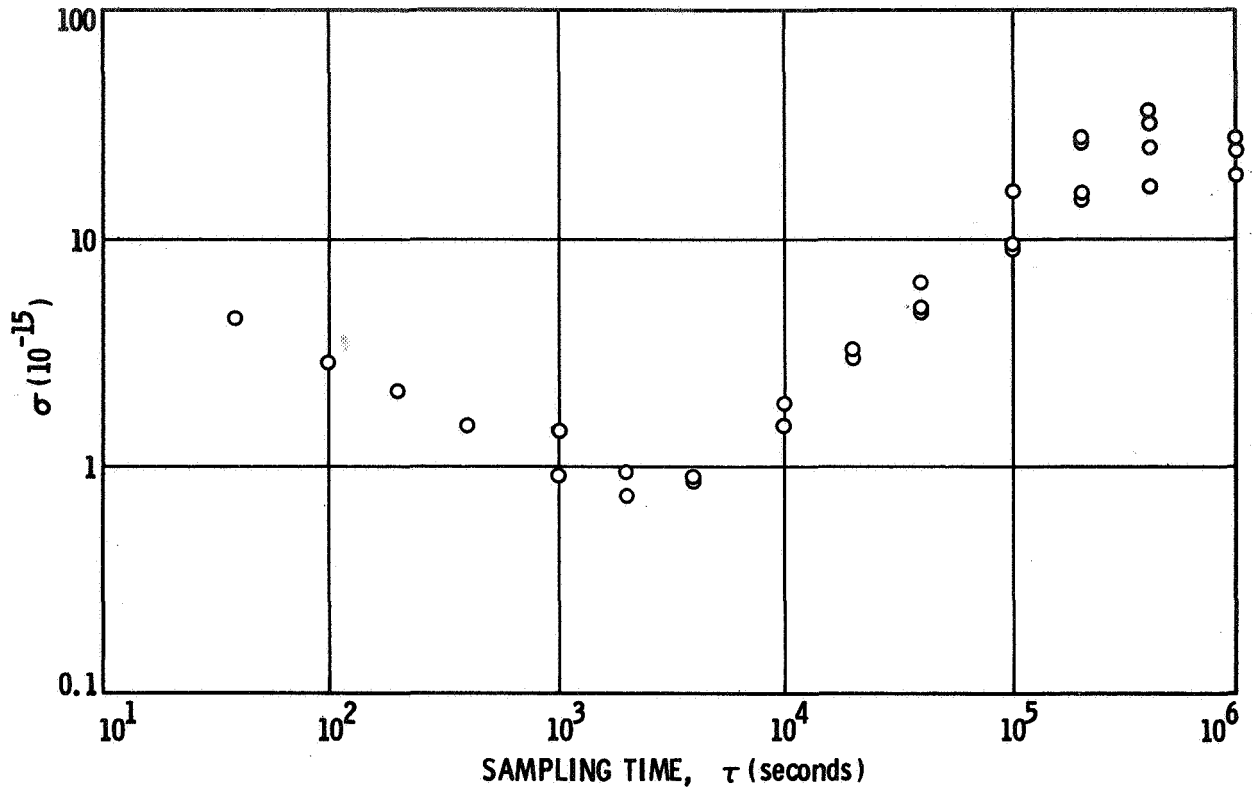


Figure 21. DSN-2 Three Corner Hat Analysis

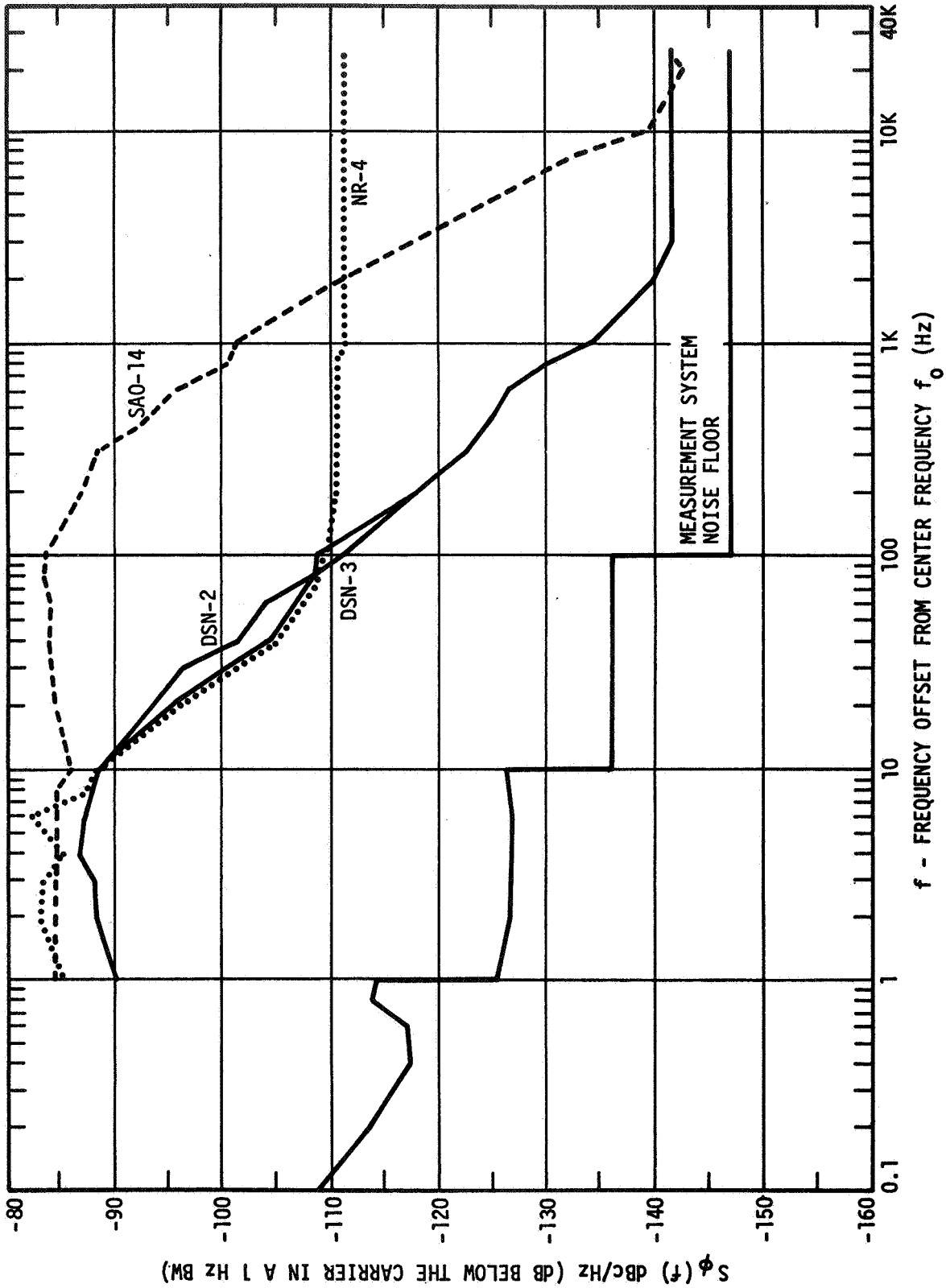


Figure 22. 100 MHz Phase Noise

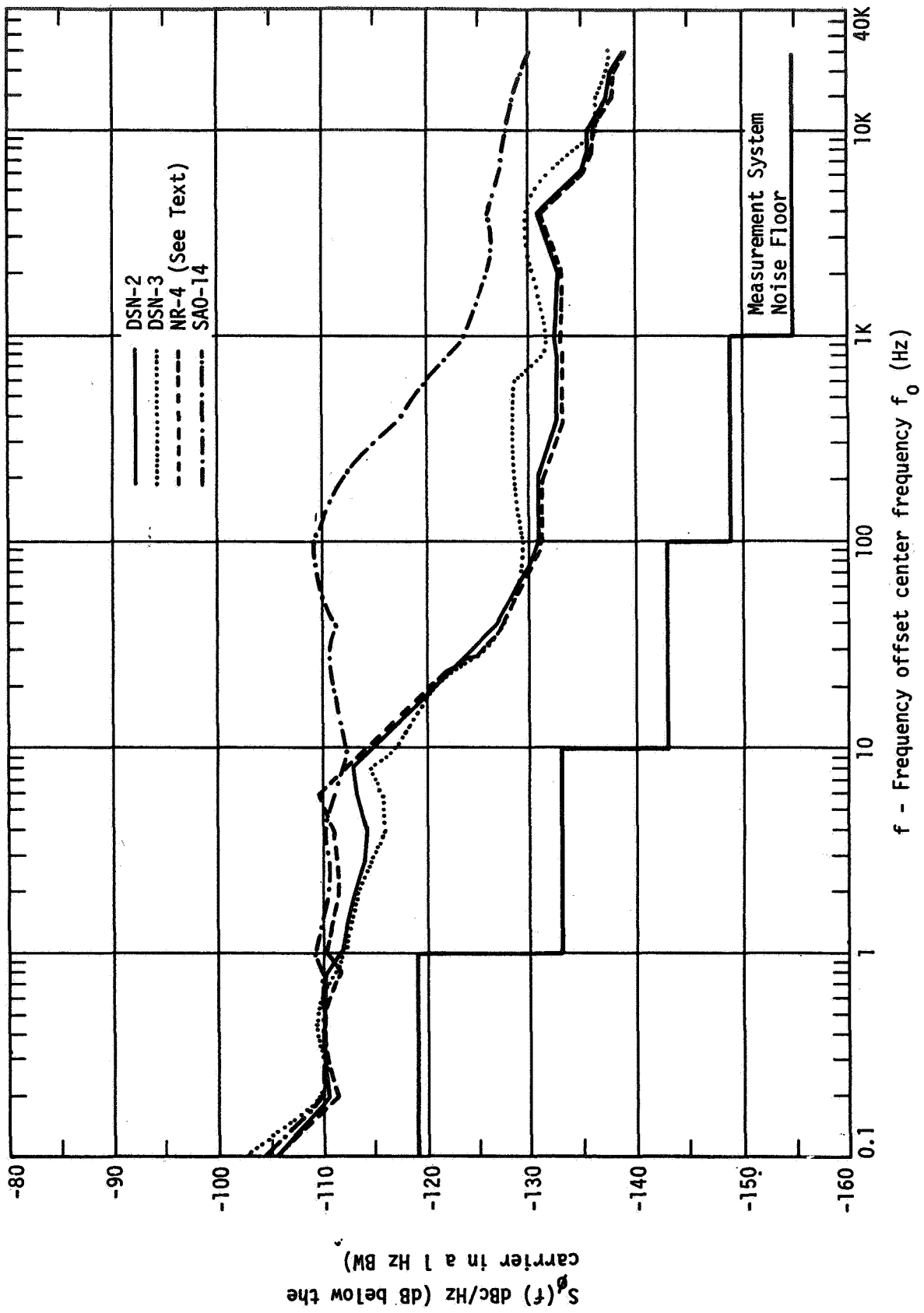


Figure 23. 5 MHz Phase Noise

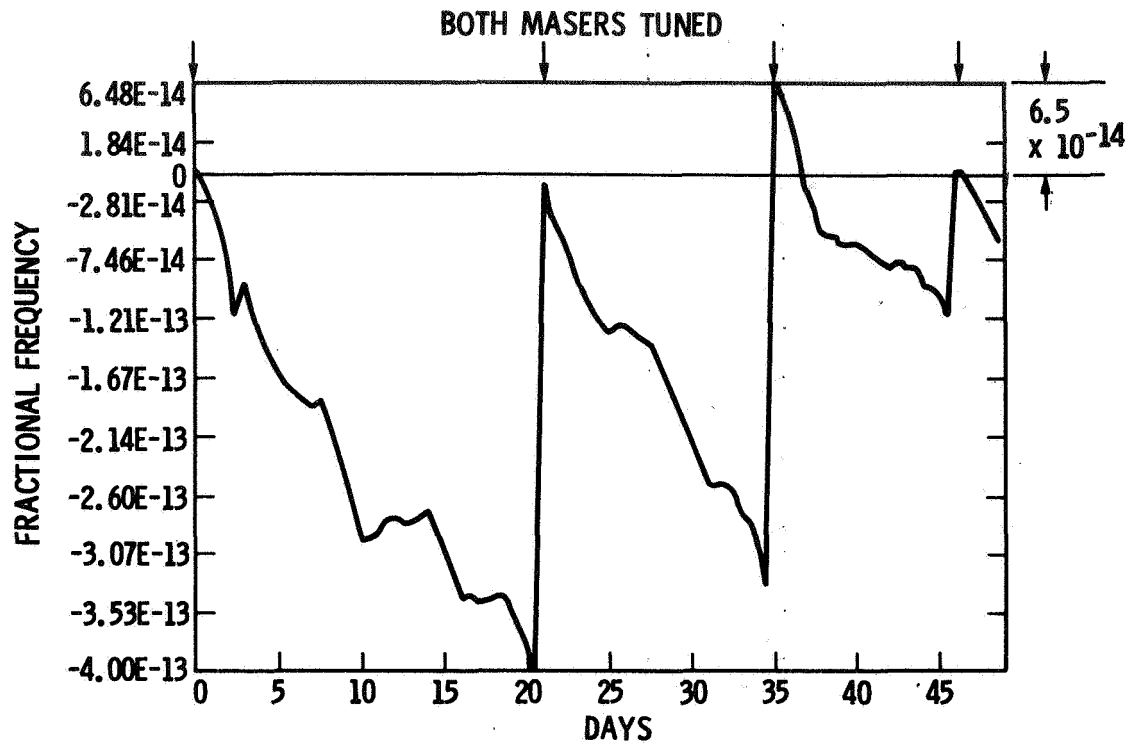
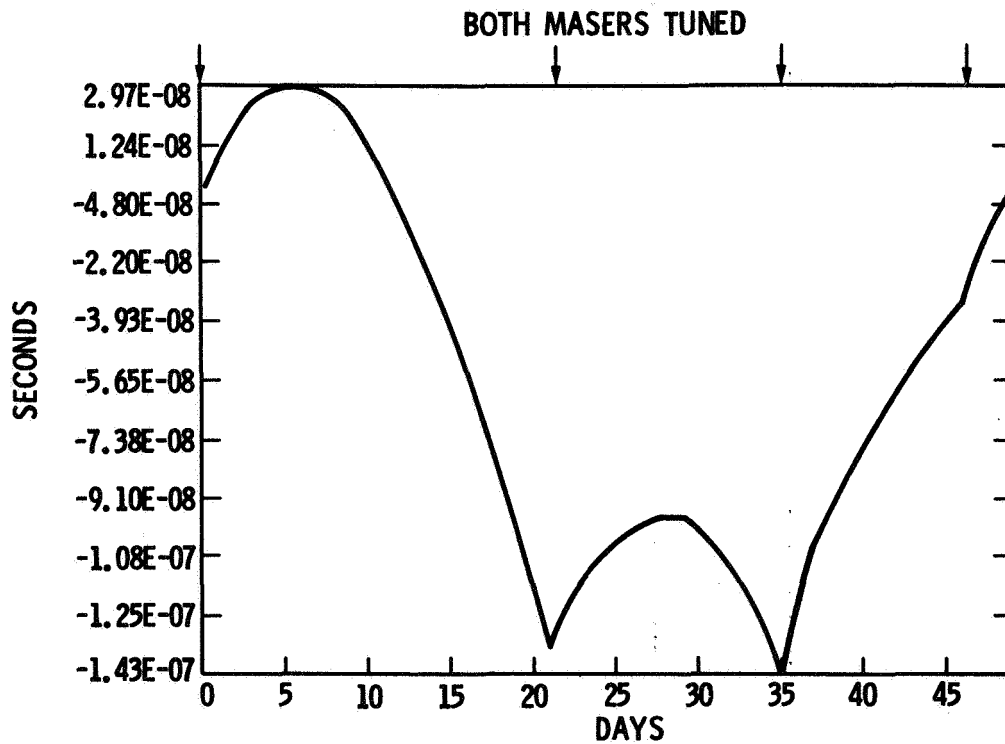


Figure 24. Tuning Repeatability of NR-4 and SAO-14



**PLOT OF TIME RESIDUALS AFTER REMOVING A MEAN
FREQUENCY OFFSET OF -1.64×10^{-13}**

Figure 25. Time Residuals Between NR-4 and SAO-14

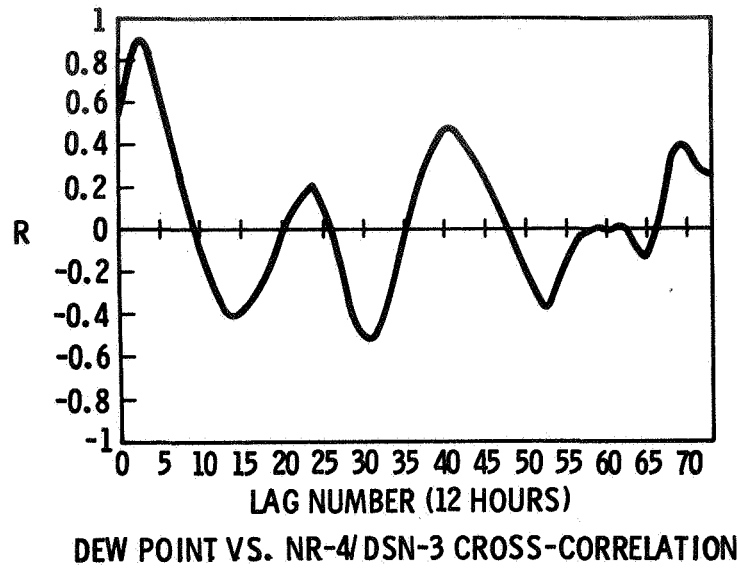


Figure 26. Dew Point vs. NR-4/DSN-3 Cross-Correlation

Table 2. Coefficients: Masers vs. Dew Point

FREQUENCY STANDARD PAIR	R_{PEAK}	DELAY (DAYS)
NR-4/ DSN-3	0.895	1.5
SAO-14/ DSN-3	-0.729	0
NR-4/ SAO-14	0.911	1.0
DSN-2/ DSN-3	0.878	2.5
DSN-2/ SAO-14	0.861	2.0
DSN-2/ NR-4	0.789	3.5

COEFFICIENTS: MASERS VS. DEW POINT

Table 3. Reliability

	SAO-14	NR-4
GROUP I NOT AFFECTING RELIABILITY	1	2; 10%
	2	11; 55%
	3	0; 0%
	11; 68%	13; 65%
TOTAL		
GROUP II AFFECTING RELIABILITY	4	3; 15%
	5	1; 5%
	6	3; 15%
		5; 32%
TOTAL		
OUT OF SERVICE	SAO-14	NR-4
	906; 100%	564; 100%
	14; 1.6%	7; 1.25%
	3; 0.3%	7; 1.25%
TOTAL DAYS AND PERCENTAGE OF MASER DOWNTIME		14; 2.5%

QUESTIONS AND ANSWERS

DR. WINKLER:

I have a suggestion concerning that hump, that mysterious hump beyond 400,000 - 500,000 seconds. We have seen in several of our data a weekly spectrum line, and it's typical for human activity. And there is even multiples of that because when we start a week, on Monday or Tuesday, you pick up sometimes again on Thursday or Friday. There are powerful equations which go with a weekly rate. And I would suggest to take a look at that influence.

MR. KIRK:

Yes. I think that's a very good comment. -- That's the thing to look for.

FIRST EXPERIENCES WITH THE H-MASER EFOS 1

Wolfgang Schlüter, Klemens Nottarp, Dieter Feil
Institut für Angewandte Geodäsie (IfAG; Abt. II DGFI),
Frankfurt am Main,
Sonderforschungsbereich 78 Satellitengeodäsie (SFB 78),
TU-München
Federal Republic of Germany

Giovanni Busca
ASULAB, S.A., Neuchâtel
Switzerland

ABSTRACT

The H-Maser developed at ASULAB, S. A., Neuchâtel/Switzerland called EFOS 1 (Etalon Frequence Oscilloquartz) has been moved from Neuchâtel to the Satellite Observation Station Wettzell, Federal Republic of Germany. The results are given on the performance measurements, on the dependence on external temperature and on external magnetic field, which are derived

at ASULAB by comparison with the H₁-Maser. The experiences on the transportation of the H-Maser in operation are presented and the installation at Wettzell is described. The H-Maser-frequency is compared with the Caesium-oscillators of the station to derive the long term behavior.

INTRODUCTION

The Institut für Angewandte Geodäsie acting within and on behalf of the Sonderforschungsbereich 78 (Satellitengeodäsie) is operating the satellite observation station Wettzell 400 km east of Frankfurt. The station Wettzell is equipped with a satellite laser ranging system, which will be extended to track the moon, and with satellite Doppler receivers. A radiotelescope for geodetic VLBI is under construction. A time and frequency system is available at the station to support the measurements with the required precise time- and frequency-informations [Schlüter et al. 1981]. To achieve highest accuracy in the VLBI-measurements a H-maser will be used. The Swiss laboratory ASULAB/Oscilloquartz offered to build a H-maser for these purposes; after that they decided to start the development of a commercial maser. The EFOS 1 Maser (Etalon Frequenz Oscilloquartz) has been conceived in order to obtain optimum frequency stability for averaging times between 100 s and 10 000 s for the requirements in VLBI. Additionally the design goals are high reliability, easy maintenance and cost effectiveness. The design of the maser was described by Busca in [Busca et al., 1982].

After the factory acceptance test the maser was delivered to IfAG on July, 23 1982. The maser was transported to Wettzell in

full operation. The time and frequency system at the station in Wettzell consists now of 3 Cs-clocks, 4 Rb-clocks, 1 H-maser (EFOS 1) and 3 BVA-quartzcrystal oscillators. The constellation of the frequency generators at Wettzell does not allow to determine the maser frequency drift on the basis of measurements over a period of 3 month. This paper describes the results of the acceptance test performed at the laboratory of ASULAB using their maser H1 and the first experiences at Wettzell station.

MASER PERFORMANCE DERIVED DURING THE ACCEPTANCE TEST AT ASULAB

The acceptance test of the H-maser EFOS 1 has been performed in the period from 19th to 22nd July 1982 at the laboratory of ASULAB. The test procedure includes

- the thermal sensitivity
- the magnetic sensitivity
- the frequency stability (1s, 10s, 100s, 1000s)

The conditions for the test procedures were not the best: A few hours before starting the acceptance test it was necessary to replace the high voltage ion pumps power supply which required interruption of about 3 hours of the masers normal operation. Later during frequency stability test a main power failure occurred (thunderstorm) which caused a complete interruption of the reference maser H1 and the air conditioning system.

It is clear best performance results could not be achieved under such conditions. In the following the test results are presented and also those results are given which have been determined from measurements preceding the acceptance test.

a) thermal sensitivity

The temperature was changed stepwise (from 22.8 °C to 18.8 °C) and the corresponding frequency shift was measured by comparison with the frequency of the reference maser H1, which was kept at a constant temperature. The thermal sensitivity was obtained as

$$\Delta f/f = +1.7 \times 10^{-13} / \text{degree Kelvin.}$$

As the thermal test were performed only some hours after the high voltage power supplies replacement, the frequency of EFOS 1 was not stabilized enough and the detected frequency change was not only caused by the temperature change. These data do not correspond to the measurements preceding the acceptance test, made under stable conditions which give a thermal sensitivity of

$$\Delta f/f = -2 \times 10^{-14} / \text{degree Kelvin.}$$

b) magnetic sensitivity

Two thin square coils were used to simulate variations of the vertical components of the ambient magnetic field. The maser frequency (EFOS 1) was measured by comparison with the frequency of the undisturbed second maser H1 in the following sequence. The ambient field increment was changed twice from + 500 mGauss to - 500 mGauss without frequency measurement to eliminate the possibility of transient hysteresis effects. After that 5 cycles of frequency measurements (100 s) have been performed by an ambient field of + 500 mGauss resp. - 500 mGauss and by a C-field of 415 microGauss. The sensitivity was obtained as

$$\Delta f/f = - 1.4 \times 10^{-13} / \text{Gauss}$$

c) Stability Test

Obviously under the given environmental conditions the frequency stability test results can not be as good as under stable conditions.

The Allan Variances derived under the test conditions are given in table 1 compared to the results obtained under stable con-

τ in s	test conditions		stable conditions	
	$\sigma (\tau)$	number of samples	$\sigma (\tau)$	number of samples
1	4.1×10^{-13}	100	1.5×10^{-13}	100
10	6.7×10^{-14}	100	1.9×10^{-14}	100
100	7.7×10^{-15}	100	6.5×10^{-15}	100
1000	3.5×10^{-15}	63	1.7×10^{-15}	100
10000	-	-	2.6×10^{-15}	18

Table 1, frequency stability of EFOS 1 derived during the acceptance test and derived under stable conditions.

ditions. The measurement system bandwidth was 1 Hz for the test conditions and 6 Hz for the previous measurements. Consequently the 1 s and 10 s values measured under stable conditions have been normalised to 1 Hz bandwidth. The frequency stability measurement system has been described in [Busca et al., 1982].

TRANSPORTATION FROM ASULAB/NEUCHÂTEL TO WETTZELL

The H-maser was transported from Neuchâtel to Wettzell in full operation without interruption (figure 1). The transportation took around 24 hours with 10 hours driving on a distance of about 650 km. 1 Stop during night time was necessary, which was used to charge the batteries.

INSTALLATION AT WETTZELL

The maser was installed in a small cellar room of about 2.5 m^2 , which is thermally isolated (cold thermostat). The maser was put on a sand-filled trough in which a granite plate is "swimming" to protect the maser against vibrations transferred by the ground. The complete trough stands on a 2 cm thick rubber plate (figure 2).

After the transportation and the installation of the maser, low current degaussing was needed.

The temperature in the maser room climbed up to 27° C in July and August mainly caused by the hot summertime we had in Europe. Now the temperature is 25° C . The room is isolated in such a manner that no daily temperature variations were observed.

MASER FREQUENCY CHANGE DUE TO TRANSPORTATION

Before the acceptance test the maser cavity was tuned by spin-exchange technique using the maser H1 as a reference. The tuning was done for two different values of the "C" field

(namely 83 μ Oersted and 415 μ Oersted). The results show that the cavity tuning setting was independent of the "C" field within the error of 1×10^{-14} . The nominal "C" field value was set and the synthesizer frequency was adjusted to the value required for compensating the evaluated Wall shift ($- 2 \times 10^{-11}$) and the second order Doppler shift ($- 4.3 \times 10^{-11}$). The maser frequency was compared with a commercial Cs-standard and a relative frequency off-set of 4.5×10^{-13} was found. After the installation at Wettzell the maser frequency was compared with the 2 Cesium standards and a frequency off-set of $< 1 \times 10^{-12}$ was measured. This implies that no major changes of the maser frequency occurred during the transportation.

THREE MONTHS EXPERIENCES AT WETTZELL

The maser frequency was controlled against the frequencies generated by the Cs-Standards over a period of about 80 days. Phase measurements of the 5 MHz signal of the maser against the 5 MHz output of the Cs-standards have been carried out with a HP-5370 A counter. To eliminate the noise of the Cs-standards a mean value was determined by measuring of $10 \times 100\,000$ samples of the time elapsed between the zero point crossings of the EFOS-frequency and Cs-standards-frequency. The precision of the mean phase measurement is better than 0.1 ns. The results of the measurements are plotted in figure 3. The measurements were performed against the two Cs-clocks (CS 7/Ser. No. 131 and CS 8/Ser. No. 173). Curve I shows the LORAN C comparisons of the CS 7 (daily phase value correction is taken into account) and gives the frequency relation to UTC (USNO-MC). The second curve (II) shows the comparison of the two used Cs-standards and curve III and IV give the maser-frequency compared to the Cs-standards.

The first change in the slope appears in curve I, II and III and happen after the installation of a BVA-quartz oscillator next to the CS 7 frequency generator (Mod. Jul. date = 45 199). A correlation of both events, the BVA-installation and the slope change, can not be excluded.

A slight change occurs in the curve III and IV (on Modified Julian date = 45 214). The change is obviously caused by a change of the maser frequency, possibly due to thermal effects (figure 4).

The maser stopped its operation on Mod. Jul. date = 45 226 due to a power interruption at the station over three hours. Possibly the vacuum became too low and the maser stopped the oscillation. The correct vacuum was restored after 2 days elapsed. The following frequency comparisons indicate only a small difference against the frequency before the maser interruption (2×10^{-13}).

The last change of frequency in figure 3 appears on the curve II and IV on MJD = 45 255. The CS 8-standard was moved from the temperature uncontrolled laboratory room to a separate, isolated cellar (cold thermostat) which has been finished at that time.

The measurements plotted in figure 3 were fitted by a linear approximation. The slope was determined for the curve 2, 3 and 4 within $< \pm 3\text{ns/d}$ and for the curve I within $< \pm 10\text{ns/d}$. The residuals are given in figure 5. The Allan Variance was estimated as

$$\sigma_{\text{EFOS-CS}} \sim 2.5 \times 10^{-13} \text{ (over 1 day)}.$$

It is obvious, that this value is mainly influenced by the Cs-standard behavior. The Allan Variance estimated from the CS 7 against CS 8 measurements is

$$\sigma_{\text{CS } 7/\text{CS } 8} (1 \text{ day}) \sim 6 \times 10^{-13}.$$

Assuming the same quality for both Cs-standards the performance of the Cs-oscillators could be estimated as

$$\sigma_{\text{CS}} (1 \text{ day}) \sim 6 \sqrt{2} \times 10^{-13} \sim 4 \times 10^{-13}$$

It has to be pointed out, that the H-maser performance could not be estimated on the basis of the measurements over a 3 month period by the clock ensemble of Wettzell. From the given results it could be stated, that the 1 day behaviour of the maser is better than from the Cs-standards. To have results for more than $\tau = 1$ day, longer undisturbed series of observations are needed. However no systematic frequency drift of the maser could be ascertained, which will show up as a parabolic curve in the figure 3. An upper limit of the maser frequency drift from the present data can be roughly estimated as $< 1 \times 10^{-14}$ /day.

Studies on oscillator performance have been started by e.g. comparing the phase of the maser frequency against the Cs-clocks and the BVA quartz-oscillators. Currently no results are available. To demonstrate that good results will be expected the phases of a BVA oscillator and of a Cs-oscillator against EFOS are plotted in figure 6. The smooth curve is the phase of the BVA-crystal-oscillator. Full scale of each record is about 10 ns.

References:

- [1] Schlüter, W.;
Nottarp, K.: Applications of Time and Frequency in Geodesy, IETE, Vol 27, No. 10, 1981
- [2] Busca, G.;
Addor, F.;
Hadorn, F.;
Prost, L.;
Brandenberger, H.;
Thomann, P.;
Johnson, L.: Preliminary Measurements on EFOS 1 H-Maser, paper presented at the 36th annual Symposium on Frequency Control, 1 - 4 June 82, Philadelphia, U.S.A.

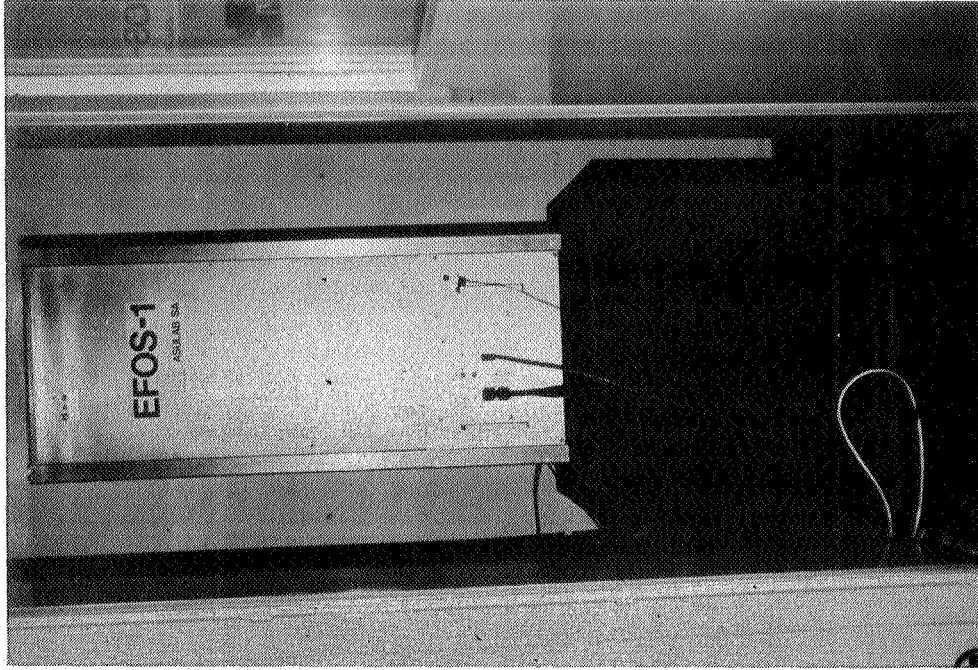


Figure 2 - Maser installed at
Wettzell.

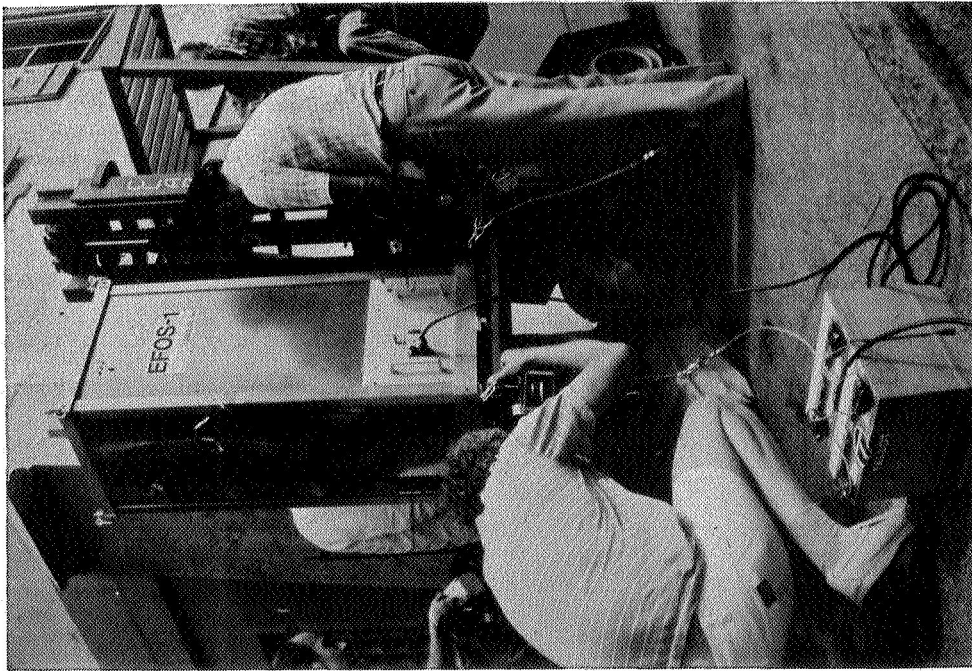
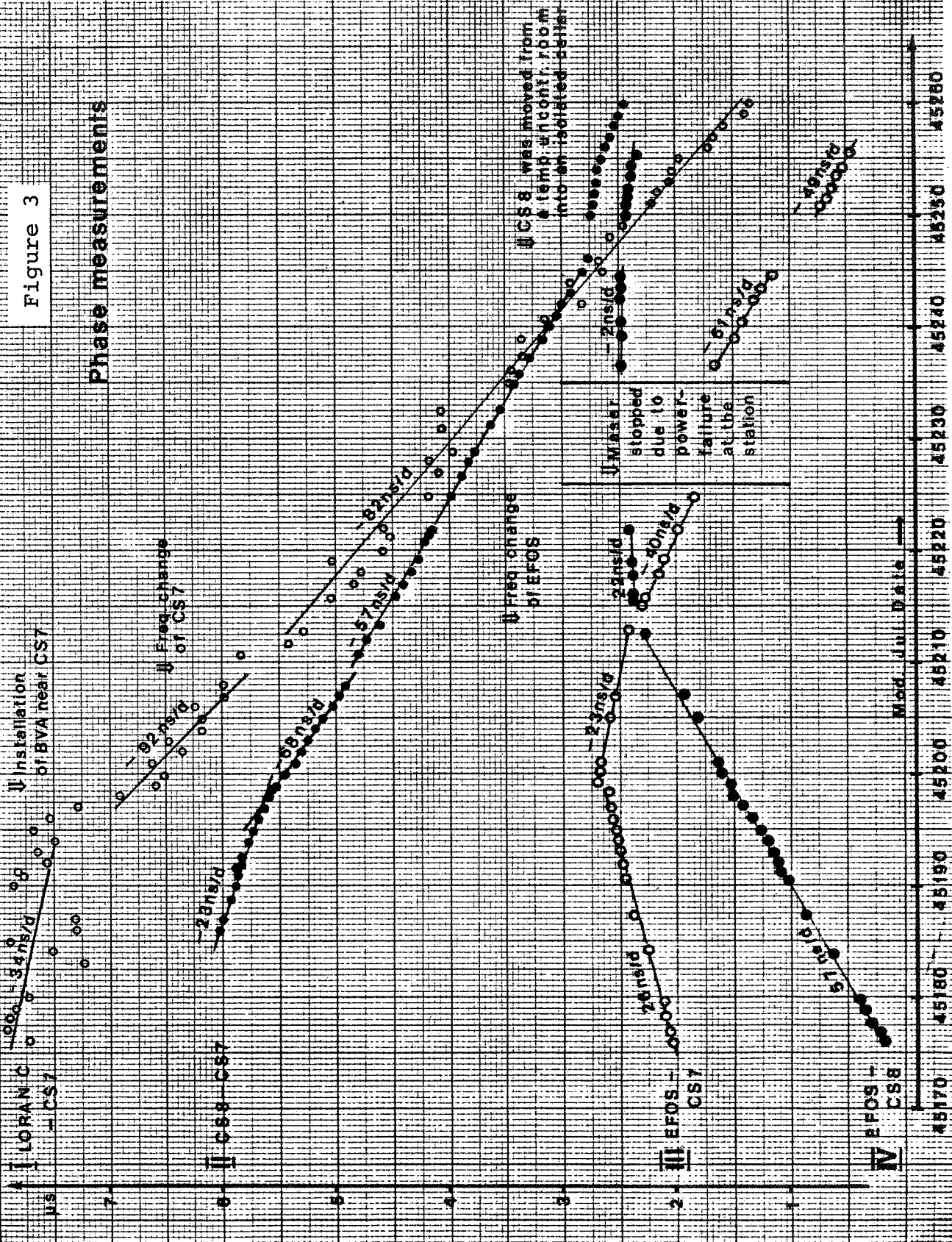


Figure 1 - Transportation of the
Maser from Neuchâtel
to Wettzell in operation.

Figure 3

Phase measurements



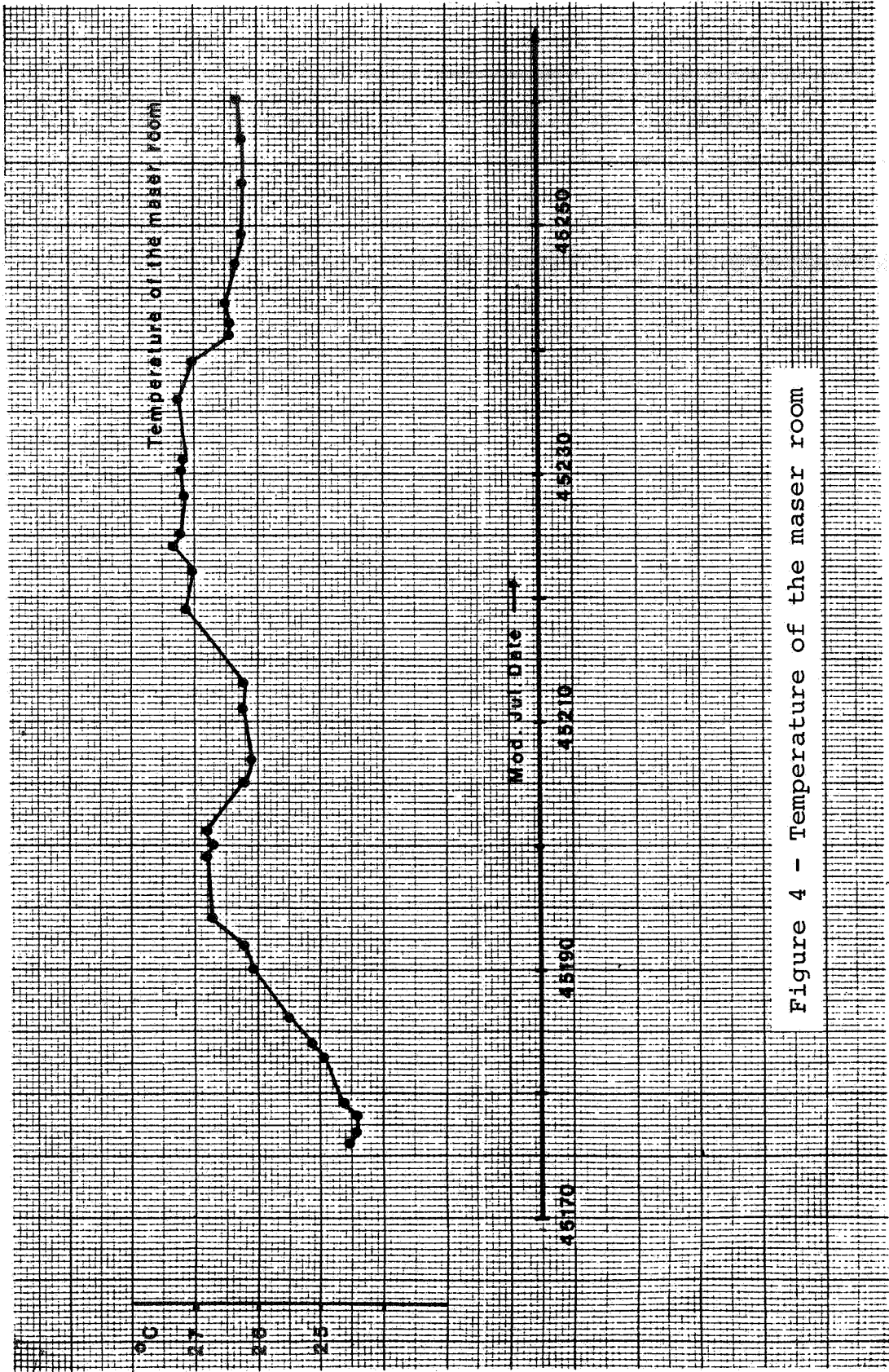
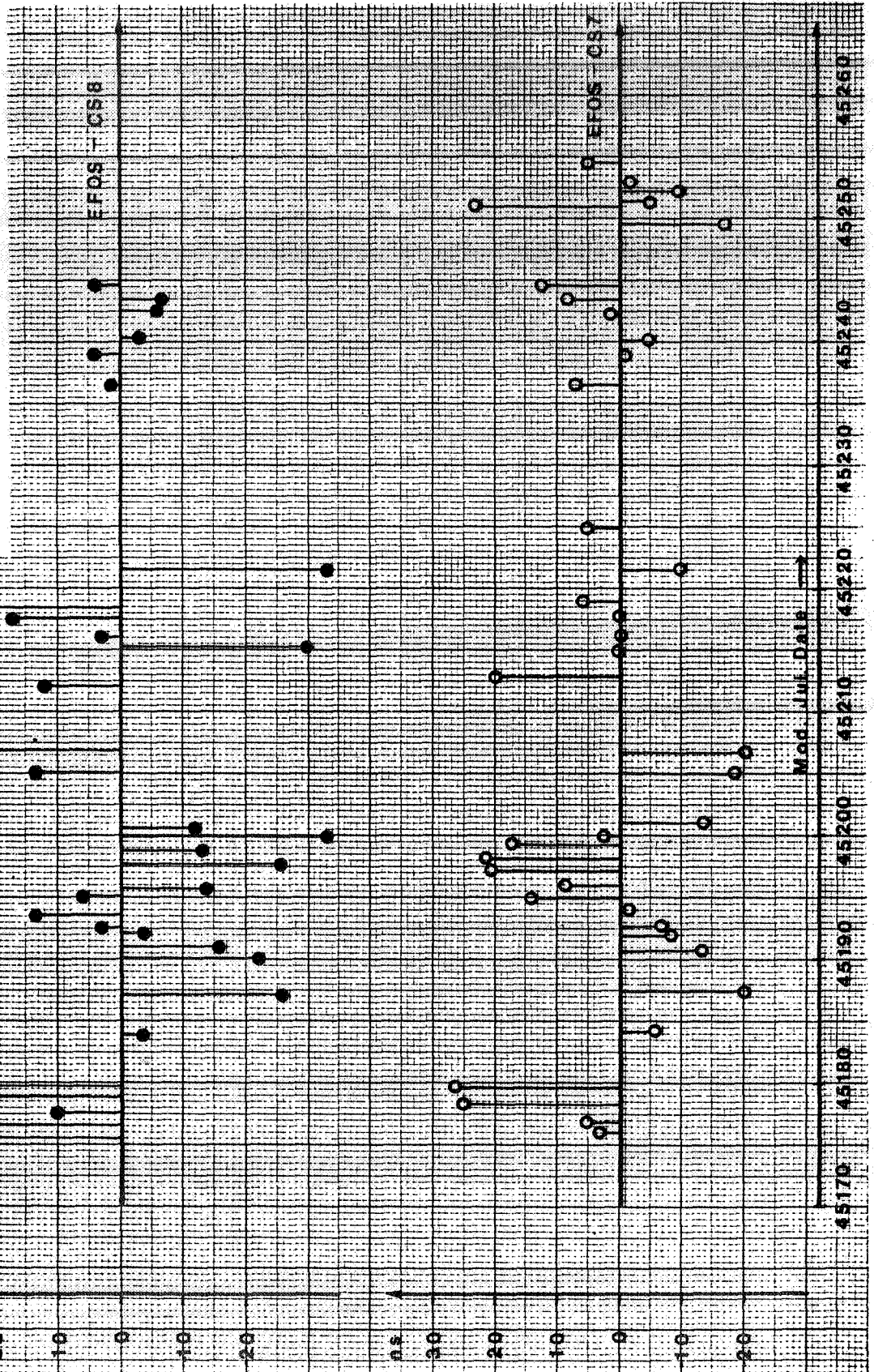


Figure 4 - Temperature of the maser room

Figure 5 - Residuals of the phase measurements after a linear fit.



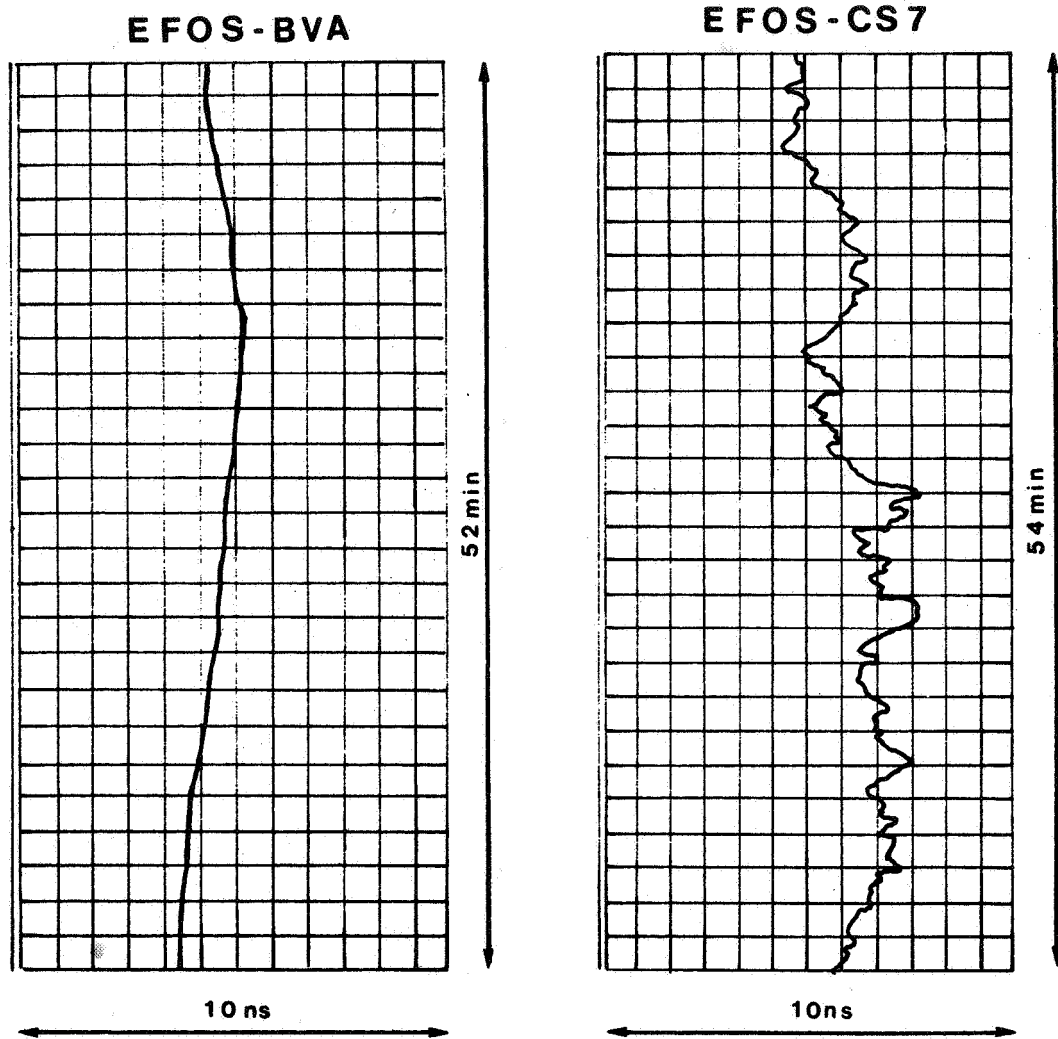


Figure 6 - Phase - comparisons of
the BVA-quartz oscillators
against EFOS, CS-oscillator
against EFOS

QUESTIONS AND ANSWERS

DR. COATES:

Any questions?

MR. SAM WARD, Jet Propulsion Laboratory

I noticed that after the power failure, the drift term changed. Is there any explanation for that?

MR. BUSCA:

After the power failure, this is the drift we had before. This is after only a rate of twenty nanoseconds per day. I have no explanation, maybe it's due to thermal effects because the cellar room is not well insulated.

MR. LAUREN J. RUEGER, JHU/APL

Do you have a means to flux tune the masers after you are on the station site?

MR. BUSCA:

No.

DR. COATES:

Did everybody understand that? Your answer was "no", right?

MR. BUSCA:

Yes.

A COMMERCIAL HYDROGEN MASER, PROGRESS REPORT

M. Dials and L. Wert
Efratom
Division of Ball Corporation
Irvine, California

ABSTRACT

Efratom Systems Corporation has been participating in an NBS Industrial Research Associate Program since July, 1981. One of the goals of this program is to produce new and improved small passive hydrogen masers. Efratom will then develop a commercially available full production hydrogen maser.

This paper describes the design of the new small passive hydrogen maser prototype and some anticipated design changes between the version reported in this paper and the commercial versions.

Specifications of the commercial hydrogen maser and performance data of the prototype are given.

INTRODUCTION

This paper describes a program that has been in progress for about a year and a half to design, build and test a Compact Passive Hydrogen Maser atomic frequency standard, in a form suitable for quantity production, with the goal of making this instrument widely available in the commercial market place. The design is derived from the extensive technology in passive hydrogen masers, evolved over the past five years at the National Bureau of Standard by Dr. Fred Walls and his co-workers.

Efratom Systems Corporation has entered into the Industrial Research Program with NBS to effect the transition of the laboratory accomplishments to the level of a practical and economically producible system. It is a major objective of this program to achieve small size and high reliability, while preserving the extraordinary performance already demonstrated by the NBS passive maser.

System design

Figure 1 shows the overall compact hydrogen maser block diagram. The description of operation of the passive hydrogen has been presented in previous NBS publications [1,2,3,4], therefore only the changes in the new design will be described.

Physics package

The primary change in the physics package (see figure 2) is the use of a quadrupole magnet as the state selector. (The old design uses a hexapole magnet.) The use of a quadrupole has two advantages. First, it permits a reduction in the length of the physics package from 36 to 19.5 inches. Second, it increases the efficiency of state selection thereby allowing a reduction in the flux of molecular hydrogen required to achieve an acceptable signal to noise. The use of a quadrupole should allow at least a factor of two reduction in the present H₂ consumption rate. This latter advantage of the quadrupole is extremely important because it has a very beneficial impact on the requirements for the maser vacuum system and H₂ storage, allowing a significant decrease in the overall size and weight of the maser without sacrificing reliability.

Frequency synthesizer

A new synthesizer was designed for the maser to provide finer output frequency adjustment resolution than was available with the commercial synthesizer used in the old design. The new synthesizer can adjust the output 5.0 MHz in 2×10^{-4} steps over a range of $\pm 2 \times 10^{-1}$

Two synthesizers have been built, and spectral purity and output isolation measurements were made with the following results:

L(f)@ 5 MHz	-116 dB @ 1 Hz
	-140 dB @ 10 Hz
	-160 dB @ 100 Hz
Isolation (Output to Output)	119 dB

Dissociator

Three dissociator cell sizes were tried, and it was found that a smaller cell is generally more efficient. Also, if RF power is scaled in accordance with cell size, there is some indication that a small cell may be more reliable.

As a result of these studies a cell size of 19 mm O. D. by 46 mm long was chosen. Once fabricated, the pyrex cell is annealed for approximately eight hours with hydrogen flowing through it.

The dissociator electronics is a single transistor self-excited oscillator, based on the design used in EFRATOM's rubidium oscillator. High electric fields are present before the discharge is ignited; these fields are sufficient to ignite the discharge. Once lit, the field intensity is substantially reduced and coupling to the plasma is evenly distributed over the cell surface. The nominal D.C. operating power of this circuitry is about 2.0 watts. This low power dissipation has several advantages:

- 1) No active cooling is required
- 2) Only about a third of this power (.7 watts) is dissipated in the bulb, thereby keeping the temperature rise low, which should help increase life
- 3) The relatively low energy plasma will keep deterioration of the bulb's inside wall to a minimum, thereby increasing life

Dissociation efficiency was measured comparing input power to atom flux for various dissociator configurations. Measurements of atom flux were performed using a kapton-platinum recombination detector in a balanced bridge. Some test results are shown in figure 4. For further information see [5].

Performance Data

Figures 3, 5 and 6 show data taken at NBS on the NBS small passive hydrogen maser. The primary differences between the NBS maser and the new commercial maser (CPHM) are:

- 1) CPHM has a new microwave amplifier that improves noise figure by about 3.5 dB. This should improve short term performance by a factor of about .67.
- 2) CPHM has the new frequency synthesizer
- 3) CPHM uses a quadrapole state selector with shorter beam optics
- 4) CPHM has a new hydrogen pressure servo loop which will directly servo hydrogen atom density in the storage bulb
- 5) CPHM has magnetic shielding around the source end to reduce the maser sensitivity to changes in ambient magnetic field

Figure 3 shows Allan variance data that was obtained by comparing the NBS passive hydrogen maser against three other clocks. The clocks were NBS-4 (a stable laboratory cesium standard) and the two best commercial cesium clocks in the NBS ensemble. Three-cornered hat analysis was performed on three sets of clocks, each set having the maser as one member. The RMS of this data is shown in figure 3.

It should be noted that frequency drift is not removed from the data. Also other measurements of the maser versus the NBS ensemble have not shown a flicker floor for the maser, with data that extends out to thirty-two days.

Figure 5 is a plot of the fractional frequency deviation of the NBS passive maser versus NBS-4 for one day averages. Only an average frequency offset is removed from the data. A linear least squares curve fit to the data shows a drift of about 1×10^{-16} /day. (Note: the reported accuracy of NBS-6, the primary frequency standard, implies an ability to measure absolute frequency drift of 3×10^{-16} /day for long data sets. Given this limit, we have not been able to find a measureable drift in the maser for data runs up to 72 days in length.)

Figure 6 is a plot of the time difference between the maser and NBS-4. Again, only an average offset frequency has been removed. The peak-to-peak deviation for the pair is 10 ns over 38 days.

Figures 7 and 8 are the preliminary specifications for the commercial hydrogen maser. Some of the specifications are derived from data obtained on the NBS small passive hydrogen maser. The specifications will be updated when more data become available on the CPHM, and the device is more fully characterized.

Acknowledgements

We would like to thank all the people in the Time and Frequency Division at NBS for their help. We are especially grateful to Dr. Fred Walls for his help in all areas of maser technology, Dave Howe for his help on the microwave cavity, Dave Allan and Jim Barnes for their help on data analysis, and Dr. Karl Persson for his work on the dissociator.

REFERENCES

1. Walls, F. L., and Howe, D. A., Proc. 12th Annual Precise Time and Time Interval Planning Meeting (1980).
2. Howe, D. A., Walls, F. L., Bell, H. E., and Hellwig, H., Proc. 33rd Annual Symposium on Frequency Control (1979).
3. Walls, F. L., and Hellwig, H., Proc. 30th Annual Symposium on Frequency Control (1976).
4. Walls, F. L., Proc. 8th Annual Precise Time and Time Interval Planning Meeting (1976).
5. Persson, K., and Walls, F. L., NBS Report "Investigation of the Hydrogen Source for Masers", to be published.

CPHM BLOCK DIAGRAM

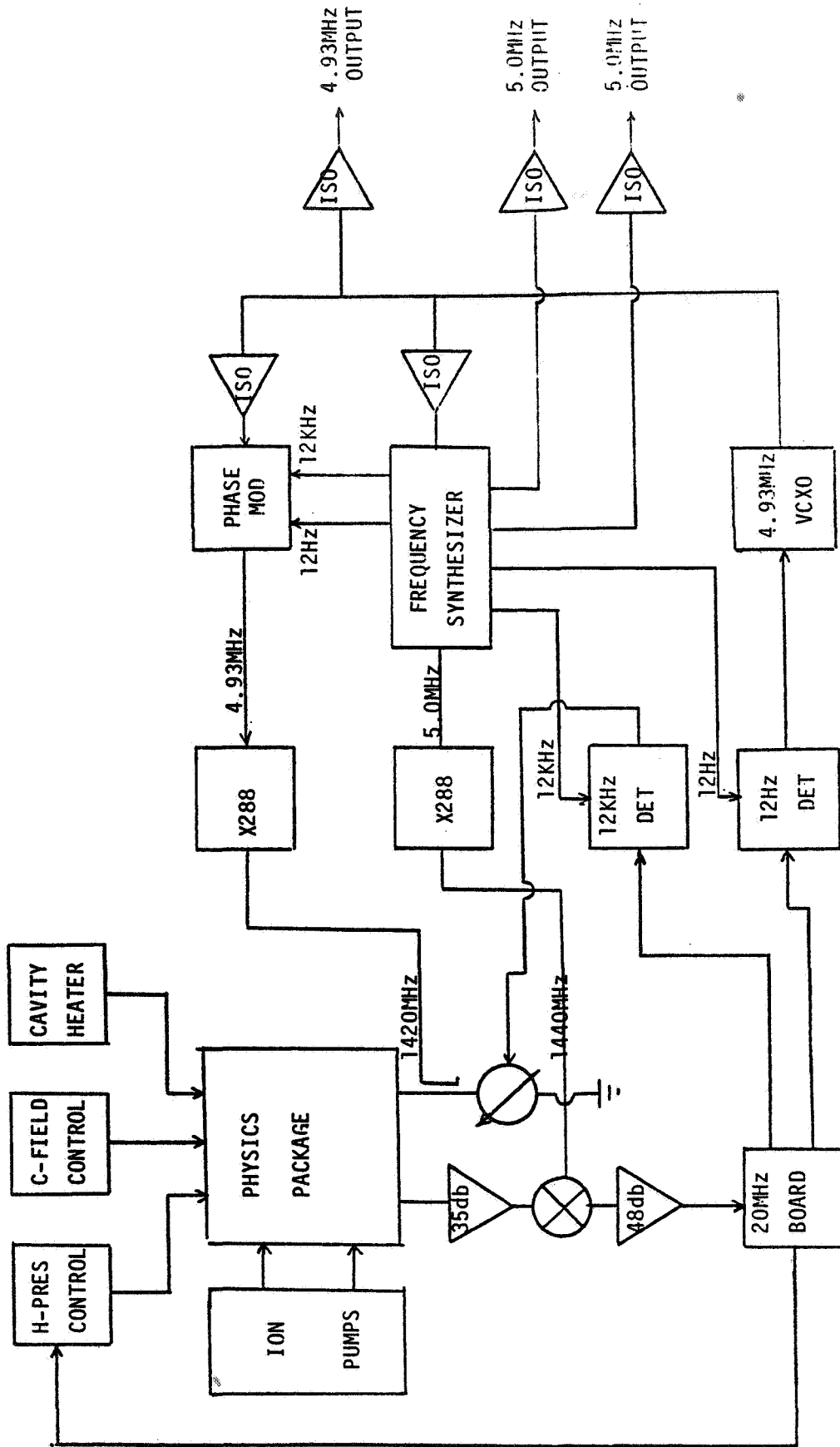


FIGURE 1

PHYSICS PACKAGE

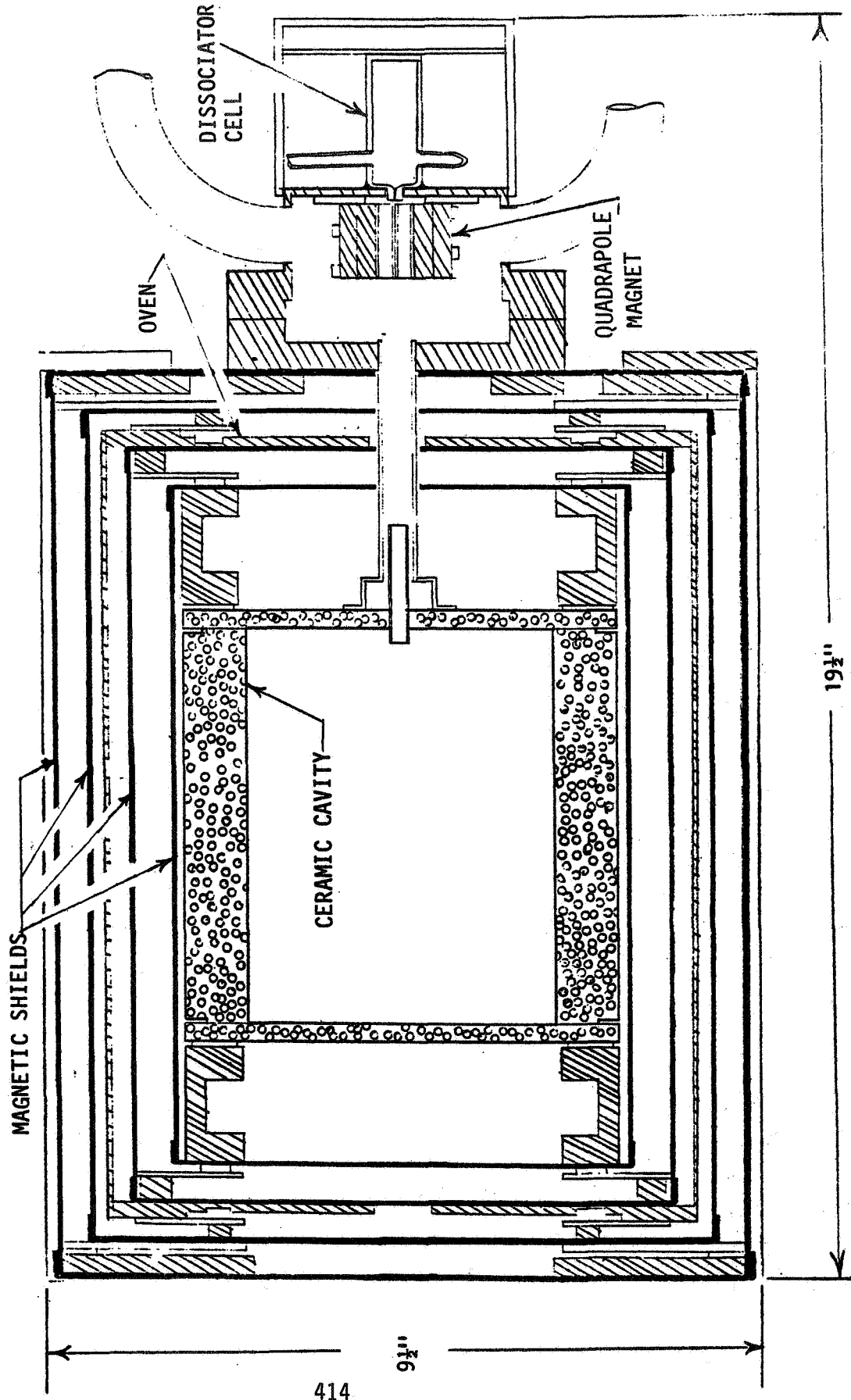


FIGURE 2

PASSIVE HYDROGEN MASER STABILITY

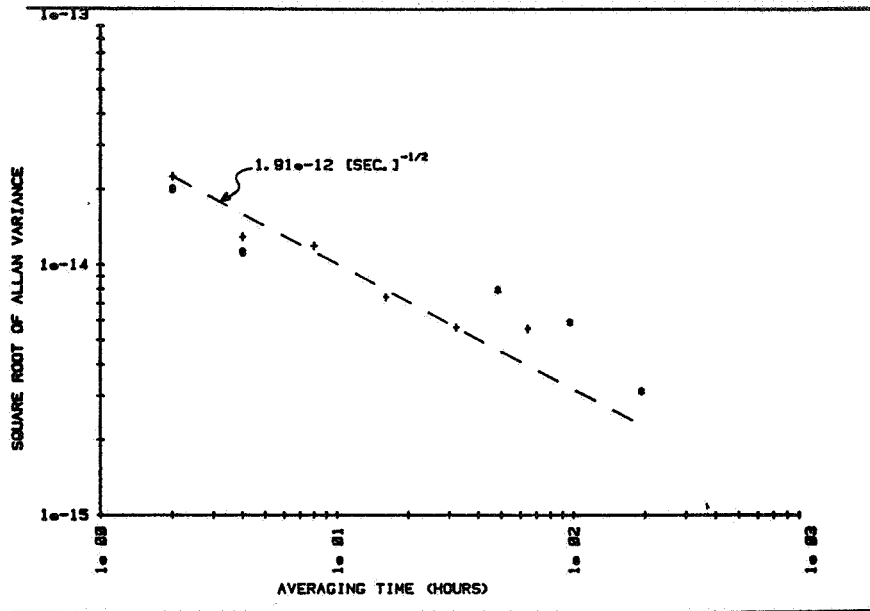


FIGURE 3

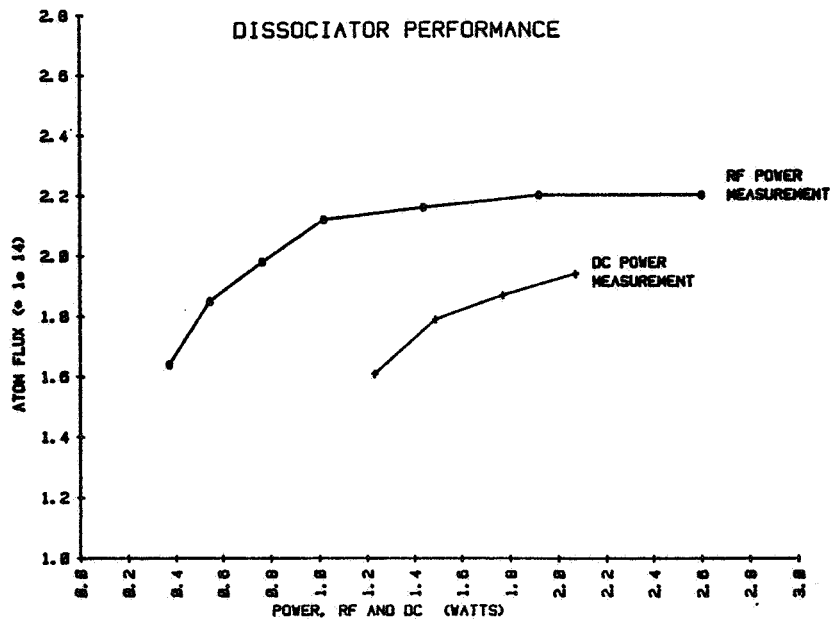


FIGURE 4

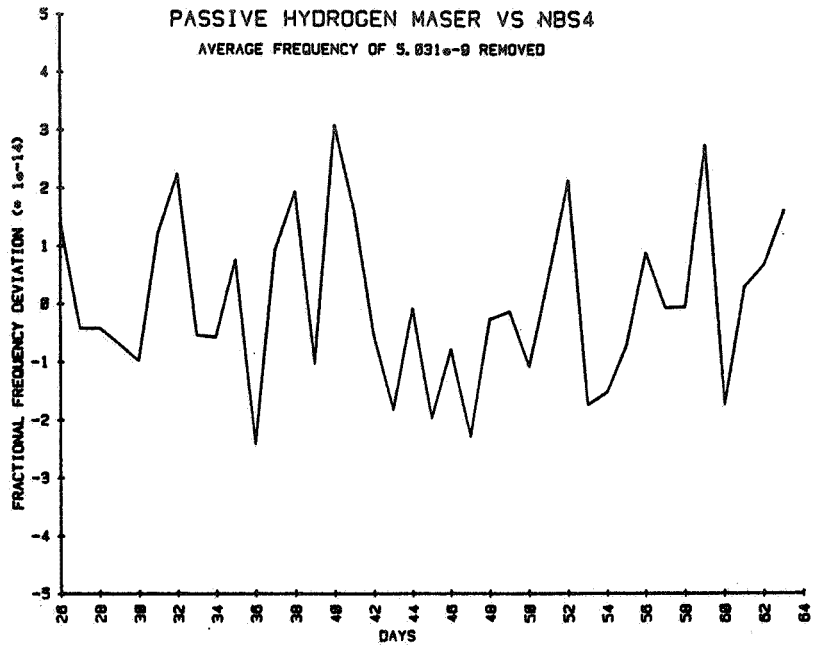


FIGURE 5

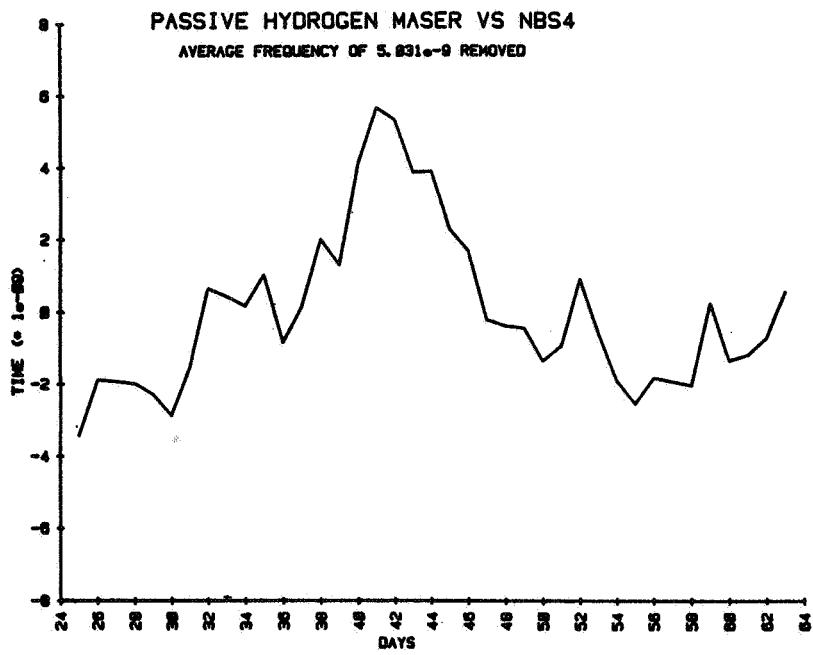


FIGURE 6

Specifications

PASSIVE HYDROGEN MASER PRELIMINARY SPECIFICATIONS

Output	5.0 MHz Sine wave, 1 Vrms, 50 Ω , 2 buffered outputs
Isolation(Output to Output)	>110 dB
Signal-to-Noise Ratio	-113 dB at 1 Hz
L(f) at 5 MHz	-135 dB at 10 Hz -155 dB at ≥ 100 Hz
Short-Term Stability	$\sigma_y = 2 \times 10^{-12} \tau^{-1/2}$ for $1s < \tau < 10,000s$
Long Term Drift	$< 1 \times 10^{-15}$ /day (Note 1)
Max. Frequency Change Over Life of Unit	$< \pm 1 \times 10^{-12}$
Retrace (Turn Off, Turn On)	$< 5 \times 10^{-13}$
Temperature Coefficient	$< 5 \times 10^{-14}$ /°C
Magnetic Field Sensitivity	$1 \times 10^{-13} \Delta f/f$ for Δ ext. field of ± 1 gauss (Note 2)
Input Power (Steady State)	<70 watts
Input Voltages	+28 VDC (Note 3) ± 18 VDC + 9 VDC
Warmup Time	~ 24 hours to lock
Operating Temperature Range	+10°C to + 35°C (Note 4)
Size	19" rack, ~ 14 " high x 24" deep
Weight	60 lbs - 80 lbs
Anticipated Life	>5 years

FIGURE 7

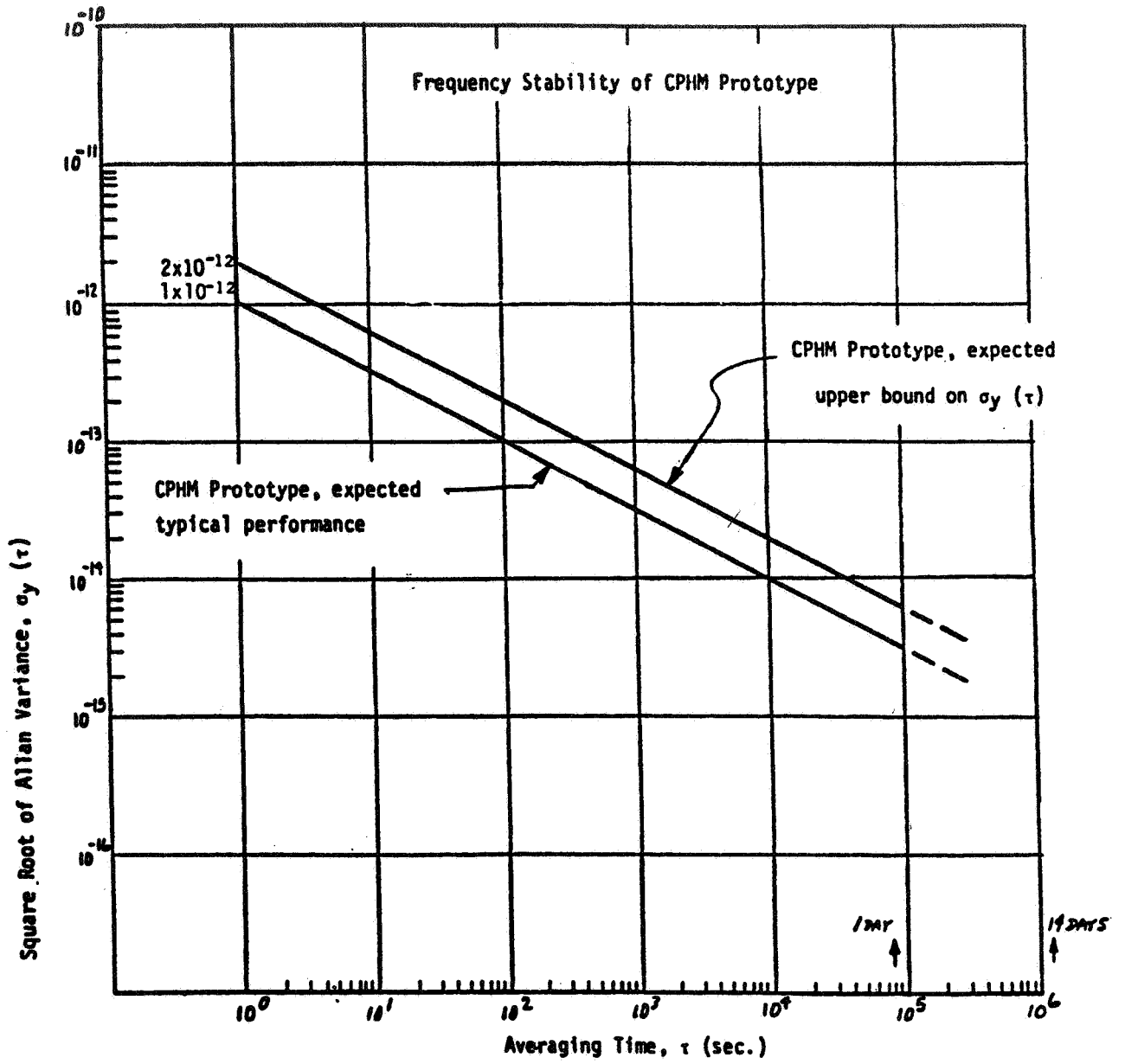


FIGURE 8

QUESTIONS AND ANSWERS

MR. SAM WARD, JPL

Have you any idea as to what is causing the drift?

MR. DIALS:

Basically, like I said, we can't find any left in this particular unit.

MR. SAM STEIN, NBS

I just wanted to say that work has been going on at NBS passive masers since about 1973, and that work was supported the whole time by the Naval Research Laboratory.

AUDIENCE:

What improvement did you find by replacing the hexapole magnet by the quadrupole magnet? Did you improve the efficiency of the source? Have you explained how that happens.

MR. DIALS:

We haven't measured that yet. That particular unit with the quadrupole; we just started looking for the hydrogen line a couple of weeks ago.

The reason we did, we expect to improve the overall size, the overall link, and secondly, we expect to improve the efficiency and we think, based on talks with Harry Peters and some other papers, that we'll buy something on the order of a factor of two to four improvement on the hydrogen line Q. But we have not measured that yet.

DR. COATES:

Thank you.

THE NASA/GSFC HYDROGEN MASER PROGRAM:
A REVIEW OF RECENT DATA

Mary Chiu, Alvin G. Bates, Lauren J. Rueger
(Johns Hopkins University/Applied Physics Laboratory);
Victor S. Reinhardt, Peter Dachel, Richard Kunski, Robert Kruger
(Bendix Field Engineering Corporation);
S. Clark Wardrip (NASA/Goddard Space Flight Center)

ABSTRACT

The NASA/Goddard Space Flight Center Hydrogen Maser Program has had as goals for many years the development of improved field operable hydrogen masers, the improvement of existing field operable hydrogen masers and the development of novel hydrogen maser frequency standards. This paper presents a review of recent data, taken both in the laboratory and in the field, in these areas. Data is presented on the phase and frequency stability, over time periods extending to one week, of the new NR field operable hydrogen masers developed by the Applied Physics Laboratory (APL) and the older NX and NP field operable hydrogen masers developed by Goddard Space Flight Center and maintained and upgraded by Bendix Field Engineering Corporation (BFEC). Data is presented on the NR masers in the laboratory showing frequency stabilities well into the 10^{-15} range and phase stabilities well into the 100 ps range for periods of up to one day. Data is presented on upgraded NP masers in the laboratory showing that the frequency stability has been improved substantially to virtually the NR level. VLBI data is presented on the phase difference between NX-2 at Owens Valley, California and NR-2 at Fort Davis, Texas for a one week period showing, after removal of a constant frequency drift, a 350 ps RMS phase stability. The role of a temperature control chamber for hydrogen masers developed by BFEC in improving the long term stability of hydrogen masers is discussed.

Extensive development work is being performed by both APL and BFEC to improve the performance of hydrogen masers beyond their current levels. A quartz cavity liner designed to retrofit into existing NR, NP, and NX microwave cavity structures has been developed by BFEC and APL in a cooperative effort. This liner has been installed in an NR maser and has been shown to reduce the cavity temperature coefficient by a factor of 8. Data is presented showing the stability of this maser against other NR masers. A completely quartz cavity and storage bulb

ABSTRACT (cont)

structure, called the integral cavity, which will also retrofit into the NR, NX, and NP masers is being developed by BFEC and APL in another cooperative effort. This structure should reduce the cavity temperature coefficient by a factor of 25 or more and should improve the maser's frequency stability under mechanical shock. Data is presented on the recent progress in the development of an external bulb variable volume hydrogen maser primary frequency standard.

INTRODUCTION

The NASA/Goddard Space Flight Center Hydrogen Maser Program has had as its goals for many years the development of improved field operable hydrogen masers, the improvement of existing hydrogen masers, and the development of novel hydrogen maser frequency standards. This paper represents a review of recent data taken both in the laboratory and in the field in these areas. The paper is broken into two basic sections reporting on data taken by Bendix Field Engineering Corporation and the Applied Physics Laboratory of Johns Hopkins University, the two main contractors to the NASA Hydrogen Maser Program.

BENDIX FIELD ENGINEERING

The Bendix Field Engineering Corporation (BFEC) has supported the NASA Goddard Space Flight Center hydrogen maser program for the past ten years. Recently, BFEC has expanded its support in response to the increasing demands of the NASA Crustal Dynamics Project and the NASA research program. Both hydrogen maser maintenance and operations and hydrogen maser research and development are now performed at BFEC's new 4500 square foot Hydrogen Maser Facility located at BFEC Headquarters in Columbia, Maryland.

Thermal Chamber for Hydrogen Masers

Figure 1 shows a thermal chamber developed by BFEC to improve the long term frequency stability of hydrogen masers by improving their thermal environment. These chambers typically reduce room temperature fluctuations by a factor of about 100 and typically keep the temperature of the hydrogen maser from fluctuating no more than 10-20mC in a laboratory environment (1C room temperature fluctuations). Figure 2 shows the thermal chamber with a side panel removed. This shows some of the main features of the thermal chamber:

1. Completely field dismantlable so the unit can be brought into a room through a 30 inch door.
2. Uses thermoelectric coolers for high reliability.

3. Has 18 Rotron fans to create an 1800cfm air flow in the chamber to reduce the effects of temperature gradient changes. (The thermal conductivity of the moving air is equivalent to that of aluminum.)
4. Shock mounts on the chamber and the fans to eliminate 60Hz vibration problems.
5. A failsafe thermostat to prevent accidental overheat of the maser in case of chamber failure.
6. Separate fuses for the thermoelectric coolers and the fans so individual failures in these devices will not keep the chamber from operating.
7. Remote and local alarm outputs.

The chamber has also been successfully used to improve the long term stability of Hewlett Packard high performance cesium standards.

Figure 3 shows typical thermal chamber performance in a good laboratory environment. The figure shows NR-1's upper cabinet temperature and the corresponding air temperature outside the box(smoothed with a 1.5hr time constant temperature probe). In station environments where the temperature has varied as much as 10K, the temperature in the chamber has varied less than 0.1K.

VLBI Data

Figures 4 and 5 show a 7 day phase(group delay) intercomparison between NR-2 at Fort Davis, Texas and NX-2 at Owens Valley, California by very long baseline interferometry(VLBI)(ref1). Figure 4 shows the phase difference in seconds with only a frequency offset term removed from the data(as well as nonclock VLBI terms such as earth rotation). Notice that the data has the quadratic behavior associated with uniform frequency drift. Figure 5 shows the same data with a uniform frequency drift term also removed. The least squares fit used to generate this figure produced clock parameters as follows:

$$\begin{aligned}
 x_0 &= 5686.83(10)\text{ns} \\
 y_0 &= -236.26(04)\text{E-14} \\
 D_0 &= -1.16(01)\text{E-14/Day}
 \end{aligned}$$

The RMS phase(group delay) deviation from the fit was 347ps.

Repair and Upgrade of Hydrogen Masers

Figure 6 shows several NASA NP and NX hydrogen masers being repaired and upgraded in BFEC's Hydrogen Maser Facility. The upgraded NP and NX masers have received new cavity thermal controls, synthesizers, VXCO's, receiver components, and distribution amplifiers and have had the physics packages rebuilt. Figure 7 shows the before upgrade and the after upgrade frequency stabilities of NP-2 measured against NR-6 from 1 to 1000

seconds averaging time. Notice the almost one order of magnitude improvement in performance. Figure 8 shows the frequency stability of the upgraded NP-2 and the non-upgraded NP-3 measured against NX-3 from 10^3 to 10^5 seconds averaging time. NP-2 and NX-3 were in thermal chambers and NP-3 was not. Thus the factor of ten or more long term stability improvement shown is due both to the maser upgrade and the use of the hydrogen maser thermal chambers.

Quartz Cavity Retrofits for NP, NX, and NR Hydrogen Masers

BFEC and APL have a joint effort to improve the temperature coefficient and the mechanical stability of NP, NX, and NR hydrogen masers with retrofitable quartz cavities. There are 2 retrofitable designs being developed. The Hybrid Cavity shown in Figure 9 uses a quartz cylinder coated on the outside with silver as an internal liner in the microwave cavity. This reduces the temperature coefficient of the microwave cavity by about a factor of 5, but still allows the microwave cavity's frequency to be set with tunable end plates and allows one to use temperature tuning of the cavity as with the conventional aluminum cavity. The Hybrid Cavity is being tested in NRB by APL and is reported on in the APL section. The temperature coefficient of NRB with the Hybrid Cavity has been measured by APL as $6.9(9) \times 10^{-15}/C$.

The second retrofitable design being developed is the Integral Cavity whose main components (storage bulb not shown) are shown in Figure 10. In the integral cavity all the parts making up the microwave cavity are made of quartz. After trimming the cavity to the proper frequency, all the pieces (including the storage bulb) will be fused or cemented together. This design will have a cavity temperature coefficient a factor of 25 smaller than a conventional aluminum cavity and should achieve greater mechanical stability because of the fusing of the pieces. An integral cavity has already been fabricated and will be tested in NRX. It has not been determined yet whether temperature or varactor tuning will be used.

External Bulb Hydrogen Maser

The External Bulb Hydrogen Maser is a variable volume hydrogen maser being developed by BFEC for NASA. The purpose of the maser is to provide a primary hydrogen maser frequency standard which will eliminate teflon wall frequency shifts and other accuracy limiting frequency shifts to the 1×10^{-14} level(ref2). As part of the development effort, the maser has been tested with a 1/2 mil thick teflon film bulb and a long time constant collimator (without the external bulb). The results of that test demonstrating an operating line Q of $6.5E9$ are shown in Figure 11. The maser has also successfully operated at 90C. Currently the maser is being rebuilt to overcome magnetic problems.

NR MASER STABILITY DATA

The NR maser, shown in Fig.12, has several advantages over the earlier NX and NP masers. Their biggest advantage is an internal 64-channel microprocessor. This microprocessor provides diagnostic and monitoring information on many maser operations, and provides automated control for cavity tuning. Cavity tuning can be accomplished by autotuning against another maser or the crystal oscillator internal to the maser; or by programming the microprocessor to adjust the cavity for a predicted drift. Stability data on several NR masers are presented. These data were measured in the Time and Frequency facility of The Johns Hopkins University Applied Physics Laboratory.

Maser Intercomparisons

Stability measurements between two or more masers are accomplished by offsetting the frequency of one of our masers, NR-6, by -5×10^{-8} . The signal from NR-6 can then be mixed with the signal from a second maser at 200 MHz to obtain a 10 Hz beat. An HP 5300 time interval counter is then used to measure the phase difference between NR-6 and a second maser. This measurement technique using an offset maser provides a 20 million multiplication factor for the time interval measurement; one millisecond on the counter corresponds to 50 picoseconds of phase difference at 200 MHz.

During all the data runs to be presented, NR-6 was located in an environmental control chamber; and was programmed to compensate for a predicted cavity drift. At regular intervals, but not during any of the data runs presented here, NR-6 was tuned.

Recently we began using an automated system for recording phase difference measurements between three maser pairs (all referencing NR-6) at intervals of 100 seconds, onto floppy disks. This system allows continuous phase difference information over long periods of time. Temperature data for the room and the maser environmental chambers are also recorded at hourly intervals.

Figure 13 shows the residuals to a least squares fit of the phase difference between NR-3 and NR-6 over a seven day span. (This treatment of the data is consistent with that of the VLBI users). NR-3 was located in an environmental chamber; NR-3 was not autotuning during this time. Over the majority of the data span, the residuals remained within $\pm .5$ ns, with extremes of ± 1.0 ns. Within this data are two relatively large phase jumps of approximately .5 ns. These jumps are artifacts of our measurement system, which we are working on eliminating. Even with these jumps, the RMS deviation of the week long data was 0.316 ns.

The Allan Variance of the (NR-3) - (NR-6) data shown in Fig.13, removing the two discontinuities, is shown in Fig.14. The Allan Variance of both the raw data and the residuals (i.e. drift removed data) are shown.

Error bars are given for the drift rate removed data but similar error bars apply for the raw data. These error bars were estimated by

$$\text{Error} = \pm 1/\sqrt{(N-2)} \%$$

where N is the number of adjacent time intervals of length tau (τ). The factor of two is required because the raw data is in phase rather than frequency. Both masers were assumed to contribute equally to the noise, and hence a factor of $2^{-1/2}$ was included in the calculations.

Figure 14 shows that NR-3's stability at 100,000 seconds is 4×10^{-15} for the drift rate removed data.

Figure 15 again shows the residuals to a least squares fit of the phase difference between NR-B and NR-6. NR-B has the integral cavity liner with the improved temperature coefficient, approximately $7 \times 10^{-15}/^{\circ}\text{C}$. A week long data span is shown. NR-B was not autotuning, and was located in an environmental control chamber. However, NR-B's chamber was operating near its upper temperature control limit, causing larger variations as shown in the temperature plot in Fig. 15. One would not expect temperature variation as large a factor in NR-B's performance as other NR masers without a quartz liner and, in fact, the residuals plotted in Fig. 15 show a peak-to-peak variation of only $\pm .5$ ns. The RMS deviation of the data over the seven days was only 0.251 ns. (Again there appeared a single discontinuity resulting from the measurement system.)

The Allan Variances with the drift rates removed of NR-5, NR-B, and NR-2 whose residuals were not shown, are plotted in Fig. 16. Shorter term data was measured only on NR-2. All masers were measured relative to NR-6 and the variances and error bars were calculated in the same manner as that described earlier for NR-3. NR-5 and NR-2 were autotuning while NR-B was not.

Figure 16 coupled with Fig. 14 on NR-3's stability, illustrates the range of performance in the hydrogen masers APL has completed. Their stabilities are seen to be well into the 10^{-15} range for taus (τ 's) of 500 - 100,000 seconds when drift is removed.

NR-1 Long Term Stability

NR-1 maser resides at APL on a long term basis and serves as our laboratory standard. Taking advantage of NR-1's availability, we investigated the performance of a hydrogen maser being operated as a clock relative to our laboratory's cesium option 004 Hewlett-Packard frequency standards.

For ten months, from September 1981 through June 1982, we maintained

a continuous record of the phase difference between NR-1* and our Cesium 793. The phase difference was measured at 5 MHz using a dual balance time delay mixer with a beat frequency of about .25 Hz relative to each standard. In our Time and Frequency Laboratory within APL we maintain three cesium standards. Timing information is reported to BIH (Bureau International de l'Heure) on these three cesiums relative to our paper clock, and the USNO (United States Naval Observatory) Master Clock #1, with whom we transfer time using portable cesium clocks. BIH, in turn, calculates and publishes bimonthly, the rates of the reporting clocks relative to UTC (Universal Time Coordinated). Figure 17 shows both the bimonthly clock rates of our three cesium standards published by BIH, and the derived clock rate of NR-1.

Figure 17 shows that, as a clock, NR-1 performed as good or better than the best ten month data span of any of the three cesiums. In fact, the actual performance of the NR-1 maser is most probably masked by the limited resolution in the BIH published data, given only to ± 10 ns; and by the performance of the cesium transfer standard.

Another advantage of the NR-1 hydrogen maser operating as a clock is the ability to set the frequency without adversely affecting the inherent stability of the device. This is not true of present cesiums.

After our ten month data run comparing NR-1 to Cesium 793, the maser operating conditions were changed; NR-1 was placed in a continuous auto-tune mode. This operating mode allows the cavity bit register to automatically adjust to compensate for the cavity frequency drift. The cavity register value was printed out at four hour intervals and later converted to the frequency shift through a measured value of the frequency shift per cavity register bit**. Figure 18 shows these cavity register drift corrections plotted over a four month interval.

A rather significant piece of data on the maser's performance was obtained quite unintentionally. During the four month time period, our room air conditioner suffered a failure over a weekend when no one was present to immediately correct the situation. NR-1 was in an environmental control chamber, but the room temperature rose above the box's control limit. The spike in the data of Fig. 18 is the cavity register trying to compensate for the temperature control failure. The behavior of NR-1 after temperature control was restored is worthy of note; the cavity came back to the same frequency as that just before the temperature control failed. This behavior

* During this time period, NR-1 was in an environmental control box for temperature control. NR-1 was not autotuning during this time.

** The frequency shift per bit for NR-1 during this time period was 2.03×10^{-16} /bit.

following a failure is a great advantage for our masers operating in remote areas where short term failures, such as the one just described, are more likely to occur.

Ignoring the temperature control failure, the drift corrections to the cavity shown in Fig.18 appear to increase in a nearly linear manner with time. A quadratic least squares fit of the data was calculated, which gives the linear daily drift of the cavity as:

$$-4.90 \times 10^{-15}/\text{day}.$$

Higher order terms of cavity drift as a function of time are insignificant relative to the linear term. The data in Fig.18 are frequency corrections made to cavity to compensate for its drift, therefore, the increasing frequency compensates for a cavity frequency that is drifting downward in frequency.

In addition to the cavity register data shown in Fig.18, two determinations of the NR-1 cavity drift were made; one in early August 1981, and the other in late February 1982. The total change in NR-1's cavity register value over a period of 78 days, was obtained in each case and an average daily drift rate was calculated. These calculations agreed to within 10% of the daily cavity drift calculated for the four month data shown in Fig.18.

Linear Daily Drift (averaged over 78 days):

$$-4.4 \times 10^{-15}/\text{day} \quad \text{period ending} \\ 4 \text{ August } 1981$$

$$-5.1 \times 10^{-15}/\text{day} \quad \text{period ending} \\ 24 \text{ February } 1982$$

The cavity drift rate of NR-1 has remained essentially constant over a time period of greater than one year with an uncertainty of $\pm 5 \times 10^{-16}/\text{day}$.

ACKNOWLEDGEMENTS

The authors would like to acknowledge C. Knight of Interferometrics Incorporated for reducing the VLBI data shown.

REFERENCES

1. A. R. Whitney, et. al., "A Very Long Baseline Interferometer for Geodetic Applications", Radio Science, Vol. 11, Number 5, pp 421-432(May 1976)
2. V. S. Reinhardt, "Variable Volume Maser Techniques", Proceedings of the 8th Annual NASA/DOD Precise Time and Time Interval Planning Meeting (Washington, DC, 1976)

FIGURES

- Figure 1. Hydrogen Maser Thermal Control Chamber
- Figure 2. Thermal Chamber with Side Panel Removed
- Figure 3. Thermal Chamber Performance in a Laboratory Environment
- Figure 4. VLBI Phase Comparison Between NR-2 and NX-2 - Frequency Offset Removed
- Figure 5. VLBI Phase Comparison Between NR-2 and NX-2 - Frequency Drift Removed
- Figure 6. Hydrogen Masers Being Repaired and Upgraded at the BFEC Hydrogen Maser Facility
- Figure 7. NP-2 Short Term Frequency Stability Before and After Upgrade
- Figure 8. NP Maser Long Term Stability Before and After Upgrade
- Figure 9. Hybrid Cavity Design
- Figure 10. Integral Cavity for NP, NX, and NR Retrofit
- Figure 11. Line Q of External Bulb Maser with Film Storage Bulb Verses Hydrogen Flux
- Figure 12. NR Maser
- Figure 13. Residuals to Least Squares Fit of Phase Difference Between NR-3 and NR-6, Over Seven Day Span
- Figure 14. Allan Variance of (NR-3)-(NR-6), Removing the Two Discontinuities
- Figure 15. Residuals to Least Squares Fit of Phase Difference Between NR-B and NR-6
- Figure 16. Range of Performance in Hydrogen Maser APL Has Completed
- Figure 17. APL Clock Rates
- Figure 18. NR-1 Cavity Register Drift Corrections, Plotted Over Four Months

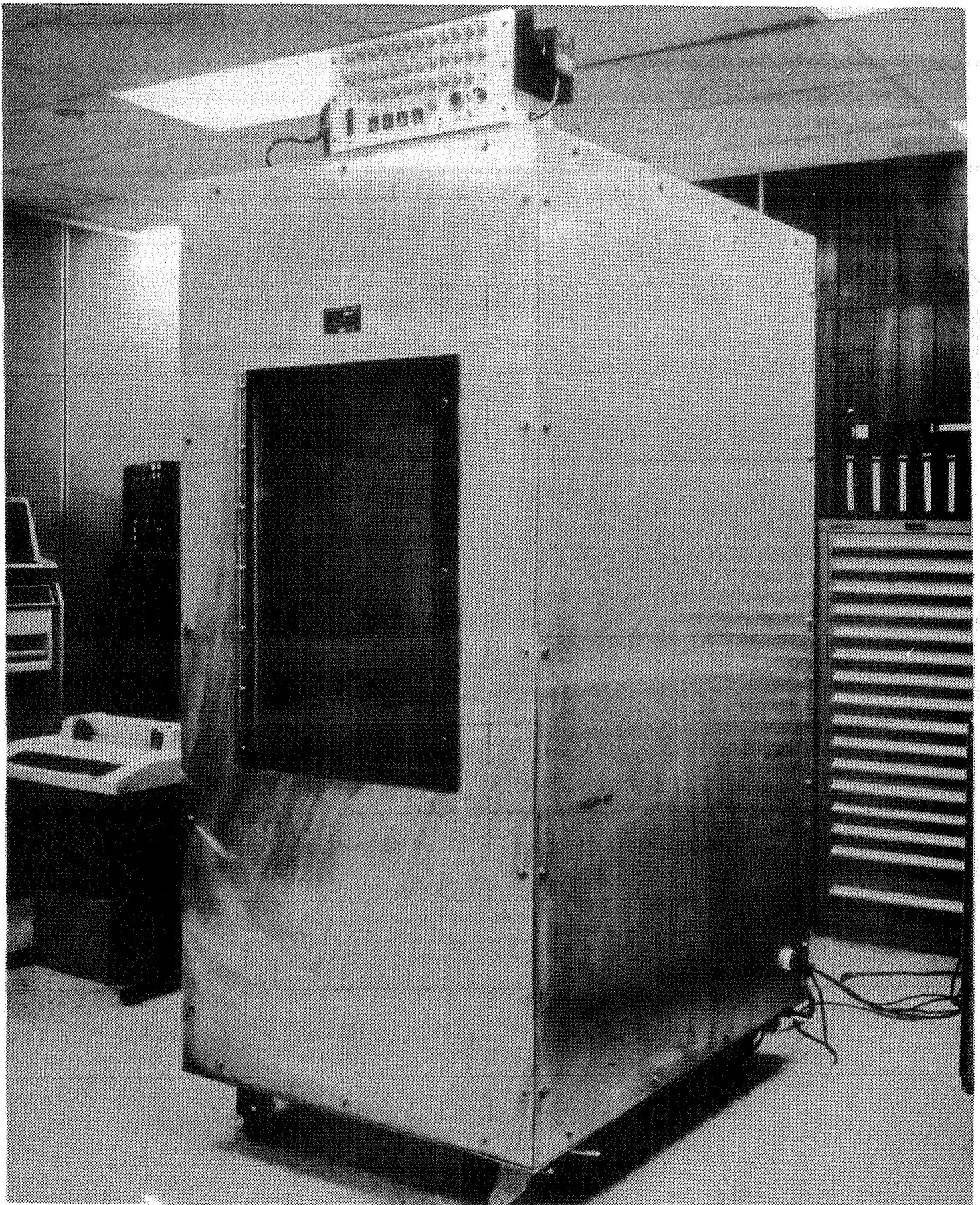


Figure 1. Hydrogen Maser Thermal Control Chamber

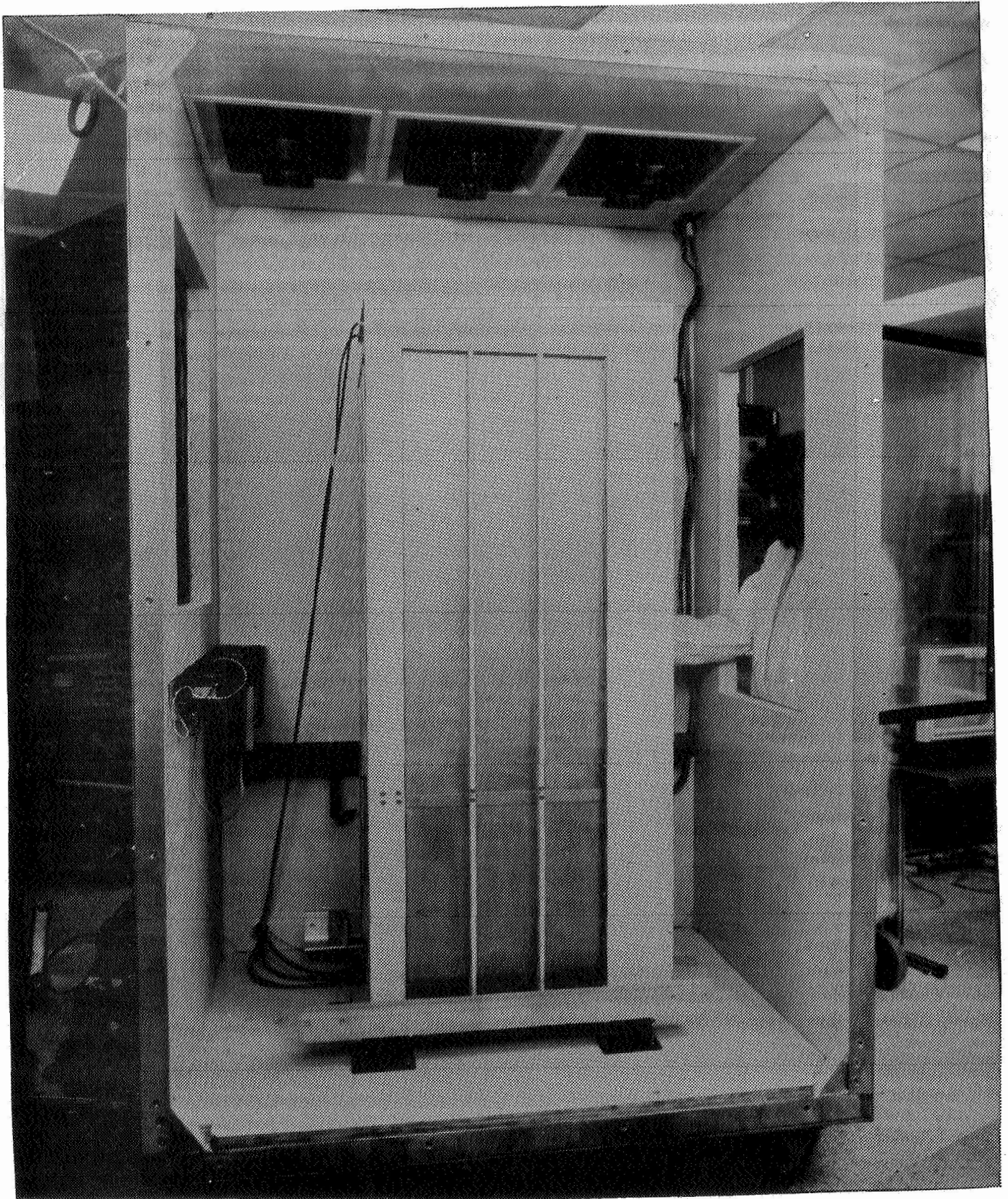
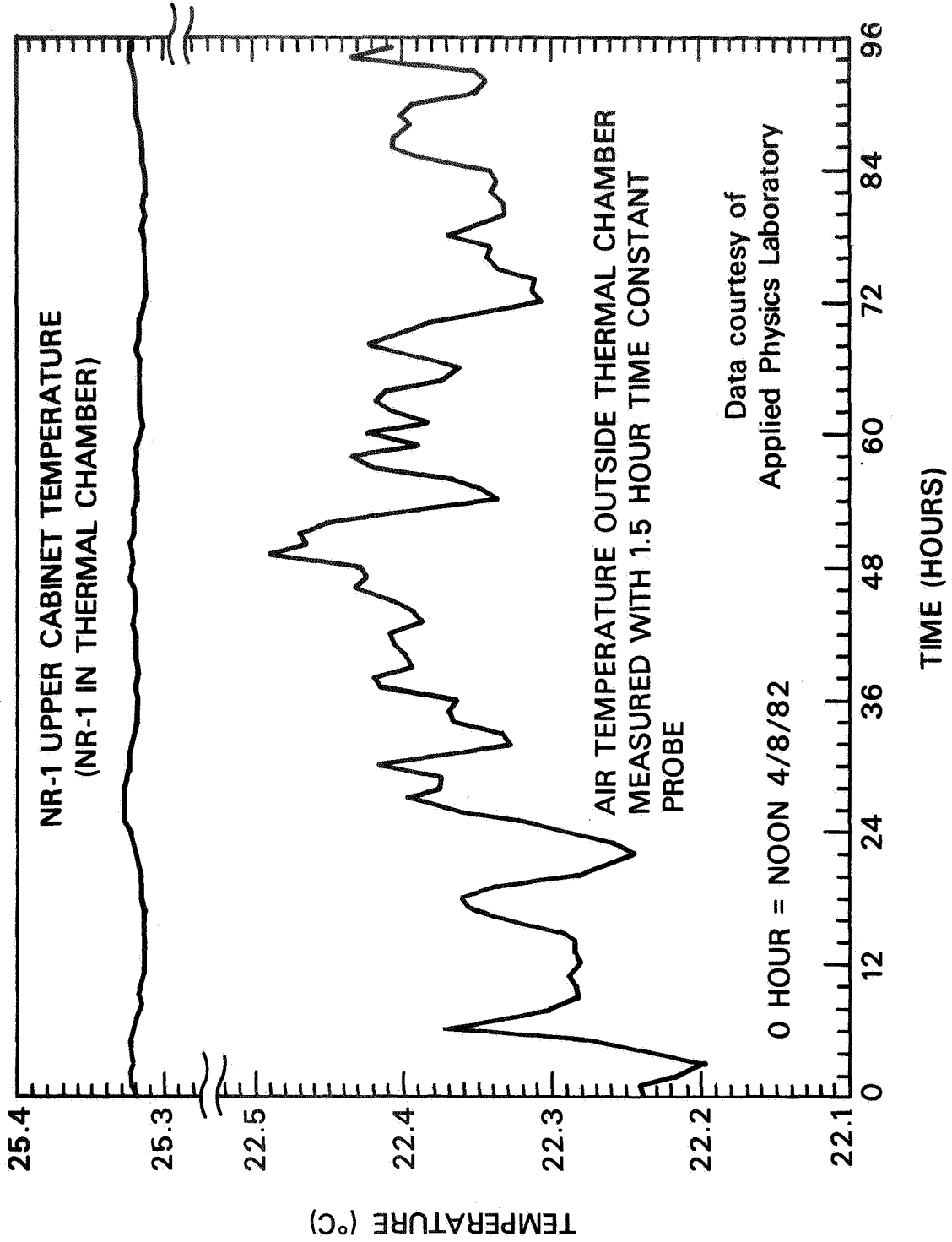


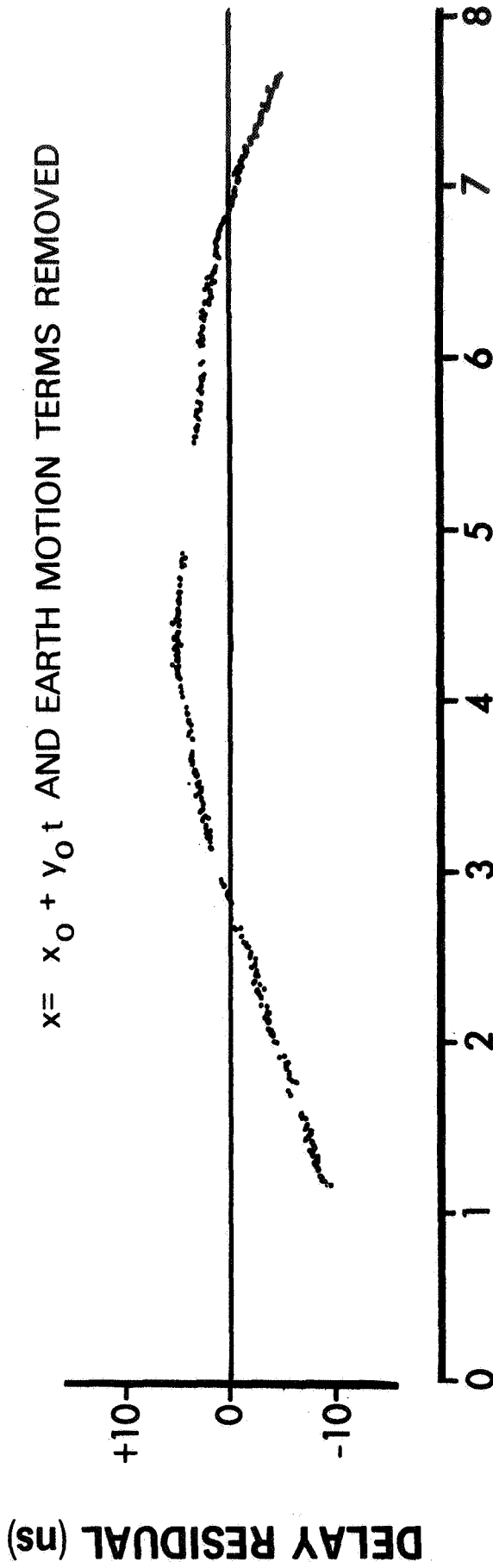
Figure 2. Thermal Chamber with Side Panel Removed



**Simultaneous Temperature Data Taken at Applied Physics Laboratory
Inside and Outside Thermal Chamber**

Figure 3. Thermal Chamber Performance in a Laboratory Environment

**VLBI GROUP DELAY DIFFERENCE
 BETWEEN NX-2 AT OWENS VALLEY, CALIFORNIA
 AND NR-2 AT FORT DAVIS, TEXAS**



ELAPSED TIME (DAYS FROM 9/26/80, 00:00 UTC)

Data COURTESY of
 C. KNIGHT, PHOENIX CORP.

Figure 4. VLBI Phase Comparison Between NR-2 and NX-2 -
 Frequency Offset Removed

**VLBI GROUP DELAY DIFFERENCE
 BETWEEN NX-2 AT OWENS VALLEY, CALIFORNIA
 AND NR-2 AT FORT DAVIS, TEXAS**

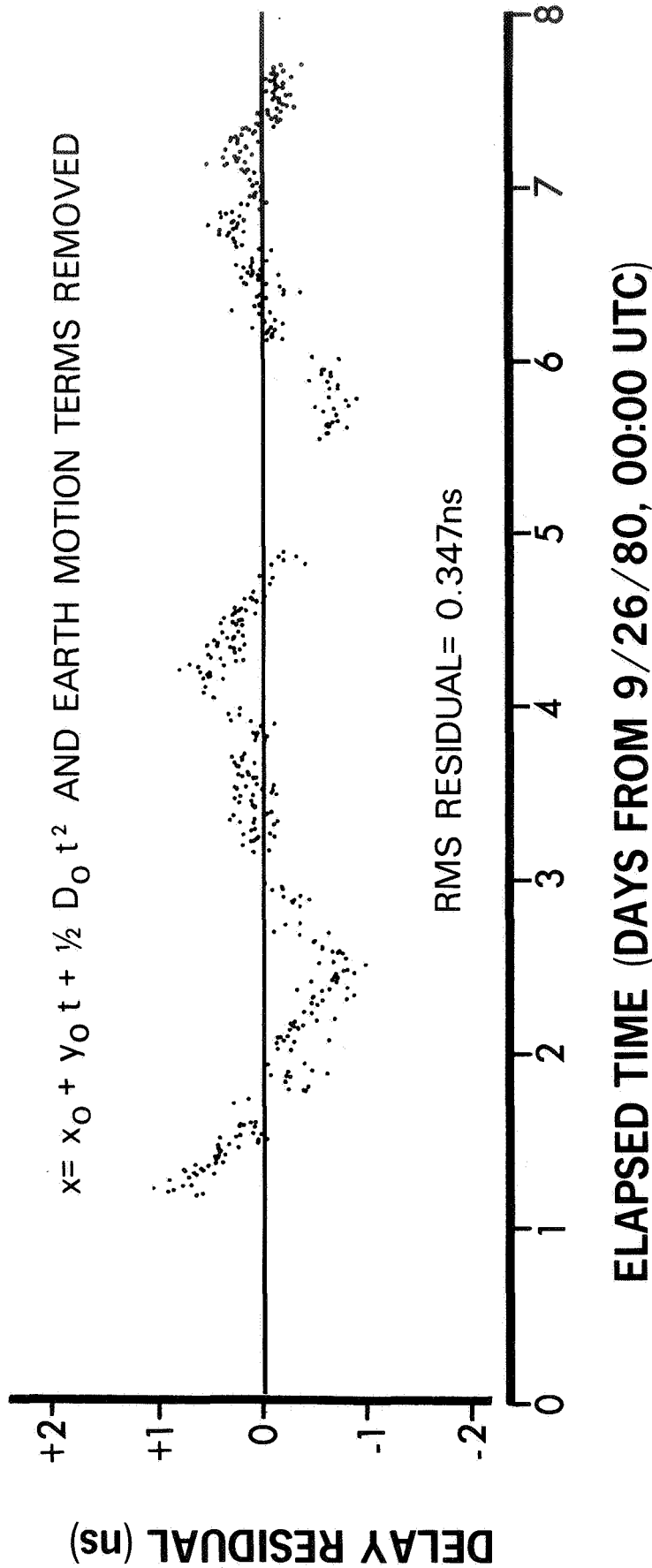
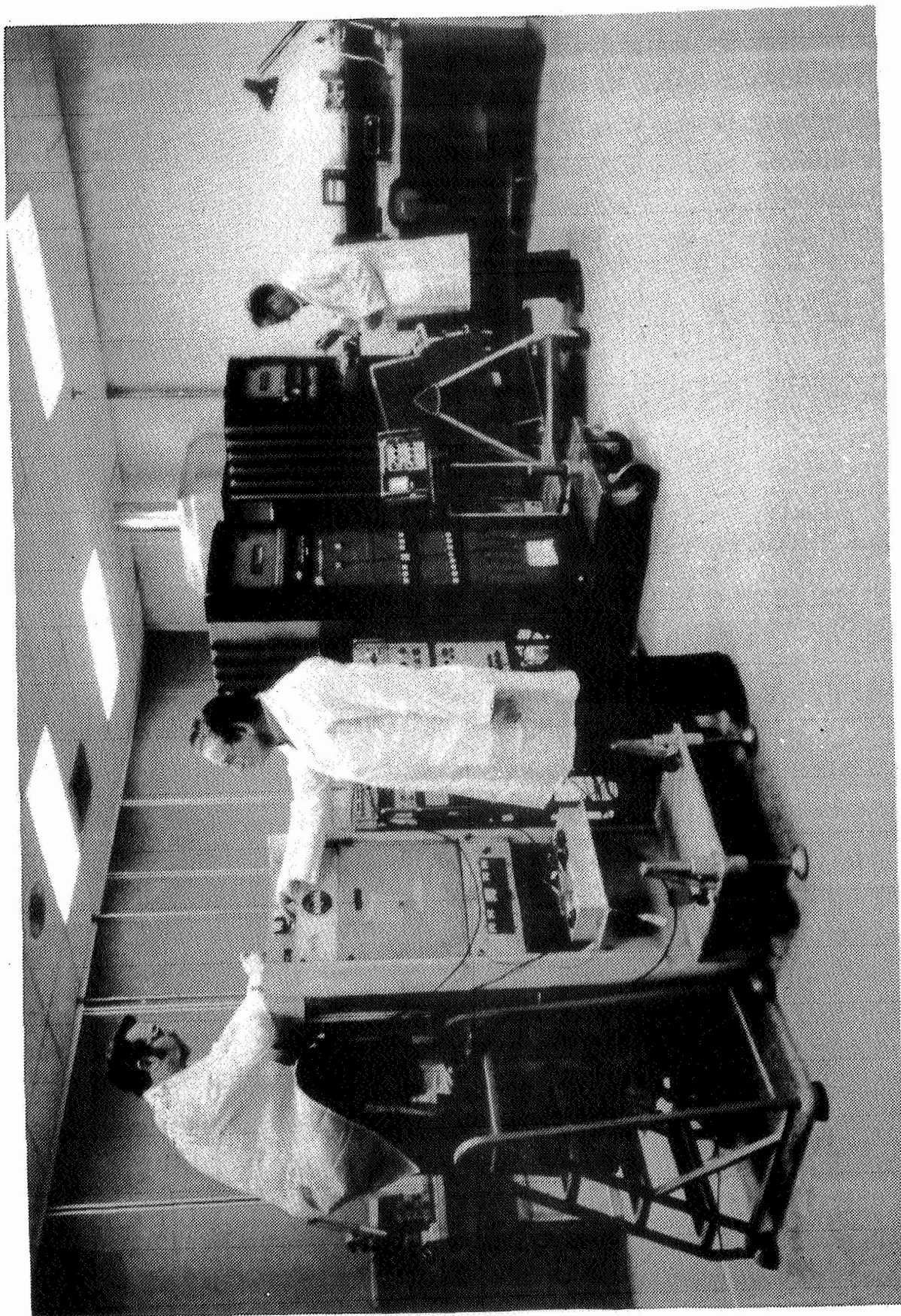


Figure 5. VLBI Phase Comparison Between NR-2 and NX-2 -
 Frequency Drift Removed

Data COURTESY of
 C. KNIGHT, PHOENIX CORP.



BENDIX LABORATORY/RETROFIT AREA FOR NP AND NX MASERS

Figure 6. Hydrogen Masers Being Repaired and Upgraded at the BFEC Hydrogen Maser Facility

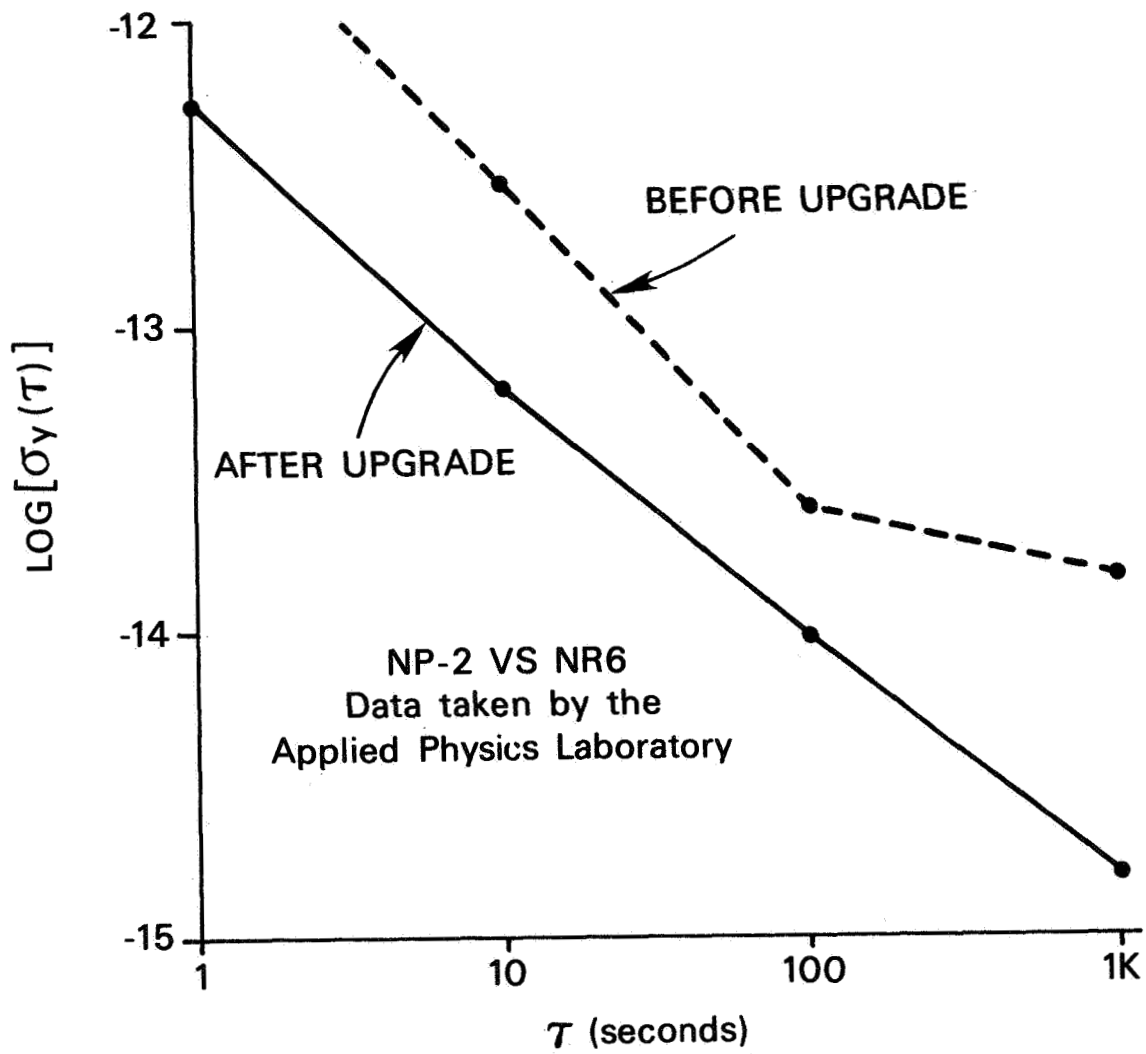


Figure 7. NP-2 Short Term Frequency Stability Before and After Upgrade

COMPARISON OF NP MASER STABILITY WITH AND WITHOUT THERMAL CHAMBERS

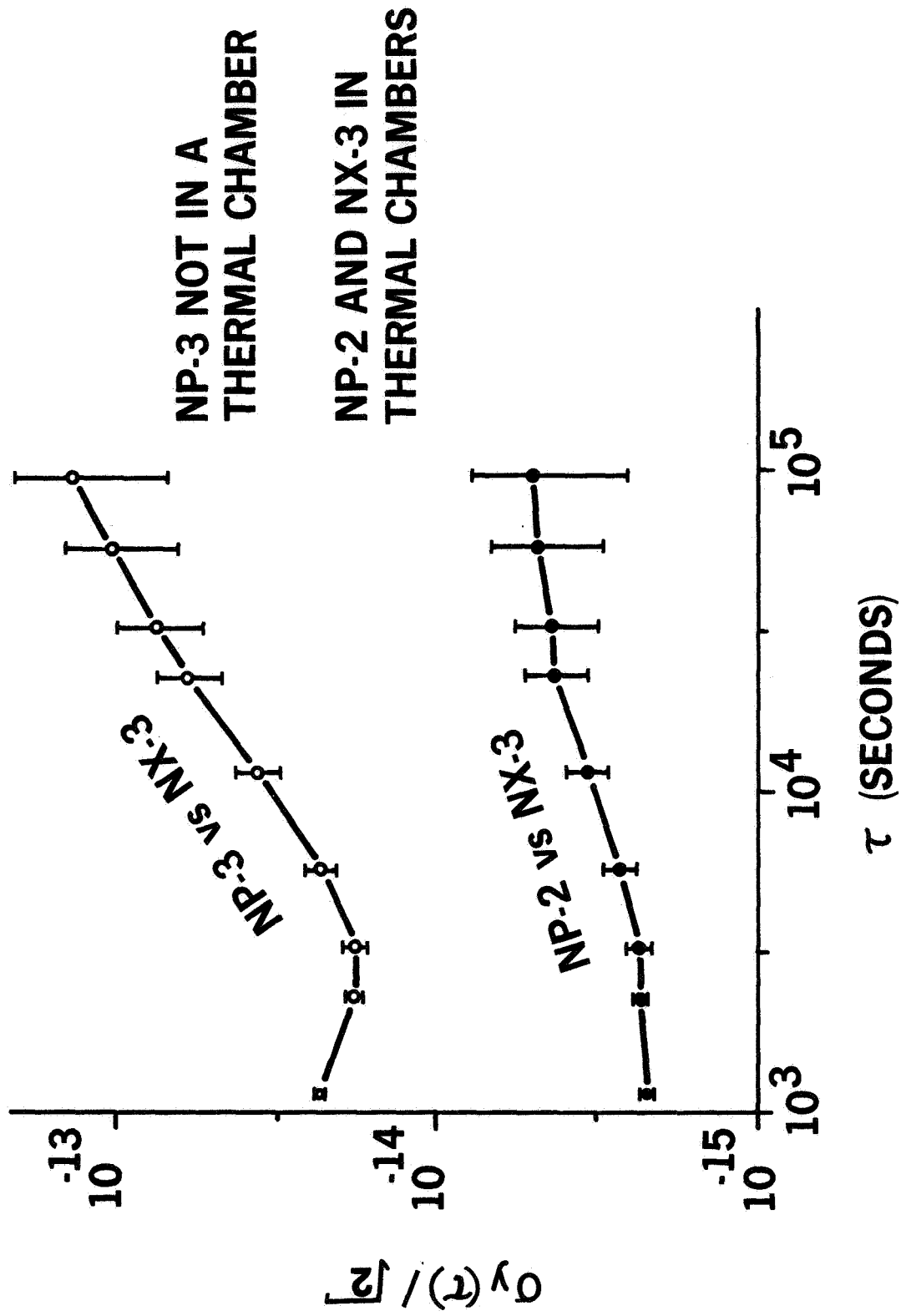


Figure 8. NP Maser Long Term Stability Before and After Upgrade

INTEGRAL FUSED QUARTZ CAVITY - STORAGE BULB

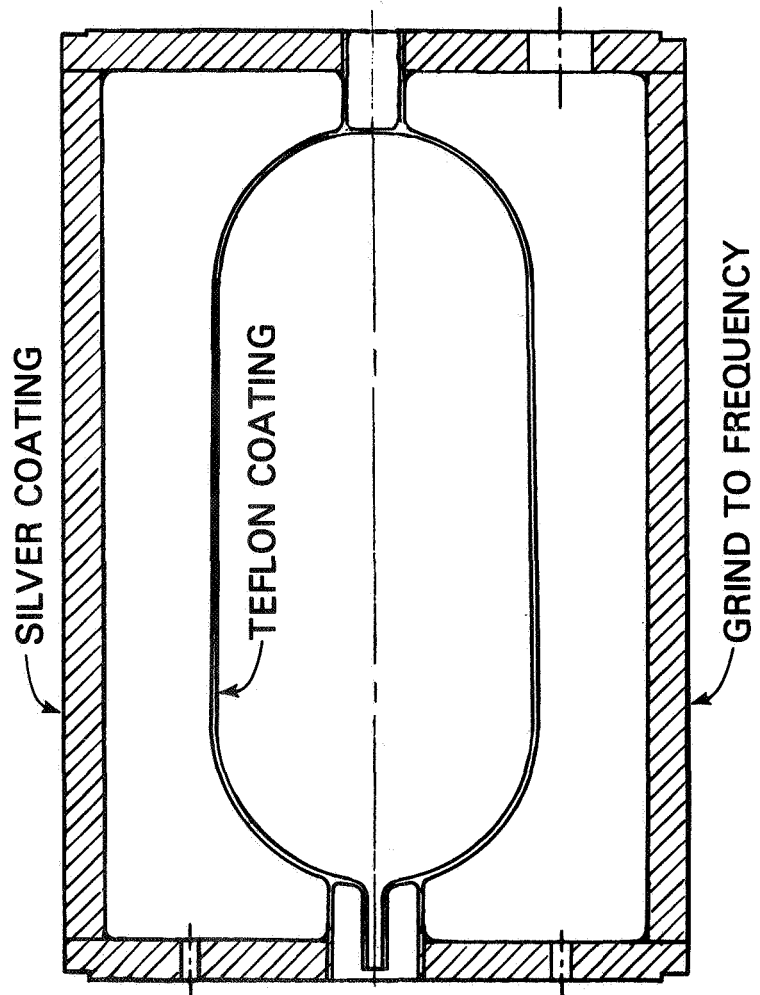


Figure 9. Hybrid Cavity Design

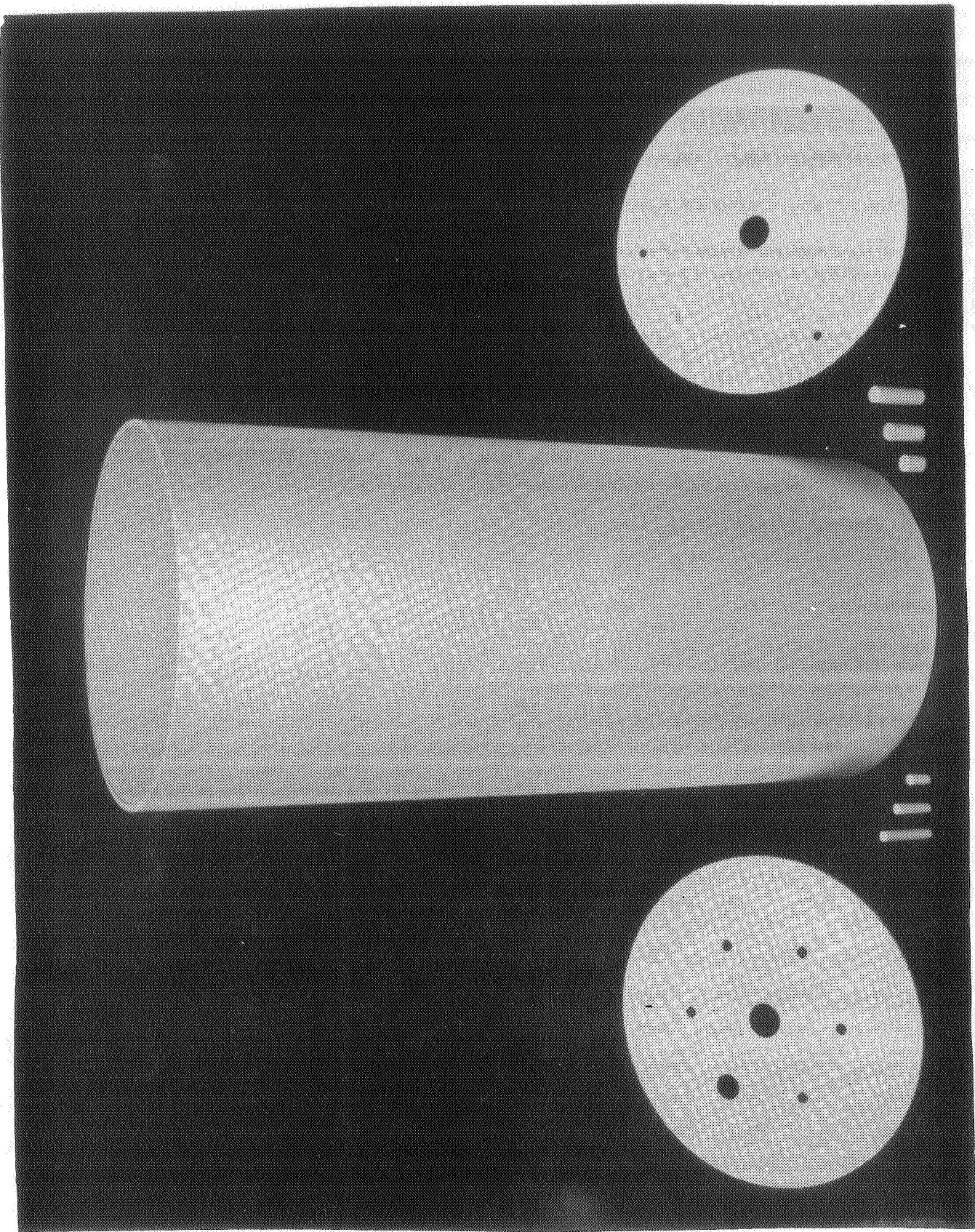


Figure 10. Integral Cavity for NP, NX, and NR Retrofit

OPERATING LINE Q AND I.F. VOLTAGE FOR FILM BULB IN EXTERNAL BULB MASER

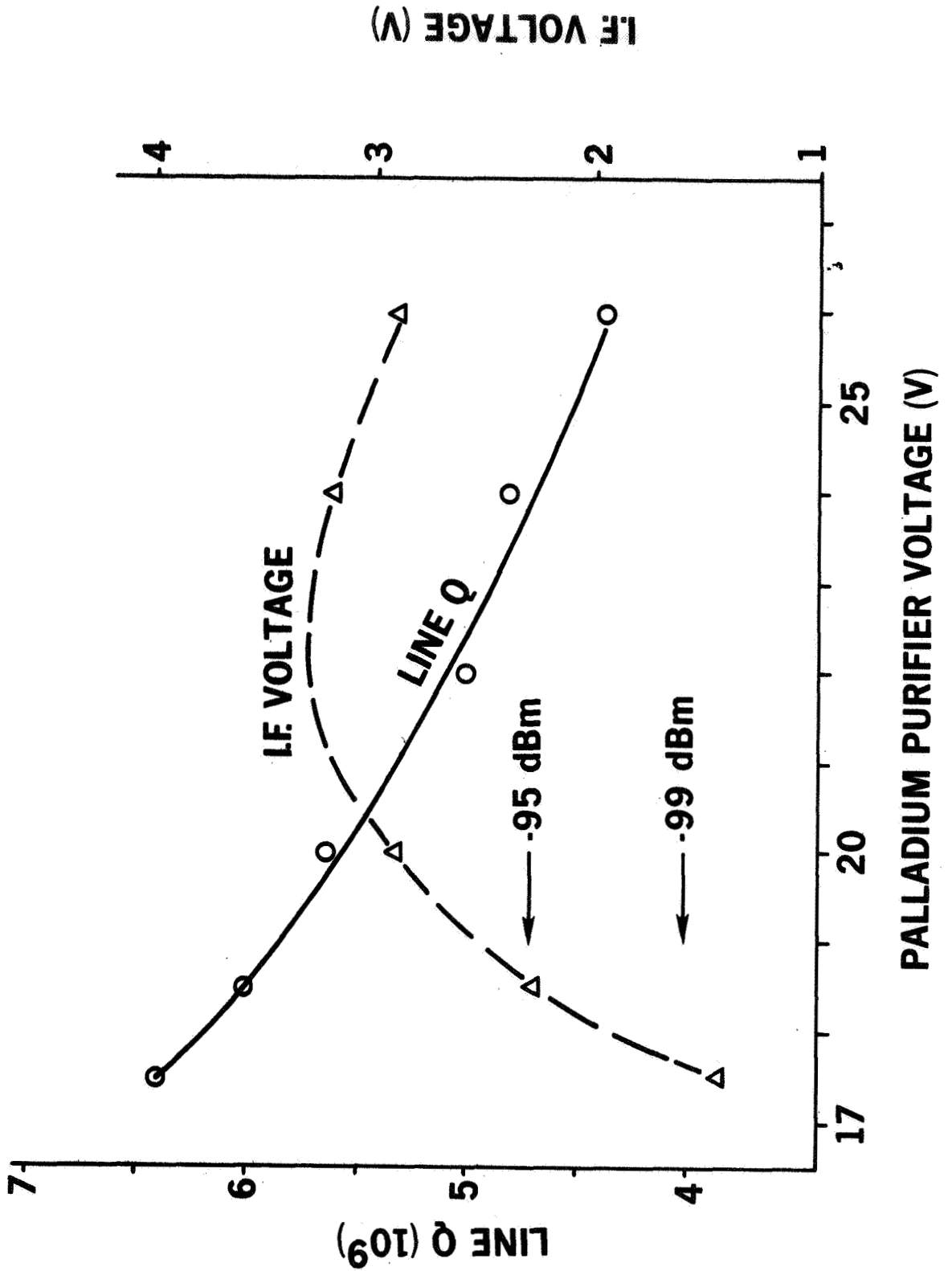


Figure 11. Line Q of External Bulb Maser with Film Storage Bulb Versus Hydrogen Flux

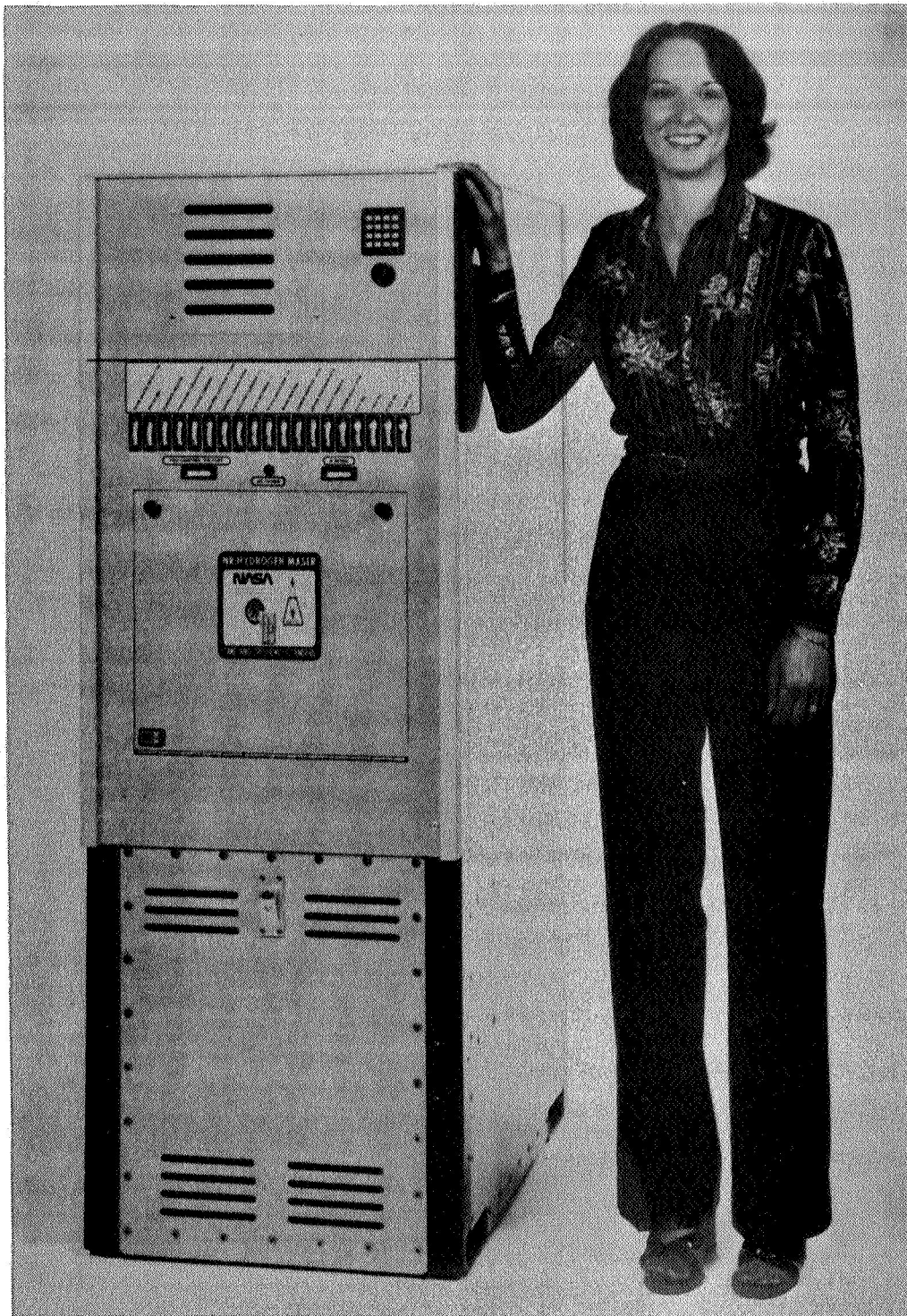
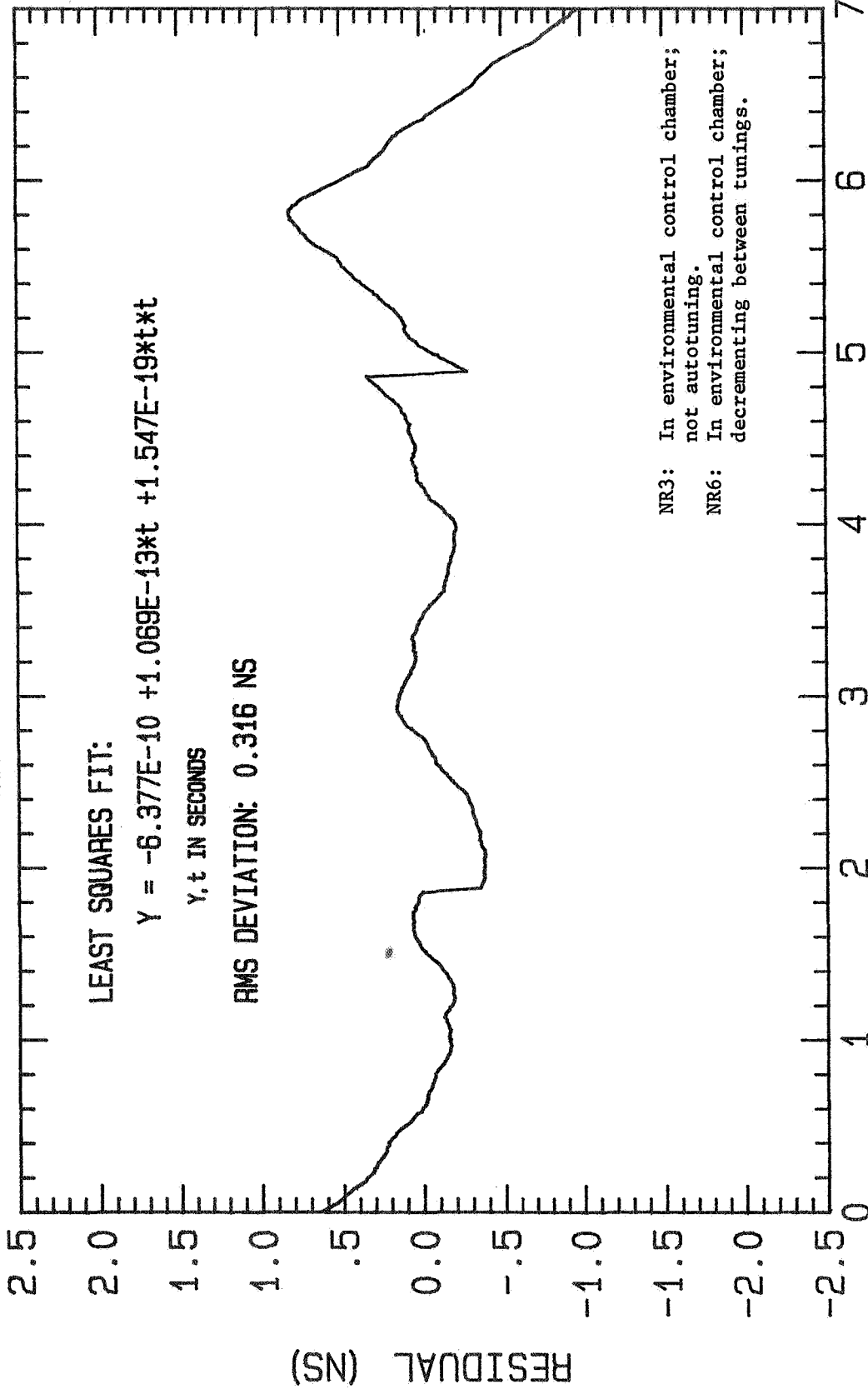


Figure 12. NR Maser

RESIDUALS: NR3-NR6



DAY NUMBER (1000 SEC DATA)

Figure 13. Residuals to Least Squares Fit of Phase Difference Between NR-3 and NR-6, Over Seven Day Span

ALLAN VARIANCE: NR3-NR6

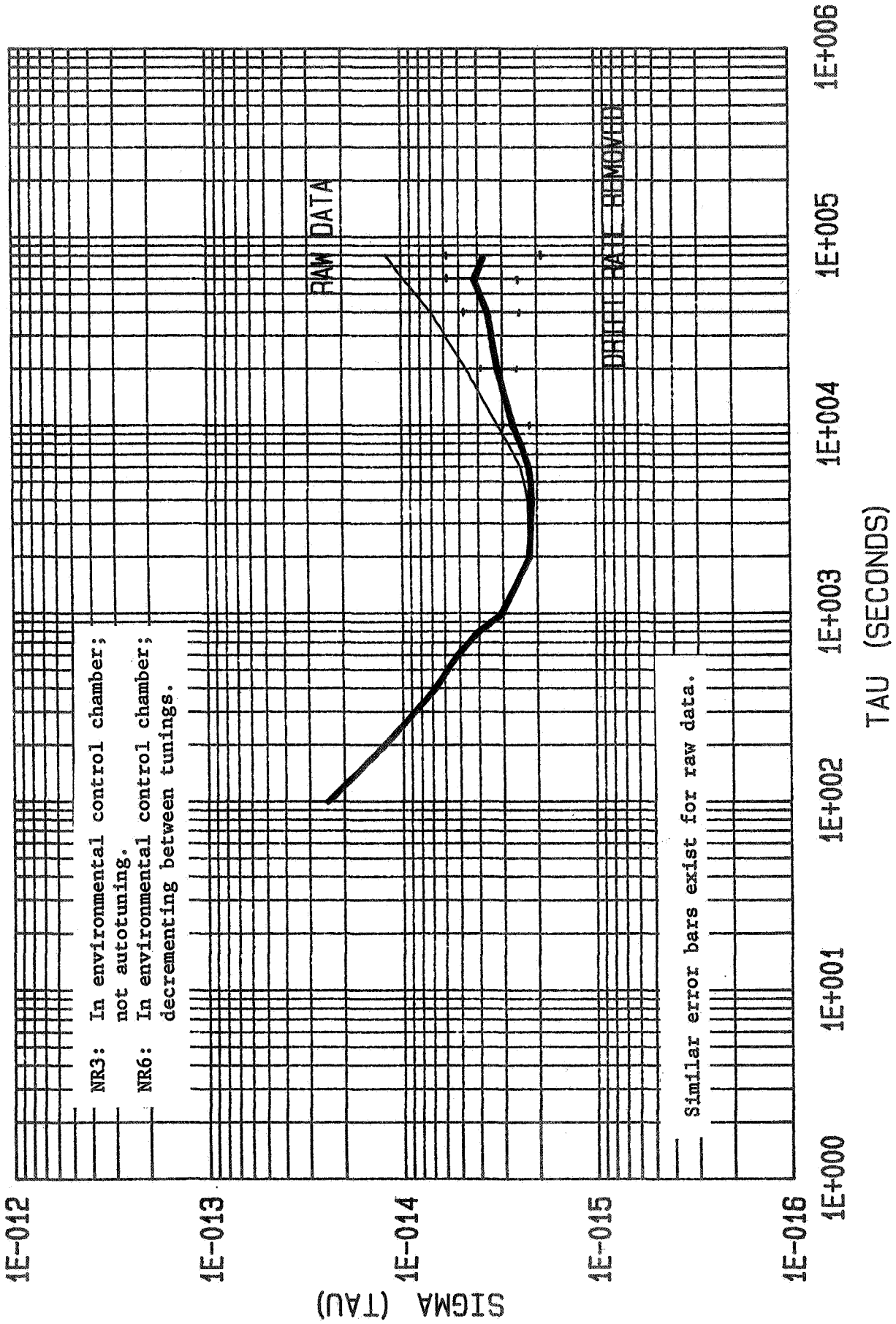


Figure 14. Allan Variance of (NR-3)-(NR-6), Removing the Two Discontinuities

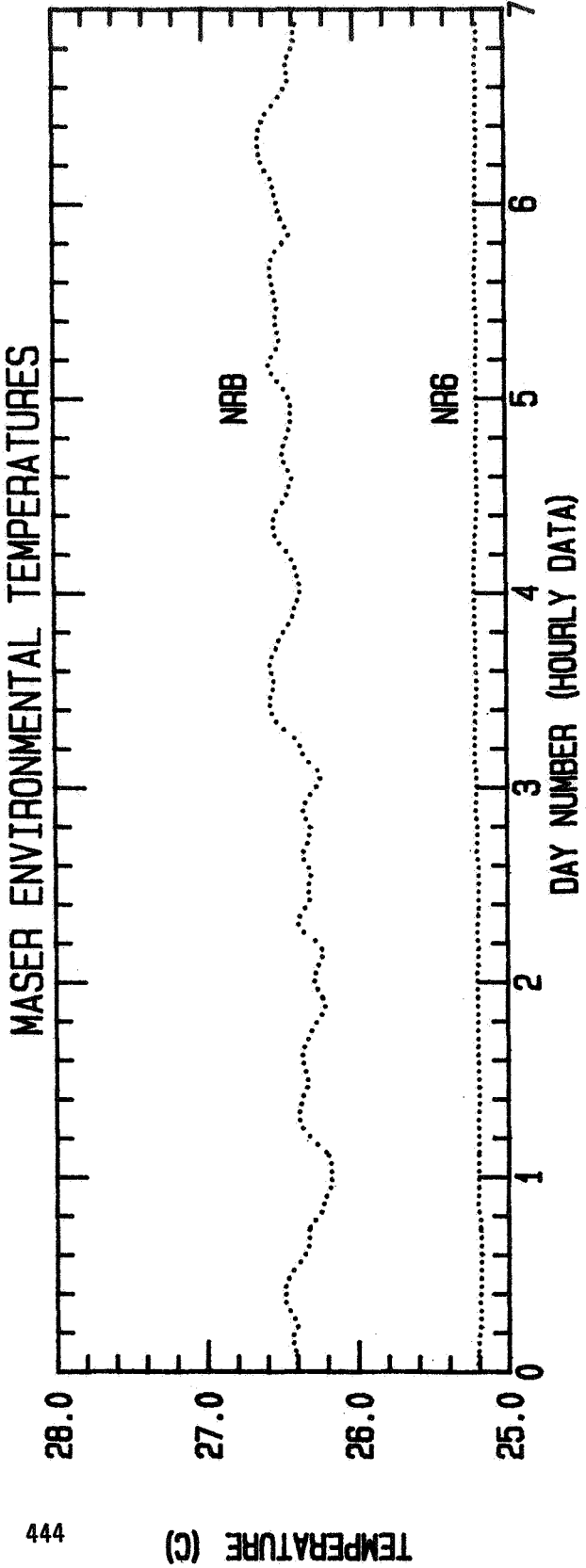
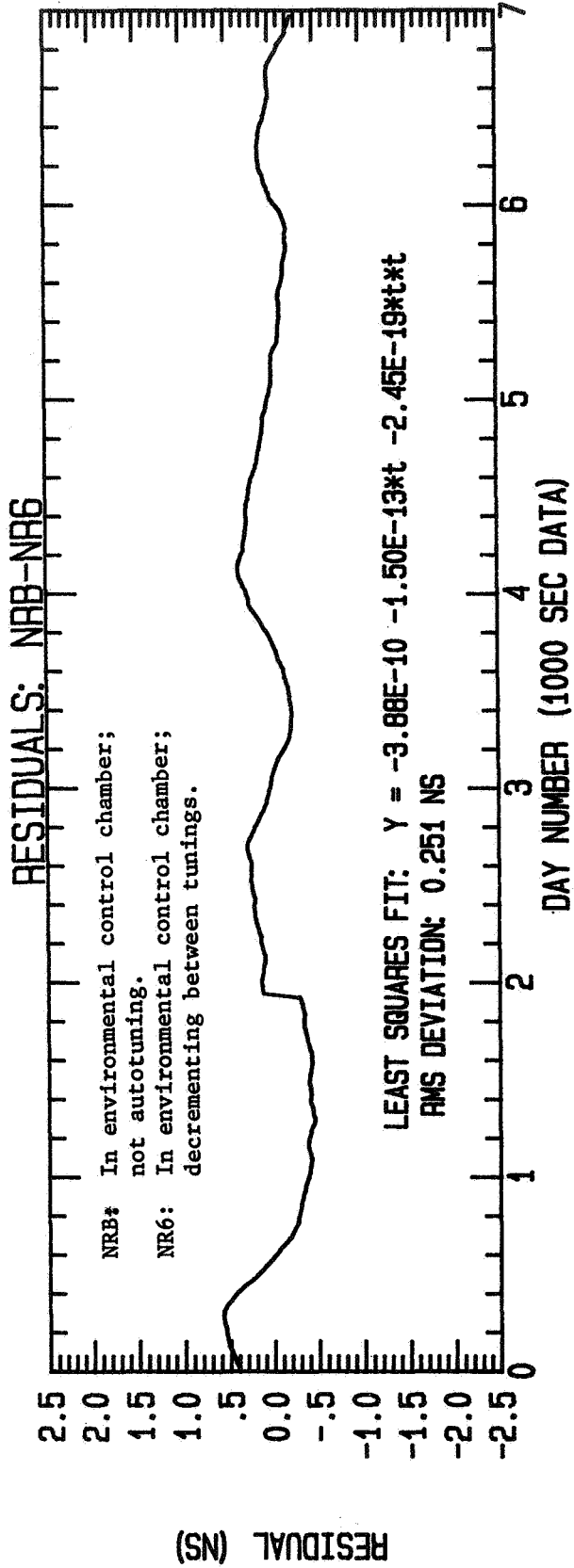


Figure 15. Residuals to Least Squares Fit of Phase Differences Between NR-3 and NR-6

ALLAN VARIANCE

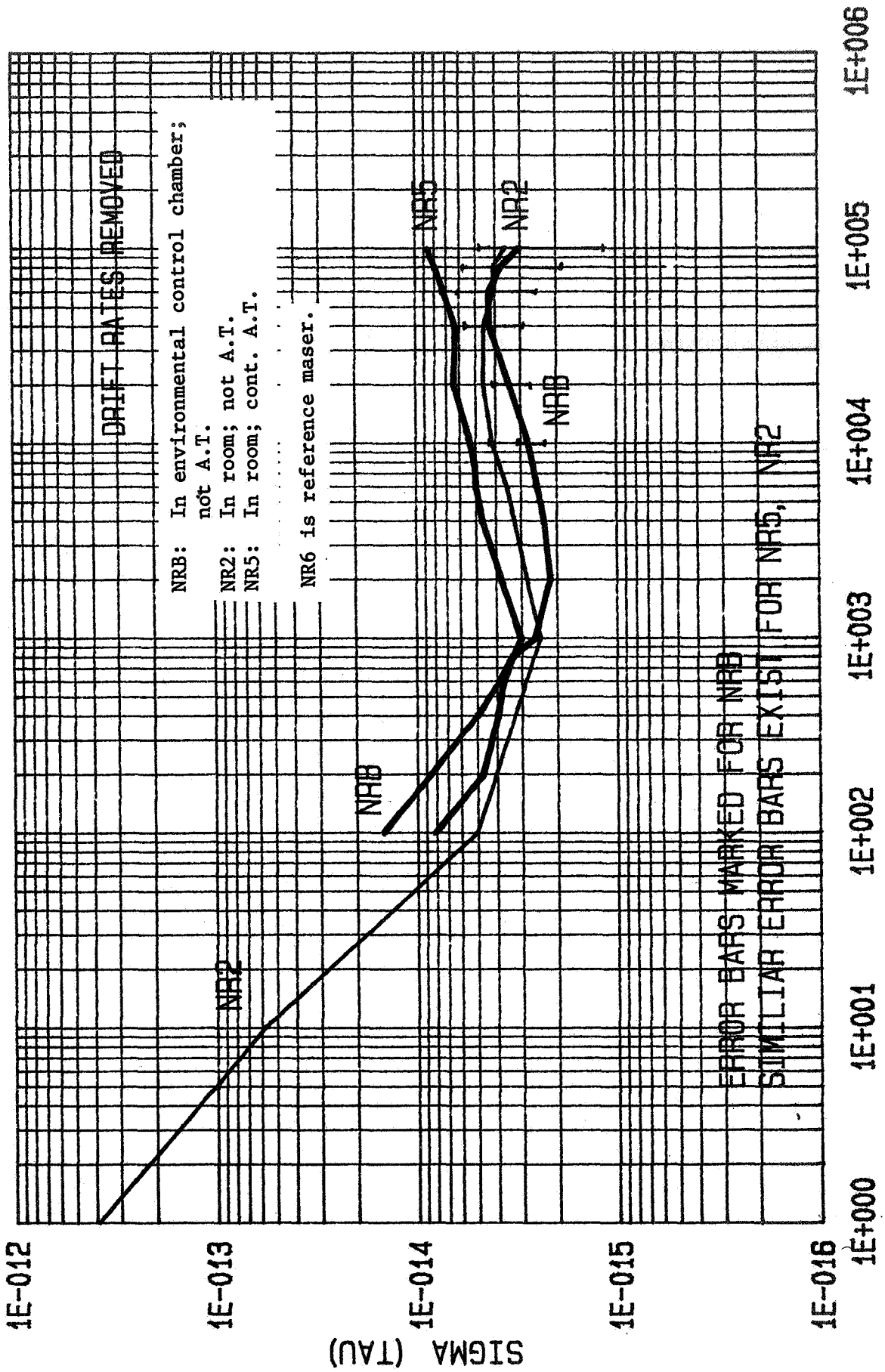


Figure 16. Range of Performance in Hydrogen Maser APL Has Completed

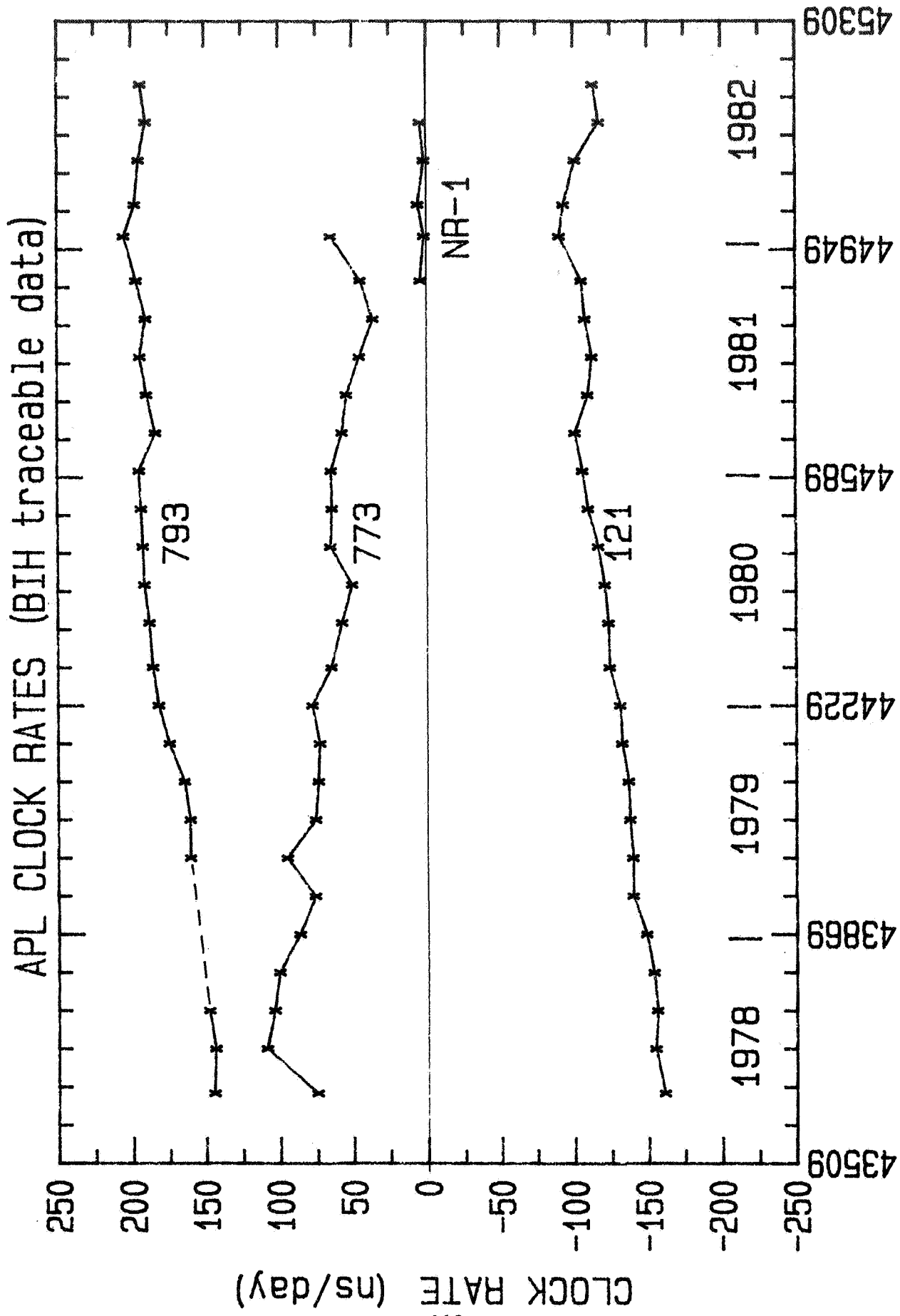


Figure 17. APL Clock Rates

NR1: DRIFT CORRECTIONS TO CAVITY

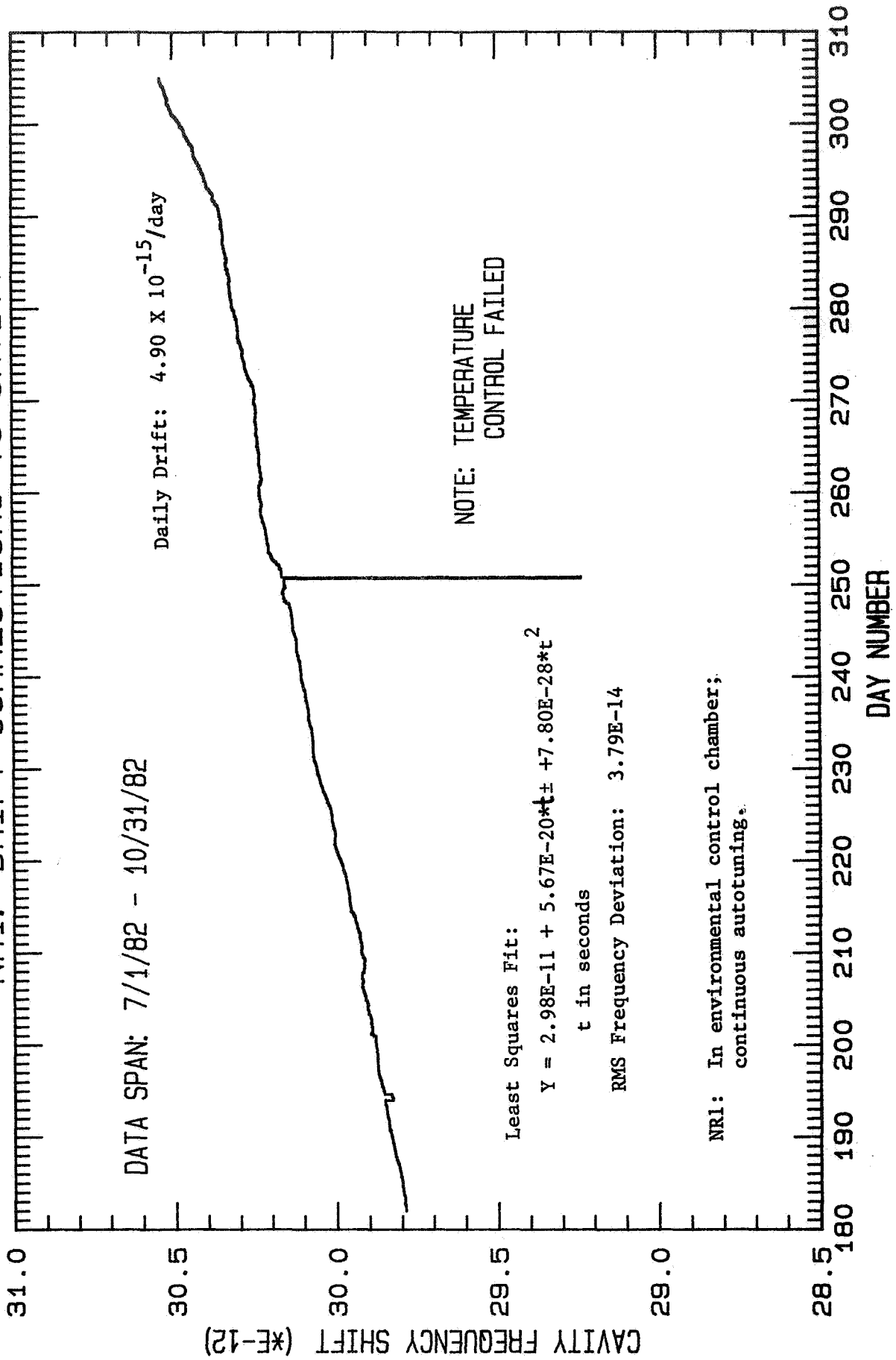


Figure 18. NR-1 Cavity Register Drift Corrections, Plotted Over Four Months

QUESTIONS AND ANSWERS

None for Paper #19

DR. COATES:

Earlier this afternoon, we were talking about frequency standards and clocks. From here on, we're talking about networks for synchronizing various clocks and, of course, you really have to have both in order to have viable precision time and time interval systems.

The first paper in this session is entitled, "Timing Subsystems Development/Network Synchronization Experiments" by Ken Backe.

TIMING SUBSYSTEM DEVELOPMENT -
NETWORK SYNCHRONIZATION EXPERIMENTS

K. R. Backe
CNR, Inc.
220 Reservoir Street
Needham, MA 02194
Telephone: (617) 449-4902

ABSTRACT

In the predominantly digital Defense Communication System (DCS), a requirement exists to coordinate clocks at geographically distinct nodes to handle switched digital traffic and provide a general timing capability. The characteristics of the nodal clocks, link equipment delay/phase relationships, transmission medium, and synchronization technique all affect system performance and must be considered when attempting network-wide clock alignment. This paper describes a program in which several experimental timing subsystem prototypes were designed, fabricated, and field tested using a small network of troposcatter and microwave digital communication links. This equipment was responsible for modem/radio interfacing, time interval measurement, clock adjustment and distribution, synchronization technique, and node-to-node information exchange. Presented are discussions of the design approach, measurement plan, and performance assessment methods. Recommendations are made based on the findings of the test program and an evaluation of the design of both the hardware and software elements of the timing subsystem prototypes.

INTRODUCTION

The DCS network involves a large number of links and nodes with various categories of transmission media, including troposcatter (TROPO), line-of-sight microwave (LOS), satellite, and cable. The variety of transmission equipment that is available now, or planned as part of an all-digital network, makes a complete and comprehensive evaluation of system performance difficult; therefore, an emphasis in the experimental work reported on here has been toward synchronization performance in a three

node network at RADC, Rome, NY.

As speed, size, and complexity of military communications systems increases, characteristics of the frequency sources that clock digital information play a more dominant role in determining the overall effectiveness of the system. If the desired goal is to provide a synchronous non-interrupted digital network, then even a modest amount of clock disciplining would greatly ease the problem. Since each separate node would have a frequency/time source, it has traditionally been considered paramount that each be of highest quality to minimize clock-to-clock relative drift and maximize the time between buffer resets (which interrupts digital traffic). In practice, the continuous traffic goal is unattainable when operating in an independent clock mode; buffer resets would still be required. This places the burden on the clocks themselves and the system designer is forced to specify highly accurate, highly stable, and very costly standards. For planned networks with literally hundreds of nodes, the cost is substantial.

A directed-control disciplined network rests the network frequency (phase) reference with one or at most, a few of the best sources while subordinate clocks are manipulated to follow the characteristics of the selected references. These manipulated clocks need only be lesser-quality (i.e., quartz) standards since their individual frequency trends are not mapped throughout the network.

An active clock control situation must rely on a timing/synchronization technique to carry out the timing function and insure a stable, reliable system. The focus of the Timing Subsystem Development program was to design, build, and test equipment to achieve this end using an existing Air Force network for evaluation [1]. Although several techniques have been proposed and studied [2] - [6], as yet an actual field implementation had not been attempted.

This paper begins with a brief review of time transfer techniques and objectives. The microprocessor-based link termination and processing equipment is described revealing the hardware and software components of the system. Following an overview of the RADC network configuration, a summary stemming from laboratory experience and field experiment findings forms the base on which relevant observations, conclusions, and recommendations are presented.

BACKGROUND

The primary mechanism for clock comparison is the transfer of digital data over links terminated by node processing equipment. At any node, incoming data is clocked into a buffer by signals derived from the receiver-demodulator bit tracking loop. This clock signal exhibits fluctuations and drift behavior as a result of transmit clock variations, medium variability, and tracking loop dynamics. In a synchronous network, the received data is later clocked out of the buffer by the node clock and multiplexed or switched with other data from other terminated links for retransmission; the objective being to coordinate the collection of node clocks so that buffers do not overflow or deplete. For normal communication, relative synchronization of the nodes is sufficient and the node clocks need not be phased identically as long as their mutual average frequency offsets are zero. In addition, a timekeeping function would involve the desire to meet the above objective with zero phase offset between node clocks. Combined with removal of ambiguity, phase-aligned clocks serve as the basis for a time-of-day distribution system. A scheme of this type has obvious advantages when the network is referencing universal time such as UTC. Time is marked at each end of the link in terms of a periodic Time Reference Pulse (TRP) which is synchronous with the high rate data clock. If ambiguity issues are ignored in this discussion, it can be simply stated that the time transfer objective is to align TRP transmissions.

The data required in the clock control loop processor will depend on synchronization technique selected (timing algorithms reside in firmware) but, in general will consist of time measurements from two nodes, A and B, of a TRP. Node B measures the elapsed time of the incoming TRP from node A relative to its own clock, resulting in the quantity t_A . Similarly, at node A the TRP from node B is measured relative to the local clock producing t_B . Defining the clock TRP emission times on a reference time scale to be t'_A and t'_B , the four parameters are:

- t'_A = node A transmit TRP relative to node A reference
- t_B = node B receive TRP relative to node A reference
- t'_B = node B transmit TRP relative to node B reference
- t_A = node A receive TRP relative to node B reference

Considering a path delay from A to B as \mathcal{J}_{AB} , it can be shown that for a single-ended transfer, TRP arrival time at node B relative to node A is:

$$\mu_{AB} = t'_A - t_A + \mathcal{J}_{AB}$$

and TRIP arrival time at node A relative to node B is:

$$\mu_{BA} = t'_B - t_B + \mathcal{J}_{BA}$$

For double-ended exchanges the clock difference is:

$$\mu = 1/2 (t'_A - t_A - t'_B + t_B)$$

Path delay can be computed as:

$$PD = 1/2 [(t_A + t_B) - (t'_A + t'_B)] \text{ assuming } \mathcal{J}_{AB} = \mathcal{J}_{BA}$$

All parameters are to be interpreted as elapsed time measurements. Figure 1 illustrates these clock error and path delay calculations for single- and double-ended exchanges using TRP's derived from Time Reference Information Packets (TRIP's).

In a synchronous network, incoming data enters an elastic store at a rate determined by the receiver tracking loop output, but is clocked out of the store at a rate determined by the local node clock. Differences are accommodated as long as buffer capacity is not exceeded, and data is transmitted out of the node without the need for pulse stuffing. Although not classified as synchronous, the independent clock approach follows this methodology but, buffer resets are inevitable when input/output rates differ without correction.

With the current timing subsystem design, implementation of the various timing techniques differs only in the way references are selected or combined. Considering the once-per-second update rate, processor execution speed for each technique is not significant and, in each case, the result is a clock phase or frequency shift command to alter the node reference 1-pps signal. Similarly, the phase control indirectly affects buffer clocks causing the rate of fill or depletion to change. With independent clock operation, the phase shift control is zeroed.

TIMING SUBSYSTEM PROTOTYPE

The basic function of the Timing Subsystem (TS) is to combine locally-made timing measurements with other timing information transmitted from connected nodes in order to compute local clock error relative to a master reference. The nature of this reference is determined by the synchronization technique in effect. Then, based on the computed clock error, the TS corrects its local node clock and transmits local timing information to other nodes. A photograph of the three TS prototypes and development station is shown in Figure 2.

The TS is configured of several modules, each with a particular function. Many of these modules are under the control of a Central Processing Unit (CPU) which determines the order of events, performs arithmetic tasks, and collects information for performance evaluation and general system monitoring. Each TS contains the following sections; CPU, time interval measurement unit, clock control and distribution, frequency synthesizer, multiplexers for data input and output, and other interface circuitry. A block diagram is shown in Figure 3.

NODE CONTROL COMPUTER AND SOFTWARE

The TS is microprocessor-based equipment designed around the Motorola 6800 8-bit MPU and support devices. Floating point arithmetic functions are handled by a separate arithmetic processor chip. Figures 4 and 5 depict the bus-oriented control processor and I/O structure. During design, an effort was made to keep as much of the hardware as possible under computer control. This maximized the flexibility of the system by shifting much of the application-specific configurations to the software. Similar to the hardware structure, nodal software is divided along functional boundaries. Many routines are entered through external interrupt and relative asynchronism between routine execution is controlled by a special interrupt dispatcher that maintains a prioritized queue of scheduled processes [7]. The interrupt dispatcher determines the order of events and insures that no process will begin unless certain conditions have been satisfied. Figure 6 is a functional block diagram illustrating the various program modules incorporated in the TS software.

The user interface to the timing subsystem consists of a software monitor and debugger that allows the operator to set

up experiments by defining memory locations and initiating a run. The monitor responds to simple commands and is always available to the user (even during an experiment). Several timing functions and system configurations may be invoked by manipulating the set-up parameters through the operator keyboard. In this light, the TS can be considered a programmable device cable of clock error measurement, control, and distribution.

Software development was made less cumbersome through the use of a microcomputer development system. It can also be used as an intelligent terminal to provide general communication and data-logging functions. Experiment set-ups can be stored on disk and down-loaded to the TS.

LINK TERMINATION

Special-purpose link termination processors support the clock data communications through service channel multiplexers. These can be wired to accommodate many of the standard military data rates. In particular, they follow the Synchronous Data Link Control (SDLC) protocol. Information frames contain the timing and status indicators and are of programmable length (typically 536 bits). A flag detect circuit provides a pulse to the time interval measurement unit to mark time-of-arrival at the same point for each frame. A 16-bit cyclic redundancy check feature identifies the presence of bit errors. Due to the fact that critical timing information is contained in these frames, errored TRIP's are discarded.

TIME INTERVAL MEASUREMENT

The basic criteria required to determine clock error is derived from direct measurement of once-per-second pulses from divided-down, buffered 5 MHz frequency standard outputs. Resolution of +/- 10 ns is obtained through the use of a 100 MHz counter with multiple output registers. On each connecting link there is a transfer of timing events and control signals. This data is transferred in blocks (TRIP's) separated by frame markers that emanate from each node at a rate of once-per-second. TRIP data format is shown in Figure 7. Time-of-arrival resolution is 10 ns and the data rate is 4 KHz via the service channel for all nodes.

CLOCK CORRECTION AND PERFORMANCE ASSESSMENT

The fundamental function performed by the clock correction control loop is the generation of a set of reference frequencies, derived from a 5-MHz node reference, to avoid buffer overflow or depletion. The unperturbed standard output is called the station standard and the adjusted version of this signal is called the node reference. A phase shifting device implements the correction in response to a digital control command. The shifted output from this device then goes to a digital clock which supplies a 1-pps time reference to all equipment at the node, and in particular, to the time-of-arrival measurement device.

TS-based performance assessment consists of storing a series of 10-minute averages of computed clock error, path delay (for double-ended exchanges only), and averages of node reference clock vs. up to three external 1-pps signals. By connecting external pulses for comparison, nodal drift may be compared to any other clock or, by trace-back through additional receivers, to a LORAN-C signal, and ultimately, to U.S. National Time Standards.

NETWORK CONFIGURATION

TROPO AND LOS LINKS

A small tandem network (three nodes, two single-ended links) consisting of a troposcatter and microwave link was configured at RADC, Rome, NY. The RADC test sites included modem and radio equipment to support the links. Figure 8 indicates the geographical layout of the sites used in the field test program. The Verona and GAFB locations were connected by a LOS link through a repeat station at Stockbridge (normally left unattended). Philco-Ford LOS baseband modems operating at 3.088 MHz were used in conjunction with Philco-Ford LC-8D radios broadcasting in the 8 GHz region. A one-way medium-only delay of 138.3 μ s over 25.7 miles was observed. Timing variations were typically less than 10 ns.

An important aspect of the link selection process was to evaluate the performance of a fading channel when used to support a timing function. At the time, the Youngstown-to-

Verona TROPO path (168 statute miles) was available and configured with Raytheon DAR-IV digital modems and AN/TRC-132A radios operating at 3.5 MHz over the 4.4 - 5.0 GHz band (C band), respectively. A one-way medium delay of 910.1 μ s with variations of about ± 20 ns was verified [8].

CONNECTING THE TIMING SUBSYSTEM

At each link termination site, the TS units were connected directly to modems and radios. A MUX hierarchy was not used. TRIP flag sequences generate a reference pulse at each receiver to stop the interval counter. Combined with transmit timing information contained in the TRIP, a clock error term can be computed. For single-ended transfers, average path/equipment delay must be included to eliminate a phase offset that would otherwise be the result.

As an example of node configuration, Figure 9 shows the connections required at the Verona site as middle node in a tandem network. In an effort to improve monitorability and measurement reliability, NBS-developed Frequency Measurement Terminals (FMT's) were used to measure the same pulses that the TS's were logging. Also, from each FMT, a decoded LORAN-C 1-pps signal was connected to one of the TS auxiliary inputs for direct comparison to the nodal station standard. Thus, each TS measured and stored the LORAN-C signal relative to its adjusted clock; giving a level of redundancy. This provided a means to evaluate clock trends compared to an unadjusted ultimate reference or, any other site standard.

MEASUREMENT AND REFERENCE FACILITIES

The choice of frequency source for each TS station centered around availability. If at a given site, a frequency source was not available, the TS employed its own internal source to allow stand-alone operation. During the design phase of this program, it was anticipated that, in certain tests, the TS's would be equipped with atomic standards. Therefore, space was provided in the chassis for such units. However, two of the three TS's also contained VCXO's for stand-alone operation and to compare the performance of these devices with higher quality standards. Under this configuration, the TS oscillator was used to drive the internal synthesizer and frequency distribution system. It was observed that the characteristics of the quartz devices are quite satisfactory when operated in the slaved mode. Furthermore,

the high servo update of 1 per second is well-matched to the use of quartz sources in the subsystems.

A single telephone interface was wired using data couplers furnished by the FMT's. Nodal management, setup, and parameter transfers were accomplished by accessing each TS individually. Through this technique, control and management functions were handled by using a remote terminal and dialing telephone numbers. This is acceptable for a small network but a large network (i.e., greater than six nodes) would benefit from a node management protocol (for the purpose of network configuration) gaining TS control through TRIP data packet exchanges originating from a single controller and propagating around the network.

EXPERIMENTS

EQUIPMENT DELAY

The TS equipment can be used to measure round-trip delay in modems and radios if they can be configured in loop-back mode. Actually, for the purpose of directly measuring round-trip path and equipment delay, a loop-back through the transmission path with a single TS both as source and sink yields the cumulative delay of all link elements. Generally, a survey of individual delays of each piece of link equipment is required to properly configure an experiment. This procedure will help to identify any asymmetric signal propagation properties so they can be accommodated at set-up time. For double-ended exchanges, any difference in opposite-path delays will manifest itself as a phase offset superimposed on clock-correction terms. Directed-control schemes rely on frequency averaging so equipment delay compensations need not be included if frequency tracking is the desired result.

FIELD EXPERIMENTS

Emphasis in the experiment series was placed on observing basic network synchronization through node-to-node clock error logging. Time did not permit more extensive evaluation of such things as: phase alignment, alternate tracking loop bandwidths, multiple stage acquisition strategies, and tier-type self-organizing timing techniques. Furthermore, due to link equipment availability, only a tandem, single-ended exchange network configuration was possible.

The Seneca, NY, LORAN-C station was considered to be the ultimate network reference. This station is slaved to the Dana, IN, East coast chain master. Since experiments were concerned with frequency alignment, a calibration procedure determined the relative frequency drift between the LORAN pulse and each site standard. GAFB and Verona employed rubidium sources. Youngstown used a cesium clock. Through receivers located in each FMT (one at each site) LORAN-node relative frequency trends were measured and plotted as shown in Figure 10. Small variations are smoothed so the plots represent average trends. Data was gathered over a period of about eight days. Notice that each site standard is drifting in the same direction. Although not usually the case, it was assumed that each source was drifting at a constant rate; short-term stability tends to be better for rubidium sources than for cesium clocks. Most importantly, this frequency comparison forms the basis for evaluating node performance, since the TS's use the site standards directly as a timing source to drive station interval measurement devices and synthesizers, and all performance assessment measurements are made relative to each site standard.

Testing consisted of a series of six relatively short experiments. Run times varied between 24 and 48 hours. Each used the directed control type of synchronization, one with automatic master selection. Typically, an experiment session proceeds as follows:

- Select an ultimate, unadjusted reference through which the performance of each node can be compared.
- Determine the frequency offset of each site standard compared to the ultimate reference.
- Configure the network for a timing experiment, including node parameters and connections for evaluation equipment.
- Permit experiment to run for at least 24 hours so that acquisitional effects, and other short-term perturbations, do not significantly affect the measurement series.
- Compare resulting time interval measurements of the adjusted TS clock with those of each unadjusted site standard. These measurements can be collected through

either the FMT, TS, or both.

- Plot the frequency offset between the TS adjusted clock and the unadjusted site standard (maintain directionality).
- Add or subtract the frequency offset of the site standard compared to the ultimate reference. The result is the net frequency error. Frequency comparisons may be either node-to-node or node-to-ultimate reference.

Table 1 summarizes network performance for each of the six experiments. Experiment 4 ran with the original version of time reference distribution including the path length counter [4]. Experiment 5 used master/slave for synchronization but superimposed a much larger frequency offset on the master node to simulate a poor clock. Reading across Table 1 illustrates that each TS was able to accommodate the added offset which was set at 2.8×10^{-9} . Experiment 6 incorporated the use of a quartz VCXO in the GAFB slave node to evaluate its performance as a station standard. To the limits of available measurement capability, the quartz slave performed admirably with only slightly higher short-term fluctuations. In each case, test results show that the network had in fact, achieved frequency alignment and stable operation. For these experiments, inverse tracking loop noise bandwidths were 45 Hz and 450 Hz for LOS and TROPO links, respectively.

CONCLUDING REMARKS

Observations made during performance evaluation indicate that steady-state frequency tracking between geographically distant nodes was achieved. By referencing an unadjusted clock, the relative drift of each of the nodal clocks was compared. Experiments support conclusions from [8] that timing information can be successfully transferred over both LOS and TROPO channels. For this series of experiments, time interval measurements were triggered directly from received packets. When a multiplexer hierarchy exists, alternate reference pulse extraction schemes through MUX or radio framing patterns, are within the capabilities of the existing TS design.

It should be evident that the timing subsystem prototypes are capable of implementing and evaluating many different arrangements in network architecture and synchronization technique. Recently, a set of desirable attributes for the DCS switched digital network was proposed [9], [10] as enhancements to a basic directed control approach offering features considered important in a military environment. The TS prototypes can easily be programmed to employ these attributes.

The TS hardware is arranged around a general-purpose microprocessor architecture and the I/O devices can deliver a wide range of data rates and MUXing schemes. The equipment was found to be quite reliable with a computed MTBF of 1400 hours [11] substantiated by zero failures in the field after periodic use over a span of about six months. Generally, microprocessor-based designs are particularly suitable for use in timing and synch applications.

Considering the somewhat restricted testing schedule for this program, it is strongly encouraged that further experimentation be undertaken. To investigate some of the more pressing issues, additional tests should include the evaluation of: acquisition and tracking strategies, single-ended vs. double-ended exchanges, precise time techniques, and the level of network automation. For example, a network management protocol could be easily implemented through existing overhead space in the TRIP's. This would centralize control for start-up and monitoring purposes but would not jeopardize the function of distributed references and self-organization.

In military applications requiring clock control, survivability, reliability, maintainability, and monitorability take on much more emphasis: the timing subsystems reported on here already possess these features to some degree. A more difficult problem is that of selecting a general approach for a timing technique, and more precisely, phase referencing or frequency alignment. A directed control system (master/slave) is most often recommended as the best compromise, especially if one of the more urgent requirements is to eliminate digital traffic interruptions inherent in independent clock networks. Mutual synch systems are not considered good candidates for DCS applications [1], [5], [6]. Several tactical programs (JTIDS, SEEK-TALK) specify the use of high quality frequency standards [12] maintaining that buffer resets will be infrequent when clocks

run independently. Even a minimal timing function would improve link availability and overall reliability while at the same time make possible replacement of some expensive standards with quartz sources.

The Timing Subsystem Development program has demonstrated that communication link termination, clock control and correction, network synchronization and performance assessment capabilities can be implemented using a single microprocessor-controlled device. Furthermore, there is ample evidence that the current design can support the interfacing and processing requirements for advanced testing well into the foreseeable future.

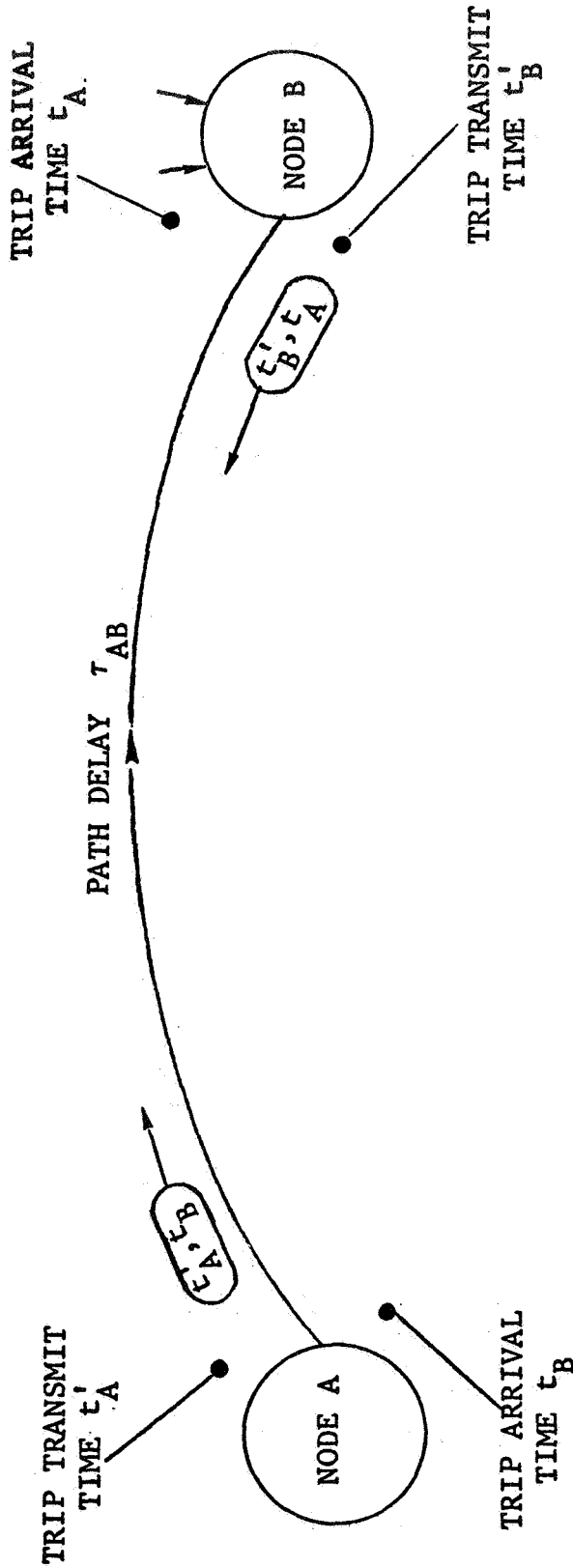
ACKNOWLEDGMENTS

The work reported on in this paper was supported by the Rome Air Development Center under Contract No. F30602-78-C-0287. The principal investigators at CNR were: Dr. P. Bello, Dr. P. Alexander, K. Backe, and D. Miller. CNR would also like to acknowledge the assistance and encouragement given by the RADC Project Engineer, W. Cote, and Site Supervising Engineers, J. Findley, and D. Mangold. Many other RADC personnel including W. Voss, W. Schneider, J. Pritchard, and J. Krause also made substantial contributions to the successful operation of the field equipment.

REFERENCES

- [1] CNR, Inc., "Timing Subsystem Development," Final Technical Report, RADC-TR-82-124, May 1982.
- [2] H. A. Stover, "Time Reference Concept for the Timing and Synchronization of the Digital DCS," DCASEF TC39-73, July 1973.
- [3] H. A. Stover, "Improved Time Reference Distribution for a Synchronous Digital Communications Network," Proceedings PTTI Meeting, November 1976, pp. 147-166.
- [4] Clarkson College of Technology, "A Study of Microprocessor Implementation of Time Reference Distribution," RADC Phase Report TR-77-20, June 1977.
- [5] Harris Corp., "Study of Alternative Techniques for Communication Network Timing/Synchronization," Final Report, March 1977.
- [6] M. Willard, et al., "DCS Synchronization Subsystem Optimization/Comparison Study," Harris Corp., Final Report, November 1979.
- [7] CNR, Inc., "Timing Subsystem Development - Computer Program Manual," Prepared under Contract No. F30602-78-C-0287 with RADC, September 1981.
- [8] CNR, Inc., "System Timing and Synchronization," Final Technical Report on Contract No. F30602-76-C-0347 with RADC, May 1978.
- [9] H. A. Stover, "Attributes for Timing in a Digital DCS," Defense Communications Engineering Center, Publication No. 1-80, July 1980.
- [10] H. A. Stover, "Network Timing/Synchronization for Defense Communications," IEEE Trans. on Communications Vol. COM-28, August, 1980, pp. 1234-1244.
- [11] CNR, Inc., "Timing Subsystem Development - Reliability and Maintainability Analysis," Prepared under Contract No. F30602-78-C-0287 with RADC, December 1981.

- [12] D. B. Brick and F. W. Ellersick, "Future Air Force Tactical Communications," IEEE Trans. on Communications, Vol. COM-28, August 1980, pp. 1551-1572.



$$\begin{aligned}
 \text{TRIP ARRIVAL TIME AT B (RELATIVE TO A)} &= t'_A - t_A + \tau_{AB} && \text{SINGLE-ENDED COMPUTATION} \\
 \text{TRIP ARRIVAL TIME AT A (RELATIVE TO B)} &= t'_B - t_B + \tau_{BA} && \\
 \text{CLOCK ERROR (EQUAL DELAYS) } u &= \frac{1}{2}(t'_A - t_A - t'_B + t_B) && \text{DOUBLE-ENDED COMPUTATION} \\
 &= \text{CLOCK A - CLOCK B} && \\
 &= \text{(START-TO-STOP TIME)} &&
 \end{aligned}$$

$$\text{PATH DELAY } \tau_{AB} = \frac{1}{2} \left[(t_A + t_B) - (t'_A + t'_B) \right] \quad \text{ASSUMING } \tau_{AB} = \tau_{BA}$$

Figure 1 Clock Error and Path Delay Calculations for Single- and Double-Ended Exchanges

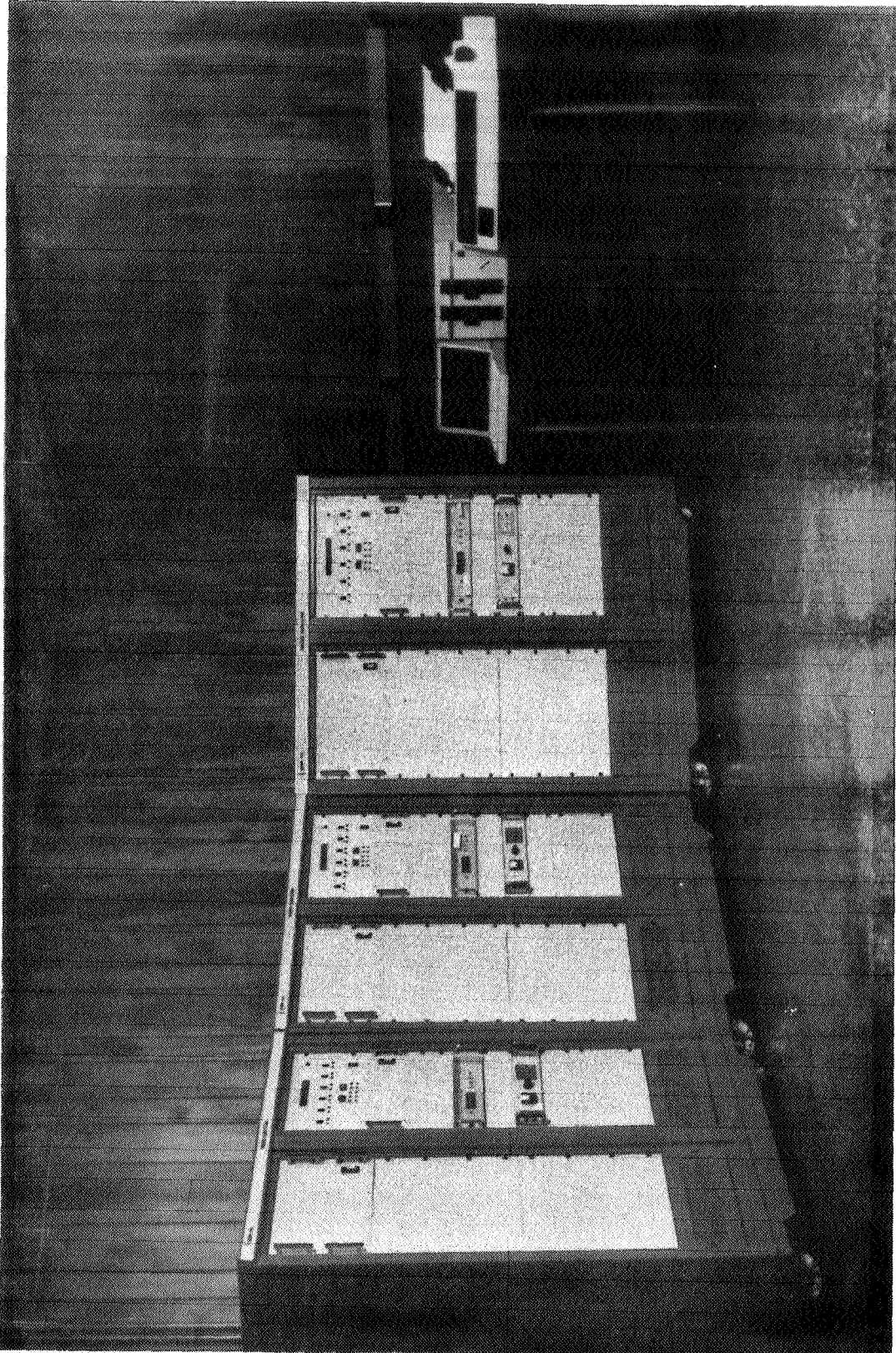


Figure 2 Timing Subsystems (3) with Microcomputer Development Station

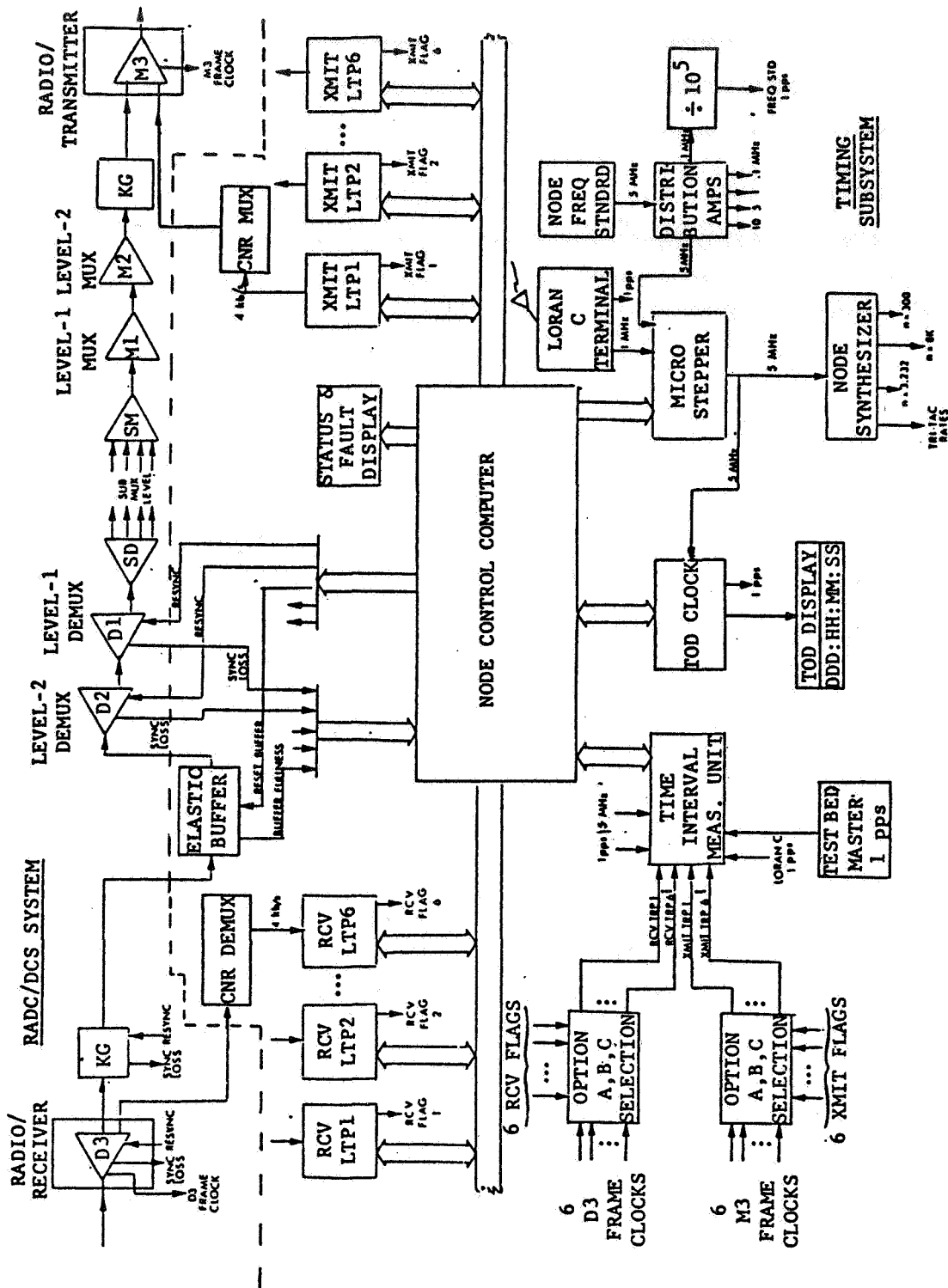


Figure 3 Block Diagram of Timing Subsystem Showing Interfaces with Link Multiplexers

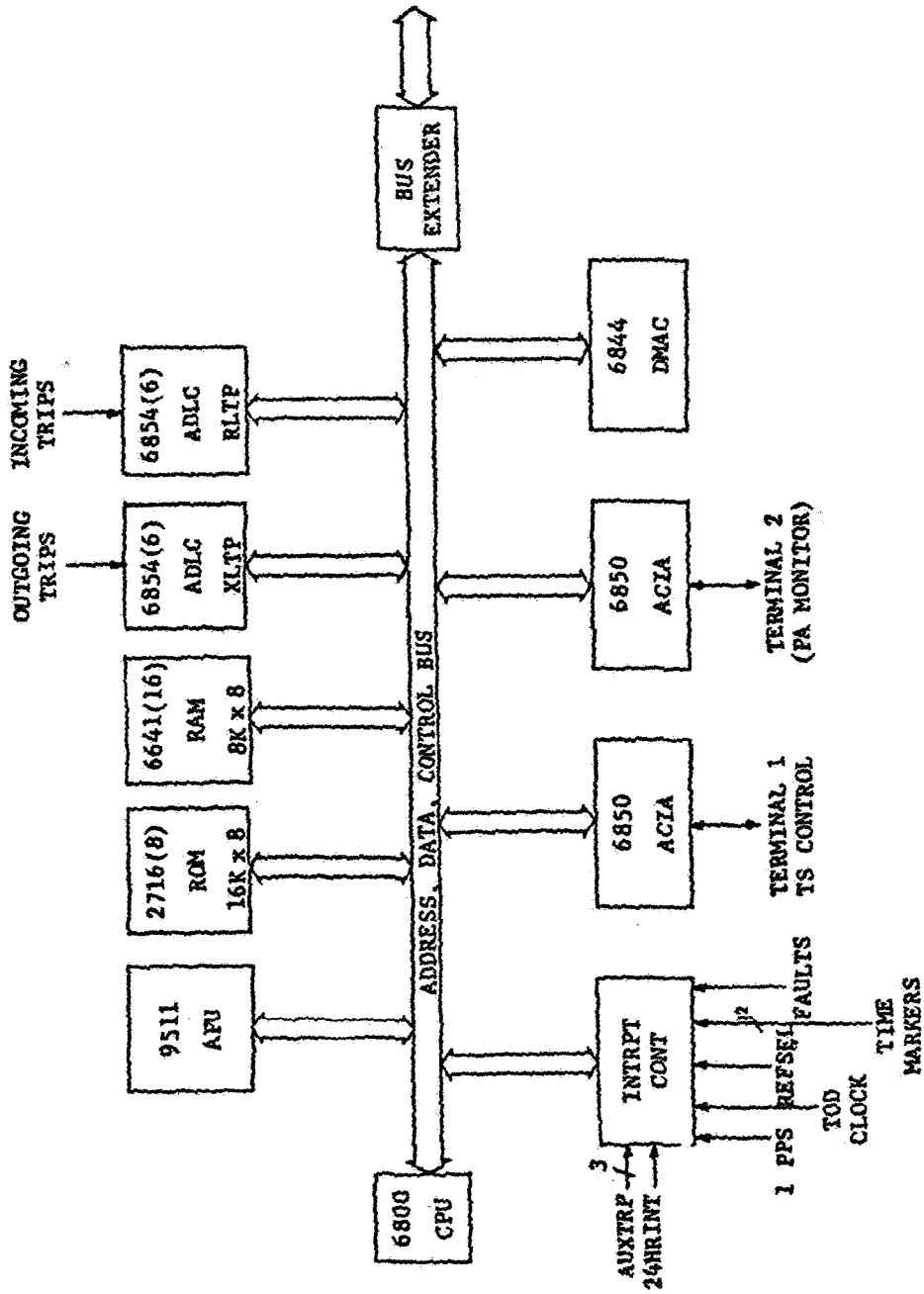


Figure 4 Node Control Processor

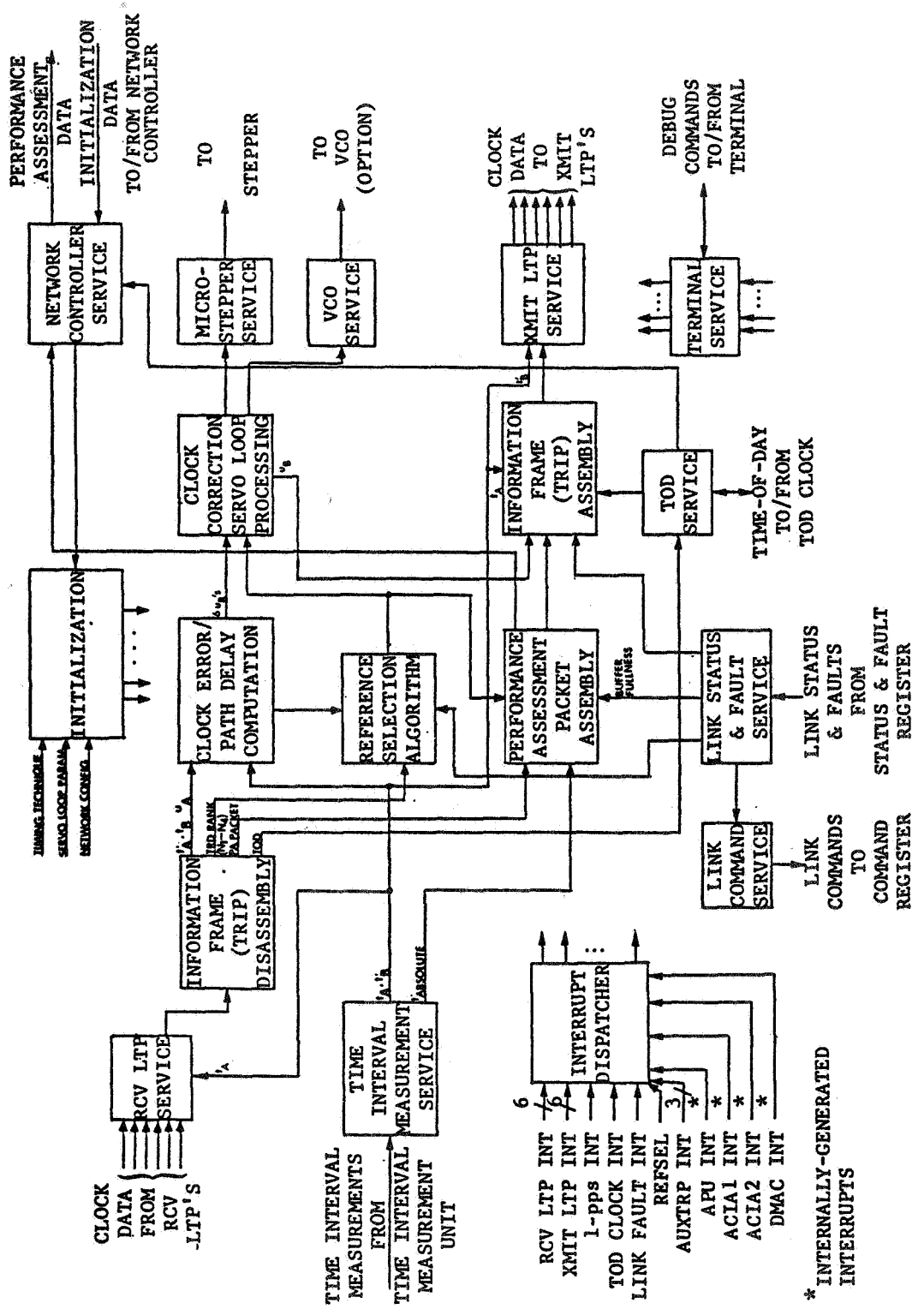


Figure 5 Node Control Computer Functional Block Diagram

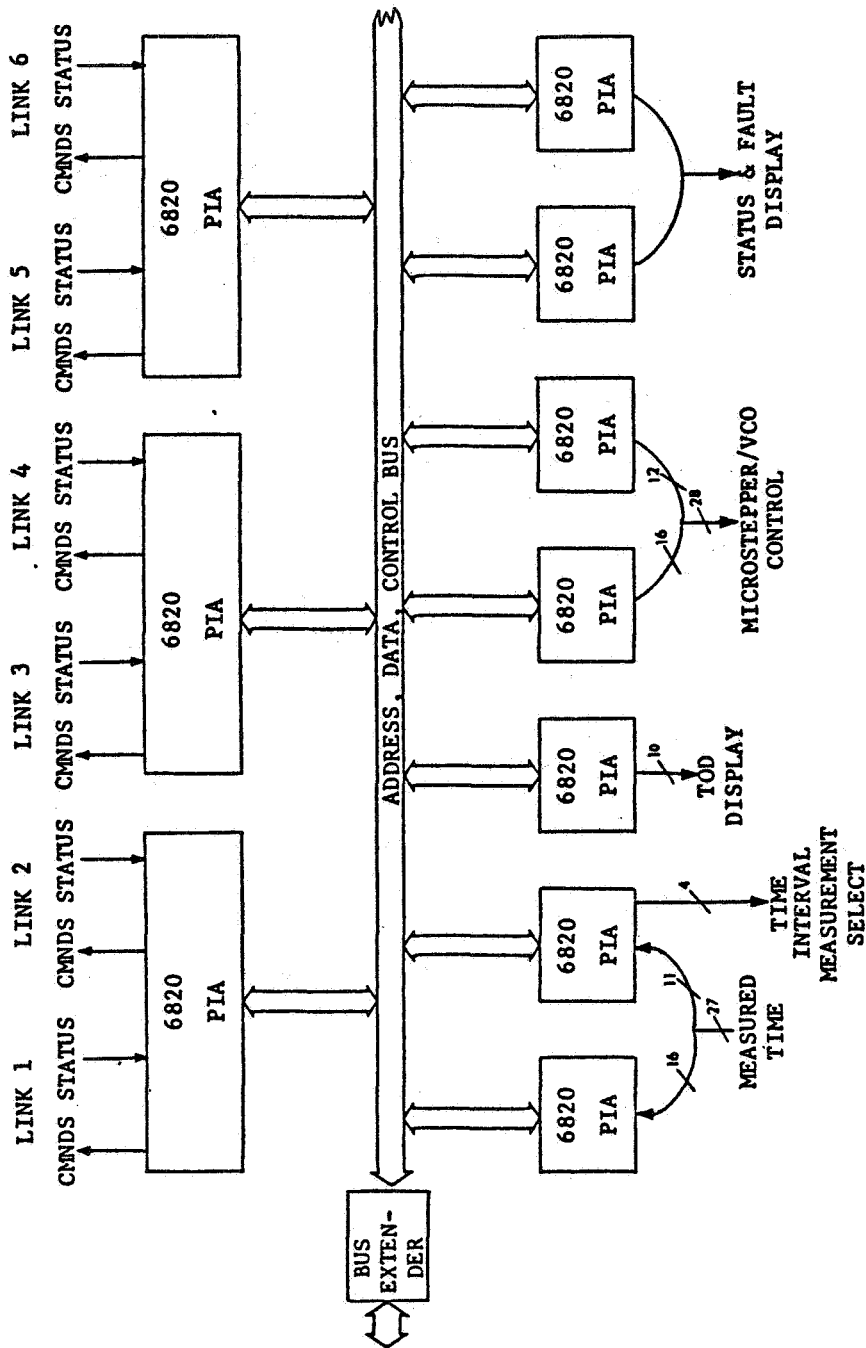
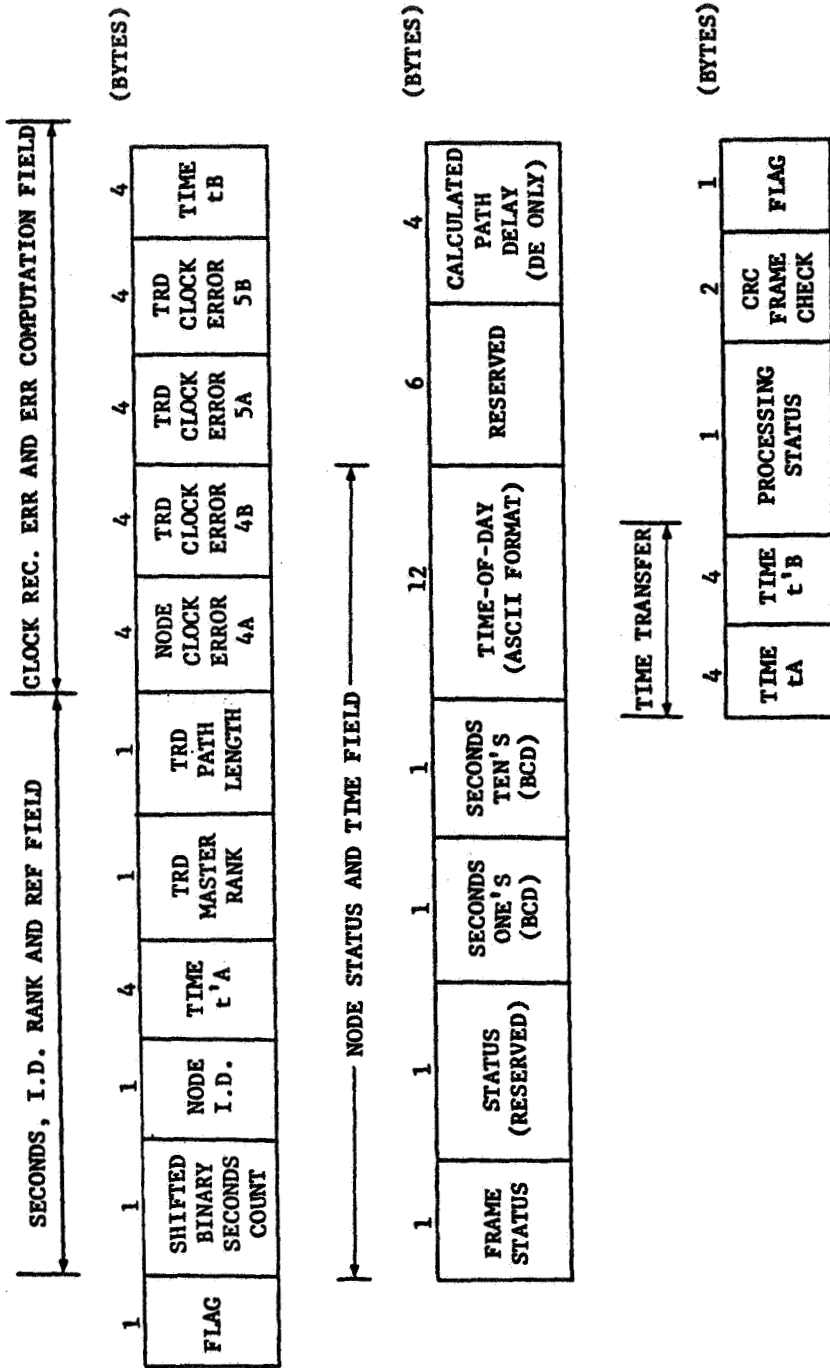


Figure 6 Parallel I/O



[TOTAL NUMBER OF BYTES = 67]

[TOTAL NUMBER OF BITS = 536]

Figure 7 Clock Data TRIP Format

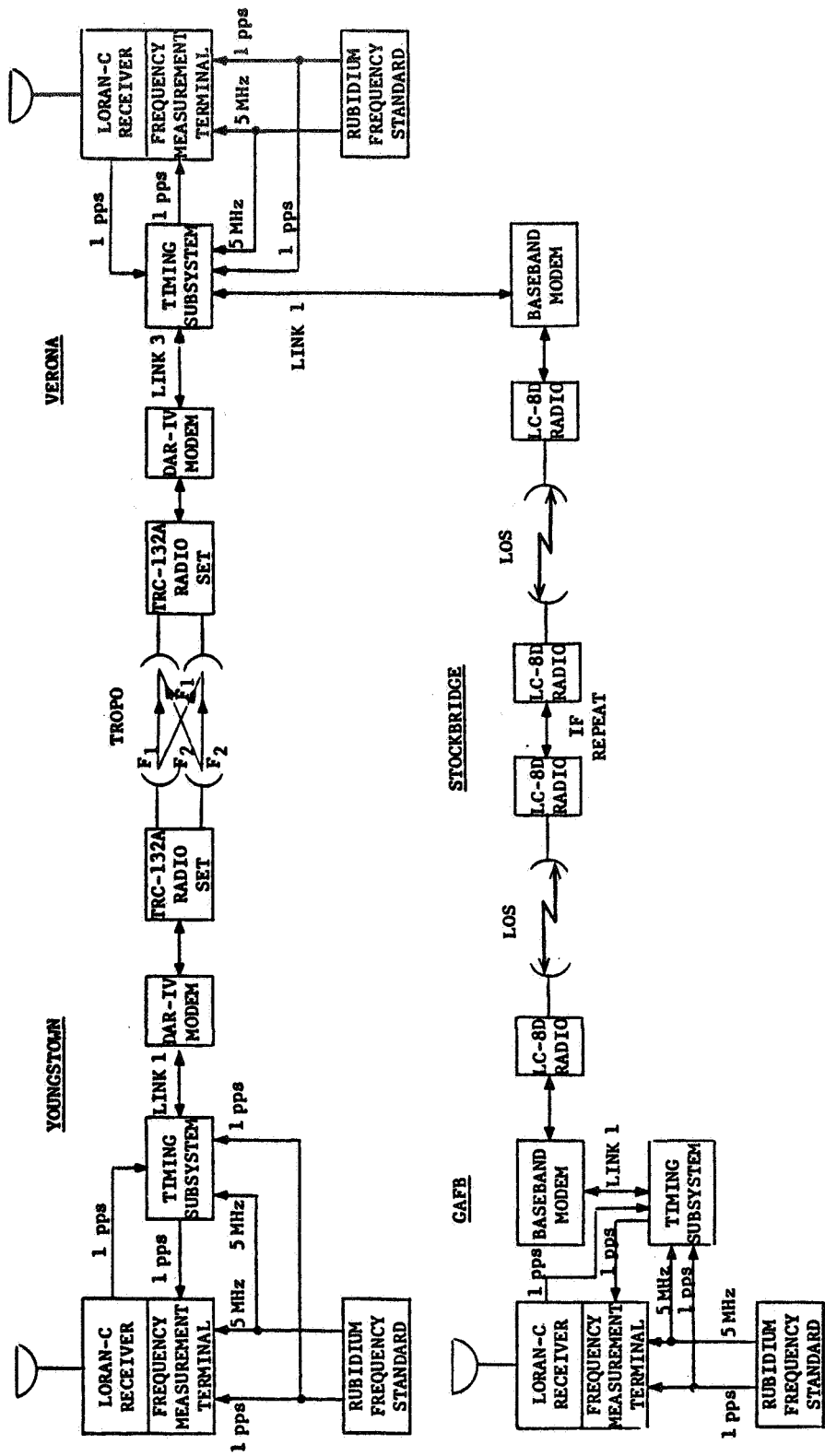
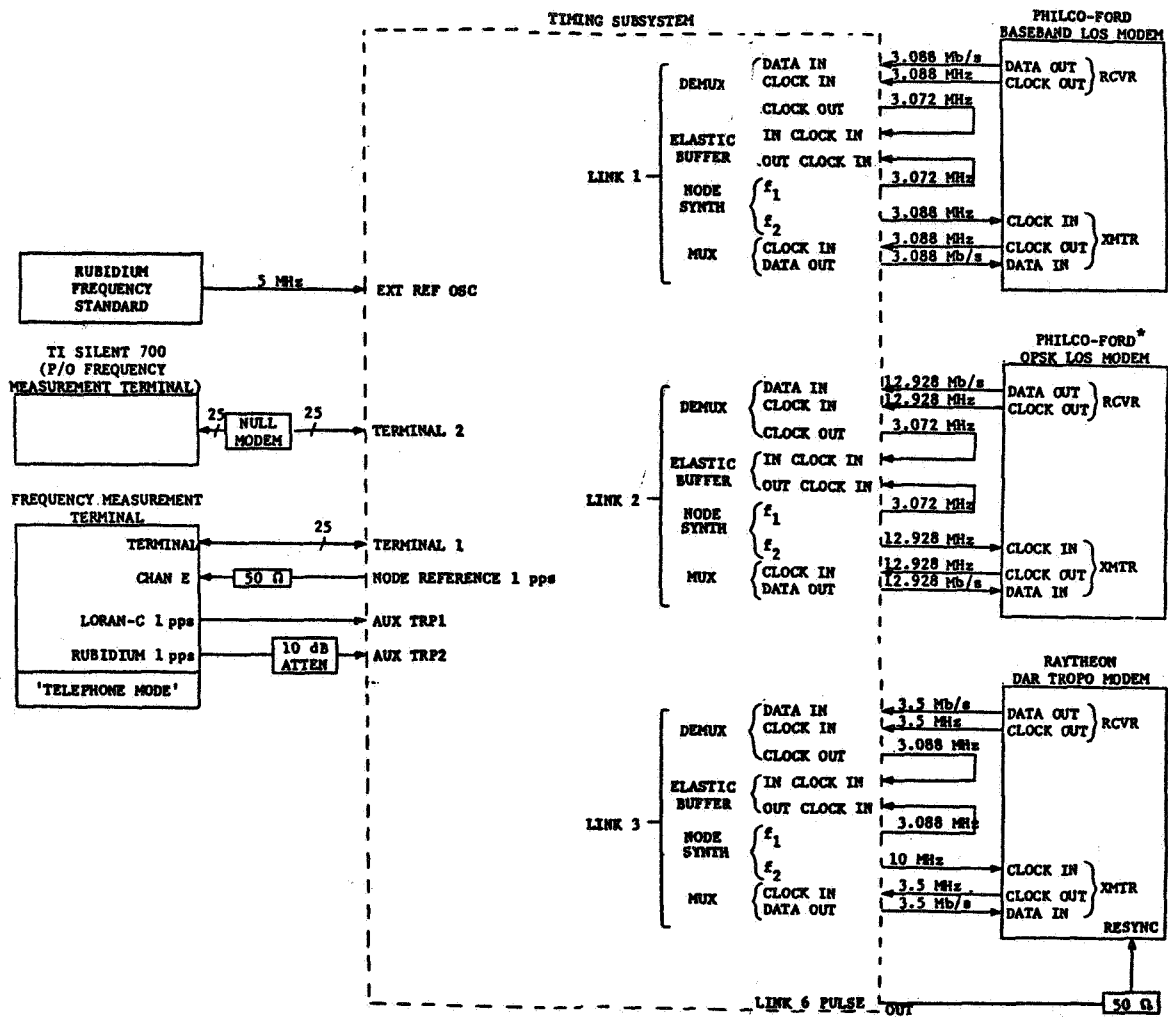


Figure 8 Three-Node Tandem Network with LOS and TROPO Links



* This link not used.

Figure 9 Node Configuration (Verona)

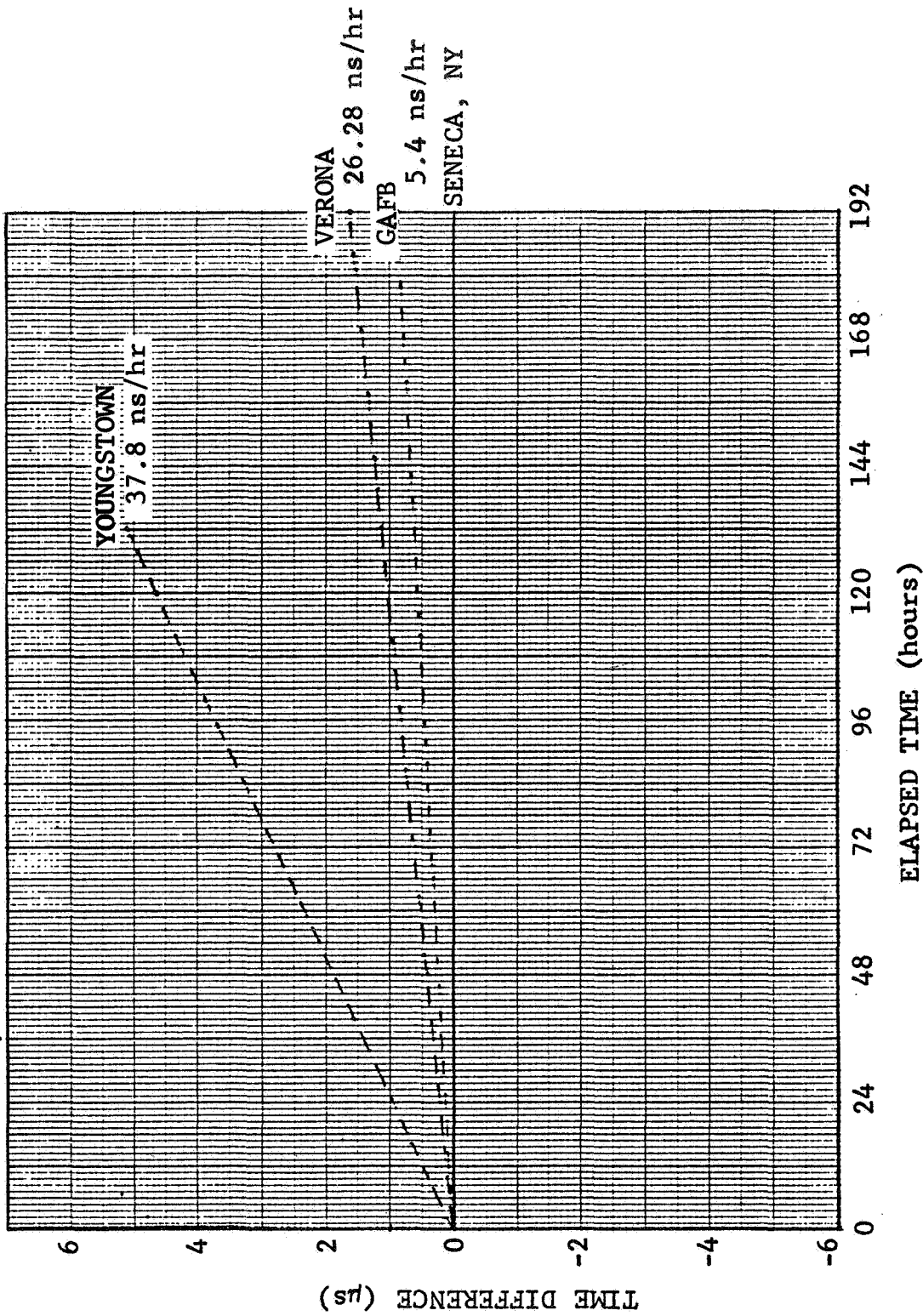


Figure 10 Seneca, NY, LORAN-C Station Frequency vs. Unadjusted Node Frequency Standards

TABLE 1
SUMMARY OF NETWORK SYNCHRONIZATION PERFORMANCE*

EXPERIMENT	TYPE	FREQUENCY OFFSET AS COMPARED TO LORAN-C SENECA, NY			
		YOUNGSTOWN	VERONA	GAFB	
Site Standard	Free Running Rubidium Standard	1.05×10^{-11}	7.3×10^{-12}	1.5×10^{-12}	
1	2N-M/S	1.05×10^{-11} (Master)	1.03×10^{-11}	--	
2	2N-M/S	--	2.3×10^{-12} (Master)	2.3×10^{-12}	
3	3N-T-M/S	1.05×10^{-11} (Master)	1.05×10^{-11}	1.05×10^{-11}	
4	3N-T-TRD	1.05×10^{-11} (Master)	1.05×10^{-11}	1.05×10^{-11}	
5	3N-T-M/S Master-Lrg. Freq. Offset	2.8099×10^{-9} (Master)	2.8×10^{-9}	2.8×10^{-9}	
6	3N-T-M/S Slave VCO	2.8099×10^{-9} (Master)	2.8×10^{-9}	2.81×10^{-9}	

* Read across to determine node-to-node frequency offset.

QUESTIONS AND ANSWERS

None for Paper #20

AEROSPACE GUIDANCE AND METROLOGY CENTER (AGMC)
Inertial Navigation/Calibration/Precise Time and Frequency Capabilities

Larry M. Galloway and James F. Barnaba
Newark Air Force Station, Ohio

ABSTRACT

The Aerospace Guidance and Metrology Center was conceived in 1959 to be the US Air Force Inertial Navigation and Metrology Center. This paper will show the mission capabilities of the Inertial Navigation Maintenance Center and the Air Force Measurement and Standards Laboratory. Highlighted will be the precise time and frequency program developed by AGMC to support Air Force precise time and frequency requirements worldwide. A description of the past, present, and future precise time and frequency activities will be presented.

This paper is not intended as a technical presentation, but as a discussion of the US Air Force capabilities at Newark AFS. It's important to note that Newark AFS is located in Newark, Ohio, not Newark, New Jersey, as is often thought.

As you can tell from the name Aerospace Guidance and Metrology Center (AGMC), the mission at Newark AFS is twofold. One is the Inertial Guidance or Inertial Navigation mission and the other is the Air Force Metrology Center.

First, we will briefly tell you a little about what is referred to as the inertial navigation side of the house. Most of the 2600 or so people who work at AGMC are involved with the diagnostic testing, overhaul, repair, and checkout of inertial guidance systems for missiles and inertial navigation units for aircraft. This is a highly specialized career field and one of the reasons that Newark Air Force Station is unique.

The Missile Inertial Guidance System workload in the past included the Atlas and Titan, along with the current Minuteman System. Aircraft Inertial Navigation Systems serviced at AGMC include the A-7, F-4, F-111, and the C-5A.

The other unique mission at Newark Air Force Station is the Air Force Metrology Center. As you probably know, metrology is the science of measurement and in general, we are talking about calibration. The number of personnel assigned to the Metrology Directorate at AGMC is only about 220. However, a lot of responsibility is involved. The Air Force Measurement and Standards Laboratory is located at AGMC with direct traceability to NBS and the USNO. The underground laboratory complex consists of four floors

descending in a tier with the lowest level at a depth of 55 feet. The concrete walls enclosing the laboratory taper from 6 feet at ground level to 7 feet at bottom level. The floor at bottom level is 11 feet thick. This large mass of concrete provides excellent thermal stability and vibration damping necessary for a laboratory performing state-of-the-art measurements. The standards at AGMC are used to calibrate the Air Force Base Standards in precision measurement equipment laboratories (PMELs) located throughout the world. Major measurement areas at AGMC include force, temperature, pressure, vibration, sound, vacuum, flow, mass, dimensional, optics, DC, low frequency RF, microwave, infrared, laser, and precise time and frequency.

This brings us to the major portion of this paper, the Precise Time and Frequency Program at AGMC. In the 1960s, most PMELs had frequency calibration requirements; for example, oscillators in frequency counters, but very few, if any, precise time requirements. Several Air Force activities had timing requirements, such as the Baker Nunn sites, Satellite Control Facility sites, and one or two classified precise time users. Rather than having precise time available in the PMELs, time was supplied to Air Force activities worldwide directly from AGMC utilizing two person clock teams. In the beginning, civilians were utilized, but today trained military personnel perform most portable clock timing requirements. A two week precise time-keeping school has been established by the United States Air Force Air Training Command, Lowry AFB, Colorado. All military and civilian personnel must attend this training prior to assuming timekeeping duties.

Our Precise Time and Time Interval (PTTI) program has been quite successful using the Hewlett-Packard E21-5061A Flying Clock, the Frequency Time Systems 4010 Light Weight Clock, and the Austron 1210 Crystal Clock. As more precise time requirements evolved, the expense of portable clock trips became prohibitive.

Alternate methods of providing precise time had to be developed. One method being applied is self-sufficiency where the user buys equipment and takes care of his own timing requirements. Examples of this would be TV Line-10, Loran-C, and various satellite timing receivers. Another method being utilized is to establish additional sources of precise time in certain geographical areas. Examples of this are the timing centers for the Eastern and Western Test Ranges, the Precise Time Reference Station at Elmendorf, Alaska, and the Precise Time and Frequency Consoles (PTFC) placed in certain PMELs. The PTFC provides an inexpensive timekeeping system that allows a trained technician to maintain and provide time service to selected AF users. Currently 26 PTFC systems are located strategically throughout the Air Force's approximately 129 Precision Measurement Equipment Laboratories.

Most Air Force precise time users require 100 microsecond timing accuracy. As a result, very few field sites are supported directly from AGMC today. Looking toward the future, we envision more self-sufficiency and more utilization of satellite timing methods.

Well, as you have probably noticed, not much has been said about frequency capability. In the 1960s, each Air Force PMEL was supplied with a VLF frequency comparator. This scheme worked quite well until the Navy VLF stations switched to (minimum shift keying) MSK. A few MSK converters were purchased and sent to labs who were totally dependent on those VLF stations; however, a lot of locations still seemed to have reception problems and it became difficult to determine if it was personnel problems or equipment problems for two reasons:

- a. The decline of expertise of PMEL technicians.
- b. The VLF receivers were getting very old, unreliable, and difficult to keep in repair.

Currently we are in the process of replacing the old VLF frequency comparator receivers with the new automatic Loran-C frequency monitors.

We have addressed the AGMC support of Air Force precise time and frequency requirements and have only one final aspect to cover. Just a few years back, it was determined that the cost of maintaining Air Force atomic standards was quite high. A feasibility comparison study was conducted and the decision was made to establish a Technology Repair Center (TRC) within the Maintenance Directorate. The TRC is responsible for repair and calibration of atomic standards. A large bench stock of components, cesium and rubidium tubes, and trained electronic technicians allow our TRC to provide quality repair and calibration service with a quick turnaround to all customers. Presently we provide repair service by Memorandum of Agreement (MOA) to Baker-Nunn, Satellite Control and Communication facilities, and other DOD agencies. Any DOD agency wishing to use our services should contact the appropriate AGMC office.

In summary, AGMC has a dynamic viable Precise Time and Frequency program that can provide repair service and portable clock timing to approved customers. We provide 0.5 microseconds time transfers at AGMC, 1 microsecond for trips less than 5 days, and at all other times, 2 microseconds. We encourage consultation with AGMC on any time/frequency requirement that you may have.

QUESTIONS AND ANSWERS

DR. COATES:

Questions? Yes?

MR. MIKE GARVEY, FTS

I'd like to comment at the risk of sounding overly commercial. FTS now manufactures the satellite receiver which you showed. The performance of this system is currently limited by the update maintenance capabilities of the Navy. And, I have had some discussions. I think very properly so, with people here at this meeting who realize the potential of this service and the importance of a proper maintenance of that. I think your evaluation of a few hundred microseconds is certainly within the realm of possibility, but I don't think it's customarily quite that large.

MR. GALLOWAY:

Yes. I am completely with agreement of that. We realize that the filter factor of this can resolve that to a number quite smaller than that. But typically, we send this particular instrument to a location and allow it to remain on site approximately five days.

So, in general, we're using Quartz type reference frequency and as you know, with the instrument, the reference frequency can be a major error, so that's the reason. And the truth, if you'd like to be very specific about the number, we believe that we can do a bit less than fifty. Twenty-five is about what we like to talk about.

DR. COATES:

Thank you, Larry.

PORTABLE CLOCK ANALYSES

F. Neville Withington
U.S. Naval Observatory
Washington, D.C.

ABSTRACT

The portable clock remains the most frequently used means of time dissemination and of calibration of precise clocks to the U.S. Naval Observatory Master Clock (USNO MC). Because of this, portable clock trips and the factors that influence the confidence placed in the measurements obtained must be understood. In this paper, the general philosophy of trips and some of the error factors that can occur are discussed. The stability of individual USNO portable clocks is determined by analysis of pre- and post-trip measurements obtained through the USNO data Acquisition and Control System. Using these data, this paper explores their historical accuracy and determines error budgets. The feasibility of determining a statistical "reliability factor" based on the pre- and post-trip readings of an individual clock is also examined. From these studies the dependability and reliability of portable clock trips as a whole, may be concluded.

(ABSTRACT ONLY)

PAPER NOT SUBMITTED

QUESTIONS AND ANSWERS

MR. SAM WARD, Jet Propulsion Laboratory

It's not necessarily a question, but more a statement. Since the pre and post measurements were made in the same environment, one would expect that a stable cesium would get the same answers.

The, how much time offset you can expect when you return is a function of how long it was in some environment, especially magnetic that caused it to, change its rate. And longer trips the measurements, the guesses that we have made is what the longest trip that would be practical before that you got diminishing returns (at one time, I think, we thought it was seven, ten days).

But there's really no relationship between the length of the trip away and the behavior of the clock.

MS. NEVILLE:

And the behavior of the--

MR. WARD:

And the behavior, except for the performance of that individual clock.

MS. NEVILLE:

Right. Which of course, this may be another factor as well.

DR. WINKLER:

I would like to make a comment here which may be useful, to illustrate the direction of these efforts. We are making a major effort to improve the accuracy of portable clock time transfers and the estimate of errors that is an extremely important function. The clock that is very expensive, and one of the results which you see are these searches, which, I must say are excellent to find an objective measure.

Now, such an objective measure as Ms. Neville has shown, can be composed, must be composed of several factors. One of them is documentation. It is utterly necessary, and yet it is more difficult than anyone would think it is to extract from our portable clock carriers the necessary information.

It's a constant struggle. It's, well there are many reasons why that is difficult, but it is absolutely essential.

I think the lesson to be learned from the data shown until now (and I hope that efforts like this will continue) is that a portable clock trip has about the same limitations as any enterprise. There has to be some judgement, how much money you want to spend, and how much is really required.

Well, we do make that selection in some of our clock trips. We send the very best clock which we have. Incidentally your clock 1452 or 3, I think, is older than three years. We do not have any clock which is younger than that at the moment because last year we had absolutely zero dollars available for clock purchases.

MR. MCCULLOUGH, Oceanographic

It, would seem that since the oscillators are banging around in the magnetic fields, the temperature fields and so forth, have those functions been monitored to find out what's going on on a trip, and secondly, have those function been simulated in the laboratory to see what kind of parametric changes to expect?

MS. NEVILLE:

Dr. Winkler can answer that.

DR. WINKLER:

Over the years we have made extensive tests. In fact, one of the best tests ever made was in conjunction with Professor Alley's experiments on a P-3, portable clock (in fact, a very good one) was mounted without protection in the same aircraft, and measured continuously against the clock set. The time base, which was available on that clock set was better than one nanosecond.

And, the greatest effect was during takeoff and landing. You can see that this produced a shock, which produces an almost instantaneous phase offset. The longer lasting frequency changes, or, the residual frequency changes almost have to be considered as partly to be expected. If you use a clock which, for instance the regular 5061 would have an Allan variance for a one day interval of about one part 10 to the 13th. So it's to be expected that your rate will vary by about a part in 10^{13} after a week or so.

What one has to separate is the systematic effects. And coming back to a question of tests, for instance a good test for a portable clock is to turn it upside down in the laboratory. And measure the frequency shifts after one day. We discussed that about 4 years ago, here in the same conference. At that time, I think, somebody I forgot who, brought my attention to the effect in this case is due to the temperature change in the clock. When you do that the temperature gradient will be inverted. There

is one thing frequency shift is a good indication how the clock will perform during the trip when it is exposed to temperature variations. Magnetic fields, correct it should be measured. But all of this goes back to the need to document what's happening. There are some clock trips which are carried out beautifully without any mishap whatsoever. The clock is protected, temperature changes are modest, you don't go from a hot exterior to an air-conditioned interior and so on.

So, in this case I think a greater weight has to be assigned. That is exactly what the cesium is trying to accomplish through assigned weights on the basis of a documented history of the portable clock.

Thank you.

SOME TIME TRANSFER EXPERIENCES WITH INDIAN
EXPERIMENTAL SATELLITE APPLE

B. S. Mathur, P. Banerjee, A. sen Gupta, Mithlesh Saxena
A. K. Hanjura and A. K. Suri
National Physical Laboratory, New Delhi, India

and

C. L. Jain, K. Kumar, M. R. Sivaraman and Sheela
Space Applications Centre,
Ahmedabad, India

ABSTRACT

Clock synchronization and Time Dissemination Experiments in India by means of satellite Symphonie were earlier reported by this group in 10th, 11th and 12th PTTI Meetings. In this paper we report some time transfer experiences with Indian Experimental Satellite APPLE. The satellite APPLE is not stable in its geostationary orbit and its position varies over a large range as compared to Symphonie. In view of this, accuracies and precision achieved are not as good as those reported earlier. But it gave us an opportunity to try out new techniques not attempted earlier with satellite Symphonie, such as active TV technique, transmission of satellite position data along with time code, time signal monitoring with direct reception sets and satellite ranging from three earth stations. Using ranging data obtained from clock synchronization experiments, orbital elements of APPLE were also computed.

These experiences with APPLE will be quite useful in terms of Indian efforts to provide time dissemination services via Indian Domestic Satellite INSAT on an operational basis.

(ABSTRACT ONLY)

PAPER NOT PRESENTED

SESSION V

SYNCHRONIZATION

RADIATION STUDIES AND QUARTZ TECHNOLOGY

Dr. John R. Vig, Chairman
Army Electronics Technology
and Devices Laboratory

SYSTEMATIC EFFECTS IN GPS TIME TRANSFER

W. J. Klepczynski
U. S. Naval Observatory
Washington, D.C.

ABSTRACT

Values of the differences between the USNO Master Clock (MC) and GPS and Space Vehicle time obtained from horizon to horizon tracking of a satellite are examined in order to discover the existence of systematic effects. Differences between the transmitted satellite ephemeris and a batch-processed ephemeris will be compared with the time transfer data to see if correlations exist. In addition, simultaneous common-view time-transfer data will be inspected for systematic effects.

(ABSTRACT ONLY)

PAPER NOT SUBMITTED

QUESTIONS AND ANSWERS

PROFESSOR ALLEY, University of Maryland

Where will the new stations be?

MR. W. J. KLEPCZYNSKI, U.S. Naval Observatory

I don't know exactly where they are going to be. I saw a list of about 10 or 12 distributed geographically throughout the world, but don't ask me for an exact location right now.

MR. R. J. MCCONAHY, JHU/APL

In the SATRAK system we have had a considerable amount of experience with the GPS ephemerides, and we do use the Dahlgren batch fit ephemerides for our processing and we can confirm what you have observed here. However, the big effect is the upload time, that is, the time from the injection of the message into the satellite to the time in which you read it out. They actually take their Kalman filter and make a prediction over about a 26-hour span, and this is then uploaded into the satellite and read out from the memory of the satellite into the navigation message every hour, and that is what you are seeing, so what it does is degrade with time. If you would look at this rather close to an upload time, I think you would see quite different characteristics.

The other thing is that Dahlgren can produce for you a fit not only to the ephemeris but to the clock. In other words, they can produce a joint fit to both the clock coefficients and the ephemeris, and I think if you would use that you would see even less dispersion, probably, then you saw in your own plots.

Thank you.

MR. W. J. KLEPCZYNSKI:

Well, one of the aspects that we are interested in is using GPS as a real time distribution system.

MR. MCCONAHY:

Yes, I understand that, but in order to analyze exactly the way the ephemeris enters into your errors and corrections, I thought that --

MR. KLEPCZYNSKI:

Okay, okay.

MR. R. CRUTCHFIELD, IBM Corporation

We have the contract for the GPS control segment. One gentlemen asked the question where the new monitor station sites are going to be: Diego Garcia, Kwajalein, Hawaii, Colorado Springs, and Ascension.

I wanted to make another point on your first slide, where you mentioned that by January 15th 1983 they are going to change to the new NAV method. Actually, our plan is on December 28th to remove the long-term bias and drift from the clock that you saw, all the charts had bias and drift on them, but by January 15, you're right, that's when we will go to the new NAV method.

Now one other question I wanted to ask you; I find your results quite interesting, did you look at multipath as a possible problem?

MR. KLEPCZYNSKI:

No.

MR. CRUTCHFIELD:

We noticed with the receiver we had in Gaithersburg that multipath would give you a quite repeatable pseudo-range error every day, it will look the same every day.

MR. KLEPCZYNSKI:

Yes. Okay, but the comparison between the two ephemerides doesn't depend on that.

MR. CRUTCHFIELD:

Yes, I agree. That seems to rule that out.

ARCHITECTURE AND PERFORMANCE OF A NEW GPS TIME TRANSFER AND POSITIONING RECEIVER

T.I. Kido, P.C. Ould, and R.J. Van Wechel
Interstate Electronics Corporation
Anaheim, California

ABSTRACT

This paper describes the Interstate Electronics 4200 GPS Receiver System that has been developed for time transfer and low dynamic positioning applications. The receiver employs the NAVSTAR Global Positioning System (GPS) L₁ C/A-code and has three optional solution modes for the clock/navigation state estimation:

- A time transfer-only mode while tracking at least one satellite, with a solution set containing user-clock and oscillator-bias states. Typically this mode can be used for about 12 hours per day with the current NAVSTAR GPS satellite constellation.
- A two-dimensional (2-D) navigation-plus-time transfer mode, with a solution set containing clock and oscillator bias, plus user latitude and longitude states. This mode is operable on three satellites simultaneously, which makes it usable for about 4 hours per day with the current GPS constellation.
- A three-dimensional (3-D) navigation-plus-time transfer mode, with a solution set as for 2-D except for the addition of an altitude state, making it usable for about 2 hours per day at present.

The system consists of a separate preamplifier/antenna and processing unit (5-1/4 inches high by 17-1/4 inches wide by 24 inches deep). The processor has the following four circuitboard assemblies: (1) an RF converter that converts the preamplifier output to baseband for digitizing; (2) a digital signal processor containing a digital correlator, numerically controlled oscillators, and a code generator; (3) a tracking controller equipped with a user clock, digital phase-stepper that fully synchronizes the 1-pps output signal to the nanosecond level, and a microprocessor that operates in conjunction with the signal processor to close the tracking loops; and (4) a data processor for executive control, input/output management, and clock/navigation state estimation.

The processing unit can optionally use either an external frequency reference or its own crystal oscillator. The control/display unit, which is built into the processor's front panel, has a four-line, 40-character liquid crystal display and a 4X4 keypad for mode control and data input. Standard computer interfaces are included.

The paper also summarizes the results of system performance in terms of both single- and multiple-satellite operation.

INTRODUCTION

The Interstate 4200 GPS receiver has been designed for time transfer, 2-D positioning, and 3-D positioning. The time transfer function is handled in a manner that is completely compatible with the time transfer community. A fully synchronized 1-pps output is supplied. The receiver can handle positioning applications in either an absolute- or relative-navigation mode. It can also be used at either fixed or mobile sites.

The receiver operates on the GPS L_1 C/A-code via a single-channel, sequential multiplex. A broadband RF converter converts the GPS signals to baseband, where they are digitized before being processed in a digital signal processor.

The receiver design capitalizes on the latest advances in electronic technology. Two advanced 16-bit microprocessors with 32-bit internal arithmetic are used: one for the carrier and code tracking loop filters, and the other for the clock and navigation state estimation software.

The system's state estimation filter is a five-state U-D factorized¹ Kalman-filter formulation with a state vector consisting of clock bias, oscillator bias, latitude, longitude, and altitude. For time transfer, only the first one or two clock states are estimated. The two clock states with latitude and longitude are estimated for 2-D positioning and time transfer; all five states are estimated for 3-D positioning and time transfer.

The receiver thus permits maximum use of satellites now orbiting in the Navstar constellation. At fixed sites, time transfers with the system can be realized for about 12 hours per day in most areas, by using only one satellite. This makes time transfer an immediately feasible application. On mobile sites — particularly ships — time transfer and 2-D positioning can be achieved with three satellites during about 4 hours per day. With four satellites, a redundant solution in the 2-D mode yields improved accuracy. The 2-D GPS solution, it has been shown,² always yields a more accurate horizontal solution, when altitude is known precisely, than does the 3-D solution for the same number of satellites. The 3-D positioning mode now can be used for about 2 hours per day in most areas, either for precise receiver location in time transfer or for applications where specifically a 3-D position solution is needed.

These combined time transfer/positioning features make the compact receiver especially suitable for fixed instrumentation systems; portable, van-based tracking systems; and shipboard navigation systems.

OVERALL CHARACTERISTICS

Figure 1 shows the 4200 receiver system. Its major characteristics are summarized in table 1.

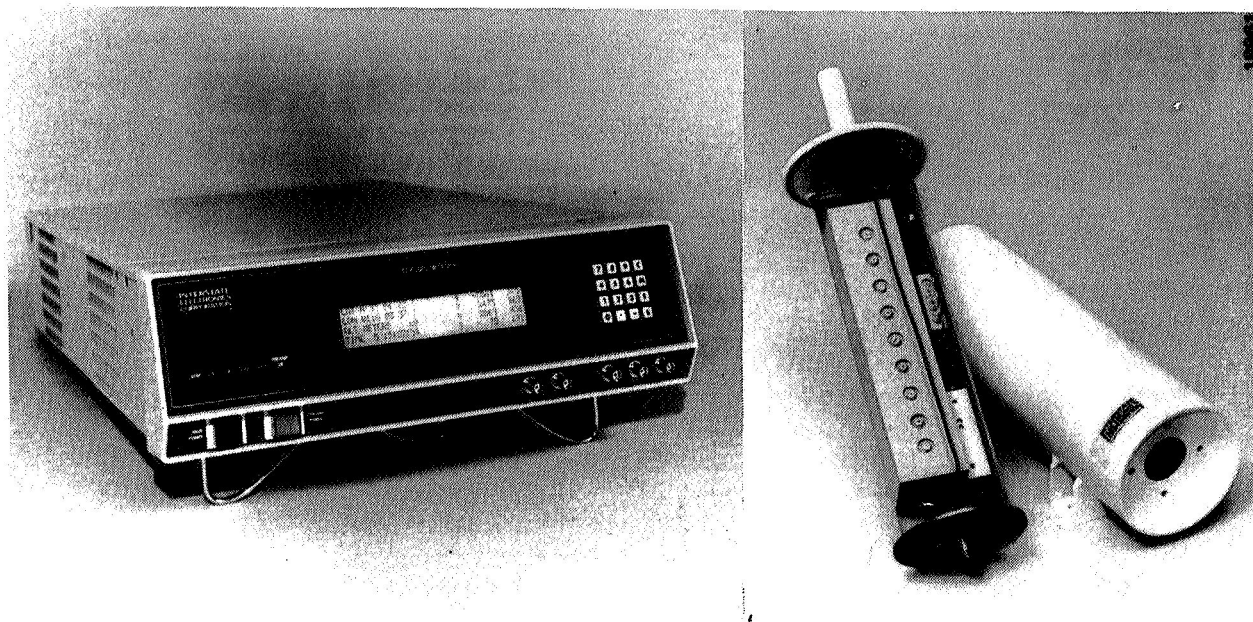


Fig. 1 — GPS receiver with antenna/preamplifier

Mounting and Access

The antenna/preamplifier assembly may be mounted either on a tripod or fixed mast with no additional ground plane structure at a distance of up to 200 feet from the receiver. The receiver itself either can be rack- or bench-mounted. The major processing modules can be reached or removed through the front panel, which hinges up and locks in place. The power supplies, reference oscillator, and line filter can be accessed simply by removing the top cover. Reference inputs and signal outputs are accessible on both the front and rear panels.

Table 1—4200 GPS receiver system characteristics

Antenna	
<ul style="list-style-type: none"> ● Polarization ● Gain 	<p>Righthand circular 0 dB at 5-deg elevation 5 dB at 90-deg elevation</p>
Preamplifier	
<ul style="list-style-type: none"> ● Gain ● Noise Figure ● Bandwidth ● Size 	<p>42 dB 3.2 dB, typical 36 MHz 16 in. L, 4.75 in. dia</p>
Receiver	
<ul style="list-style-type: none"> ● Input <ul style="list-style-type: none"> ● RF ● Reference ● Sync (Optional) ● Power ● Output <ul style="list-style-type: none"> ● Time ● Data* ● Size 	<p>1575.42 MHz at 50 ohms; C/A-code at 1.023 Mb/s 5 MHz at 50 ohms 1 pps at 50 ohms 115-230 VAC, 50-60 Hz</p> <p>1 pps synchronized to GPS/UTC time 5.115 MHz synchronized to 5-MHz reference</p> <p>Latitude (deg, min., sec, tenths of sec); longitude (deg, min., sec, tenths of sec); altitude (m); time of Day (hr, min., sec); clock error (nsec); oscillator error (fractional); Kalman measurement residuals:</p> <ul style="list-style-type: none"> ● Range (m) ● Range rate (m/sec) <p>Satellite view times</p> <p>5.25 in. H, 17.25 in. W, 24.00 in. D (rack-mounting option)</p>
<p>*Available on liquid crystal display, RS-232 serial I/O, and IEEE 488 parallel I/O (optional)</p>	

Power

The unit requires only primary AC power for basic operation. Conversion between 60 Hz/115 VAC and 50 Hz/230 VAC operation can be accomplished by changing a few jumper wires, but without changing any component. The main circuit breaker (mounted on the rear panel) applies standby power to the reference oscillator and enables the operate power switch (located on the front panel). This switch supplies operating voltages to all unit components and can be interlocked via the control keypad to preclude any unintentional power shutdown.

Display/Keypad

Since the system is all-digital except for the RF converter, no manual adjustment is necessary. All control and data entries are made through the 16-element keypad. These entries are prompted and echoed on the display unit, a four-line by 40-character liquid crystal device.

Expansion Capability

Although the unit is fully operational in its self-contained state, the data and control bus may be extended to an external unit to expand its processing capability, as shown in figure 2. The unit bus is based on the Motorola VERSAbus,* which makes it compatible with either a Motorola EXORmacs* development system or a single-board computer such as the VME 68/2.* Extension to either type of unit permits the user to gain access to raw tracking and data block information in memory. This extended processing capacity may be used to expand the clock/navigation state filter or collect, process, and record data for experimental purposes.

Outputs

Two RS-232 ports are available for outputs. One port can be converted (optionally) to a GPIB port. These ports are usable to output data to printers or recorders, and they also provide for input/output of differential correction parameters when two 4200 GPS receivers are used for relative navigation or time transfer applications. Additionally the ports accommodate remote control and monitoring in unattended-mode situations.

HARDWARE

Figure 3 is a block diagram of the system highlighting its modular approach.

The receiver employs digital baseband correlation^{3,4} rather than analog IF correlation of the signals with the reference code. The receiver chassis includes four main modules: (1) the RF converter, (2) signal processor, (3) controller, and (4) data processor. Each module is a plug-in unit that is removable through the receiver's hinged front panel.

**VERSAbus, EXORmacs, and VME 68/2 are trademarks of Motorola, Inc.*

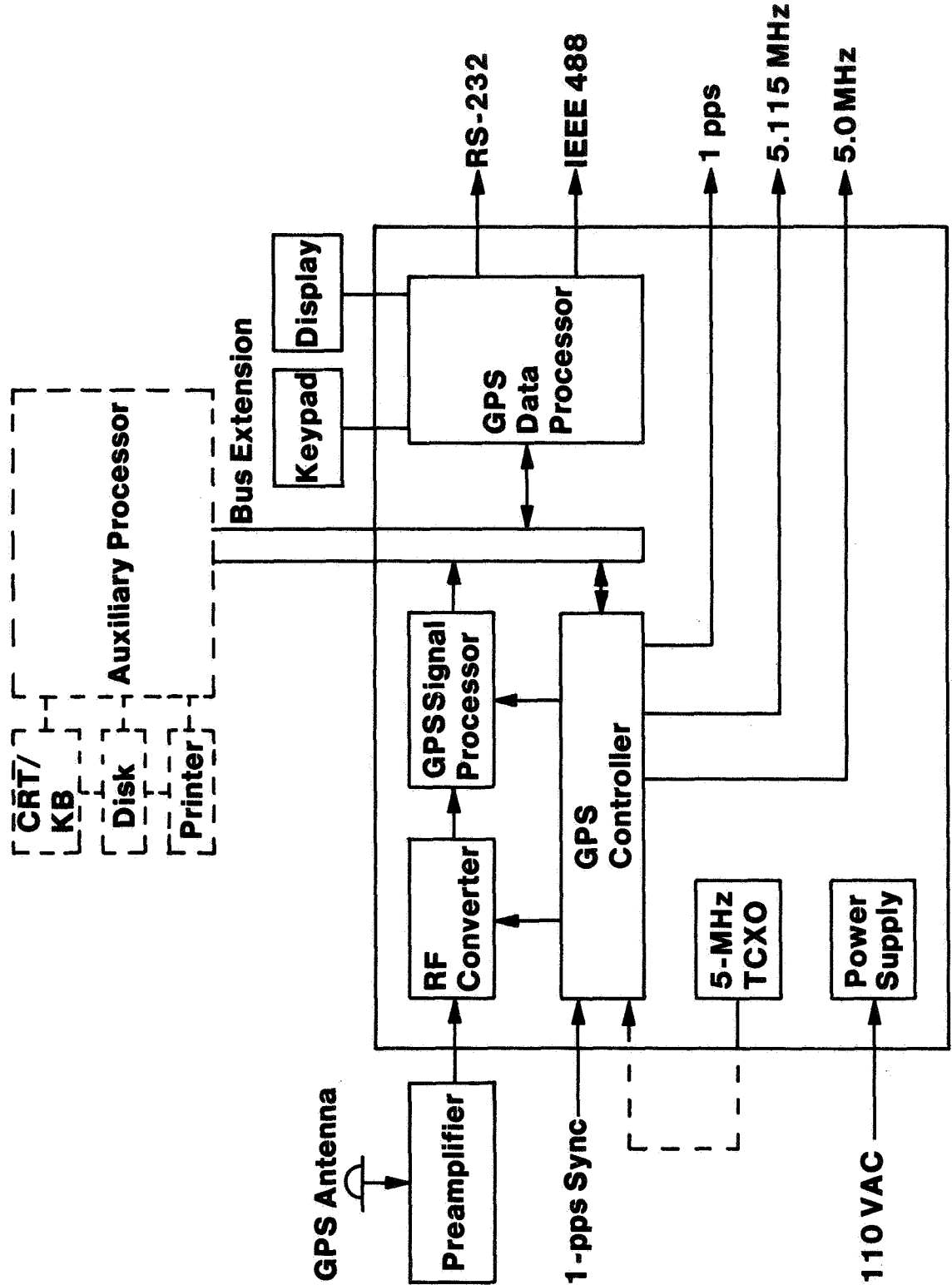


Fig. 2 — System architecture

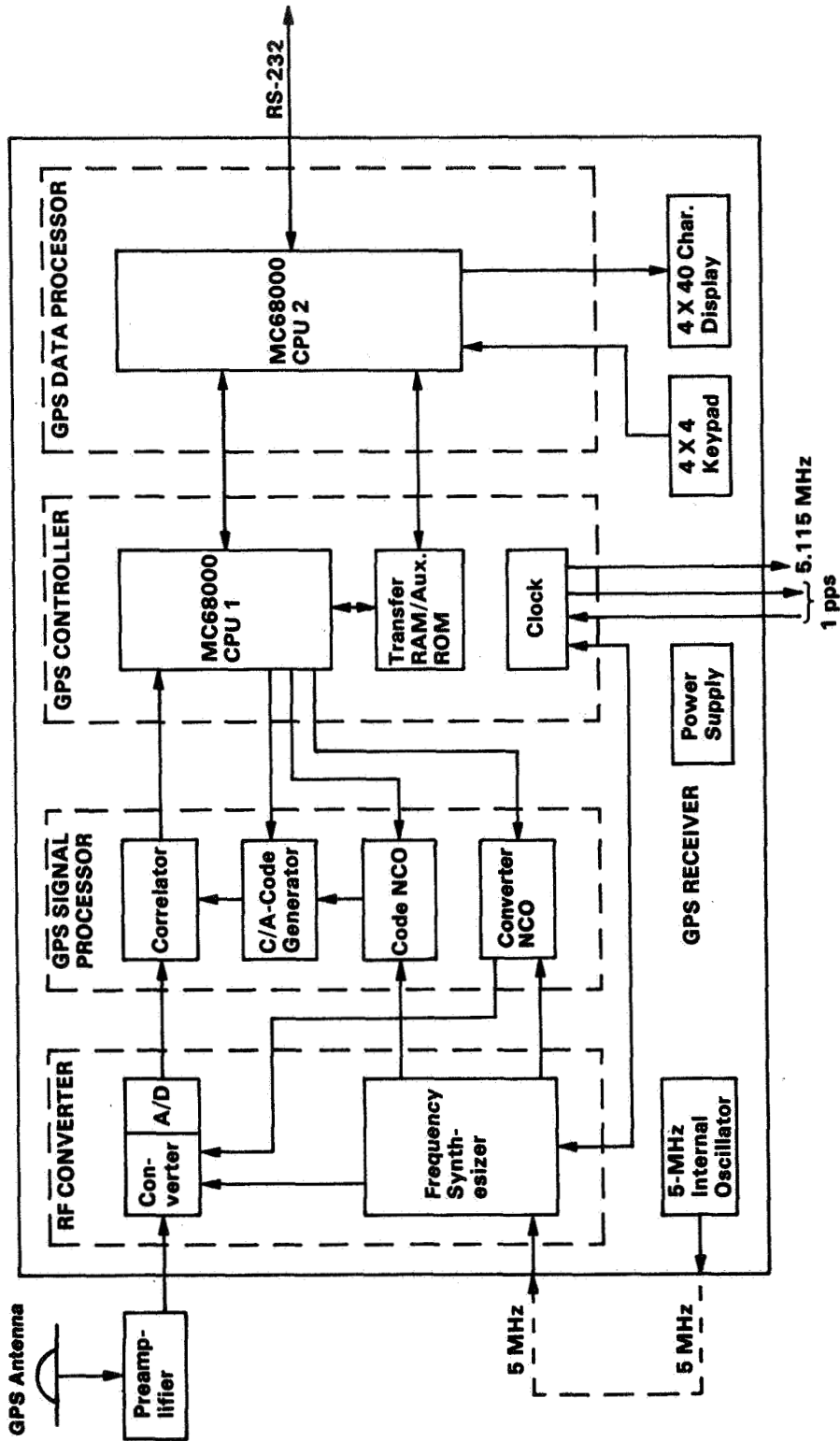


Fig. 3—Block diagram of receiver hardware

Antenna/Preamplifier

The antenna/preamplifier is a separate unit that is powered through a coaxial cable connecting to the main chassis. Figure 4 shows the configurations of both the antenna/preamplifier and the down converter. This circuitry converts an input 1575.42-MHz GPS signal to baseband in-phase (I) and quadrature (Q) components, which then are digitized to 1-bit words. All subsequent processing is performed digitally.

RF Converter

The RF converter module includes a frequency synthesizer that synthesizes all signal frequencies received from the 5-MHz internal or external reference. A digitally controlled synthesizer in the module generates a finely controlled, phase-shifted 0.115-MHz signal from the 5-MHz input. In conjunction with this phase-shifted signal, a 5.115-MHz signal is generated that can be shifted in very fine phase steps (1/1000 cycle or about 0.2 nanosecond) under the data processor's control. (See figure 5.) This 5.115-MHz signal is then used to generate all references and clocks for the system, and allows phase control to precisely align the output 1 pps to estimated GPS or UTC time. It also provides the feature, if desired, of correcting frequency offsets in the 5-MHz reference, which would be present in the use of the internal crystal oscillator. In this case the crystal reference oscillator can be corrected up to ± 0.25 Hz to approximate the corrected satellite oscillator while a satellite is being tracked. The mechanism for supplying digital inputs to the digitally controlled synthesizer is the clock bias state from the Kalman filter. The phase-shifting allows the clock bias state to be driven to zero, which, if continued over a period of time, effectively corrects for the offset of the 5-MHz reference oscillator.

The converter module is constructed with off-the-shelf components and its overall volume is approximately 100 cubic inches. Simplicity of the design also lends itself to production in hybrid form for applications where size and power consumption are critical factors.

GPS Signal Processor

The GPS signal processor (figure 6) operates on the sampled baseband data from the RF converter to generate the I and Q components of the early, on-time, and late correlation coefficients from which all tracking and data recovery parameters are derived.

In its current configuration, the processor consists of 112 standard integrated circuits on a 126-square-inch (or 9-by-14-inch) circuitboard. Straightforwardness of the baseband digital processing accommodates production of the signal processor in custom gate-array devices to achieve cost-effective, low-power systems.

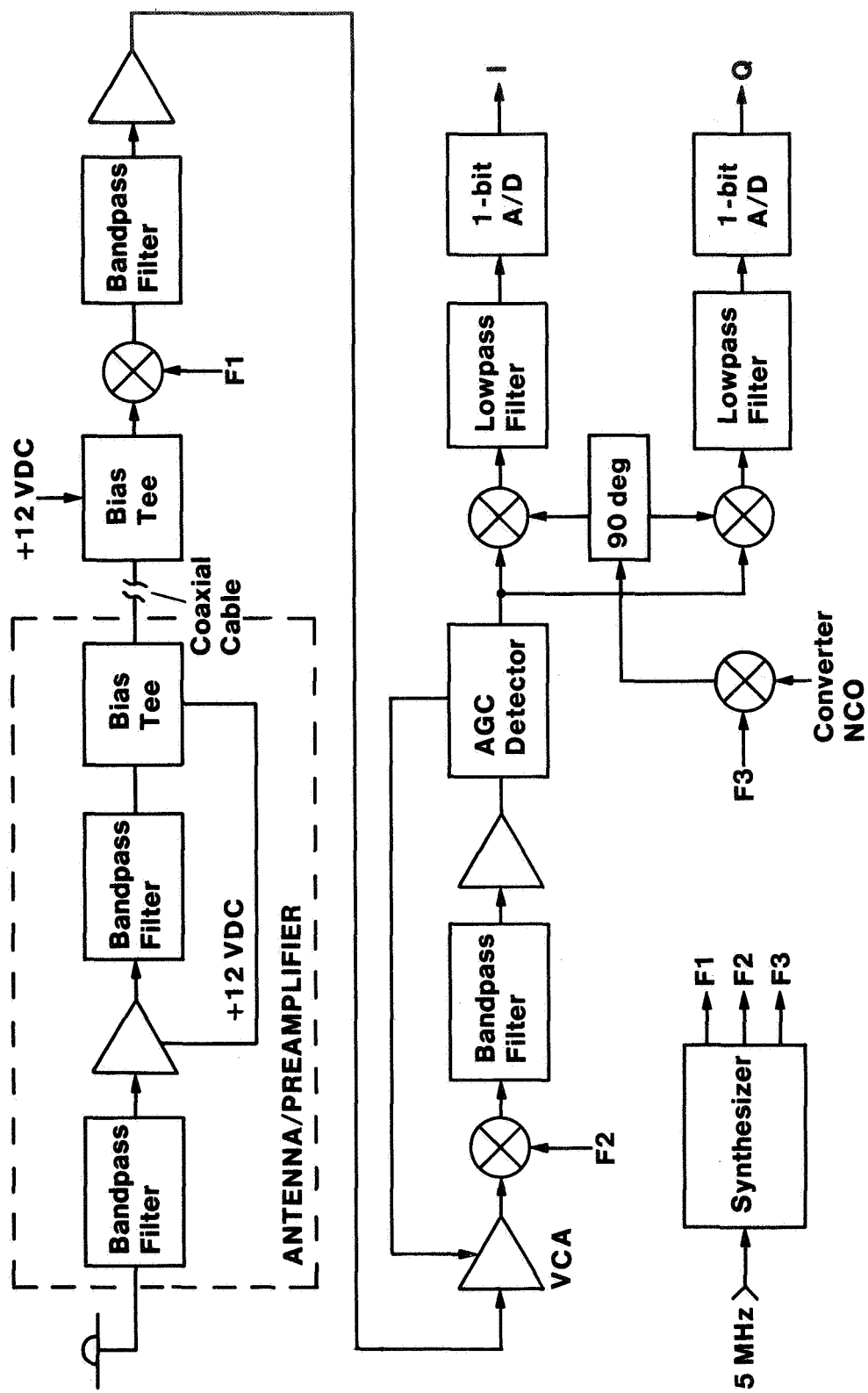


Fig. 4—Antenna/preamplifier and RF converter

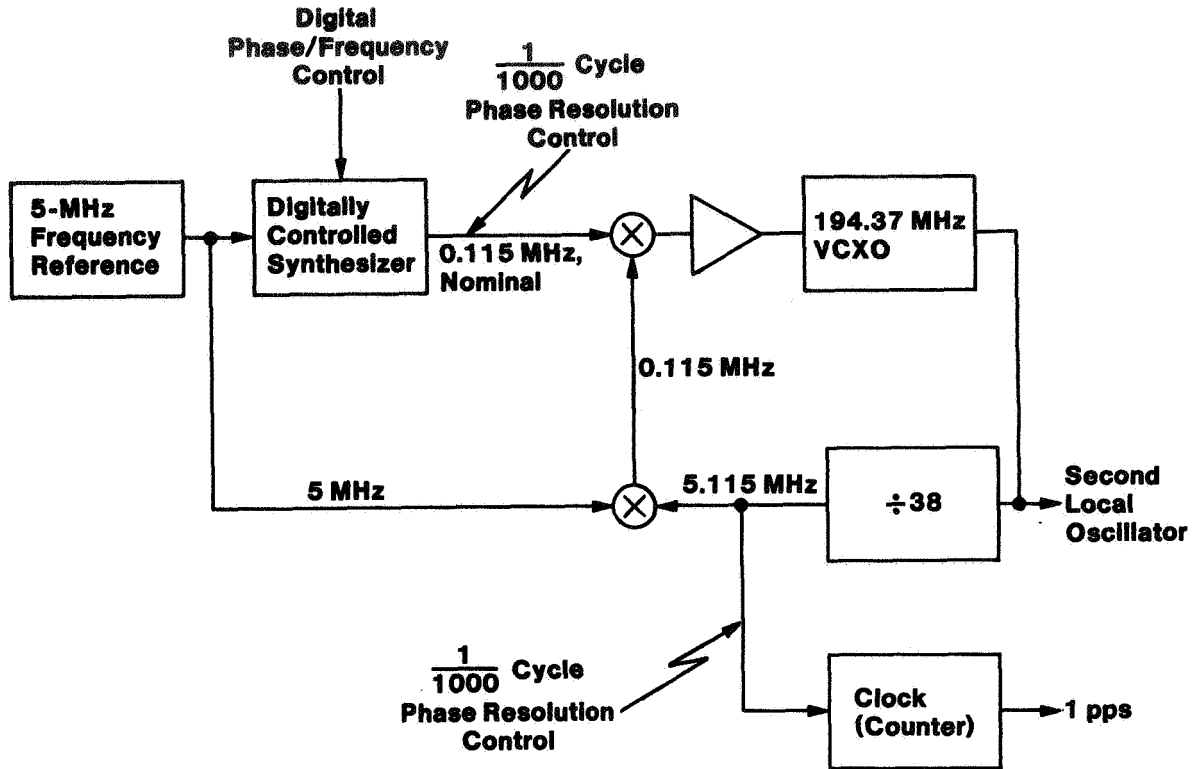


Fig. 5— Operation of digital phase-shifter

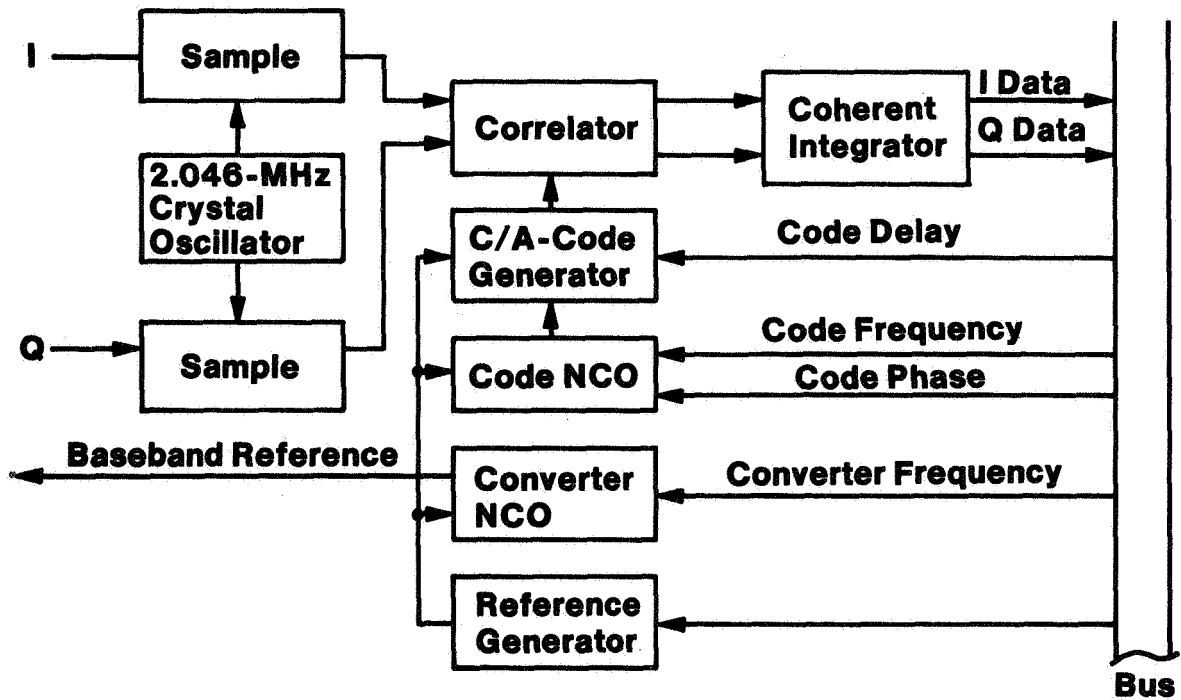
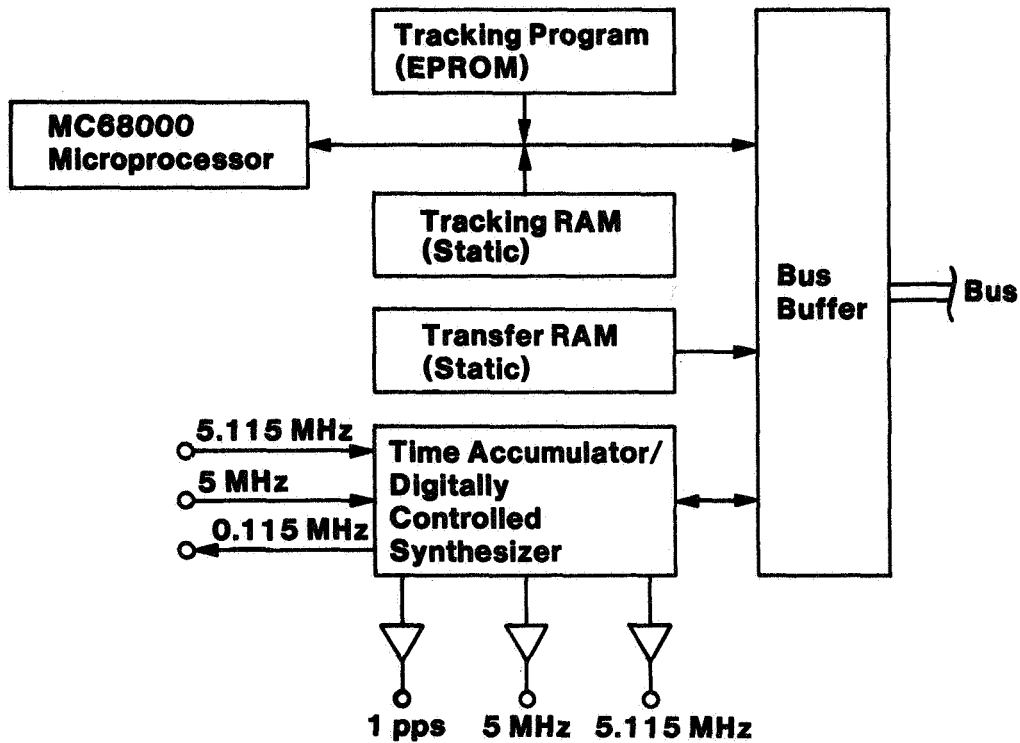


Fig. 6— GPS signal processor

GPS Controller

The GPS controller module (figure 7) is a microprocessor-based loop filter for the code and carrier loops. This module also includes a time accumulator and digitally controlled synthesizer. Communications with the GPS data processor module are provided through the transfer RAM.

Firmware for the controller module is written in MC68000 assembly language. The controller's primary functions are the search algorithms, code-loop and carrier-loop filtering, and decoding of the data block.



18968

Fig. 7—GPS controller

GPS Data Processor

The GPS data processor (figure 8) is a general-purpose, microprocessor-based computer that performs the system's executive function and executes the clock/navigation software algorithms.

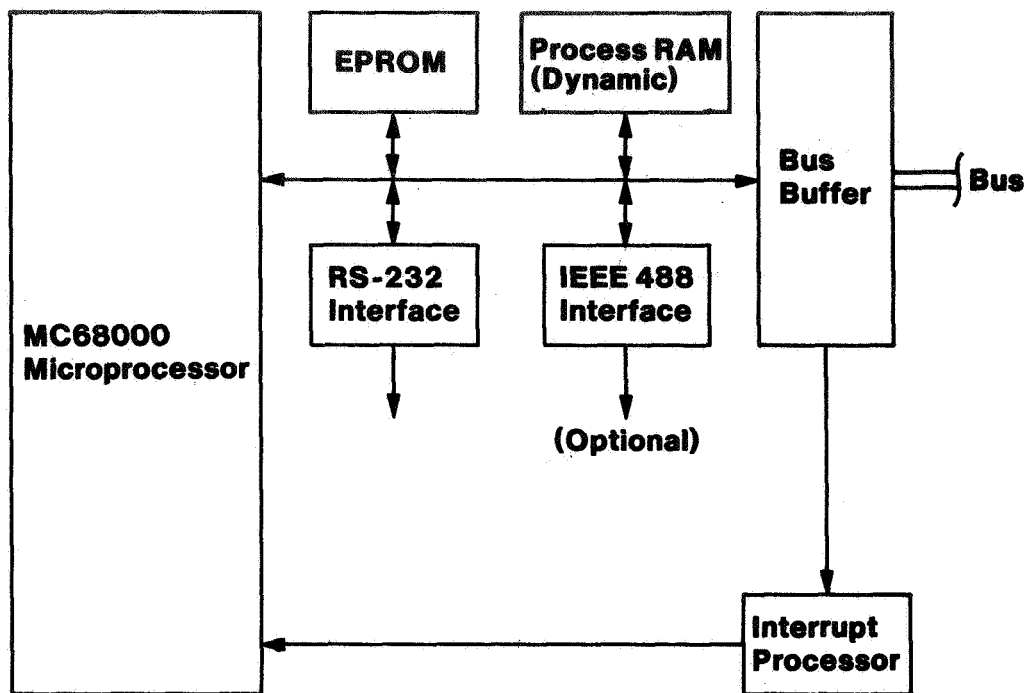


Fig. 8— GPS data processor

SOFTWARE DESIGN

During initial checkout and development of the 4200 GPS Receiver System, the software used was developed on a single MC68000-based microprocessor⁴ as a developmental tool for evaluating the receiver system; thus, because this software was initially designed for only one microprocessor, it operates in a serial mode to perform all system software functions and therefore sequences between satellites at the rather slow rate of 10 seconds. New software is being developed at Interstate to capitalize on the use of two microprocessors in the design; this will yield sequencing between satellites at the rate of every few milliseconds.

Phase Correction Feature

Figure 9 highlights the overall interaction between the software in the system's two microprocessors and its hardware. Of particular interest in this block diagram is the interaction and control of the digitally controlled synthesizer in the GPS controller module. As noted previously, this synthesizer provides the option of fine phase control on the input 5-MHz signal and also allows optional alignment of the 1-pps signal to corrected time. Under software control, this permits a continuous phase correction to be made which can, in effect, correct for the offset of the reference oscillator. The basis for these corrections is the clock-bias state from the Kalman filter, which is zeroed by this phase correction process.

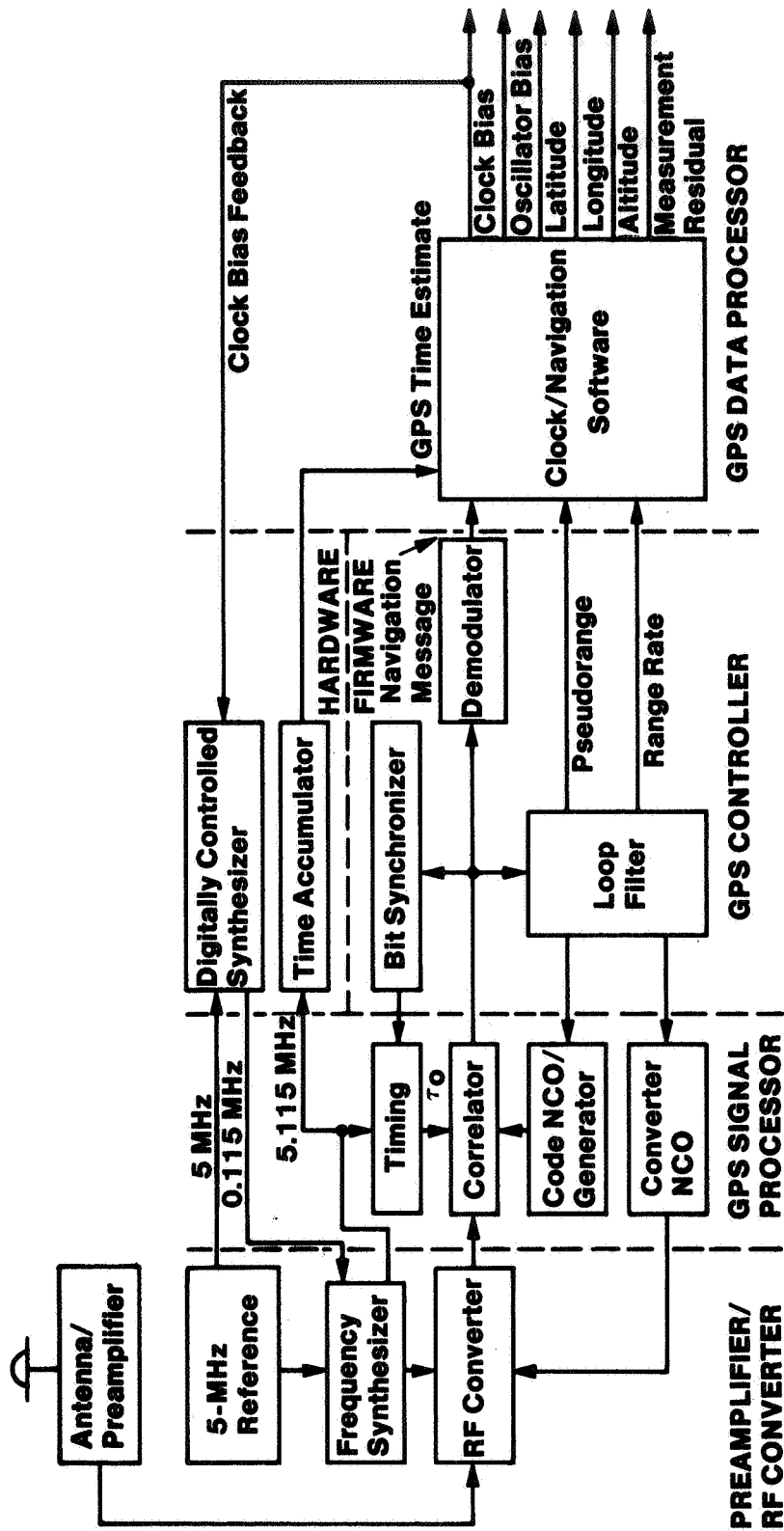


Fig. 9—System functional block diagram

Clock/Navigation

The clock/navigation software (figure 10) estimates clock and navigation states based on pseudorange and range-rate measurements from up to four satellites. A Kalman filter is employed for state estimation using the Bierman U-D factorized measurement-update algorithm¹ to ensure numerical stability in the filter covariance computation. The filter state vector includes two clock-error states (i.e., clock and oscillator biases) and three position states (geodetic latitude, longitude, and altitude relative to the earth reference ellipsoid).

Basic inputs to the clock/navigation software processor are pseudorange and range-rate measurements, and satellite-navigation-message data blocks. The data block parameters with the GPS orbit and clock correction algorithms⁵ are used to compute the satellite orbit and corrections which are applied to pseudorange and range-rate measurements. The corrected measurement set and satellite orbit, computed at the corrected time of signal transmission, are input to the filter.

The clock/navigation state filter operates in discrete time steps and is synchronized with the receiver measurement cycle. The filter states are partitioned to facilitate reduced satellite tracking and optional solution mode (i.e., time transfer, 2-D navigation, or 3-D navigation) processing. In the reduced-state operation, the filter updates only the mode selected states (may be reduced to a single clock-bias state) and retains the keyboard-entered values for the remaining states. The Kalman measurement residuals, which are an indication of filter convergence, are also output and displayed along with the estimated state vector. (The measurement corrections include compensation terms for satellite clock offset, relativistic effects, ionospheric and tropospheric propagation delays, and cable and RF hardware filter delays.)

TIME TRANSFER OPERATIONAL MODES

Various time transfer modes are available for use with this system. The following list suggests many possibilities:

- Using either the internal crystal oscillator or an external atomic reference, the internal clock may be fully synchronized to GPS or UTC time by the internal digital phase shifter (figure 5). The 1-pps output is then aligned to corrected time.
- The internal clock may be left alone and monitored by the GPS measurements. The clock error can be output on the digital interface, or displayed.
- The internal clock can be driven into synchronization by an externally supplied 1-pps clock. In this case, the 5-MHz reference must also be supplied externally. The external clock can then be monitored, and its error from GPS or UTC time measured and then output on the display or digital interface.

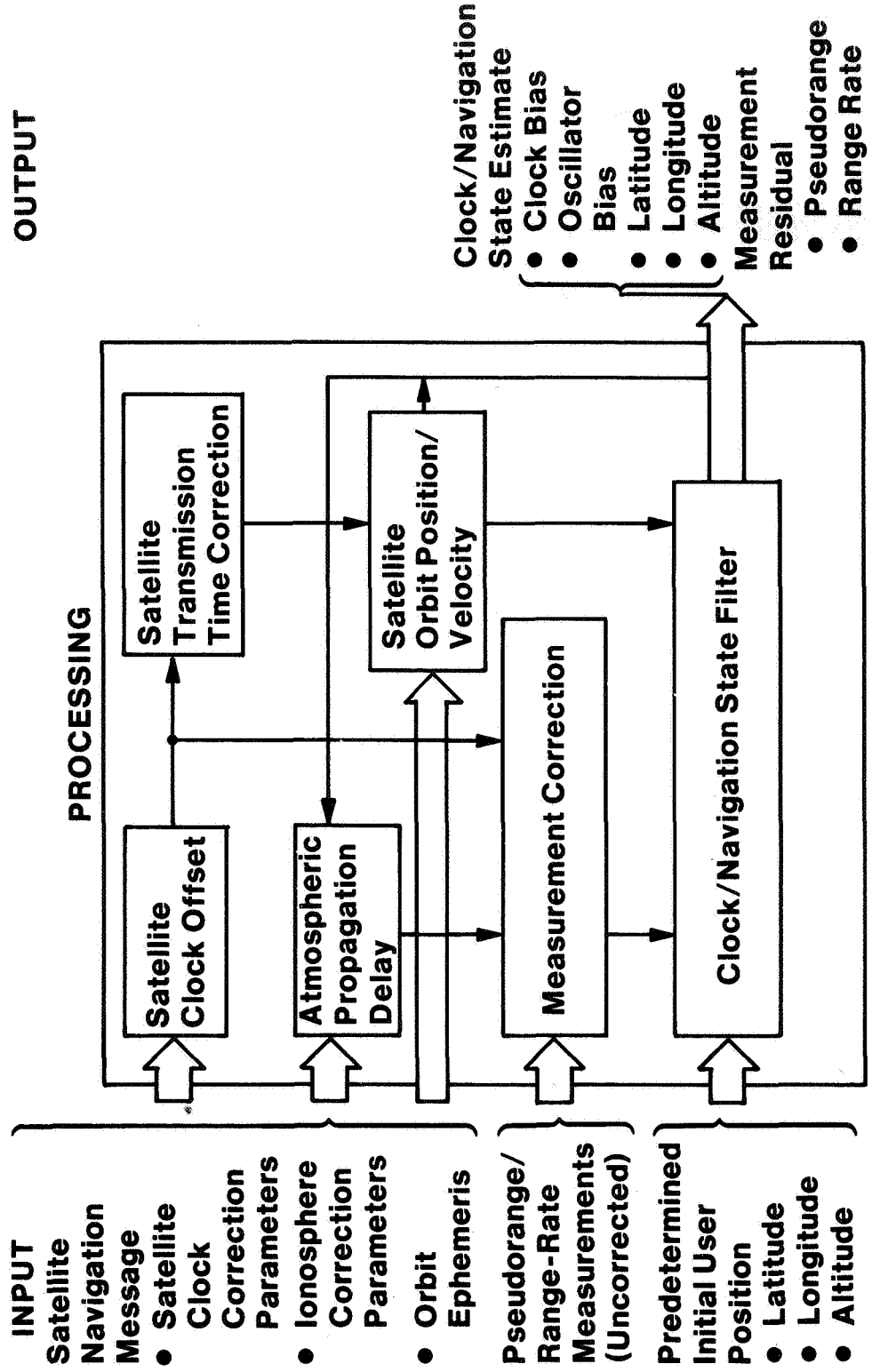


Fig. 10 — Clock/navigation software

SYSTEM PERFORMANCE

A computer-aided analysis of the receiver system's clock/navigation filter was undertaken to determine system performance in the 2-D navigation and time transfer modes, using actual NAVSTAR GPS satellite measurements.

2-D Navigation Capability

A number of position fixes (with the receiver antenna's fixed location at Interstate Electronics/Anaheim, California) were derived to verify the system's 2-D positioning capability. Each fix was independent and based on tracking of typically four GPS satellites for a period of less than one hour. The satellite data was processed sequentially, one satellite every 10 seconds. Table 2 summarizes the resulting antenna-location latitudinal and longitudinal state estimates for six independent position fixes, and figure 11 plots the position fix points relative to the latitudinal and longitudinal coordinate axes. The six sample points (identified by ID number in table 2) lie in a rectangular area with dimensions less than 18 by 25 meters; except for two extreme points (ID numbers 1 and 6), the remaining four points fall in a 10-by-10 meter area.

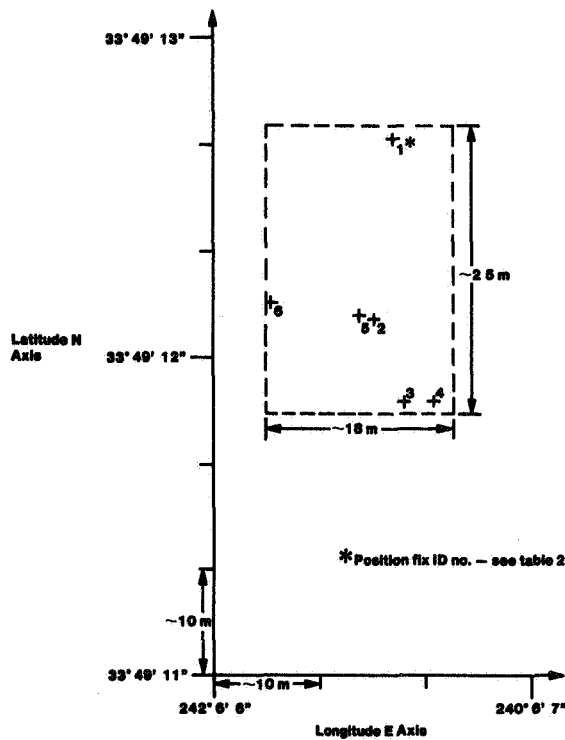


Fig. 11— 2-D position fix scatter

18875

Table 2—2-D position fix (antenna fixed location) sample results

Position Fix ID	Date (1982)	GMT (hr:min.)	NAVSTAR	2-D Position State Estimate	
				Latitude (N)	Longitude (E)
1	27 Jul.	23:33	1,4,6	33°49'12.63"	242°6'6.55"
2	22 Nov.	14:57	3,4,5,6	33°49'12.09"	242°6'6.49"
3	22 Nov.	16:27	3,4,5,6	33°49'11.83"	242°6'6.58"
4	23 Nov.	15:19	3,4,5,6	33°49'11.84"	242°6'6.67"
5	24 Nov.	14:58	3,4,5,6	33°49'12.10"	242°6'6.45"
6	25 Nov.	15:14	3,4,5,6	33°49'12.13"	242°6'6.17"

Time Transfer Capability

Time transfer mode outputs were analyzed for cesium-oscillator and crystal-clock-oscillator states. Figures 12 and 13 show the computer-derived time history plots for the filter-estimated cesium-oscillator and clock states respectively.

The cesium oscillator's bias state (figure 12) does not appear to be fully converged, as evidenced by the magnitude level of the estimated oscillator error. In figure 13, the clipping of points (or quantization effect) in the clock bias was caused by the computer routine plotting the clock bias with a large offset and not the result of either the GPS receiver hardware or software.

Figure 14 is a time history plot of the filter-estimated crystal-oscillator bias state. The magnitude level of the filter convergence appears to be consistent with expected crystal oscillator performance.

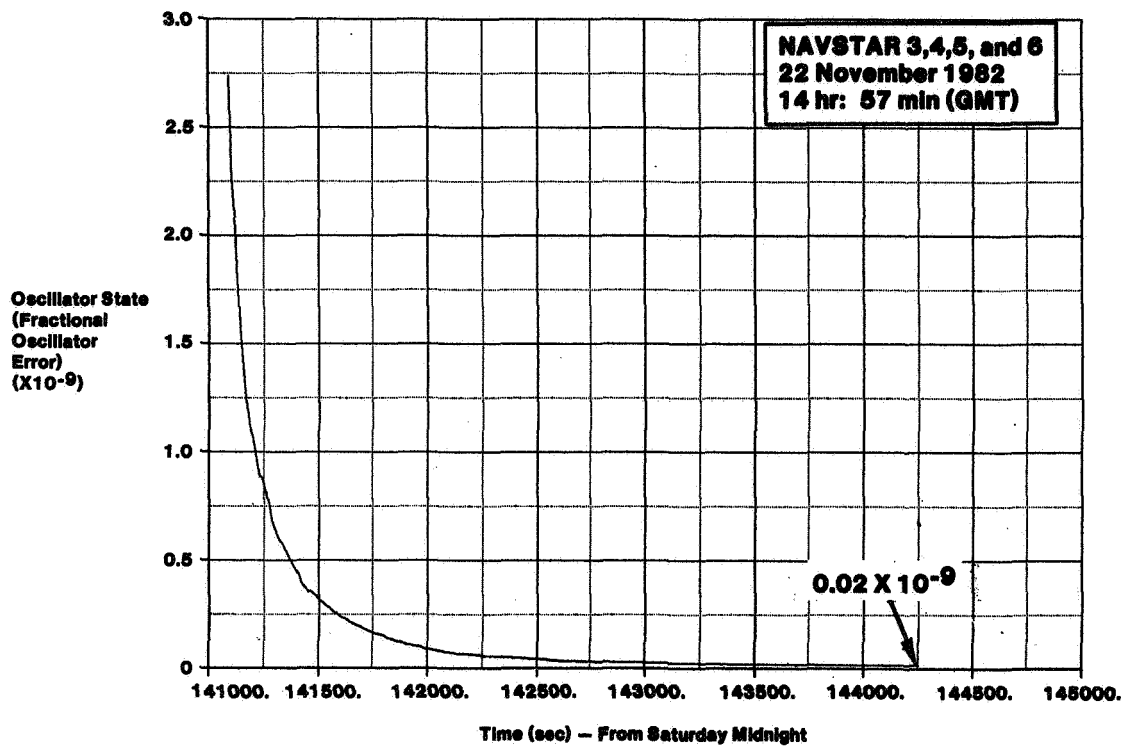
Future Effort

These preliminary results are based on initial receiver system data acquisition and filter processing. Extensive GPS tracking data collection and analysis of filter data processing are planned for further evaluation of the 4200 receiver system's performance; this future effort will include a variance measure of the system's time transfer stability.

ACKNOWLEDGMENTS

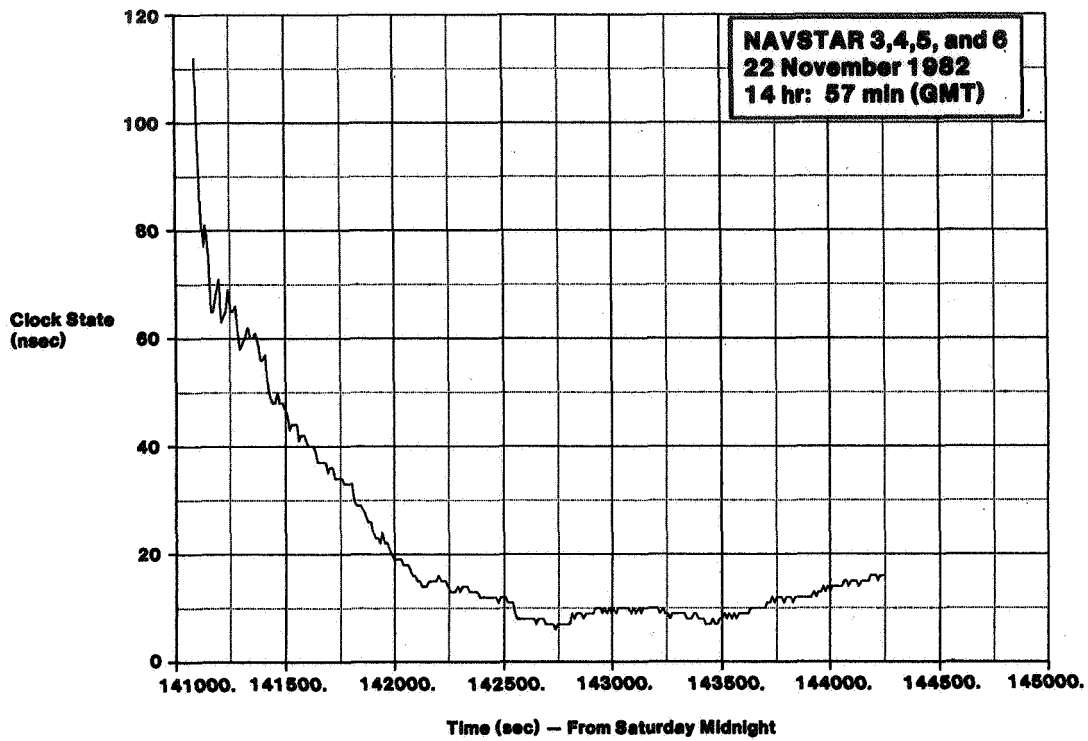
The authors acknowledge the assistance and support of numerous Interstate Electronics personnel and consultants who aided in development of the 4200 GPS Receiver System, particularly Dr. A.J. Mallinckrodt, for consultation on measurement and clock corrections; Dr. G.J. Bierman, for consultation on the U-D factorized measurement-update algorithm; Ms. C. Walls and Mr. E. Benton of Interstate Electronics for firmware and software development; Mr. S. Young of Interstate Electronics for the logic design of the GPS signal processor module and GPS controller module; Mr. J. Soapes of Interstate Electronics for the display/keypad interface as well as overall

hardware unit design; Mr. C. Craig of Interstate Electronics for design of the antenna/preamplifier and RF converter; Mr. A. Kurlovich for design of the frequency synthesizer and final timing-error calibration; Mr. C. Ota for an outstanding job of mechanical design; and last but not least, Messrs. D. Beech, H. Morris, and C. Hoefener of Interstate Electronics for managerial support to the project.



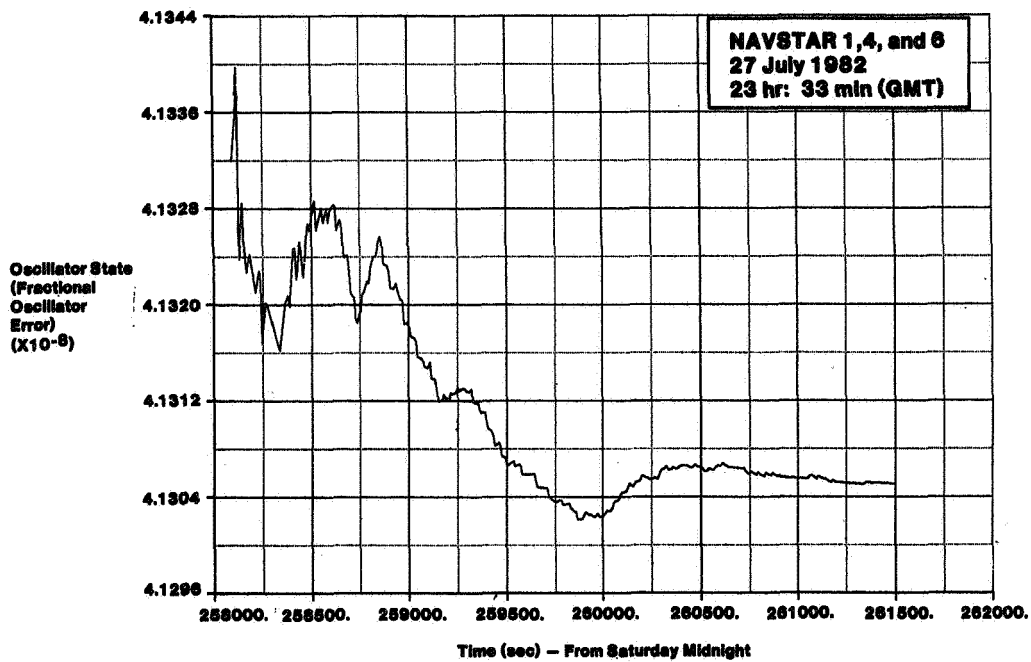
18872

Fig. 12— Time transfer mode output—cesium-oscillator state estimate



18973

Fig. 13—Time transfer mode output—clock (w/cesium oscillator) state estimate



18974

Fig. 14—Time transfer mode output—crystal-oscillator state estimate

REFERENCES

1. G.J. Bierman, *Factorization Methods for Discrete Sequential Estimation*, Academic Press, New York, 1977.
2. R.J. Milliken and W. Kizner, "A Comparison of Two- and Three- Dimensional Navstar Navigation Solutions," IEEE 1978 National Aerospace and Electronics Conference, NAECON 78, Vol. 1, pp. 22-31.
3. P.C. Ould and R.J. Van Wechel, "All-Digital GPS Receiver Mechanization," *Navigation: Journal of The Institute of Navigation*, Vol. 28, No. 3, Fall 1981, pp. 178-188.
4. P.C. Ould and R.J. Van Wechel, "Design Approach for a Microprocessor-Based GPS Time Transfer Receiver," *Proceedings of the Thirteenth Annual Precise Time and Time Interval (PTTI) Applications and Planning Meeting*, December 1981, NASA Conference Publication 2220.
5. Space Vehicle Navigation Subsystem and NTS PRN Navigation Assembly/User System Segment and Monitor Station, Rockwell Interface Control Document MH08-00002-400, Revision G, 6 August 1979.

QUESTIONS AND ANSWERS

MR. P. HOYUP, NASA/GSFC

Is this unit available in the market currently?

MR. R. J. VAN WECHEL, Interstate Electronics Corporation

Well, we have built our first prototype and that is what you see there, and it will be available, yes.

MR. HOYUP:

Do you have a schedule for delivery?

MR. VAN WECHEL:

Well, I think it will be 6 to 9 months. It will be by quote out of the plant, and if you're really interested, come and see me but I think it will be in the 6 to 9 month range.

MR. HOYUP:

Thank you.

QUESTION FROM THE AUDIENCE:

What will be a typical price? Can you estimate that?

MR. VAN WECHEL:

Well, I don't know whether I ought to do that at this meeting. I would like to talk to you about it afterwards.

DR. VIG, Army Electronics Technology and Devices Laboratory

Why not this meeting?

MR. VAN WECHEL:

Well, it's really going to be quoted out of the company. There isn't a catalog price on it right now.

DR. VIG:

Do you have a ball park estimate?

MR. VAN WECHEL:

In singles, it will be in the \$70,000 range, as a ball park figure.

MR. D. MCCULLER, Oceanographics

A quick comment on the country coordinates for those of you who are not familiar with it, we weren't. They are done in State coordinates in this country, and those are converted rigorously to North American datum of 1927. This is not the same as WGS-72, which are the satellite coordinates. There are two versions of that, the broadcast the precise ephemeris, from the transit satellite which is your best reference system at the moment. If you make a first-order correction from NAD-27 to the satellite, WGS-72, in our area you are off about 16 meters. If you make no correction in our area you are off about 30 meters, so it isn't surprising to hear that you're off a little bit. That might be encouraging.

MR. VAN WECHEL:

That is encouraging. We were wondering about that.

MR. MCCULLER:

Then in the last step, if you want to get down to the meter level you would have to go to the precise ephemeris, and you need a correction from DMA on that to make that last correction. You can get, within about a week's time you can get a benchmark in your area that is within a meter or two.

MR. VAN WECHEL:

I see.

MR. MCCULLER:

Thank you.

INTERCONTINENTAL TIME AND FREQUENCY TRANSFER
USING A GLOBAL POSITIONING SYSTEM TIMING RECEIVER *

Philip A. Clements
California Institute of Technology
Jet Propulsion Laboratory, Pasadena, California

ABSTRACT.

The Deep Space Network (DSN) has a requirement to maintain knowledge of the frequency offset between DSN stations within 3×10^{-13} and time offset within 10 microseconds. It is further anticipated that in the 1987-1990 era the requirement for knowledge of time offset between DSN stations will be less than 10 nanoseconds.

The Jet Propulsion Laboratory (JPL) is using the Global Positioning System (GPS) Space Vehicles, as a development project, to transfer time and frequency over intercontinental distances between stations of the DSN and between the DSN and other agencies. JPL has installed GPS timing receivers at its tracking station near Barstow, California and at its tracking station near Madrid, Spain.

The details of the experiment and the data are reported. There is a discussion of the ultimate capabilities of these techniques for meeting the functional requirements of the DSN.

INTRODUCTION

The Jet Propulsion Laboratory (JPL) operates the Deep Space Network (DSN) for the National Aeronautics and Space Administration (NASA). The DSN contains three complexes located in California, Spain and Australia which allow a continuous view of non-earth orbiting spacecraft. The DSN has a requirement to maintain knowledge of frequency offset between complexes of $3 \times 10^{-13} \Delta f/f$, and a knowledge of time offset to within 10 microseconds. It is further anticipated that in the 1987-1990 era the requirement for knowledge of time offset between DSN complexes will be less than 10 nanoseconds. Clearly, new measurement techniques will be needed to meet these requirements.

Among the new measurement techniques being investigated by JPL, to meet these requirements, is the use of Global Positioning System (GPS) timing receivers. The GPS timing receivers presently being used by JPL were developed and built by the National Bureau of Standards (NBS). Part of this development was funded by JPL.

* The research described in this paper was carried out by the Jet Propulsion Laboratory, California Institute of Technology, under contract with the National Aeronautics and Space Administration.

Description of the Receivers

The NBS receiver is described in last years proceedings (ref. 1), it uses only the one frequency containing the CA code which is transmitted by each space vehicle. The receiver locks on the space vehicle's signal, therefore it needs only a small omnidirectional antenna rather than a steerable dish. The receiver is controlled by an internal microprocessor that automatically handles schedules, length of reception time and other tasks. Once the receiver is set up, normal operation only requires occasional human intervention. For instance, the reception time is decremented 4 minutes every day which of course is a little different than a sidereal day. This is done to make it a bit more convenient by having to deal only with whole minutes. It is necessary to adjust the schedule every few weeks to keep the viewing angles correct.

Configuration of the System

At present JPL has two GPS timing receivers, one is located at the Goldstone Tracking Station Complex (GTS) near Barstow, California. This receiver gets its 1 second timing pulse from a cesium clock, Goldstone clock 5, GTS(C15) which is located about 20 Km from a hydrogen maser clock Goldstone Station Reference GTS(SR) which is at another station in the same complex. The hydrogen maser clock is the same one used in Very Long Baseline Interferometry (VLBI) which measures, among other things, the time offsets between the DSN complexes. A clock trip using a portable cesium clock is made once a week between GTS(C15) and GTS(SR). These clock trips are done in conjunction with the regularly scheduled weekly VLBI measurements.

The second GPS timing receiver is located at the DSN tracking station near Madrid, Spain. The Madrid receiver gets its timing pulse from a hydrogen maser clock which is that station reference clock MAD(SR). MAD(SR) is another hydrogen maser clock used in the VLBI measurements and is at the other end of the weekly VLBI measurement between California and Spain.

Two other receivers involved in this test were located at NBS in Boulder, Colorado and at the United States Naval Observatory (USNO) in Washington, DC. The NBS receiver is identical to those used at JPL, it gets its timing pulse from the NBS clock 9 which is a clock in the NBS ensemble. A daily offset of clock 9 to UTC(NBS) is available at months end and of course the receiver is accessible by telephone with a modem. The USNO GPS timing receiver is a Stanford Telecommunications receiver of similar functional design to the NBS receiver. Its schedule is decremented approximately 28 minutes per week (1). The receiver gets its timing pulse from UTC(USNO, MC). There are corrections available to UTC(USNO).

¹The USNO receiver schedule is decremented 27 minutes one week and 28 minutes the alternate week. This allows an approximation to a sidereal day. This will be changed to 4 min/day decrement starting around the first of 1983.

Procedures for gathering and processing the data

The receivers will store internally one to two weeks of data depending on how much data is acquired each day. The data from the receivers are acquired by telephone usually once a week. In the use of the NBS type receiver, the receivers themselves are accessed. In the case of the USNO receiver, the data is acquired from a public database service provided by USNO. In both cases the data are transmitted at a 300 baud rate and are received and printed out on a terminal. The data are then input by hand into a Hewlett Packard 9845 calculator.

All of the data were taken as a mutual view of the space vehicle by pairs of timing receivers. This method promises the best results and is the simplest with respect to processing the data. As more space vehicles are added to the GPS constellation, there will be additional opportunities for mutual view around the world.

The receivers are programmed to take data for 10 minutes (600 seconds). These data are then reduced in the receiver to a single data point which represents the time offset between the local clock and the GTS clock. The difference between the two values of local clock and GTS time is then calculated. This is done for each space vehicle that is available for mutual view each day. These values are then averaged to produce a single value for the day. If data points are missing, then a linear interpolation is made on the original measurement.

Results

The first and easiest measurement that was made was between clock 5 at GTS and NBS clock 9. Easiest because the NBS receiver was already set up and operating. The distance between stations is approximately 1200 Km and regular clock trips are made between GTS and NBS so the measurements can be verified.

Figure 1 shows the results of the UTC (NBS) - GTS (clock 5) with the Cesium portable clock trips results also shown. Because of different antennas being used at NBS a receiver calibration was not available, therefore the 1st clock trip was used as a calibration. The second trip disagreed by 36 ns and the third by 5 ns.

This receiver is now probably a de facto permanent installation at GTS and will probably eliminate the need for most future clock trips between NBS and GTS.

A second GPS timing receiver was installed at the DSN station in Spain. A schedule of mutual observation of two space vehicles (SV5 and SV8) was started. These are the only two space vehicles that are mutually observable from both complexes. The space vehicle observation schedule was made to have the same angle of observation from both stations. Some slight adjustments were made to equalize the angles from 41° to 45° above the horizon. The space vehicles are over Greenland at observation time and seen within a few degrees of each other in the sky at each station.

A clock offset measurement is made every day from each space vehicle and the mean is used as the value of the clock offset. The same procedure for getting a value of clock offset is used between GTS(C15) and MAD(SR) and between UTC(NBS) and GTS(C15) with the exception that only two space vehicles are available. A plot of the clock offset values is seen in Figure 2. Figure 3 is the same graph with a frequency offset removed.

The frequency offset between the GTS(C15) and MAD(SR) was calculated using 10 days of data. The calculations assumed statistical independence between the measurements using the two space vehicles. A typical offset measurement was $9.5 \times 10^{-13} \Delta f/f$ with a (confidence) standard deviation of the mean of $2.8 \times 10^{-14} \Delta f/f$. This is within the requirements to have knowledge of frequency offset to within the $3 \times 10^{-13} \Delta f/f$ DSN specification.

Confirmation by independent GPS measurements

Unlike the clock offset measurements between GTS and NBS, the measurements from California to Spain cannot be confirmed by frequent clock trips. One attempt at confirmation was a daily indirect time difference measurement made through the U.S. Naval Observatory (USNO). This was accomplished in two steps: First, there was a daily mutual view schedule maintained by NBS, USNO and Goldstone. Second, USNO and Madrid maintain a mutual view schedule, which results in daily time offset measurement between their clocks. These direct and indirect time offset measurements between Goldstone and Madrid are nearly statistically independent.

Figure 4 shows the differences in the measurement of the time offset between Goldstone and Madrid by two different paths. There was a mean offset of 140 ns. An explanation of this could be an error in the coordinates of the receiver. There is some reason to believe this is true at Goldstone and there have been no checks made at Spain. The new firmware to be installed in the NBS designed receivers in 1983 will contain a navigation program. Then it will be possible to verify the antenna location within a few meters.

A good candidate for the cause of the daily variation is the different scheduling methods used by JPL and NBS and that used by USNO. This problem should clear up in 1983 when USNO starts decrementing 4 minutes/day. At that time the test will be rerun. Some of the daily variations are probably caused by ionospheric changes. There is no attempt to account for this in the NBS and JPL receiver at this time but one would expect this error to be less than is presently seen.

Confirmation using VLBI measurements

Approximately once every week a VLBI measurement is made between GTS and MAD and between GTS and the DSN Australian complex. One of the results of the VLBI measurement is the time offset between the involved stations. By using the regular clock trips between GTS(C15) and GTS(SR), the GPS timing receiver

results can produce an approximately weekly time offset between GTS(SR) and the MAD(SR) - Figure 5. These time offset measurements can be compared to the time offset results of the VLBI measurements as seen in Figure 6.

A linear fit on each of the two sets of data shows an excellent agreement. These measurements will be continued throughout 1983. It is planned to make measurements internal to the stations to find the difference between the VLBI and the GPS measurements.

CONCLUSIONS

1. The present GPS timing receivers can meet the 1985 requirements specified for the DSN. With better data collection and the addition of software filters in the data processing, there is reason to believe the intercontinental time measurements, with the existing equipment, can approach an accuracy of 10-20 nanoseconds. Certainly, one can expect to further refine the measurement of frequency offset.
2. The GPS and VLBI measurements of time offset will compliment each other for some time to come.
3. It has been shown that the GPS timing receiver is an operational item of equipment capable of replacing regular clock trips over short distances and shows promise of replacing clock trips over intercontinental distances.

ACKNOWLEDGEMENTS

The author wishes to thank Mr. David Allan, Mr. Dick Davis of NBS for their technical assistance. Mr. Paul Wheeler and others on the staff of USNO were extremely helpful and generous in scheduling their receiver. Appreciation is given to the staff of DSN station 61 in Spain, in particular Sr. José Alonso and Sr. Delgado Muñoz for their time and effort beyond their regular duties. The receiver at Goldstone was operated by Mr. Jesse Myers, which is also much appreciated.

REFERENCES

1. Unprecedented Syntonization and Synchronization Accuracy via Simultaneous Viewing with GPS Receivers; Construction Characteristics of an NBS/GPS Receiver, D.D. Davis, et al., Proceedings of the 13th Annual Time and Time Interval Applications and Planning Meeting.

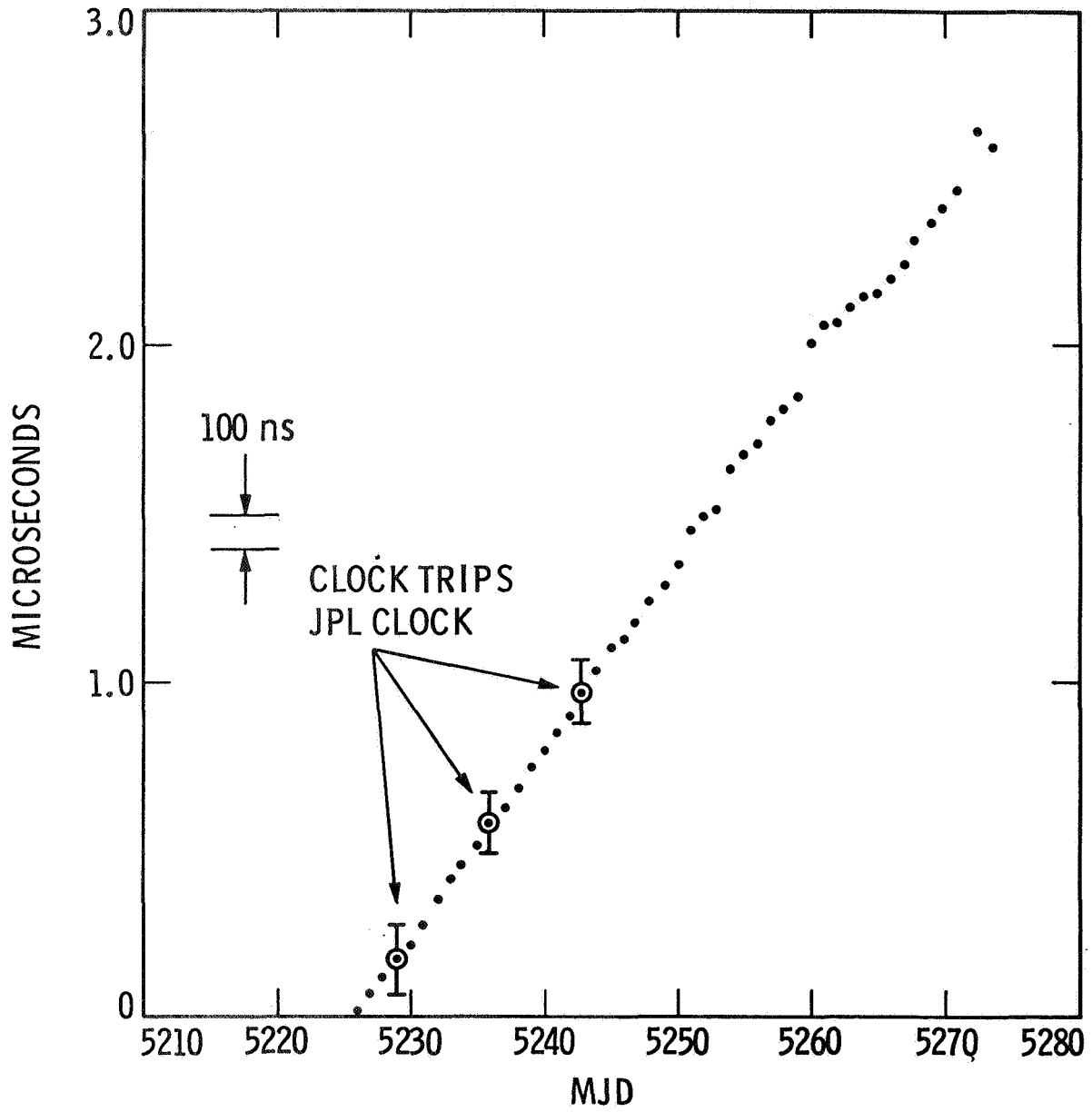


Figure 1. UTC (NBS) - Goldstone (Clock 5)

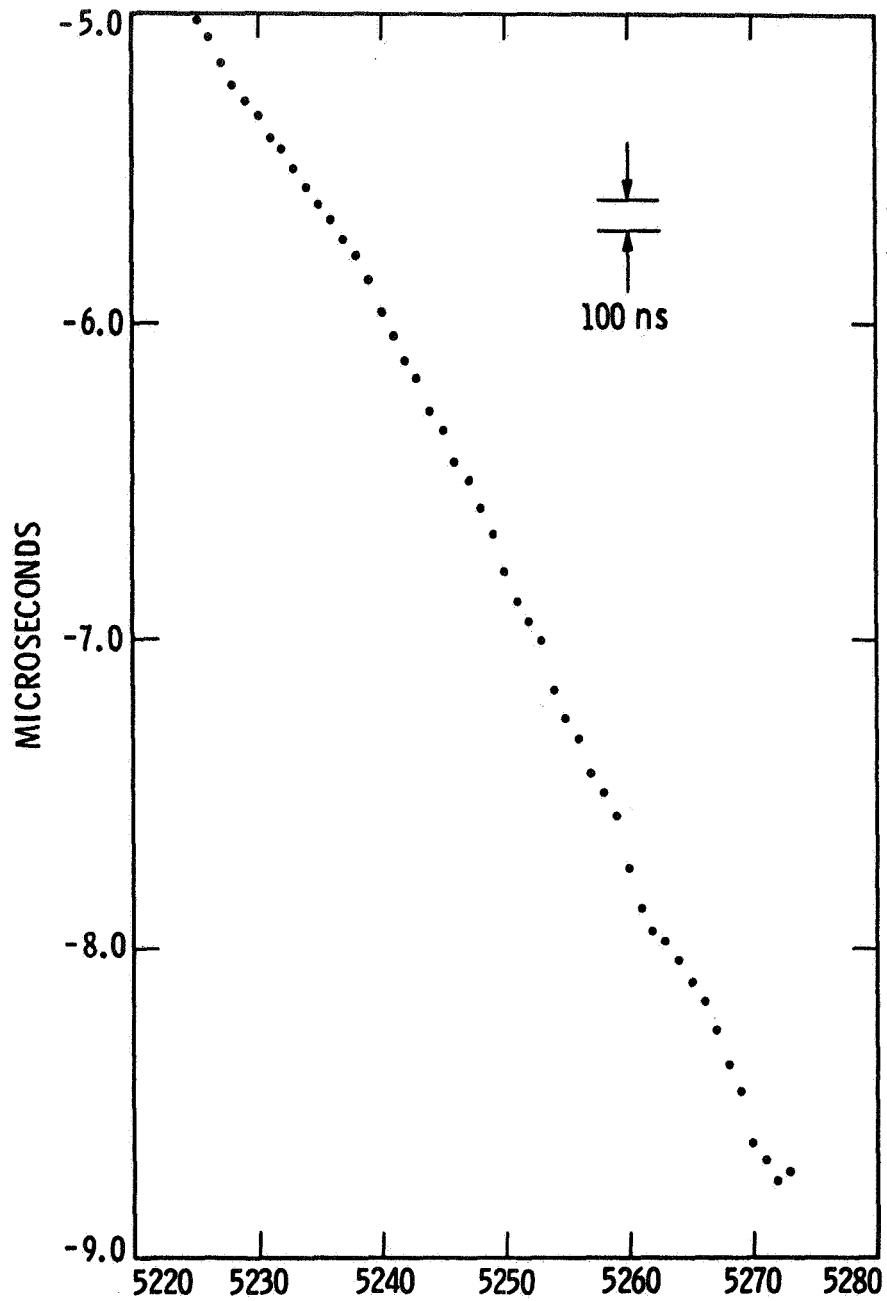


Figure 2. Goldstone - Madrid as Directly Measured by CPS Timing Receivers [Goldstone (Clock 5)] - [Madrid (Station Reference)]

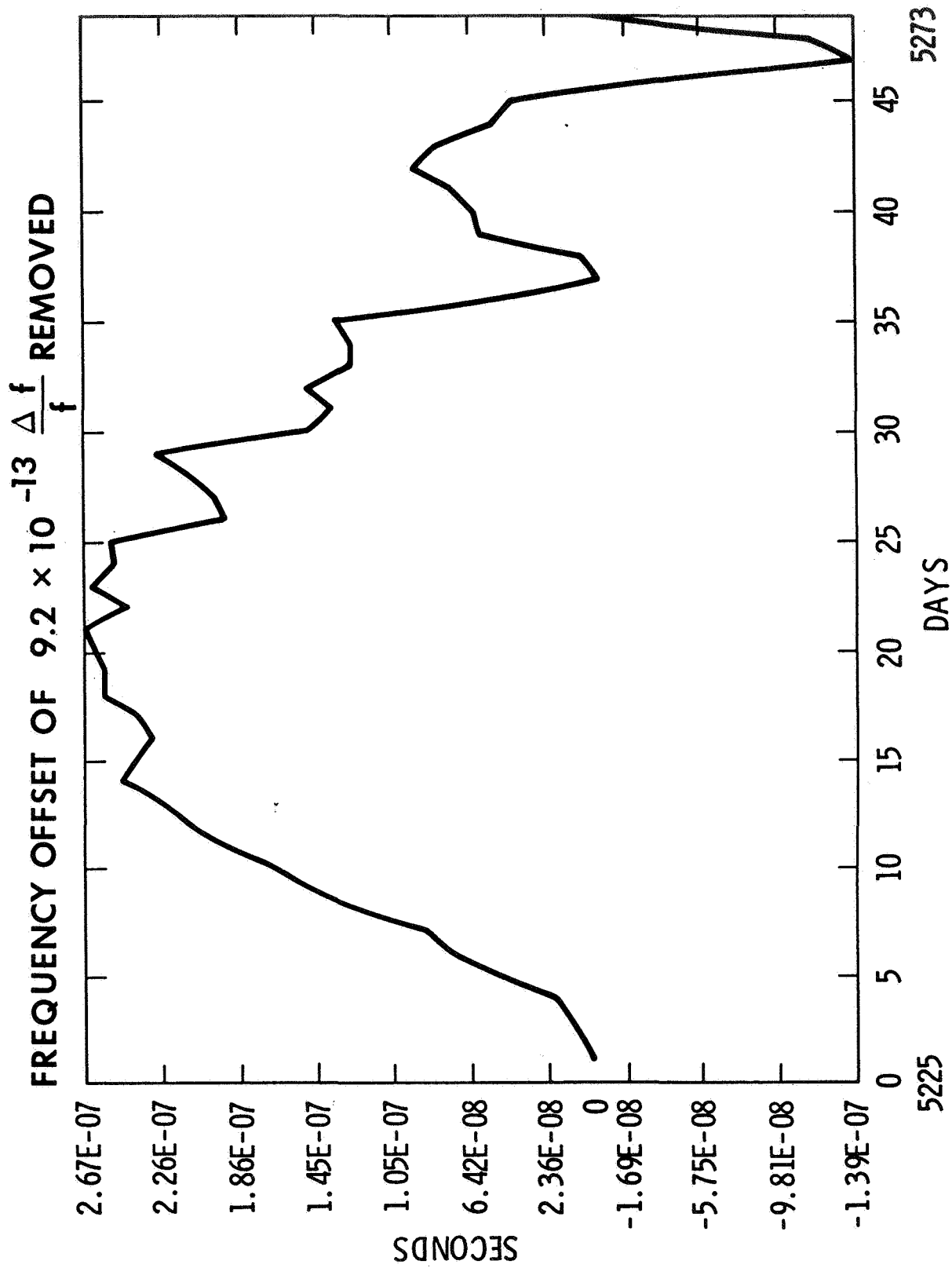


Figure 3. Goldstone (Clock 5) - Madrid (Station Reference)

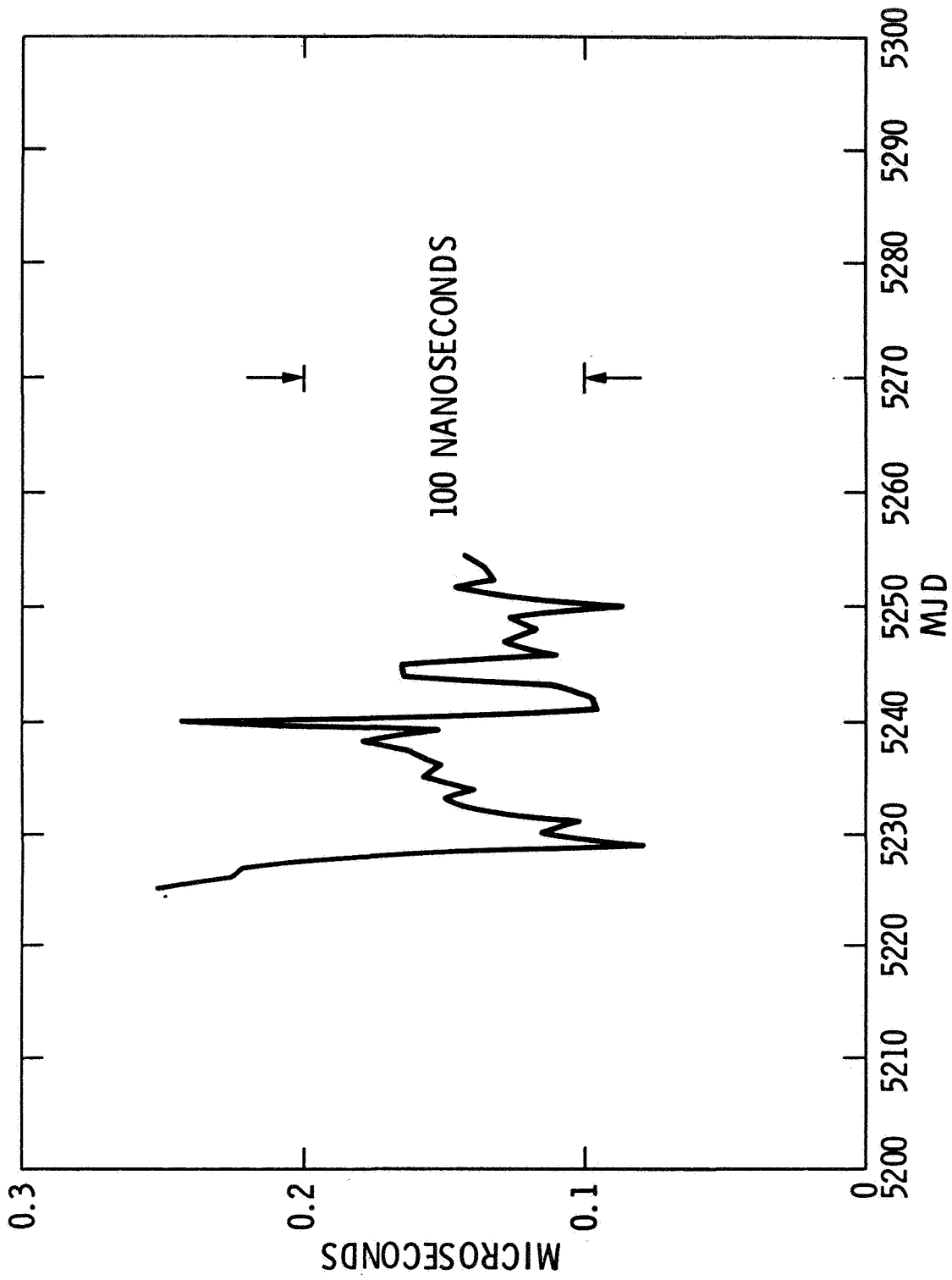


Figure 4. Difference Between Goldstone to Madrid Time Directly and Through USNO

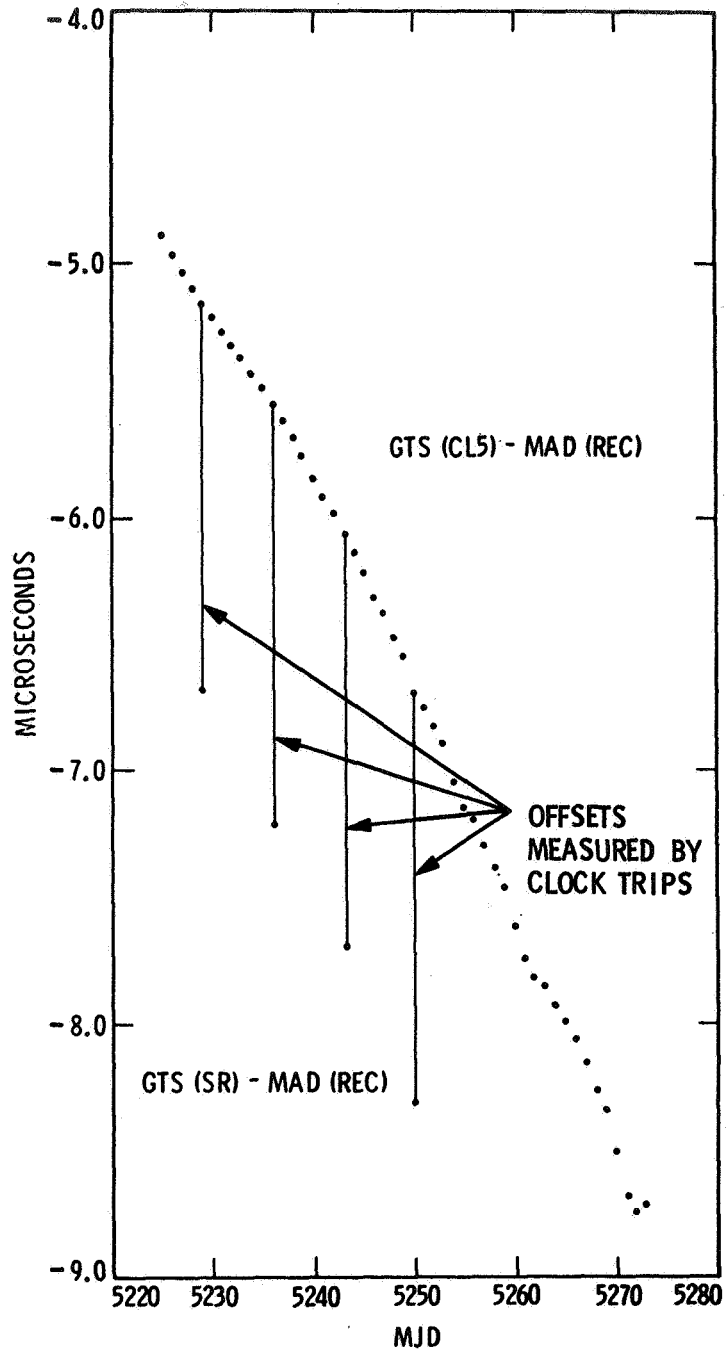


Figure 5. Goldstone - Madrid Directly Showing Offset to Goldstone (Station Reference)

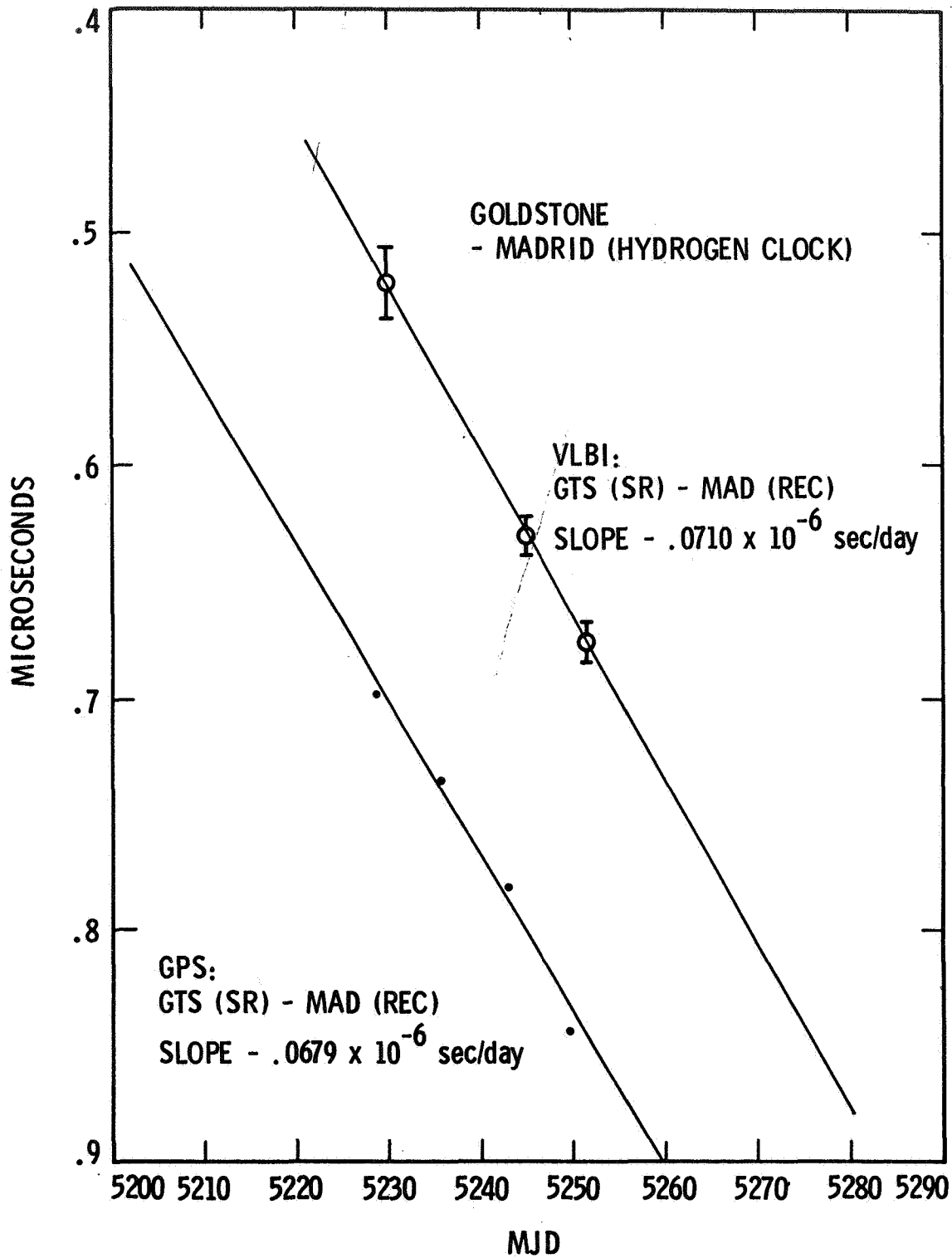


Figure 6

QUESTIONS AND ANSWERS

DR. G. M. R. WINKLER, U.S. Naval Observatory

If you make comparisons where you use one intermediate station, it is extremely important to select observations which are simultaneous pair-wise, in other words, to establish the difference between station A and B at the same time and between B and C, possibly at another time, but again pair-wise at the same time. These times don't have to be identical but they must be identical until we can verify the origin of these biases which were discussed in the first paper. When one makes a bias observation, then you can see that the time transfer undergoes a change, and unless you establish exactly theorized simultaneity, you will of course have errors due to that change.

MR. P. A. CLEMENTS, Jet Propulsion Laboratory

They are almost simultaneous. The USNO decrements 27 minutes one week and 28 minutes the other week, whereas we are decrementing 4 minutes a day, so there is some of that going on, and the two receivers that look directly, they are right in step with each other. We decrement 4 minutes a day with those, so that could be a source of error, sure.

TEST RESULTS OF THE STI GPS TIME TRANSFER RECEIVER*

David L. Hall, Jim Handlan** (HRB-Singer) and
Paul Wheeler (U.S. Naval Observatory)

ABSTRACT

Global time transfer, or synchronization, between a user clock and USNO UTC time can be performed using the Global Positioning System (GPS), and commercially available time transfer receivers. This paper presents the test results of time transfer using the GPS system and a Stanford Telecommunications, Inc. (STI) Time Transfer System (TTS) Model 502. Tests at the GPS Master Control Site (MCS) in Vandenburg, California and at the United States Naval Observatory (USNO) in Washington, D.C. are described. An overview of GPS, and the STI TTS 502 is presented. A discussion of the time transfer process and test concepts is included.

INTRODUCTION

This paper describes test results using the Stanford Telecommunications Inc. (STI) Time Transfer System (TTS) Model 502 to perform time transfer between a user clock and Universal Time Coordinated (UTC) available from the United States Naval Observatory (USNO). The time transfer procedure makes use of the STI TTS 502 receiver and the Global Positioning System (GPS) to synchronize a user's clock to UTC in a two step procedure:

- 1) time transfer between the user's clock and the GPS Master Clock (located at Vandenburg, California) using observations of GPS satellites,
and
- 2) transformation between the GPS Master Clock and UTC time based on USNO synchronization data.

A brief description of the GPS system is provided along with a discussion of the time transfer procedure used at the USNO to synchronize UTC and GPS MCS time. More detail is available in the literature (References (1) and (2), respectively). A description of the time transfer procedure using the

* This work was sponsored by the United States Government. The views and conclusions contained in this document are those of the authors and should not be interpreted as necessarily representing the official policies, either expressed or implied, of the United States Government.

** Current Address - Susquehanna University, Pennsylvania

STI TTS 502 receiver, is also presented.

Test results are described which indicate the absolute accuracy of time transfer using the STI TTS 502. These results are based on tests performed at the GPS MCS. Further test results at the USNO establish the baseline accuracy with which time transfer can be performed between a user clock and UTC.

BACKGROUND

The GPS system and commercially available receiver systems, provide the capability for a user to determine his global position, velocity and time with a high degree of accuracy. As originally planned, the GPS was to consist of a space segment of twenty-four satellites and a ground segment of a Master Control Site (MCS) and five or more Monitor Sites (MS), one of which was to be located at the USNO. The monitor sites function is to receive transmissions from each GPS satellite, referred to a local clock, and to retransmit this information to the MCS over secure data communications links. The MCS correlates this information with other data, performs the necessary calculations to determine current satellite performance parameters and uplinks this information to each GPS satellite on a daily or, as required, basis. The uplinked data provides current information on clock performance and navigation data. The satellites were intended to be equally distributed in three orbital planes inclined to the Earth's equatorial plane by 63 degrees with the ascending nodes of the orbital planes differing by 120 degree intervals.

Funding cutbacks have reduced the planned number of satellites to eighteen. This cutback will affect position/velocity determination, but have little effect on time transfer, since only one satellite needs to be visible to a user to perform time synchronization.

GPS SATELLITE SIGNAL

Reference (3) describes the GPS data transmission process and structure. Briefly, data are transmitted from the GPS satellites on two carrier frequencies, a primary, L_1 , at 1575.42 MHz and a secondary, L_2 at 1227.6 MHz. The L_1 frequency is simultaneously modulated by a precision (P) code and a coarse/acquisition (C/A) code. The L_2 frequency is modulated by either a P or C/A code. Every six seconds a 50 bps message stream is transmitted with a total frame size of 1500 bits, common to both frequency bands and to both P and C/A codes. Each frame is divided into five 300 bit subframes which are further subdivided into ten 30-bit words. Telemetry and code handover information is contained in the first two words of each subframe. Key to the time transfer process is data contained in the first three subframes. The last eight words of Subframe 1 contain clock corrections consisting of second order polynomial coefficients which represent the variation

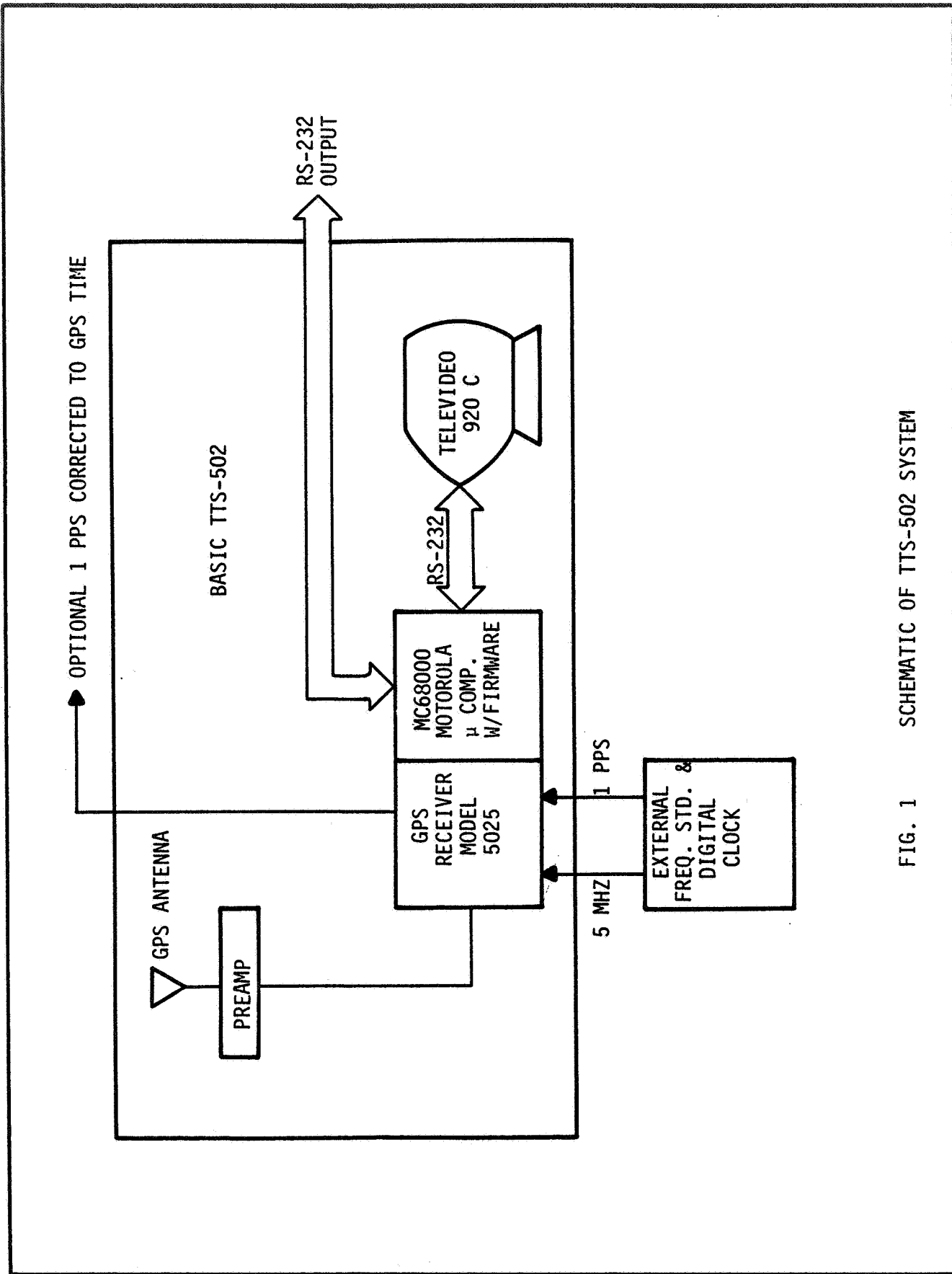


FIG. 1 SCHEMATIC OF TTS-502 SYSTEM

of the GPS satellite onboard clock with respect to the GPS master clock. Also included is an age of data word, and ionospheric delay model parameters. The GPS satellites ephemeris and age of data words are contained in Subframes 2 and 3. Subframe 4 provides an alphanumeric message for GPS users while Subframe 5 contains an Almanac (reduced accuracy version of information in Subframes 2 and 3) for each of the other GPS satellites in the constellation. Subframe 5 contains data on a single GPS satellite so that a sequence of frames is required to specify the Almanac for the complete GPS constellation.

The time transfer process using GPS requires that a user be capable of receiving, demodulating and decoding the transmitted data stream from a visible GPS satellite. The observed GPS satellite transmits the onboard satellite clock time (and corrections to the GPS master clock), which allows the user to compare the "observed" GPS time with time from his own clock. Corrections for propagation delays are required including free space instantaneous distance from GPS satellite to user, tropospheric/ionospheric delays, and equipment delays. Applying these corrections allows a measurement of the difference between the GPS master clock and the user's clock. The STI TTS Model 502 performs such a measurement for a user at a known location.

STI TIME TRANSFER SYSTEM

The STI Time Transfer System is shown schematically in Figure (1) and described in detail in Reference (4). The system consists of a GPS antenna, a preamplifier, time transfer receiver/processor and alphanumeric terminal for control of the receiver/processor. An external user clock (e.g., Cesium Beam Standard) is connected to the TTS 502 including a 5 MHz and 1 pps input. Firmware in the Motorola microprocessor provides several functions, including the following.

- 1) Scheduling the receiver to observe user selected GPS satellites. An automatic update option allows a user to specify an initial observation schedule. The microprocessor then uses the GPS ephemeris data to compute look angles accounting for orbit precession.
- 2) Perform raw time transfer observations every six seconds as scheduled, including;
 - a) derive satellite transmission time,
 - b) compute satellite clock error with respect to GPS system time,
 - c) compute GPS satellite position at the GPS system time,
 - d) estimate propagation delays (ionospheric, tropospheric, receiver constant bias),
 - e) compute satellite to station range,
 - f) determine the user clock error (difference between instantaneous user clock time and

corrected GPS time).

- 3) Perform data smoothing for a single pass of raw time transfer measurements.
- 4) Data display and formatting.
- 5) Operator interface (via the televideo 920C terminal) for data base update (user location, receiver bias) and mode control.

The TTS 502 thus allows a user clock to be compared with the GPS system time. The differences are output to the televideo 920C CRT screen and (optionally) to external peripherals via an RS-232 output channel. Correction to UTC time may be performed by inputting linear slope and offset coefficients which represent the variation between GPS system time and UTC time.

TIME TRANSFER CONCEPT

The concept of time transfer using GPS satellites is illustrated in Figure 2. The GPS satellite system will ultimately consist of a space segment of eighteen satellites distributed in three orbital planes inclined to the Earth's equatorial plane. Each satellite contains onboard an atomic clock (Rubidium or Cesium). A GPS ground segment includes a Master Control Site (MCS) and five or more Monitor Sites (MS). The monitor sites receive transmissions from each of the GPS satellites, referred to a local clock, and retransmit this information to the MCS over secure data communication links. The MCS correlates the data and performs calculations to determine current satellite performance parameters, including clock performance, and uploads data to each GPS satellite on a daily or as required basis. This process is shown schematically in Figure 2 as an upload/download from the MCS to a GPS satellite on the left hand side of Figure 2.

Each GPS satellite continually transmits a message which repeats every six seconds. The message is available to users with special GPS receivers and contains a time signal, correction parameters between the particular GPS satellite clock and the GPS master clock, propagation correction parameters for ionospheric delay, the satellites ephemeris and clock age data. Other data in the message concerns the ephemerides of all the other GPS satellites in the constellation.

Daily, for each GPS satellite the U.S. Naval Observatory's (USNO) prototype TTS performs a comparison between the individual GPS satellite clocks and the USNO master clock (hereafter referred to as Universal Time Coordinated (UTC)). In addition, the USNO compares UTC and the GPS time system. This data (viz., the correction between UTC and GPS, and the correction between UTC and the GPS satellite clocks) is published by the USNO on a daily basis

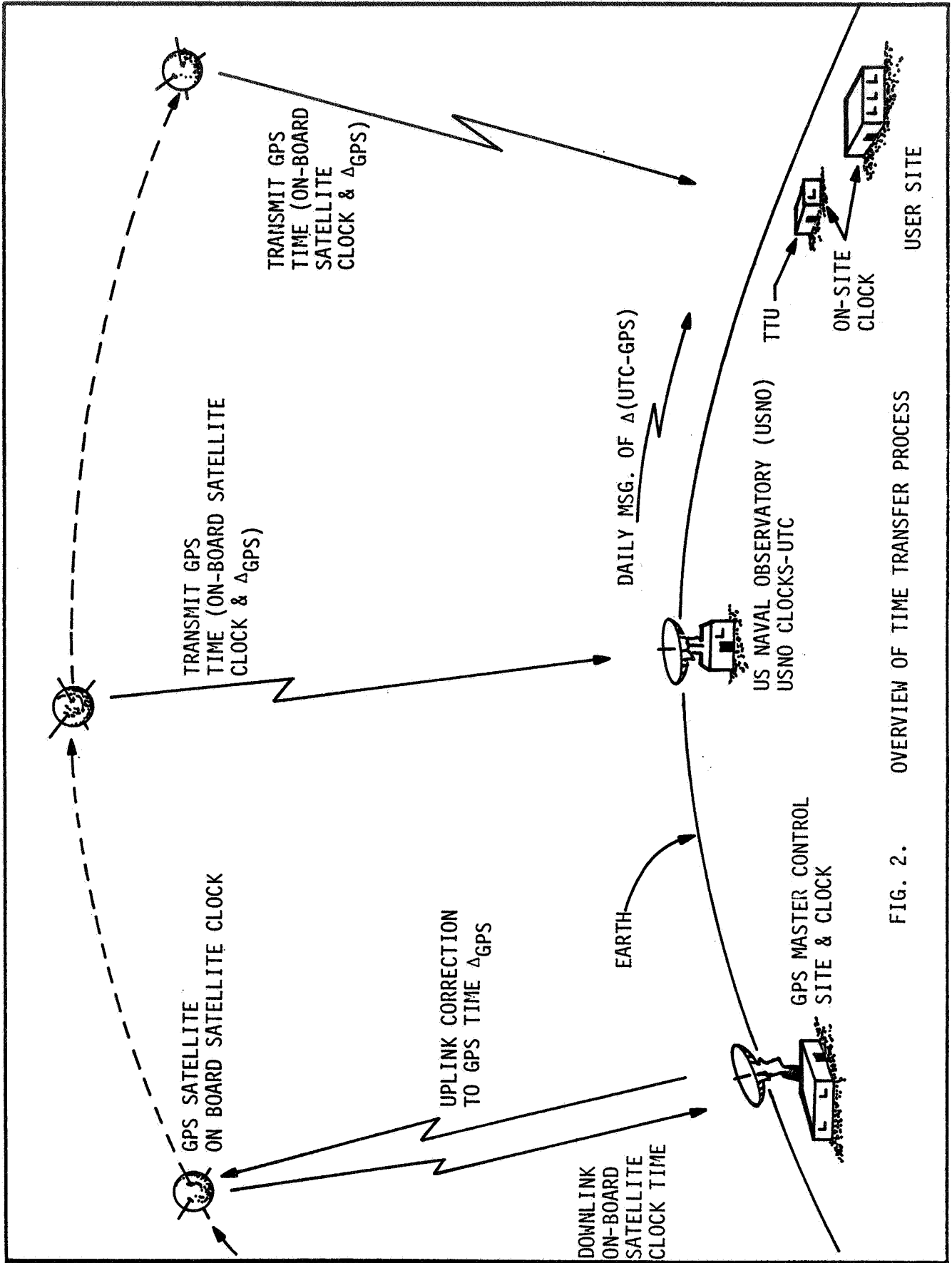


FIG. 2. OVERVIEW OF TIME TRANSFER PROCESS

via the USNO Time Service Series 4. This process is depicted in Figure 2 in the center of the figure.

As the GPS satellite becomes visible to the user site, the on-site TTS receives the GPS signal and compares the GPS time (via the onboard GPS satellite clock and GPS correction parameters) to the user's clocks. The TTS equipment and software perform a running comparison between the site clock and GPS time. The data from the USNO is then applied to correct the UTC time.

TEST PROCEDURES

During June 17 to 19 of 1982, tests of the STI TTS Model 502 were performed at the GPS MCS in Vandenburg, California and during August and September at the USNO in Washington, D.C. These tests established measurements of the fundamental accuracy of time transfer using the STI TTS 502 and the accuracy of the process of time transfer from a user clock to UTC time.

GPS MCS TESTS

In order to establish an accuracy baseline of the Time Transfer Unit, an accuracy test was performed at the GPS MCS. The test is shown schematically in Figure 3. Two TTS-502 receivers (serial #002 and 003) were set up in the GPS Master Site Integration Facility (MSIF) located at Vandenburg AFB. A USNO portable cesium clock (PC 837) was used as an intermediate standard for input to each TTS receiver. Time transfer observations were made via the time transfer TTS-502 receivers and the GPS system. These observations provided measurements of the offset between PC837 and GPS system time, as shown schematically as the output of a TTS receiver at the bottom of Figure 3. The observations were scheduled in accordance with the visibility of the GPS satellites at the MCS and to obtain a variety of time transfer measurements under all conditions (e.g. low and high elevation angles, day and night observations, etc.). The TTS-502 receivers were initialized to collect 10 minutes of data per visible GPS satellite. A round robin scheme provided for ten minute data collection on each GPS satellite (SV numbers 4, 5, 6, 8 and 9) in sequence. The TTS-502 smoothed the raw time transfer data, which were observed every six seconds throughout the ten minute data collection span, using a running 20 point linear least squares fit. A total of 149, ten minute data sets were observed during June 17 through 19.

During the same period, direct measurements of the offset between PC837 and GPS system time were obtained using the USNO 5328 counter, as shown in Figure 3. The counter measured, hourly, the offset between PC 837 and the Vandenburg Monitor Station (VMS) clock. Cable delays were measured by a 5370 Time Interval Counter to an accuracy of about 4 nsec. The difference between the VMS clock and GPS system time is monitored by GPS MCS personnel, as described in reference (5). A transformation was derived between PC837 and GPS system time using the USNO counter observations and the VMS-GPS

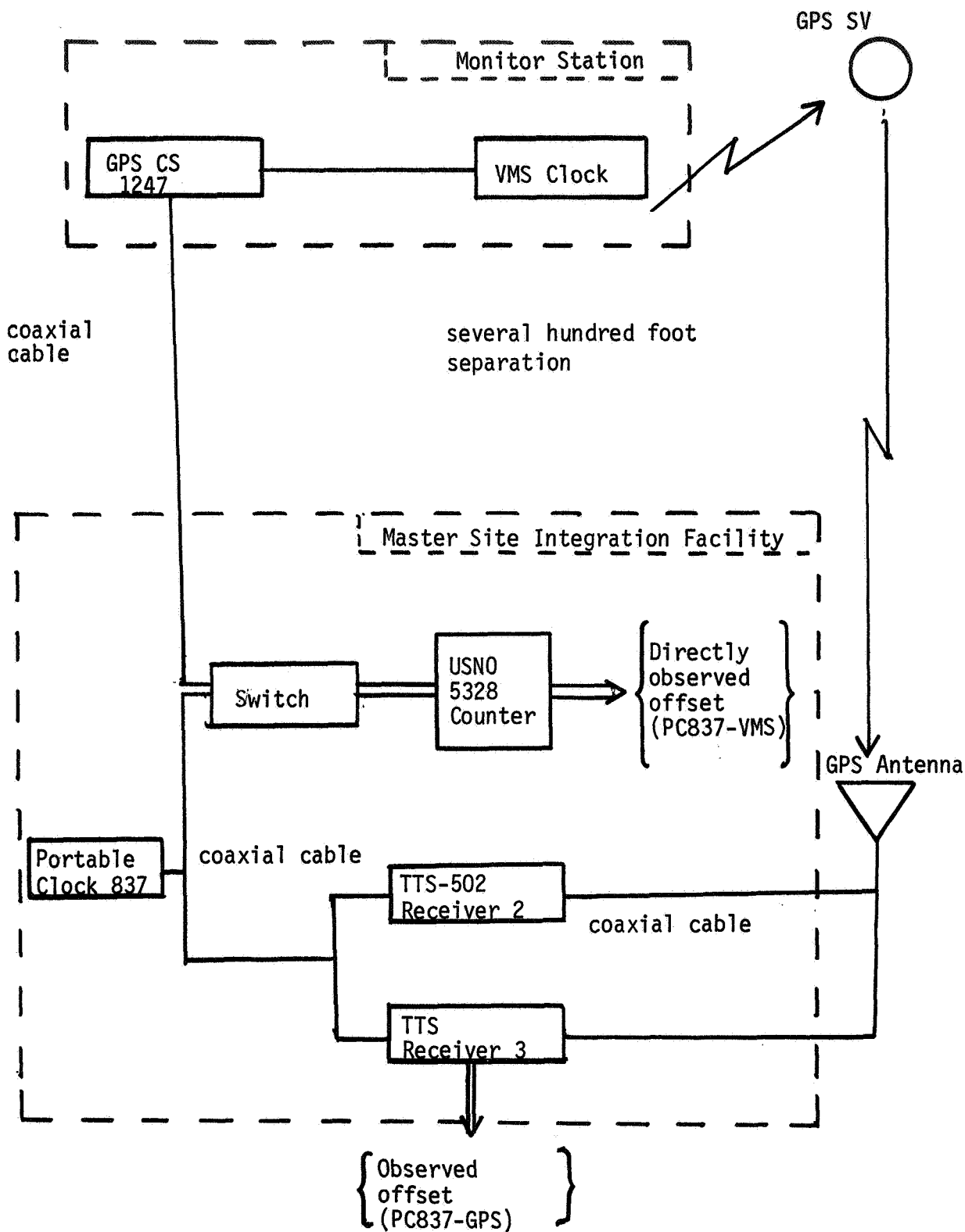


FIGURE 3: GPS MCS Accuracy Baseline Test

offset. The relation is:

$$(\Delta t)_{\text{PC837-GPS}} = (0.041147 \text{ nsec/min})(T - T_{\text{EPOCH}}) - 44531.7 \text{ nsec}$$

where $T_{\text{EPOCH}} = \text{day } 170, 4^{\text{h}}, 15^{\text{m}}, 0^{\text{s}}$ and T is the observation time. An uncertainty of ± 12.8 nsec is associated with the transformation, due to the errors associated with measuring the cable delays, noise in the USNO 5328 counter, and uncertainty in the GPS MCS determination of the relation between VMS time and GPS system time. The absolute error in the TTS-502 time transfer observations can be determined by an expression of the form,

$$(\text{TTS-502 Error}) = (\Delta t)_{\text{PC837-GPS}} - (\Delta t)_{\text{TTS-502 observations}}$$

where

$(\Delta t)_{\text{TTS-502 observations}}$ are the observations indicated as the output of the TTS-502 receivers (shown schematically at the bottom of Figure 3).

USNO VERIFICATION TESTS

Verification tests of the TTS-502 receiver, serial number 003, were performed at the USNO on August 19 through September 28 of 1982. The tests provided a measurement of the accuracy with which time transfer can be performed between UTC and GPS using the TTS-502 and the GPS satellite system.

The test compared the prototype TTU currently at the USNO with the TTS-502. In particular, the prototype USNO TTU is currently being used to perform time transfer between the GPS master clock to UTC time, and the individual GPS on-board satellite clocks to UTC time (Reference (3)). This is done at the USNO by connecting a physical UTC time signal into the prototype TTU and allowing the TTU to perform the time synchronization measurement. The results of these measurements are published daily by the USNO in a Time Series Report #4. The TTS-502 was simply set up beside the prototype TTU at the USNO. A UTC time signal was input to the TTS-502 as a system clock. Then, a comparison was made between the GPS time synchronization performed by the prototype TTU and that performed by the TTS-502. This test simply compares the operation of the prototype and new TTU units. Excluding observational noise which results directly from each TTU (viz. receiver noise, etc.), the time transfer measurements should be nearly identical, considering that the observational conditions are nearly identical (i.e., same GPS satellite, same elevation angle, same ionospheric delays, etc.)

A total of 154 passes of data were obtained for four GPS satellites (SV# 5, 6, 8 and 9). Each pass of data was smoothed by a linear least squares fit to result in a single smoothed time transfer observation. The analysis of these 154 smoothed observations is described in the next section.

TEST RESULTS

The results of both the GPS MCS tests and the USNO tests indicate that the TTS-502 receivers provide the capability to perform time transfer measurements to an absolute accuracy which is well within the 100 nanosecond budget for the receivers.

GPS MCS TEST RESULTS

Figure 4 shows a histogram of the data collected at the GPS MCS. The histogram includes all data collected during June 17 to 19, for receiver serial numbers 002 and 003, excluding GPS satellite number 4. Receiver #002 shows an absolute bias of -56.0 nsec with a standard deviation of 9.8 nsec. Receiver #003 exhibits a bias of -51.0 nsec with a standard deviation of 15.0 nsec. As shown on Figure 4, the one sigma uncertainty of the zero point calibration is ± 13 nsec.

Subsequent to the GPS MCS test, STI discovered a calibration error in the TTS-502 due to the algorithm used to correct for quantization effects. The resulting recalibration reduced the TTS-502 bias error by approximately 25 nanoseconds. Note that the STI recalibration was not fortuitous based on knowledge of the GPS MCS tests. STI personnel did not have the results of the GPS MCS test when the recalibration was performed. Thus, the absolute bias in the STI TTS-502 receivers is in the range of -26 to -56 nanoseconds with observational noise of 9 to 15 nanoseconds. It should be noted that the MCS GPS tests were conducted in an uncontrolled environment with variations in temperature, atmospheric pressure and humidity. Moreover, the data used to obtain the noise and bias figures, included observations of all GPS satellites (excluding number 4), day and night observations, and high and low elevation angles. Control of the ambient environment and careful selection of observations should decrease the observation noise.

USNO TEST RESULTS

Receiver #003 was moved to the USNO for further testing during August 19 through September 28. A total of 154 passes of time transfer data were collected in accordance with the previously described USNO test procedures. The data consisted of time transfer measurements between UTC and GPS system time using both the TTS-502 receiver and the USNO prototype receiver. Three basic analysis were performed including; (1) a comparison of the TTS-502 and USNO prototype receivers, (2) an analysis of the ability of a linear model to represent the TTS-502 time transfer data, and (3) an analysis of the accuracy with which the UTC-GPS offset can be predicted using a linear model. Each of these is described below.

First, a comparison was made between the TTS-502 time transfer data and that observed by the USNO prototype. Based on the results of the GPS MCS tests it was expected that the comparison of the TTS-502 and USNO prototype would

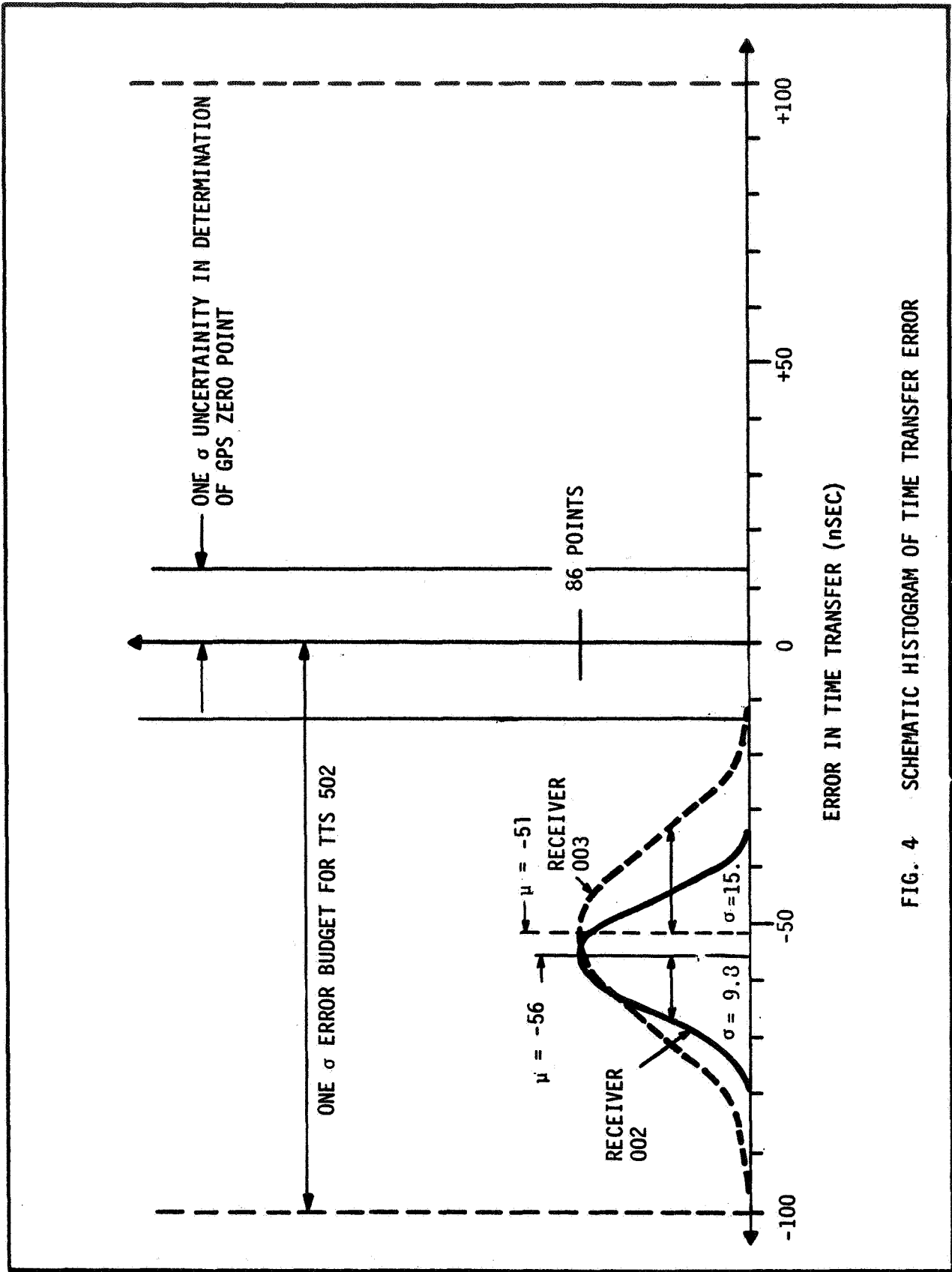


FIG. 4 SCHEMATIC HISTOGRAM OF TIME TRANSFER ERROR

yield an offset within a factor of two of the expected error of the TTS-502.

A linear regression was performed between the TTS-502 data and the prototype data. The resulting linear relation is,

$$(\text{TTS-502 Offset}) = (1.000) (\text{Prototype Offset}) + 170.\text{nsec.}$$

Figure 5 shows a histogram of the residuals about the linear expression. Clearly, a constant bias of 170 nanoseconds exists between the TTS-502 and the prototype receivers. This is significantly larger than the measured (-51 nsec) bias of the TTS-502 receiver. The standard deviation of the residuals about the regression line was 8.1 nsec.

During the USNO testing, another time transfer receiver from the Naval Research Laboratory (NRL) was brought to the USNO by Mr. Jay Oaks. Initial results indicate that the TTS-502 compares well with the NRL receiver. Further tests are required to resolve the offset issue. STI plans to recalibrate the prototype receiver during December 1982.

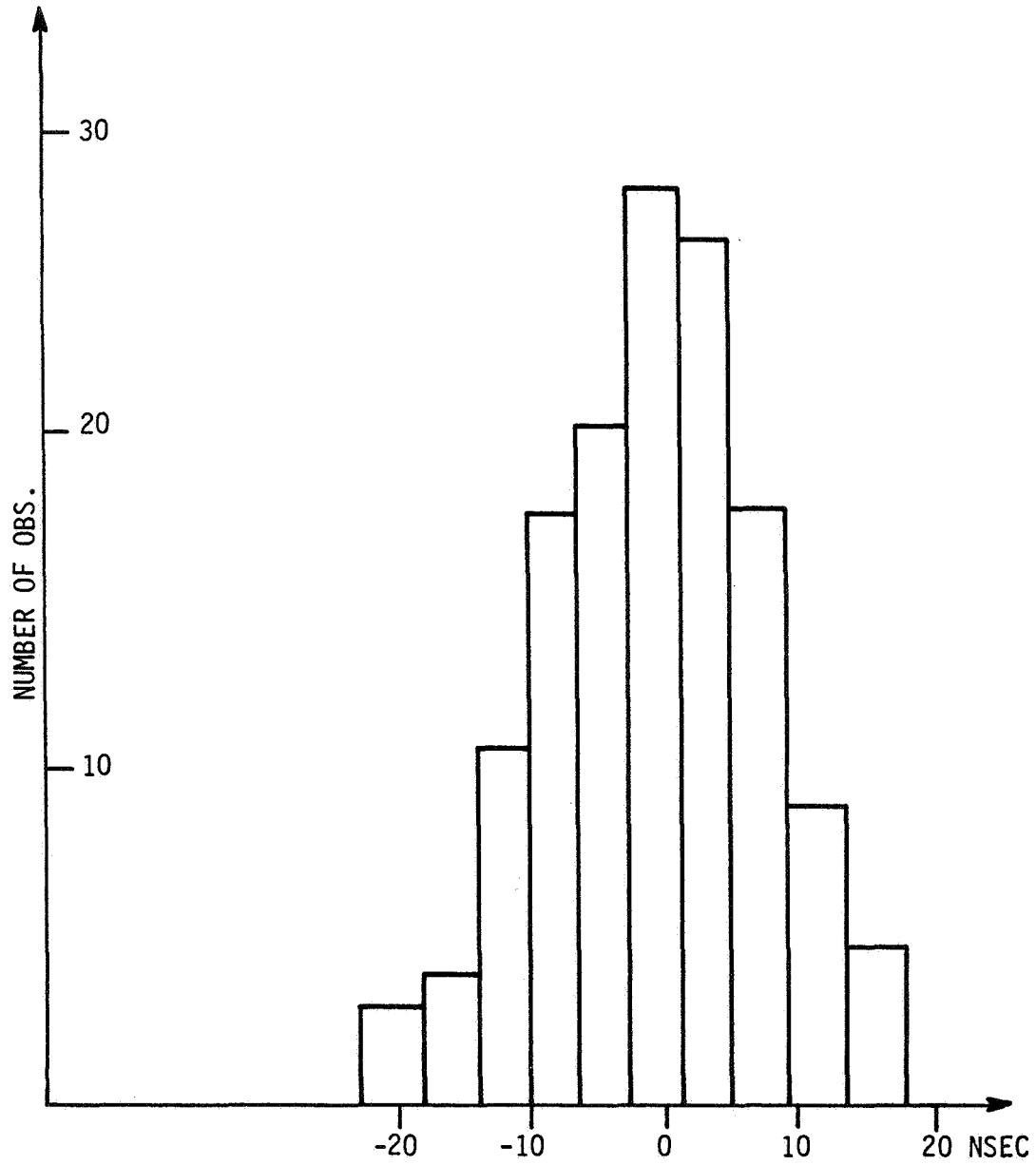
The second analysis performed on the USNO data was to model the observed TTS-502 data by a linear model. The data were fit by linear regression over several data collection spans. Expressions were obtained of the form,

$$(\text{GPS} - \text{UTC Offset}) = A(\text{Observation Time} - \text{Epoch}) + B$$

where the observation time is the starting time of the tracking of a GPS satellite in Julian days (format DDDD.DD). The epoch was chosen as Modified Julian day number 45198.0. The quantity A is the slope of the variation of the GPS to UTC time scales (microseconds per day), and B is the offset (microseconds) between GPS and UTC time at epoch.

Linear regressions were performed using all satellite data for several data collection spans ranging from a few days to the entire data collection span of 40 days. For each regression, the standard deviation of the residuals about the regression equation was computed. The results are shown in Figure 6 which plots the standard deviation of the residuals as a function of the data collection span. It might be expected that the standard deviation would be small for short data collection intervals, indicating a "local fit" phenomena, and subsequently increasing and leveling off for the data collection span for which the linear model is valid. At some point, the standard deviation of the residuals would increase when a data span is reached for which the linear model becomes invalid. Such a phenomena is shown in Figure 6. The linear model provides a good fit for a data collection span of less than 35 days. Beyond that interval, the linear model seems to break down. Because of the abrupt change of the standard deviation of the residuals, it might be suspected that some change in the GPS time scale was effected at Modified Julian day number 45233. Similar changes in the GPS system time scale have occurred in the past. However, over a collection interval of up to 35 days, a linear relation provides a good model to represent the time transfer data.

COMPARISON OF PROTOTYPE/TTS-502



SLOPE = 1.000
OFFSET = 170 NSEC
 $\sigma = 8.1$ NSEC

FIG. 5 HISTOGRAM OF RESIDUALS ABOUT THE LINEAR REGRESSION OF PROTOTYPE/TTS-502

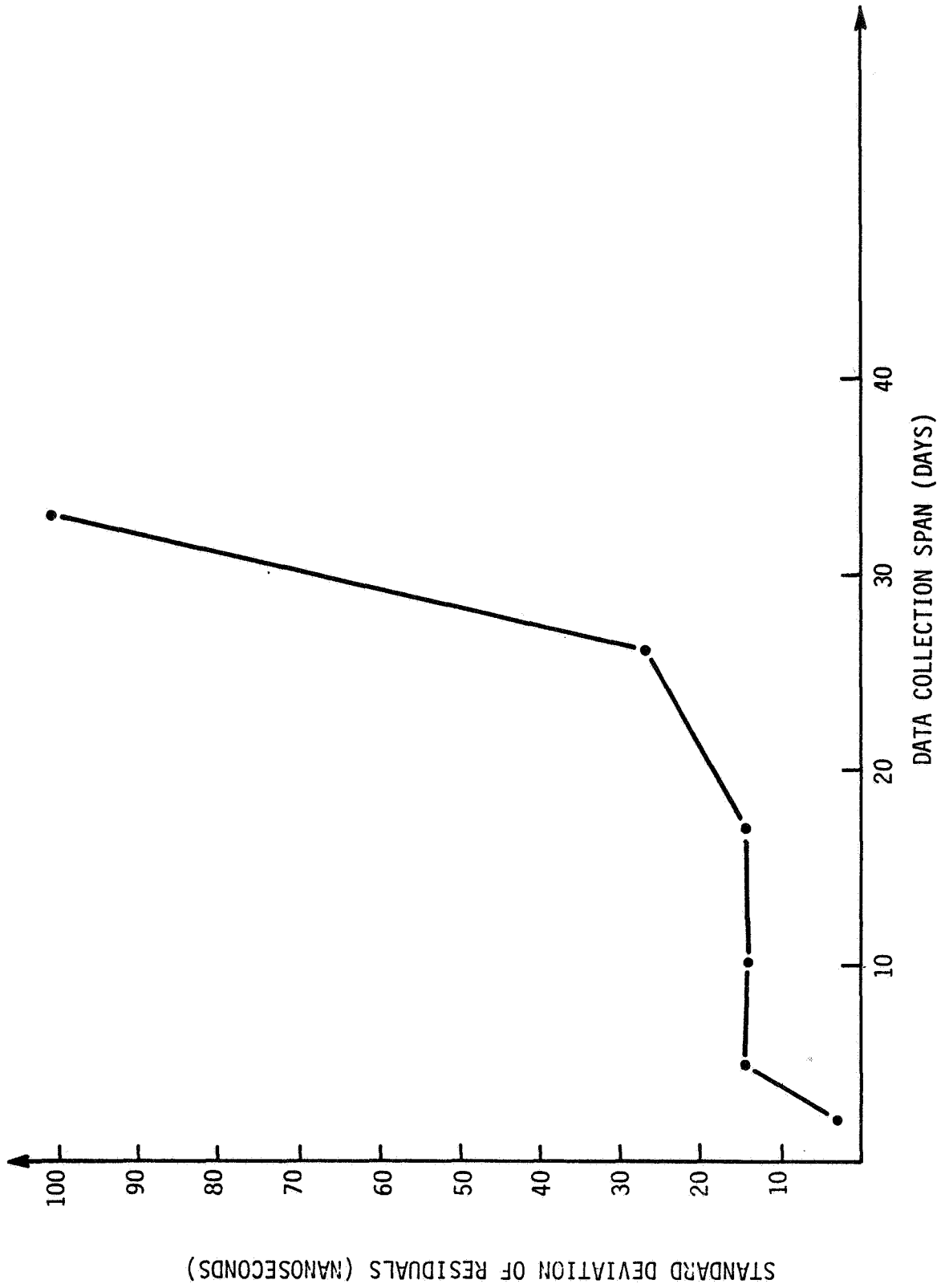


FIG. 6 STANDARD DEVIATION OF THE RESIDUALS ABOUT THE REGRESSION VS COLLECTION

The final analysis of the USNO data was an investigation of the ability of a linear model to predict the offset between GPS and UTC time. Specifically, the TTS-502 data was fit by a linear regression over a 26 day subinterval of the 40 day span of collected time transfer data. An equation of the form,

$$(\text{GPS} - \text{UTC Offset}) = A (\text{Observation Time} - 45198.0) + B$$

was obtained by least squares fit of the TTS-502 data for Modified Julian days 45198 to 45224. Five separate regression equations were obtained, one for each GPS satellite (numbers 5, 6, 8 and 9) and one regression which included all four satellites. Figure 7 lists the regression equation coefficients, the number of observations included in the fit, and the standard deviation of the residuals about the regression equation.

Each of these equations, or linear models for a 26 day span of time transfer observations, was used to predict the GPS-UTC offset for times beyond the end of the fitting interval (i.e., beyond Modified Julian day 45224). These predictions were compared against the actual TTS-502 observational data beyond day 45224. The comparison,

$$\text{Prediction Error} = (\text{Predicted Offset}) - (\text{TTS-502 Observed Offset})$$

was made to determine how the linear fit degrades beyond the end of the fitting interval. Figure 8 graphs the prediction error versus prediction interval (observation time -45224) for all four GPS satellites. The error degrades quadratically with prediction interval. However, a linear model yields a prediction error of less than 100 nanoseconds for a prediction interval of four to five days, using a 26 day calibration span.

GPS SV NUMBER	NUMBER OF OBSERVATIONS	REGRESSION EQUATION COEFFICIENTS		STANDARD DEVIATION RESIDUALS (μSEC)
		SLOPE (A) μSEC	OFFSET (B) μSEC	
5	17	0.110	-39.5	0.013
6	27	0.109	-39.1	0.017
8	27	0.111	-39.2	0.041
9	19	0.110	-39.1	0.019
ALL	90	0.110	-39.1	0.027

FIG. 7 REGRESSION EQUATIONS FOR A 26 DAY OBSERVATION SPAN

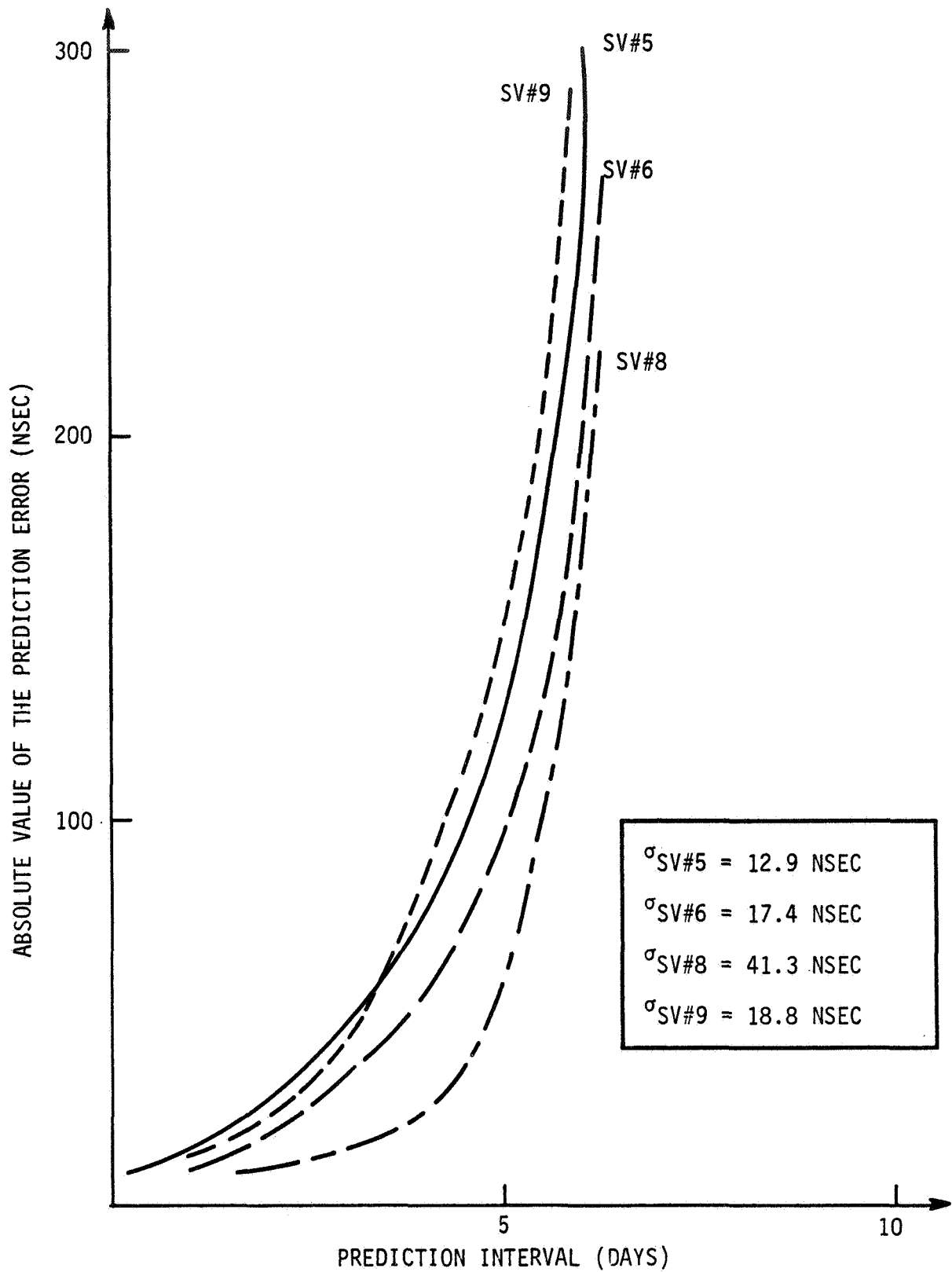


FIG. 8 PREDICTION ERROR VERSUS PREDICTION INTERVAL FOR 26 DAY CALIBRATION INTERVAL

ACKNOWLEDGEMENTS

The authors would like to acknowledge the help and advice of Dr. Winkler of the USNO in obtaining the USNO observational data. Mr. R. Sholley of HRB-Singer provided assistance in the final data reductions. Finally, Mr. F. Varnum of the GPS MCS supported the collection of the GPS MCS data. This work was supported by the Naval Research Laboratory.

REFERENCES

- (1) Global Positioning System, The Institute of Navigation, Washington, D.C., 1980.
- (2) Putkovich, K., "Initial Test Results of USNO GPS Time Transfer Unit", Proc. 34th Annual Frequency Control Symposium, USAERADCON, Ft. Monmouth, NJ 07703, May 1980.
- (3) System Specification for the NAVSTAR Global Positioning System, USAF Space and Mission Systems Organization, 31 January 1979.
- (4) Van Dierendonck, A. J., Hau, Q. D., McLean, J. R., and Denz, "Time Transfer Using NAVSTAR GPS", Stanford Telecommunications, Inc., Technical Memorandum, STI-TM-9828, 1 September 1981, 1195 Bordeaux Drive, Sunnyvale, CA 94086.
- (5) Varnum, F. and Chaffee, J., "Data Processing at the Global Positioning System Master Control Station", paper presented at the International Doppler Positioning Symposium in New Mexico, 1981.

QUESTIONS AND ANSWERS

MR. D. W. ALLAN, National Bureau of Standards

A question regarding the bias and the distribution of that bias: The 9.8 and 15 nanosecond widths, were those calculated from the 10-minute averages for all of the data taken for a receiver? I'm not sure how that 9.8 nanosecond width was calculated.

MR. D. L. HALL, HRB-Singer, Inc.

Yes. Basically, we used each data point as a smooth data point that contained for, say, a 10-minute span, that 9.8

MR. ALLAN:

So each data point was a 10-minute average?

MR. HALL:

That's right.

MR. ALLAN:

And that's the distribution of those 10-minute averages?

MR. HALL:

That's correct.

MR. ALLAN:

Okay. I think in principle, from the work we have done at the Bureau, we have seen distributions between receivers looking at the same satellite that are roughly on an order of magnitude better than that, and I wonder if you have any feeling for the source of that distribution?

MR. HALL:

No. I did want to say, though, that those numbers represented observations that were taken both at low elevations, high elevations, all times of the night and day, and so it is not the best case. When we looked at using, say, a single satellite, using night observations, high elevations, we could certainly reduce those noise figures by certainly 4 or 5 nanoseconds but not by an order of magnitude.

MR. ALLAN:

That certainly explains a lot of it.

RADIATION HARDNESS OF EFRATOM M-100
RUBIDIUM FREQUENCY STANDARD

Thomas C. English and Henry Vorwerk
Efratom
Division of Ball Corporation
Irvine, California

and

Norman J. Rudie*
IRT Corporation
San Diego, California

ABSTRACT

The effects of nuclear radiation on rubidium gas cell frequency standards and components are presented, including the results of recent tests where a continuously operating rubidium frequency standard (Efratom, Model M-100) was subjected to simultaneous neutron/gamma radiation. At the highest neutron fluence [7.5×10^{12} n/cm²] and total dose [11 krad(Si)] tested, the unit operated satisfactorily; the total frequency change over the 2½ hour test period due to all causes, including repeated retraction from and insertion into the reactor, was less than 1×10^{-10} . The effects of combined neutron/gamma radiation on rubidium-frequency-standard physics-package components were also studied, and the results are presented.

INTRODUCTION

The use of atomic frequency standards in space during the last decade and the employment of these devices in a growing number of military applications has resulted in continuing efforts to assess and ensure their operation in nuclear radiation environments. In this paper, the focus will be on rubidium gas cell frequency standards in general, and the Efratom, Model M-100, military rubidium frequency standard (RFS) in particular.

This paper is divided into two main parts. The first is a brief review of previous unclassified work in this area, including the effect of total dose and dose rate on an operating RFS and some of its components. The second presents new results that show the effects of neutrons on an operating RFS and certain RFS subsystems and components. These new results are of special interest for military applications that require the use of an RFS in a nuclear radiation environment.

PREVIOUS WORK

Whereas the general principles that govern the effects of nuclear radiation on atomic frequency standards have been enumerated previously,¹ not much has been published that deals with the direct, experimental assessment of these effects for RFS's. Almost all of the previous unclassified work was done by Rockwell International (RI) in conjunction with the NAVSTAR Global Positioning System (GPS). This system uses satellite-borne atomic clocks to provide military navigation of unprecedented accuracy. Most of the clocks used in this system have been built by Rockwell. They are a space-qualified version of the Efratom Model FRK-H RFS and include an Efratom-supplied physics package.

The first radiation test^{2,3} of an RFS by Rockwell was carried out in March 1974. In this test, an unmodified, Efratom, Model FRK, commercial RFS was irradiated with a total dose of 10 krad(Si) from a C_{60} gamma source at a constant rate over a one hour period while the unit was operating. This device, which was not radiation hardened in any way, exhibited a fractional frequency change of $+6 \times 10^{-11}$ due to the irradiation. This frequency increase resulted from a change in the characteristics of the electronics in the servo loop. The fact that the RFS photocell current changed by less than 1% during the irradiation showed that the rubidium lamp, physics package optics, and photocell were essentially unaffected by the radiation.

A second test² was carried out by Rockwell on an engineering model of the actual space clock (RFS) to determine the effect of dose rate. This unit was exposed to the maximum dose rate available from the RI flash x-ray facility ($\sim 4 \times 10^8$ rads(Si)/sec). An upper limit of <1 nsec was set on any accumulated phase error due to this dose rate and it was also observed that the radiation had a negligible effect on the physics package.

Samples of glasses that have been used in RFS's were also tested by Rockwell. In these tests^{4,5} aluminosilicate⁶ and borosilicate⁷ glasses were irradiated with up to 1 Mrad total dose from a C_{60} source. Light transmission at the rubidium resonance-line wavelengths⁸ was monitored for cumulative doses of 30 krad, 100 krad, 300 krad, and 1 Mrad. The results for the three samples of each glass type and the two wavelengths⁹ are summarized in Fig. 1. At the highest dose of 1 Mrad, the decrease in light transmission was 3.1% and 2.6% for the aluminosilicate and borosilicate samples, respectively.

PRESENT WORK

The purpose of the present work was to assess experimentally the effect of neutron irradiation on an operating, Efratom, Model M-100, military rubidium frequency standard (RFS), and also on certain RFS subsystems and components. This work¹⁰ was carried out in two parts using the General Atomic, Mark F TRIGA reactor in San Diego. The first part tested the complete RFS, and the second part tested RFS subsystem and components. The two tests were conducted one month apart.

IRRADIATION OF OPERATING RFS

The model M-100 RFS used for these tests was an engineering model¹¹ that differed from a standard production unit only in having a slightly modified frame and thicker-than-normal PC boards. The unit was operated continuously during the entire irradiation test and the following variables were also monitored continuously: the output frequency,¹² the dc output voltage of the photocell amplifier, the servo control voltage to the voltage-controlled crystal oscillator (VCXO), and the baseplate temperature (which varied from 42°C to 47°C during the test).

Irradiation Sequence

The unit was irradiated at four different levels. The irradiation sequence for each level consisted of the following four steps.

1. Attach two dosimeters to the side of the unit receiving the most radiation and insert the unit into the reactor tube.
2. Let the unit run undisturbed, with the reactor off, for 5 - 10 min.
3. Turn on the reactor at a low power level, thereby providing a constant irradiation, and maintain this for approximately 5 min.
4. Turn off the reactor and remove the unit immediately. Remove the two dosimeters and allow the unit to run undisturbed for at least 5 min (retraction period).

After the final irradiation sequence, the power to the unit was turned off for approximately 5 min and the unit restarted, after which it was left running for 45 min.

The purpose of the retraction operation was to minimize the total dose due to gamma radiation that results from the short-lived induced radioactivity of the reactor coolant after the reactor is turned off. In these tests all neutron fluences were expressed in terms of the 1 MeV neutron fluence that would produce the same damage to a silicon sample as the actual neutron fluence, i.e., as 1 MeV-silicon-damage-equivalent fluences.¹³

Test Results

The test data were taken over a four hour period that included a 90 min warmup and a 45 min restart test after completion of all irradiation. Relevant portions of these data have been compressed¹⁴ to fit on a single 8½ x 11 figure (see Fig. 2). Based on the test data, the following observations can be made.

1. The net change¹⁵ in fractional frequency due to all causes [including insertion and retraction] over a 2½ hr period [including irradiation to 7.5×10^{12} n/cm² and 11.2 krad(Si)] was less than 1×10^{-10} .
2. Frequency changes of from -2×10^{-11} to -5×10^{-11} were produced when the unit was retracted. These frequency changes were most likely due to changes in the orientation of the unit relative to the ambient magnetic field. They were not a result of irradiating the unit.
3. Changes in fractional frequency due to irradiation by combined neutron/gamma radiation were only a couple of parts in 10^{11} for up to 3×10^{12} n/cm² and 4.4 krad(Si) (levels 1 - 3).
4. Changes in fractional frequency during the last irradiation step [from 3×10^{12} to 7.5×10^{12} n/cm², and from 4.4 to 11.2 krad(Si)] were less than 1×10^{-10} except for a slow (~ 20 s) negative frequency transient of $\sim 1.5 \times 10^{-10}$ that occurred during the latter portion of the level 4 irradiation.
5. The dc photocurrent dropped drastically due to irradiation but this had only a small effect upon the performance of the unit as a frequency standard.
6. The short-term frequency stability of the unit was degraded by about a factor of two due to the irradiation (levels 1 - 4).
7. After the restart of the unit, subsequent to the level 4 irradiation, the retrace was within 2×10^{-11} of the frequency prior to turn off (normal behavior).
8. Over the 2½ hr duration of the test, the VCXO control voltage decreased from 10 V to 9V. For a free-running VCXO not locked to the atomic resonance, this would correspond to a fractional frequency change of approximately $+8\frac{1}{2} \times 10^{-8}$ which amounts to about one tenth of the electrical trim range of the VCXO.¹⁶

Decrease of dc Photocurrent

The dc photocurrent was monitored indirectly during these tests by observing the dc output voltage of the photocell amplifier. The photocell is operated in the short-circuit mode and under normal conditions the dc output voltage of the photocell amplifier is proportional to the dc photocurrent. Estimates^{10,17} of the change in this dc output due to radiation-induced changes in input offsets, bias voltage and current, show that it is a small fraction of a percent for irradiation by 1×10^{12} n/cm² and 1.5 krad(Si). This means that the observed decreases in dc output voltage (ranging from 55% to 78%) are due almost entirely to corresponding decreases in dc photocurrent.

At first glance, two mechanisms for this decrease in photocurrent appear

possible. The first of these is a decrease in the intensity of the light incident on the photocell surface. This mechanism would also produce a light shift in the resonance cell. Bench tests to simulate this effect indicate that the light shift is an order of magnitude larger than the observed frequency changes and has the opposite sign. This strongly suggests that changes in light intensity are not responsible for the observed decreases in dc photocurrent. The irradiation tests subsequently carried out on RFS subsystems and components (as will be shown) also support this conclusion. The only mechanism left is photocell degradation. Data¹⁸ on photocell degradation due to nuclear radiation show that for the irradiation levels used here, gamma radiation has little effect but neutrons can produce large decreases in photocurrent of the magnitude observed. As will be discussed later in this paper, direct tests on RFS photocells show clearly that considerable degradation does, in fact, occur.

The main effect of photocell degradation is a deterioration of the short-term frequency stability. Experimentally, a decrease of a factor of two was observed and this is consistent with bench test simulations of the effect.

IRRADIATION OF SUBSYSTEMS AND COMPONENTS

A month after the irradiation of the complete Model M-100 RFS, a second nuclear irradiation test on certain subsystems and components (see Table 1) was carried out using the same reactor under very similar conditions.

SUBSYSTEM IRRADIATION

The two subsystems irradiated were independent and nearly identical, each being comprised of the following M-100 subassemblies (Fig. 3).

1. Photocell-cavity-shield assembly, including cavity-thermostat board.
2. Lamp board and rubidium lamp
3. Power-supply board.

Items 2 and 3 were standard, unmodified, production items. Item 1 was also a standard production item except that the rubidium resonance cell and the Mylar window on the cavity had been removed to allow a completely unobstructed optical path from outside the assembly directly to the active surface of the photocell inside the microwave cavity. Both cavities were heated in the normal way, their temperatures being individually thermostatically controlled and continuously maintained at 75°C. The two assemblies differed only in that the photocells were from different manufacturers (Table 1).

Items 1 and 2 of each subsystem were mounted in the standard M-100 configuration thereby allowing light from each lamp board to be monitored by its

respective photocell. Both subsystem frames were rigidly bolted together so that the entire dual-subsystem unit could be easily inserted into the nuclear reactor for irradiation. Also included as part of this "inboard test fixture" was a standard M-100 servo board that was used to monitor the dc photocurrent of photocell #2 (PC2).

Irradiation Sequence

Like the previous test on the complete M-100, the two subsystems were irradiated at four different levels. The irradiation sequence, which was similar, was as follows.

1. Attach two dosimeters on the side of the unit receiving the most radiation and one dosimeter on the opposite side. Insert the unit into the reactor.
2. Let the unit run undisturbed, with the reactor off, for 5 - 10 min.
3. Turn on the reactor at a low power level, thereby providing a constant irradiation, and maintain this for approximately 5 min.
4. Turn off the reactor and remove the unit immediately. Remove the three dosimeters and allow the unit to run undisturbed for at least 5 min.

Outboard Photocell Test Fixture

Each frame was designed to allow its respective photocell-cavity-shield assembly to be easily removed and then subsequently reinserted into the same position relative to the lamp board. Prior to reactor insertion, each photocell-cavity-shield assembly was removed one-at-a-time and inserted into another test fixture that remained permanently outside the reactor during the entire test period. In what follows, this test fixture will be referred to as the "outboard photocell test fixture." This fixture, which is shown schematically in Fig. 4, consisted of an M-100 lamp board with rubidium lamp, an M-100 servo board, and an M-100 power supply board. The main purpose of this fixture was to provide a stable source of optical radiation for testing each of the two inboard photocells before and after each irradiation level. Since the lamp board, lamp, and power supply board in this fixture were not irradiated, they could be relied upon to provide constant illumination for the duration of the test.

The outboard photocell test fixture had two important modifications that greatly increased its versatility. The first modification allowed sinusoidal modulation of the light beam at the RFS modulation frequency (127 Hz) using the modulation signal from the servo board. The amplitude of this modulation was kept small compared to the dc light level so that the dc measurements were unaffected by it. The purpose of the modulation was to allow determination of the effect of the irradiation on the ac response of the two photocells. The second modification allowed the photocell Thévenin

equivalent shunt resistance¹⁹ (R_S) to be measured^{20,21} by insertion of a 100 Ω resistor in series with the photocell. The shunt resistance is an important photocell parameter in our application because its value largely determines²⁰ the amount of photocell-amplifier additive noise in the vicinity of the RFS modulation frequency which, in turn, influences the short-term frequency stability of the RFS. The shunt resistance must be 1 k Ω or greater for satisfactory operation of the M-100.

In summary, then, the following photocell variables could be monitored using the outboard photocell test fixture: dc photocurrent, ac photocurrent at 127 Hz, and shunt resistance, all under conditions of constant illumination.

Measurement Sequence

Prior to level 1 irradiation, the outboard photocell test fixture was used to characterize both photocells by measuring the dc photocurrent, the ac photocurrent,²² and the shunt resistance for each.²³ Each photocell was subsequently characterized again between irradiation levels and at the end of level 4.

During the time that the photocells were inserted in the reactor, the dc photocurrent of each was monitored continuously. The current of photocell #1 (PC1) was monitored using the photocell amplifier on the outboard-photocell-test-fixture servo board, and the current of photocell #2 (PC2) using the photocell amplifier on the inboard servo board.

Test Results

Dc Photocurrent The inboard and outboard measurements of dc photocurrent for the two photocells are listed in Table 2 and the outboard results (constant illumination) are plotted in Fig. 5 as a function of neutron fluence and total dose (as measured by the two dosimeters on the side of the unit receiving the most radiation). For the highest cumulative irradiation tested, namely 6.15×10^{12} n/cm², the dc photocurrents of both photocells dropped to approximately 40% of the pre-irradiation values. Both photocells exhibited similar dc photocurrent degradation.

Ac Photocurrent The dc and ac photocurrents are compared in Table 3 where it can be seen that the ac photocurrent is degraded to a greater extent than the dc photocurrent.²² Note that at the highest fluence of 6.15×10^{12} n/cm² the normalized ac photocurrents were about 70% of the normalized dc photocurrents.

Shunt Resistance Fig. 6 shows the results for photocell shunt resistance as a function of neutron fluence and total dose. The Ferranti photocell (PC1) shunt resistance increased slowly with cumulative neutron fluence and total dose. The increase was from an initial value of about 2 k Ω to a final

end-of-test value of about 3 k Ω . The International Rectifier photocell (PC2) showed a different behavior. Its shunt resistance increased slightly at first, starting at 11 k Ω , and thereafter decreased, reaching an end-of-test value of about 6.5 k Ω . In no instance did the shunt resistance for either photocell drop below 2 k Ω as a result of irradiation. Since the requirement for satisfactory RFS operation is 1 k Ω or greater, the effect of the radiation on shunt resistance is of no practical importance for the M-100.

Rubidium Light Source

The test results in Table 2 also show that the M-100 rubidium light source (lamp board and lamp) is virtually unaffected by the radiation even at the highest level of 6.2×10^{12} n/cm² and 9.2 krad(Si). This follows from the close tracking of the inboard and outboard values for both photocells. The tracking is not perfect but the differences (up to several percent) that do exist can probably be attributed to small misalignments in the relative positions of the photocell assemblies and the lamp boards from measurement to measurement. (The positioning mechanisms did have some "slop" in them and examination of the insertion/removal processes²⁴ shows that such misalignment "errors" could have occurred.)

If small light intensity changes of a few percent are occurring, there are several possible mechanisms that might be responsible. For example, radiation-induced offsets in the lamp-thermostat op amp can, in principle, produce changes in lamp temperature. A calculation of the size of this effect for 1×10^{12} n/cm² and 1.5 krad (Si) predicts a temperature change of 0.02°C or less. Since a 1°C increase in lamp temperature is required to produce a $\sqrt{7}$ % increase in light intensity, this effect is expected to be insignificant.

Changes in light intensity due to effects of nuclear radiation on the lamp oscillator circuitry are also expected to be small but precise calculations are not possible in this case because of a lack of knowledge as to how critical parameters (such as base-emitter impedance) are altered and how the amount and frequency of the rf power delivered to the lamp affect the light output. In any event, it is clear from the experimental results that any changes in light intensity that do occur, do not exceed several percent at most.

COMPONENT IRRADIATION

The optical materials listed as S1 through S5 in Table 1 were also irradiated to determine the effects of simultaneous neutron/gamma radiation on their light transmittance. These are materials that are used in the light paths of Efratom's RFS's.

Transparency Test Fixture

The transparency test fixture is shown in Fig. 7. This fixture contains an RFS rubidium lamp board and lamp which produces rubidium light. The rubidium light is incident upon an interference filter which passes rubidium D₁ resonance light (794.8 nm). The D₁ light is detected by a photocell mounted approximately 5/8" below the filter. Sample transparency is determined by inserting the sample into the light beam and measuring the amount of transmitted light.

The glass samples used were in the form of glass tubes,²⁵ nominally 2" long. To measure the light attenuation produced by a glass tube, it was positioned as shown in Fig. 7, intercepting all of the D₁ light incident upon the photocell. The mica and Mylar samples were in the form of thin disks (see Table 1) approximately 5/8" in diameter. These disks were glued to a flat aluminum plate, concentric with a 1/2" hole through the plate, as shown in Fig. 8. To measure light attenuation, the plate was inserted into the sample holder slot shown in Fig. 7 (with the glass tube removed). In this configuration, D₁ light could reach the photocell only by passing through the sample.

The mica and Mylar samples could be positioned quite precisely in the test fixture and, in addition, they were of uniform thickness without any obvious optical distortion. This was not the case for the glass samples, each of which had slight irregularities that affected the light transmission due to small variations in reflection and refraction as the tube was rotated about its own axis in the test fixture. To avoid these changes in transmitted light due to this extraneous effect, care was taken during the tests to orient each glass tube in the same way each time it was inserted into the transparency test fixture. This precaution reduced these effects to an insignificant level. (They weren't very large anyhow.) In addition, for each glass sample tested, a nearly identical control was used as a reference. The sample was irradiated in the reactor, the control was not.

Measurement Procedure

Prior to level 1 irradiation the light transmission of each sample and control was measured in the transparency test fixture. The samples, S1 - S5, were then placed behind the inboard test fixture on the carriage that was used to transport the test fixture to the reactor core. The samples remained at this location on the carriage until all irradiation was complete (levels 1 - 4). They were then removed and their light transmission, along with that of the controls, was measured again in the transparency test fixture to determine the effect, if any, of the radiation.

Dosimetry

The dosimeters on the rear of the inboard test fixture (one for each level)

were used to determine the cumulative neutron fluence to the optical samples. This amounted to 2.7×10^{12} n/cm², compared to the corresponding figure for the front of the inboard test fixture of 6.2×10^{12} n/cm² (plus 9.2 krad(Si) total dose, 98% of which is due to gamma radiation). The difference in these neutron fluences can be attributed mostly to scattering of the incident neutrons by the test fixture. Since the gamma radiation is attenuated very little by the test fixture, the cumulative gamma dose to the glass is expected to be ~ 9 krad(Si).

Test Results

The transparency test fixture was observed to be stable to a few tenths of a percent over the more than three hour duration of the optical sample test. It is therefore expected that changes in sample light transmission of $\lesssim 1\%$ could have been detected. The observed changes in light transmission for all samples and controls (after vs. before, and sample vs. control both before and after) were of the order of a few tenths of a percent with the exception of the Schott 8436 glass where the after vs. before readings for the transmitted light were -1.2% and -1.0% for the sample and control, respectively. The fact that both sample and control showed nearly identical 1% decreases is most likely due to a short-term fluctuation in the test apparatus rather than to any change in sample or control transparency. It is therefore reasonable to conclude that, to within the experimental uncertainty of several tenths of a percent, no radiation-induced transparency changes occurred for any of the optical materials tested.

SYNTHESIS OF RESULTS

In the tests carried out on the complete Model M-100 RFS, it was concluded that the decrease in the dc photocurrent due to irradiation was due almost entirely to photocell degradation. This conclusion is supported by the results of RFS subsystems and components, namely, the constancy of the light output from the lamp board during irradiation, the absence of any radiation-induced changes in the transparency of the optical materials,²⁶ and, of course, the degradation of the two photocells tested.

Photocell Degradation

The dc photocurrent of the complete RFS tested is plotted against neutron fluence in Fig. 5 assuming that the illumination of the photocell remained constant during the test (a good assumption, as pointed out above). The photocell used in this unit was neither an IR nor a Ferranti photocell but rather one manufactured by Silicon Sensors, Inc.. Consequently, the significance of Fig. 5 is that there are considerable variations in photocell degradation from one manufacturer to the next. For the three curves shown, the max/min variation ranges from 1.5 at 6.5×10^{11} n/cm² to 2.0 at 6.5×10^{12} n/cm². It is highly significant that for the worst degradation

shown, the complete M-100 still operated satisfactorily.²⁷

EXTRAPOLATION TO HIGHER RADIATION LEVELS

The results obtained in the two parts of this investigation are based on neutron irradiation up to 7.5×10^{12} n/cm² and 6.2×10^{12} n/cm², respectively. Since data points were also taken at lower fluences, a straight-forward extrapolation to at least 1×10^{13} n/cm² is possible for certain portions of the RFS.

Transparency of Optical Components The optical materials tested received a maximum fluence of 2.7×10^{12} n/cm² which is estimated from the front/rear dosimetry data to correspond to a fluence of 5×10^{12} n/cm² to a complete RFS. At this level of irradiation, no change in transparency was observed and the experimental uncertainty sets an upper limit on changes in light transmission of a few tenths of a percent. It therefore seems unlikely that a fluence of 1×10^{13} n/cm² to an RFS will produce significant darkening of any of the optical materials. Independent data on the effects of neutron fluences of 1×10^{13} n/cm² and greater for glass and mica also support this view.²⁸

As regards the glass alone, there is additional direct evidence that it can withstand neutron irradiation in excess of 10^{15} n/cm². During the Rockwell Efratom rubidium lamp investigation for the Global Positioning System (GPS),²⁹ in which one of us (T.C.E.) was directly involved, a number of rubidium lamps were neutron activated as part of a program to determine the quantity of rubidium in rubidium lamps. The first step in the activation process is to irradiate the filled lamp (less base) with neutrons. This was done in the General Atomic TRIGA, Mark I reactor³⁰ in San Diego. Lamps were typically irradiated simultaneously with a $\sim 2 \times 10^{15}$ n/cm² of 1 MeV-equivalent neutrons and ~ 7 Mrad gamma total dose.¹⁰ The irradiated lamps were made of Corning 1720 glass and Schott 8437. Schott 8437 is very similar to the Schott 8436 glass that Efratom presently uses in all its RFS lamps (both are alkali-resistant borosilicate glasses).

Several of the irradiated lamps were used in Rockwell/Efratom GPS rubidium clocks that are in GPS satellites presently orbiting the earth. The glass of these lamps had a slight yellowish cast after irradiation but there were no indications during acceptance testing that they performed in any way that was different from an unirradiated lamp.³¹

Photocell Degradation Extrapolation of the normalized dc photocurrent for the IR photocell to 1×10^{13} n/cm² using Fig. 5 gives a value of $\sim 40\%$. Assuming that the normalized ac response is $\sim 60\%$ of the normalized dc response gives a normalized ac response of $\sim 25\%$ at 1×10^{13} n/cm². This is low but nevertheless adequate since the complete M-100 tested showed satisfactory operation for about a factor of two lower value at 7.5×10^{12} n/cm²

using the Silicon Sensors photocell.²⁷

Electronics The hardness of the electronics at 1×10^{13} cannot be extrapolated from our results and will require an additional hardness assessment at this level.

SUMMARY AND CONCLUSIONS

Separate tests were conducted on an Efratom, Model M-100, military, radiation-hardened, rubidium frequency standard (RFS), and on certain RFS subsystems and components by subjecting them to combined neutron/gamma radiation from a nuclear reactor. The results of these tests allow the following conclusions to be drawn.

Complete RFS

1. The Model M-100 RFS, which was operated continuously during the test, performed satisfactorily up to and including the highest radiation levels tested [7.5×10^{12} n/cm² and 11 krad(Si)]. Over the $2\frac{1}{2}$ hr duration of the test, the overall frequency change due to all causes (including insertion into and retraction from the reactor) was less than 1×10^{-10} .
2. As a result of irradiation of the unit at the highest level, the short-term frequency stability decreased by about a factor of two. The tests conducted show that this decrease was due to a degradation of the performance of the photocell in the unit. This result is of particular significance since the photocell used in this unit showed the greatest degradation of the three photocells irradiated. In the future, use of either Ferranti or IR photocells should result in the unit meeting its original short-term stability spec even after irradiation to 7.5×10^{12} n/cm² and 11 krad(Si).³²
3. The free-running VCXO frequency (had the VCXO not been locked to the atomic resonance) was shifted by only about one tenth of its electrical trim range due to the irradiation. For this reason there is no danger of the control voltage being shifted beyond the control limits due to irradiation, or the unit failing to reacquire lock when turned off and then turned on again.
4. After the final irradiation of the unit, it was turned off for five minutes and then turned on again. Retrace was within 2×10^{-11} of the frequency prior to turn off (normal performance).

Subsystems and Components

5. Samples of all materials used in the optical paths of Efratom rubidium frequency standard (RFS's) were tested for radiation-induced changes in the optical transmission of rubidium D₁ resonance light (at 794.8 nm). For simultaneous neutron fluences and total doses up

to 2.7×10^{12} n/cm² and ~ 9 krad(Si), respectively (corresponding to $\sim 5 \times 10^{12}$ n/cm² and ~ 9 krad(Si) to a complete RFS), no changes in the optical transmission of any of the materials were observed, to within the experimental uncertainty of a few tenths of a percent. Transmission measurements for rubidium D₂ light (780.0 nm) were not made, but because of the close proximity of the D₁ and D₂ spectral lines (~ 15 nm separation) it is quite unlikely that D₂ transmission behaves in a different manner than D₁ transmission. This latter conclusion is also supported by measurements of total light intensity from rubidium lamps operating in the same radiation environment (see below).

6. The experimental results for two rubidium lamps, lamp boards, and power supply boards, all continuously operating in a nuclear radiation environment, can be used to set an upper limit on radiation-induced changes in the total light output of an Efratom RFS rubidium light source. For the highest irradiation level tested (6.2×10^{12} n/cm² and 9.2 krad(Si) total dose), this limit amounts to several percent and corresponds to the experimental uncertainties in the measurements. In addition, calculations based on the known behavior of electronic components under irradiation make it virtually certain that changes in light intensity due to radiation-induced changes in lamp-oven temperature are significantly less than one percent.
7. Rubidium lamps made by Efratom were neutron activated to determine their rubidium fills for the GPS program. During neutron activation these lamps received a neutron fluence in excess of 10^{15} n/cm² and a gamma dose of ~ 7 Mrad. (These radiation levels are $\sim 300\times$ and $\sim 600\times$ greater, respectively, than those used in our tests.) Subsequent to neutron activation these lamps passed GPS acceptance testing and there were no indications that they operated in any way that was different from that of an unirradiated rubidium lamp. Six of these lamps are now in GPS satellites orbiting the earth. Of these six, the one that has been turned on is still operating satisfactorily after two years.
8. Two different RFS photocells were tested for degradation after simultaneous exposure to neutrons and gamma radiation (see Fig. 5). For the highest radiation levels of 6.2×10^{12} n/cm² and 9.2 krad(Si), the dc photocurrents dropped to approximately 40% of their initial, pre-irradiation values (under conditions of constant illumination with unfiltered rubidium light).
9. The ac photocurrents of the two photocells due to light modulation at 127 Hz (the RFS modulation frequency) were also measured under the same conditions and were found to degrade somewhat more rapidly than the corresponding dc photocurrents (see Table 3). At the highest irradiation level, the ac photocurrents, normalized to the pre-irradiation values, amounted to $\sim 70\%$ of the corresponding normalized dc photocurrents.
10. The photocell shunt resistances were also measured and found to be

affected by simultaneous neutron and gamma irradiation (see Fig. 6), but even at the highest irradiation level (6.2×10^{12} n/cm² and 9.2 krad(Si) total dose) the shunt resistances of both photocells were in excess of 3 k Ω . Since the shunt resistance must be 1 k Ω or greater for satisfactory M-100 operation, shunt resistance changes due to irradiation at up to 6.2×10^{12} n/cm² and 9.2 krad(Si) are of no importance for the M-100.

11. Straightforward extrapolation of the results of this paper indicates that the physics package optical components and photocell are most likely hard at neutron fluences of 1×10^{13} n/cm². The hardness of the electronics at this level of irradiation is presently unknown and requires a separate assessment.

ACKNOWLEDGEMENTS

The authors would like to thank George Malley for his innovative and expert mechanical efforts in the construction of the test fixtures. The professional competence of the IRT reactor crew is also greatly appreciated.

REFERENCES AND FOOTNOTES

*Efratom Consultant

1. T.M. Flanagan and R.E. Leadon, "Radiation Effects in Crystal and Atomic Frequency Standards," Proc. PTTI 7, 125 (1975)
2. Thomas C. English, "Discussion Forum: Atomic Frequency Standards, Rubidium," Proc. PTTI 10 199 (1978)
3. E.M. Hicks and F.K. Koide, Test Report No. 74-220-RT-012, Autonetics Division, Rockwell International, March 1974.
4. Rockwell Autonetics Internal Letter No. 74-551-010-103 from J.T. Blandford to L.S. Mims, 23 Sept. 1974.
5. Norman J. Rudie, Principles and Techniques of Radiation Hardening, Vol. 1. Second Edition (Western Periodicals Co., 13000 Raymer, North Hollywood, Calif. 91605) 1980, p. 11-19.
6. Corning 1720 glass, 0.11 cm thick sample
7. Corning 7070 glass, 0.16 cm thick sample
8. 794.8 nm (D₁) and 780.0 nm (D₂)
9. All readings for 780.0 nm and 794.7 nm were the same to within 0.1%
10. Thomas C. English and Henry Vorwerk, "M-100 Radiation Hardness Test," Parts 1 and 2 (Efratom Systems Corporation Internal R & D Reports, May 1982 and November 1982, respectively; unpublished.)
11. S/N E-002. It came off the assembly line in November 1981. The frame and PC board modifications mentioned were originally intended to improve the mechanical rigidity.
12. Measured against an Efratom, Model FRT-H, RFS using a Tracor, Model 527A Frequency Difference Meter.
13. For the test reactor used, a neutron fluence of 10^{12} n/cm² also results in a total radiation dose of 1.5 krad(Si). Of this total dose, only 2% is due to neutrons, the remainder being due to gamma radiation that is present with the neutrons. All other types of radiation (e.g., α , β) are negligible.
14. In order to fit the data on one 8½ x 11 figure, part of each of the following were omitted from Fig. 2: Initial warmup prior to level 1 sequence retraction period for each level, restart data. Also not shown in Fig. 2 are transient frequency changes that occur during a one minute interval when the unit is retracted, and later when it is reinserted into the reactor.
15. $y(\text{end of } 2\frac{1}{2} \text{ hr}) - y(\text{beginning of } 2\frac{1}{2} \text{ hr})$ where y = fractional frequency offset from reference.
16. The crystal used in the M-100 is an unswept, AT cut, third overtone, 10 MHz quartz crystal manufactured by Colorado Crystal

17. "Hardness Assessment of the Efratom Rubidium Frequency Standard, Model M-100" (Consultant's report to Efratom dated July 24, 1979, available on request.)
18. H.Y. Tada and J.R. Carter, Jr., Solar Cell Radiation Handbook, JPL Publication 77-56 (NASA & JPL, Nov. 1, 1977), Figs. 3.6, 3.18 and p. 3-49.
19. "Silicon Photovoltaic Detectors and Detector/Amplifier Combinations" (EG&G Electro-Optics Application Note D3011B-1, 1 August 1975).
20. T. English, "Noise Sources in the FRK Photocell and Photocell Amplifier, Part 1" (Efratom Systems Corp. Internal R & D Report, 1 August, 1978).
21. For normal operation of the photocell in the short-circuit current mode, the shunt resistance can be computed from

$$R_S(\Omega) = 100 \Omega \times \frac{i}{(i - i_0)}$$

where i_0 = dc photocurrent without series resistor

i = dc photocurrent with series resistor

22. Due to the complexity of the test and the time factor (the unit was radioactive after the first irradiation and could only be handled for a very short period between irradiations) the ac photocurrent was not measured between levels 1 and 2, or between levels 2 and 3.
23. When a photocell-cavity-shield assembly was inserted into the outboard photocell test fixture for characterization, the photocell's dc and ac photocurrents were measured using the photocell amplifier on the fixture's servo board. Since this servo board was not irradiated, its performance could not be affected in any way by nuclear radiation.
24. The insertion/removal processes mentioned here refer to the insertion/removal of a photocell-cavity-shield assembly relative to an inboard or outboard lamp board.
25. Flat glass plates would have been more desirable but they were not conveniently available.
26. The samples of optical materials were at ambient temperature when irradiated, whereas in an RFS they operate at elevated temperatures. However, it was not convenient in these tests to irradiate the samples at temperatures above ambient.
27. Efratom no longer uses Silicon Sensors photocells in any of their RFS's due to the low shunt resistance of these devices.
28. Ref. 5, Ch. 11.
29. This investigation began in February 1979 and continued through 1981.
30. This reactor is different than the TRIGA, Mark F reactor used in the RFS irradiation experiments.
31. No "before-and-after" tests of light transmission were performed on these lamps.

32. A typical M-100 has a short-term stability (σ_y) that is a factor of two better than spec. Using either a Ferranti or IR photocell should reduce the deterioration of short-term stability due to irradiation from a factor of two to about a factor of $1\frac{1}{2}$.

TABLE 1
OPTICAL MATERIALS USED IN RFS COMPONENT IRRADIATION TEST

Item	Description ^a	RFS Function ^b	Used in Efratom RFS Model(s) ^c
PC1	Silicon solar cell, International Rectifier P/N 49-2835, 1.0 O.D.	Photodetector	A
PC2	Silicon solar cell, Ferranti MS11B, 1.0 O.D.	Photodetector	A
S1	Transparent mica window, 0.5 D. X 0.004 thk	Lamp oven window	A
S2	Transparent Mylar window, 0.5 D. X 0.003 thk	Microwave cavity window	A
S3 ^f	Corning 7740 ^d glass tube, 1.0 D. X 0.060 wall	Rb resonance cell ^e	M-100, FRK
S4 ^f	Schott 8435 glass tube, 0.875 D. X 0.065 wall	Rb lamp	A
S5 ^f	Corning 1720 glass tube, 1.0 D. X 0.070 wall	Rb resonance cell	M-1000

^a All dimensions in inches.

^b Dimensions in RFS may differ somewhat from that of irradiation sample.

^c A denotes all models: M-100, FRK, M-1000.

^d Pyrex (trade name of Corning Glass).

^e Cells produced in Munich use Schott Duran 50 glass which is nearly identical to Corning 7740 glass (Pyrex).

^f For samples S3, S4, S5, controls (designated S3C, S4C, S5C) were also used for comparison. The samples were irradiated, the controls were not.

TABLE 2
EFFECT OF IRRADIATION ON DC PHOTOCURRENTS

Measurement Point ^a	Normalized dc Photocurrent, I/I ₀ (%)					
	PC1 (International Rect.)		PC2 (Ferranti)			
	Inboard ^b	Outboard	Inboard ^c	Outboard	Inboard	Outboard
BL1	100	100	100	100	100	100
AL1	81	78	85	90	85	91
BL2	80		90			
AL2	75	73	81	86		
BL3	75		82			
AL3	58	56	64	70		
BL4	57		68			
AL4	38		40			
AL4 + 1 hr	40	37	43	44		

^a BL1 = before level 1 irradiation
AL1 = after level 1 irradiation, etc.

^b Uses outboard servo board

^c Uses inboard servo board

TABLE 3

COMPARISON OF AC AND DC PHOTOCURRENTS ^{a,b}

Measurement Point ^c	dc Photocurrent I/I ₀ (%)		ac Photocurrent i/i ₀ (%)		ac Photocurrent as % of dc Photocurrent	
	PC1	PC2	PC1	PC2	PC1	PC2
BL1	100	100	100	100	100	100
AL3/BL4	56	70	39	57	69	81
AL4 + 1hr	37	44	23	34	63	76

^a Normalized to pre-irradiation values

^b Outboard measurements

^c BL1 = before level 1 irradiation

AL3 = after level 3 irradiation, etc.

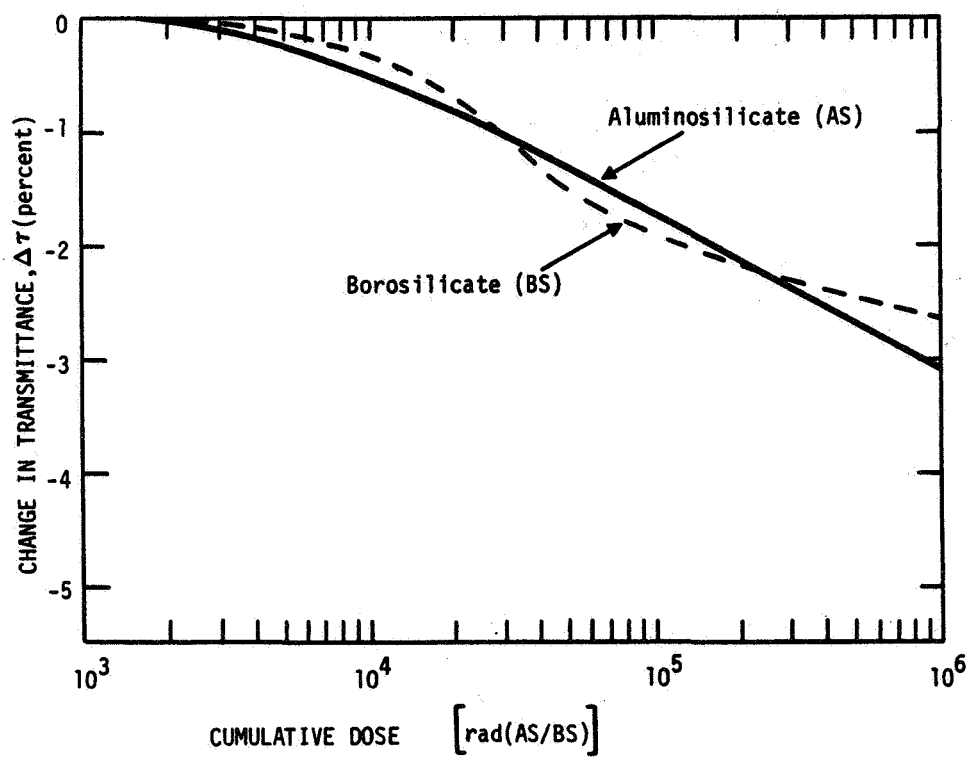


FIGURE 1. Nominal change in transmittance as a function of total dose for two glasses.

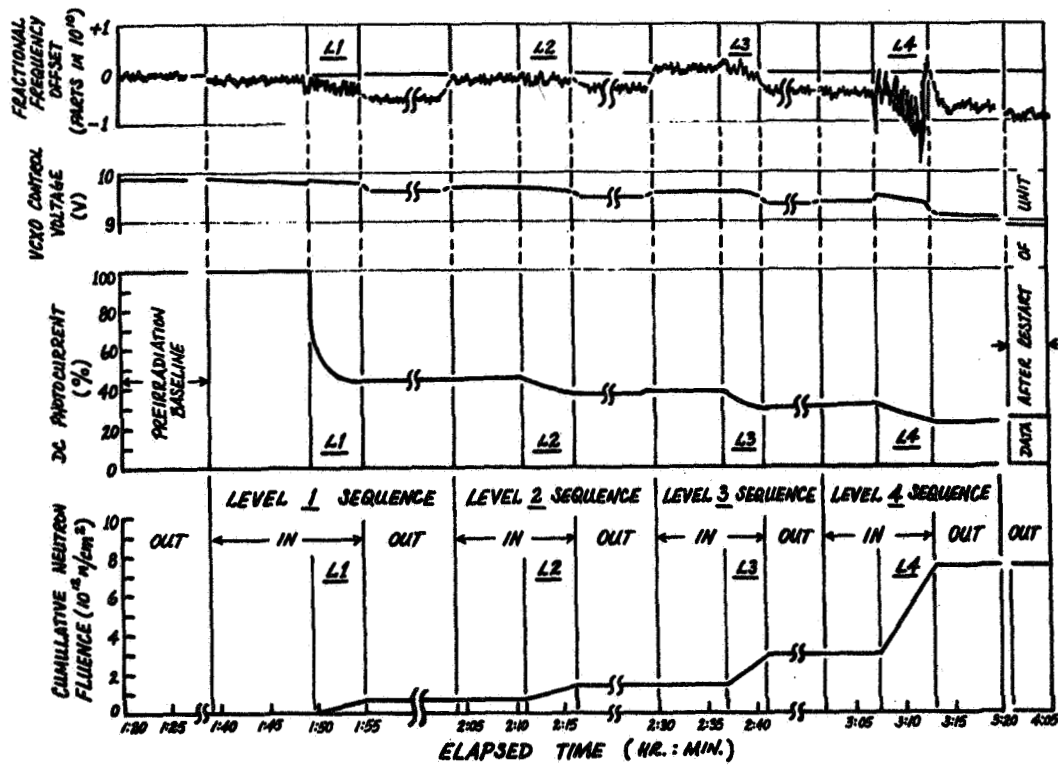


FIGURE 2. Effect of combined neutron/gamma radiation from a nuclear reactor on an operating Efratom M-100 rubidium frequency standard.

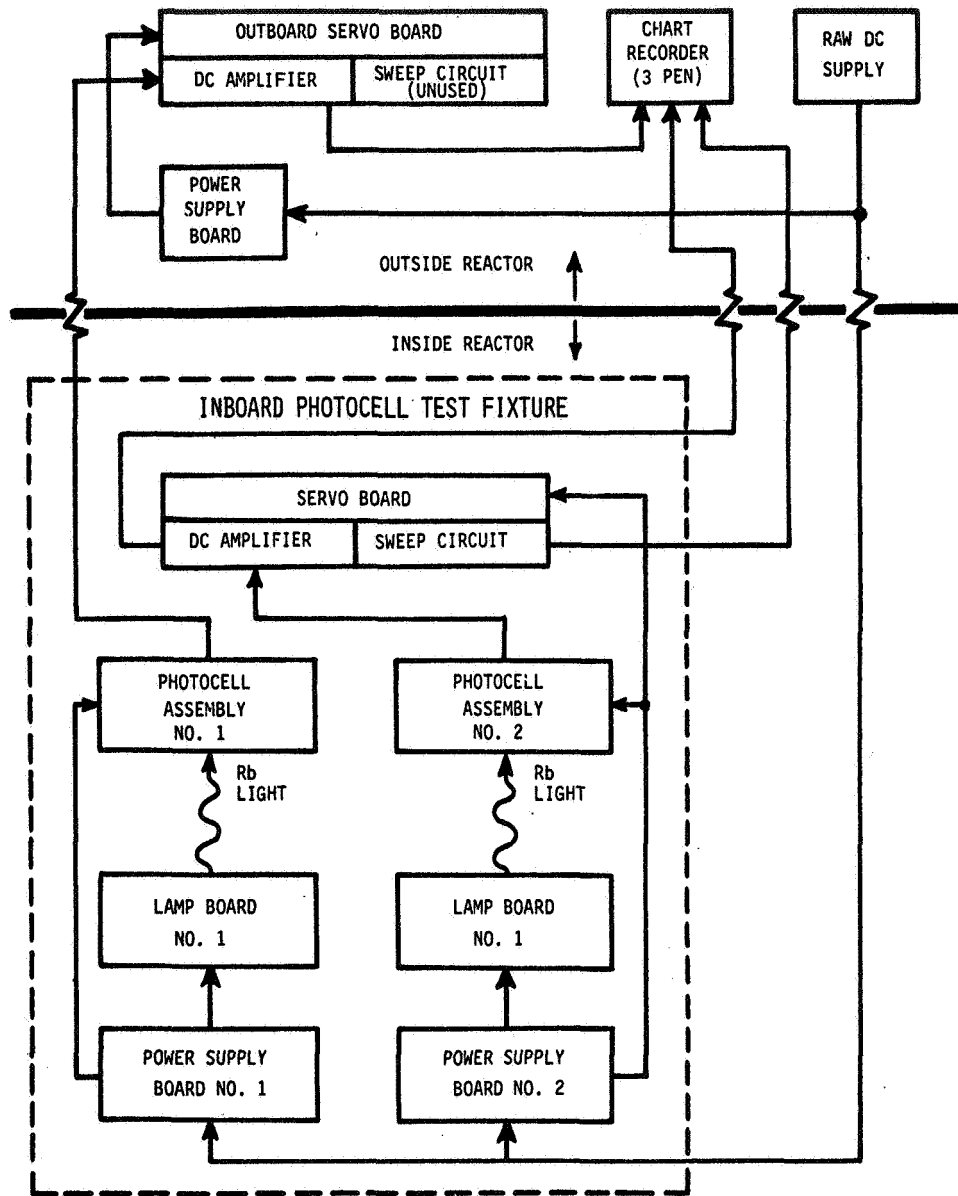


FIGURE 3. Block diagram of inboard photocell test fixture and associated test equipment.

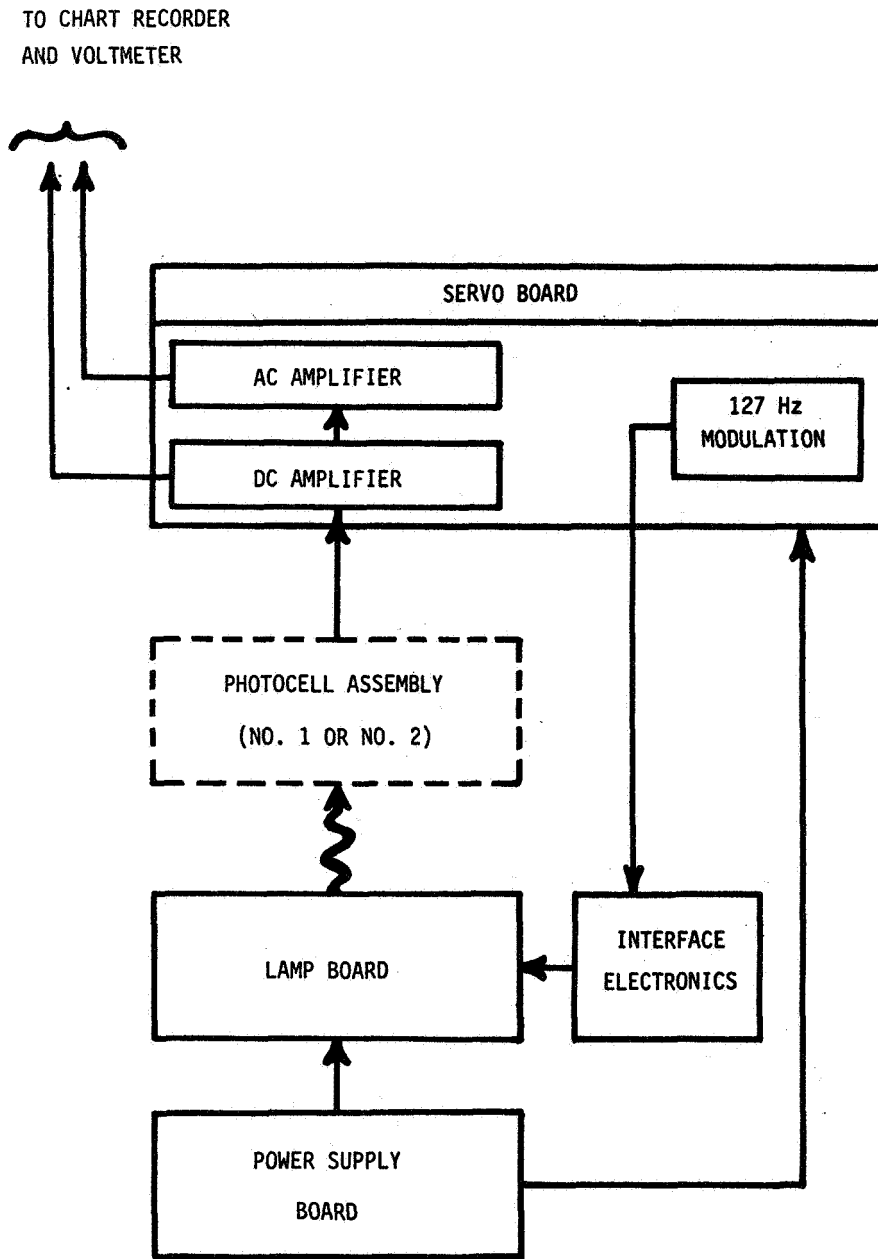


FIGURE 4. Block diagram of outboard photocell test fixture.

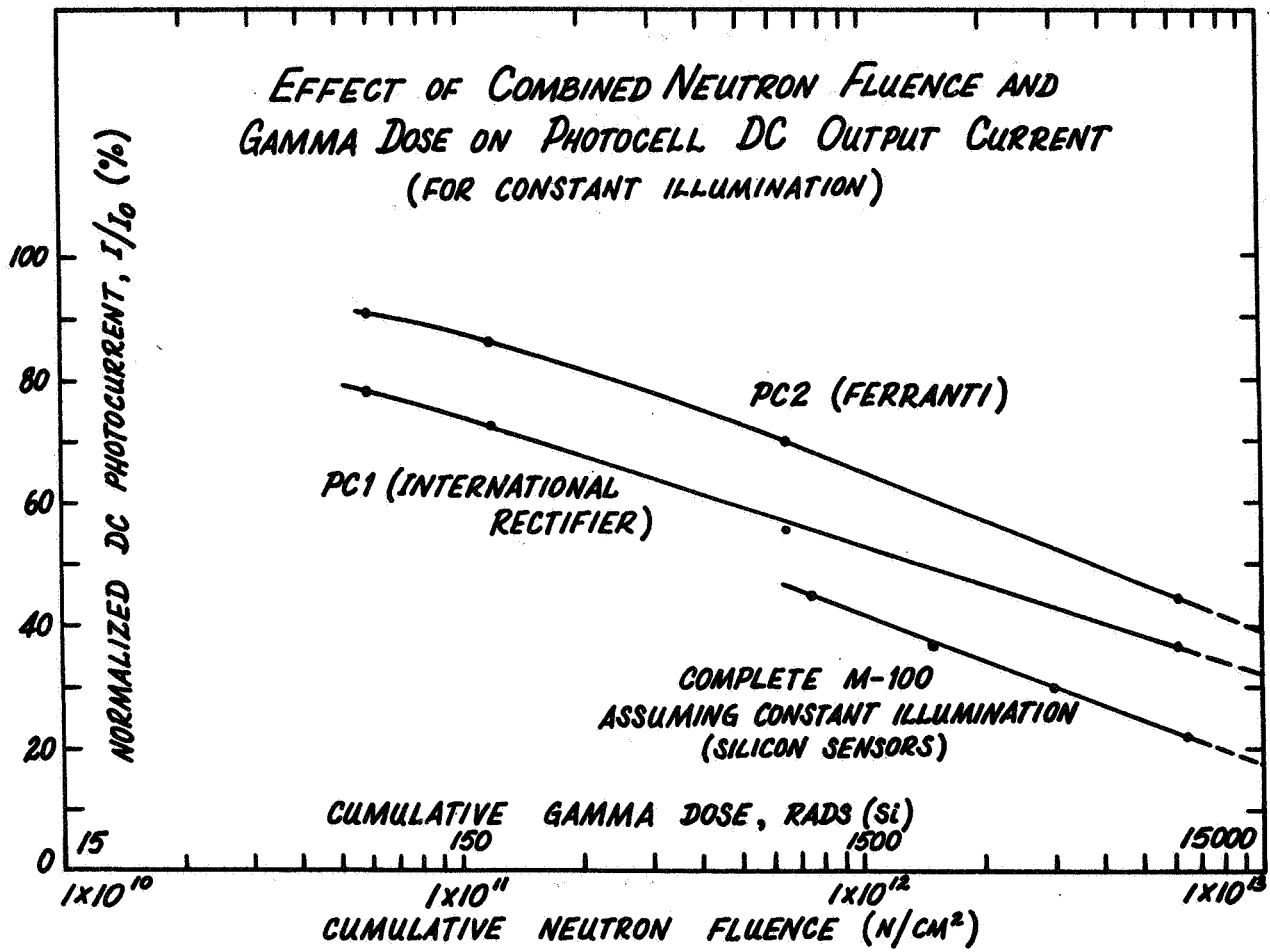


FIGURE 5

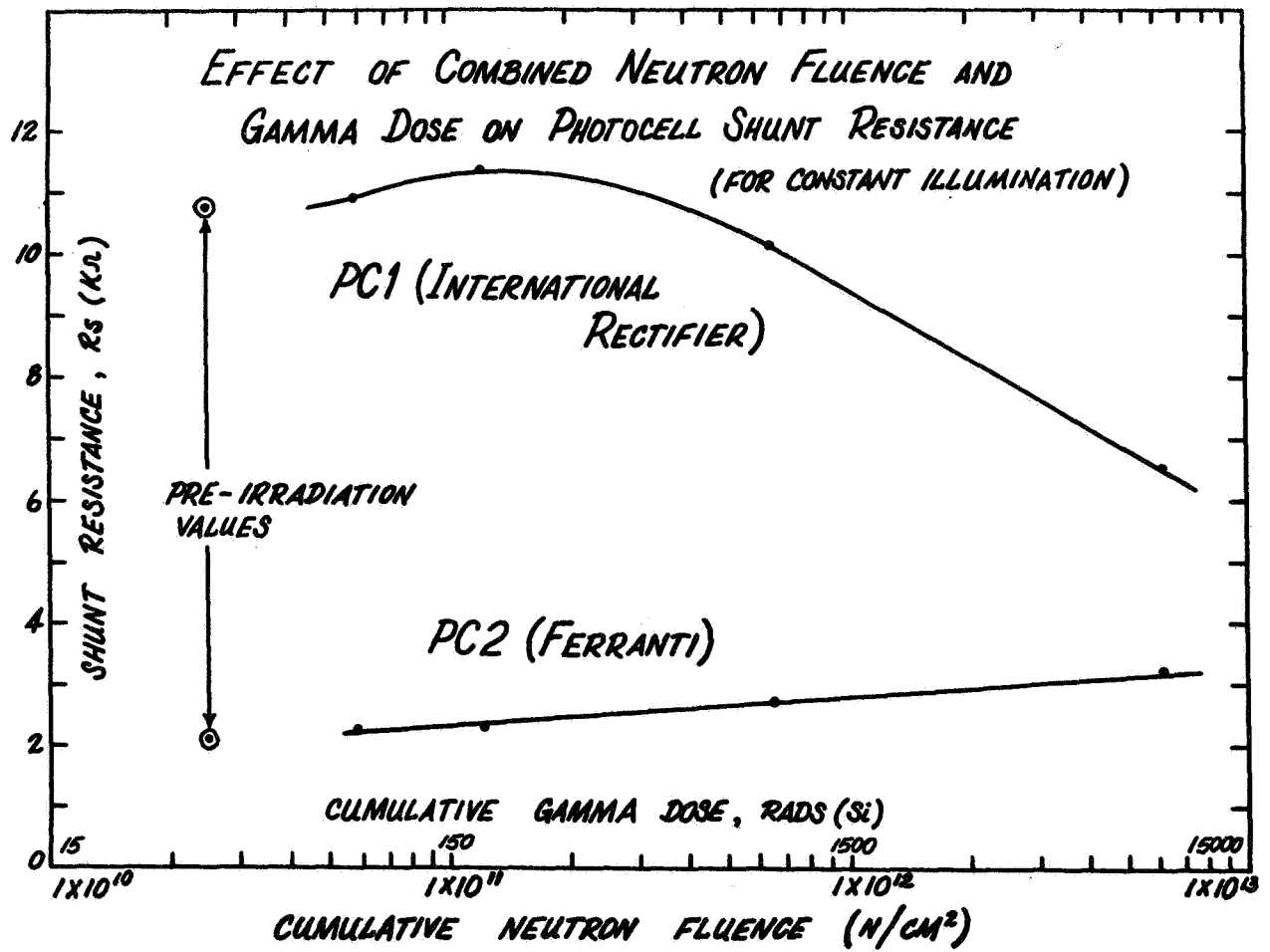


FIGURE 6

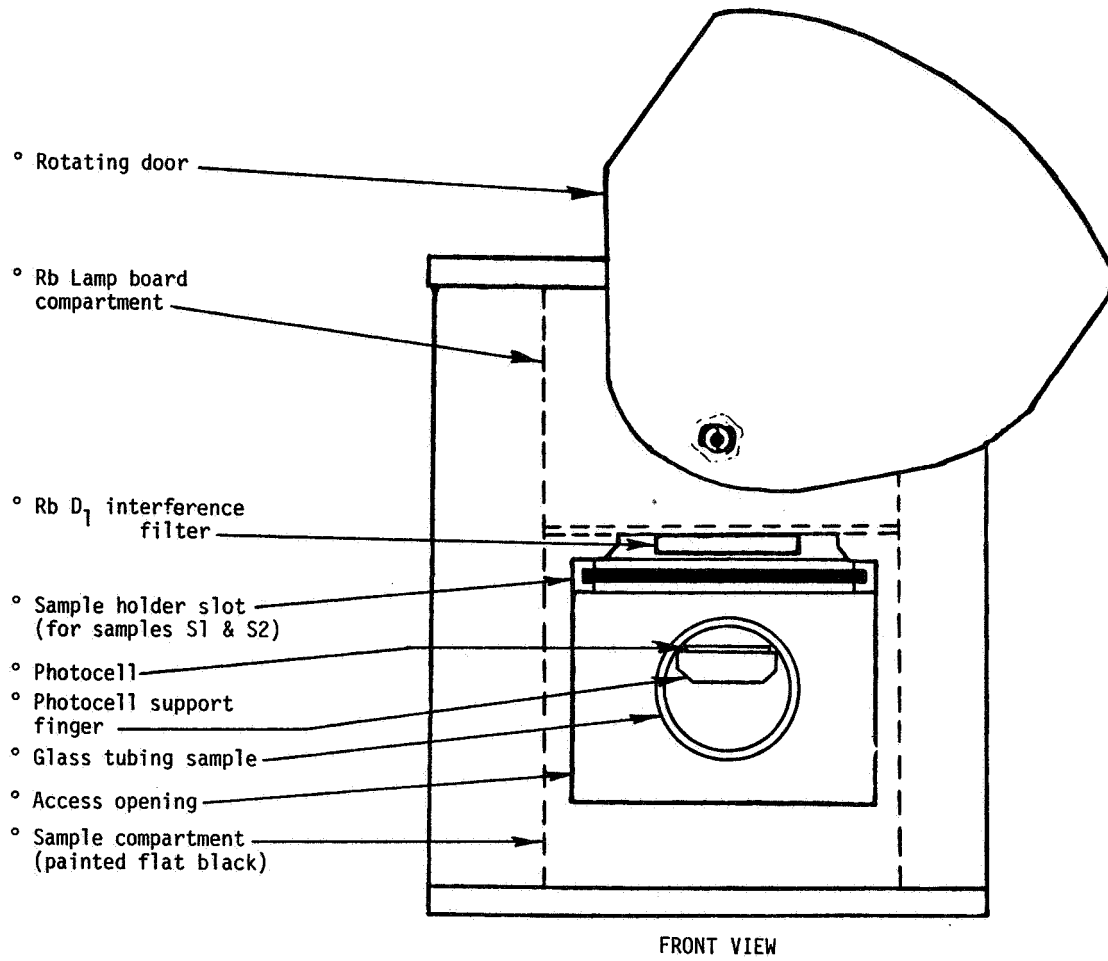


FIGURE 7. Transparency test fixture.

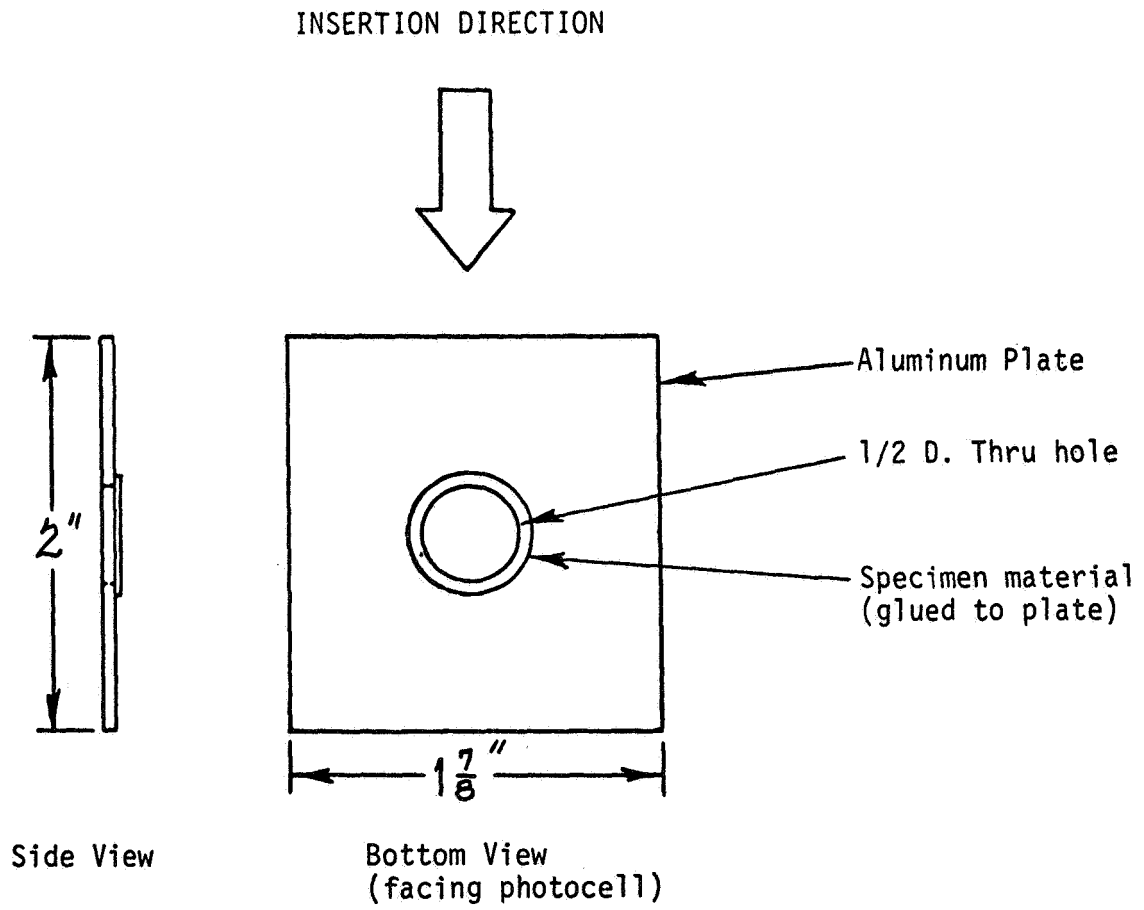


FIGURE 8. Sample holder used for samples S1 and S2.

QUESTIONS AND ANSWERS

None for Paper #28

AK-cut Crystal Resonators

Alfred Kahan and Ferdinand K. Euler
Solid State Sciences Division
Rome Air Development Center
Hanscom AFB, MA 01731

ABSTRACT

Calculations have predicted the existence of crystallographically doubly rotated quartz orientations with turnover temperatures which are considerably less sensitive to angular misorientation than comparable AT- or BT-cuts. We have arbitrarily designated these crystals as the AK-cut. We report experimental data for seven orientations, ϕ -angle variations between 30-46° and θ -angle variations between 21-28°, measured on 3.3-3.4 MHz fundamental mode resonators vibrating in the thickness shear c-mode. The experimental turnover temperatures of these resonators are between 80°C and 150°C, in general agreement with calculated values. The normalized frequency change as a function of temperature has been fitted with a cubic equation.

INTRODUCTION

In a previous publication,¹ the turnover temperatures, T_{t0} , of crystallographically doubly rotated quartz plates vibrating in the thickness shear mode were calculated. It was shown that in addition to the usual rotation angles associated with the AT-, FC-, IT-, SC-, RT-, and BT-cuts, there is another crystallographic region which yields T_{t0} values in the temperature range of practical interest to temperature controlled resonators. These crystal orientations, vibrating in the thickness shear c-mode, were arbitrarily designated as AK-cuts. The frequency as a function of temperature characteristics of the AK-cuts are located between the AT- and BT-cuts, but the T_{t0} values are considerably less sensitive to angular orientation than any of the other cuts. In this paper, we give additional theoretical results related to the AK-cut, and at the same time report experimental confirmation of turnover temperatures on 10 MHz, 3rd overtone, resonators fabricated from seven different crystallographic orientations.

The computations performed in this investigation are based on elastic constant values, c_{pq} , of quartz published by Bechmann, Ballato, and Lukaszek,² hereafter referred to as BBL(1962), and on a set of temperature coefficients of the elastic constants, $T_n(c_{pq})$, derived in Ref. 3, and hereafter referred to as BBL(1963) LSF. These temperature coefficients are based on the least squares fit (LSF) of experimental data published by Bechmann, Ballato, and Lukaszek (BBL) in 1963.⁴ A $T_n(c_{pq})$ set has been derived in BBL(1962) and another set has been published by Adams, Enslow, Kusters, and Ward,⁵ and we refer to this set as Adams et al. In Ref. 3 we compared and discussed the limitations associated with the different sets, and their ap-

plicability to predict the frequency-temperature behavior of arbitrary doubly rotated crystal orientations. This topic has also been treated in Refs. 6 and 7. For reasons outlined in these references, we find the BBL(1963) LSF set more satisfying than the one derived in BBL(1962). For the crystallographic region associated with the AK-cuts, all three sets give similar general results and predict the existence of this cut, but actual T_{t0} values for a specific pair of rotation angles depend on the particular set used in the computations. In this paper, we intend to illustrate general results, and we limit the computations, with one exception, to the BBL(1963) LSF set of temperature coefficients of elastic constants.

CALCULATED TURNOVER TEMPERATURES

Figure 1 depicts the plate geometry and crystallographic coordinate systems used in this investigation. The orientation of the plate is described by angles (ϕ, θ) where ϕ and θ are rotations around the z- and x-axis, respectively. In this nomenclature, ϕ -angle limits are $0^\circ < \phi < 60^\circ$ and θ -angle rotations are $0^\circ < \theta < 90^\circ$. The angular rotations associated with the AK-cuts are approximately between $\phi = 30^\circ$ and $\phi = 47^\circ$, and between $\theta = 17^\circ$ and $\theta = 30^\circ$. For example, one specific (ϕ, θ) combination is $(40.9, 21.0)^\circ$. In another commonly used notation, this rotation is on the "negative theta" side and is designated as $(19.1, -21.0)^\circ$.

Figure 2 shows the calculated (ϕ, θ) loci for selected turnover temperatures between 75°C and 160°C of AK-cut c-mode vibrations. The temperature coefficients of the elastic constants are valid between -200°C and $+200^\circ\text{C}$. For AT-cut crystals, $\phi = 0^\circ$, the turnover temperatures throughout this temperature range are single value functions of the θ -angle, and are obtained at θ -angles slightly larger than 35.25° . In the 50°C to 100°C range, the AT-cut T_{t0} shifts by 2.6°C per minute of arc. The AT-cut angle equivalent to $T_{t0} = 200^\circ\text{C}$ is $\theta = 36.70^\circ$. For AK-cut crystals, the lowest possible T_{t0} , based on BBL(1963) LSF parameters, is approximately 75°C , and for a specified ϕ -angle there are two θ -angles which give identical T_{t0} . For a selected T_{t0} , the (ϕ, θ) loci exhibit concentric quasi-elliptical characteristics, with the angular boundaries increasing with T_{t0} . The distortions in the $T_{t0} = 140^\circ\text{C}$ and $T_{t0} = 160^\circ\text{C}$ curves at the higher ϕ -angles and upper θ -angle segments are due to the interference of the T_{t0} branch containing the AT-type turnover temperatures. This can be deduced from Ref. 1, Fig. 9. The (ϕ, θ) locations of the experimental resonators are shown in Fig. 2 by dots, with the experimental T_{t0} values indicated. (These will be discussed further on.)

The primary advantage of AK-cut crystals, that is, the relative insensitivity of T_{t0} to inaccuracies in (ϕ, θ) , is implicit in the curves shown in Fig. 2. For example, at $\phi = 37^\circ$ the tolerance on the θ -angle for the T_{t0} to be between 75°C and 85°C is $\Delta\theta = \pm 1.9^\circ$. In contrast, for the same T_{t0} range, the tolerance for the AT-cut is $\Delta\theta = \pm 2'$, approximately 60 times more sensitive. The T_{t0} position of the b-mode BT-cut ($\phi = 60^\circ$) is less sensitive to θ -angle changes than the AT-cut, and the comparable angular tolerance is $\Delta\theta = \pm 14'$.

Figure 3 shows a comparison of the (ϕ, θ) loci for $T_{t0} = 90^\circ\text{C}$ calculated with $T_n(c_{pq})$ values based on Adams et al, BBL(1962), and BBL(1963) LSF. All three sets show the quasi-elliptical nature of the curves, but vary in detailed numerical results. For a given (ϕ, θ) , Adams et al parameters yield the lowest T_{t0} values, the BBL(1963) LSF set predicts higher T_{t0} , and BBL(1962) gives the highest T_{t0} values. A similar order is followed in calculating the lowest possible T_{t0} for the AK-cuts, approximately 55°C for Adams et al, 75°C for BBL(1963) LSF, and 85°C for BBL(1962). These results also point out the difficulty in comparing theoretical predictions with experimental data. The $T_n(c_{pq})$ values are derived from the first, second, and third order temperature coefficients of frequencies measured on a set of (ϕ, θ) orientations. Their applicability to a particular crystallographic region may depend on the (ϕ, θ) distribution of the original data set. To the best of our knowledge, data points from the (ϕ, θ) region defining the AK-cut were not included in any of the three data sets. For AK-cut calculations there is then neither an a priori preference for selecting a particular $T_n(c_{pq})$ set, nor is there any confidence that the predicted T_{t0} values will be observed. For reliable computations, it is essential to collect experimental data weighed heavily with (ϕ, θ) orientations applicable to the crystallographic region of interest, and then based on this data derive a "local" set of c_{pq} and $T_n(c_{pq})$.

EXPERIMENTAL PROCEDURES AND RESULTS

The primary objective of this investigation was to confirm the existence of thickness shear c-mode vibrations yielding turnover temperatures in the 80°C to 200°C temperature range for crystallographic orientations which are unrelated to angular values usually associated with the general class of doubly rotated AT-cuts.

The initial evaluation of the AK-cut crystals comprises seven (ϕ, θ) orientations. Figure 4 shows the (ϕ, θ) positions of the selected cuts, and the Miller indices of the lattice planes associated with this crystallographic region. The primary (ϕ, θ) selection criterion was ease of orientation and fabrication. Three rotations, $(30, 24.44)^\circ$, $(36.58, 28.45)^\circ$, and $(46.10, 23.59)^\circ$ are low index lattice planes, $[111]$, $[323]$, and $[312]$, respectively. Another three rotations, $(40.9, 21.0)^\circ$, $(40.9, 23.59)^\circ$, and $(40.9, 27.0)^\circ$ are situated along the $[211]$ and $[212]$ planes, and the seventh $(36.0, 24.44)^\circ$, is obtained by a 6° rotation from $[111]$. The crystals were machined into plano-plano plates, beveled at the edges, and the disks were fabricated into 10 MHz, 3rd overtone, resonators at Frequency Electronics, Inc., using established manufacturing processes. The exact 10 MHz frequency value was not a fabrication requirement.

The resonators were placed in a heater and connected through a π -network to a network analyzer. A programmable synthesizer provided a stepwise variable frequency. Temperature was measured with a thermocouple attached to the resonator enclosure and connected to a digital thermometer. A data bus connected these components to a desktop computer and printer for automatic data recording. A programmable temperature controller provided linear ramps with adjustable rates, e.g. 0.1 or $0.2^\circ\text{C}/\text{minute}$. The control-

ling computer program called for repetitive frequency sweeping through the series resonance in 100 steps with 1 msec per step, and determined the resonance frequency as function of temperature with temperature intervals of typically 0.5 to 1°C between data points. For mode spectra determination, the frequency was swept over several MHz in steps of 1 or 2 Hz at constant temperature.

Figure 5 shows the normalized measured frequency change $(f_{\text{meas}} - f_0)/f_0$, with f_0 being the frequency at 25°C, as a function of temperature for the $(36.0, 24.44)^\circ$ cut in the fundamental and in the 3rd overtone modes. The turnover temperatures are 84°C and 82°C for the fundamental and 3rd overtone, respectively. At T_{t0} , the curves show maxima, similar to the b-mode BT-cut. Whereas, the c-mode SC-cut turnover changes from minimum to maximum as T_{t0} shifts from below to above the inflection temperature, the curvature found with AK-cut crystals is unrelated to the inflection temperature. For this particular AK-cut orientation, the inflection temperature is calculated to be at -793°C , a meaningless number. The other fabricated resonators also have turnover temperatures in the fundamental mode, and their T_{t0} values were indicated in Fig. 2. Some experimental points lie above, some below, and some almost coincide with predicted values. Considering the simplified mathematical formalism utilized for these computations, and the inaccuracies of the $T_n(c_{pq})$ values, the general agreement between theory and experiment is surprising and gratifying. However, detailed comparisons of this data with calculated results based on the $T_n(c_{pq})$ sets are not too meaningful.

The frequency as a function of temperature curves are fitted by a normalized cubic equation in the form

$$\Delta f/f_0 = (f - f_0)/f_0 = \sum_{n=1}^3 a_n (T - T_0)^n$$

where $T_0 = 25^\circ\text{C}$ and f_0 is the frequency at $T_0 = 25^\circ\text{C}$. The resulting coefficients a_n are listed in Table 1 together with the standard deviations of the fits which are reasonable and consistent. The normalized frequency differences between measured and calculated values based on the cubic equation are also plotted in Fig. 5. Throughout the entire measured temperature range, 25°C to 145°C, the data is equally well described by the cubic equation, and the deviations from the cubic are substantially less than $\pm 1 \times 10^{-6}$. The frequency-temperature characteristics of the corresponding 3rd overtone curves were also fitted by the cubic equation. For this particular (ϕ, θ) combination, the fundamental and the 3rd overtone T_{t0} agree within 2°C. As shown in Table 1, this is not the case for other (ϕ, θ) orientations. For $(30.0, 24.44)^\circ$, the 3rd overtone T_{t0} is 27°C higher, and for $(36.58, 28.45)^\circ$ and $(46.1, 23.50)^\circ$ the fundamental mode T_{t0} is higher by 23°C and 41°C, respectively. These discrepancies do not necessarily imply inconsistencies in data or calculations. In the first order approximation, the frequency-temperature characteristics of fundamental and overtone modes are also related, in a complicated fashion, by the temperature coefficients of the electromechanical coupling factors. At the present time, we have not included this effect in our mathematical formalism. Our initial measurements

Table 1. Temperature Coefficients of Frequency for Experimental AK-cut Crystals.

Orientation		measured T_{t0}	temperature coefficients			standard deviations	ΔF (see text)
ϕ	θ		a_1 /°C	a_2 /°C ²	a_3 /°C ³		
Fundamental mode							
30.00°	24.44°	145°C	4.35×10^{-6}	-22.3×10^{-9}	22.6×10^{-12}	1.0×10^{-7}	14.2×10^{-9}
36.00°	24.44°	84	3.58	-29.2	-11.9	0.8	31.3
36.58°	28.45°	101	4.50	-27.8	-14.8	0.8	31.2
40.90°	21.00°	129	7.31	-30.6	-33.9	3.7	41.0
40.90°	23.59°	113	6.48	-30.8	-47.7	4.5	43.4
40.90°	27.00°	107	6.18	-32.0	-42.5	2.3	42.6
46.10°	23.59°	154	11.90	-31.8	-72.3	3.7	60.0
3rd overtone mode							
30.00°	24.44°	172	5.04	-22.8	25.1	1.6	11.9
36.00°	24.44°	82	3.90	-31.2	-28.6	1.5	36.2
36.58°	28.45°	78	3.43	-28.1	-70.5	4.0	39.0
46.10°	23.59°	113	7.77	-36.3	-55.9	4.0	51.2

pertained to the 3rd overtone modes, and the corresponding T_{t0} values were the ones indicated in Ref. 1, Fig. 14.

Table 1 also lists values for

$$\Delta F = \left| \Delta f / f_0 (T = T_{t0} \pm 1) - \Delta f / f_0 (T = T_{t0}) \right|,$$

the difference between the calculated normalized frequency at T_{t0} and $T_{t0} \pm 1^\circ\text{C}$. This quantity is a measure of the "flatness" of the frequency-temperature curve at T_{t0} . The values range from 14×10^{-9} to 60×10^{-9} , and there seems to be some correlation between these values and the ϕ -angles. Comparative values for AT-cut range from $\Delta F = 21.5 \times 10^{-9}$ for $T_{t0} = 85^\circ\text{C}$ to $\Delta F = 40.0 \times 10^{-9}$ for $T_{t0} = 160^\circ\text{C}$.

Figure 6 shows the mode spectrum for the fabricated resonators vibrating in the fundamental b- and c-modes measured at room temperature. All (ϕ, θ) pairs show similar patterns. The amplitude of the lowest c-mode resonance is very large, and we designate this frequency, for each respective (ϕ, θ), as f_0 . The f_0 modes have been aligned in Fig. 6, but the f_0 values actually vary between 3.36 and 3.41 MHz. The f_0 mode is followed by a series of anharmonic modes of various strengths. Some anharmonic modes are as strong as f_0 . The abundance of anharmonic modes is a characteristic feature of doubly rotated cuts, and no efforts were made to suppress unwanted vibrations. The vibration patterns associated with the anharmonic modes have not

Table 2. Comparison of Fundamental b- and c-mode Frequency Separation.

ϕ	θ	$(f_b - f_c)/f_b$	
		calculated	experimental
30.0°	24.44°	14.6%	13.4%
36.0	24.44	11.6	11.1
36.58	28.45	5.7	5.5
40.9	21.0	14.3	14.7
40.9	23.59	10.4	10.1
40.9	27.0	5.1	5.2
46.1	23.59	7.2	6.9

been identified. The dashed lines indicate the b-modes. Table 2 lists the b- to c-mode frequency separations for the seven orientations. There is close agreement between calculated and experimental values.

Figure 7 shows the corresponding 3rd overtone c-mode spectra, with the exception of (40.9, 23.59)°. The increased number of modes is consistent with the increased number of allowable vibrations. The arrow indicates the relative $3f_0$ positions, and the spectra are aligned at $3f_0$. For several orientations, there are a large number of strong resonances below $3f_0$, and there is no one dominant resonance that can be designated as the equivalent to f_0 . This poses a problem in evaluating the temperature characteristics $f(T)$ of the resonators. Do we choose the lowest frequency, the strongest amplitude, or the mode closest to $3f_0$? For some resonators we have measured $f(T)$ for several modes, and in some cases we do find considerable differences in their T_{t0} . The data listed for the 3rd overtone in Table 1 correspond to the lowest observed frequencies.

The real difficulty encountered in evaluating the 3rd overtone modes is that for the three $\phi = 40.9^\circ$ orientations we are unable to observe turnover temperatures. The resonances are close together, vary considerably in strength with temperature, become coupled, and they are very hard to follow and identify with changes in temperature. The mode spectra data indicate that considerable work is needed to optimize disk geometry and suppress anharmonic vibration patterns. Figure 8 shows the 3rd overtone resonance for (36.0, 24.44)°. The Q-value is approximately 1.5×10^6 , that is of the same order of magnitude as high precision 10 MHz, 3rd overtone, AT-cut resonators.

OPTIMIZED ORIENTATIONS

The most important resonator performance characteristic is the frequency-temperature behavior. The claim for the AK-cut crystals relates to turnover temperature insensitivity to angular orientations. The large (ϕ, θ) choice available for specific T_{t0} values of AK-cuts may also allow one to optimize the resonator design to some additional performance parameter. The primary concern is the temperature coefficient of frequency near T_{t0} . A small value is desired, but constraints are imposed by the electromechanical coupling factors, and the b- to c-mode frequency separations.

Figure 9 shows a plot of the normalized frequency differences ΔF between T_{t0} and $T_{t0} \pm 1^\circ$ as a function of ϕ -angles for the BBL(1963) LSF $T_{t0} = 90^\circ\text{C}$ curve shown in Fig. 3. The ΔF values are not exactly symmetric around the 90°C turnover temperatures and we have calculated ΔF both at 89°C and at 91°C and selected the larger value. The solid line of this curve corresponds to the lower and the dashed line to the upper θ -angle. The ΔF values range from approximately 22×10^{-9} at the lower ϕ -angles to 42×10^{-9} at the upper ϕ -angles, with ΔF for the lower θ -angle always less, by $2-3 \times 10^{-9}$, than for the upper one. This is also consistent with the experimental ΔF increase with the ϕ -angles, shown in Table 1.

For low ΔF values, one would select low ϕ -angles and the lower θ -angle. The corresponding ΔF value, at $T_{t0} = 90^\circ\text{C}$, for the AT-cut is 22.8×10^{-9} and for the BT-cut 62.2×10^{-9} . Hence, the magnitude of the frequency-temperature curvature of the AK-cut is between that of the AT- and BT-cuts. For higher T_{t0} values, the ΔF values for both the AT- and BT-cuts increase with T_{t0} , whereas for some AK-cut (ϕ , θ) combinations ΔF decreases with increasing T_{t0} .

Figure 10 shows the b- and c-mode electromechanical coupling factors, k_b and k_c , as a function of ϕ for $T_{t0} = 90^\circ\text{C}$. Data for the lower θ -angle is drawn with a solid line and for the upper θ -angle with a dashed line. The AK-cut operates in the c-mode, and, ideally, a strong k_c and weak k_b is desired. However, for most angles, k_b is substantially stronger than k_c . For the lower θ -angle k_c becomes equal to k_b at $\phi = 38^\circ$. At the higher ϕ -angles k_c continues to increase while k_b decreases. For the upper θ -angles, k_b is stronger than k_c up to approximately $\phi = 40^\circ$.

Figure 11 shows the relative frequency separations, in percent, between the b- and c-modes as a function of ϕ -angle for $T_{t0} = 90^\circ\text{C}$. The curve corresponding of the upper θ -angle starts approximately at 11%, dips to 6% and increases to 8% at the high ϕ -angle. In contrast, the curve corresponding to the lower θ -angle peaks at 14%. There is no established criterion for a minimum b- to c-mode frequency separation or relative strengths of electromechanical coupling factors. The recently developed doubly rotated SC-cut, $(21.93, 34.24)^\circ$, may be applied as a guideline for the AK-cut. For SC-cut crystals, the frequency separation is 9.1%, $k_b = 5.0\%$, and $k_c = 4.6\%$. This coupling factor criterion will limit the AK-cut mostly to the lower θ -angle and to ϕ -angles from $\phi = 37^\circ$ to $\phi = 40.8^\circ$. The ΔF value in this ϕ -angle range increases from 30.7×10^{-9} to 41.7×10^{-9} . In addition, the frequency separation criterion will completely eliminate the upper θ -angle for practical resonators. For a given T_{t0} , the optimum resonator design will then be a compromise between fabrication tolerances on the ϕ - and θ -angles, and the constraints imposed by k_b , k_c , and the b- to c-mode frequency separation.

Acknowledgments. We wish to thank Robert J. Andrews and Cherrille D. Stewart for their technical assistance with measurements and curve fitting computations.

REFERENCES

1. Kahan, A. (1982) Turnover temperatures for doubly rotated quartz, 36th Annual Frequency Control Symposium, 170-180.
2. Bechmann, R., Ballato, A.D., and Lukaszek, T.J. (1962) Higher-order temperature coefficients of the elastic stiffnesses and compliances of α -quartz, Proc. IRE, 50, 1812-1822.
3. Kahan, A. (1982) Elastic constants of quartz and their temperature coefficients, 36th Annual Frequency Control Symposium, 159-169.
4. Bechmann, R., Ballato, A.D., and Lukaszek, T.J. (1963) Higher-Order Temperature Coefficients of the Elastic Stiffnesses and Compliances of α -Quartz, USAELRDL TR 2261.
5. Adams, C.A., Enslow, G.M., Kusters, J.A., and Ward, R.W. (1970) Selected topics in quartz crystal research, 24th Annual Symposium on Frequency Control, 55-63.
6. Kahan, A. (1982) Elastic Constants of Quartz, RADC-TR-82-117.
7. Kahan, A. (1982) Temperature Coefficients of the Elastic Constants of Quartz, RADC-TR-82-224.

FIGURE CAPTIONS

- Figure 1. Singly and doubly rotated crystal plates. Coordinate system.
- Figure 2. Calculated (ϕ, θ) loci of selected turnover temperatures, T_{t0} , for AK-cut crystals. Dots indicate the position of experimental resonators and their measured T_{t0} values.
- Figure 3. Calculated (ϕ, θ) loci for $T_{t0} = 90^\circ\text{C}$, based on three sets of temperature coefficients of the elastic constants.
- Figure 4. Rotation angles of seven experimental AK-cut resonators, indicated by solid circles. Also shown are the Miller indices of lattice planes used for orientation.
- Figure 5. Measured frequency-temperature characteristics for fundamental and 3rd overtone modes. Also shown are the differences between measured and fitted normalized frequencies.
- Figure 6. Fundamental c- and b-mode spectra measured for seven AK-cuts.
- Figure 7. 3rd overtone c-mode spectra measured for six AK-cuts.
- Figure 8. Example of 3rd overtone AK-cut resonance curve.
- Figure 9. Calculated frequency offsets between $T_{t0} = 90^\circ\text{C}$ and 91°C for AK-cuts.
- Figure 10. Calculated electromechanical coupling factors k_b and k_c for AK-cuts with turnover at 90°C .
- Figure 11. Calculated b-mode to c-mode frequency separation for AK-cuts with turnover at 90°C .

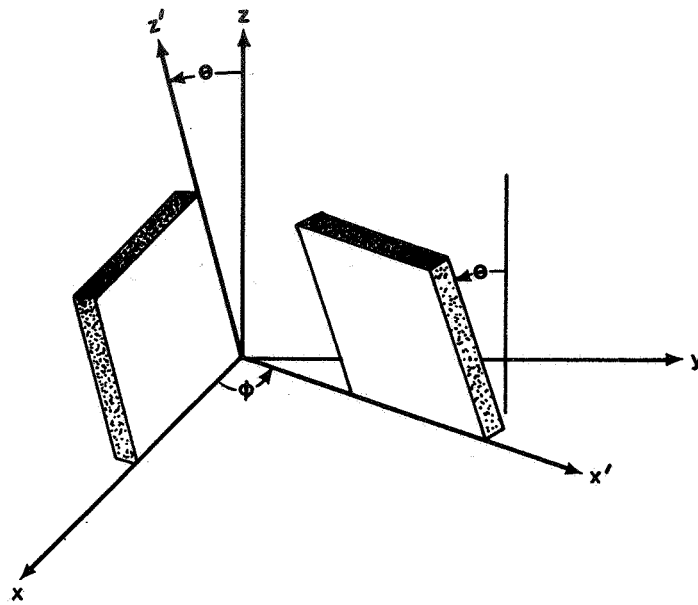


Figure 1. Singly and doubly rotated crystal plates. Coordinate System.

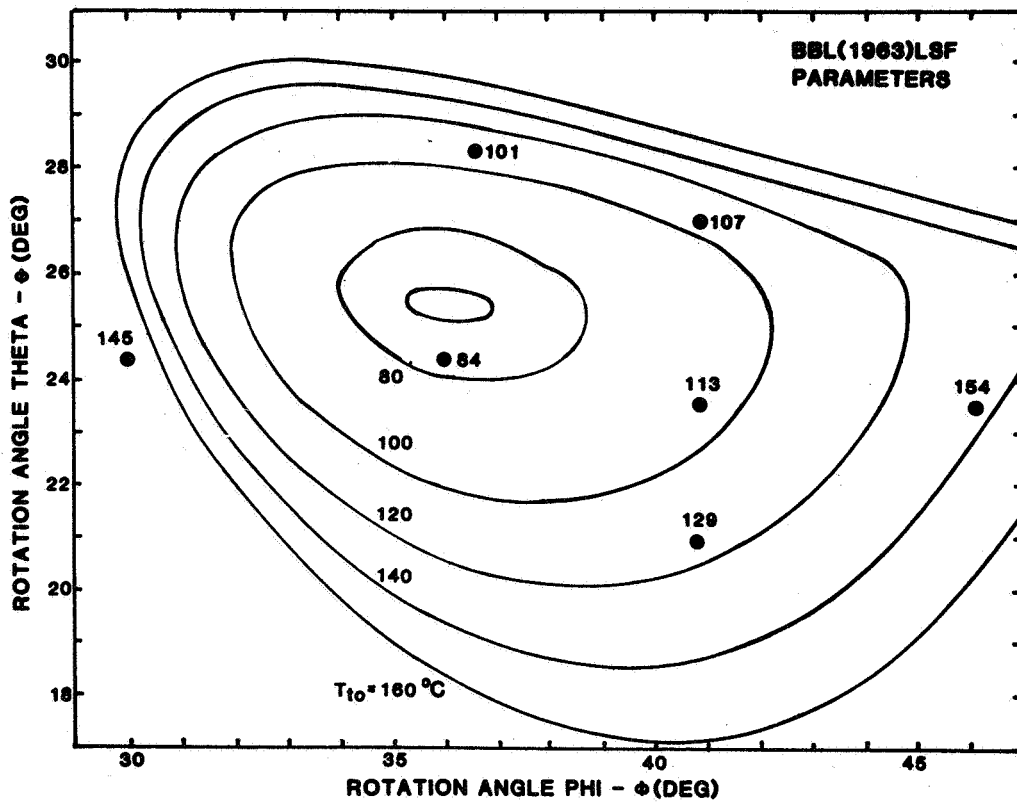


Figure 2. Calculated (ϕ, θ) loci of selected turnover temperatures T_{t0} for AK-cut crystals. Dots indicate the positions of experimental resonators and their measured T_{t0} values.

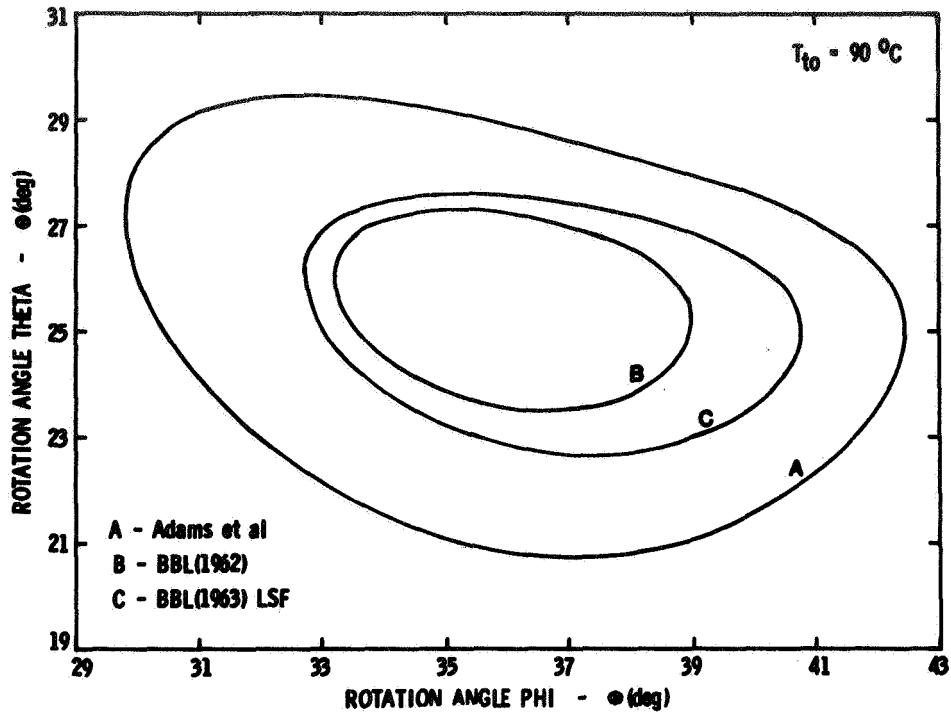


Figure 3. Calculated (ϕ, θ) loci for $T_{t0} = 90^{\circ}\text{C}$, based on three sets of temperature coefficients of elastic constants.

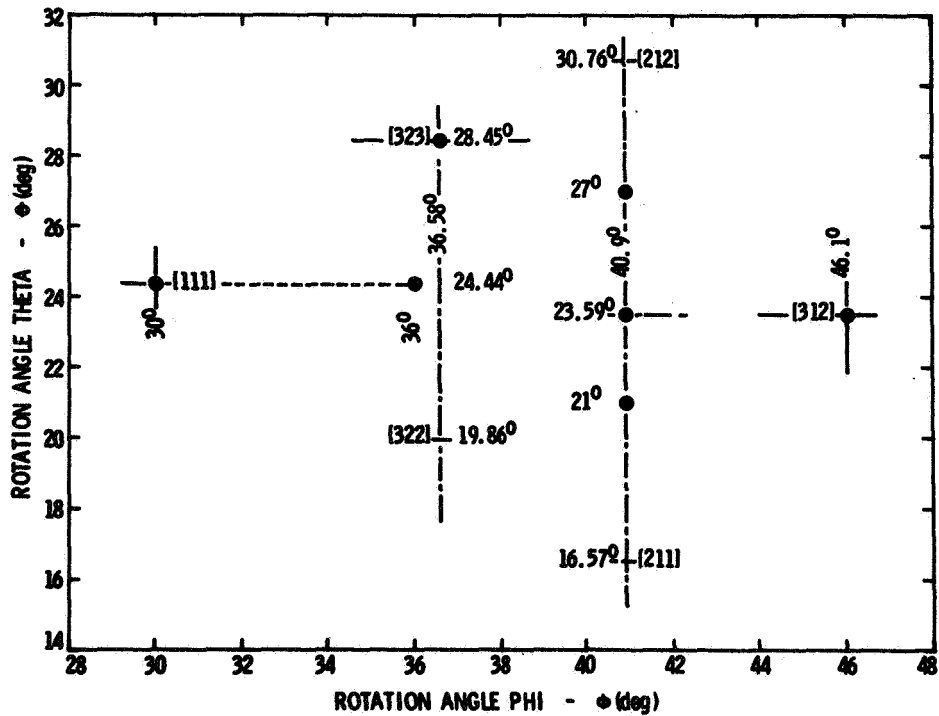


Figure 4. Rotation angles of seven experimental AK-cut resonators (solid circles). Also shown are the Miller indices of lattice planes used for orientation.

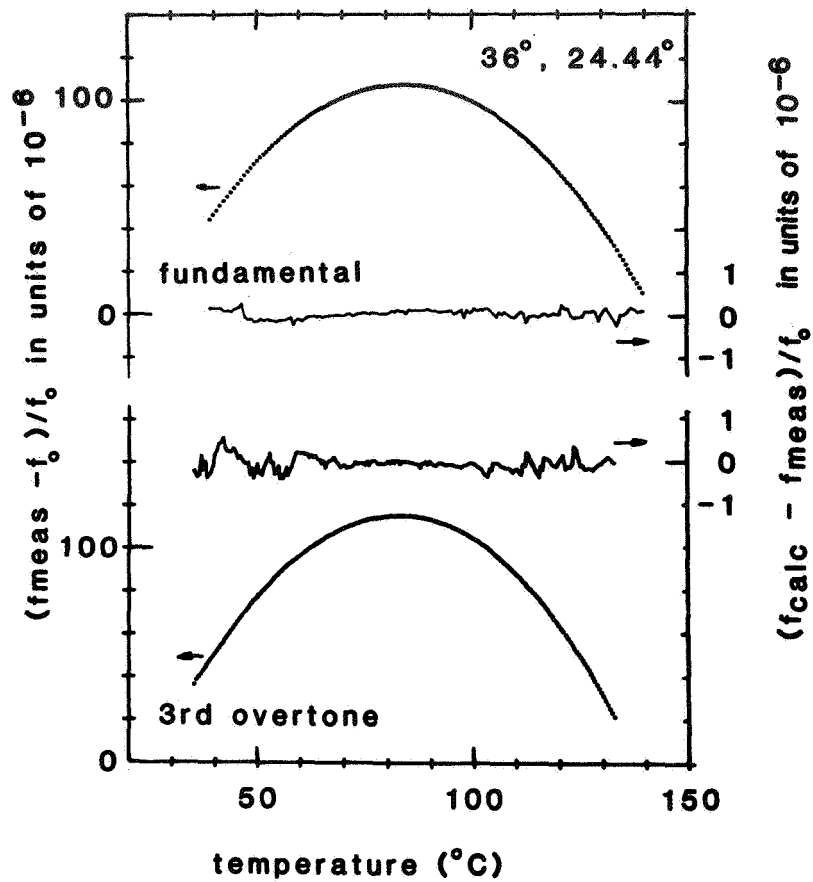


Figure 5. Example of measured frequency-temperature characteristics for fundamental and 3rd overtone modes. Also shown are the differences between measured and fitted normalized frequencies.

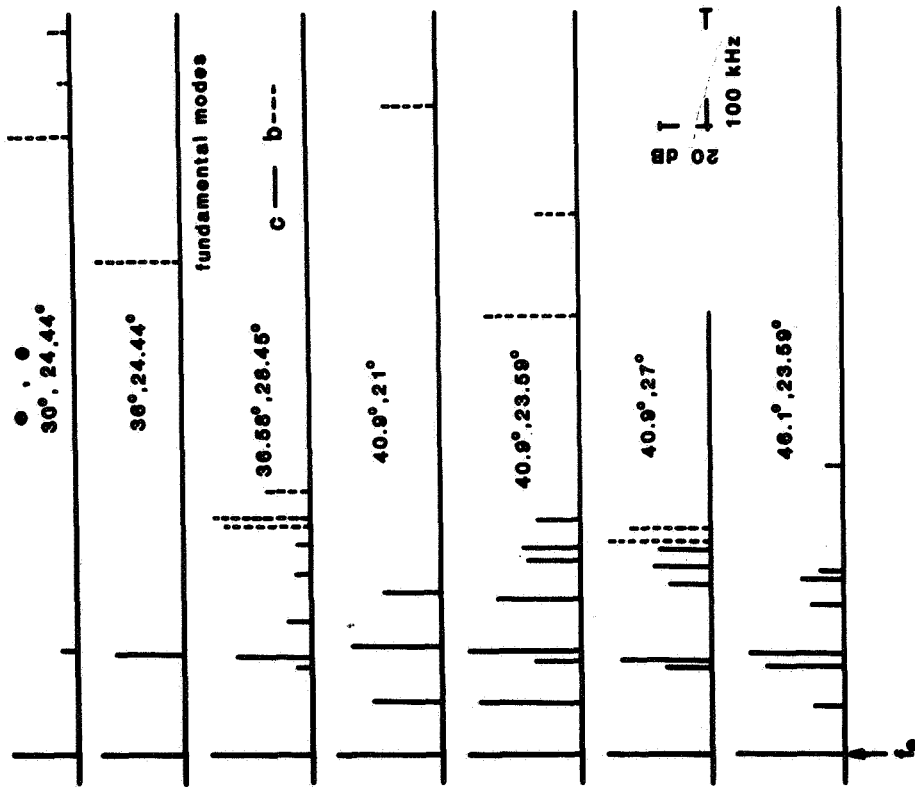


Figure 6. Fundamental c- and b- mode spectra, measured for seven AK-cuts.

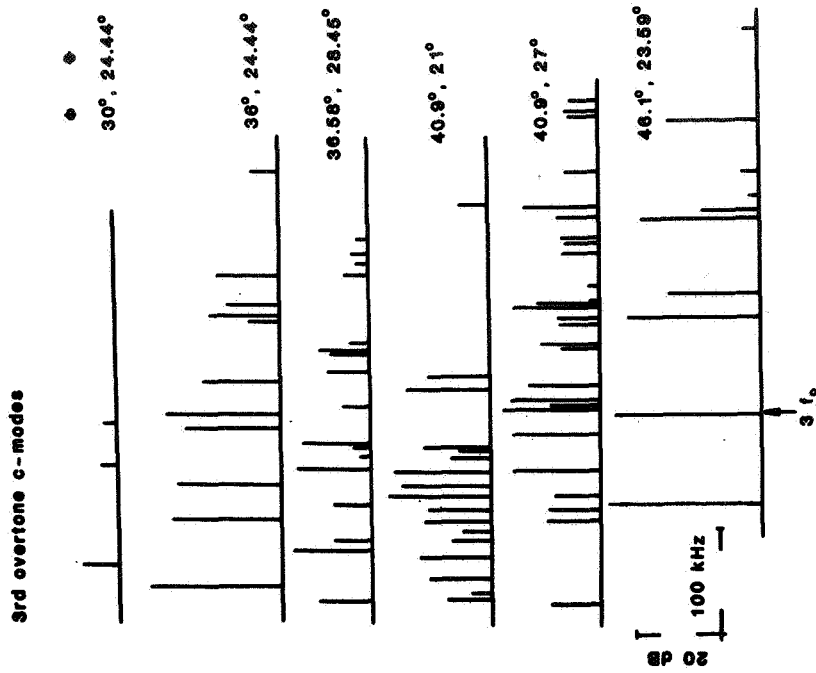


Figure 7. 3rd overtone c-mode spectra, measured for six AK-cuts.

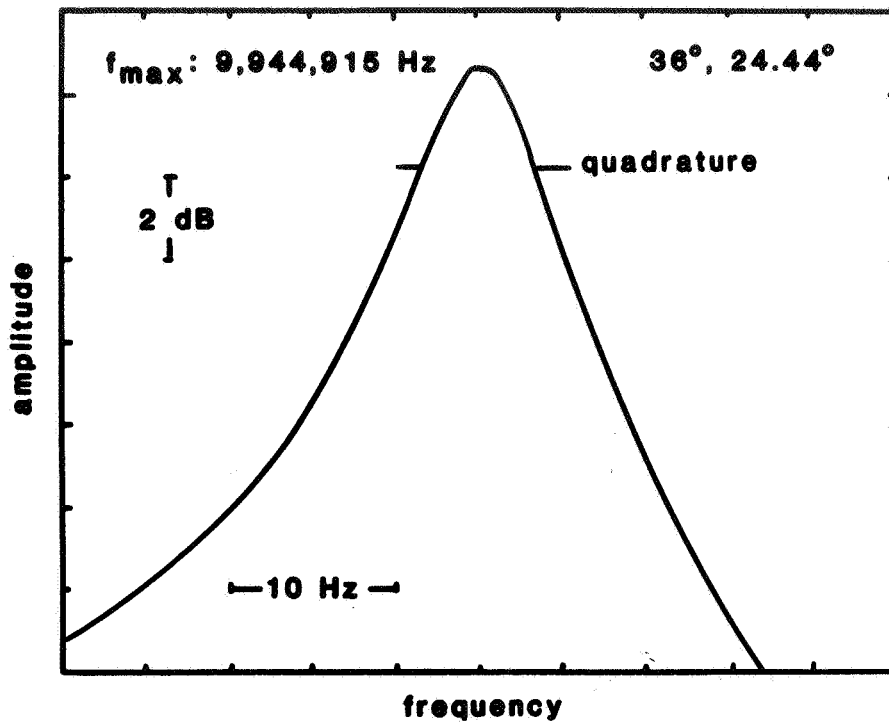


Figure 8. Example of 3rd overtone AK-cut resonance curve.

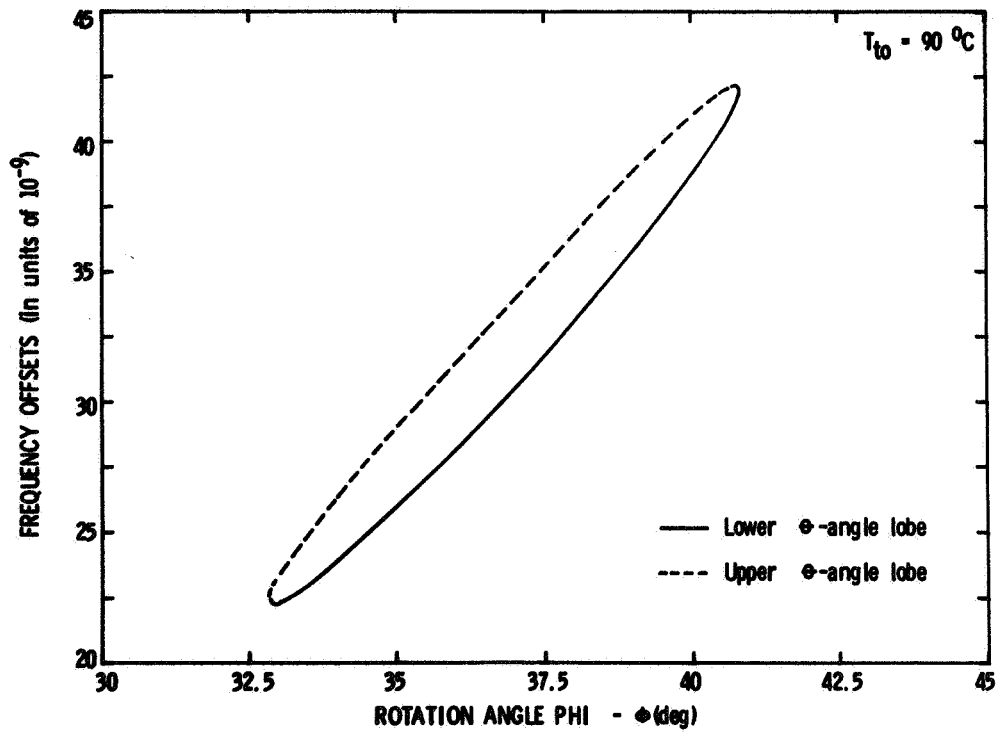


Figure 9. Calculated frequency offsets between $T_0 = 90^\circ\text{C}$ and 91°C for AK-cuts.

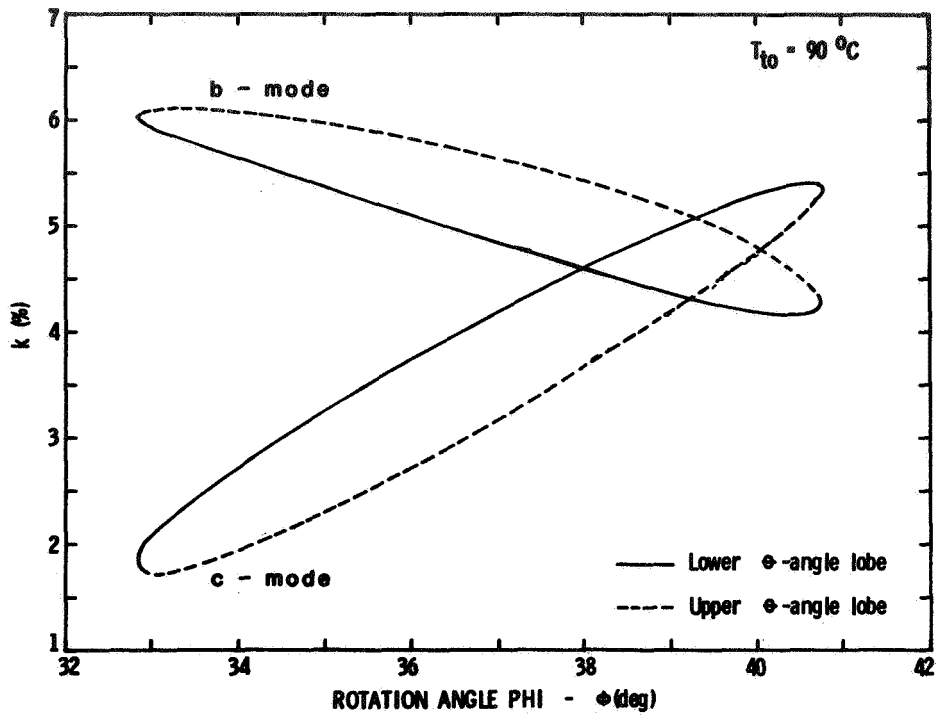


Figure 10. Calculated electromechanical coupling factors k_b and k_c for AK-cuts with turnover at 90°C .

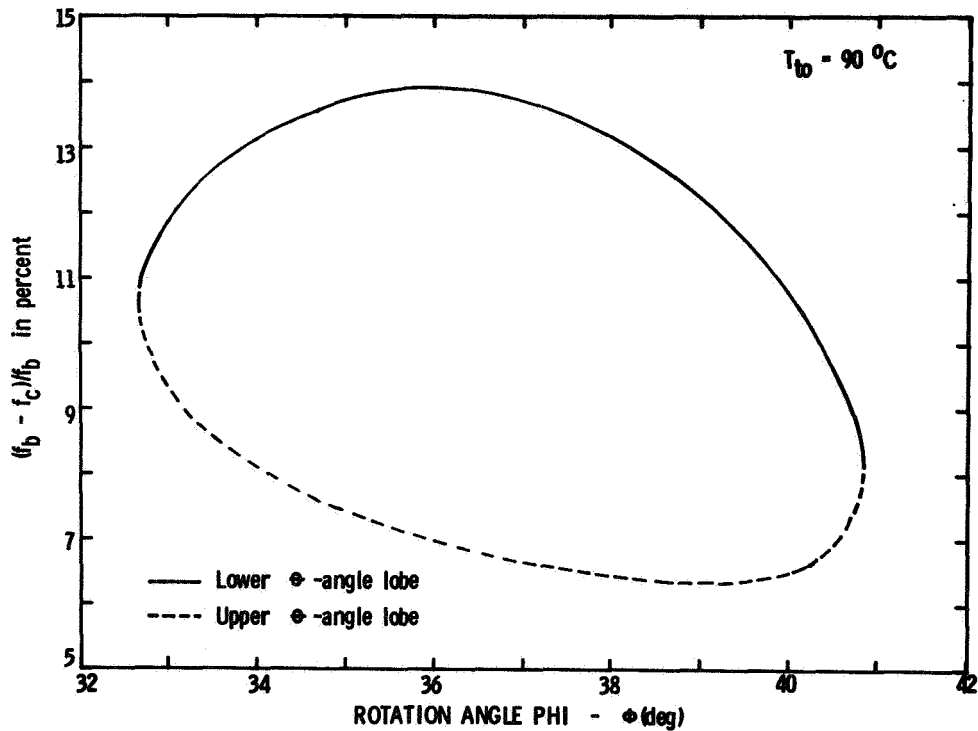


Figure 11. Calculated b-mode to c-mode frequency separation for AK-cuts with turnover at 90°C .

QUESTIONS AND ANSWERS

None for Paper #29

SOME NEW RESULTS ON IRRADIATION CHARACTERISTICS OF
SYNTHETIC QUARTZ CRYSTALS AND THEIR APPLICATION
TO RADIATION HARDENING

HARISH BAHADUR and R. PARSHAD,
National Physical Laboratory,
Hillside Road, New Delhi - 110 012,
India.

ABSTRACT

The paper reports some new results on irradiation characteristics of synthetic quartz crystals and their application to radiation hardening. The present results show how the frequency shift in quartz crystals can be influenced by heat processing prior to irradiation and how this procedure can lead to radiation hardening for obtaining precise frequencies and time intervals from quartz oscillators in space.

In line with the thinking already proposed (H. Bahadur and R. Parshad, Proc. 12th PTTI Conference, pp. 829-849, 1980) for explaining some of the irradiation characteristics of natural crystals, for the present work, it was assumed that the positive frequency shift in irradiated synthetic crystals is due to crystal imperfections. The crystal imperfections in synthetic crystals were sought to be removed by appropriate annealing (slow heating to 240°C followed by slow cooling). Different annealed crystals on irradiation gave either a negative frequency shift, thus simulating the behavior of natural crystals or almost a zero frequency shift. This result would be due to the positive frequency contribution of remanant crystal defects matching the negative frequency contribution of the A-centers of the crystal lattice.

The experimental results indicate a new way of radiation hardening.

This work was supported in part by a Homi Bhabha Fellowship awarded to H. Bahadur.

INTRODUCTION

By now, intense work¹⁻³⁷ on irradiation characteristics of natural and synthetic quartz crystals has been carried out. The main results are the following. For optically clear natural quartz crystals, γ - and X-irradiation produce a negative frequency shift culminating in most cases to a saturation state for prolonged radiation doses. For synthetic crystals the results are more complex and varying. For unswept crystals of lower grade⁸, or premium Q¹⁶, the frequency increases with the dose. For swept crystals of the lower grade, the frequency remains constant with irradiation dose while for the premium Q crystals, the results are varying (frequency increase or constant) depending upon the nature and technique of sweeping¹⁶ or a constancy of frequency followed by decrease¹⁸.

For natural crystals, investigations in this laboratory^{28,36,37} showed that on irradiation, while the optically clear quartz gave the frequency characteristics following the literature results (negative frequency shift), but for the non-optically clear quartz the initial decrease of frequency was followed by an increase. This increase can be so much as to have the new resonance frequency greater than the starting frequency before irradiation.

We were led to believe that the ensuing positive frequency shift (after the initial negative shift) was due to the role of crystal defects present in the non-optically clear natural quartz, these defects also producing the relative opacity of the crystals. That crystal defects were present in such crystals was also adduced by results of investigations of EPR and thermoluminescence of these crystals.³⁸ However, these studies will not be discussed in the present paper.

Parallel with the role of defects in causing positive frequency shifts in natural crystals, it was thought that the overall positive frequency shift in synthetic crystals⁸ right from the time of irradiation was due to the greater density of defects present in such crystals (particularly in those produced at the time of Capone et.al.'s publication: Ref.8). The above thinking led us to the attempt of removing or decreasing the crystal defects by appropriate annealing before subjecting the crystal to γ -irradiation. The results have been rewarding and are detailed below. As would be seen, the results have not only fundamental interest but also indicate a new way of radiation hardening so desirable for use of crystals in satellite-borne frequency standards and other associated applications.

EXPERIMENTAL RESULTS

The various synthetic crystal AT-cut resonators studied were drawn from both unswept and swept materials and oscillated in different frequency regions such as 1, 3.5 and 5 MHz. Swept crystals were Sawyer material and their sweeping was done at Sandia Laboratories, Albuquerque, NM. The unswept synthetic crystal resonators were assembled by Andhra Electronics, India. The resonators were used as the frequency determining elements in a self-oscillating modified Colpitts oscillator circuit. The crystals were γ -irradiated in steps from a ^{60}Co source to different cumulative doses.

At the outset, before giving results for individual crystals, it should be stated that all the crystals, swept and unswept, gave on irradiation an initial frequency instability before the frequencies took up steady values. In this paper, the experimental results about only the steady frequency drifts will be described and discussed.

In the following are given the experimental results for the swept and unswept crystals separately. The studies on the swept crystals were done with the aim to effectively judge the results on the unswept synthetic crystals, all subjected to the same irradiation environment.

Swept Synthetic Crystals

Two swept resonators (designated as Resonators I and II) were operated in their third overtone in the frequency region of 3 MHz. Figures 1 and 2 represent the irradiation results. It can be observed that the steady frequency following the initial instability is unchanged as a result of irradiation.

Unswept Synthetic Crystals

The experimental results for unswept crystal resonators designated as Resonators III, IV and V are given in tables I to III. As can be seen from the tables, for all the resonators the post-irradiation frequencies, following the literature results, were greater than those of the virgin crystals, the frequencies showing a saturation for extended doses. At this stage, the synthetic crystals already irradiated were annealed. In the annealing procedure, the resonators III, IV and V were gradually heated to a maximum temperature of 240°C in a thermostat. They were kept at this temperature for a few hours (~ 5 hrs) and were subsequently cooled slowly at the rate of about $5^{\circ}\text{C}/\text{hr}$ to room temperature. The annealing process would, of course, also fully or partially bleach the crystals. It was interesting to observe that the resonance frequencies of the annealed crystals were lower than those of the original virgin crystals.

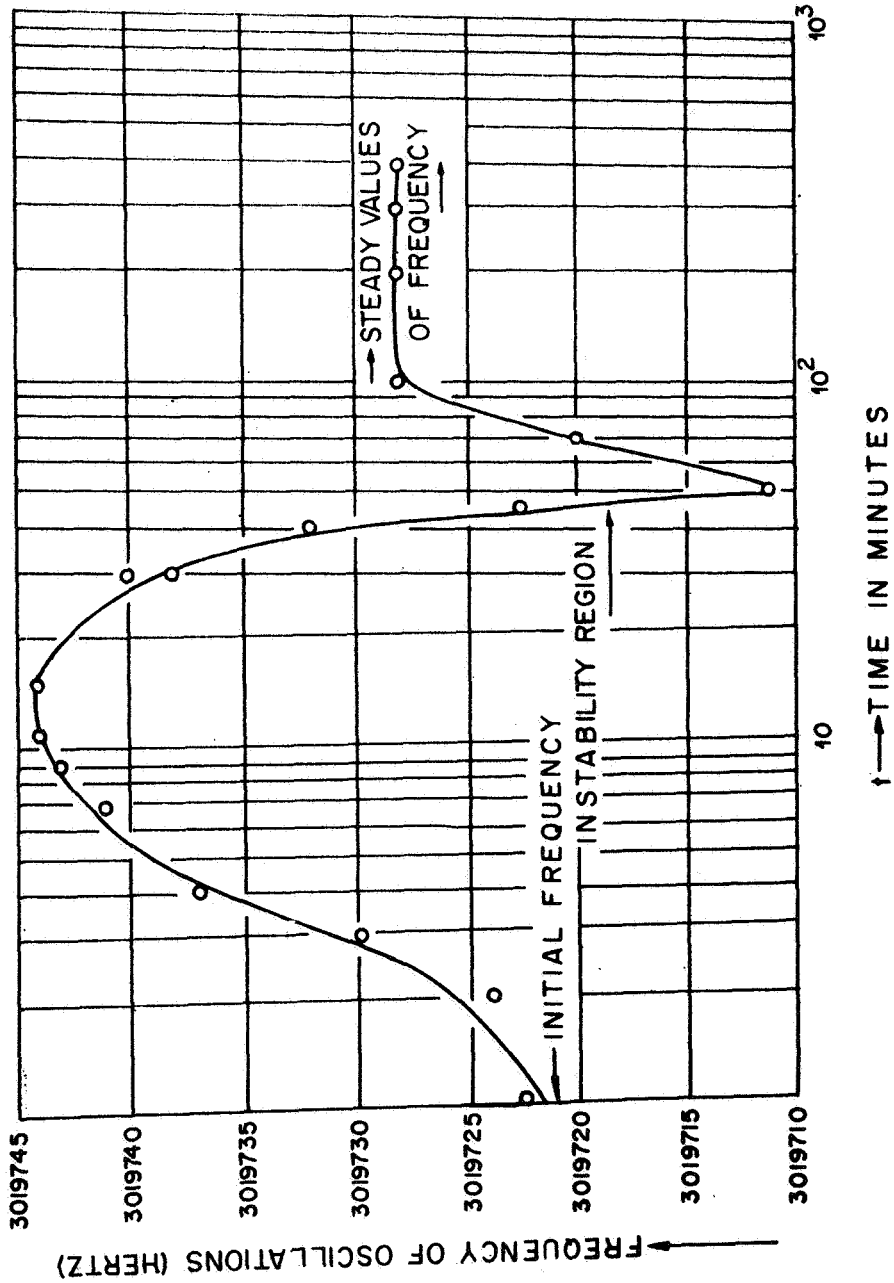


Fig. 1 Post-irradiation frequency characteristic of a swept synthetic quartz resonator after irradiation by a dose of 1.5 MRads of γ -rays using ⁶⁰Co. The crystal is designated as resonator I in the text.

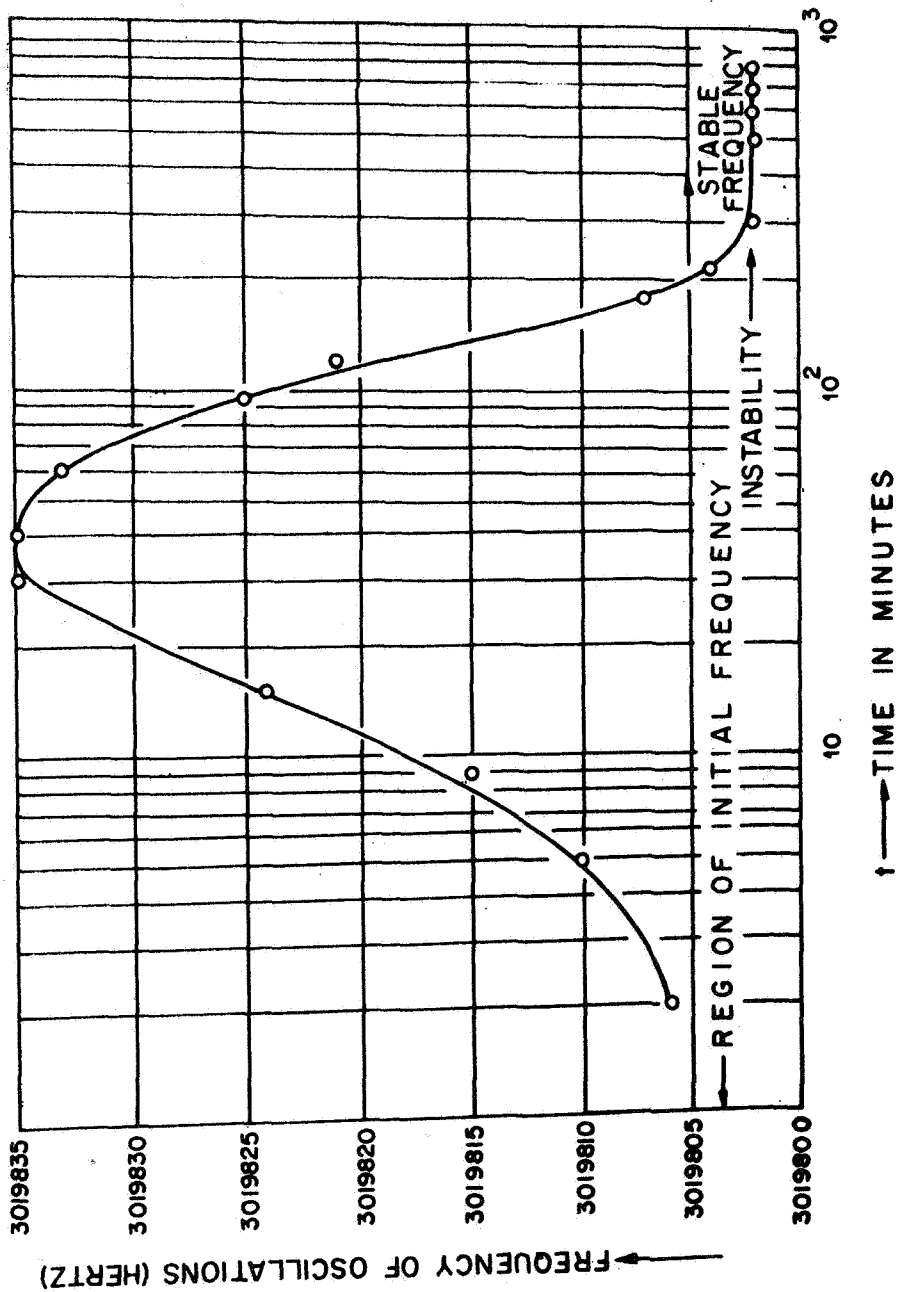


Fig. 2 Post-irradiation frequency characteristic of a swept synthetic quartz resonator after irradiation by a dose of 1.5 MRads of γ -rays using ^{60}Co . The crystal is designated as Resonator II in the text.

TABLE - I

Frequency behavior of a 5-MHz (unswept) synthetic quartz crystal (Resonator III) on γ -irradiation.

Virgin crystal frequency = 5000217 Hz.

Dose	Steady frequency	Steady frequency offset
25 kRads	5000253 Hz	+36 Hz
50 kRads	5000268 Hz	+51 Hz
100 kRads	5000270 Hz	+53 Hz
200 kRads	5000273 Hz	+56 Hz

At this stage the crystal was annealed. Frequency of annealed crystal was 4999792 Hz (\sim 480 Hz lower than the frequency of the virgin crystal). Further irradiation showed the following results.

Dose	Steady frequency	Steady frequency offset with respect to the frequency of the annealed crystal.
100 kRads	4999775 Hz	- 17 Hz
200 kRads	4999765 Hz	- 27 Hz

TABLE - II

Frequency behavior of a 3.5 MHz (unswept) synthetic quartz crystal (Resonator IV) on γ -irradiation.

Virgin crystal frequency = 3500125 Hz.

Dose	Steady frequency	Steady frequency offset
25 kRads	3500153 Hz	+14 Hz
50 kRads	3500158 Hz	+33 Hz
100 kRads	3500158 Hz	+33 Hz
200 kRads	3500160 Hz	+35Hz

At this stage the crystal was annealed. Frequency of annealed crystal was 3500079 Hz (\sim 45 Hz lower than the frequency of the virgin crystal). Further irradiation showed the following results.

Dose	Steady frequency	Steady frequency offset with respect to the frequency of the annealed crystal.
100 kRads	3500086 Hz	+7 Hz
200 kRads	3500084 Hz	+5 Hz

TABLE - III

Frequency behavior of another 3.5 MHz (unswept) synthetic quartz crystal (Resonator V) on γ -irradiation.

Virgin crystal frequency = 3500087 Hz.

Dose	Steady frequency	Steady frequency offset
25 kRads	3500107 Hz	+20 Hz
50 kRads	3500120 Hz	+33 Hz
100 kRads	3500123 Hz	+36 Hz
2000 kRads	3500123 Hz	+36 Hz

At this stage the crystal was annealed. Frequency of the annealed crystal was 3500056 Hz (~ 30 Hz lower than the frequency of the virgin crystal). Further irradiation showed the following results.

Dose	Steady frequency	Steady frequency offset with respect to the frequency of the annealed crystal.
100 kRads	3500062 Hz	+6 Hz
200 kRads	3500065 Hz	+9 Hz

Regarding the irradiation characteristics of the annealed crystals, they changed rather drastically. For resonator III, the post-irradiation frequency was even less than the frequency of the bleached and annealed crystal (serving as the equivalent virgin crystal for the present series of experiments). Thus this crystal, in the way visualized by us, simulated the behavior of a natural crystal. Resonators IV and V gave post-irradiation frequencies almost the same as they were before the second irradiation.

DISCUSSION OF RESULTS

The prominent results that stand out from our investigations are that on annealing the synthetic crystals the irradiation-frequency behavior changed characteristics rather drastically. In one resonator the characteristic became the same as of natural crystals (frequency decreasing with irradiation dose). The other two resonators studied showed almost a constant frequency characteristics (a residual positive frequency shift). The resonator with the negative frequency shift validates the assumption that the positive frequency shift due to irradiation of unannealed crystals is a result of crystal defects and therefore on removing or decreasing the defects on annealing, the frequency behavior would simulate that of the natural crystals. For these crystals, the negative frequency shift is of-course due to the contribution of the A-centers formed from their precursors, the so-called $[Al/M^+]^0$ — centers⁴.

In the context of the above, the irradiation characteristics of the other resonators giving almost zero or residual positive frequency shift must be due to the positive frequency contribution of the remanant crystal defects (remaining after non-ideal annealing) almost matching the negative frequency shift.

Here, it may be of interest to observe that the frequencies of the annealed crystals (before second irradiation) were even less than those of the original virgin crystals. It has been shown earlier³⁸ that neutron-irradiated crystals and those subjected to high enough temperatures ($\sim 1000^{\circ}C$) and rapid enough cooling gave increased hardness and modulus of rigidity, all this leading to increase of resonance frequency. In the light of these results, the decrease of the observed resonance frequency by annealing indicates reduction or elimination of crystal imperfections, the premise on which the work of the present paper is based.

Apart from the fundamental interest of the investigations, the results have the immediate application in that more controlled annealing procedure would yield exact radiation hardening comparable to those of swept crystals (Figures 1 and 2) for satellite-borne frequency standards and other associated uses.

ACKNOWLEDGMENTS

The authors appreciate the help of Dr. J.C. King of Sandia Laboratories, Albuquerque, NM in providing swept crystals for the present studies and wish to acknowledge the cooperation of Dr. M.M. Gupta, Mr. N.K.Ray and Mr. N.Kumar of Institute of Nuclear Medicine and Allied Sciences, New Delhi for various facets of irradiation.

REFERENCES

1. J.C. King, Proc. Internat. Conf. Evaluation of Space Environment on Materials, Center Spatial de Toulouse, June 17-21, 1974.
2. C. Frondel, Amer. Mineralogist 30, 416 (1945).
3. C. Frondel, Amer. Mineralogist 30, 432 (1945).
4. J.C. King, Bell Syst.tech.J. 38, 573 (1959).
5. R.A. Poll and S.L. Ridgway, IEEE Trans. Nuclear Sci. 13, 130 (1966).
6. D.B. Fraser, J. Appl.Phys. 35, 2913 (1963).
7. D.B. Fraser, Physical Acoustics, Ed. W.P. Mason, 5, Academic Press, New York, 59 (1968).
8. B.R. Capone, A. Kahan, R.N. Brown, and J.R. Buckmelter, IEEE Trans. Nucl. Sci., 17, 217 (1970).
9. T.M. Flanagan and T.F. Wrobel, IEEE Trans. Nuclear Sci. 16, 130 (1969).
10. E.P. EerNisse, Tech. Memo. Sandia Laboratories, SC-TM-70-417, July 1970
11. B.R. Capone, A. Kahan and B. Sawyer, Proc. Annual Frequency Control Symp., 25, US Army Electronics Command, NJ, 1971, p.109.
12. A. Kahan, B.R. Capone and R.N. Brown, Tech. Memo. LQ-16, Air Force Cambridge Res. Lab. , Bedford, Mass., March 16, 1973.
13. J.C. King (Ed.), Radiation Effects, 26, No.4 (1975).
14. T. Aoki, K. Norisawa, and M. Sakisaka, Japan. J. Appl. Phys. 15, 2131 (1976).
15. ibid, 15, 749 (1976).
16. Paul Pellegrini, F. Euler, A. Kahan, T.M. Flanagan and T.F. Wrobel, IEEE Trans. Nucl. Sci. 25, 1267 (1978).
17. F. Euler, P. Ligor, A. Kahan, P. Pellegrini, T.M. Flanagan, and T.F. Wrobel, Proc. Annual Frequency Control Symp., 32, US Army Electronics Command, Atlantic City, NJ, 1978, p.24.
18. H.G. Lipson, F. Euler and P.A. Ligor, Proc. Annual Frequency Control Symp. 33, US Army Electronics Command, Atlantic City, NJ, 1979, p.122.
19. F. Euler, H.G. Lipson and P.A. Ligor, Proc. Annual Frequency Control Symp., 34, US Army Electronics Command, Atlantic City, NJ, 1980 .
20. J.C. King and H.H. Sander, IEEE TRans. Nucl. Sci. 19, 23, (1972).
21. E.F. Hartman and J.C. King, Proc. Annual Frequency Control Symp. 27, US Army Electronics Command, Atlantic City, NJ p. 124, (1973).
22. J.C. King and H.H. Sander, Radiation Effects 26, 203, (1975).

23. E.F. Hartman and J.C. King, Radiation Effects, 26, 219 (1975).
24. J.C. King and H.H. Sander, IEEE Trans. Nucl. Sci. 20, 117 (1973).
25. Harish Bahadur and R. Parshad, Rev. Sci. Instrum. 51, 1420 (1980).
26. T.J. Young, D.R. Koehler and R.A. Adams, see (17) (p.34).
27. D.R. Koehler, see (18).
28. H. Bahadur and R. Parshad, Indian J. Phys. 53(A), 239 (1979).
29. J.C. King and D.B. Fraser, Proc. Annual Frequency Control Symp. 16, US Army Electronics Command, Atlantic City, NJ 1962, p.7.
30. F.B. Johnson and R.S. Pease, Phil. Mag. 45, 651 (1954).
31. J.C. King, Final Rep. Fundamental Studies of the Properties of Natural and Synthetic Quartz Crystals., Jan.15,1960 (Contract DA 36-039 Sc-64586).
32. H.G. Lipson, F. Euler and A.F. Armington, Proc. Annual Frequency Control Symposium, 32, US Army Electronics Command, NJ (1978), p.11.
33. David L. Griscom, Proc. Annual Frequency Control Symposium, 33, US Army Electronics Command, NJ, (1979).
34. L.E. Halliburton, M.E. Markes and J.J. Martin, Proc. Annual Frequency Control Symp. US Army Electronics Command, 34, (1980).
35. L.E. Halliburton, N. Koumavakalis, M.E. Markes and J.J. Martin, J. Appl. Phys. 52, (5), 3565 (1981).
36. H. Bahadur and R. Parshad,, Phys. stat. solidi (a)67, 683 (1981).
37. H. Bahadur and R. Parshad, Proc. Second International Symp. Radiation Physics, Penang, Univ. Sains, Malaysia, 25-30 May, 1982.
38. Harish Bahadur, "Investigations on Oscillating and Structural Characteristics of Quartz Crystals" Ph.D dissertation, Univ. of Delhi, Department of Physics, 1978.

QUESTIONS AND ANSWERS

None for Paper #31, Not Presented at PTII

ONE NANOSECOND TIME SYNCHRONIZATION
USING SERIES AND GPS

L. A. Buennagel
D. J. Spitzmesser
L. E. Young
Jet Propulsion Laboratory
Pasadena, California

Abstract

Subnanosecond time synchronization between two remote rubidium frequency standards is verified by a traveling clock comparison. Using a novel, code ignorant Global Positioning System (GPS) receiver developed at JPL, the SERIES geodetic baseline measurement system is applied to establish the offset between the 1 Hz. outputs of the remote standards. Results of the two intercomparison experiments to date are presented as well as experimental details.

INTRODUCTION

Traveling clock intercomparisons with better than a nanosecond agreement demonstrate that time synchronization is now possible using a new technique. The technique is known as Satellite Emission Range Inferred Earth Surveying (SERIES) and was developed at the Jet Propulsion Laboratory by a group with a background in Very Long Baseline Interferometry (VLBI.) The traditional sources for VLBI are quasars, distant and dim astronomical objects. The quasar signal strengths are five or six orders of magnitude less than the GPS satellite signals. Using brighter sources permits relaxing the severe discipline imposed on VLBI researchers, such as long observation times as well as high instrumental and frequency standard stabilities. The major departure from the VLBI approach is the absence of any bit stream alignment or correlation in the data reduction stage. The major inheritance for SERIES from the VLBI tradition is an irreverence for "codes"; indeed, it has been said that no one knows the code being broadcast by the quasars, but that has not kept them from being successfully used.

The SERIES technique, then, is built around a novel GPS receiver, one that does not have a preset bit stream generator inside; there is nothing correlating with the received signal. Instead, the SERIES receiver collapses the received spread spectrum signal, extracting the transitions of the spaceborne pseudorandom code generator. These transitions provide the event common to both stations for the baseline parameter estimation, the primary SERIES application.

EXPERIMENTAL OBSERVATION

The situation for a SERIES experiment is indicated in FIGURE 1. A GPS satellite is shown illuminating two SERIES stations, each with a rubidium standard. In this case, the standards are assumed to be synchronized, thus their ticks are shown aligned vertically. Moreover, at the moment depicted, exactly an integral number of half wave lengths of the transition fit between the satellite and the lower station antenna. For the assumed case of no phase delays in the receiver, the square wave output of the SERIES receiver is in phase with the received transition and with its station clock.

Note the second station's receiver output. A non-integral number of wavelengths fit in the path between the satellite and the antenna. With the assumed zero delay in the receiver, the square wave output has a phase shift relative to its own station clock. Each station's measured receiver phase is recorded. During data reduction, the receiver phases measured at the same time at the two stations are differenced. This phase difference is modeled as propagation delay due to the projection of the baseline onto the line of sight to the satellite. In addition, since the two standards are never synchronized in phase or frequency, effects of these two offsets are present in the difference data and must be solved for in the parameter estimation. It is the estimation of these effects that permits the SERIES technique to provide time synchronization.

Each square wave coming from the receiver looks like any other, so there is an ambiguity as to just which event in the train of square waves either station saw. This ambiguity can be removed either by adequate prior knowledge of the baseline or by a fuller treatment of the data as a Doppler differential positioning problem. For the demonstration goals of the current SERIES task, the a priori baseline data was provided at about the 100 meter level. The Doppler approach is being implemented and is expected to remove this requirement for the SERIES system.

PORTABLE STATION

Figure 2 shows the station used in the SERIES system. One such single man station is placed at each end of the line to be measured. The camper shell is required for shelter but is not very full. The whole system occupies three half-electronic equipment racks, a total of about eighty inches of front panel space. The receiver takes eight inches, the rest is taken up by off-the-shelf items for the data system such as a nine track tape deck, a computer, the HP5370A Time Interval Counter which is the main measurement device and the station's rubidium standard.

Behind the camper is the system antenna, which is rolled over the marker defining the end of the baseline. A stylus drops from the base of the mount in order to measure any geometric offset from the intended position. Above the wagon and pedestal are the television pan and tilt mount for steering the antenna, the dish or main reflector and finally the feed and ground plane. The dish is a homemade affair of bent aluminum and half inch wire mesh. The feed is a helix wound on a 16oz. plastic drinking cup and the ground plane is a 10 inch pie pan.

BASELINE ESTIMATION

Whatever doubts that may have been raised about the seriousness of this effort should be allayed by Figure 3, which depicts how well the parameter estimation process treated the observations. This figure shows the plot of the residuals to the data taken on the 24th of August, 1982; the other experiment to date, on the 23rd of August, had similar results. The baseline being measured at the time of these experiments was approximately 21 kilometers long, at JPL's Goldstone tracking complex in Southern California. The computed phase difference was derived from the five parameter solution: the three dimensional vector between the stations, the epoch offset between the station clocks and the frequency offset between those clocks. Plotted on a full scale of 4 nanoseconds are 101 residuals, which have an RMS scatter of .6 nanoseconds, typical for experiments run for this baseline. While they are not identified in the figure, observations on all five GPS satellites are present, normally one after the other for good sampling of the baseline components. This estimation was limited to the two and a quarter hours that all five satellites were in common view.

The time at which the epoch offset estimate is correct is the start of the observation run; this was chosen as the time to express the intercomparison results and is indicated on the residual plot by the vertical arrow. Also on the residual plot are two gaps, the first for a traveling clock visit to station A, and again, half an hour later, for a visit to station B.

CALIBRATIONS

The transitions extracted by the SERIES receiver are found in three guises as broadcast by each GPS satellite, one at 1.023 MHz. on the upper broadcast frequency, designated L1, and two at 10.23 MHz., one on L1, and a second on the lower frequency, designated L2. A measurement of the delay from the L1 10.23 MHz. transition to that on L2 permits a direct calibration of the ionospheric delay along the line of sight to the satellite, much as in the standard GPS (two channel) receiver. The SERIES system obtains this calibration for each observation, removing ionospheric delay as an error source.

Because the SERIES system was not designed for time synchronization, two ancillary measurements were required for absolute clock difference measurements. During each day's experiment, the phases of certain local oscillators at each station were measured relative to the station clock using the same Time Interval Counter as was used for the other phase measurements.

In addition, it was necessary to measure the differential total delay through the two stations. This calibration was made on the 25th of August. Both stations were located at Station A and operated as on other occasions, except that the geometry was known and the clock bias was eliminated by operating both stations from the same frequency standard. The parameter estimation results were used to derive the differential total system delay. Again, "differential" is used because the absolute system delay is not obtained but only the difference between the two stations. The system differential as well as the second day's single cycle ambiguity were applied to obtain the final SERIES value for the station clock offsets.

TRAVELING CLOCK

The independent verification of the station clock offsets was a traveling clock measurement. The measurement setup is indicated in Figure 4, with the traveling clock visiting station A. The HP5370A Time Interval Counter (TIC) measures the offset between the host clock and the traveling clock. (By way of comparison, the figure notes the use of the TIC for the baseline estimation setup; in this case, the TIC is started on the host clock tick and stopped at a predetermined point on the receiver output waveform.)

Figure 5 presents the traveling clock data for the 24th of August. Each dot plots the average of 100 measurements of the time delay between the 1 Hz. outputs of the station clock and traveling clock. Typical RMS deviations of each of the 100 measurements were a half nanosecond. The lines, here hand drawn, depict the fit to the data taken at each station. A third order polynomial was used in order to interpolate the two station clock offsets to a common epoch. The RMS errors to the fits were about a half nanosecond. The common epoch for this day's intercomparison with the parameter estimation results is indicated by the vertical arrow. Note that the 1300 nanosecond offset exceeds the SERIES ambiguity interval of 997 nanoseconds. One ambiguity interval was added to the parameter estimate for this date.

The sequence of data points, alternating between the two stations, shows there were two and a half round trips for the traveling clock; the same was done on the 23rd. The effort spent on the repeated trips gave us confidence that there were no clock breaks in the traveling clock. Pains were taken in the measurement technique to insure

repeatability, such as using digital voltmeter settings to define the reference points on the clock output wave forms, and using the same cables for connecting the traveling clock at each station. The traveling clock measurement can be seen to be accurate to about 0.5 nanosecond. This is reasonable performance for the HP 5065A Rubidium standard with $(\Delta f)/f$ at one hundred seconds of 5×10^{-13} , given a mean of about 10 minutes between measurements:

$$(5 \times 10^{-13}) \times 10 \text{ min} \times 60 \text{ sec/min} \times \text{square root}(2 \text{ clocks}) = 0.4 \times 10^{-9} \text{ sec.}$$

RESULTS

The results are tabled in Figure 6. The second column contains the SERIES determined offset between the two station clocks at the date and time listed in the first column. The third column contains the traveling clock estimate of the clock offsets, interpolated by means of the polynomial to the time shown in the first column. The difference between the methods was .6 nanoseconds for the first day and -.6 nanoseconds for the second.

In summary, the subnanosecond intercomparison of the clock offsets shows the SERIES technique to have more than just promise as an economical and flexible method for time synchronization with performance that will not degrade should the satellite codes involved pass from public access.

The authors would like to acknowledge the able assistance given to this experiment by Earl Lobdell, Sharon Schmitt, Ben Johnson, Bob Newsted, Mark Smith, and Jess Myers.

**1 NANOSECOND TIME SYNCHRONIZATION
USING SERIES**

(SATELLITE EMISSION RANGE INFERRED EARTH SURVEYING)

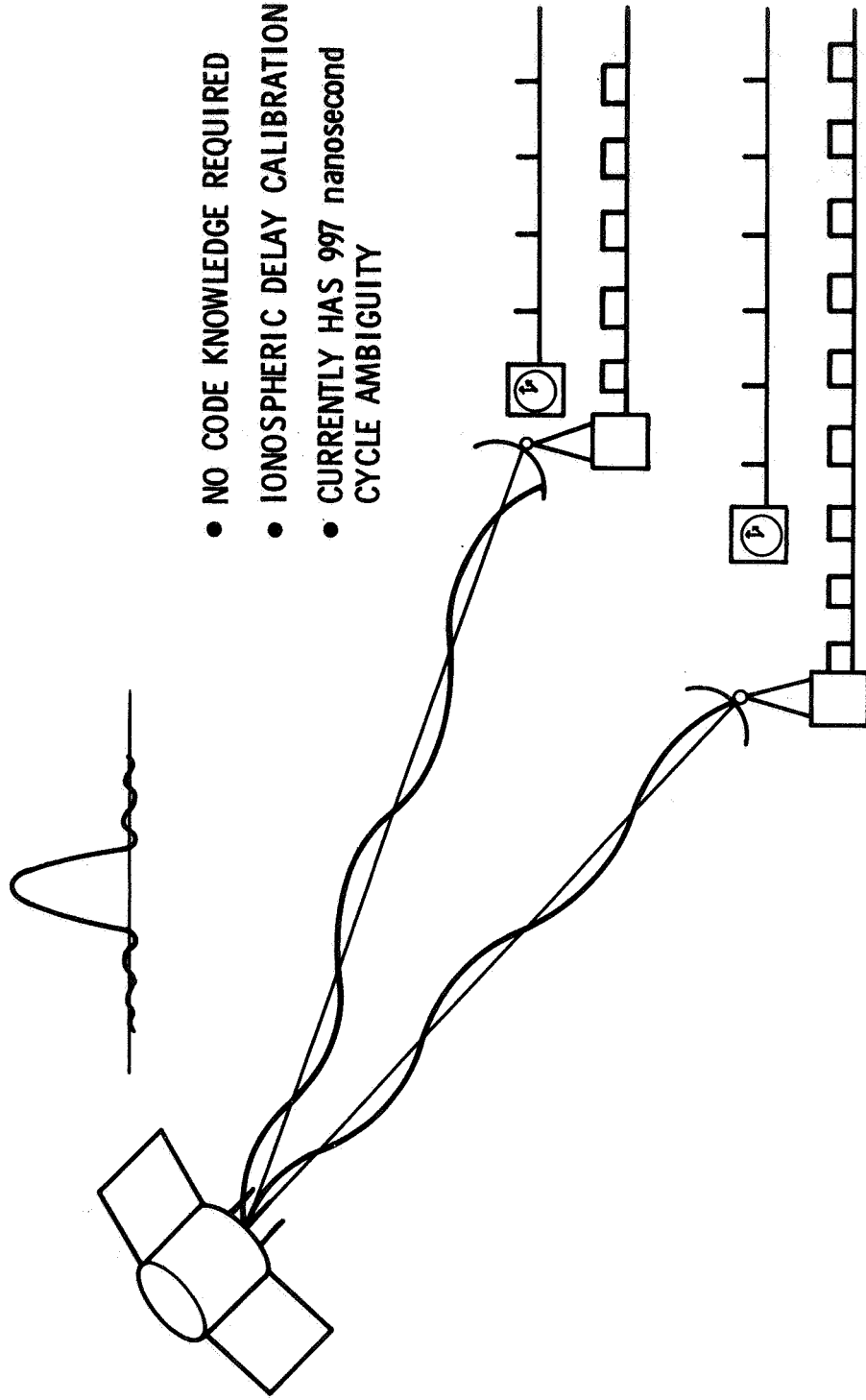


Figure 1. SERIES observable for parameter estimation.



Figure 2. SERIES portable station.

24 AUGUST 1982
 DIFFERENTIAL TIME OF ARRIVAL MINUS COMPUTED
 21,463 METER BASELINE

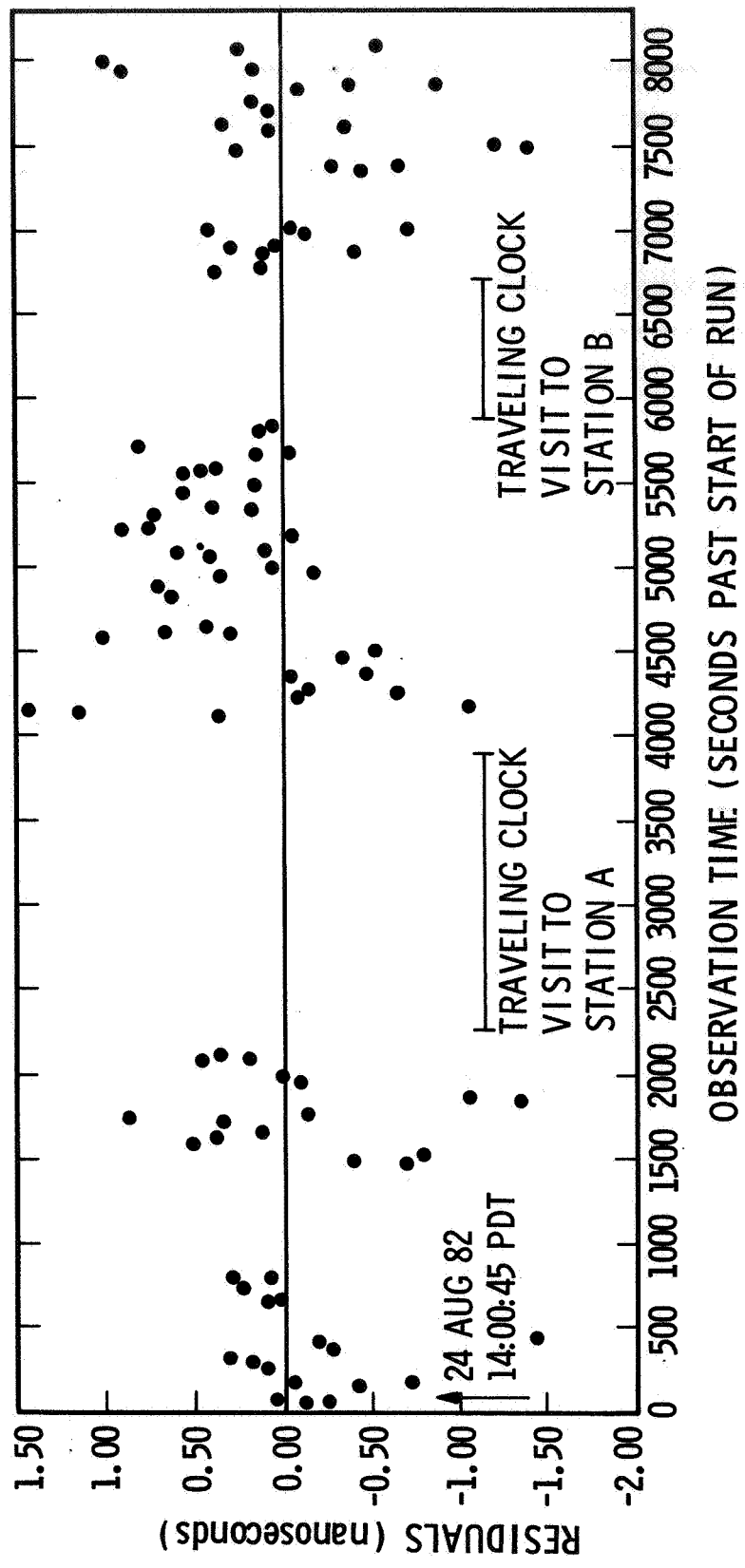


Figure 3. Residuals to differenced delay measurements.

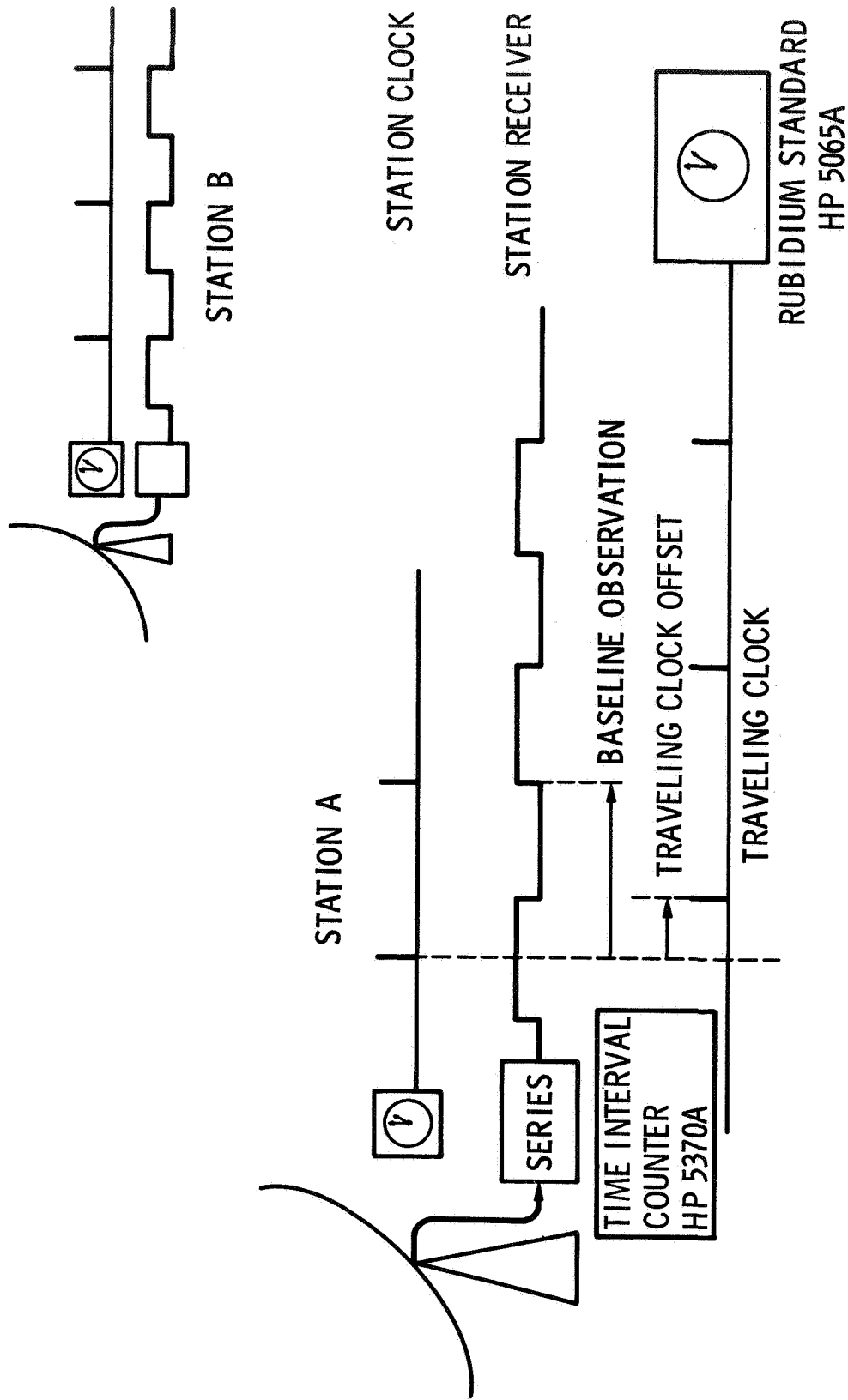


Figure 4. Measurement during traveling clock visit.

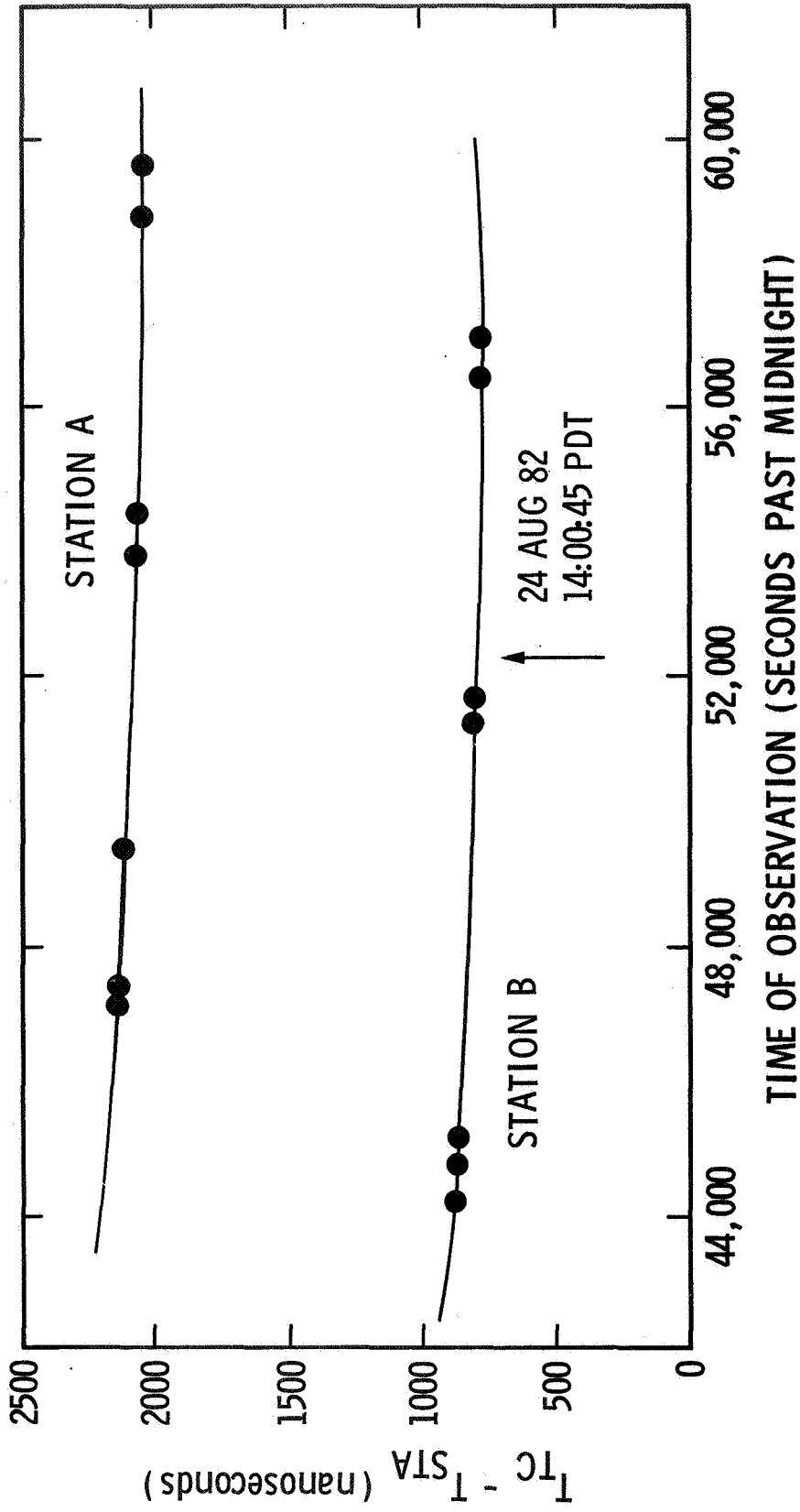


Figure 5. Offsets to traveling clock for each station.

	$t_{\text{STA A}} - t_{\text{STA B}}$ SERIES RECEIVER	$t_{\text{STA A}} - t_{\text{STA B}}$ TRAVELING CLOCK	DIFFERENCE BETWEEN 2 TECHNIQUES
23 AUG 82 14:36:45 PDT	-189.7 ns	-190.3 ns	+0.6 ns
24 AUG 82 14:00:45 PDT	-1302.0 ns	-1301.4 ns	-0.6 ns

- SERIES MEASUREMENT INCLUDES
- MEASURE MIXER PHASE AT EACH RECEIVER
- COLOCATE TO CALIBRATE TOTAL SYSTEM DELAY

Figure 6. Comparison of SERIES and traveling clock values.

QUESTIONS AND ANSWERS

MR. D. W. ALLAN, National Bureau of Standards

One comment and two questions: I believe that is the 5370 counter, is it not?

MR. L. A. BUENNAGEL, Jet Propulsion Laboratory

53 or 5070, I don't know. The digit is at the wrong place.

MR. ALLAN:

Okay, fine. How do you determine the ephemeris for the satellite? What do you use for the ephemeris estimation?

MR. BUENNAGEL:

Okay. We have two problems. First of all it is a steered antenna, as you see, so we need to know where to point. For that, the Vandenberg Master Control Station provides, on a week or two basis depending on when we are calling up, et cetera, orbital parameters which are an almanac class message in the upload. Post facto, some two weeks or so after the observation, we get a tape from Anderle's group at the Naval Surface Weapons Center. I do not know what that tape is, and I have questions about it. I am afraid that it is the prediction tape sent to Vandenberg. The hope, in contrast, is that really is, as advertised, the 5-minute center positions of the satellites, so we use the post facto for the ephemeris positions of the satellites.

MR. ALLAN:

The second question is, how large a baseline do you think you can go up to?

MR. BUENNAGEL:

This experiment was terminated at the line shown here by bringing one end of the baseline back to JPL. That's 171 kilometers, a factor of eight. We expect to be able to do that. Our experience has been that we do better the further out we get. I do not want to advance an estimate that we are going to move baselines further out. We'll see what happens.

DR. KELLOGG, Lockheed

When you talk about some nanosecond precision, or whatever you choose to call it, the difference between the two, you described an antenna built in not only an imprecise manner but one which gave one pause. The distances you are measuring are from the phase center of an antenna to some

other source, using VLBI techniques. Is the phase center of this tracking, non-rigid antenna reproducible within the sub-nanosecond level, converting to the speed of light, that's a pretty few centimeters?

MR. BUENNAGEL:

You are striking on an article of faith of the VLBI community that I personally have called into question. The argument goes, suppose there is a phase center not at the assumed geometric intersection of axes, which is the solution point. If it is off-axis, which would be argued against on the basis of symmetry, you would not be sampling that component because it is normal to the incident ray wavefront. If it is along axis of the antenna, it is indistinguishable from a clock term, which then in turn is lumped into the final step, namely the differential total station delay calibration required.

So you have ferreted out a nice matter. I have given the doctrine, the dogma, on how to deal with that, but I have my doubts, and given some time I want to investigate that.

DR. KELLOGG:

I'm glad you do. Thank you.

MR. BUENNAGEL:

A question in the back?

MR. J. M. PRZYJEMSKI, Draper Laboratories

Have you at any time measured any of these baselines using, perhaps, a surveying technique?

MR. BUENNAGEL:

Yes. We have measured baselines of zero meters out to two meters, 150 meters, and now this one, which are in fact known to three more places than I put on the graph.

MR. PRZYJEMSKI:

So that would be a third means of supporting these time transfer results that you have.

MR. BUENNAGEL:

The result of the comparison on this longest baseline is in agreement with the hybrid of the National Geodetic Survey answer and a VLBI measurement along the baseline of 2.2 centimeters length at the current time, but that really is a result that has to be described elsewhere, under other circumstances.

MR. PRZYJEMSKI:

I see. Another comment is, you mentioned that the further your baseline, the better you feel the results might be.

MR. BUENNAGEL:

No, just the better they appear to be.

MR. PRZYJEMSKI:

They appear to be. Would you feel that your ability to measure or compensate for differential ionospheric delays might cause you to have a greater error with increasing baseline length.

MR. BUENNAGEL:

In fact, none of the solutions to date have used the ionosphere calibration delay information. This six-tenths of a nanosecond agreement that we have here doesn't use that information. Moreover, it doesn't use any kind of atmosphere correction. At Goldstone that may not be so terrible, because it is very dry, its level, the winds are still. It is obvious that the more we push this, the more we are going to have to use other forms of data.

MR. PRZYJEMSKI:

Did you use L1N02?

MR. BUENNAGEL:

We do routinely record that. It was touted as our first product but in fact we don't use it in any of that.

MR. PRZYJEMSKI:

Certainly that would give you a good result if the baseline was short, where the differential on the ionosphere may have a small or negligible effect on the result.

MR. BUENNAGEL:

We are a little bit pessimistic right now because the noise on the ionosphere delay is worse than the gain you get back putting in the corrections.

MR. PRZYJEMSKI:

I see. Thank you very much.

DR. VICTOR REINHARDT, Bendix Field Engineering Corporation

What technique do you use to extract the time ticks without knowing the code?

MR. BUENNAGEL:

It is described as a power divide, shift, and multiply technique. It is documented in a patent application on file under the name of Peter McDoren, the person who developed this technique. I am not a radio person. I cannot go into the details of that. I believe that you can find this application that has been documented.

I would enjoy a question from Dr. Alley, my former employer.

PROFESSOR ALLEY, University of Maryland

Thank you. I am a little surprised you have such good agreement on this traveling clock, Al. Did you take precautions to protect it during this transit?

MR. BUENNAGEL:

I have been alerted to expect challenge on that side. I am hiding behind the word "agreement" here. You will notice that there was some rigor used here, namely, more than one round trip and more than one day, as I have noted. I doubt that there was any protection at all. It was placed gently in a car and driven but beyond that, I did not make the trip myself so I do not know what the protection was.

PROFESSOR ALLEY:

I see. Thank you.

MR. BUENNAGEL:

Dr. Winkler?

DR. WINKLER:

Two things: The principle of collapsing a pseudo random noise code consists in compensating for the phase modulation. In case of simple ± 180 degree phase modulation, at whatever rate and in whatever pseudo random sequence, if you multiply your I.F. frequency by two, the result will always be zero phase angle, whether it is 180 or zero, and exactly the same thing can be done with whatever phase modulation you have, just that it has to be more complicated. This in fact is the technique which is used to track the pseudo random noise with VLF receivers.

But I have another question: You have emphasized that you don't need the code but you do need the ephermeris, and of course in the moment the code is withdrawn I doubt that you will have the ephermeris without being authorized.

MR. BUENNAGEL:

That, I think, will be a politcal question, and the answer thus far has been that because we are a nontactical user, that we may have the solution after the fact, two weeks, et cetera. Again, in a tactical or a real time point of view, that is terrible, but relative to the VLBI experiment that runs for days itself before the data is gathered, let alone the solution, 2 weeks is wonderful.

MR. L. J. RUEGER, JHU/APL

I was wondering if you could support the independent phase stability of these rubidium standards to that quality actually as independent time pieces, because half a nanosecond over that length of time is really quite remarkable.

MR. BUENNAGEL:

Again, I am hiding behind the word "agreement". I am familiar with documented properties, et cetera, but I think we have something.

DR. VIG:

Thank you for a most interesting paper, as evidenced by the number of questions.

NEW AUTO-TUNING TECHNIQUE FOR THE HYDROGEN MASER

R. L. Sydnor and L. Maleki
Jet Propulsion Laboratory
California Institute of Technology
Pasadena, California

ABSTRACT

Auto-tuning of the maser cavity compensates for cavity pulling effect, and other sources of contribution to the long term frequency drift. Schemes previously proposed for the maser cavity auto-tuning can have adverse affects on the performance of the maser. In this paper we propose a new scheme based on the phase relationship between the electric and the magnetic fields inside the cavity. This technique has the desired feature of auto-tuning the cavity with a very high sensitivity and without disturbing the maser performance. Some approaches for the implementation of this scheme and possible areas of difficulty are examined.

Introduction

The dominant cause of the long term frequency drift in the hydrogen maser is the slow change in the dimensions of the high Q cavity. Since the dimensions of the cavity must be held stable to approximately one angstrom to maintain the frequency of the maser to one part in 10^{15} , it is difficult to directly measure and control. This dimensional change must be overcome in some indirect manner which senses the cavity frequency offset and tunes the cavity back to resonance. Aside from overcoming the cavity pulling effect, auto-tuning can also enhance the performance of the maser by reducing the sensitivity to pressure variations, and compensating for anomalous frequency shifts often encountered in the hydrogen maser.

A number of techniques have been previously proposed for cavity auto-tuning.¹⁻⁴ These techniques are essentially based on either the modulation of the atomic line width, or the sensing of the cavity resonance. The technique proposed in this paper is based on the latter effect, and utilizes the phase relationship between the electric and the magnetic fields in a finite Q cavity.

In the remainder of this paper brief discussions of cavity auto-tuning methods based on atomic line width modulation and on resonance sensing will first be presented. The description of the auto-tuning scheme based on phase detection will then be given. Finally, a discussion of the potential advantages and disadvantages, and possible means of the implementation, of the method will be made.

Cavity Auto-Tuning Techniques Based on Line Width Modulation

The line width modulation technique is based on the influences of the quality factor, Q , of the atomic line, the Q of the maser cavity, and the mistuning of the cavity on the output frequency, f_0 of the maser. Designating the deviation of the oscillator frequency from true resonance by Δf_0 , the cavity frequency mistuning by Δf_c , and the cavity and line quality factors by Q_c and Q_1 , respectively, we may write,

$$\Delta f_0 = (Q_c / Q_1) \Delta f_c \quad (1)$$

According to equation (1), the mistuning of the cavity may be determined by changing the atomic line width. There are several ways in which this may be accomplished. In the first, and most common way, it is accomplished through the controlled modulation of the atomic beam flux, which in turn influences the contribution of the spin exchange effect to the line width.¹

The modulation of the atomic flux may be accomplished in a number of ways, including the modulation of the input power of the hydrogen gas dissociator. The most popular method for atomic beam flux modulation however involves the chopping of the beam and thus controlling the number of atoms which enter the maser storage bulb in the cavity. The resulting change in the maser output frequency is detected and used to determine the cavity mistuning and thus to control the effect of the cavity drift. While this method has the advantage of simplicity and effectiveness, it nevertheless suffers from a number of problems including reproducible control of the beam chopper and adverse influence on the performance of the maser due to periodic alteration of the signal-to-noise ratio in the maser and the effect of the varying output power on the phase transfer function of the electronics.

Another technique for varying the width of the atomic line that has been attempted is the introduction of inhomogeneities in the magnetic field in the maser cavity. The resulting frequency change in the maser output frequency would be detected and used as above. This technique has not been used because of the difficulty in achieving the proper kind of controlled inhomogeneity.

Cavity Resonance Sensing Technique

A number of techniques have been devised, in connection with the development of the passive hydrogen maser,² to auto-tune the cavity by sensing the cavity resonance. One such technique² involves the injection of a signal which has been square-wave frequency modulated by an amount approximately equal to the band-width of the cavity, and is centered on the atomic line. If the cavity is not tuned correctly, the two signals will be attenuated by different amounts as they traverse the cavity. This modulation of the amplitude of the injected signals is then used to generate an error signal which corresponds to the difference between the cavity resonance frequency, and the frequency of the injected reference signal.

A somewhat similar technique employs a signal centered on the atomic line which has been modulated by a sine wave to produce two side-bands

approximately one cavity band-width apart, with a carrier suppressed far enough to not perturb the maser operation.³ The modulation of the amplitude is again used to generate an error signal which is used to tune the cavity to resonance. Finally, in yet another technique⁴, the cavity center frequency is square wave modulated about the hydrogen line frequency. The modulation of the amplitude is again used to measure the frequency offset.

While all three techniques mentioned above are effective in cavity auto-tuning, they nevertheless involve either the introduction of a signal in the cavity, or modulation of the cavity frequency. In either case it is difficult to prevent the introduction of noise in the cavity and modification of the maser performance. Furthermore, these techniques are difficult to implement, and require the use of low noise and high performance electronic components which are difficult to develop.

Cavity Resonance Sensing by Phase Comparison

In a resonant cavity the energy is stored in both the electric and the magnetic fields. For a cavity of infinite Q, the **E** and **H** fields are in temporal and spatial quadrature. For a lossy cavity the temporal phase becomes an arccotangent function of the fractional frequency offset of the signal frequency from the cavity center frequency, normalized to the cavity bandwidth. This fact is illustrated by the input impedance of the cavity shown in the Smith chart of Figure (1). The cavity input impedance is small far from resonance, and complex near resonance. At resonance, the input impedance is real. This, too, implies that the phase of the electric and the magnetic fields may be used to determine the cavity resonance.

The development of a cavity auto-tuning system based on the ideas sketched above can be illustrated by the following, not necessarily optimum, technique. Two co-located, weakly coupled probes, one loop and one dipole, can be used to detect the magnetic and the electric fields in the cavity. Signals from each probe may be compared in phase in a manner similar to that illustrated in figure (2). A deviation of phase from 90 degrees as detected by the phase detector in figure (2) will then signal the departure of the cavity from resonance condition. The signal from the phase detector may be used in conjunction with the varactor to auto-tune the cavity back to resonance.

The sensitivity of this technique in tuning the cavity may be illustrated by a simple calculation. Let us assume typical values of 35000 for the Q of the maser cavity, and 10^9 for the hydrogen line Q. Designating BW for the cavity bandwidth we have $BW=40571$ Hz with these parameters. The cavity bandwidth corresponds to a phase shift of 90 degrees. Assuming a sensitivity of 1×10^{-6} radian for the phase detector, the technique will be sensitive to a fractional frequency deviation of 4.6×10^{-16} .

The implementation of the phase sensing of the cavity resonance will require careful design of the probes and their location, as well as low noise amplifiers for the detection of the signal. Nevertheless, this method, unlike the other cavity sensing techniques mentioned above, dispenses with

the need of injecting signals in the cavity and therefore does not adversely affect maser performance.

Summary

We have examined a sensitive technique for auto-tuning of the hydrogen maser cavity. The technique is based on detecting the phase relationship between the magnetic and the electric fields in the cavity with appropriate probes to maintain the resonance condition.

Because of dispensing with the need of signal injection in the cavity, or modulation of the cavity frequency, the proposed scheme has the apparently attractive feature of auto-tuning the cavity without adversely influencing the maser performance. It is clear, however, that the implementation of this technique in the hydrogen maser requires care to insure effective tuning without disturbance of the maser performance. In particular, light coupling of the **E** and **H** probes requires low noise amplifiers with little sensitivity to temperature variations. The position of the probes in the cavity, and with respect to each other, should also be carefully chosen to ensure maximum signal with minimum disturbance to the maser power.

Preliminary investigations in our laboratory, however, has yielded promising results for this technique. We are also investigating probe configurations and sensing schemes that will enable the implementation of this technique effectively, in newly designed and existing masers.

Acknowledgements

This paper presents the results of one phase of research carried out at the Jet Propulsion Laboratory, California Institute of Technology, under contract sponsored by the National Aeronautics and Space Administration.

REFERENCES

1. Kleppner, D., Goldenberg, H. M. and Ramsey, N. F., Phys. Rev. 126, 603 (1962).
2. Audoin, C., Revue Phys. Appl. 16, 125 (1981).
3. Wang, H. T. M., Proc. 34th An. Symp. on Freq. Control, (Philadelphia, PA, 1980) p. 364.
4. Peters, H. E., Proc. 36th An. Symp. on Freq. Control, (Philadelphia, PA, 1982) p. 240.

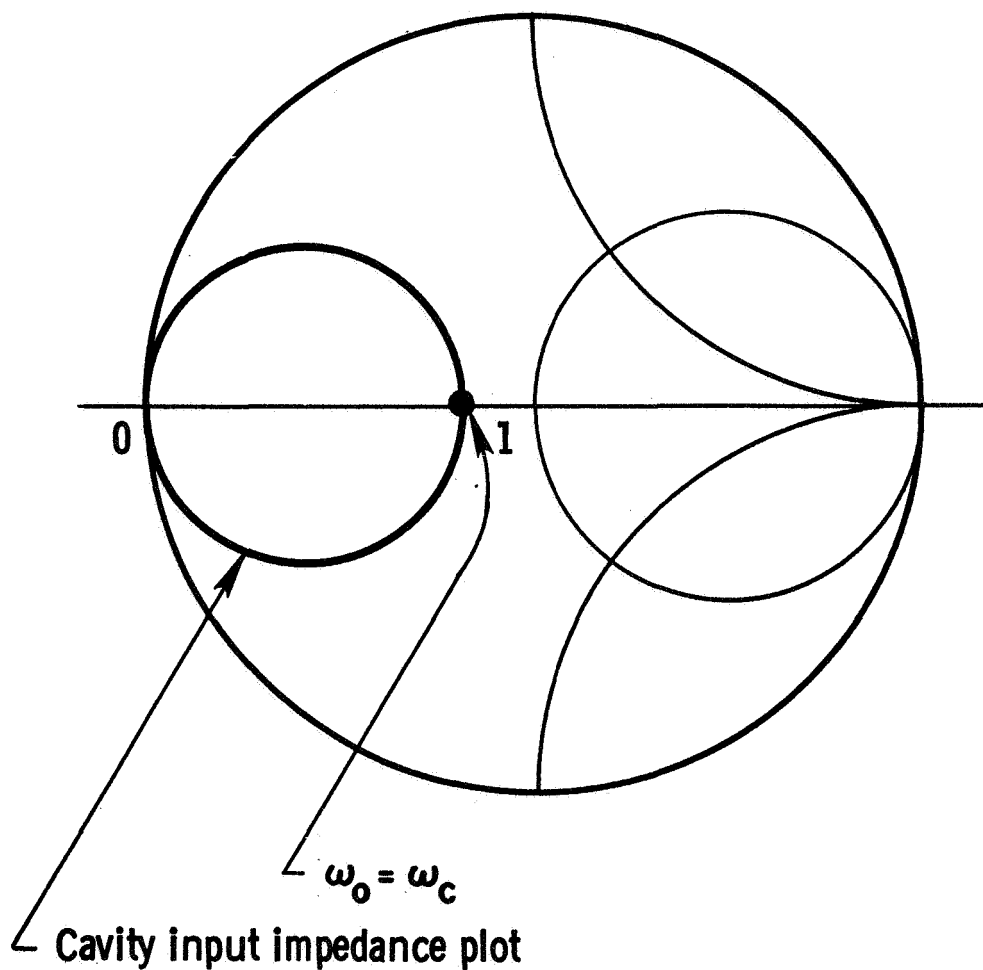
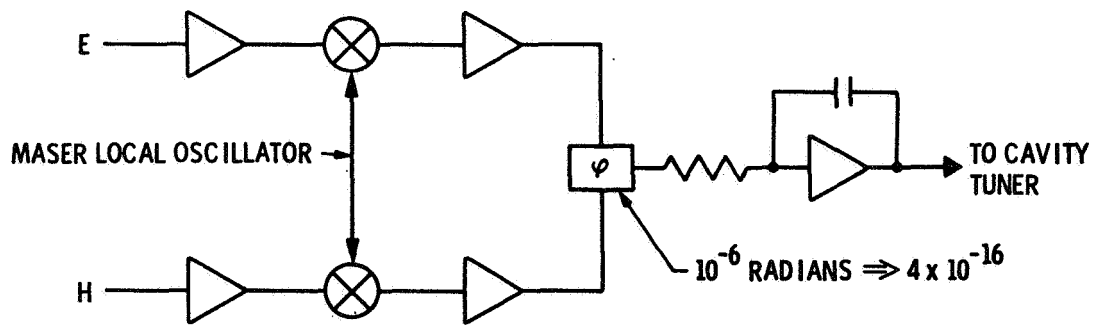


Fig. 1 Normalized cavity input impedance versus frequency presented on a Smith chart.



ELECTRONIC BLOCK DIAGRAM

FIGURE 2

QUESTIONS AND ANSWERS

DR. R. F. C. VESSOT, Center for Astrophysics, Smithsonian Observatory

I guess it was expected. I look upon this process as a sort of a horse race between the stability of electronics and the stability of the cavity, and it appears to me that no one knows really which way it will go. We are trying it, too, but we have found that we can inject substantial signals in the cavity without sensibly changing the output frequency. It's the old Bloch-Segert effect, and Bloch and Segert are correct. If one is very modest in his injection power and spaces it far enough away, there is another way that you can operate without suffering too badly.

It is clear that something ought to be done. I just feel that there is more than one approach to this that has about the same promise, including looking again for cavities that don't move.

DR. R. L. SYDNOR, Jet Propulsion Laboratory

I agree with you. We have not been able to duplicate the injection of signals into the maser cavity without altering the frequency, and Al Kirk has made a number of measurements of this trying out different amplitudes and positions away from the center frequency. It depends partly on how finely you measure how much offset you have, so we're not too happy with that since we have not been able to do it successfully. If you can do it successfully it sounds like a great idea.

SESSION VI

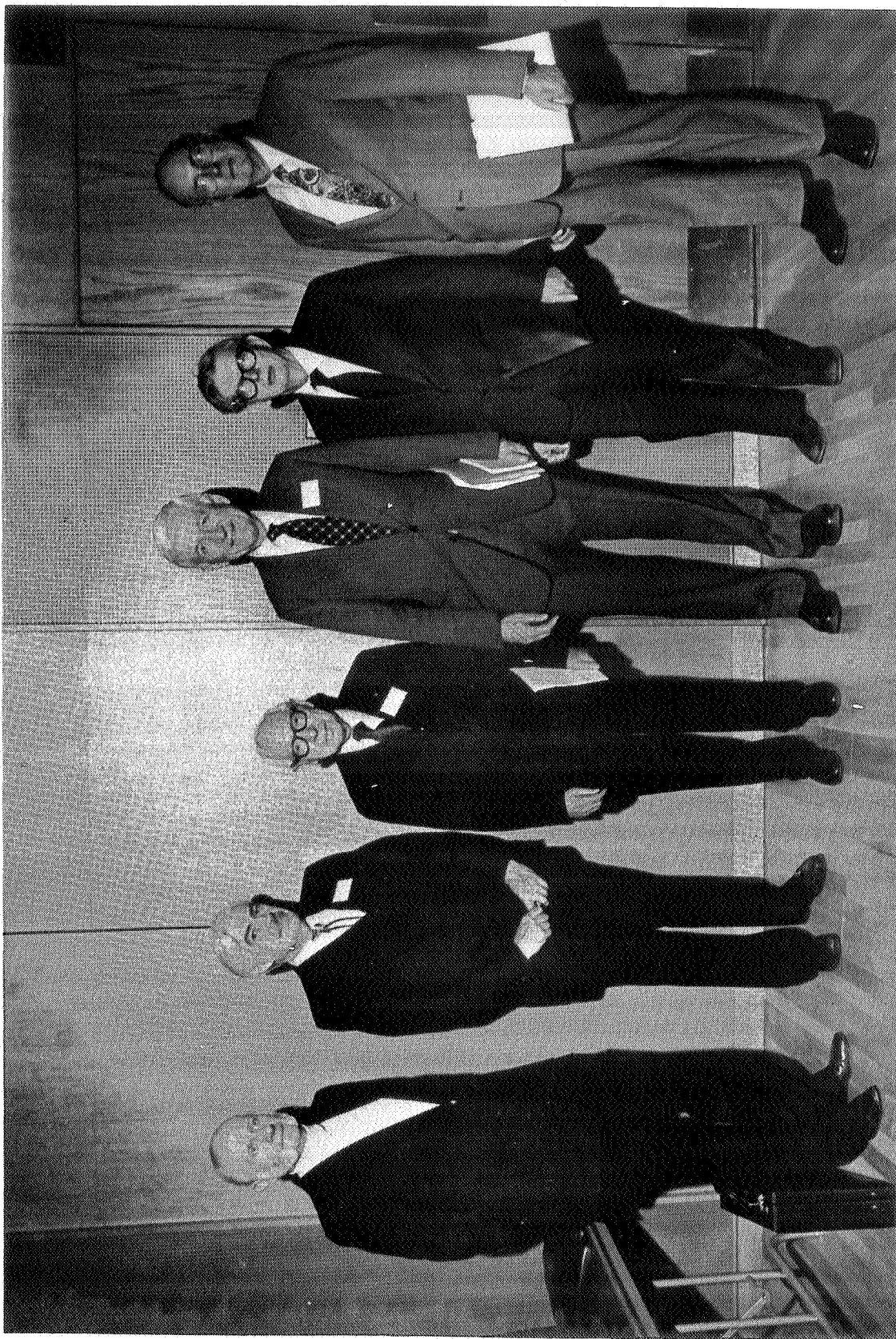
DISTINGUISHED SCIENTIST PANEL DISCUSSION

Dr. Richard L. Sydnor, Chairman
Jet Propulsion Laboratory

INTRODUCTION TO
DISTINGUISHED SCIENTIST PANEL

DR. R. L. SYDNOR: I am very pleased to introduce our panel here. I think they actually probably don't need any introduction. Professor Rabi, of course besides his innumerable prizes and awards, positions in and out of the Government and academia, is well-known as the man that probably started the whole development of the atomic standards we have today.

We have collected these people at great expense to come and discuss some of their views with you. I will let Professor Rabi introduce the panel and lead the discussion. Professor Rabi?



Distinguished Scientist Panel (from left to right): H. G. Dehmelt, R. V. Pound, I. I. Rabi, N. F. Ramsey, R. H. Dicke, and C. H. Townes



Distinguished Scientist Panel (from left to right): N. F. Ramsey, C. H. Townes, H. G. Dehmelt,
I. I. Rabi, R. H. Dicke, and R. V. Pound

DISTINGUISHED SCIENTIST PANEL

Panel Chairman: Professor I. I. Rabi, Columbia University

Thank you. I am delighted to see what happened to a suggestion that I happened to make years ago at a Richtmeyer lecture, it was either in 1944 or 1945. It is something which I didn't publish. I was asked to give this Rickmeyer lecture at the annual meeting of the American Physical Society and also the American Physics Teachers.

This was during the war, and as you might guess, we were very busy. The question was what to talk about, and so I began to think of what we were doing, not in the war but what had happened before on the state-of-the-art. Now as an admirer of Einstein through high school, college, and graduate school, I was very familiar with his notion of an atomic clock. When he spoke of a clock in relativity and so on, he meant that somehow in nature there was such a thing as a clock, which is working according to the laws of nature, such as they are.

So that seemed to be the ideal thing. We always thought it was, and then I realized that, to give this talk, there was an atomic clock, and there was the atom, there were those frequencies. And I suggested this, not in any detail, but enough: This would open a rather basic field of using the basic clock of Einstein for other scientific or practical purposes. I didn't write this out but I gave this at a lecture.

Present at the lecture was the science writer for the New York Times, William Lawrence, and he published it in the New York Times, in a column, about the atomic clock. That is the way this thing was born, came to public attention, as far as I know. I have never investigated it historically but there is a fine paper here, which I have not yet read, by Norman Ramsey which goes much deeper into the subject. My points are personal reminiscences, not historical in the sense of a historian's footnotes.

This is about as far as I went. Of course, this received quite a bit of publicity from the New York Times, absolutely free, unintended publicity, and I was approached, I think it was by the Bulova Watch Company, who wanted to give me \$100,000 to make this clock. My interests were otherwise and I really had never worked for a private concern, and I turned it down. But Gerald Zacharias took it up, and other people in England, the Bureau of Standards, and so on.

And cesium, I think I mentioned cesium, I'm not sure, cesium seemed to be an ideal substance for this thing. I don't think it can be patented because it was announced. My name wasn't on the publication but a famous reporter was on it, so that's about the historical basis, the only real connection I have had with the atomic clock.

I did feel then, and certainly now, that when you have a new device, you open up a new avenue in physics, great things are bound to happen in time, because I don't think, much as it may look right now when we have a unified field

theory and all that sort of thing, that physics by its very nature will not be a closed system; that nature will hold surprises for us all the time.

A story which I have told often is my visit to Max Born in 1928 with Professor Otto Stern. When we came in, I stood in great awe of Born for all his works, in a certain sense the founder of the use of matrices in quantum mechanics, Max Born announced as we came in that "Physics will be over in 6 months."

It was quite a blow. I was a fresh-caught Ph.D., I was a post-doc, and there it was, over in 6 months. He said, "Of course, there will be a lot to do but physics as we know it will be over because the shock of the DIRAC equation and what it did for the electron was really traumatic." It came right out of the relativistic equation, right out of relativistic wave mechanics.

And he said, "Of course, in 6 months we will have the proton. Of course, there will be a lot to do." And I thought to myself, "This is a great man but he has limitations."

To use Einstein's models, "der lieb gott" dear God is not so limited in physics with the DIRAC equation. And this has happened: As the advances in instrumentation have been made, more and more new phenomena have been discovered, unexpected phenomena.

To me the most remarkable thing, apart from the electron spin, was the polarization of electrons, beta decay the same as mu mesons. If you are a simpleminded experimental physicist and think of an electron or a mu meson, it is a marvelous thing. It has a spin, it has a magnetic moment, it has mass, all sorts of charge. I don't think that we will know all about it or do know all about it, despite the fact that we have excellent equations which will describe a lot of the phenomena we know.

So my feeling was and is that if we drive our experimental techniques to the limit to which we can, it has always turned out in the past that a new phenomenon will be discovered, a new aspect of nature. One of them now that is just being talked about, that people all over the world are working on it, is the possible decay of the proton. We're not accustomed to the proton decaying but we have not lived 10^{31} years and we can't say too much about it.

But almost everything -- and go to the history of physics -- almost everything which was deeply believed as an article of faith has usually been, turned out to be wrong, possible irrelevant. So I am delighted that this measurement of time, particularly time intervals, is moving ahead as rapidly as it has been. I am sure in some respects, either in atomic physics or nuclear physics or astronomy, and maybe even geology -- although one doesn't think of precision measurements of time with respect to geology, I think it will come in -- that you are opening a new field for greater and greater understanding of time.

I just wanted to add that we do have senses which give us a direct feeling for and understanding of space but not of time. Time is really an artificial thing, and dependent very much on the invention of a clock. We have not yet, to my mind, decided what a good clock is, a sensitive clock to measure divisions. What a real good clock is, I don't know, but what time means in quantum mechanics, basically when you get down to it I know how you put it in an equation but I don't know how to talk about it, let's say, to my grandson who is not a scientist.

So I am just quite inspired to be with a group of people who are so interested in pressing on with this problem of time and this measurement, particularly the interval measurements.

Now we are supposed to have a discussion amongst the people here. We have gotten together beforehand and have come to no conclusion on what to present to you, both for your entertainment and possibly edification, and perhaps a deeper look into how these things were and these eminent scientists we have assembled here.

I have no way of starting, except I think I will start with my right, with Norman, especially since Norman has a paper here on the whole business.

DISTINGUISHED SCIENTIST PANEL

Panel Member: Professor Norman F. Ramsey, Mt. Holyoke College

After Dr. Rabi's remarks, I shall add an additional reference to the paper on the History of Atomic Clocks which many of you received as a preprint at this meeting. This reference will be to Rabi's Richtmeyer Lecture and to the New York Times.

I think Dr. Rabi was unduly modest in listing his contributions to the precision measurement of time. This whole subject, in my opinion, really goes back to his earliest work on the molecular beam magnetic resonance method; the invention of magnetic resonance method for molecular beams is where the precision clock started even though the work at that time was initially directed towards the measuring of magnetic moments. The magnetic resonance method was a great invention, enabling magnetic moments to be measured to parts in 10^5 or better instead of 5% or worse.

For my remarks I have chosen to review the history of three important atomic clock developments subsequent to Rabi's initial invention of the molecular beam magnetic resonance method. These developments are ones with which I was particularly concerned. One development was the transition from the period of the resonance method as primarily a method of measuring magnetic moments to essentially molecular beam spectroscopy or radio frequency spectroscopy, as we eventually called it in an earlier paper. My second topic will be the early history of the separated oscillatory field methods and the final topic will be the early history of the hydrogen maser.

When Dr. Rabi first proposed the molecular beam magnetic resonance method, he had the courage to start two different projects on it at the same time. Kusch, Rabi and Zacharias developed a technique for measuring magnetic moments of alkalis while Kellogg, Rabi, Ramsey and Zacharias did the same thing for the proton and the deuteron. We knew the latter would be more difficult. On the other hand the proton and deuteron were particularly important nuclei to measure.

Starting from the point of view of trying to measure the magnetic moment, the first results for the proton were in some respects pleasing and some respects terribly disappointing. What we expected to get was a nice, sharp resonance from which we could determine the peak of the curve. Instead we got something much even worse than the top figure of my transparencies [Fig. 7 of Phys. Rev. 56, 737 (1939)]. Unfortunately, it was so bad I don't know anywhere that that is preserved. There was a somewhat bigger peak in the middle but just a bunch of fuzz in the background which we couldn't interpret. Nevertheless we found that that central peak shifted with the magnetic field the right way for a magnetic moment, and then we discovered that with deuterium we got a good peak. In this way we could get the magnetic moments, but it was clear that we ought to get better resolution to see how much of the peculiar

resonance shape was apparatus effect and how much of it was perhaps something intrinsic. There was also the problem at that stage though, since I was a Ph.D. student, what does the Ph.D. student do for his Ph.D?

It was decided that I should study this fuzzy background for my Ph.D. thesis while Kellogg and Zacharias were constructing the next round of equipment which was going to have higher resolution. Basically, what I found during the summer -- this was during the summer of 1938 -- was that if one lowered the amplitude of the oscillating magnetic field the resonance shape got steadily better. Unfortunately I dropped the amplitude in too-small steps. I would drop it a factor of two and when I found it was much better, another factor of two. I should have done it in factors of 10 and it would have gone a little faster. It took about 2 days to get one of those curves, because each point was taken very slowly. At low enough oscillating field amplitude it became apparent that there were several resonances, as in a spectrum.

At this point it began to become clear that we were studying spectroscopy, not just measuring magnetic moments. There really did seem to be at least five resonances and perhaps six, if you wanted to consider one as a double resonance (Fig. 8 ibid.). At the end of that summer, the newer modifications of the apparatus being made by Zacharias and Kellogg were completed, and then we obtained the bottom curve (Fig. 6 ibid.).

It was essentially this work that marked the transition of the magnetic resonance method from just the measuring of magnetic moments to spectroscopy. Also, a key thing was that the distance in frequency between the left most peak and the right most peak was independent of the strength of the magnetic field and therefore did provide something that was field-independent as is required for a clock. Other than that, the device was really more of a magnetometer.

In the summer of 1938, I also did similar studies with deuterium. Initially there appeared to be a single, nice isolated peak, but when I studied it with a little more care over that summer it became apparent that there were really subsidiary resonances in the background there, too. [Fig. 1 of Phys. Rev. 57, 681 (1940)]

Again with the improved apparatus that was being made during the same summer, we later obtained a resonance curve similar to the bottom curve where there was clearly one very marked resonance and several subsidiary ones. At this point it was quite clear that we were studying radio-frequency spectroscopy, the first step to something that would be a good basis for an atomic clock. Again, the separations of the subsidiary curves from each other were approximately magnetic field independent.

A year or so later Kusch, Millman, and Rabi found a resonance with lithium 7 in zero magnetic field, by looking at a transition for which there was a relative reorientation of the electron and nuclear spins. Such a fixed frequency resonance provided the bases for an atomic clock.

I think these comments essentially cover the period of transition from magnetic moment measurement to the potential, at least, of a clock. Subsequently many developments led to the later clocks.

Now the second thing I would like to say a little bit about is the development of the separated oscillatory field method which is used in almost all of the cesium clocks.

In the case of the invention of the separated oscillatory field I had just gotten a new job at Harvard and I was trying to build up an experiment. One of the experiments that I wanted to do was to do a more precise job in measuring the interactions that we had discovered with H_2 and D_2 . In one sense the obvious way to do so was to make the apparatus longer because by the Heisenberg uncertainty principle, the longer the atoms are in the apparatus, the longer the time Δt and hence the smaller the ΔE , the uncertainty in the width of the resonance.

But I also knew from our Columbia experiences that this didn't work. It didn't work for the following reason: if one increased the apparatus much longer than we had at Columbia, the inhomogeneities in the magnetic field were so great that the line became broader rather than narrower because the field was lower at say the final end of the oscillatory field region than it was at the beginning. The question was, how do you overcome this. While I was still building the new apparatus and not quite sure how to overcome this difficulty, I was giving a course on physical optics at Harvard. The time came to talk about the Michelson stellar interferometer. One of my friends in Cambridge, England, describes the Michelson stellar interferometer as follows: If you have two stars that you want to distinguish, if you have a big telescope that doesn't quite separate the two, and if you borrow a can of black paint and paint over all the middle of the telescope except for leaving two little slits at the edge, you double the resolution of the apparatus and can thereby resolve the stars. This procedure has the added advantage that it doesn't make any difference how bad the glass is in between because, clearly, what is under the black paint won't make any difference.

Well, I was in the midst of describing this in these terms to my class, when I thought, "Wouldn't it be nice if we could do the same thing with our magnetic field, some how wipe out the middle of it." Eventually I realized that the analog in that case would be to put an oscillatory field at the beginning and an oscillatory field at the end, whence indeed one obtains a resonance that is twice as sharp as it was before, and in addition it doesn't make any difference if one has moderate fluctuations of the magnetic field in-between, because they average out correctly. That is essentially the origin of the idea from which, the separated oscillatory field resonance method came. Subsequently many modifications and further extensions were added.

The third thing, I would say just a word on is the invention of the hydrogen maser. I have an analogous history in that case. For this history I am especially sorry that Professor Zacharias is not here. I was hoping that he would be. One of the things that stimulated this invention was the disappointment I felt when Zacharias proposed the so-called fountain experiment. This

was a brilliant idea. Namely, he was going to do molecular beam experiments much sharper than people had done before, increasing the time and getting the benefit of the Heisenberg uncertainty principle by having the beam shoot up and then fall down under gravity. It is well known that anything, whether it is baseballs or atoms, take around a second to go up 16 feet or so and come back down again, and therefore we would get an immensely fine resolution.

Unfortunately, this experiment failed to succeed because there weren't enough very slow molecules. They just weren't there, presumably due to scattering. The Maxwellian velocity distribution in practice dropped off to zero, so although the experiment was a failure the idea was a good one. I was thinking, "Why didn't I think of that?" Well, at the same time I was also, in my split personality, helping with the design of a big accelerator being built at Cambridge with a 236-foot diameter ring, and we were proposing this to be constructed. This machine was eventually constructed but the time of concern was in the early phases of it.

There is always the worry when you are proposing a multimillion dollar machine: "What do you do when it fails?" Well, one thing would be to convert the tunnel to a great molecular beam. You would have the molecular beam go around in a circle and keep it there a long time, and hence get a very high precision. I realized you could do this with an inhomogeneous magnetic field to confine the beam to a ring. Then I also realized, alas, that this is just the wrong thing to do because if you have an inhomogeneous magnetic field and are trying to look at the spectrum with high precision, you of course broaden all the lines. If you have an inhomogeneous field and some of the atoms are in one field and some in another, it would be fine for trapping the atoms but it would be no good from the point of view of spectroscopy. Incidentally, something like that is currently done now by Wolfgang Paul with neutrons, but for measuring the neutron half-life.

Well, having realized that problem, then I also realized what was really needed. It was much better to have an intense interaction for a very short period of time rather than an inhomogeneous field essentially present all the time. The limiting case to that was to put a box around the ring, essentially a long tube and have the confined atoms there. Well, then I realized that you could do even better than that if you closed up the ends of the tube. If the atoms are going to hit the walls of the tube, you might as well let them hit the ends as well. Eventually this led to an experiment which was done by Dan Kleppner working with me for his Ph.D. thesis, the so-called broken atomic beam experiment where we made a box and a beam of atoms came in, as in a molecular beam resonance experiment. We let them undergo four or five collisions and come out in a different direction, and measured their transition and did indeed get a resonance, but it then became apparent to both Dan and myself that we would do very much better with atomic hydrogen than with cesium, which was being used for the first run. Cesium tended to stick on the surfaces, but then hydrogen has the disadvantage of being very hard to detect. So we thought maybe we could detect the radiation, and then eventually realized we could in fact detect the radiation very well. Then we also recognized that the system could be a self-oscillator or an atomic hydrogen maser, analogous to the molecular ammonia maser that had been developed earlier by Charles Townes.

It is from this that the idea for the atomic hydrogen maser came. We realized that atoms could be used in such a confined box. This also differed from what had been done, say in optical pumping, where at that time extensive amounts of buffer gases were used to narrow the lines and retain the atoms.

In this case we realized we could do it with aligned beams from using the molecular beam technique, and then have a box initially with paraffin-coated walls. Then we discovered experimentally that it was better to do it with Teflon, which has been essentially the standard thing in hydrogen masers since.

Well, so much for past history. I'll conclude with a brief remark about the future, I fully echo Dr. Rabi's views that there is much to be said for precision measurements. Out of them come unexpected things. At one time we thought that there would be no interest in clocks if they were more accurate than a part in 10^7 , and now it is quite clear that each time we make a step forward, there is a small revolution. Now most highly accurate measurements are reduced to the measurement of a frequency because frequencies can be measured so well. Precision measurements of almost all quantities now remind me of my mother's story of a doctor who could cure only one disease -- stomach ache -- but he became a great doctor because he also knew how to reduce all other diseases to a stomach ache.

Well, this is basically the procedure for almost all precision measurements at the present time. We know how to measure one thing very accurately -- time and frequency -- and therefore the big advances in all other measurements have come from figuring out how to reduce those measurements to measurements of time or frequency. As a result, precision time and time interval measurements are at the heart of nearly all precision measurements at the present time, and I believe that in the future this will be more true rather than less true.

Thank you.

DISTINGUISHED SCIENTIST PANEL

Panel Chairman: Professor I. I. Rabi, Columbia University

Thank you very much. We now, I suppose, have done the pre-War effort which resulted in the measurement of time with atomic clocks, we will go on to Professor Townes. I don't know whether he got into this act before the War but he certainly did after the War. That will perhaps conclude the Columbia contribution.

DISTINGUISHED SCIENTIST PANEL

Panel Member: Professor Charles A. Townes, Berkeley University

Thank you very much. It is a great pleasure to be with this group of people again, whom I used to see frequently and from whom I have received a great deal of instruction and inspiration, but I have been out of the field now for some time.

Looking back, one can see in this field, as I think in so many fields, a burst of activity in a field which was considered classical and more or less finished. I think that is very typical of how science has developed. I was with Bell Telephone Laboratories during the early forties, and I was doing microwave spectroscopy, one very precise measurement of the frequency of microwave lines. Bell Laboratories was one of the most expert places in time measurement. Quartz crystal oscillators were the thing, and they were fantastically good, at least as good as a part in 10^8 , and if one had a collection of them then perhaps you could approach a part in 10^9 , and that seemed just awfully good. Of course, we do a million times better now but there were people who had been working on it a good fraction of a lifetime. They knew all the answers. They had worked on it very hard. Quartz crystals were supreme, and they had just reached the limit of the technique.

What was needed, of course, was a completely different approach which by now has changed the situation, and furthermore, in changing the situation has made the quartz crystal people look again and find in fact they could do a lot better with quartz crystals than they ever thought they could before. As I say, I think that is fairly typical of how scientific fields develop. Currently the quartz crystal people are doing remarkably well and considerably better than what was felt to be the limit.

And I might quote the field of amplifiers, where people have worked on sensitive amplifiers for many years, derived theories showing what the limits were, and the limits were good but not as good as we have today. When maser amplifiers came along, which improved the sensitivity by a couple of orders of magnitude, then people began to think again about some of the classical techniques and new techniques. Now many of the classical techniques do almost as well as masers, and the whole field has proliferated into a wide variety of techniques for very fine amplifiers, simply because people were forced to challenge, to look rather more thoroughly than they had before.

In each case you see new ideas have come in from elsewhere to stimulate the field to get going again.

Now when I was trying to measure the frequency of lines, there was some very remarkable work that Bob Pound had done, stabilizing microwave oscillators on cavities, and that was spectacular in its day, giving fantastic stability. You've got the stability of a cavity rather the stability of an electron tube as an oscillator, and we used some of those to stabilize oscillators

but it became apparent to me that while actually microwave lines and microwave spectroscopy was just developing, they were essentially as good as quartz crystals and probably better than cavities.

As everybody is pretty well aware now, I think, there are two aspects to getting high precision. One is getting good enough signal-to-noise, and that could easily be done in microwave lines or, for that matter, in stabilization on a cavity. The other was a high enough Q, and one which is stable and not affected by the surroundings. Microwave lines had a higher Q than normal cavities by an order of magnitude or so, and so pretty quickly I was examining the theory of how well one could do by stabilizing on molecular lines.

Now I have never really built an atomic clock myself, at least not purposely. I was interested in the theory, I was interested in using them, and I built them somewhat more accidentally. Harold Lyons built a clock based on stabilizing a microwave oscillator on the ammonia line, in much the kind of general technique that Bob Pound had introduced, and I remember very well his wanting to call it an atomic clock, and I kept saying, "Well, it really is a molecular clock." But this was 1948 and he said, "Well, you know, everybody pays much more attention to the atom these days. It's got to be an atomic clock and there are atoms in it after all."

Now the trouble with molecular lines for a random gas was that the Q was still not terribly high, so a frequency could be pulled by a variety of external influences, and of course this is where Dr. Rabi's suggestion of using molecular beams and a variety of other techniques for longer-lived transitions obviously in the long run would be more stable.

Nevertheless, when the maser came along the maser added one thing, in giving a spectacularly pure frequency. Its long-term stability at that time was not terribly good. It was better than gas lines because we were using a molecular beam. It had a longer transit time so it had an improved Q by, again, another order of magnitude or so, and it was a pretty good clock but its real contribution, I think, was the purity of the spectrum over short lengths of time.

And then Norman Ramsey's invention of the hydrogen maser added that to a really very high Q system and made us a beautiful clock.

Now I think another interesting aspect of the developments of fields when there are breakthroughs and new ideas introduced, is their proliferation into other fields. Norman has mentioned some of that, the use of these new ideas in a wide variety of ways, and of course time has been very important in a variety of aspects. But when I had to face giving this talk and read what we were supposed to do, to talk about the historical context of development, I decided that maybe I had better go back and look at some of my papers and see what I was saying at that time, in order not to kid myself as to, in retrospect, how things looked.

I am going to put you through the reading of a paragraph of one paper of 1961, which was one of the applications of precise time or precise frequency measurements. Now in 1961 there were a few lasers in existence, just a few types, and this was a meeting of the Second International Quantum Electronics Conference. It happened to be meeting in Berkeley, and I had been in Washington for a couple of years and really not doing very much physics but I was supposed to give an introductory talk, so I had to say, "Well, let's look at the future, what kinds of things might be done." You may be surprised at what I said at that time, simply because it all seems so obvious now, but because I was saying it at that time to a sophisticated group of people, we'll have to assume it wasn't completely obvious. Here is what I talked about, one of the things, one of about five experiments I talked about:

"Maser techniques will probably make possible frequency multiplication from a radio frequency of microwave range into the visible and ultraviolet regions." Now I said "maser" which I was using at that time in a general sense; the maser, of course, the principle is operated at any frequency.

"It should be remembered that physicists have never directly measured the frequencies of infrared and optical radiation but rather they measure wavelengths in this region and then compute frequency from a knowledge of the velocity of light, accurate to about a part in a million which was the accuracy of the velocity of light at that time. Frequency multiplication up to visible regions should allow these frequencies to be directly counted, and hence measured in terms of our standard of time. Our standard of length is now defined in terms of the wavelength of visible light; hence, a measurement of its frequency should allow immediately a determination of the velocity of light to a precision as great as that to which length is defined. The measurement of frequencies in the optical region to precisions greater than about 1 part in 10^8 , to which length is now defined, will in fact connect length and time together through the velocity of light so firmly that perhaps separate standards of length and time would no longer be appropriate. Time, which can be measured and defined more precisely than can length, might be taken as a fundamental defined unit and length then derived from it by taking the velocity of light," and so on.

Well, as I say, all that seems fairly obvious at this time. I had to go and describe how one could hope to get frequency multiplication and beats and so on in the optical region in order to get that, and I don't think it was taken awfully seriously at the time but of course people have done very beautiful work in this range now, and we in fact, now use time as a standard of length.

A couple more things I want to mention as a way in which these things come back on themselves, spread out into other fields, and interact: I haven't worked in this field for a long time. As I say, I never really built any good clocks because I was mainly interested in using them and in the theory, but much of my work depends on that and quite recently I have been interested in interferometry, spatial interferometry, Michelson type spatial interferometry, and

I want to remind you of what time really was at some time in the past, and that is a measurement of the rate of the rotation of the earth. That was the definition of a second. We no longer use that as a standard anymore because that rate can't be measured accurately enough, and anyhow it's not all that constant.

Nevertheless, the rate of rotation of the earth is still of some importance to various things, such as navigation and the study of the earth itself, and interferometers built primarily from astronomical interest, spatial interferometers which measure the position of stars, are now going to give us a substantial improvement, I think, in the measurements of the rates of rotation of the earth.

There are a number of kinds: radio interferometers, and you know the connection between radio interferometers and timekeeping, radio interferometers which will measure positions of quasi-stellar objects, for example. There are infrared and optical interferometers, I happen to be working on infrared but optical interferometers are being built of good quality, and all of these will measure stellar positions considerably more accurately than we have been able to do in the past. It seems really quite likely we will be able to approach a precision of about a part in 10^9 in the rate of rotation of the earth in one day, and of course in longer times the precision can build up.

Now the measurement of the rotation of the earth is a kind of a dirty problem, though. It's not exactly fundamental physics. The real limitations in the long run are the behavior of the atmosphere, because we have to propagate waves through the atmosphere in order to measure the position of stars, and the motion of bedrock. Those are going to be the primary limitations. As we improve techniques, we will find out a good deal more about just what those limitations are, and of course already the motions of bedrock, continental drift, and tidal motions and so on are being determined, and presumably all of this will contribute to some extent to atmospheric and earth physics.

I think that is all the comments I will try to make at this point.

DISTINGUISHED SCIENTIST PANEL

Panel Chairman: Professor I. I. Rabi, Columbia University

Thank you.

We did not get together and tell one another stories of what we were going to tell you, and this has been fascinating to me and perhaps the rest of you as the story comes out from Norman Ramsey and Charlie Townes.

I did say somewhat humorously that these frequency measurements that you are doing, time measurements, will ultimately be related to geology. There you are. Townes has just closed this, so there is no field in which this time measurement, especially intervals and perhaps in very short intervals, will not yield a great deal of basic knowledge. Of course, I spoke a little earlier more in fundamental knowledge, the use of the whole concept of time and its relation to the structure of physics.

One of the most fascinating series of experiments, which fascinated me through the years, were the experiments which were done in Heidelberg and the use of this technique developed by Kastler of optical pumping, which later on found use in Kastler's laboratory in Paris. These methods and these techniques were used to demonstrate mostly quantum mechanical properties of light and the analogies and very brilliant theory, and beautiful experiments, but I was very much impressed that in Heidelberg these methods were applied to molecular beams yielded new results of a fundamental nature.

I hope to hear and learn more of the thinking of our next speaker, of those experiments and the fascinating things he is doing now on a man-made artificial atom, namely having a single electron or positron floating around under his control at his time. Won't you please --

PROFESSOR DEHMELT: Mr. Chairman, as the youngest member of this group, may I pass for the moment?

PROFESSOR RABI: Very good. To whom do you wish to pass the torch?

PROFESSOR DEHMELT: Well, the next man in line.

PROFESSOR RABI: We have two. Which one?

PROFESSOR DEHMELT: Dicke.

PROFESSOR RABI: Alright, you are nominated.

PROFESSOR DICKE: I don't know whether I should pass or not.

PROFESSOR POUND: We'll have to get out the birth certificates.

PROFESSOR RABI: Well, the rules are such you don't have to give a reason for passing.

DISTINGUISHED SCIENTIST PANEL

Panel Member: Professor Robert H. Dicke, Princeton University

Well, I thought I might say something about the origin of the rubidium clock that occurred in the early fifties and mid-fifties at Princeton, but I think before starting on that I should remark that it is rather interesting to look at the membership of this panel to discover, really, with the exception of Hans, two roots only -- the Columbia root and the Radiation Laboratory, with overlapping membership.

I was one of those who after the War, with microwave techniques in hand, thought it would be nice to use these for doing some physics, and I thought, "What kind of physics?" Well, I thought, what are really the most fundamental things you could hope to do? One of these that occurred to me was, look at the structure of hydrogen in an excited state.

Well, I started work on this but discovered that Willis Lab at Columbia had already a head start, so I stopped that, and then went at a harder experiment which was the G factor of the electron. When I talked to a famous theorist at Princeton about this he said, "Dicke, why do you waste your time? Everybody knows you can calculate that number."

But that experiment, really, I tried a number of approaches and it really ultimately turned out to be too hard. Had I waited some 20 years, I think it might have been successful and I may just have carried it off, to trap a single electron or three electrons and to measure this.

Well, from this we turned to --

PROFESSOR RABI: If I may interject at this point in this story, on your very good advice, when Otto Stern decided to measure the magnetic moment of the proton it looked rather absurd to the theorists because they knew what it would be it has a spin $1/2$ and an electronic charge, so again this question came, "Why are you wasting your time?"

Well this was at a meeting with a number of theorists, and Otto Stern passed around pieces of paper for each one to put down the value which he would find. It seemed to be a rather absurd proceeding because they knew what it would be from the DIRAC theory on the electron and the proton.

PROFESSOR DICKE: The same scheme. It happens twice, the same mistake.

PROFESSOR RABI: He passed this around and got all these things together, and later on when he did measure it, of course they were all wrong and it was about three times as great, a circumstance which is not yet understood. So don't listen too hard to theorists.

Listen very carefully but don't follow their advice. That's more important. Listen very carefully but don't follow their advice.

PROFESSOR DICKE: I knew the story. It's really surprising to have the same thing happen twice.

Well, the next two experiments of a precision type that are of importance that were successful, was an experiment by Jim Whitke, one of my graduate students, on the hyperfine structure of hydrogen in the ground state, and Ed Land, who measured the G factor in hydrogen. For these experiments and others that we were doing, we never used the atomic beam technique. We always used the gas cell approach of various kinds, and it early became clear that one needed to do something about the doppler width problem there if you wanted to get the highest precision.

And so the concept that one was familiar with, the concept of collision broadening a spectral line, the concept of collision narrowing came along, that you could reduce the effect of doppler under the right conditions if you introduced a buffer gas that would actually narrow the line. Jim Whitke first used this technique in his measurements of hydrogen.

At about the same time, Pete Bender did an optical pumping experiment on -- it must have been sodium that he used with a buffer gas, and about that time Tom Curver, who unfortunately died last year at a very early age, thought he would like to put his hand to the question of using these various techniques -- optical pumping, the collision narrowing of spectral lines -- on an alkaline metal to see what the possibilities of producing an atomic clock that way might be.

His area was pretty much his own. He was then later on joined by Carrol Alley, who is here in the audience, as a graduate student to work on this project, and then later on he collaborated with Arditi.

He thought carefully about the problem of using alkali metal to get this collision narrowing of spectral lines, to use optical pumping to get signal strength, and then the kind of circuitry that would go with this, and decided on rubidium. I guess that was a choice that continues to be the best one to this day. He had some good reasons for doing this.

The optical pumping was the kind that my student, Bruce Hawkins, had developed at Princeton. That was the same time as Kastler's work. We weren't familiar with Kastler's work but Kastler was clearly well ahead of us.

He sort of accidentally noticed that -- I think this was before Hans Dehmelt's discovery of intensity pumping, but when that came along that produced a greatly enhanced signal -- so I guess that is about all to be said on that. The first work on this was about 1953 or 1954, somewhere in there, and he continued to be interested in this for quite a long time, and later on it was taken up by others, and this is basically the origin of the rubidium clock.

I think that is all I have to say.

DISTINGUISHED SCIENTIST PANEL

Panel Chairman: Professor I. I. Rabi, Columbia University

I think rubidium had another role, wasn't there, Charlie? Wasn't rubidium what you used for the maser?

PROFESSOR TOWNES: No, we used ammonia.

PROFESSOR RABI: Ammonia, yes. I confused Zieger, who worked with you on ammonia, who previously had worked with me on rubidium.

PROFESSOR TOWNES: Oh, yes. Well, we needed Zieger's help, certainly. We also needed the big nitrous elements which ammonia had.

PROFESSOR RABI: Those are interesting questions. Since we are reminiscing about old times and how things came to be, as you know, Charlie Townes was at Columbia while we were doing the molecular beam work. Of course, to understand what was happening in these experiments with molecular beams and selection of states, with all due respect to Professor Ramsey, we knew about atomic spectroscopy and the spectroscopy of the waves which we used. They were not exactly microwaves then, but the important thing was the Einstein -- I come back to Einstein all the time -- induced transitions in an excited state in the molecular beams at those levels, at those frequencies which were being used, would live a very long time and we wanted, then, the atoms to move from one state to another, from a lower state to a higher state and also from a higher energy state to a lower energy state, and there you used Einstein's induced transitions, the idea which he introduced back in 1916 for the famous paper. He had arrived at the Planck formula but really was the basis for what happened later in the whole quantum theory, and leading to the Heisenberg dispersion principle.

It seemed that we might use something of this sort but when we calculated, the intensity was low. The question was, how could this radiation be detected? In preparing this famous lecture -- "famous" in the sense that I talked about it first -- the Rickmeyer lecture in 1924, I thought about this matter, and this was in 1924. Great, great improvements had been made in electronics. I said earlier about the detection of these transitions which led to the measurement of moments, that they could not be detected by electromagnetic means -- it was too weak -- but that you had to see the effect on the atom, and that's what the atomic method was about, but then in writing this I said, "Is this really true now?"

I went and spoke to buddy, Ed Purcell, and spoke to Henry Tani about this. They felt yes, the method was sensitive enough that they could detect those transitions, and induced radiation from those atoms. I also had my doubts about this and talked to Felix Wacht. This was during the War, and East and West were rather concentrated in Cambridge. Purcell was at the Radiation Lab and Wacht was at the Harvard Electronic Lab. This all occurred at the same time, as a result of my being asked to do the Rickmeyer lecture.

Various things indirectly came out of this, and one is the atomic clock and the other is the nuclear magnetic induction and other things like that. Something which was impossible, seemed to be impossible in 1940 -- as I was talking last night -- as the result of a war, a lot of people working in their field, it became possible four years later.

And now we have Professor Pound. We have two Harvard people now.

PROFESSOR POUND: Two what?

PROFESSOR RABI: Two Harvard people.

PROFESSOR POUND: Two Harvard people? Well, why not?

PROFESSOR RAMSEY: I am now at Mt. Holyoke, Professor Rabi.

DISTINGUISHED SCIENTIST PANEL

Panel Member: Professor Robert V. Pound, Harvard University

I thank Charlie Townes for perhaps, at least in part, giving some explanation of what I am doing here because I was asking myself that and I thought probably you were all asking that even more, because not many of you probably have coupled my role with atomic clock development.

It does happen that this project which in fact I got into by strict accident in the Radiation Lab -- it wasn't on the route of Radiation Lab's commitments, in fact -- the business of stabilizing microwave oscillators grew out of some customer of mine. I was in the business of making mixers and things like that for microwaves at the time, and Bob Dicke and I used to talk a good deal and Bob had introduced the concept of the "magic T" and a customer of mine asked me, had I any good ideas as to how to make a microwave discriminator. I said surely that has to be based on a "magic T" and after a few scribblings on paper, I came up with a thing that would play the role at microwaves, the thing that was used as a frequency discriminator in ordinary, low-frequency radio.

Then I said, "Gee, I think that could be used for purposes of stabilizing microwave oscillators, and so on the side I gave that a try and I was rather surprised at how much it did. Previous to that, if you took a couple of microwave oscillators like Klystrons and you tuned them, say, within 30 MHz of one another so that you used a 30 MHz receiver, communications receiver to listen to the beat note between them, you didn't hear anything much at all but a lot of hash and trash and so forth. I discovered that by making two of these things you could get a pair of 10 GHz oscillators so that they beat together and produced an audio tone. You used to be able to go up and down the corridors where you could hear my audio tone going, sort of wiggling around, but you know, it was wandering on the order of 100 cycles or so with a 10 GHz base, and I was sort of impressed that you could do this.

Actually, it has been mentioned that obviously -- Charlie said that the obvious next direction was to use, instead of a cavity -- which after all isn't a fundamental phenomenon and isn't the highest Q in the world, but to use instead an atomic or a molecular spectral line as the reference. In fact, you will find in my paper of 1946 that I so suggested, first of all using the cavity that was used to stabilize the oscillator as an absorption cell for studying microwave absorption, and then mentioned the use of what now would be called the Q-dip method, I believe, to lock the oscillator ultimately to the absorption line that might be so contained.

In fact, in the spring of 1945 some of my colleagues had the kindness, including Professor Rabi, of recommending me to the Society of Fellows at Harvard. Rabi claims he never would do that again.

But that is a special organization which gives one a 3-year term as a fellow of the Society of Fellows, and in order to get that way you had to go to an interview. I went to an interview in March of 1945, in which interview there were such persons as Alfred North Whitehead, and Paul Buck, Dean of the Faculty at Harvard, Faculty of Arts and Sciences, and a few other well-known people. Arthur Darby Knox, who was a professor of history of religion, who told me in his Cambridge, England accent that I would have to speak up because Professor Whitehead was quite hard of hearing, and here I was a 25-year-old who was to explain what he had in mind for the future to this committee.

What did I have in mind? I had in mind the development of an atomic clock for the purpose of comparing atomic to gravitational time, because I had been recently reading an article -- actually it was written by an Englishman named J. B. S. Haldane, who was interpreting and promoting the theories of E. A. Milne which suggested that there were two different time scales, kinematical and dynamical time, one of which being atomic and the other being orbital, and that his theory suggested that these two scales drifted with respect to one another by the fraction which represents the time of observation over the age of the universe.

Well, I looked at three years and the Hubble constant of that era, and that was a ratio of about 10^{-9} , and I knew that I could probably make an atomic clock that was good enough but I couldn't see how to measure gravitational time to that precision because I knew that the earth's rotation fluctuated by the order of a second per year if you measured it by looking at the star transits and so forth.

But I happily, or perhaps unhappily -- well, I guess it is happily -- a big diversion or deviation from that route occurred because of my collaboration with Purcell and Tari in the project that Rabi mentioned, in the first experiment which successfully detected magnetic resonance of nuclei in solids, which in fact weren't solid as we thought they were. That diversion took me away from that direction, although I must say that the concept of finding a reference system that would be useful for ultimate atomic clocks was always somewhere in the back of my mind. One of the reasons I embarked in the trade of pure electric quadrupole resonance, a field which Professor Dehmelt here scooped me on in a certain sense, I thought that there would be a case where there would be a high Q available. If one went to a pure electric resonance at a few thousand MHz and had dipole-to-dipole linewidths only, there should have been a Q of 10 million or so and those were big numbers in those days.

Well, I didn't get back into an active role with respect to the use of ultimate high-precision devices until suddenly the Mossbauer effect appeared on the scene, and we moved rather rapidly, and some of you may know about our employment of that method to measure the effect of the gravity on effective frequency of photons. There we measured shifts of 2 times 10^{-15} fractionally to 1 percent accuracy. We have been upstaged in the conclusions from those

measurements in more recent times by Bob Vessot and his colleagues at the Smithsonian and NASA, using the hydrogen maser in the rocket probe where the gravitation red shift was measured to better than a part in 10^{14} . However, they were measuring a much better effect than what we measured, so that the fractional precision of the measurement still belongs, the extreme in that area still belongs to the Mossbauer effect, and I thought I would just mention that in more recent times we have been playing with Mossbauer resonance whose Q is 10^{15} , 2 times 10^{15} .

Here is an absorption line -- I could show you a transparency that shows such an absorption line but I think you can imagine it -- in the Mossbauer effect one has an emitter radiating gamma rays through an absorber, and if the two are stationary with respect to one another and if a lot of other conditions are satisfied, there is an absorption of the gamma rays by a resonance process in the absorber, but if you move the one slowly with respect to the other, the doppler effect of that motion is sufficient to reduce the amount of absorption by putting things out of resonance.

The speed that is required to reduce the absorption for the case of zinc 67 is .15 microns per second, which is a rather slow motion. It is the kind of motion that results from about a meter per year, I guess, and you have to compare that with the velocity of light -- in other words, it is a meter over a light year -- for the fractional effect.

Now Professor Townes also mentioned that ultimately the use of time in the optical domain should be available by successful multiplication or a derivative of some device that is a coherent source in the optical domain, which can then be controlled or locked to some reference device, and I say that with this new Mossbauer effect we are able -- if someone will kindly develop a coherent oscillating source -- one can use the Mossbauer absorption as an absolute reference with a stability -- well, the resonance full width is 10^{-15} , so I think following the enhancement over the natural resonance widths of most other atomic clock references, this should get us into the domain of 10^{-21} , which is sort of another domain of interest.

Uhhappily, the attack time or the feedback rate that you could use for these things is rather slow because the signal-to-noise ratio is relatively poor, and it takes maybe an hour to develop a decent picture of that line shape at the present time.

One last remark, I think -- oh, I might have mentioned that in addition to the role of the original the ideas of stabilizing microwave oscillators, in 1949-50 Ed Purcell and I collaborated on an experiment which became published under the title, "A Spin System at a Negative Temperature." We introduced the concept of negative temperatures, which particularly pointed to the phenomenon of induced emission as a contributor to radiospectroscopy under the conditions of having inverted population states. I think that also played a role in the development and understanding of the techniques that led to the maser, at least so the Smithsonian people told me when they asked for the crystal we used in that as a part of their laser exhibit a few years ago.

But finally I was going to remark that there is also the question as to whether quantum mechanics is really at issue in things, say, like the problem with the Mossbauer effect, in addition to the fact that it is unlikely that it is going to end up being a maser in its own right. The case that I mentioned, for example, is a wavelength of .13 angstroms or a frequency of 2.5 times 10^{19} Hz, which is sort of high. It has a line width, therefore, of 25 kHz.

Now in some very narrow resonances, like in NMR, you find there are transient effects. For example, if you do magnetic sweeping in an NMR experiment, instead of seeing a nice absorption line, you see a thing which Purcell and I called the "wiggles" back in 1946 when we first had this annoying effect. When you sweep through a resonance, you do start to get an absorption but then there is a beat that appears. You can develop exactly the same picture by a combination of single-tuned circuits, tuning one and shock-exciting the other, and the after-ring of the shock excitation beats with the one that the frequency is moving away and you see the thing as a wiggle.

It turns out that in the Mossbauer effect you have precisely the same effect: Namely, if you look at this ultra-narrow resonance line of zinc 67, which has a dip in the ordinary way if you sweep through it quite slowly, you start sweeping through a little faster, the lines start to become a little unsymmetric in shape, and if you sweep through it in a time which is short compared with the coherence time, which is 10 microseconds, of this resonance, what do you get? You get the wiggles, exactly the same as in this quasi-classical case of the NMR line.

One of the curious things that is a pedagogical problem is that the wiggle, if you go with an absorber, then in the first wiggle the intensity transmitted through the absorber is greater than this intensity would have been at those times without an absorber, and maybe I will just leave you with the challenge of figuring out how that can possibly be. Who made the energy that appears in this overshoot, as it might be called? But it does tell one that the correspondence principle, and the fact that it is no problem to answer this problem if you think of the whole system as classical.

DISTINGUISHED SCIENTIST PANEL

Panel Chairman: Professor I. I. Rabi, Columbia University

Well, before we turn to the next speaker, Professor Dehmelt, I want to make a confession of which I am very proud and which has had an important part in the history of microwave spectroscopy.

During the war, I happened to be more or less in charge of magnetrons, and finding radar for higher and higher frequencies and better definition. One of the problems which we set ourselves was 1-centimeter radar. For that we had to make a 1-centimeter magnetron which would give power, and of course the Klystron that would go with it.

We worked at this, and it's a hit-and-miss affair but we finally got a magnetron that worked with high efficiency and a lot of power and got a Klystron made in that region and set up a wonderful radar. The radar was tried and we got some wonderful pictures of New York harbor with fine definition of all the streets and the piers and so on. Of course, when the rains came it turned out that we were precisely on the water absorption line. I knew we were in great danger of being there but once you've made a magnetron, scaling is easy for the circuits once you have it. So this is fine. We'll get this made, see how it works and then scale to the appropriate frequency.

Fortunately, the war ended before we could get this scaling done, and as a result we had those Klystrons, surplus, cheap -- and the Government sold them -- easily available for experimenters, and therefore microwave spectroscopy at that time. I'm not sorry the war ended and we were not able to fix the radar. It was a 1 centimeter radar but not an all-weather radar.

But it shows that if you are in a new field, even mistakes can be of positive value.

PROFESSOR TOWNES: A great contribution to science. It has to be opportunistic.

PROFESSOR RABI: It has to be opportunistic, yes, and use everything just as Chicago did. You use the squeal in the hog.

Now I will turn to Professor Dehmelt.

DISTINGUISHED SCIENTIST PANEL

Panel Member: Professor Hans Dehmelt, University of Washington

I have a paper which hopefully will address itself to the points which the chairman has raised, and also to entertain you to some degree.

In these days of cost-benefit, the case history of non-mission oriented work leading nevertheless to very useful contributions to development of new frequency standards may be of some interest. Having been a radio amateur since age 10, in my work in Kauffman Institute on radio frequency spectroscopy research for nuclear quadrupole resonants in solids was a natural choice. However, solids are complex and the electrons seemed to be a much more interesting particle than the closing nucleus for which I had just found the search for resonance in 1950.

Also, my teacher, Richard Becker, one day in his electricity and magnetism lecture, had drawn a dot on the blackboard, declaring, "Here we have an electron." Minding Heisenberg's admission that physics should concern itself with absorbers, I have wondered ever since how one might go about in the laboratory to localize an electron in free space.

For the time being, then, however, I made do with my nuclear quadrupole resonance spectrometer in a search for the 400 MHz hyperfine line in potassium vapor, but I couldn't find it. Having been invited to work in Walter Gordy's laboratory in this country, I had more luck with the atomic resonance spectrum of atomic phosphorus in a high-pressure buffer gas. That was about in 1953-54. Now at last I had measured something on the free atom, namely its hyperfine structure. However, signal-to-noise was poor so I turned to the trigger techniques pioneered by our Chairman, Rabi, and by Block, Lamb, and my fellow colleagues Dicke and others. Adding a new wrinkle, I hoped -- as it turned out it was previously proposed by Kastler -- namely, alignment by electron impact -- I built a planar plasma diode filled with mercury vapor, and searched for a permanent resonant signal in the DC diode current but I couldn't find it.

However, shining filtered light from a mercury rectifier on it, I found the resonance in the transmitted light, and this was the origin of the transmission monitoring technique now used in the rubidium clock.

In the mercury experiment I also learned about spin exchange between electrons and atoms. The easy availability of polarized alkali atoms gave me the idea for my free electron spin resonance experiment, based on the back and forth spin exchange between electrons and optically pumped sodium atoms. To realize the long interaction and relaxation times necessary here for this kind of a spin-exchange polarization experiment, I fell back on my high-pressure buffer gas work on the atomic phosphorus.

Having very little money, I first demonstrated in a simple optical pumping experiment using adiabatic field and spin reverser, relaxation times approaching a second for sodium in a 30 torr buffer gas of argon. The correspondingly sharp $\Delta f = 0,1$ hyperfine resonances suggested by this had considerable application potential in magnetometers and frequency standards. Nevertheless, my brethren at the University of Washington, where I then was a visiting Assistant Professor, were not overly impressed by my efforts and in fact had invited me to shop around for another job.

So I contacted Martin Packard at Varian Associates, and also demonstrated my experiments to Felix Bloch, whose nuclear induction technique formed one of the cornerstones of this young company, Varian Associates. This led to a very successful collaboration in which Bell and Bloom at Varian quickly repeated my optical pumping experiments and also detected the 0-0 hyperfine transition in sodium in the transmitted light. No isotropic filter was used then. This simple approach has recently been revived for the least expensive rubidium clocks.

In my paper on the mercury work, I also had proposed radio frequency spectroscopy on trapped ions. This line of work in my lab at the University of Washington now has culminated in the magnesium monoion oscillator, an individual laser-cooled magnesium ion in a small ion trap. Well, I should mention that after our chairman, George Menley, got around to have a look in my laboratory, he did invite me to stay on as an Assistant Professor in 1956, so I am still with the University of Washington.

My collaborators, Roland Nagoni and Gary Jennings, just have measured the width of this trapped magnesium ion of the optical resonance line, which is just like a sodium-D line. The result: namely, within our limits the natural line establishes an ion temperature of about 5 milli-Kelvin.

The ultimate accuracy of a monoion oscillator laser frequency standard might approach -- I mean accuracy -- 1 part in 10^{18} . I should say "resolution" in order not to get in any big claims about how much one can split the line.

Again, the sideband cooling technique was first searched for by David Vineland and myself, not on an atomic ion for frequency standard purposes, but in our monoelectron oscillator work at the University of Washington. The goal of this work is the study of the finer structure of this most important elementary particle, namely, the electron and the positron.

I do not presume to know what frequency standards with 1 part in 10^{18} accuracy will be good for. However, for example, nobody also seems to know very well if two atoms of the same element will actually prove to be identical to that accuracy. And harking back on points raised before, maybe sequels of the Hubble expansion of the universe will become detectable in the laboratory. The important thing, again, seems to be to build one, and of course this is what you have also dedicated your efforts to.

I thank you for your attention.

DISTINGUISHED SCIENTIST PANEL

Panel Chairman: Professor I. I. Rabi, Columbia University

Well, I should perhaps mention that Professor Dicke really also tried to construct an atom.

PROFESSOR DICKE: That was an experiment that failed.

PROFESSOR RABI: Well, an experiment that failed. I have always thought about that because it was a brilliant experiment, and I know that in my case, and I collaborated with people like Norman Ramsey and Jerald Zacharias and Kusch -- that if the experiment was such that I could do it, it always succeeded, because I am not an experimenter and it had to be very simple, and others who are brilliant will always add wonderful things to it, which one deeply appreciates.

Well, I think it has been a good afternoon in the sense that it is almost 2 hours and we have lost very few customers, and the doors were open.

So I think it has been and I hope it has been entertaining, but I hope sort of inspirational of various attempts which have been made along this direction. Some have succeeded. Some did not succeed so well and haven't been pursued, but there is a very wide field and I think the richness of the field has been demonstrated by the last few speakers. Some of the new fields suggested are very intriguing, like geophysics and astrophysics. In other words, it's a great and wonderful field. I congratulate you for being in it, and I hope this has been a useful meeting. We thank you for your attention.

In the name of my colleagues, I thank you, there will be no encore and we will go on.

14TH ANNUAL PRECISE TIME AND TIME INTERVAL REGISTRATION

David W. Allan
National Bureau of Standards
325 Broadway
Boulder, CO 80303

Carroll O. Alley
University of Maryland
Dept. of Physics and Astronomy
College Park, MD 20742

Moltan P. Ananda
Aerospace Corporation
2350 E. El Segundo Blvd.
El Segundo, CA 90009

Philip E. Angerhofer
U.S. Naval Observatory
34th & Massachusetts Ave., NW
Washington, DC 20390

Claude Audoin
Laboratoire de L'Horloge Atomique
Batiment 221
Universite de Paris-Sud
91405 ORSAY, France

Kent R. Backe
CNR, Inc.
220 Reservoir St.
Needham, MA 02194

Wayne Bailey
Dept. of National Defence/CSE
101 Colonel By Drive
Ottawa, Canada K1A0K2

James F. Barnaba
Aerospace Guidance and Metrology Center
Newark Air Force Station
Newark, OH 45055

James A. Barnes
National Bureau of Standards
325 Broadway
Boulder, CO 80303

Andrew Barszczewski
National Research Council
N.A.E. Bldg U-61
Ottawa, Ontario, Canada K1A0R6

Charles A. Bartholomew
Naval Research Lab
Code 7960
Washington, DC 20375

Alvin G. Bates
Johns Hopkins Univ./APL
Johns Hopkins Rd.
Laurel, MD 20707

Charles R. Baugher
NASA
ES-63
Marshall Space Flight Center, AL 35812

Roger E. Beehler
NBS 524.00
325 Broadway
Boulder, CO 80303

Henry M. Beisner
IBM
18100 Frederick Pike
Gaithersburg, MD 20760

Jose S. Benavente
Instituto Y Observatorio de Marina
S/N General Pujale
San Fernando (Cadiz), Spain

Harry R. Betz
Lockheed Missiles and Space Company, Inc.
1111 Lockheed Way
Dept. 62-81 (DVO/LMSC)
Sunnyvale, CA 94086

Robert N. Blackwood
Blackwood Associates, Inc.
17904 Ednor View Terrace
Ashton, MD 20861

Martin B. Bloch
Frequency Electronics, Inc.
55 Charles Lindberg Blvd.
Uniondale, L.I., NY 11553

Eric L. Blomberg
KERNCO, Inc.
28 Harbor St.
Danvers, MA 01923

Edwin Bondurant
Satellite Business Systems
8003 Westpark Drive
McLean, VA 22102

Susan E. Borutzki
Jet Propulsion Lab
4800 Oak Grove Drive
Pasadena, CA 91109

William C. Brown
NASA
48 Lakeside Drive
Greenbelt, MD 20770

Ellis H. Bryant
The Weatherchron Co.
4881 Powers Ferry Rd., NW
Atlanta, GA 30327

Albert A. Buennagel
Jet Propulsion Lab
1748 N. Pepper Dr.
Pasadena, CA 91001

Lawrence A. Buennagel
Jet Propulsion Lab
1748 N. Pepper Dr.
Pasadena, CA 91001

Robert Burgoon
Hewlett Packard
5301 Stevens Creek Blvd.
Santa Clara, CA 95050

Giovanni Busca
Asulab S.A.
6 Max Meuron
Neuchatel, Switzerland 2001

Jose E. Calavia
Bendix Field Engineering
One Bendix Rd.
Columbia, MD 21045

Richard J. Carlson
Communications Security Est./Dept.
National Defence
101 Colonel By Drive
Ottawa, Ontario, Canada K1A0K2

Clifford F. Casey
Computer Sciences Corporation
6565 Arlington Blvd.
Falls Church, VA 22046

Frederick L. Casselman
Sylvania Systems Group
77 A St.
Needham Heights, MA 02194

David N. Chalmers
U.S. Naval Observatory
34th & Massachusetts Ave., NW
Washington, DC 20390

Fritz Chang
EG&G
35 Congress St.
Salem, MA 01970

Laura G. Charron
U.S. Naval Observatory
34th & Massachusetts Ave., NW
Washington, DC 20390

Mary C. Chiu
Johns Hopkins Univ./APL
Johns Hopkins Rd.
Laurel, MD 20707

Randolph T. Clarke, III
U.S. Naval Observatory
34th & Massachusetts Ave., NW
Washington, DC 20390

David A. Clayton
Offshore Navigation, Inc.
5728 Jefferson Highway
New Orleans, LA 70123

Philip A. Clemets
Jet Propulsion Lab
4800 Oak Grove Drive
Pasadena, CA 91109

Robert J. Coates
Goddard Space Flight Center
Code 904
Greenbelt, MD 20771

Jimmie B. Collie
NAVELEX
34th & Massachusetts Ave., NW
Washington, DC 20390

William V. Collings, Jr.
Pan American World Airways
Bldg 989 MU840
Patrick AFB, FL 32935

Cindy M. Collins
Pan American World Airways
Bldg 989 MU840
Patrick AFB, FL 32935

Gordon A. Corcoran
Geodetic Survey of Canada
Dept. of Mines & Resources
615 Booth St.
Ottawa, Ontario, Canada K1A0E9

Cecil C. Costain
National Research Council of Canada
Division of Physics
Ottawa, Ontario, Canada K1A0R6

Walter E. Cote
USAF/RADC
916 Schuyler
Rome, NY 13440

Duncan B. Cox, Jr.
The Charles Stark Draper Lab, Inc.
555 Technology Square
Cambridge, MA 02139

Evano L. Cunha, Chief
AFGL Research Library
SULLA, Stop 29
Hanscom AFB, MA 01731

Richard C. Cutchfield
IBM Corporation
21 First Field Rd.
Gaithersburg, MD 20760

Leonard S. Cutler
Hewlett Packard
3500 Deer Creek Rd.
Palo Alto, CA 94304

Normand N. C. Cyr
Laval University
139 St. Laurent
Quebec, Canada G1R1V1

Peter R. Dachel
Bendix Corporation
One Bendix Rd.
Columbia, MD 21045

Charles L. Daves, Jr.
Hughes Aircraft Co.
P.O. Box 31979
Aurora, CO 80041

Derek A. Davidson
University of New Brunswick
Dept. Surveying Engineering
Fredericton, N.B., Canada E3B5A3

Duane G. Davis
Hughes Aircraft Co.
P.O. Box 31979
Aurora, CO 80041

Rudolf Decher
NASA/MSFC
Huntsville, AL 35812

B. Louis Decker
DMA Aerospace Center
402 Devon Court
Ballwin, MO 63011

Hans G. Dehmelt
University of Washington
Seattle, WA 98195

Bearl F. Dennison
Hughes Aircraft Co.
P.O. Box 31979
Aurora, CO 80041

Edoardo Detoma
Bendix Field Engineering Corp.
Goddard Space Flight Center
Greenbelt, MD 20771

Michael A. Dials
EFRATOM
10213 W. Powers Ave.
Littleton, CO 80127

John G. Dick
Caltech
1201 E. California Blvd.
Pasadena, CA

Christina E. Dise
U.S. Naval Observatory
34th & Massachusetts Ave., NW
Washington, DC 20390

Robert W. Donaldson
Westinghouse Electric Corp.
P.O. Box 1897, MS 929
Baltimore, MD 21203

Robert E. Downs
Johns Hopkins Univ./APL
Johns Hopkins Rd.
Laurel, MD 20707

James D. Echols
Austron, Inc.
1915 Kramer Lane
Austin, TX 78758

Robert F. Ellis
Austron, Inc.
1915 Kramer Lane
Austin, TX 78758

Thomas C. English
EFRATOM Systems Corp.
18851 Bardeen
Irvine, CA 92626

James H. Ewing
Gawler-Knoop Co.
9209 Wendell St.
Silver Spring, MD 20901

Sheila C. Faulkner
U.S. Naval Observatory
34th & Massachusetts Ave., NW
Washington, DC 20390

Michael C. Fisher
Hewlett-Packard Co. MS 25
5301 Stevens Creek Blvd.
Santa Clara, CA 95050

Paul Forman
Smithsonian Institution
NMAH-5025
Washington, DC 20560

D. Earl Fossler
Track Systems
Division of Trak Microwave Corp.
4726 Eisenhower Blvd.
Tampa, FL 33614

George T. Fouratt
I.T.T.
1122 Patterson Rd.
Santa Maria, CA 93455

Daniel J. Freedman
Bendix Field Engineering Corp.
One Bendix Rd.
Columbia, MD 21045

Jerome P. Friedrichs
Motorola, Inc.
2553 N. Edgington
Franklin Park, IL 60131

Harold C. Friend
DCA, DCEC
1860 Wiehle Ave.
Reston, VA 22090

Dan Fryberger
Interstate Electronics Corp.
1745 Jefferson Davis Highway, Suite 601
Arlington, VA 22202

Larry M. Galloway
AGMC/MLSR
Newark Air Force Station
Newark, OH 43055

Michael R. Garvey
Frequency and Time Systems
34 Tozer Road
Beverly, MA 01915

Carl R. Gast
Trak Microwave
4722 Eisenhower Rd.
Tampa, FL 33609

R. J. Gerhars
Dept. of Defense
USANVL Bldg. 357
Ft. Belvoir, VA 22060

Asbjorn M. Gjelsvik
The MITRE Corp.
Box 208
Bedford, MA 01730

Robert M. Glasmeier
U.S. Air Force
Newark AFS Ohio MLE
Newark, OH 43055

Thomas J. Goblick
MIT Lincoln Laboratory
Wood Street
Lexington, MA 02173

Seymour Goldberg
EG&G Inc.
35 Congress St.
Salem, MA 01970

Earl Grant
U.S. Army Communications Command
P.O. Box 75
WSMR, NM 88002

Charles A. Greenhall
Jet Propulsion Lab
4800 Oak Grove Drive
Pasadena, CA 91109

David L. Hall
HRB Singer
P.O. Box 60, Science Park Rd.
State College, PA 16801

D. Wayne Hanson
National Bureau of Standards
325 Broadway
Boulder, CO 80302

Tadayoshi T. H. Hara
International Latitude Observatory
of Mizusawa
2-12 Hoshigaoka
Mizusawa, Iwate, Japan 023

James L. Harrigan
Naval Observatory
532 Twentieth Street NW, Apt 571
Washington, DC 20006

Robert W. Harris
Telecom Australia Research Labs
Box 249, Clayton
Vic 3168 Australia

Fred Harrison
Austron, Inc.
1915 Kramer Lane
Austin, TX 78758

Nelson J. Hayes
TRW
One Space Park, MS Bldg S, Rm 2470
Redondo Beach, CA 90278

Charles P. Henry
Marktron
13975 Conn. Ave
Silver Spring, MD 20906

Robert J. Hesselberth
Spectracom Corp.
320 N. Washington St.
Rochester, NY 14625

William H. Horton
Piezo Technology Inc.
2525 Shader Road
Orlando, FL 32804

Quyen D. Hua
Stanford Telecommunications, Inc.
1195 Bordeaux Drive
Sunnyvale, CA 94086

Peter S. P. Hui
GSFC, Code 725
Greenbelt, MD 20771

John F. Hynes
U.S. Air Force
1842 EEG (AFCC)
Scott AFB, IL 62225

Michael Jaffe
P.O. Box 560547
Miami, FL 33156

Chiranjiv L. Jain
Space Applications Centre,
(ISRO) Government of India
SAC P.O., Jodhpur Tekra,
Ahmedabad-380 053
Ahmedabad, Gujarat, India 380 053

Charles J. Jensik
Piezo Crystal Co.
100 K Street
Carlisle, PA 17013

Gao Jing-Hao
Beijing Institute of Radio Metrology
and Measurement
Post Box 3930
Beijing, China
Peoples Republic of China

Andrew C. Johnson
U.S. Naval Observatory
34th & Massachusetts Ave., NW
Washington, DC 20390

Charles B. Johnson
Austron, Inc.
1915 Kramer Lane
Austin, TX 78758

Alfred Kahan
USAF/RADC
Hanscom AFB
Bedford, MA 01731

William Kellogg
Lockheed Research Lab
3251 Hanover St.
Palo Alto, CA 94304

Robert H. Kern
KERNCO
4 Barbara Road
Danvers, MA 01923

Tom I. Kido
Interstate Electronics Corporation
707 E. Vermont Ave.
Anaheim, CA 92803

Dieter Kirchner
Technical University of Graz
A-8010 Graz Inffeldgasse 12, Austria

Albert Kirk
Jet Propulsion Lab
4800 Oak Grove Drive
Pasadena, CA 91109

William J. Klepczynski
U.S. Naval Observatory
Washington, DC 20390

Robert M. Kovacs
Kentron International Inc.
P.O. Box 1207
A.P.O. San Francisco, CA 96555

Ralph Kriss
Bendix Field Engineering Corp.
One Bendix Road
Columbia, MD 21045

Robert L. Kruger
Bendix Field Engineering Corp.
One Bendix Road
Columbia, MD 21045

Anthony J. Kubik
U.S. Naval Observatory
34th & Massachusetts Ave., NW
Washington, DC 20390

Paul F. Kuhnle
Jet Propulsion Lab
4800 Oak Grove Dr.
Pasadena, CA 91109

Vic Kunkle
True Time Division
3243 Santa Rosa Avenue
Santa Rosa, CA 95401

Ryszard Kunski
Bendix Field Engineering Corp.
One Bendix Rd.
Columbia, MD 21045

Paul Kushmeider
NASA/GSFC
Code 854.1
Greenbelt, MD 20771

Tae M. Kwon
Litton Guidance & Control
5500 Canoga Ave., MS25
Woodland Hills, CA 91364

Jean-Daniel Lavanceau
LT International
5106 Benton Ave.
Bethesda, MD 20814

Julis C. Law
Jet Propulsion Lab
4800 Oak Grove Drive, MS 503-101
Pasadena, CA 91109

Felix Lazarus
Hewlett-Packard (Schweiz) AG
19 Chemin Chateau-Bloc
1219 Le Lignon
Geneva, Switzerland

Christoph L. C. Lehner
DFVLR/GSOC-ZDBS
Postfach 156
Weilheim, West Germany 8120

David L. Lerner
Technical Services
P.O. Box 8
Lytle Creek, CA 92358

Vestal R. Lester
Hughes Aircraft Co.
Centinella & Teale Streets
Culver City, CA 90230

Lindon L. Lewis
National Bureau of Standards
325 Broadway
Boulder, CO 80303

Mark J. Lister
NRL, Code 7966
4555 Overlook Ave., SW
Washington, DC 20375

Theodore A. Long
Develco, Inc., Engineering Dept.
404 Tasman Dr.
Sunnyvale, CA 94086

Lute Maleki
Jet Propulsion Lab
4800 Oak Grove Drive
Pasadena, CA 91109

Richard H. Maurer
Johns Hopkins Applied Physics Lab
Johns Hopkins Road
Laurel, MD 20707

Charles May
Johns Hopkins University/APL
Johns Hopkins Rd.
Laurel, MD 20707

William K. May
Commandant (G-ONSOD/43)
U.S. Coast Guard HQ Bldg.
Washington, DC 20593

Thomas B. McCaskill
NRL, Code 7966
4555 Overlook Ave., SW
Washington, DC 20375

Raullo J. McConahy
Johns Hopkins Univ/APL
Johns Hopkins Rd.
Laurel, MD 20707

Arthur O. McCoubrey
National Bureau of Standards
Gaithersburg, MD 20760

James R. McCullough
Woods Hole Oceanographic Inst.
37 Sacenessct Road
Falwmlt, MA 02540

Michael McGuire
Hewlett-Packard Co.
3500 Deer Creek Road
Palo Alto, CA 94304

John W. McIntyre
Johns Hopkins Univ/APL
Johns Hopkins Road
Laurel, MD 20707

Marvin Meirs
Frequency Electronics, Inc.
55 Charles Lindberg Blvd.
Mitchel Field, NY 11553

Walter C. Melton
Stanford Telecommunications, Inc.
1195 Bordeaux Dr.
Sunnyvale, CA 94086

Gilles Missout
HYDRO Quebec
566 Beaumont
St. Bruno, Quebec, Canada J3NPR3

Billy B. Moon
AGMC/MLEA
Newark Air Force Station, OH 43055

Ivan I. Mueller
Ohio State University
Dept. of Geodetic Science & Surveying
1958 Neil Avenue
Columbus, OH 43210

Louis F. Mueller
Hewlett-Packard
5301 Stevens Creek
Santa Clara, CA 95050

Arvid E. Myers
U.S. Naval Observatory
34th & Massachusetts Ave., NW
Washington, DC 20390

Hartmut H. Nau
DFVLR
Munchner Street
8031 Wessling, Fed. Rep. Germany

Uri Naveh
Tadiran
909 3rd Ave.
New York, NY

Philip J. Norton
NAVASTROGRU, Systems Department
SPM 233
Pt. Mugu, CA 93042

Klemens Nottarp
Institut fur Angewandte Geodasie
Satellitenbeobachtungsstation Wettzell
8493 Kotzting, Fed. Rep. Germany 8493

Jay Oaks
Naval Research Laboratory
Code 7966
4555 Overlook Ave., SW
Washington, DC 20375

John T. Ohara
Marktron, Inc.
57 W. Timonium Rd.
Timonium, MD 21131

Bengt L. Ohman
Swedish Telecommunications Administration
11 Marbackagatan
S-123 86 Farsta, Sweden

George W. Oja
Navy Metrology Engineering Center
P.O. Box 2436
Pomona, CA 91769

William S. Orr
Geophysical Research Corp.
18131 East 4th St.
Tulsa, OK 74108

James W. O'Toole
Naval Surface Weapons Center
Dahlgren, VA 22448

Benjamin Parzen
Frequency Electronics, Inc.
3634 Seventh Ave.
San Diego, CA 92103

Iancu Pascaru
Frequency Electronics, Inc.
55 C. Lindberg Blvd.
Mitchel Field, NY 11553

Hays Penfield
Smithsonian Astrophysical Obs.
60 Garden St.
Cambridge, MA 02138

Harry Peters
Sigma Tau Standards Corp.
Box 1877
1014 Hachberry Lane
Tuscaloosa, AL 35403

H. E. Petrey
Defense Mapping Agency (Ret.)
A1 6424 54th Ave. N.
St. Petersburg, FL 33709

Edward A. Pettit
Eastern Space & Missile Center
Range Systems Management
ETR/RSM
Patrick AFB, FL 32925

David H. Phillips
2901 Accokeek Rd. W.
Accokeek, MD 20607

Paul J. Pointek
Dept. of Defense
9800 Savage Rd.
Ft. Meade, MD 20755

Robert V. Pound
Harvard University
Lyman Laboratory of Physics
Cambridge, MA 02178

Joseph M. Przyjemski
C.S. Draper Labs MS-92
555 Technology Sq.
Cambridge, MA 02139

Gerard L. Punt
KODE, Inc.
2752 Walnut Ave.
Tustin, CA 92680

Marilyn P. Raines
U.S. Naval Observatory
34th & Massachusetts Ave., NW
Washington, DC 20390

Norman F. Ramsey
Mount Holyoke College
21 Silver St.
South Hadley, MA 01075

Victor S. Reinhardt
Bendix Field Engineering Corp.
One Bendix Road
Columbia, MD 21045

Leslie W. Renfrey
Royal Australian Navy
1601 Massachusetts Ave
Washington, DC 20036

William J. Riley
EG&G, Inc.
35 Congress St.
Salem, MA 01970

Allan S. Risley
Frequency & Time Systems, Inc.
34 Tozer Rd.
Beverly, MA 01915

Charles K. Roberts
U.S. Naval Observatory
Washington, DC 20390

Tecwyn Roberts
NASA/GSFC
Code 800.3
Greenbelt, MD 20771

H. G. Robinson
Duke University
Physics Department
Durham, NC 27706

Ronald C. Roloff
Bendix Field Engineering Corp.
8005 McKenstry Dr.
Laurel, MD 20707

Vincent J. Rosati
U.S. Army ERADCOM
DELET-MQ-0
Fort Monmouth, NJ 07703

David E. Ross
Systems Development Corp.
2500 Colorado Ave. Drop 31-04
Santa Monica, CA 90406

Harold Roth
RADC/ES
Hanscom AFB
Bedford, MA 01731

Lauren J. Rueger
Johns Hopkins University/APL
Johns Hopkins Rd.
Laurel, MD 20707

William A. Ryan
NAVOBSY
2518 E. Meredith Dr.
Vienna, VA 22180

Mehjabin Saifi
Bendix Field Engineering Corp.
One Bendix Road
Columbia, MD 21045

Herbert Schild
DFVLR, Inst. for HF-Technik
D-8037 Wessling, West Germany

Bernard R. Schlueter
Oscilloquartz S.A.
16 Brevards
CH2002 Neuchatel, Switzerland

Wolfgang Schlueter
Institut fur Angewandte Geodasie
11-Weinbergstrasse
Frankfurt/M. Fed. Rep. Germany D6000

John G. Schmid
USAF AFSC WSMC
RSDE
Vandenberg AFB, CA 93437

Manfred Schneider
Institut fur Astron. und Physik. Geodasie
21 Arcisstrasse
D8000 Munchen, Fed. Rep. Germany

Anthony R. Seabrook
Royal Greenwich Observatory
Hersthonceaux Castle
Hailshah, East Sussex, England BN27 1RP

Gunter Seeber
Astronomische Station
Institut fur Erdmessung
5 Nienburgerstrasse
Hannover, West Germany

Hermann Seeger
Geodatisches Institut, Univ. Bonn
Nuss Allee 17
D5300 Bonn, Fed. Rep. Germany

Leonard F. Shepard
Time System Technology, Inc.
52 Morris Ave.
Lake Grove, NY 11755

Charles F. Shultheis
Defense Communications Engineering Center
Code R420
1860 Wiehle Ave.
Reston, VA 22090

Henry M. Sielski
Computer Sciences Corp.
8728 Colesville Rd. Offc 1032
Silver Spring, MD 20910

Alexander Skopetz
NASA/GSFC
11911 Galaxy Lane
Bowie, MD 20715

James A. Slater
Defense Mapping Agency
6500 Brookes Lane
Washington, DC 20315

Arthur E. Smith
Trajectory Inst. Div. Code 3421.3
Pacific Missile Test Center
Pt. Mugu, CA 93042

Robert C. Smythe
Piezo Technology Inc.
2525 Shader Road
Orlando, FL 32804

Kent L. Sorensen
TRW, Inc.
#1 Space Park Drive MS S-2470
Redondo Beach, CA 90278

Straton M. Spyropoulos
U.S. Naval Observatory
34th & Massachusetts Ave., NW
Washington, DC 20390

Thomas M. Stalder
Bendix Field Engineering Corp.
One Bendix Rd.
Columbia, MD 21045

Siegfried K. Starker
DFVLR, Fed. Rep. Germany
Munchuerstr
D-8031 Wessling, Fed. Rep. Germany

Sarah B. Stebbins
Naval Research Laboratory
4555 Overlook Ave., SW
Washington, DC 20375

Louis E. Stein
Westinghouse Electric Corp.
P.O. Box 1897 (MS929)
Baltimore, MD 21203

Samuel R. Stein
National Bureau of Standards
325 Broadway
Boulder, CO 80303

C. S. Stone
Brightline Corporation
P.O. Box 1016
Cedar Park, TX 78613

Harris A. Stover
Defense Communications Engineering Center
1860 Wiehle Ave.
Reston, VA 22090

David Y. Stowell
MITRE
1820 Dolley Madison Blvd.
McLean, VA

John T. Strain
FET
13975 Conn. Ave. #210
Silver Spring, MD 20906

Alvin Strauss
Frequency Electronics, Inc.
55 Charles Lindberg Blvd.
Mitchel Field, NY 11055

Su Bing-Wei
Beijing Institute of Radio Metrology
and Measurement
Post Box 3930
Beijing, Peoples Republic of China

Joe J. Suter
Bendix Field Engineering Corp.
One Bendix Rd.
Columbia, MD 21045

Richard L. Sydnor
Jet Propulsion Lab
4800 Oak Grove Drive
Pasadena, CA 91109

David A. Symonds
Piezo Technology, Inc.
Orlando, FL 32804

Aujinobu Takahashi
9208 Springhill Lane Apt. 204
Greenbelt, MD 20770

Philip E. Talley
Aerospace Corp.
2350 East El Segundo Blvd.
El Segundo, CA 90245

Michel Tetu
E. E. Dept., Laval University
Bldg. Pouliot
Quebec, Canada G1K7P4

Charles N. Townes
University of California
Berkeley, CA 94720

Hugo W. Tschiesche
Standard Elektrik Lorenz AG
42 Hellmuth-Hirth-Strasse
Stuttgart-40, Fed. Rep. Germany D7000

Jay W. Tuttle
KODE, Inc.
2752 Walnut Ave.
Tustin, CA 92680

A. J. Van Dierendonck
Stanford Telecommunication, Inc.
1195 Bordeaux Drive
Sunnyvale, CA 94086

Jacques J. V. Vanier
Laval University
Dept. of Electrical Engineering
Bldg. Pouliot, Room 3306
Quebec, Canada G1K7P4

Robert J. Van Wechel
Interstate Electronics Co.
707 E. Vermont Ave.
Anaheim, CA 92803

Robert F. C. Vessot
Smithsonian Institution
60 Garden St.
Cambridge, MA 02138

John R. Vig
U.S. Army ERADCOM Technology and
Devices Lab
Attn: DELET-MQ
Fort Monmouth, NJ 07703

Charles H. Volk
Aerospace Corporation
P.O. Box 92957
Los Angeles, CA 90009

H. Beat Wackernagel
USAF Space Command/D06
Peterson AFB, CO 80914

Elbert J. Walker
Hughes Aircraft Co.
P.O. Box 31979
Ayrora, CO 80041-0979

William C. Walker
Pan Am World Airways
Bldg. 989 MU 840
Patrick AFB, FL 32925

Donald J. Walt
89th FMS/MAAP
Bldg P17 Bolling AFB
Washington, DC 20332

Harry T. M. Wang
Hughes Research Laboratory
3011 Malibu Canyon Road
Malibu, CA 90265

Samuel C. Ward
Jet Propulsion Laboratory
4800 Oak Grove Drive
Pasadena, CA 91109

S. Clark Wardrip
NASA/GSFC, Code 854.1
Greenbelt, MD 20771

Werner A. Weidemann
Efratom Cal., Inc.
18851 Bardeen Ave.
Irving, CA 92691

Gary Westerhout
U.S. Naval Observatory
34th & Massachusetts Ave., NW
Washington, DC 20390

Robert W. Wettingfeld
Code 7752
Naval Research Lab
4555 Overlook Ave., SW
Washington, DC 20375

Paul J. Wheeler
U.S. Naval Observatory
34th & Massachusetts Ave., NW
Washington, DC 20390

Joseph D. White
U.S. Naval Research Lab
Mail Code 7962
Washington, DC 20375

Gary G. Whitworth
Applied Physics Lab/JHU
Johns Hopkins Rd.
Laurel, MD 20707

Warren L. Wilson
Fairchild Test Systems
707 Spindrift Dr.
San Jose, CA 95134

Thomas E. Wishard
Stanford Telecommunications, Inc.
1195 Bordeaux Dr.
Sunnyvale, CA 94086

Frances Neville Withington
U.S. Naval Observatory
34th & Massachusetts Ave., NW
Washington, DC 20390

Donald C. Wood
National Security Agency
Attn: R611
Ft. George Meade, MD 21012

Raymond F. Woolley
CECOM
DRSEL-PC-I-PS
Ft. Monmouth, NJ 07703

Woody Wordsworth
Austron, Inc.
1915 Kramer Lane
Austin, TX 78758

James L. Wright
Pan American Airways
Bldg. 989, MU840
Patrick AFB, FL 32925

Nicholas F. Yannoni
Rome Air Development Center/ESE
Hanscom AFB
Bedford, MA 01731

Robert R. Zeigler
Piezo Systems
100 K St.
Carlisle, PA 17013

BIBLIOGRAPHIC DATA SHEET

1. Report No. CP 2265		2. Government Accession No.		3. Recipient's Catalog No.	
4. Title and Subtitle Proceedings of the Fourteenth Annual Precise Time and Time Interval (PTTI) Applications Planning Meeting				5. Report Date February 1983	
				6. Performing Organization Code 814.2	
7. Author(s) Schuyler C. Wardrip, Editor				8. Performing Organization Report No.	
9. Performing Organization Name and Address Goddard Space Flight Center Greenbelt, Maryland 20771				10. Work Unit No.	
				11. Contract or Grant No.	
				13. Type of Report and Period Covered	
12. Sponsoring Agency Name and Address Naval Observatory; NASA Goddard Space Flight Center; Naval Electronic Systems Command; Naval Research Lab; Defense Communications Agency; Chief of Naval Operations; National Bureau of Standards; Army Electronics Technology & Devices Lab; Rome Air Development Center				14. Sponsoring Agency Code	
				15. Supplementary Notes	
16. Abstract These proceedings contain the papers presented at the Fourteenth Annual Precise Time and Time Interval (PTTI) Applications and Planning Meeting, including questions and answers following presentations. The purpose of the meeting was to give PTTI managers, systems engineers, and program planners a transparent view of the state of the art, an opportunity to express needs, a view of important future trends, and a review of relevant past accomplishments; to provide PTTI users with new and useful applications, procedures, and techniques; to allow the PTTI researcher to better assess fruitful directions for research efforts.					
17. Key Words (Selected by Author(s)) Time, time transfer, time dissemination, time measurement, hydrogen masers, masers			18. Distribution Statement Unclassified Unlimited STAR Category 36		
19. Security Classif. (of this report) Unclassified		20. Security Classif. (of this page) Unclassified		21. No. of Pages 670	22. Price*